Current Clinical Urology
Series Editor: Eric A. Klein

Pat F. Fulgham
Bruce R. Gilbert *Editors*

Practical Urological Ultrasound

Humana Press

Current Clinical Urology

Eric A. Klein, MD, Series Editor
Professor of Surgery
Cleveland Clinic Lerner College of Medicine Head,
Section of Urologic Oncology
Glickman Urological and Kidney Institute
Cleveland, OH

For further volumes:
http://www.springer.com/series/7635

Pat F. Fulgham • Bruce R. Gilbert
Editors

Practical Urological Ultrasound

Humana Press

Editors
Pat F. Fulgham, MD, FACS
Department of Urology
Texas Health Presbyterian Dallas,
Dallas, TX, USA

Bruce R. Gilbert, MD, PhD, FACS
Hofstra North Shore LIJ
School of Medicine
The Arthur Smith Institute for Urology
New Hyde Park, NY, USA

ISBN 978-1-58829-602-3 ISBN 978-1-59745-351-6 (eBook)
DOI 10.1007/978-1-59745-351-6
Springer New York Heidelberg Dordrecht London

Library of Congress Control Number: 2013933861

Printed on acid-free paper

Humana Press is a brand of Springer
Springer is part of Springer Science+Business Media (www.springer.com)

To Martin I. Resnick, MD (1943–2007) whose innovation and leadership are an enduring inspiration.

Foreword

Hark! Sound belongs to the masses! Similarly, ultrasound is not the private domain of the designated "imagers" in medicine but belongs to all members of the healing arts to the extent they wish to learn and employ it. Sound is the great equalizer providing a measure of social equality within medicine that unlike its royal sisters of imaging (i.e., fluoroscopic, computed tomographic, or magnetic resonance) is available equally and inexpensively (portable units are now <$50,000) to all.

As with endoscopy, urologists have the opportunity to be leaders in this field, and within the chapters of this book are the tickets for admission. Within these 14 chapters, all aspects of ultrasonographic urology are addressed. Drs. Pat Fulgham and Bruce Gilbert have graced us with a "labor of love," three years in the making; such is their belief, which I share, that ultrasound is the future of urology and needs to be accepted as an essential part of the urologist's training and practice. This is "opportunity come knocking".

The organs of our specialty are largely hidden from "view"—ultrasound makes them all visible, uncloaking the future and empowering physicians to favorably alter time's course on behalf of each patient. Will more renal, testicular, and possibly bladder tumors be "discovered?" Absolutely. Will their early discovery and treatment lead to a state much like we have seen with PSA and prostate cancer, in which the incidence of metastatic disease dramatically decreases and the longevity curve for each cancer is Turned "upward?" Only carefully done studies will tell, but already this technology is proving its worth as now follow-up studies for renal stones can be done with the ultrasound unit in the office, thereby saving the patient the time, money, and X-ray exposure of numerous "low-dose" CT scans.

I urge each urologic surgeon to embrace this technology in the fullest sense of its potential, for it is the ticket to a new realm of medicine, one in which we predict and thus prevent the disease before it occurs, proactively diagnose an impending illness prior to the development of debilitating symptoms, and treat/cure a malady in the most minimalist fashion, for the earlier

the diagnosis, the less the cost in dollars and human suffering for the cure. With apologies, here be at long last a non-Macbethian future in which:

> Life's defined in a passing shadow, a skilled imager
> Who scans and sets this 10 minutes upon the stage.
> And then recorded evermore.
> It is a tale.
> Told by a transducer, full of sound—not fury,
> Signifying everything.

August 9, 2012 Ralph V. Clayman

Preface

The genesis of this book was the conflicted conviction that ultrasound has a critical role to play in the management of urologic patients but that it would never be considered an integral part of the specialty of urology until there was a body of scholarly literature on the subject generated by urologists.

Urologists had been performing and interpreting transrectal ultrasound of the prostate for many years and routinely interpreting ultrasound examinations of the kidneys, bladder, and male genitalia, but comparatively few urologists were both performing and interpreting all of these studies on their patients. Therefore, the necessary preamble to this work was the identification of a group of urologists who were clinical experts in all aspects of urologic ultrasound. This group, the American Urological Association's (AUA) National Urologic Ultrasound Faculty, founded in 2007, began the ambitious project of educating themselves about the fundamentals of ultrasound physics, the biologic effects of ultrasound, patient safety, and scanning technique.

A standard curriculum was developed to transmit this enhanced information about ultrasound to practicing urologists, many of whom had already been performing transrectal ultrasound for two decades. The American Urological Association Office of Education has offered this curriculum, including hands-on training, to thousands of urologists in the United States and around the world.

The anticipated and hoped for consequence of clinicians acquiring a thorough understanding of ultrasound technology and technique was the rapid extension of ultrasound to new applications and clinical procedures. This has come to pass. As a consequence, there has been a heightened interest in establishing accepted indications for imaging procedures and guidelines for performing high-quality studies. With the guidance of the AUA, the American Institute of Ultrasound of Medicine (AIUM) has established *Practice Guidelines for the Performance of Ultrasound in the Practice of Urology*™ published in 2012. The AIUM now offers, for the first time, practice accreditation for urologic ultrasound.

Urologists have now begun to publish original research on the basic science of ultrasound as well as many clinical studies. Ultrasound education has become a more formal component of residency training in urology.

With these foundational pieces in place, we felt it was time to bring the information together in a single work conceived and written exclusively by clinical urologists. As such, we hope the information will be both authoritative and practical.

Dallas, TX, USA Pat F. Fulgham, MD, FACS

Preface

Imaging in medicine has been, and will likely remain, the primary modality for identification of altered structure due to disease processes. As a noninvasive, safe, and relatively inexpensive imaging modality, ultrasound has been embraced by many medical specialties as the "go to" technology.

With ever-changing technology and regulatory requirements, this book was envisaged to provide a compendium of information for the practicing urologist, beginning with the physical science of ultrasound and continuing through clinical applications in urology. It is our hope that this will be the first of many literary endeavors of urologists for urologists interested in performing and interpreting urologic ultrasound studies.

Ultrasound has often been referred to as the urologist's stethoscope because much of the genitourinary system is not easily evaluated by physical examination and requires imaging for diagnosis. Therein lies one of the unique aspects of ultrasound studies performed and interpreted by urologists. The mandate to examine the patient coupled with the urologist's experience in both surgical and medical treatment engenders an unparalleled ability to meld the healer's art with advanced imaging technology. It is our fervent hope that this text might encourage more urologists to embrace the art and science of ultrasound in their mission to provide excellence in patient care.

New Hyde Park, NY, USA — Bruce R. Gilbert, MD, PhD, FACS

Acknowledgements

Pat F. Fulgham MD, FACS

This book would not have been possible without the dedication and expertise of our contributing authors, many of whom are leading the way in research and developing new applications in urologic ultrasound.

Dr. Claus Roerhborn brought the practice of office-based ultrasound with him from Germany in 1983. Dr. Marty Resnick enlisted Claus to help educate a generation of urologists. They developed the early AUA Office of Education courses on urologic ultrasound which became the basis for much of the material in this book.

Special thanks to Dr. Bruce Gilbert whose knowledge and patience were the perfect modulating qualities for helping bind the complex pieces together into a cohesive "whole." His passion for teaching is infectious.

Angela Clark provided invaluable assistance in manuscript preparation, image preparation and labeling, graphics production, and research. Her talented project management, including dogged pursuit of the "finished product," has been the glue holding the project together.

Finally, thanks to my family whose forbearance permitted me the many distracted hours of writing and editing necessary to complete what proved to be a multiyear journey. It was a "task" in one sense but also a joy to see urologists take ownership of ultrasound as an invaluable tool in the management of their patients.

Bruce R. Gilbert MD, PhD, FACS

This book was the vision of my coeditor, colleague, and friend Dr. Pat Fulgham. Through his leadership over this past decade, he has helped elevate the art of urologic ultrasound to a subspecialty within urology. He is a gifted surgeon, articulate spokesman, and tireless academician who accepts nothing less than perfection from himself, which is Contagious amongst all who have had the great fortune to work with him.

To the authors of this book, I am indebted. They have tirelessly given of their precious time away from family and their busy clinical practices to share their experience. Their teachings as expressed in this text form the basis of urologic ultrasound.

My wife, and best friend Betsy, has been the most supportive and loving partner through the late nights and endless weekends involved in this project. She is, and has always been, my source of inspiration.

Contents

Contributors

Chad Baxter, MD Department of Urology, David Geffen School of Medicine at UCLA, Santa Monica, CA, USA

Akhil K. Das, MD, FACS Department of Urology, Thomas Jefferson University, Kimmel Cancer Center, Philadelphia, PA, USA

Majid Eshghi, MD, FACS, MBA Department of Urology, New York Medical College, Westchester Medical Center,Valhalla, New York, NY, USA

Farzeen Firoozi, MD Department of Urology, Hofstra Northshore–LIJ School of Medicine, The Arthur Smith Institute for Urology, Center of Pelvic Health and Reconstructive Surgery, Lake Success, NY, USA

Pat F. Fulgham, MD, FACS Department of Urology, Texas Health Presbyterian Dallas, Dallas, TX, USA

Bruce R. Gilbert, MD, PhD, FACS Hofstra North Shore LIJ School of Medicine, The Arthur Smith Institute for Urology, New Hyde Park, NY, USA

Fernando J. Kim, MD, FACS Department of Surgery/Urology, University of Colorado Health Science Center, Denver Health Medical Center, Tony Grampsas Cancer Center, Denver, CO, USA

Xiaolong S. Liu, MD Department of Urology, Thomas Jefferson University, Kimmel Cancer Center, PA, USA

Rao S. Mandalapu, MD Department of Urology, Fox Chase Cancer Center, Temple University Hospital, Elkins Park, PA, USA

Lane S. Palmer, MD Hofstra North Shore-LIJ School of Medicine, Cohen Children's Medical Center of New York, Lake Success, NY, USA

Christopher R. Porter, MD, FACS Department of Surgery, Virginia Mason Medical Center, Seattle, WA, USA

Soroush Rais-Bahrami, MD Hofstra North Shore LIJ School of Medicine, The Arthur Smith Institute for Urology, New Hyde Park, NY, USA

Kyle Rove, MD Department of Urology, University of Colorado Health Science Center, Aurora, CO, USA

Mostafa A. Sadek, MD Department of Urology, The Arthur Smith Institute for Urology, New Hyde Park, NY, USA

David E. Sehrt, BS Department of Surgery/Urology, University of Colorado Health Science Center, Denver Health Medical Center, Tony Grampsas Cancer Center, Denver, CO, USA

Jennifer Simmons, MD Division of Urology, Geisinger Medical Center, Danville, PA, USA

R. Ernest Sosa, MD Division of Urology, Veterans Administration Healthcare System, New York Harbor, Manhattan, NY, USA

Peter N. Tiffany, MD Department of Urology, Winchester Hospital, Tufts University School of Medicine, Stoneham, MA, USA

Edouard J. Trabulsi, MD, FACS Department of Urology, Thomas Jefferson University, Kimmel Cancer Center, Philadelphia, PA, USA

Nikhil Waingankar, MD North Shore-Long Island Jewish Health System, The Arthur Smith Institute for Urology, New Hyde Park, NY, USA

History of Ultrasound in Urology

1

Nikhil Waingankar and Bruce R. Gilbert

Ultrasound is the portion of the acoustic spectrum characterized by sonic waves that emanate at frequencies greater than that of the upper limit of sound audible to humans, 20 kHz. A phenomenon of physics that is found throughout nature, ultrasound is utilized by rodents, dogs, moths, dolphins, whales, frogs, and bats for a variety of purposes, including communication, evading predators, and locating prey [1–4]. Lorenzo Spallazani, an eighteenth-century Italian biologist and physiologist, was the first to provide experimental evidence that non-audible sound exists. Moreover, he hypothesized the utility of ultrasound in his work with bats by demonstrating that bats use sound rather than sight to locate insects and avoid obstacles during flight; this was proven in an experiment where blind-folded bats were able to fly without navigational difficulty while bats with their mouths covered were not. He later determined through operant conditioning that the *Eptesicus fuscus* bat can perceive tones between 2.5 and 100 kHz [5, 6].

The human application of ultrasound began in 1880 with the work of brothers Pierre and Jacques Curie, who discovered that when pressure is applied to certain crystals, they generate electric voltage [7]. The following year, Gabriel Lippmann demonstrated the reciprocal effect that crystals placed in an electric field become compressed [8]. The Curies demonstrated that when placed in an alternating electric current, the crystals either underwent expansion or contraction and produced high-frequency sound waves, thus creating the foundation for further work on piezoelectricity. Pierre Curie met his future wife, Marie—with whom he later shared the Nobel Prize for their work on radioactivity [9]—in 1894, when Marie was searching for a way to measure the radioactive emission of uranium salts. She turned to the piezoelectric quartz crystal as a solution, combining it with an ionization chamber and quadrant electrometer; this marked the first time piezoelectricity was used as an investigative tool [10].

The sinking of the RMS Titanic in 1912 drove the public's desire for a device capable of echolocation, or the use of sound waves to locate hidden objects. This was intensified 2 years later with the beginning of World War I, as submarine warfare became a vital part of both the Central and Allied Powers' strategies. Canadian inventor Reginald Aubrey Fessenden—perhaps most famous for his work in pioneering radio broadcasting and developing the Niagara Falls power plant—volunteered during World War I to help create an acoustic-based system for echolocation. Within 3 months he developed a high-power oscillator consisting of a 20 cm copper tube placed in a pattern of perpendicularly oriented magnetic fields that was capable of detecting an iceberg 2 miles away and being detected underwater by a receiver placed 50 miles away [11].

N. Waingankar, MD
North Shore-Long Island Jewish Health System,
The Arthur Smith Institute for Urology,
New Hyde Park, NY, USA

B.R. Gilbert, MD, PhD (✉)
Hofstra North Shore LIJ School of Medicine, The Arthur Smith Institute for Urology, New Hyde Park, NY, USA
e-mail: bgilbert@gmail.com

P.F. Fulgham and B.R. Gilbert (eds.), *Practical Urological Ultrasound*, Current Clinical Urology,
DOI 10.1007/978-1-59745-351-6_1, © Springer Science+Business Media New York 2013

A contemporary of Fessenden and student of Pierre Curie, Paul Langevin was similarly interested in using acoustic technology for the detection of submarines in World War I. Using piezoelectricity, he developed an ultrasound generator in which the frequency of the alternating field was matched to the resonant frequency of the quartz crystals. This resonance evoked by the crystal produced mechanical waves that were transmitted through the surrounding medium in ultrasonic frequency and were subsequently detected by the same crystals [12, 13]. Dubbed the "hydrophone," this represented the first model of what we know today as sound navigation and ranging, or SONAR. Although there were only sporadic reports on the use of SONAR in sinking German U-boats, SONAR was vital to both the Allied and Axis Powers during World War II [14].

In 1928, Russian scientist Sergei Sokolov further advanced the applicability of ultrasound in his experiments at Ulyanov Electrotechnical Institute. Using a "reflectoscope," Sokolov directed sound waves through metal objects, which were reflected at the opposite side of the object and traveled back to the reflectoscope. He determined that flaws within the metals would alter the otherwise predictable course of the sound waves. Sokolov also proposed the first "sonic camera," in which a metal's flaw could be imaged in high resolution. The actual output, however, was not adequate for practical usage. These early experiments describe what we now know as through transmission [15]. Sokolov is regarded by many as the "Father of Ultrasonics" and was awarded the Stalin prize for his work [13].

In 1936, German scientist Raimar Pohlman described an ultrasonic imaging method based on transmission via acoustic lenses, with conversion of the acoustic image into a visual entity. Two years later, Pohlman became the first to describe the use of ultrasound as a treatment modality when he observed its therapeutic effect when introduced into human tissues [16]. Austrian neurologist Karl Dussik is credited with being the first to use ultrasound as a diagnostic tool. In 1940 in a series of experiments attempting to map the human brain and potentially locate brain tumors, transducers were placed on each side of a patient's head, which along with the transducers was partially immersed in water. At a frequency of 1.2 MHz, Dussik's "hyperphonography" was able to produce low-resolution "ventriculograms" [17]. Other investigators were unable to reproduce the same images as Dussik, sparking controversy that his may have not been true images of the cerebral ventricles, but rather, acoustic artifact. Dussik's work led MIT physician HT Ballantyne to conduct similar experiments, where they demonstrated that an empty skull produces the same images obtained by Dussik. They concluded that attenuation patterns produced by the skull were contributing to the patterns that Dussik had previously thought resulted from changes in acoustic transmission caused by the ventricles. These findings led the United States Atomic Energy Commission to conclude that ultrasound had no role in the diagnosis of brain pathology [18, 19].

In 1949, John Wild, a surgeon who had spent time in World War II treating numerous soldiers with abdominal distention following explosions, used military aviation-grade ultrasonic equipment to measure bowel thickness as a noninvasive tool to determine the need for surgical intervention. He later used A-mode comparisons of normal and cancerous tissue to demonstrate that ultrasound could be useful in the detection of cancer growth. Wild teamed up with engineer John Reid to build the first portable "echograph" for use in hospitals and also to develop a scanner that was capable of detecting breast and colon cancer by using pulsed waves to allow display of the location and reflectivity of an object, a mode that would later be described as "brightness mode," or simply B-mode [13, 20, 21].

Following the post-World War II resurgence of interest in cardiac surgery, Inge Edler and Hellmuth Hertz began to investigate noninvasive methods of detecting mitral stenosis, a disease with relatively poor results at the time. Using an ultrasonic reflectoscope with tracings recorded on slowly moving photographic film designed by Hertz, they were able to capture moving structures within the heart. Dubbed "ultrasound cardiography," this represented the first echocardiogram, which was capable of differentiating mitral stenosis from mitral regurgitation and detecting atrial thrombi, myxomas, and pericardial effusions [22, 23] (Fig. 1.1).

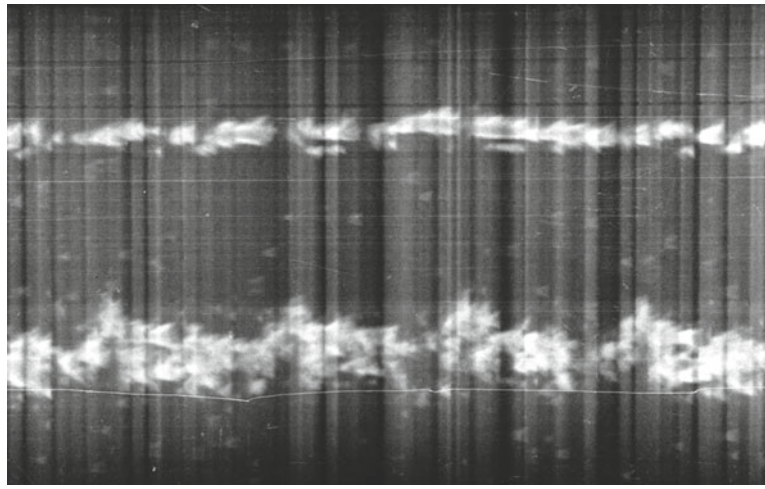

Fig. 1.1 First "motion-mode," or M-mode, tracing displaying ultrasonic tracings of moving cardiac structures. From [23]

With the support of the Veterans Administration and United States Public Health Service, Holmes et al. described the use of ultrasound to detect soft tissue structures with an ultrasonic "sonascope." This consisted of a large water bath in which the patient would sit, a sound generator mounted on the tub, and an oscilloscope which would display the images. The sonascope was capable of identifying a cirrhotic liver, renal cyst, and differentiating veins, arteries, and nerves in the neck. Consistent with the results of their predecessors, however, they were unable to produce meaningful ultrasound images of the brain [24].

The use of ultrasound in obstetrics and gynecology began in 1954 when Ian Donald became interested in the use of A-mode, or amplitude-mode, which uses a single transducer to plot echoes on a screen as a function of depth; one of the early uses of this was to differentiate solid from cystic masses. Using a borrowed flaw-detector, he initially found that the patterns of the two masses were sonically unique. Working with the research department of an atomic boilermaker company, he led a team that developed the first contact scanner. Obviating the need for a large water bath, this device was hand-operated and kept in contact with skin and coupled with olive oil. Captured on Polaroid film with an open shutter, abdominal masses could be reliably and reproducibly differentiated using ultrasound. Three years later, Donald collaborated with his team of engineers to develop a means to measure distances on the output on a cathode ray tube, which was subsequently used to determine fetal head size [13, 25, 26].

History of Doppler Ultrasound

In 1842, Christian Johann Doppler theorized that the frequency of light received at a distance from a fixed source is different than the frequency emitted if the source is in motion [27]. More than 100 years later, this principle was applied to sound by Satomura in his study on cardiac valvular motion and peripheral blood vessel pulsation [28]. In 1958, Seattle pediatrician Rushmer and his team of engineers further advanced the technology with their development of transcutaneous continuous-wave flow measurements and spectral analysis in peripheral and extracranial brain vessels [29]. Real-time imaging—developed in 1962 by Holmes—was born out of the principle of "compounding," which allowed the sonographer to sweep the transducer across the target to continuously add information to the scan; the phosphor decay display left residual images from the prior transducer position on the screen, allowing the entire target to be visualized [13]. The first commercially available real-time scanner was

produced by Siemens, and its first published use was in the diagnosis of hydrops fetalis [30, 31].

Bernstine and Callagan were the first to report the obstetric utility of Doppler in their 1964 report on ultrasonic detection of fetal heart movement, thus laying the foundation for continuous fetal monitoring [32]. The same year, Buschmann was the first to report "carotid echography" for the diagnosis of carotid artery thrombosis [33], although debate ensued as to whether ultrasound was capable of identifying the carotid bifurcation or its branches into the internal and external carotid arteries [34–37].

In 1966, Kato and Izumi developed directional Doppler that was capable of determining direction of flow [31, 38]. The following year, McLeod in the United States reported similar findings using phase shift in the United States [31, 39]. By 1967, the use of Doppler ultrasound had spread to Europe, where continuous-wave ultrasound (which does not allow precise spatial localization) was being used to diagnose occlusive disease of neck and limb arteries, venous thrombosis, and valvular insufficiency with accuracy [40]. Pulsed Doppler soon provided the capability of sampling specific Doppler signals in target tissues, a function that quickly became clinically applicable in the detection of valvular motion and differential flow rates within the heart [41].

The addition of color flow mapping to Doppler ultrasound allowed real-time mapping of blood flow patterns [42]. The limitations of color flow, including angle dependence and difficulty assessing flow in slow-flow states, were soon appreciated. These were overcome with the advent of an alternative form of Doppler, termed "Power Doppler." This alternative to routine color flow was found to be useful in confirming or excluding difficult cases of testicular or ovarian torsion and vascular thrombosis [43].

In 1989, Baba and colleagues reported on the first production of a three-dimensional ultrasonic image. Using a real-time straight or curved transducer, they were able to obtain positional information with an ultrasound device that was connected to a microcomputer, which reconstructed the data into a three-dimensional output. The authors hypothesized that this system would be ideal for the screening of fetal anomalies and abnormalities in intrauterine growth [43]. Following the development of von Ramm's three-dimensional ultrasound device, Sheikh et al. published the first use of real-time three-dimensional acquisition and presentation of data in the United States in 1991. This proved to be useful in cardiology for assessment of perfusion and ventricular function [44].

History of Ultrasound in Urology

Prostate

In 1963, Japanese urologists Takahashi and Ouchi became the first to attempt ultrasonic examination of the prostate. However, the image quality that resulted was not interpretable and thus carried little medical utility [45]. Wild and Reid also attempted transrectal ultrasound, but were met with the same result. Progress was not made until Watanabe et al. demonstrated radial scanning that could adequately identify prostate and bladder pathology. Using a purpose-built device modeled after a museum sculpture entitled "Magician's Chair," Watanabe seated his patients on a chair with a hole cut in the center such that the transducer tube could be passed through the hole and into the rectum of the seated patient [46]. Images from Watanabe's seated probe are displayed below; it is evident in Fig. 1.2b (demonstrating an area of circumscribed symmetric echogenicity, representing BPH) and Fig. 1.2c (demonstrating an asymmetric area of hyperechogenicity, representing prostate cancer) that resolution was poor and images displayed extreme contrast. Subsequent development of biplane, high-frequency probes has created increased resolution and has allowed for transrectal ultrasound to become the standard for diagnosis of prostatic disease (Fig. 1.2a–c).

In 1974, Holm and Northeved introduced a transurethral ultrasonic device that would be interchangeable with conventional optics during cystoscopy for the purpose of imaging the prostate and bladder. Their goals for this device included the ability to determine the depth of bladder tumor penetration, prostatic volume, prostatic tumor progression, and to assist with transurethral resection of prostate [47].

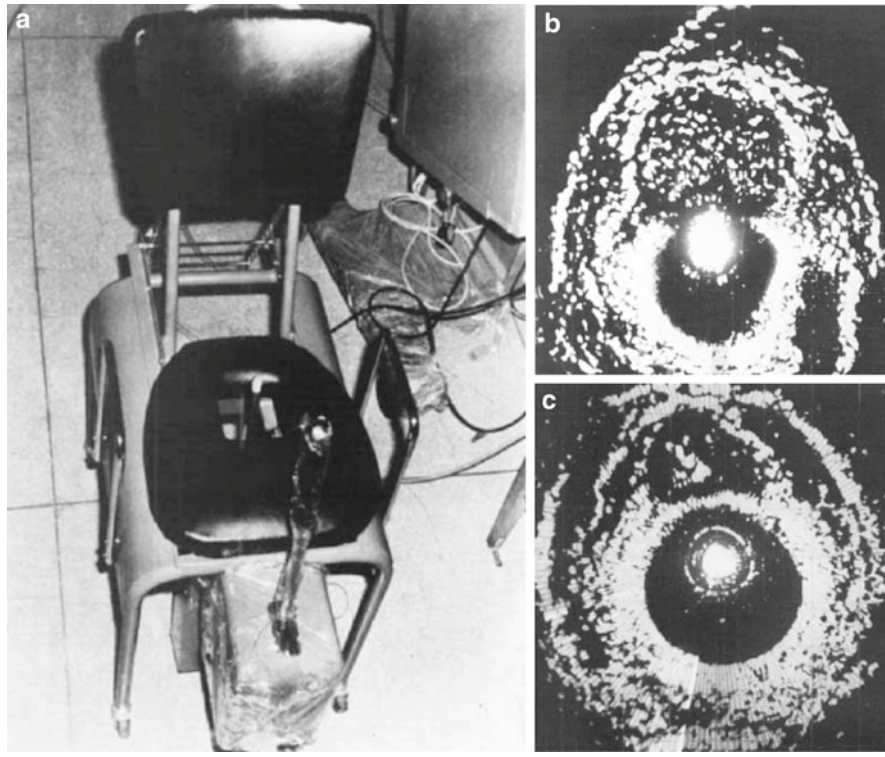

Fig. 1.2 (**a**) Watanabe's chair, (**b**) display of patient with BPH, (**c**) display of prostate cancer. This material is reproduced with permission of John Wiley & Sons, Inc. Watanabe H, et al. Development and application of new equipment for transrectal ultrasonography. J Clin Ultrasound. 1974; 2(2): p. 91–8. Copyright 1957 John Wiley & Sons, Inc

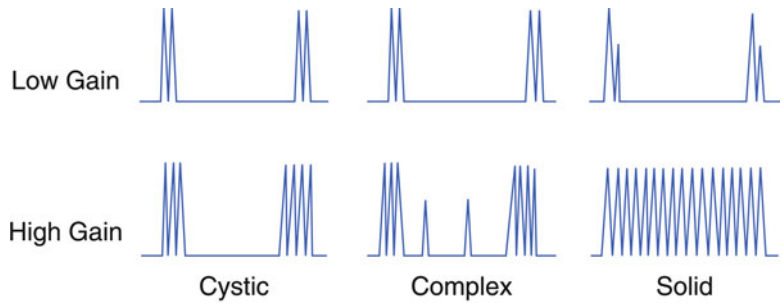

Fig. 1.3 RCC. Reprinted from The Journal of Urology, 2, Barry B. Goldberg, Howard M. Pollack, T Differentiation of renal masses using a-mode ultrasound, 2002, with permission from Elsevier

Kidney

In 1971, Goldberg and Pollack, frustrated with the inability of IVP to differentiate benign from malignant lesions, turned to A-mode ultrasound. In their report on "nephrosonography," they demonstrated in a series of 150 patients the capability of ultrasound to discern solid, cystic, and complex masses with an accuracy of 96%. The diagrammatic representation of the three ultrasound patterns they found is depicted in Fig. 1.3 above [48]. In cystic lesions, the first spike represents the striking of the front wall of the cyst, and the second spike represents the striking of the back wall. More complex lesions, therefore have return of more spikes.

Scrotum

Perri et al. were the first to use Doppler as a sonic "stethoscope" in their workup of patients with an acute scrotum. While they were able to identify patients with epididymitis and torsion of the appendix testis as having increased flow, and patients with spermatic cord torsion as having no blood flow, they also reported that false negatives in cases of torsion could result from increased flow secondary to reactive hyperemia [49, 50].

Further Advancements

Watanabe et al. demonstrated that Doppler could be used to identify the renal arteries in a noninvasive way in 1976 [51], and 5 years afterward, Greene et al. documented that Doppler could adequately differentiate stenotic from normal renal arteries [52]. In 1982, Arima et al. used Doppler to differentiate acute from chronic rejection in renal transplant patients, noting that acute rejection is characterized by the disappearance of diastolic phase, with reappearance being indicative of recovery from rejection. The authors concluded that Doppler could guide the management of rejection as an index for steroid therapy [53].

In the early 1990s, a number of authors investigated the therapeutic uses of high-intensity focused ultrasound, or HIFU. Following prior reports of histologic changes following HIFU [54], Madersbacher et al. were the first to report the safety and efficacy of HIFU in symptomatic BPH patients [55]. Its utilities in the treatments of testicular cancer [56], early prostate cancer [57], recurrent prostate cancer [58], and renal cell cancer (transcutaneously [59] and laparoscopically [60]) were soon explored as well.

The field of urology continues to demand and discover novel uses for ultrasound technology. Chen et al. used transrectal ultrasound guidance to inject botulinum toxin into the external urethral sphincters of a series of patients with detrusor external sphincter dyssynergia [61]. Ozawa et al. used perineal ultrasound videourodynamics to accurately diagnose bladder outlet obstruction in a new, noninvasive method [62]. The possibilities for the application of ultrasound in diagnosing or treating urologic patients remain endless.

Conclusion

Ultrasound is a cost-effective, accurate, easy to use, and nearly ubiquitous diagnostic tool that produces meaningful results instantly. As a standard in the urologist's office armamentarium, it can be applied to the work-up of pathology of the genitalia, pelvic floor, bladder, prostate, and kidneys. Specific uses within each organ system will be detailed throughout this book.

The history of ultrasound is quite extensive and has involved a number of groundbreaking discoveries and new applications of basic physical principles. This homage to the innovators of the past serves both to recognize prior achievements and to acknowledge that future work in the development of new applications for ultrasound will always be needed.

References

1. Corcoran AJ, Barber JR, Conner WE. Tiger moth jams bat sonar. Science. 2009;325(5938):325–7.
2. Dunning DC, Roeder KD. Moth sounds and the insect-catching behavior of bats. Science. 1965;147:173–4.
3. Mackay RL, Liaw HM. Dolphin vocalization mechanisms. Science. 1981;212(4495):676–8.
4. Ruttimann J. Frogs chat in ultrasound. Nature News, 15 Mar 2006.
5. Galambos R. The avoidance of obstacles by flying bats: Spallazani's ideas (1794) and later theories. Isis. 1942;34(2):132–40.
6. Dijkgraaf S. Spallanzani's unpublished experiments on the sensory basis of object perception in bats. Isis. 1960;51(1):9–20.
7. Curie J, Curie P. Sur 'electricite polaire dans cristaux hemiedres a face inclinees. C R Seances Acad Sci. 1880;91:383.
8. Katzir S. The discovery of the piezoelectric effect. In: Katzir S, editor. The beginnings of piezoelectricity: a study in Mundane Physics. Netherlands: Springer; 2006. p. 15–64.
9. Curie P. Radioactive substances, especially radium. Nobel Lecture, 6 Jun 1905.
10. Diamantis A, Magiorkinis E, Papadimitriou A, Androutsos G. The contribution of Maria Sklodowska-Curie and Pierre Curie to Nuclear and Medical Physics. A hundred and ten years after the discovery of radium. Hell J Nucl Med. 2008;11(1):33–8.

11. Seitz F. The cosmic inventor: Reginald Aubrey Fessenden (1866-1932). Am Philos Soc. 1999;89:41–6.
12. Chilowsky C, Langevin MP. Procedes et appareils pour la production de signaux sous-marins diriges et pour la localisation a distance d'obstacles sous-marins; French patent #502913, 1916.
13. Martin J. History of ultrasound. In: Sanders RC, Resnick M, editors. Ultrasound in urology. Baltimore, MD: Williams and Wilkins; 1984. p. 1–12.
14. Zimmerman D. Paul Langevin and the discovery of active sonar or Asdic. North Mariner. 2002; 12(1): 39–52.
15. Sokolov SY. The ultra-acoustic microscope. Zh Tekh Fiz. 1949;19:271.
16. Jagannathan J, et al. High-intensity focused ultrasound surgery of the brain: part 1—a historical perspective with modern applications. Neurosurgery. 2009;64(2):201–10. discussion 210–1.
17. Dussik K. Uber die Moglichkeit, hochfrequente mechanische Schwingungen als diagnostische Mittel zu verwerten. Z Ges Neurol Psych. 1941;174:153–68.
18. Thomas AMK, Banerjee AK, Busch U. Uber die Moglichkeit, hochfrequente mechanische Schwingungen als diagnostische Mittel zu verwerten. In: Banerjee AK, Thomas AMK, Busch U, editors. Classic papers in modern diagnostic radiology. Berlin: Springer; 2005. p. 141–61.
19. Shampo MA, Kyle RA. Karl Theodore Dussik–pioneer in ultrasound. Mayo Clin Proc. 1995;70(12):1136.
20. Thomas AMK, Banerjee AK, Busch U. Application of echo-ranging techniques to the determination of structure of biological tissues. In: Banerjee AK, Thomas AMK, Busch U, editors. Classic papers in modern diagnostic radiology. Berlin: Springer; 2005. p. 162–9.
21. Wild JJ, Reid JM. Application of echo-ranging techniques to the determination of structure of biological tissues. Science. 1952;115(2983):226–30.
22. Edler I, Hertz CH. The use of ultrasonic reflectoscope for the continuous recording of the movements of heart walls. 1954. Clin Physiol Funct Imaging. 2004; 24(3):118–36.
23. Fraser AG. Inge Edler and the origins of clinical echocardiography. Eur J Echocardiogr. 2001;2(1):3–5.
24. Holmes JH, et al. The ultrasonic visualization of soft tissue structures in the human body. Trans Am Clin Climatol Assoc. 1954;66:208–25.
25. Donald I, Macvicar J, Brown TG. Investigation of abdominal masses by pulsed ultrasound. Lancet. 1958;1(7032):1188–95.
26. Thomas AMK, Banerjee AK, Busch U. Investigation of abdominal masses by pulsed ultrasound. In: Banerjee AK, Thomas AMK, Busch U, editors. Classic papers in modern diagnostic radiology. Berlin: Springer; 2005. p. 213–23.
27. Doppler C. Über das farbige Licht der Doppelsterne und einiger anderer Gestirne des Himmels. Abh Königl Böhm Ges Wiss. 1843;2:465–82.
28. Satomura S. Ultrasonic Doppler method for the inspection of cardiac function. J Acoust Soc Am. 1957;29:1181–5.
29. Coman IM. Christian Andreas Doppler–the man and his legacy. Eur J Echocardiogr. 2005;6(1):7–10.
30. Hofmann D, Hollander HJ. Intrauterine diagnosis of hydrops fetus universalis using ultrasound. Zentralbl Gynakol. 1968;90(19):667–9.
31. Woo J. A short history of the development of ultrasound in obstetrics and gynecology. http://www.ob-ultrasound.net/site_index.html.
32. Bernstine RL, Callagan DA. Ultrasonic Doppler inspection of the fetal heart. Am J Obstet Gynecol. 1966;95(7):1001–4.
33. Buschmann W. On the diagnosis of carotid thrombosis. Albrecht Von Graefes Arch Ophthalmol. 1964; 166:519–29.
34. Brinker RA, Landiss DJ, Croley TF. Detection of carotid artery bifurcation stenosis by Doppler ultrasound. Preliminary report. J Neurosurg. 1968;29(2):143–8.
35. Grossman BL, Wood EH. Evaluation of cerebrovascular disease utilizing a transcutaneous Doppler technic. Radiology. 1968;90(3):586–7.
36. Strandness D Jr. Ultrasonic velocity determination in the diagnosis and evaluation of peripheral vascular disease. In: Symposium on ultrasound. Bloomington, IN: Indiana University Press; 1968.
37. Maroon JC, Campbell RL, Dyken ML. Internal carotid artery occlusion diagnosed by Doppler ultrasound. Stroke. 1970;1(2):122–7.
38. Kato K, Izumi T. A new ultrasonic flowmeter that can detect flow direction. In: Proceedings of the 10th scientific meeting of the Japan Society of Ultrasonics in Medicine; Springer 1966. p. 78–9.
39. McLeod F. A directional Doppler flowmeter. In: Digest of the 7th international conference on medical electronics and biological engineering; Royal Academy of Engineering Sciences 1967. p. 213.
40. Bollinger A, Partsch H. Christian Doppler is 200 years young. Vasa. 2003;32(4):225–33.
41. Baker DW, Johnson SL. Doppler echocardiograpy. In: Waag RC, Gramiak R, editors. Cardiac ultrasound. St. Louis: CV Mosby; 1974. p. 24.
42. Maulik D, et al. Doppler color flow mapping of the fetal heart. Angiology. 1986;37(9):628–32.
43. Hamper UM, et al. Power Doppler imaging: clinical experience and correlation with color Doppler US and other imaging modalities. Radiographics. 1997; 17(2):499–513.
44. Sheikh K, et al. Real-time, three-dimensional echocardiography: feasibility and initial use. Echocardiography. 1991;8(1):119–25.
45. Takahashi H, Ouchi T. The ultrasonic diagnosis in the field of urology. Proc Jpn Soc Ultrasonics Med. 1963;3:7.
46. Watanabe H, et al. Development and application of new equipment for transrectal ultrasonography. J Clin Ultrasound. 1974;2(2):91–8.
47. Holm HH, Northeved A. A transurethral ultrasonic scanner. J Urol. 1974;111(2):238–41.
48. Goldberg BB, Pollack HM. Differentiation of renal masses using A-mode ultrasound. J Urol. 1971; 105(6):765–71.

49. Perri AJ, et al. Necrotic testicle with increased blood flow on Doppler ultrasonic examination. Urology. 1976;8(3):265–7.
50. Perri AJ, et al. The Doppler stethoscope and the diagnosis of the acute scrotum. J Urol. 1976;116(5): 598–600.
51. Watanabe H, et al. Non-invasive detection of ultrasonic Doppler signals from renal vessels. Tohoku J Exp Med. 1976;118(4):393–4.
52. Greene ER, et al. Noninvasive characterization of renal artery blood flow. Kidney Int. 1981;20(4):523–9.
53. Arima M, et al. Predictability of renal allograft prognosis during rejection crisis by ultrasonic Doppler flow technique. Urology. 1982;19(4): 389–94.
54. Burgess SE, et al. Histologic changes in porcine eyes treated with high-intensity focused ultrasound. Ann Ophthalmol. 1987;19(4):133–8.
55. Madersbacher S, et al. Tissue ablation in benign prostatic hyperplasia with high-intensity focused ultrasound. Eur Urol. 1993;23 Suppl 1:39–43.
56. Madersbacher S, et al. Transcutaneous high-intensity focused ultrasound and irradiation: an organ-preserving treatment of cancer in a solitary testis. Eur Urol. 1998; 33(2):195–201.
57. Chapelon JY, et al. Treatment of localised prostate cancer with transrectal high intensity focused ultrasound. Eur J Ultrasound. 1999;9(1):31–8.
58. Berge V, Baco E, Karlsen SJ. A prospective study of salvage high-intensity focused ultrasound for locally radiorecurrent prostate cancer: early results. Scand J Urol Nephrol. 2010;44(4):223–7.
59. Kohrmann KU, et al. High intensity focused ultrasound as noninvasive therapy for multilocal renal cell carcinoma: case study and review of the literature. J Urol. 2002;167(6):2397–403.
60. Margreiter M, Marberger M. Focal therapy and imaging in prostate and kidney cancer: high-intensity focused ultrasound ablation of small renal tumors. J Endourol. 2010;24(5):745–8.
61. Chen SL, et al. Transrectal ultrasound-guided transperineal botulinum toxin a injection to the external urethral sphincter for treatment of detrusor external sphincter dyssynergia in patients with spinal cord injury. Arch Phys Med Rehabil. 2010; 91(3):340–4.
62. Ozawa H, et al. The future of urodynamics: noninvasive ultrasound videourodynamics. Int J Urol. 2010;17(3):241–9.

Physical Principles of Ultrasound

2

Pat F. Fulgham

Introduction

The use of ultrasound is fundamental to the practice of urology. In order for urologists to best use this technology on behalf of their patients, they must have a thorough understanding of the physical principles of ultrasound. Understanding how to tune the equipment and to manipulate the transducer to achieve the best-quality image is crucial to the effective use of ultrasound. The technical skills required to perform and interpret urologic ultrasound represent a combination of practical scanning ability and knowledge of the underlying disease processes of the organs being imaged. Urologists must understand how ultrasound affects biological tissues in order to use this modality safely and appropriately. When the physical principles of ultrasound are fully understood, urologists will recognize both the advantages and limitations of ultrasound.

The Mechanics of Ultrasound Waves

The image produced by ultrasound is the result of the interaction of mechanical ultrasound waves with biologic tissues and materials. Because ultrasound waves are transmitted at frequent intervals and the reflected waves received by the transducer, the images can be reconstructed and refreshed rapidly, providing a real-time image of the organs being evaluated. Ultrasound waves are **mechanical waves** which require a physical medium (such as tissue or fluid) to be transmitted. Medical ultrasound imaging utilizes frequencies in the one million cycles per second (or MHz) range. Most transducers used in urology vary from 2.5 to 18 MHz, depending on the application.

Ultrasound waves are created by applying alternating current to piezoelectric crystals within the transducer. Alternating expansion and contraction of the piezoelectric crystals creates a mechanical wave which is transmitted through a coupling medium (usually gel) to the skin and then into the body. The waves that are produced are **longitudinal waves**. This means that the particle motion is in the same direction as the propagation of the wave (Fig. 2.1). This longitudinal wave produces areas of rarefaction and compression of tissue in the direction of travel of the ultrasound wave.

The compression and rarefaction of molecules is represented graphically as a sine wave alternating between a positive and negative deflection from the baseline. A **wavelength** is described as the distance between one peak of the wave and the next peak. One complete path traveled by the wave is called a **cycle**. One cycle per second is known as 1 Hz (Hertz). The **amplitude** of a wave is the maximal excursion in the positive or negative direction from the baseline, and the **period** is the time it takes for one complete cycle of the wave (Fig. 2.2).

P.F. Fulgham, MD, FACS (✉)
Department of Urology, Texas Health Presbyterian Dallas, 8210 Walnut Hill Lane Suite 014, Dallas, TX 75231, USA
e-mail: pfulgham@airmail.net; patfulgham@yahoo.com

P.F. Fulgham and B.R. Gilbert (eds.), *Practical Urological Ultrasound*, Current Clinical Urology,
DOI 10.1007/978-1-59745-351-6_2, © Springer Science+Business Media New York 2013

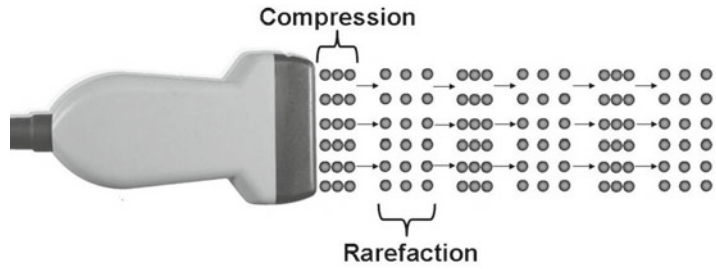

Fig. 2.1 Longitudinal waves. The expansion and contraction of piezoelectric crystals caused by the application of alternating current to the crystals causes compression and rarefaction of molecules in the body

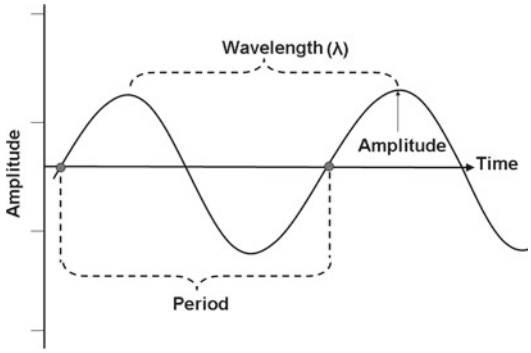

Fig. 2.2 Characteristics of a sound wave: the amplitude of the wave is a function of the acoustical power used to generate the mechanical compression wave and the medium through which it is transmitted

The velocity with which a sound wave travels through tissue is a product of its frequency and its wavelength. The velocity of sound in tissues is constant. Therefore, as the frequency of the sound wave changes, the wavelength must also change. The average velocity of sound in human tissues is 1,540 m/s. Wavelength and frequency vary in an inverse relationship. Velocity equals frequency times wavelength (Fig. 2.3). As the frequency diminishes from 10 to 1 MHz the wavelength increases from 0.15 to 1.5 mm. This has important consequences for the choice of transducer depending on the indication for imaging.

$$\upsilon = f\lambda$$

velocity = frequency x wavelength

Fig. 2.3 Since the velocity of sound in tissue is a constant, the frequency and wavelength of sound must vary inversely

Ultrasound Image Generation

The image produced by an ultrasound machine begins with the transducer. **Transducer** comes from the Latin **transducere**, which means to convert. In this case, electrical impulses are converted to mechanical sound waves via the **piezoelectric effect**.

In ultrasound imaging the transducer has a dual function as a sender and a receiver. Sound waves are transmitted into the body where they are at least partially reflected. The piezoelectric effect occurs when alternating current is applied to a crystal containing dipoles [1]. Areas of charge within a piezoelectric element are distributed in patterns which yield a "net" positive and negative orientation. When alternating charge is applied to the two element faces, a relative contraction or elongation of the charged areas occurs resulting in a mechanical expansion and then a contraction of the element. This results in a mechanical wave which is transmitted to the patient (Fig. 2.4).

Reflected mechanical sound waves are received by the transducer and converted back into electrical energy via the piezoelectric effect. The electrical energy is interpreted within the ultrasound instrument to generate an image which is displayed upon the screen.

For most modes of ultrasound, the transducer emits a limited number of wave cycles (usually two to four) called a pulse. The frequency of the two to four waves within each cycle is usually in the 2.5–14 MHz range. The transducer is then "silent" as it awaits the return of the reflected waves from within the body (Fig. 2.5). The transducer serves as a receiver more than 99 % of the time.

Pulses are sent out at regular intervals usually between 1–10 kHz which is known as the **pulse repetition frequency (PRF)**. By timing the pulse from transmission to reception it is possible to

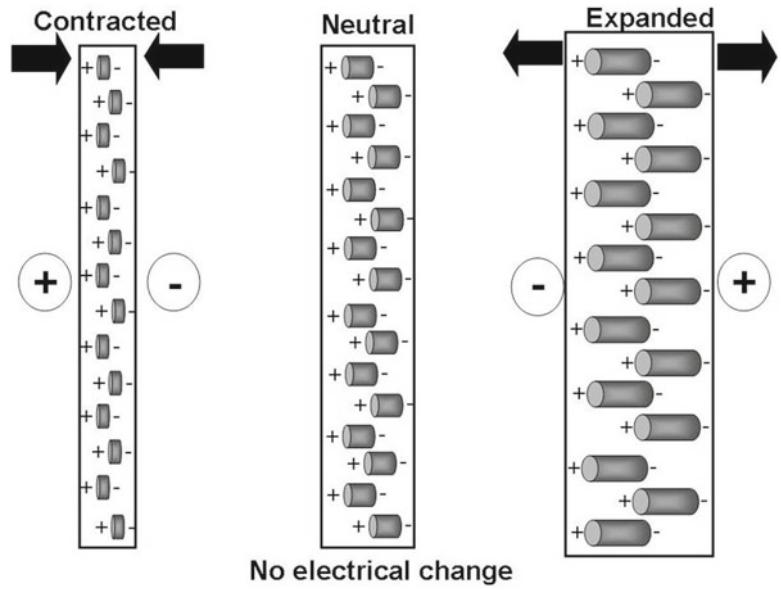

Fig. 2.4 Piezoelectric effect. Areas of "net" charge within a crystal expand or contract when current is applied to the surface, creating a mechanical wave. When the returning wave strikes the crystal, an electrical current is generated

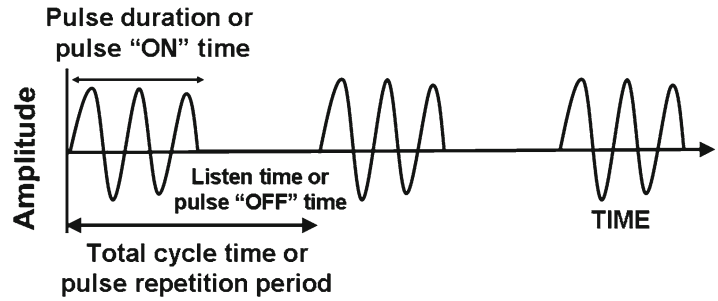

Fig. 2.5 The pulsed-wave ultrasound mode depends on an emitted pulse of 2–4 wave cycles followed by a period of "silence" as the transducer awaits the return of the emitted pulse

calculate the distance from the transducer to the object reflecting the wave. This is known as **ultrasound ranging** (Fig. 2.6). This sequence is known as **pulsed-wave ultrasound**.

The amplitude of the returning waves determines the brightness of the pixel assigned to the reflector in an ultrasound image. The greater the amplitude of the returning wave, the brighter the pixel assigned. Thus, an ultrasound unit produces an "image" by first causing a transducer to emit a series of ultrasound waves at specific frequencies and intervals and then interpreting the returning echoes for duration of transit and amplitude. This "image" is rapidly refreshed on a monitor to give the impression of continuous motion. Frame refresh rates are typically 12–30 per second. The sequence of events depicted in Fig. 2.7 is the basis for all "scanned" modes of ultrasound including the familiar gray-scale ultrasound.

Interaction of Ultrasound with Biological Tissue

As ultrasound waves are transmitted through human tissue they are altered in a variety of ways including loss of energy, change of direction, and change of frequency. An understanding of these interactions is necessary to maximize image quality and correctly interpret the resultant images.

Attenuation refers to a loss of kinetic energy as a sound wave interacts with tissues and fluids within the body [2]. Specific tissues have different potentials for attenuation. For

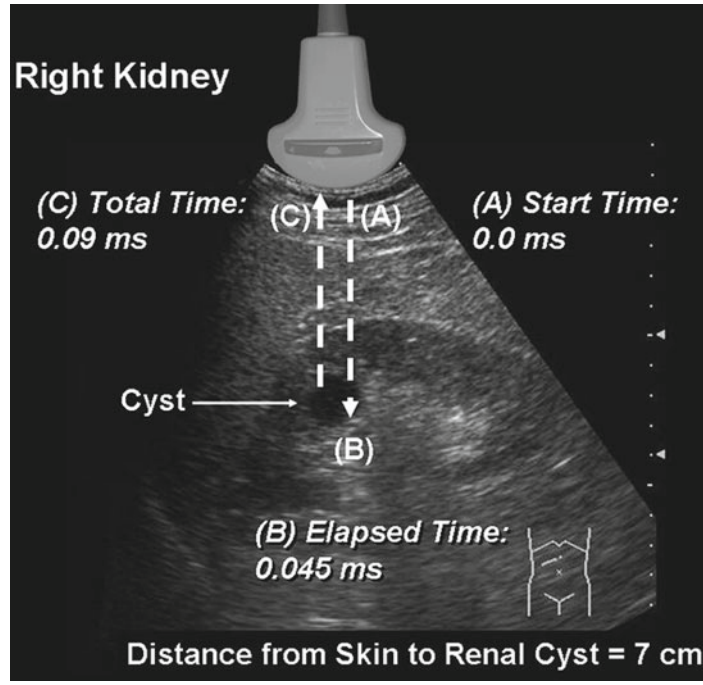

Fig. 2.6 Ultrasound ranging depends on assumptions about the average velocity of ultrasound in human tissue to locate reflectors in the ultrasound field. The elapsed time from pulse transmission to reception of the same pulse by the transducer allows for determining the location of a reflector in the ultrasound field

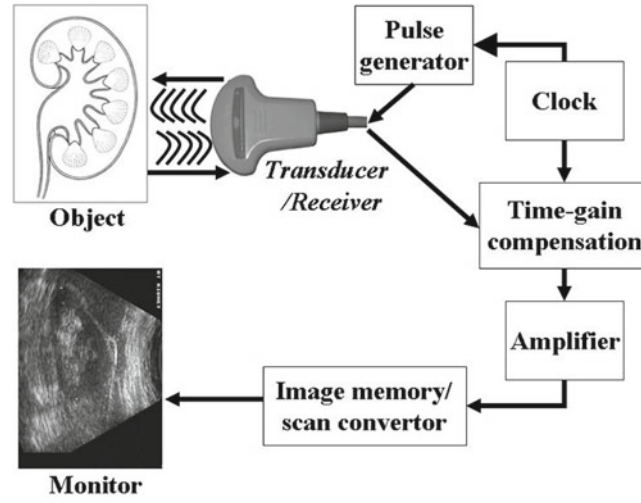

Fig. 2.7 Schematic depiction of the sequence of image production by an ultrasound device

example, water has an attenuation of 0.0 whereas kidney has an attenuation of 1.0 and muscle an attenuation of 3.3 Therefore, sound waves are much more rapidly attenuated as they pass through muscle than as they pass through water (Fig. 2.8). (Attenuation is measured in dB/cm/MHz.)

The three most important mechanisms of attenuation are absorption, reflection, and scattering. Absorption occurs when the mechanical kinetic energy of a sound wave is converted to heat within the tissue. Absorption is dependent on the frequency of the sound wave and the characteristics of the attenuating tissue. Higher frequency waves are more rapidly attenuated by absorption than lower frequency waves.

Since sound waves are progressively attenuated with distance traveled, deep structures in the body (e.g., kidney) are more difficult to image. Compensation for loss of acoustic energy by attenuation can be accomplished by the appropriate use of gain settings (increasing the sensitivity of the transducer to returning sound waves) and selection of a lower frequency.

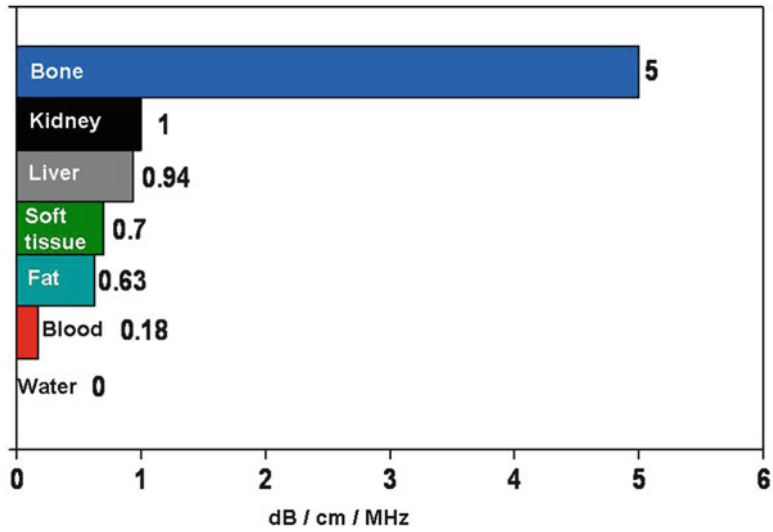

Fig. 2.8 Attenuation of tissue (Adapted from Diagnostic Ultrasound, Third Ed., Vol 1). The attenuation of a tissue is a measure of how the energy of an ultrasound wave is dissipated by that tissue. The higher the attenuation value of a tissue, the more the sound wave is attenuated by passing through that tissue

Refraction occurs when a sound wave encounters an interface between two tissues at any angle other than 90°. When the wave strikes the interface at an angle, a portion of the wave is reflected and a portion transmitted into the adjacent media. The direction of the transmitted wave is altered (refracted). This results in a loss of some information because the wave is not completely reflected back to the transducer, but also causes potential errors in registration of object location because of the refraction (change in direction) of the wave. The optimum angle of insonation to minimize attenuation by refraction is 90° (Fig. 2.9).

Reflection occurs when sound waves strike an object or an interface between unlike tissues or structures. If the object has a relatively large flat surface, it is called a specular reflector, and sound waves are reflected in a predictable way based on the angle of insonation. If a reflector is small or irregular, it is called a diffuse reflector. Diffuse reflectors produce **scattering** in a pattern which produces interference with waves from adjacent diffuse reflectors. The resulting pattern is called "speckle" and is characteristic of solid organs such as the testes and liver (Fig. 2.10).

When a sound wave travels from one tissue to another, a certain amount of energy is reflected at the interface between the tissues. The percentage of energy reflected is a function of the difference in the **impedance** of the tissues. Impedance is a property of tissue related to its "stiffness" and the speed at which sound travels through the tissue [3]. If two adjacent tissues have a small difference in tissue impedance, very little energy will

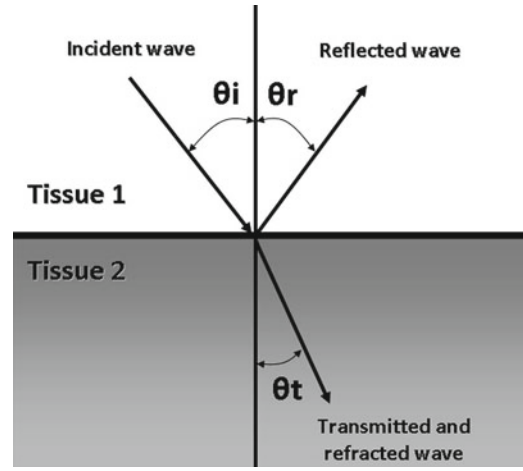

Fig. 2.9 A wave which strikes the interface between two tissues of differing impedance is usually partially reflected and partially transmitted with refraction. A portion of the wave is reflected (θR) at an angle equal to the angle of insonation (θi); a portion of the wave is transmitted at a refracted (θt) angle into the second tissue

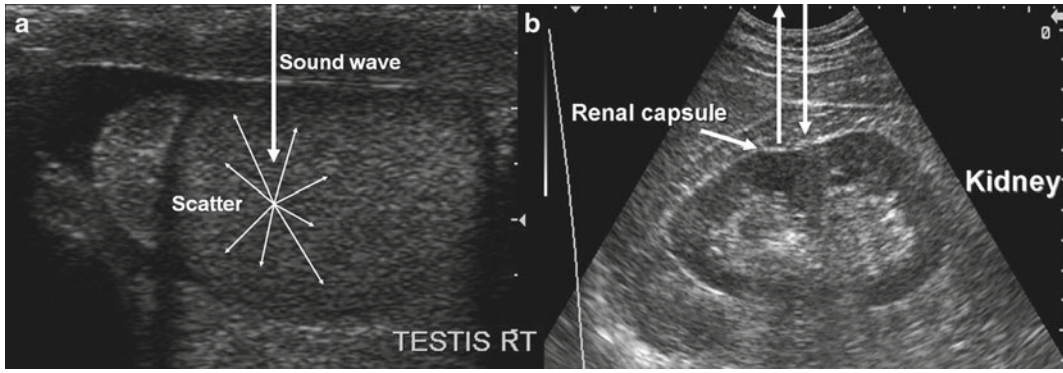

Fig. 2.10 (**a**) Demonstrates a diffuse reflector. In this image of the testis small parenchymal structures scatter sound waves. The pattern of interference resulting from this scattering provides the familiar "speckled" pattern of testicular echo architecture. (**b**) Demonstrates a specular reflector. A specular reflector reflects sound waves at an angle equal to the incident angle without producing a pattern of interference caused by scattering. In this image of the kidney the capsule of the kidney serves as a specular reflector

Table 2.1 Impedance of tissue (Adapted from Diagnostic Ultrasound, 3rd Ed, Vol. 1)

Tissue	Density (kg/m^3)	Impedance (Rayles)
Air and other gases	1.2	0.0004
Fat tissue	952	1.38
Water and other clear liquids	1,000	1.48
Kidney (average of soft tissue)	1,060	1.63
Liver	1,060	1.64
Muscle	1,080	1.70
Bone and other calcified objects	1,912	7.8

Impedance (Z) is a product of tissue density (p) and the velocity of that tissue (c). Impedance is defined by the formula: Z (Rayles) = p (kg/m^3) × c (m/s)

be reflected. The impedance difference between kidney (1.63) and liver (1.64) is very small so that if these tissues are immediately adjacent, it may be difficult to distinguish the interface between the two by ultrasound (Table 2.1).

Fat has a sufficient impedance difference from both kidney and liver that the borders of the two organs can be distinguished from the intervening fat (Fig. 2.11).

If the impedance differences between tissues are very high, complete reflection of sound waves may occur, resulting in acoustic shadowing (Fig. 2.12).

Artifacts

Sound waves are emitted from the transducer with a known amplitude, direction, and frequency. Interactions with tissues in the body result in alterations of these parameters. Returning sound waves are presumed to have undergone alterations according to the expected physical principles such as attenuation with distance and frequency shift based on the velocity and direction of objects they encountered. The timing of the returning echoes is based on the expected velocity of sound in human tissue. When these expectations are not met, it may lead to image representations and measurements which do not reflect actual physical conditions. These misrepresentations are known as "artifacts." Artifacts, if correctly identified, can be used to aid in diagnosis.

Increased through transmission occurs when sound waves pass through tissue with less attenuation than occurs in the surrounding tissues. For example, when sound waves pass through a fluid-filled

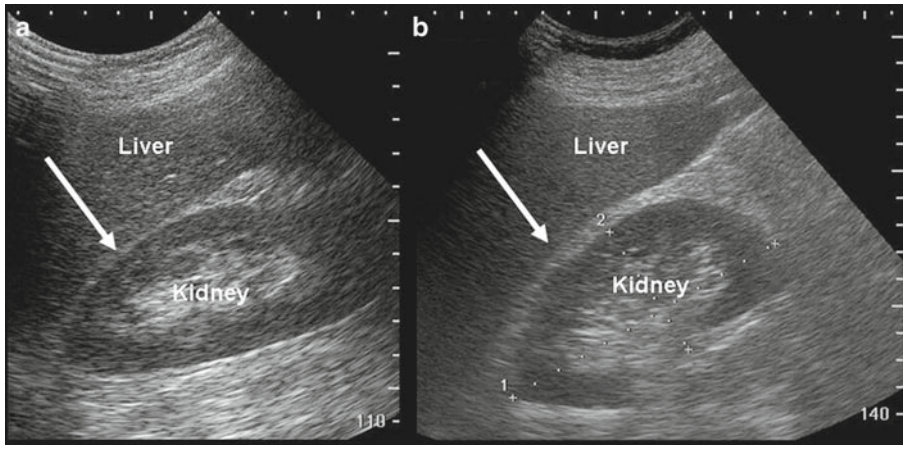

Fig. 2.11 Image (**a**) demonstrates that when kidney and liver are directly adjacent to each other, it is difficult to appreciate the boundary (*arrow*) between the capsules of the kidney and liver. Image (**b**) demonstrates that when fat (which has a significantly lower impedance) is interposed, it is far easier to appreciate the boundary between liver capsule (*arrow*) and fat

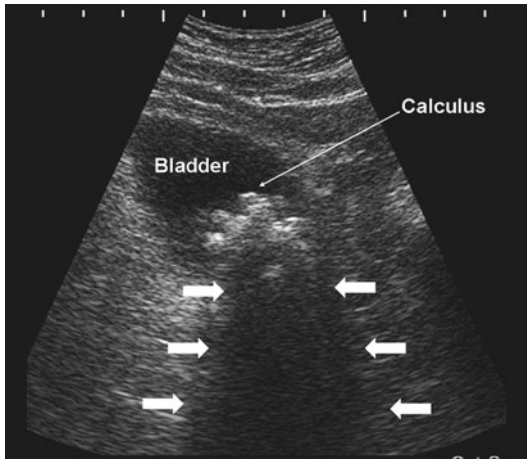

Fig. 2.12 In the urinary bladder, reflection of sound waves as the result of large impedance differences between urine and the bladder calculus (*thin arrow*). Acoustic shadowing results from nearly complete reflection of sound waves (*arrows*)

structure such as a renal cyst, the waves experience relatively little attenuation compared to that experienced in the surrounding renal parenchyma. Thus when the waves reach the posterior wall of the cyst and the renal tissue beyond it, they are more energetic (have greater amplitude) than the adjacent waves. The returning echoes have significantly greater amplitude than waves returning through the renal parenchyma from the same region of the kidney. Therefore, the pixels associated with the region distal to the cyst are assigned a greater "brightness." The tissue appears hyperechoic compared to the adjacent renal tissue even though it is histologically identical (Fig. 2.13). This artifact can be overcome by changing the angle of insonation or adjusting the time-gain compensation settings.

Acoustic shadowing occurs when there is significant attenuation of sound waves at a tissue interface causing loss of information about other structures distal to that interface. This attenuation may occur on the basis of reflection or absorption, resulting in an "anechoic" or "hypoechoic" shadow. The significant attenuation or loss of the returning echoes from tissues distal to the interface may lead to incorrect conclusions about tissue in that region. For instance, when sound waves strike the interface between testicular tissue and a testicular calcification, there is a large impedance difference and significant attenuation and reflection occur. Information about the region distal to the interface is therefore lost or severely diminished (Fig. 2.14). Thus, in some cases spherical objects may appear as crescenteric objects, and it may be difficult to obtain accurate measurements of such three-dimensional objects. Furthermore, fine detail in the region of the acoustic shadow may be obscured. The problems with acoustic

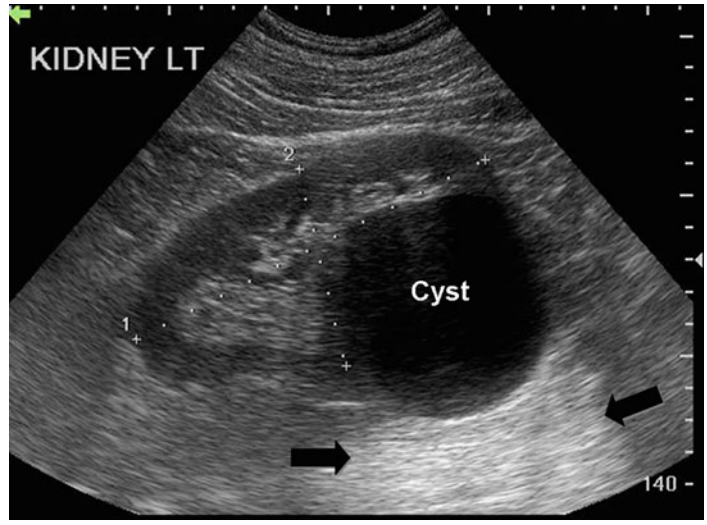

Fig. 2.13 Increased through transmission with hyperechogenicity (*arrow*) as the result of decreased attenuation by the fluid-filled cyst. This is an example of artifactual misrepresentation of tissue characteristics and must be recognized to avoid incorrect clinical conclusions

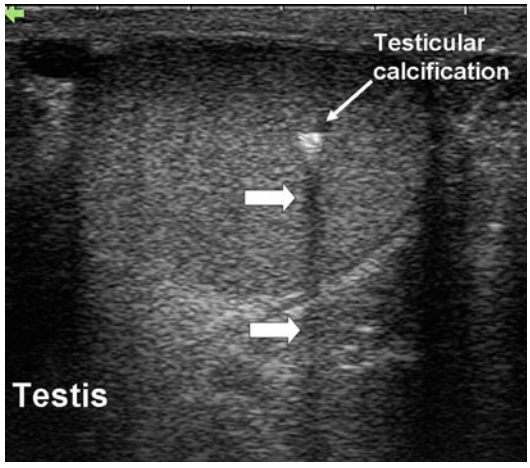

Fig. 2.14 Acoustic shadowing occurs distal to a calcification in the testis (*large arrows*). Information about testicular parenchymal architecture distal to the area of calcification is lost

shadowing are most appropriately overcome by changing the angle of insonation.

Edging artifact occurs when sound waves strike a curved surface or an interface at a critical angle. A **critical angle** of insonation is one which results in propagation of the sound wave along the interface without significant reflection of the wave to the transducer. Thus, information distal to the interface is lost or severely diminished. This very common artifact in urology must be recognized and can, at times, be helpful. It is seen in many clinical situations but very commonly seen when imaging the testis. Edging artifacts often occur at the upper and lower pole of the testis as the sound waves strike the rounded testicular poles at the critical angle. This artifact may help differentiate between the head of the epididymis and the upper pole of the testis. The edging artifact is also prominently seen on transrectal ultrasound where the two rounded lobes of the prostate come together in the midline. This produces an artifact that appears to arise in the vicinity of the urethra and extend distally. Edging artifact may be seen in any situation where the incident wave strikes an interface at the critical angle (Fig. 2.15). Edging artifact may be overcome by changing the angle of insonation.

A **reverberation artifact** results when an ultrasound wave bounces back and forth (reverberates) between two or more reflective interfaces. When the sound wave strikes a reflector and returns to the transducer, an object is registered at that location. With the second transit of the sound wave the ultrasound equipment interprets a second object that is twice as far away as the first. There is ongoing attenuation of the sound wave with each successive reverberation resulting in a slightly less intense image displayed on the screen. Therefore, echoes are produced which are spaced at equal intervals from the transducer but are progressively less intense (Fig. 2.16).

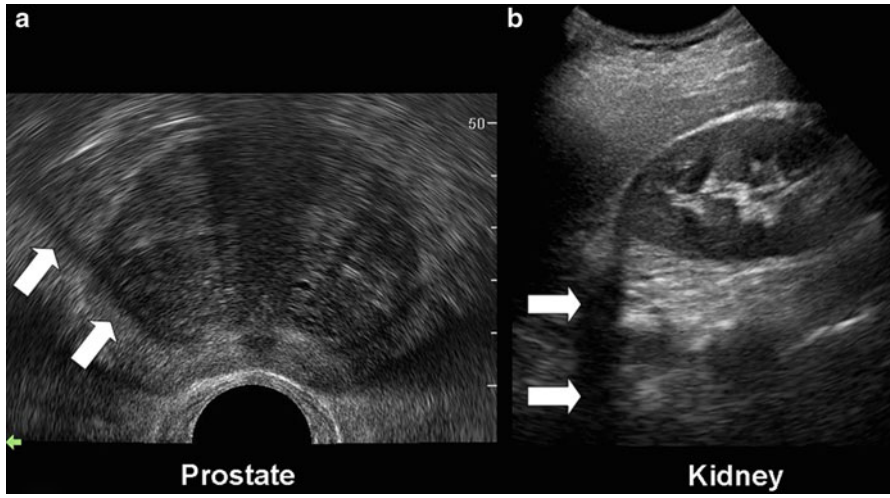

Fig. 2.15 Edging artifact (*arrows*) seen in this transverse image of the prostate is the result of reflection of the sound wave along the curved lateral surface of the transition zone (**a**). Edging artifact (*arrows*) caused by the rounded upper pole of the kidney (**b**)

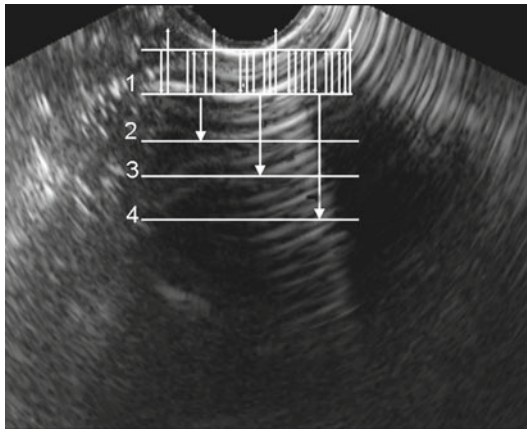

Fig. 2.16 A reverberation artifact occurs when a sound wave is repeatedly reflected between reflective surfaces. The resultant echo pattern is a collection of hyperechoic artifactual reflections distal to the structure with progressive attenuation of the sound wave

The reverberation artifact can also be seen in cases where the incident sound wave strikes a series of smaller reflective objects (such as the gas–fluid mixture in the small bowel) which results in multiple reflected sound waves of various angles and intensity (Fig. 2.17).

This familiar artifact may obscure important anatomic information and is frequently encountered during renal ultrasound. It may be overcome by changing the transducer location and the angle of insonation.

Modes of Ultrasound

Gray-Scale, B-Mode Ultrasound

Gray-scale, B-mode ultrasound (brightness mode) is the image produced by a transducer which sends out ultrasound waves in a carefully timed, sequential way (pulsed wave). The reflected waves are received by the transducer and interpreted for distance and amplitude. Time of travel is reflected by position on the image monitor and intensity by "brightness" of the corresponding pixel. Each sequential line-of-sight echo is displayed side by side and the entire image refreshed at 15–40 frames/s. This results in the illusion of continuous motion or "real-time" scanning. The intensity of the reflected sound waves may vary by a factor of 10^{12} or 120 dB. Although the transducer can respond to such extreme variations in intensity, most monitors or displays have an effective range of only 10^6 or 60 dB. Each of 512×512 or 512×640 pixels may display 2^8 or 256 shades of gray [3]. Most ultrasound units internally process and compress ultrasound data to allow it to be displayed on a standard monitor. Evaluation of gray-scale imaging requires the ability to recognize the normal patterns of echogenicity from anatomic structures.

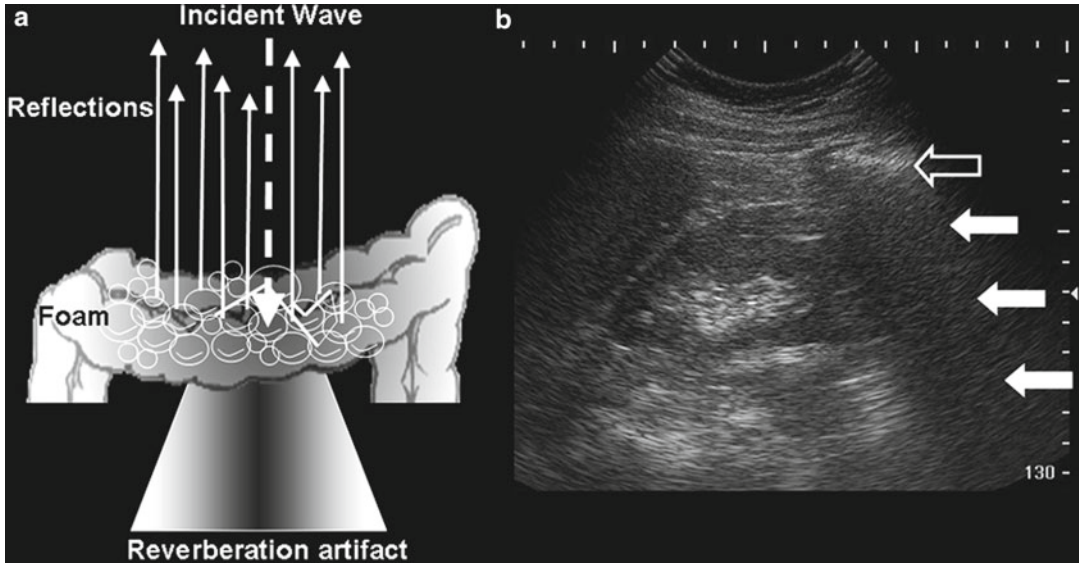

Fig. 2.17 (**a**) Reverberation artifact produced when sound waves strike a mixture of fluid and gas in the bowel. (**b**) This type of reverberation (multipath artifact) is characterized by hyperechoic areas (*open arrow*) and distal attenuation of the incident wave (*closed arrows*)

Variations from these expected patterns of echogenicity indicate disorders of anatomy or physiology or may represent artifacts.

Doppler Ultrasound

The Doppler ultrasound mode depends on the physical principle of frequency shift when sound waves strike a moving object. The basic principle of Doppler ultrasound is that sound waves of a certain frequency will be shifted or changed based on the direction and velocity of the moving object as well as the angle of insonation. This phenomenon allows for the characterization of motion, most commonly the motion of blood through vessels, but may also be useful for detecting the flow of urine.

The **Doppler Effect** is a shift in the frequency of the transmitted sound wave based on the velocity of the reflecting object that it strikes. If the reflecting object is stationary relative to the transducer, then the returning frequency will be equal to the transmitted frequency. However, if the echo-generating object is traveling toward the transducer, the returning frequency will be higher than the transmitted frequency. If the object generating the echo is traveling away from the transducer, then the reflected frequency will be lower than the transmitted frequency. This is known as the frequency shift, or Doppler shift (Fig. 2.18).

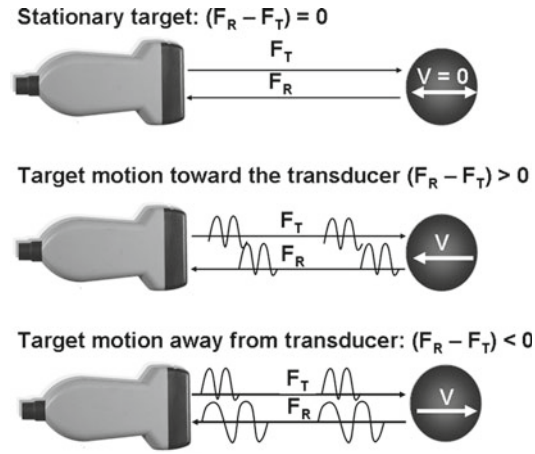

Fig. 2.18 Dopper effect. FT is the transmitted frequency. When the FT strikes a stationary object, the returning frequency FR is equal to the FT. When the FT strikes a moving object, the FR is "shifted" to a higher or lower frequency

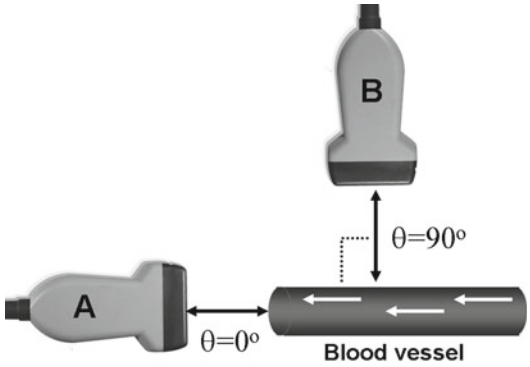

Fig. 2.19 (**A**) Maximum frequency shifts are detected when the transducer axis is parallel to the direction of motion. (**B**) No frequency shift is detected when the transducer axis is perpendicular to the direction of motion

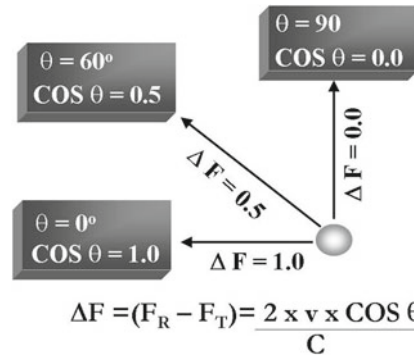

Fig. 2.20 Angle of insonation. The calculated velocity of an object using Doppler shift is dependent on the transducer angle (θ). If the transducer axis is perpendicular to the direction of flow (90°), then the cosine of θ is 0. Based on this formula for Doppler shift (ΔF), the detected frequency change would be 0. Adapted from Radiographics 1991;11:109–119

The frequency shift of the transmitted wave is also dependent on the angle of the transducer relative to the object in motion. The maximum Doppler frequency shift occurs when the transducer is oriented directly on the axis of motion of the object being insonated. That is, when the transducer is oriented parallel (angle θ=0°) to the direction of motion, the shift is maximal. Conversely, when the transducer face is oriented perpendicular to the direction of motion (angle θ=90°), there will be no shift in Doppler frequency detected (Fig. 2.19).

An accurate calculation of velocity of flow depends on the angle θ between the transducer and the axis of motion of the object being insonated (Fig. 2.20).

Color Doppler ultrasonography allows for an evaluation of the velocity and direction of an object in motion. A color map may be applied to the direction. The most common color map uses blue for motion away from the transducer and red for motion toward the transducer (Fig. 2.21).

The velocity of motion is designated by the intensity of the color. The greater the velocity of the motion, the brighter is the color displayed. Color Doppler may be used to characterize blood flow in the kidney, testis, penis, and prostate. It also may be useful in the detection of "jets" of urine emerging from the ureteral orifices. An accurate representation of flow characteristics requires attention to transducer orientation relative to the object in motion. Therefore, in most clinical circumstances the angle between the transducer and the direction of motion should be less than or equal to 60° (Fig. 2.22).

When it is not possible to achieve an angle of 60° or less by manipulation of the transducer, the beam may be "steered" electronically to help create the desired angle θ (Fig. 2.23).

Power Doppler ultrasonography is a mode which assigns the amplitude of frequency change to a color map. This does not permit evaluation of velocity or direction of flow but is less affected by backscattered waves. Power Doppler is therefore less angle-dependent than color Doppler and is more sensitive for detecting flow [4].

When a sound wave strikes an object within the body, the sound wave is altered in a variety of ways including changes in frequency and changes in amplitude (Fig. 2.24).

While color Doppler assigns the changes in frequency to a color map, power Doppler assigns changes in integrated amplitude (or power) to a color map. It is possible to assign low-level backscattered information to a color which is unobtrusive on the color map, thereby allowing increased gain without interference from this backscattered information (Fig. 2.25). Power Doppler may be more sensitive than color Doppler for the detection of diminished flow [4].

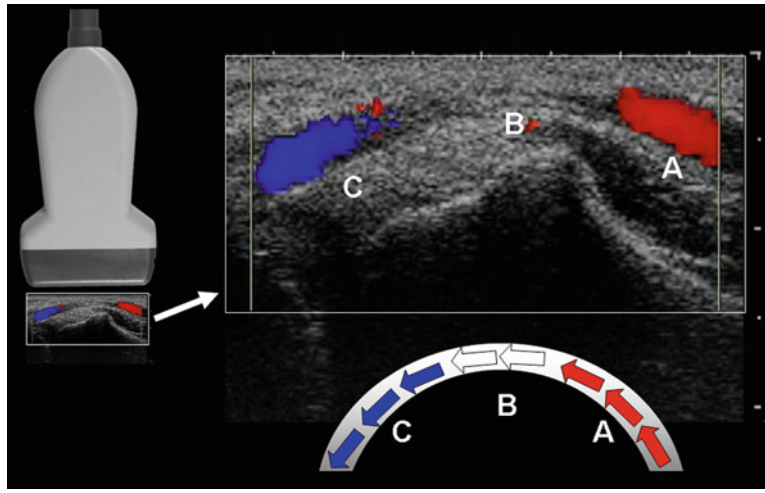

Fig. 2.21 In this image of the radial artery, blood is flowing through the curved vessel from (**A**) to (**C**). Flow toward the transducer (**A**) is depicted in *red*. Flow in the middle of the vessel (**B**) is perpendicular to the transducer axis and produces no Doppler shift; thus, no color is assigned even though the velocity and intensity of flow are uniform through the vessel. Flow away from the transducer (**C**) is depicted in *blue*

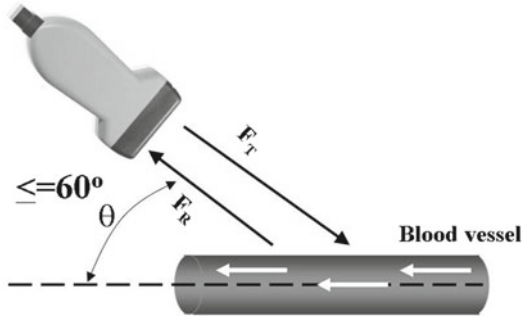

Fig. 2.22 The transducer angle should be ≤60° relative to the axis of fluid motion to allow a more accurate calculation of velocity of flow

The integrated amplitude (power) of the Doppler signal is signified by the brightness of the color. Because frequency shift is not displayed in standard power Doppler, the direction and velocity of flow are not indicated.

Color Doppler with spectral display is a mode which allows the simultaneous display of a color Doppler image and representation of flow as a wave form within a discrete area of interrogation. This mode is commonly used to evaluate the pattern and velocity of blood flow in the kidney and testis (Fig. 2.26).

The spectral waveform provides information about peripheral vascular resistance in the tissues. The most commonly used index of these velocities is the resistive index (Fig. 2.27).

The resistive index may be helpful in characterizing a number of clinical conditions including renal artery stenosis and ureteral obstruction. Since the velocity is represented on a scaler axis, it is necessary to set appropriate scaler limits to prevent artifacts. Therefore, it is necessary to know the expected velocity within vessels pertinent to urologic practice (Table 2.2). The clinical use of resistive index is described in subsequent chapters.

Artifacts Associated with Doppler Ultrasound

The **twinkle artifact** is produced when a sound wave encounters an interface which produces an energetic reflection of the sound wave. In ultrasound modes such as power and color Doppler, this can cause a distortion in the returning sound wave that gives the appearance of motion distal to that interface. The resulting Doppler signal appears as a trailing acoustic "shadow" of varying intensity and direction known as twinkle artifact. Although this artifact may be seen in a variety of clinical circumstances (e.g., twinkle artifact produced by the

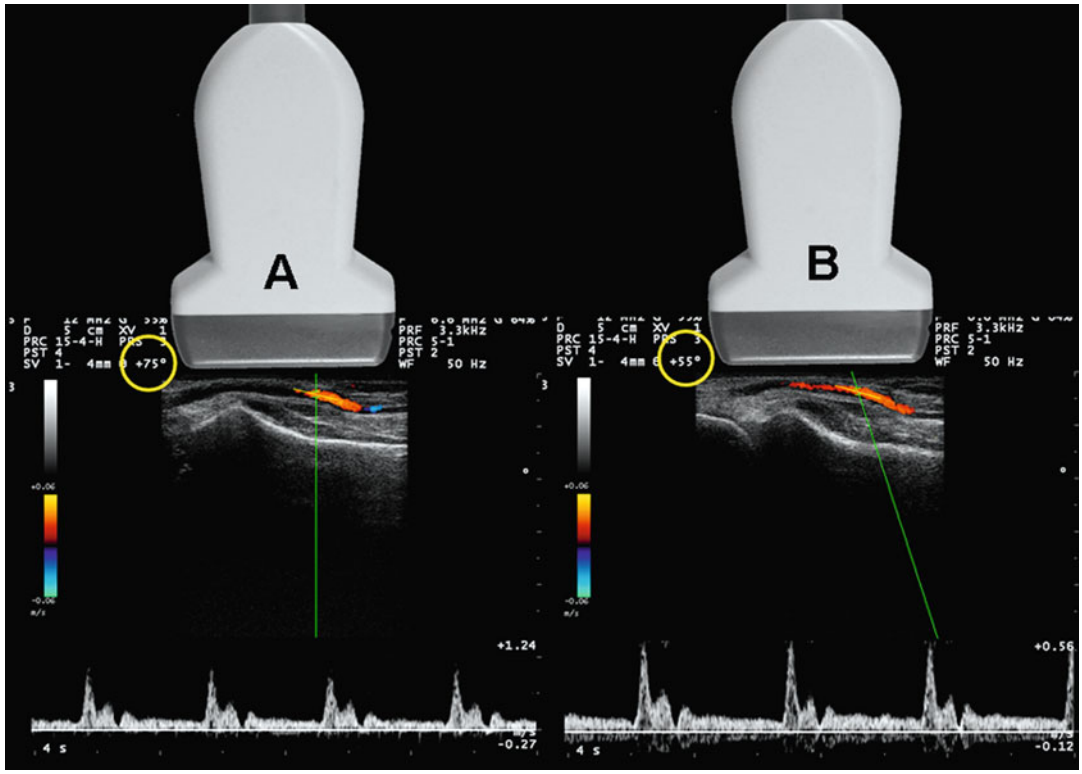

Fig. 2.23 Beam steering. In image (**A**) the angle of insonation is 75° (*yellow circle*) which is unfavorable for accurate velocity calculations. This is because the axis of the transducer is perpendicular to the vessel. In image (**B**) the beam has been "steered" to produce an angle of 55° (*yellow circle*) without changing the physical position of the transducer. The resultant velocity calculation is more accurate at 55°

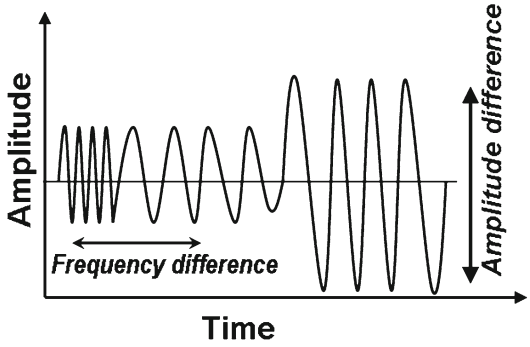

Fig. 2.24 Backscatter is defined as a combination of changes in frequency and amplitude which occur in the reflected sound wave of a primary frequency

interaction of an ultrasound wave with a Foley catheter balloon in the bladder), it is most often helpful clinically in evaluating hyperechoic objects in the kidney. Stones often have a twinkle artifact (Fig. 2.28) whereas arcuate vessels and other hyperechoic structures in the kidney usually do not. Not all calcifications display the twinkle artifact. Calcifications of the renal artery and calcifications within tumors and cysts may also produce the twinkle artifact [8].

Aliasing is an artifact which occurs when the ultrasound interrogation (determined by PRF) of an event occurs at a frequency which is insufficient to accurately represent the event. When interrogation occurs at infrequent intervals, only portions of the actual event are depicted. Aliasing occurs when the interrogation frequency is less than twice the shifted Doppler frequency (Fig. 2.29).

Normal laminar unidirectional blood flow is depicted as a single color on color Doppler. Spectral Doppler shows a complete waveform (Fig. 2.30). During color Doppler scanning,

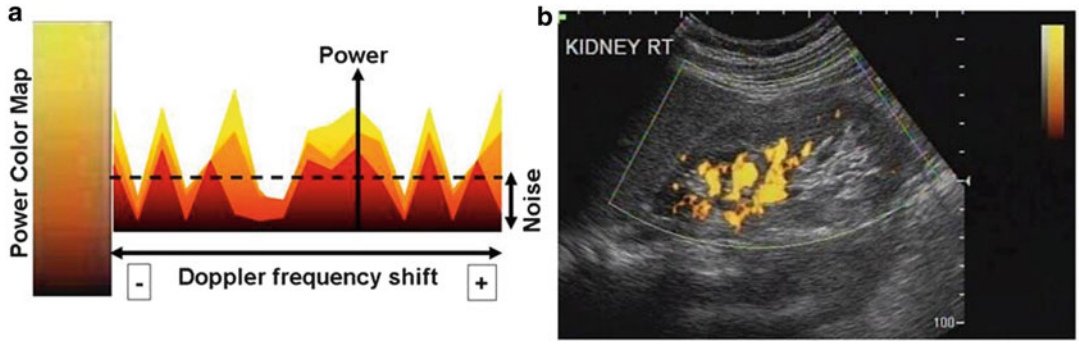

Fig. 2.25 (**a**) For power Doppler the intensity of color is related to changes in amplitude (power) rather than changes in frequency. (**b**) In this sagittal image of the kidney, power Doppler blood flow is demonstrated. Note that the color map depicted to the upper right does not have a scale since quantitative measurement of velocity is not displayed with standard power Doppler

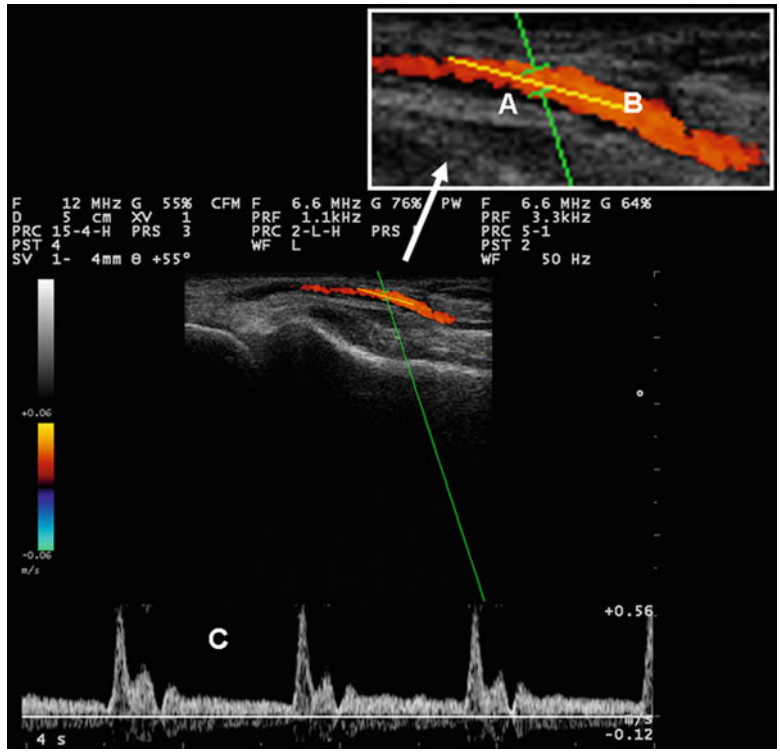

Fig. 2.26 In this example, the radial artery is shown in real-time gray-scale ultrasound with color Doppler overlay. The interrogation box or gate (**A**) is positioned over the vessel of interest. The gate should be positioned and sized to cover about 75 % of the lumen of the vessel. The angle of insonation is indicated by marking the orientation of the vessel with a cursor (**B**). The velocity of the flow within the vessel is depicted quantitatively in the spectral display (**C**)

aliasing is most commonly seen as apparent turbulence and change in direction of blood flow within a vessel. During spectral Doppler scanning the aliasing phenomenon is seen as truncation of the systolic velocity peak with projection of the peak below the baseline (Fig. 2.31).

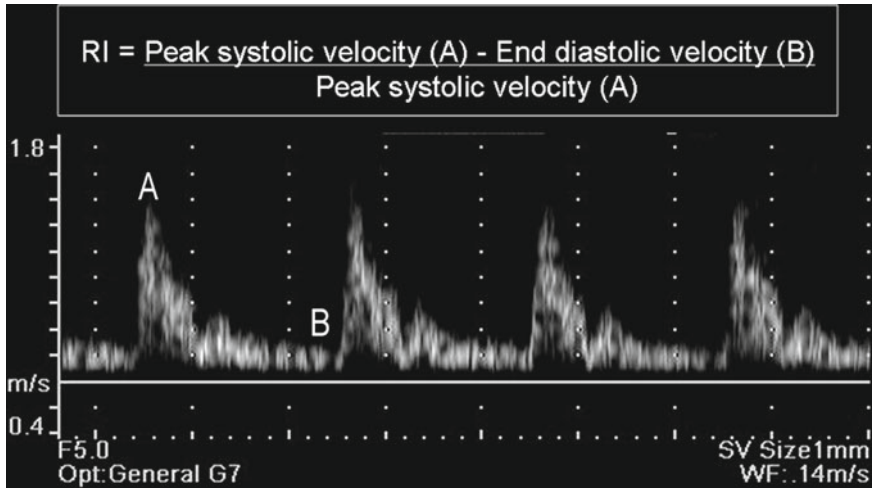

Fig. 2.27 The resistive index (RI) is the peak systolic velocity (**A**) minus the end-diastolic velocity (**B**) over the peak systolic velocity (**A**)

Table 2.2 Expected velocity in urologic vessels

Vessel	Velocity
Penile artery	>35 cm/s (after vasodilators) [5]
Renal artery	<100 cm/s [6]
Scrotal capsular artery	5–14 cm/s [7]

The measured velocity will depend on a variety of physiologic and anatomic variants

This artifact can be overcome by decreasing the frequency of the incident sound wave, increasing the angle of insonation (θ), or increasing the PRF.

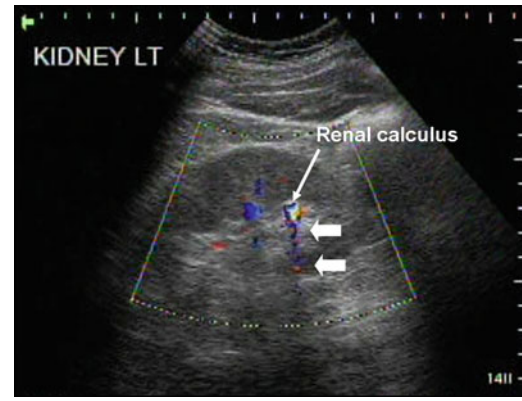

Fig. 2.28 Twinkle artifact. The effect produced by the interaction of sound waves at an interface with high impedance differences (in this case a renal calculus) which produces an artifact suggesting turbulent motion (*large arrows*)

Harmonic Scanning

Harmonic scanning makes use of aberrations related to the nonlinear propagation of sound waves within tissue. These asymmetrically propagated waves generate fewer harmonics but those which are generated have greater amplitudes (Fig. 2.32).

Since these harmonics are less subject to scattering associated with the incident wave, there is less noise associated with the signal. By selectively displaying the harmonic frequencies which are produced within the body and reflected to the transducer, it is possible to produce an image with less artifact and greater resolution.

Spatial compounding is a scanning mode whereby the direction of insonation is sequentially altered electronically to produce a composite image. This technique reduces the amount of artifact and noise producing a scan of better clarity [9] (Fig. 2.33).

Three-dimensional (3-D) scanning produces a series of images (data set) which can then be manipulated to generate additional views of the

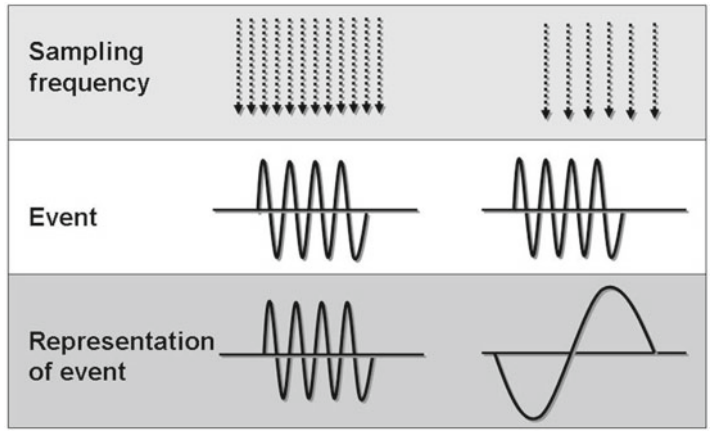

Fig. 2.29 Aliasing. In this illustration where a sine wave is the real-time event and the vertical *arrows* in the *top* panel represent the frequency of interrogation, we see that frequent interrogation produces an accurate representation of the event. An accurate depiction of an ultrasound event must meet the condition: fs ≥ 2b, where fs is the sampling frequency and 2b is the highest frequency in the event. This is known as the Nyquist limit. Less frequent sampling (on the right) results in an incorrect interpretation of the event. (Diagram adapted from Diagnostic Ultrasound, 3rd Ed., Figs. 1–40, p. 33)

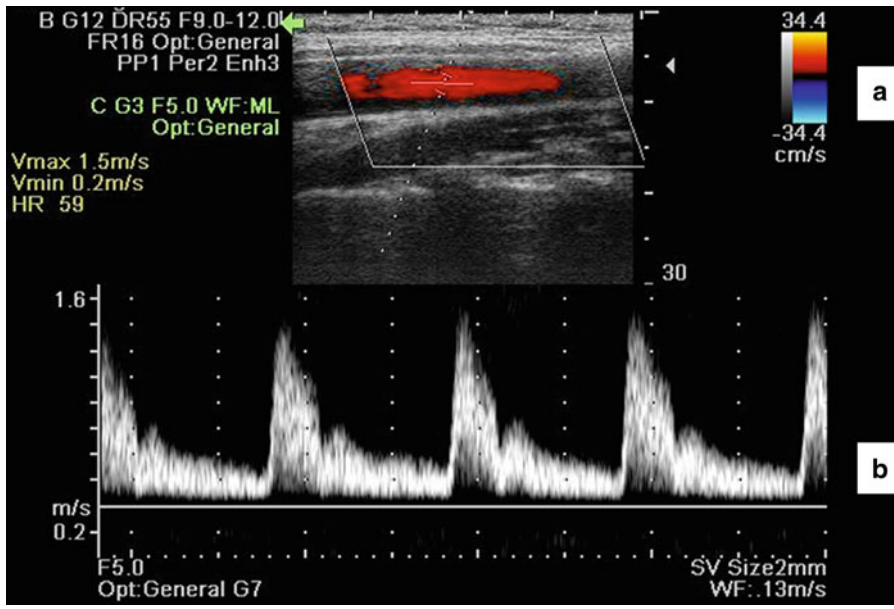

Fig. 2.30 Spectral Doppler. (**a**) Blood flow appears unidirectional on color mapping in this color Doppler image with spectral flow analysis. (**b**) The waveform is accurately depicted on spectral analysis

anatomy in question (Fig. 2.34). 3-D rendering may be important in procedural planning and precise volumetric assessments [10]. 3-D scanning may allow the recognition of some tissue patterns which would otherwise be inapparent on two-dimensional scanning [11].

Contrast Agents in Ultrasound

Intravenous compounds containing microbubbles have been used for enhancing the echogenicity of blood and tissue. Microbubbles are distributed in

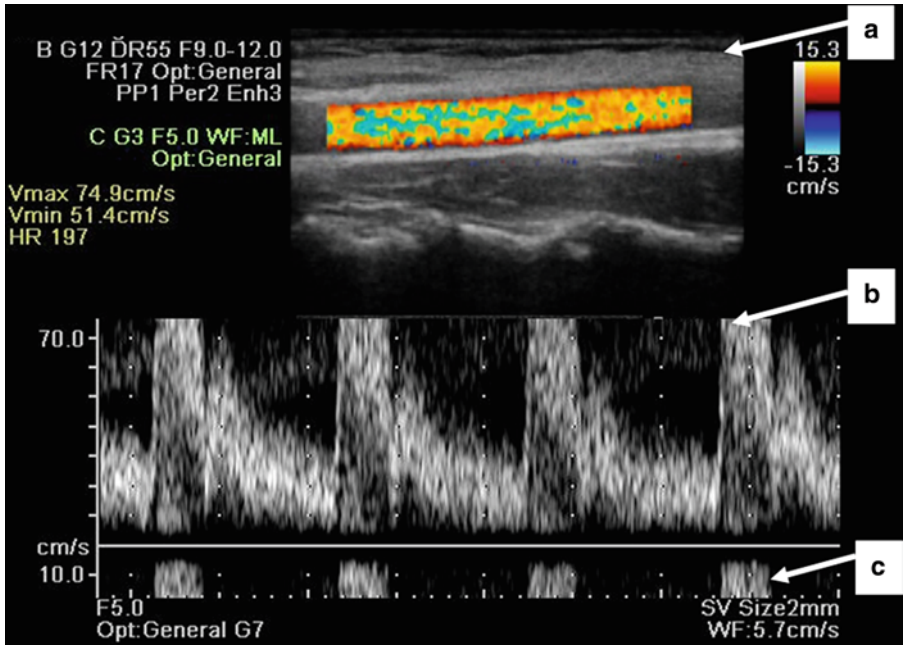

Fig. 2.31 In this color Doppler ultrasound with spectral flow, aliasing is demonstrated by apparent changes in velocity and direction on the color map assigned to the vessel (**a**). Aliasing of the spectral waveform is seen as truncation of the peak systolic velocity (**b**) with projection of the peak below the baseline (**c**)

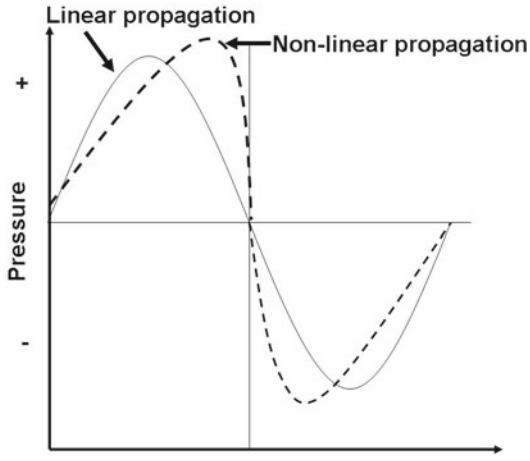

Fig. 2.32 Nonlinear propagation of sound waves in tissue results in fewer but more energetic harmonics which may be selectively evaluated in the returning echo

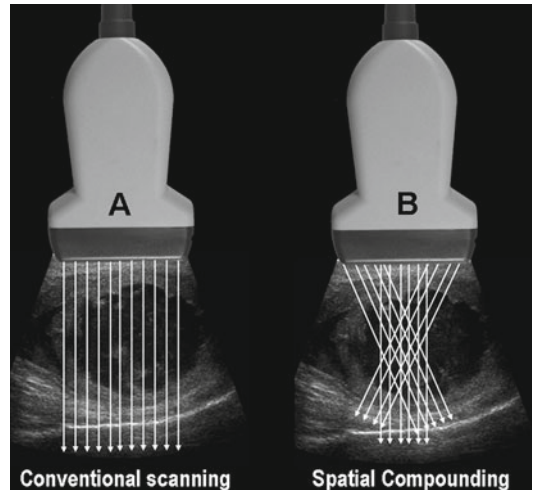

Fig. 2.33 Spatial compounding results in a composite image by combining data from multiple scanning angles produced by automated beam steering. The resulting image is more detailed with less artifact

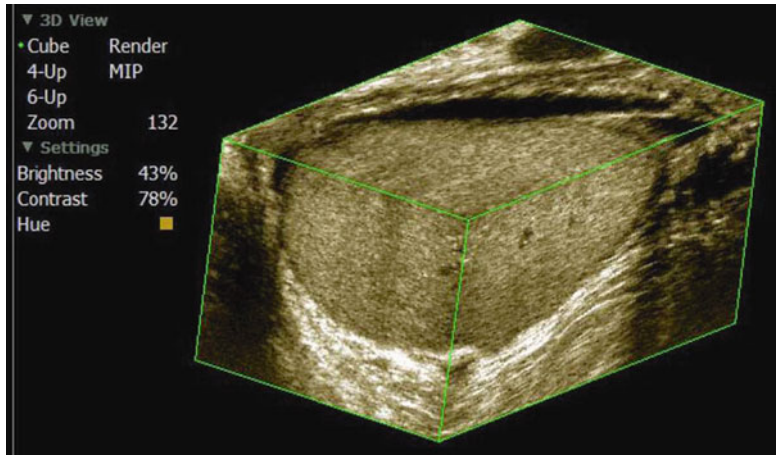

Fig. 2.34 3-D scan of the testis is a reconstructed data set from sequential 2-D images (Image used with permission. Contemporary Urology. Scrotal ultrasound. Bruce R. Gilbert, MD, PhD)

the vascular system and create strong echoes with harmonics when struck by sound waves. The bubbles themselves are rapidly degraded by the interaction with the sound waves. Machine settings producing a low mechanical index (see Chap. 4) are desirable to reduce destruction of the microbubbles. Contrast agents may be useful in prostatic ultrasound by enhancing the ability to recognize areas of increased vascularity [12]. The use of intravenous ultrasound contrast agents is considered investigational but has shown promise in a number of urologic scanning situations. The ability to demonstrate vascular enhancement without exposure to potential toxic contrast agents or ionizing radiation makes contrast-enhanced ultrasound a promising urologic imaging modality.

References

1. Mason WP. Piezoelectricity, its history and applications. J Acoust Soc Am. 1981;70(6):1561–6.
2. Rumack CM, Wilson SR, Charboneau JW. Diagnostic ultrasound. 3rd ed. St. Louis: Mosby, Inc;2005. p. 8.
3. Rumack CM, Wilson SR, Charboneau JW. Diagnostic ultrasound. 3rd ed. St. Louis, MO: Mosby, Inc; 2005. p. 12.
4. Rubin JM, Bude RO, Carson PL, et al. Power Doppler US: a potentially useful alternative to mean frequency-based color Doppler US. Radiology. 1994;190:853–6.
5. Rifkin MD, Cochlin DL. Imaging of the scrotum & penis. London: Martin Dunitz Ltd; 2002. p. 276.
6. Zucchelli PC. Hypertension and atherosclerotic renal artery stenosis: diagnostic approach. J Am Soc Nephrol. 2002;13:S184–6.
7. Bluth EI, Benson CB, Ralls PW. Ultrasonography in vascular diseases: a practical approach to clinical problems. New York: Thieme Medical Publishers; 2008. p. 87.
8. Kim HC, Yang DM, Jin W, Ryu JK, Shin HC. Color Doppler twinkling artifacts in various conditions during abdominal and pelvic sonography. J Ultrasound Med. 2010;29:621–32.
9. Merritt CR. Technology update. Radiol Clin North Am. 2001;39:385–97.
10. Ghani KR, Pilcher J, Patel U, et al. Three-dimensional ultrasound reconstruction of the pelvicaliceal system: an in-vitro study. World J Urol. 2008; 26:493–8.
11. Mitterberger M, Pinggera GM, Pallwein L, et al. The value of three-dimensional transrectal ultrasonography in staging prostate cancer. BJU Int. 2007;100: 47–50.
12. Mitterberger M, Pinggera GM, Horninger W, et al. Comparison of contrast enhanced color Doppler targeted biopsy to conventional systematic biopsy: impact on Gleason score. J Urol. 2007;178:464–8.

Bioeffects and Safety

3

Pat F. Fulgham

Urologists who perform and interpret ultrasound in their office must have a thorough knowledge of the potential bioeffects of ultrasound in human tissues and how to maintain the ultrasound equipment to protect patient safety. Diagnostic ultrasound transmits energy into the patient which has the potential to produce biological effects. The maximum output of ultrasound energy by ultrasound devices is regulated by the US Food and Drug Administration (FDA) [1]. In general, these regulations allow enough energy to accomplish diagnostic goals but prescribe a margin of safety. The total energy imparted during an ultrasound examination is controlled by the operator through (1) acoustic output, (2) selection of frequency, (3) mode of ultrasound, (4) technique, and (5) duration of the examination.

Bioeffects of Ultrasound

As ultrasound waves enter biological tissues, some of the energy is transmitted, some is reflected, and some is dissipated as heat. The interaction of ultrasound with human tissue produces **thermal effects** and **mechanical effects**.

P.F. Fulgham, MD, FACS (✉)
Department of Urology, Texas Health Presbyterian Dallas, 8210 Walnut Hill Lane, Suite 014, Dallas, TX 75231, USA
e-mail: pfulgham@airmail.net; patfulgham@yahoo.com

Thermal Effects

The most important thermal effect of ultrasound is tissue heating. Tissue heating from ultrasound is a result of **scattering** and **absorption**, two mechanisms of attenuation. Absorption of ultrasound by tissue results in the conversion of mechanical acoustic energy into heat. The amount of heat generated is directly proportional to the frequency of the wave, the amplitude of the wave, and the duration of exposure.

The work performed by ultrasound as it passes through tissue is given in Watts (*W*) which is a measure of acoustic power per unit of time. The distribution of acoustic power over area is **intensity**. Intensity (*I*) is expressed in w/cm^2. Intensity is influenced by the cross-sectional area of the ultrasound beam. The same amount of acoustic power distributed in a smaller area results in increased intensity. The amount of heating which occurs in human tissue as the result of ultrasound exposure is directly proportional to the intensity. Thus, beam focusing in a specific anatomic region will result in more heating in that area because of increased acoustic intensity at that location.

Temporal factors also influence the amount of tissue heating. The fraction of time that the transducer is producing pulses (called the *duty factor*) and the total amount of time a tissue is exposed to the beam (called the *duration time*) influences tissue heating. A low duty factor and a short duration time reduce tissue heating. In standard scanned modes of ultrasound (e.g., gray scale,

P.F. Fulgham and B.R. Gilbert (eds.), *Practical Urological Ultrasound*, Current Clinical Urology,
DOI 10.1007/978-1-59745-351-6_3,

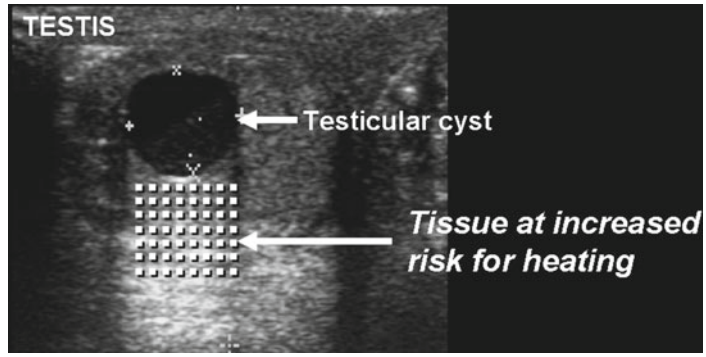

Fig. 3.1 Testicular cyst. The tissue distal to this testicular cyst (*gridded area*) is prone to more tissue heating because sound waves passing through the cyst are less attenuated than those passing through adjacent testicular parenchyma

power, and color Doppler), the transducer is being moved at frequent intervals, reducing duration time and limiting imaging of specific tissue areas. Blood flow in tissues also tends to dissipate heat, resulting in less temperature increase in the tissue.

The type of tissue being insonated influences tissue heating. Tissues which rapidly attenuate sound (i.e., tissue with high impedance, such as bone) experience more heating. Thus, soft tissue immediately adjacent to bony structures may be more prone to tissue heating. Soft tissue heating may also occur when less attenuated waves strike these tissues. This may occur in tissue distal to a fluid-filled structure such as a cyst (Fig. 3.1).

Tissue heating of up to 1°C may occur during diagnostic imaging at tissue/bone interfaces. Localized tissue heating seems to be safe up to about 2–5°C [2]. In most diagnostic scanning applications the amount of tissue heating is negligible. The beneficial effects of tissue heating are utilized in therapeutic ultrasound for joints and muscles. At high intensity levels (e.g., with high-intensity focused ultrasound (HIFU)), the biological effects of heating and cavitation are used to destroy tissue [3].

Standard gray-scale imaging generates the least tissue heating because the pulse duration is short and pulse-repetition frequencies (PRFs) are low. Color flow Doppler and power Doppler produce immediate tissue heating. Spectral Doppler imaging is an unscanned mode which uses longer pulse durations and higher PRFs (to avoid artifacts such as aliasing) and therefore has an increased potential for heating. Spectral Doppler also involves longer duration times as individual

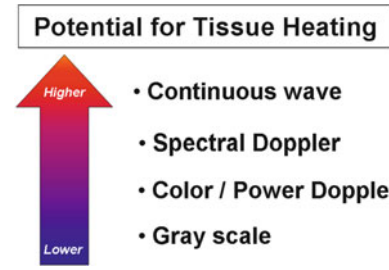

Fig. 3.2 Potential for tissue heating. Relative likelihood of tissue heating by mode of ultrasound is based in part on pulse-repetition frequency and duration of tissue exposure

vessels are interrogated in a fixed scanning position (Fig. 3.2) [4]. Tissue heating associated with routine diagnostic ultrasound is not known to produce tissue damage or to cause denaturation of proteins or to have teratogenic effects as long as scanning times are not prolonged and acoustic output restrictions are observed [5].

Mechanical Effects

Ultrasound energy generates an **acoustic field** in tissue. The acoustic field generates mechanical forces which affect tissue at the microscopic and macroscopic levels. Pressure exerted by the field creates **torque** and induces motion called **streaming**. These forces may potentially damage cells or tissues and also contribute secondarily to tissue heating.

One phenomenon associated with acoustical fields, **cavitation**, deserves special attention since it has been shown to cause tissue damage in animal models [1]. Cavitation occurs when gas bubbles within tissue begin to first oscillate

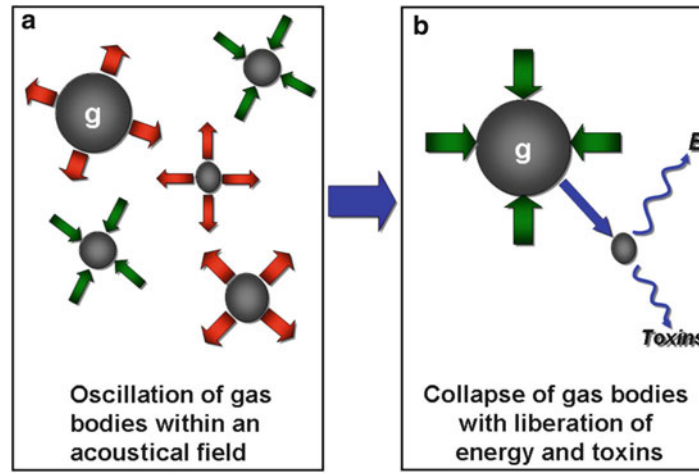

Fig. 3.3 Cavitation. (**a**) The oscillation and collapse of gas bodies (g) is cavitation. (**b**) The result of the collapse of gas bodies is the release of energy (E) and chemical toxins which may cause tissue damage

or vibrate in response to ultrasound and then to collapse. This collapse causes a violent movement of individual adjacent particles within the tissue which, in turn, causes tissue damage. This damage may take the form of ruptured cells and blood vessels or may cause chromosomal (ultrastructural) damage. In addition, the heat generated by the rapid collapse of gas bubbles may result in the formation of toxic chemical by-products (Fig. 3.3) [6].

The detrimental mechanical effects of acoustic fields are most likely to occur at gas/fluid interfaces. Thus cavitation effects (such as petechia formation) would most likely be seen in the lung or bowel. The threshold for cavitation is approximately 1 kw/cm^2 (far higher than the average intensity of 100 mw/cm^2 generated by most clinical scanners) [6].

Patient Safety

For most urologic applications, ultrasound produces energies in human tissues which are within recognized safe limits. *The single most important factor in minimizing potential adverse effects of ultrasound is the well-informed ultrasound operator* [7].

The proper selection of acoustic output, transducer frequency, and mode of ultrasound for a specific indication will mitigate risks. Expeditious and efficient scanning technique is critical to limiting overall exposure. To assist the sonographer in monitoring the bioeffects of ultrasound, the ultrasound community has adopted the output display standard (ODS) [8]. Two values are typically displayed, the **mechanical index** (**MI**) and the **thermal index** (**TI**) (Fig. 3.4). These indices are calculated estimates of the potential for bioeffects of ultrasound based on the mode of ultrasound being used, frequency, power output, and time of insonation. The MI and TI are typically displayed on the monitor during ultrasound examinations and all practitioners should be familiar with the location. It is important to understand that these indices are not safety limits and are not direct measurements.

Mechanical Index

The MI indicates the probability that cavitation will occur. For tissues not containing stabilized gas bodies (lung and intestine), the risk of cavitation is low as long as the MI is ≤0.7. For structures adjacent to lung or intestine, scanning time should be limited if the MI exceeds 0.4 (Fig. 3.5).

Thermal Index

The TI indicates the probability that tissue temperature within the sonographic field will be

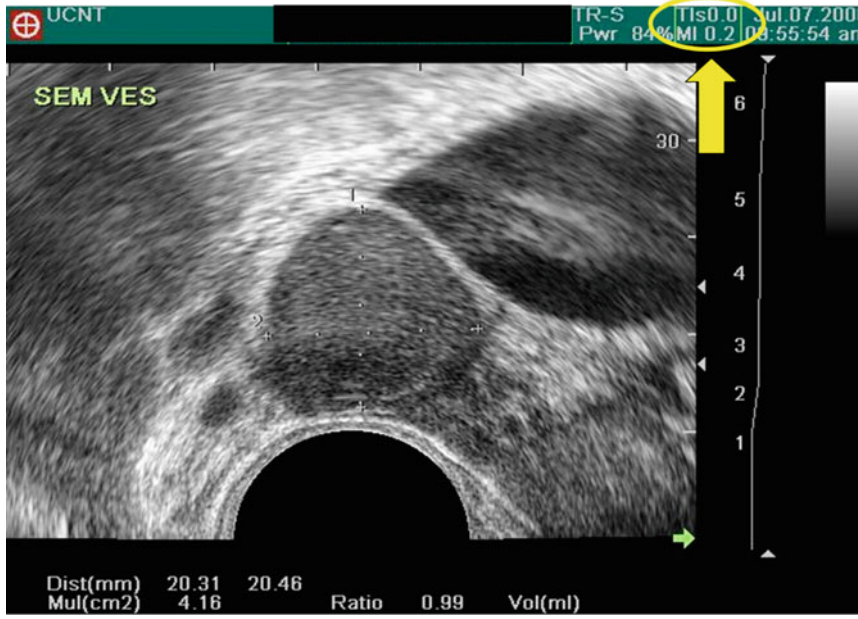

Fig. 3.4 Mechanical and thermal index. The MI and TI (*yellow* cycle) are calculated estimates of the potential for cavitation and tissue heating, based on study parameters and time of study. These are not direct measurements of either heating or pressures in the acoustical field

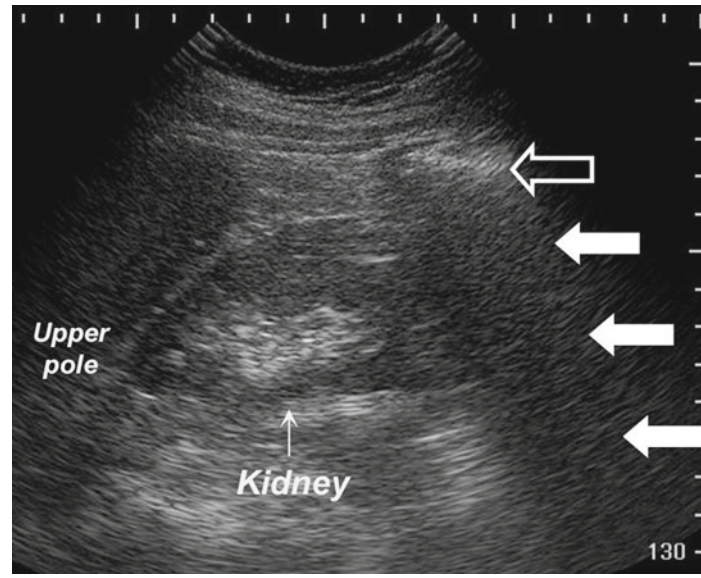

Fig. 3.5 The risk for cavitation is higher in tissues which are in proximity to gas-containing bodies such as the bowel. Here, bowel gas (*open arrow*) and the resultant distal acoustic shadowing (*white arrows*) obscures the *lower* pole of the *right* kidney (*arrow*)

increased by 1°C. The precise consequences of tissue heating are not completely understood, but even tissue temperature elevations of up to 6°C are not likely to be dangerous unless exposure time exceeds 60 seconds [2].

ALARA

In general, ultrasound performed by urologists has a low risk for patient harm as long as standard protocols are followed. Although tissue

heating may occur, there are no confirmed biologic effects of tissue heating in non-fetal scanning except when they are sustained for extended periods. "No independently confirmed adverse effects caused by exposure from present diagnostic ultrasound instruments have been reported in human patients in the absence of contrast agents. Biological effects (such as localized pulmonary bleeding) have been reported in mammalian systems at diagnostically relevant exposures but the clinical significance of such effects is not yet known. Ultrasound should be used by qualified health professionals to provide medical benefit to the patient" [9]. Nevertheless, all urologists should endeavor to follow the principles of **ALARA** which stands for "**A**s **L**ow **A**s **R**easonably **A**chievable." The ALARA principle is intended to limit the total energy imparted to the patient during an examination. This can be accomplished by (1) keeping power outputs low, (2) using appropriate scanning modes, (3) limiting exam times, (4) adjusting focus and frequency, and (5) using the cine function during documentation.

Scanning Environment

The physical environment where ultrasound examinations are performed should have adequate room for ultrasound equipment with the ability to control lighting and temperature. The exam table should have a height adjustment for sonographer comfort and ease of patient access. If there are windows in the exam room, they should have adjustable coverings to reduce the light and glare on the monitor and to preserve patient privacy. Workspace design should include adequate space to allow for safe handling of biopsy needles and specimens. Since the lighting in the room is dimmed, it may be necessary to provide a separate lighting source for the work area where biopsy samples are being transferred into specimen containers.

The goals of the optimum scanning environment should be to protect patient safety and to maximize operator efficiency and reduce the risk for work-related musculoskeletal disorders (MSDs). Occupational Safety and Health Administration (OSHA). OSHA has established an e-tool to provide guidance on operator safety in the performance of ultrasound [10]. Urologists should personally arrange the ultrasound equipment and monitor the environment in pursuit of these goals. Policies and procedures should be in place to provide for the safety of patients and personnel. Infection control policies and procedures should be in place including adherence to universal precautions and proper care, cleaning, and maintenance of ultrasound equipment.

Patient Identification and Documentation

Patient identification should be verified prior to performing ultrasound procedures. When biopsy specimens are taken, a time-out should be conducted to verify patient identity and the accurate labeling of ultrasound images and specimen containers. It is estimated, based on DNA evidence, that up to 1% of prostate biopsy specimens may be subject to incorrect patient identification [11]. Documentation and image labeling is addressed in further detail in Chap. 2. An ultrasound report should be generated. The report and images should be included in the patient's medical record.

Equipment Maintenance

Ultrasound equipment should be in good operating condition and undergo routine calibration at least once a year [12]. Equipment manufacturer specifications and federal and state guidelines for the maintenance of ultrasound equipment should be followed. Equipment should be routinely inspected and tested for electrical safety. When transporting ultrasound equipment, care should be taken to ensure that transducers are secured to the machine. The transducers are delicate and should not be dropped. Transducer cables and power cords should be secured to the machine and off the ground to prevent damage to the cables by the machine rolling over them.

Cleaning and Disinfection of Ultrasound Equipment

The ultrasound transducers, cables, and the machine itself should be cleaned immediately following each study. Ultrasound transducers have delicate parts which can be damaged by inappropriate handling, so equipment manufacturer guidelines should be followed when cleaning. The cleaning method and level of disinfection for transducers will depend on the specifics of the procedures and the nature of tissue encountered. The Centers for Disease Control (CDC) publishes guidelines for disinfection and sterilization in healthcare facilities which should be followed [13].

Applications such as abdominal, pelvic, or scrotal ultrasound are considered **noncritical** since they are performed on intact skin. The transducers and transducer holders should be cleaned immediately following the procedure. Allowing gel to dry on the probe makes cleaning more difficult. Staff should wear gloves when cleaning the probes and equipment. The probe should be disconnected from the ultrasound unit when cleaning. Ultrasound gel may be removed from the probe by wiping with a soft cloth. The transducer should be cleaned with mild soap and water or a commercial spray or wiped after every use. The ultrasound manufacturer-approved disinfectant should be used to avoid damaging the probe. When placing the probe under running water, care should be taken to keep water away from the junction of the probe and the cable. The entire body of the transducer may be immersed, but care should be taken to avoid the junction between the transducer body and the cable. Each manufacturer provides specific instructions about the proper immersion levels for probes. A small soft brush may be used to clean crevices where gel may accumulate.

When an ultrasound procedure is performed in which the probe comes into contact with mucous membranes (e.g., with transrectal ultrasound), a **high-level disinfection** process should be followed. Even when the probe covers are used, high-level disinfection after the procedure is still necessary. When cleaning the transrectal probe and attachments, staff should wear personal protective equipment including gloves and glasses. The FDA has published guidelines for the reprocessing of reusable ultrasound transducer assemblies used for biopsy procedures which should be followed [14]. The AIUM has issued guidelines on the cleaning and preparing of endocavitary ultrasound transducers between patients [15]. Transducer covers and biopsy attachments should be removed and discarded in a biohazard container. The probe should be placed under warm running water to remove residual debris and a small amount of nonabrasive liquid soap used to thoroughly cleanse the probe. Using a small brush, areas of angulation and crevices may be brushed clean. The probe should be rinsed with warm running water prior to being placed in sterilizing liquid. When immersing in a liquid, care should be **taken** to follow the manufacturer's recommended immersion level so as to not damage the probe. The transducer should be immersed in a disinfectant approved for high-level disinfection and for the specified time recommended by the manufacturer to achieve high-level disinfection. The transducer should not remain immersed in the disinfectant solution for longer than the recommended time as prolonged exposure may damage the transducer. A published list of approved high-level disinfectants for use in processing reusable medical devices is available at US Food and Drug Administration website [16]. The CDC publishes guidelines on the cleaning of medical devices on their website [13]. After high-level disinfection has been performed, the transducer should be rinsed thoroughly with sterile water, dried with a paper towel, and stored in a clean environment until its next use.

Critical disinfection is required when blood or body fluids come in contact with the transducer or needle guide. Because blood and tissue pass through prostate biopsy guides, reusable prostate biopsy guides should be heat sterilized. If reusable biopsy guides are not able to be heat sterilized, then chemical sterilization should be performed [17]. Attachments which are labeled "onetime use" should not be reused and should be disposed of in a biohazard container. When cleaning reusable biopsy attachments, they should

be placed immediately into a solution of mild soap and water. A clean and properly sized brush should be used to clean the biopsy channel and lumen of the device checking to make sure no debris remains in the channel or lumen. The attachment should be rinsed and placed in a bag for heat sterilization. Heat sterilization should be performed, and the attachments should remain in the sterile bag until ready for use.

References

1. Guidance for industry and FDA staff-information for manufacturers seeking marketing clearance of diagnostic ultrasound systems and transducers. Document issued on 9 Sept 2008. http://www.fda.gov/MedicalDevices/DeviceRegulationandGuidance/GuidanceDocuments/ucm070856.htm.
2. Bioeffects Committee of the American Institute of Ultrasound in Medicine. American Institute of Ultrasound in Medicine consensus report on potential bioeffects of diagnostic ultrasound: executive summary. J Ultrasound Med. 2008;27:503–15.
3. Susani M, Madersbacher S, Kratzik C, Vingers L, Marberger M. Morphology of tissue destruction induced by focused ultrasound. Eur Urol. 1993;23 Suppl 1:34–8.
4. Rumack CM, Wilson SR, Charboneau JW. Diagnostic ultrasound. 3rd ed. St. Louis, MO: Mosby; 2005 (Ch. 2, Page 37).
5. O'Brien WD, Deng CS, Harris GR, Herman BA, Merritt CR, Sanghvi N, et al. The risk of exposure to diagnostic ultrasound in postnatal subjects: thermal effects. J Ultrasound Med. 2008;27:517–35.
6. Church CC, Carstensen EL, Nyborg WL, Carson PL, Frizzell LA, Bailey MR. The risk of exposure to diagnostic ultrasound in postnatal subjects: nonthermal mechanisms. J Ultrasound Med. 2008;27:565–92.
7. Nelson TR, Fowlkes JB, Abramowicz JS, Church CC. Ultrasound biosafety considerations for the practicing sonographer and sinologist. J Ultrasound Med. 2009; 18:139–50.
8. American Institute of Ultrasound in Medicine. How to interpret the ultrasound output display standard for higher acoustic output diagnostic ultrasound devices: version 2 [technical bulletin]. J Ultrasound Med. 2004;23:723–6.
9. American Institute of Ultrasound in Medicine Official Statement on Prudent Use Clinical Safety. April 2012. http://www.aium.org/resources/statements.aspx Accessed 29 Jan 2013.
10. United States Department of Labor Occupational Safety and Health Administration: Hospital eTool, Clinical services sonography. http://www.osha.gov/dcsp/products/etools/hospital/sonography/sonography.html.
11. Makary MA, Epstein J, Pronovost PJ, Millman EA, Hartmann EC, Freischlag JA. Surgical specimen identification errors: a new measure of quality in surgical care. Surgery. 2007;141(4):450–5.
12. Routine quality assurance for diagnostic ultrasound equipment. Published by the American Institute of Ultrasound in Medicine; 2008. http://www.aium.org.
13. Rutala WA, Weber DJ, The Healthcare Infection Control Practices Advisory Committee (HICPAC). Guidelines for disinfection and sterilization in healthcare facilities; 2008. http://www.cdc.gov/hicpac/pdf/guidelines/Disinfection_Nov_2008.pdf Accessed 29 Jan 2013.
14. FDA public health notification: reprocessing of reusable ultrasound transducer assemblies used for biopsy procedures; 2006. http://www.fda.gov/medicaldevices/safety/alertsandnotices/publichealthnotifications/ucm062086 Accessed 22 June 2006.
15. AIUM Guidelines for Cleaning and Preparing Endocavitary Ultrasound Transducers Between Patients. Approved June 4, 2003. http://www.aium.org/resources/statements.asp.x. Accessed 29 Jan 2013.
16. FDA-cleared sterilants and high level disinfectants with general claims for processing reusable medical and dental devices, March 2009. http://www.fda.gov/MedicalDevices/DeviceRegulationandGuidance/ReprocessingofSingle-UseDevices/ucm133514.htm.
17. ANSI/AAMI ST58:1005(R)2010. Chemical sterilization and high level disinfection in health care facilities. Developed by the Association for the Advancement of Medical Instrumentation. Approved by the American National Standards Institute.

Maximizing Image Quality: User-Dependent Variables

4

Pat F. Fulgham

Introduction

Ultrasound is a tool used for the diagnosis and management of urologic disease. An ultrasound examination performed and interpreted by the clinician combines a knowledge of the underlying anatomy and disease processes with technical expertise to produce images of superior quality which answer a specific clinical question. The interpretation of urologic images is an integral part of the training of all urologists. The technical performance of the study and the ability to maximize image quality are learned skills. Current ultrasound equipment is a sophisticated combination of mechanical equipment and software which is capable of producing exquisitely detailed anatomic images. Almost all current ultrasound equipment includes preset applications which optimize machine settings for imaging of specific organs or regions of the body. These presets save a great deal of time because they set scanning parameters which are favorable for most patients. However, there are many clinical circumstances in which these presets will need to be adjusted by the individual performing the ultrasound examination. An understanding of the underlying physical principles of ultrasound, proper probe selection, and machine settings is critical to making appropriate adjustments to the equipment.

P.F. Fulgham, MD, FACS (✉)
Department of Urology, Texas Health Presbyterian Dallas, 8210 Walnut Hill Lane, Suite 014, Dallas, TX 75231, USA
e-mail: pfulgham@airmail.net; patfulgham@yahoo.com

Tuning the Instrument

The goal of adjusting machine settings is to produce "a good-quality image." Accepted characteristics of a good-quality image include (1) sufficient and uniform brightness, (2) sharp and in focus, (3) adequate size, and (4) oriented and labeled for documentation purposes. Desired attributes of an image may vary from individual to individual, but these general principles should always apply.

Several machine settings can be manipulated by the sonologist. These include but are not limited to gain, time-gain compensation (TGC), frequency, focal zones, depth/size, field of view, and cine function (Fig. 4.1).

This chapter will explore the use of each of these "user-controlled" variables emphasizing the underlying physical principles and defining the clinical circumstances under which these adjustments may be necessary.

Transducer Selection

Selection of the transducer is critical to maximizing image quality. The physical shape of the transducer may be important in certain circumstances. The image that is produced by a transducer may

P.F. Fulgham and B.R. Gilbert (eds.), *Practical Urological Ultrasound*, Current Clinical Urology,
DOI 10.1007/978-1-59745-351-6_4, © Springer Science+Business Media New York 2013

Frequently Used Adjustable Machine Settings

- Gain
- Time-gain compensation
- Frequency
- Focal zones
- Depth / Size
- Field of view
- Cine function

Fig. 4.1 There are a large number of parameters and settings which may be modified by the user. These seven represent commonly used adjustments and functions for manipulating image quality

be recognized by its shape. A linear array transducer produces a rectangular image whereas a curved array transducer produces an image which is trapezoidal in shape (Fig. 4.2).

Linear array transducers are most commonly used in urology for imaging of the testes and male genitalia. The curved array transducer is more frequently used for abdominal scanning. The curved nature of the probe allows gentle pressure on the patient's abdomen or flank resulting in contact of the entire transducer face with the skin. Curved array transducers are useful for imaging between ribs or angling beneath the pubic symphysis.

Transducers are usually multifrequency, meaning the frequency can be switched electronically over a range of frequencies (e.g., 2.5–6 mHz for an abdominal transducer). It is important to select the highest frequency which has adequate depth of penetration for the anatomic area of interest. The higher the frequency of the transducer, the greater the axial resolution and the better the anatomic representation of the image. However, there is a trade-off between frequency and depth of penetration. Imaging of the kidneys requires a lower frequency to penetrate to a depth of 6–14 cm below the surface of the skin. Thus, renal scanning is usually performed with a curved array transducer between 2.5 and 6 mHz. By contrast, because of the close proximity of the testes to the surface of the skin, scanning of the testis can be performed with high frequency transducer, producing excellent axial resolution. A linear array transducer at 12 mHz is often used for testicular ultrasound. Transrectal ultrasound of the prostate often employs a transducer of 7.5 mHz since it offers an optimal combination of depth of penetration and axial resolution for the average-sized gland (Fig. 4.3).

Interfaces

To produce the best-quality image, the sonographer should arrange the scanning environment so that the interfaces between patient, sonographer, and equipment are optimized. The patient should be positioned at a height which allows the sonographer to stand or sit in a comfortable position so that the sonographer is able to stabilize the transducer against the patient's body. This minimizes unwanted movement of the transducer and allows the sonographer to maintain the orientation and position of the transducer while adjusting machine features (Fig. 4.4).

The sonographer must have the ability to comfortably reach the physical console or touch screen in order to adjust the machine setting. Many ultrasound units provide the ability to freeze and unfreeze the transducer via a button on the transducer itself or by a foot switch. In either case the sonographer must be able to scan the patient with one hand while manipulating the console and documenting with the other hand.

The sonographer must have a clear direct view of the monitor. The angle of the monitor should be adjusted for viewing by the sonographer. The brightness settings on the monitor need to be adjusted for the conditions under which the scan is being performed. In general, dimming the room lights improves the ability to evaluate the image on the monitor.

Monitor Display

It is important when performing an ultrasound examination to understand the information that is available on the monitor. Patient demographic information, type of exam, and facility should be entered. The monitor will usually display

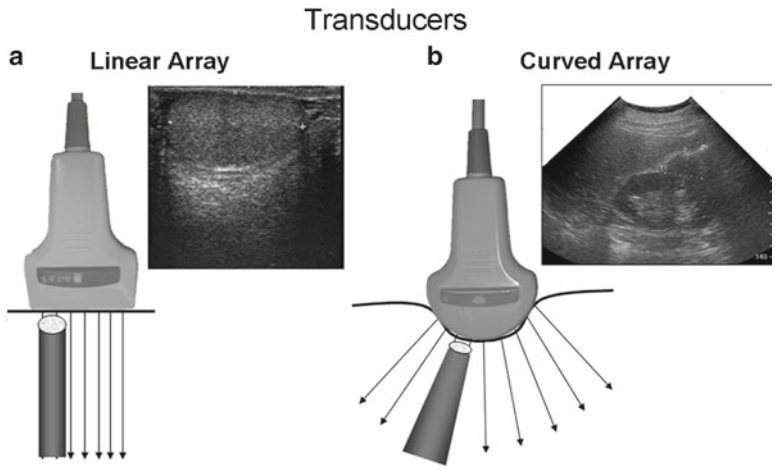

Fig. 4.2 (**a**) The linear array transducer produces a *rectangular* image field. (**b**) The curved array transducer produces a *trapezoidal* or *pie-shaped* image. The shape of the transducer affects the divergence of the sound wave as it propagates in the body

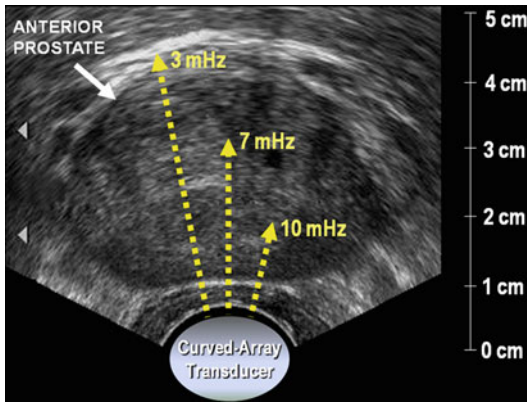

Fig. 4.3 The selection of a transducer with the frequency of 7.5 mHz reflects the trade-off between depth of penetration and good axial resolution. In this axial image of a large prostate, a *lower* scanning frequency may be needed to adequately visualize the anterior prostate

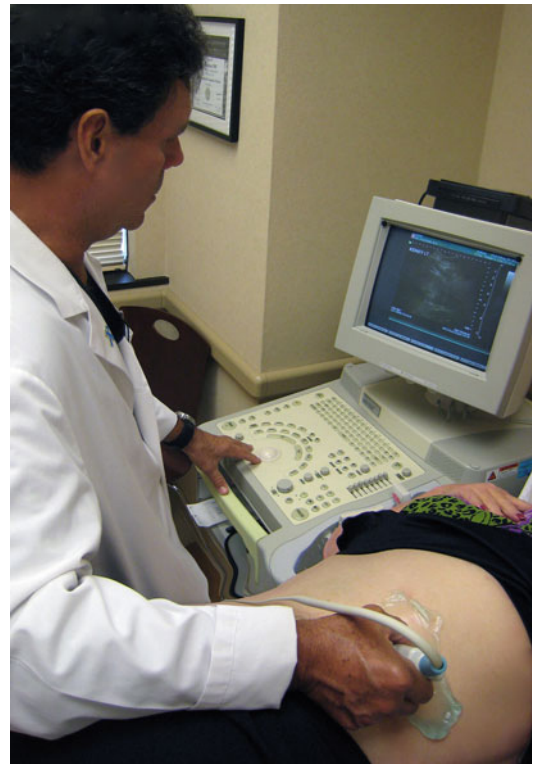

Fig. 4.4 The configuration of the equipment and proximity to the patient are critical in maximizing comfort, efficiency, and accuracy during scanning and documentation

information regarding which probe is active, the frequency of the probe, and the magnification of the image. Information regarding overall gain and other settings is available on the monitor. Typically there will be a TGC curve displayed on one side of the image as well as color bar which demonstrates the range of pixel brightness or hues available. In addition, there will be gradient markings on one side so that depth of field can be appreciated (Fig. 4.5).

By convention, when scanning organs in the sagittal view, the upper pole of the organ (e.g., kidney or testis) is to the left of the screen and the lower pole is to the right of the screen (Fig. 4.6).

In transverse scanning the right side of an anatomic structure is displayed on the left side of the

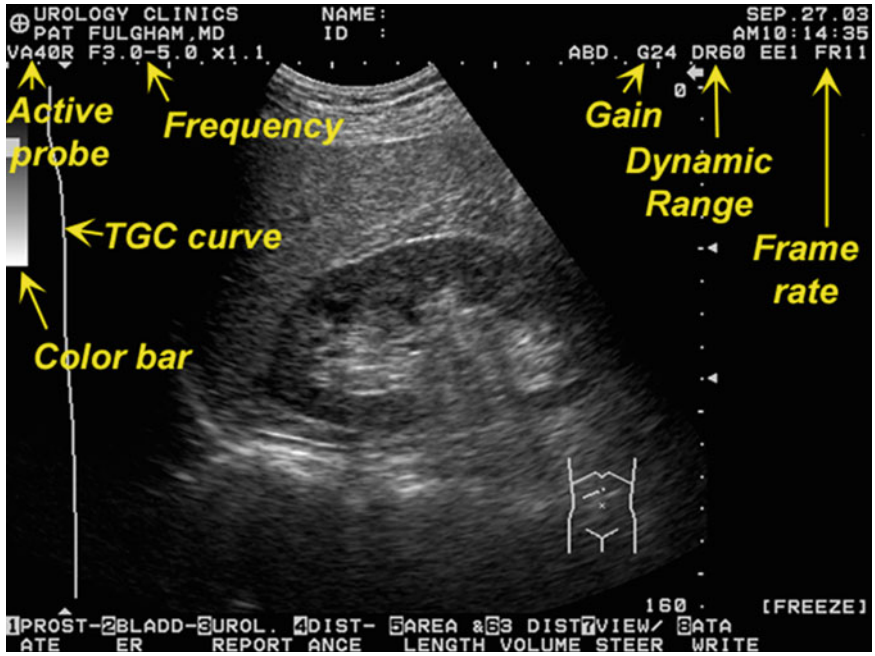

Fig. 4.5 Some of the machine settings are displayed on the monitor. Knowing where these settings are displayed and what they mean assists in optimizing image quality

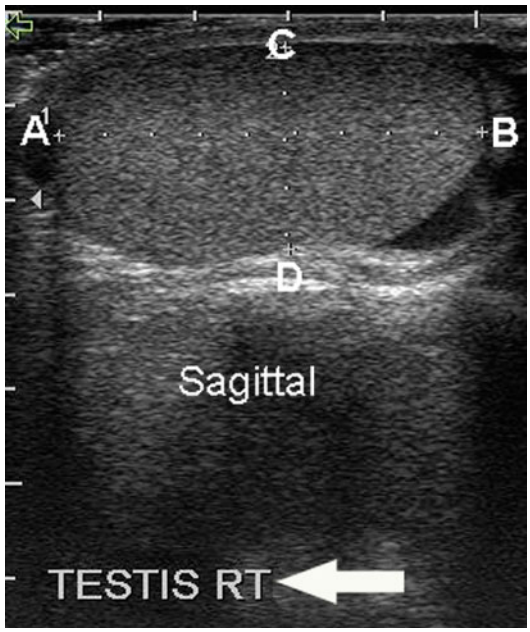

Fig. 4.6 In this sagittal image of the *right* testis, the superior pole of the testis (**A**) is to the *left* and the inferior pole of the testis (**B**) is to the *right*. The anterior aspect of the testis (**C**) is at the *top* of the image and the posterior aspect (**D**) at the *bottom*. Without the label, there would be no way to distinguish the *right* from the *left* testis

image just as it would be when evaluating a conventional radiograph. These conventions should always be followed when documenting an ultrasound examination; however, it may be useful to also demonstrate the orientation of the probe using graphics or icons. When paired structures such as the kidneys or testes are imaged, it is particularly important to designate the organ as right or left.

User-Controlled Variables

One of the most commonly required adjustments during ultrasound scanning is an adjustment to the overall **gain**. The gain is a control which determines the degree to which the electrical signal produced by a returning sound wave when it strikes the transducer will be amplified for display. This needs to be differentiated from **acoustic output** which is defined as the power or amplitude of the afferent wave which is generated by the transducer (Fig. 4.7).

Both gain and acoustic power can be controlled by the operator; however, acoustic output is limited by the manufacturer in compliance with

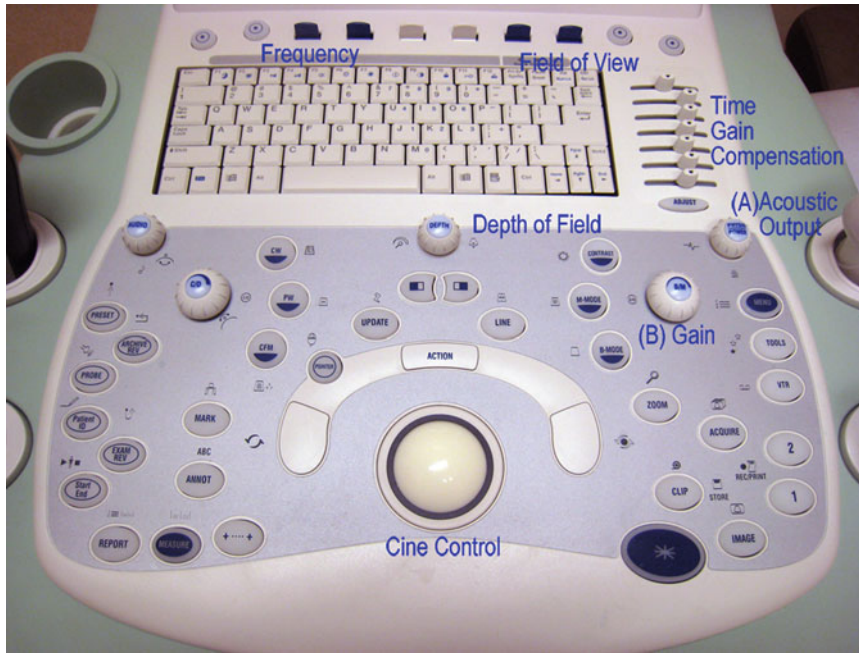

Fig. 4.7 A typical console interface showing common user-controlled variables. The acoustic output (**A**) controls the amplitude or power of the generated sound wave while overall gain (**B**) controls the degree to which the returning echo-generated electrical impulse will be amplified

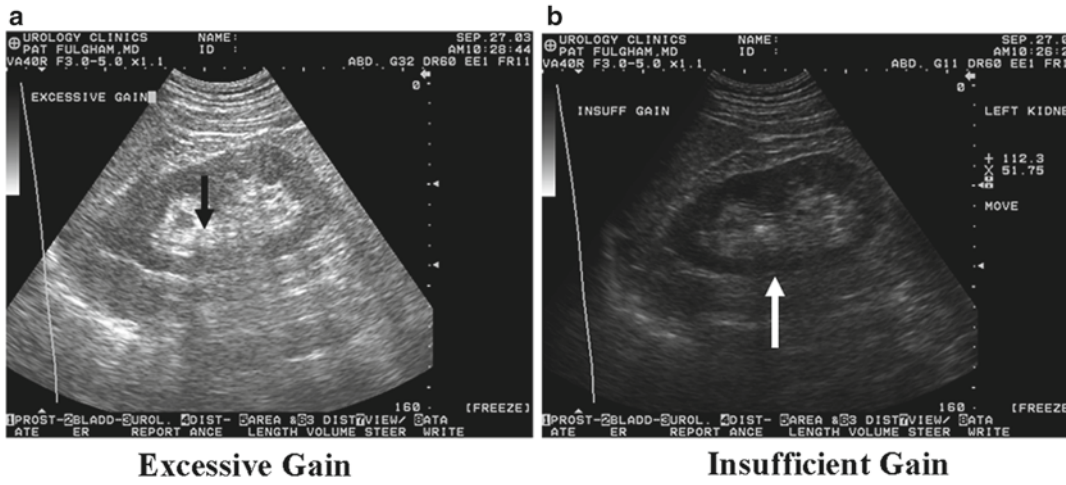

Fig. 4.8 (**a**) Excessive gain settings make it difficult to distinguish the stone (*black arrow*) in the *upper* pole of the kidney. (**b**) Insufficient gain makes it difficult to appreciate the distinction between the medial renal capsule (*white arrow*) and the perinephric fat

industrial safety standards [1]. In general, when the gain is increased the resultant image is brighter or more hyperechoic. When there is excessive overall gain, the image often appears bright and washed out. When there is insufficient overall gain, the image is often dark and it is difficult to distinguish between adjacent structures (Fig. 4.8).

It is generally more desirable to increase or decrease the gain rather than manipulate the

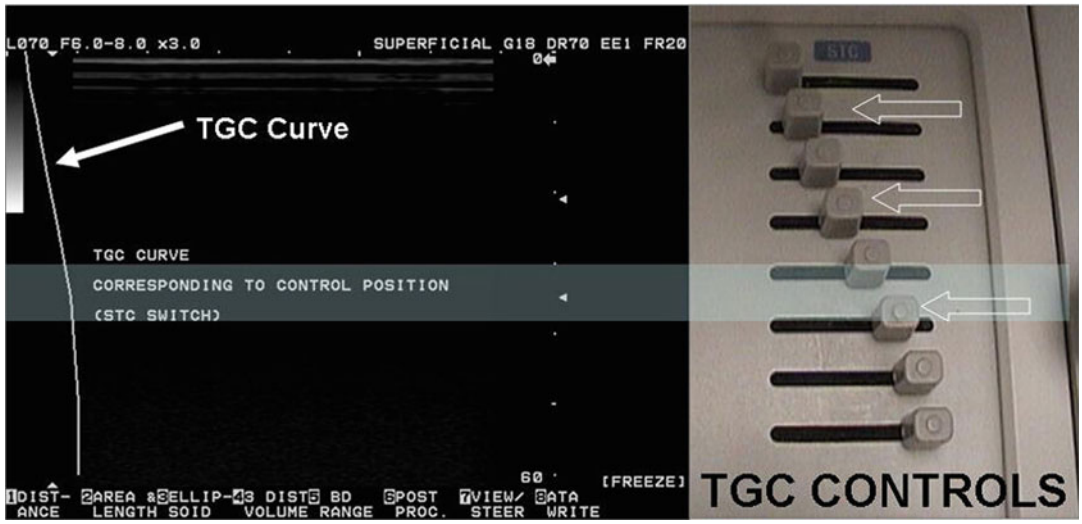

Fig. 4.9 TGC (time-gain compensation). The signal from a reflected (returning) sound wave can be amplified or diminished based on the depth of the reflector within the scanned field. The physical "sliders" (*open arrows*) correspond to the shape of the "TGC curve" (*white arrow*) on the monitor

acoustic output. However, there may be circumstances (e.g., a very thin or a very heavy patient) where increases or decreases in acoustic output would be appropriate. In every case, manipulations of gain or acoustic output are made to improve image quality. The principle of ALARA (as low as reasonably achievable) should always be honored when making these adjustments, imparting as little acoustic energy into the patient as will provide an adequate image.

Time-gain compensation is another way to control the amplification of the signal from a returning sound wave. As opposed to overall gain, the amplification of these signals can be adjusted independently by region of the scanned field. That is, the electrical signal generated by sound waves returning from a specific region inside the patient can be individually amplified using TGC controls. TGC controls usually involve a set of sliding switches which can increase or decrease the amplification of a signal at a particular depth in the scanned field. This is often displayed graphically on the monitor as a line or a curve which corresponds to the position of the physical slides on the console (Figs. 4.9 and 4.10).

TGC is most commonly used to amplify the signal strength from regions of the image where there is high attenuation of the sound waves or to decrease the amplification of the signal strength when there are areas where sound waves are unattenuated. One frequent use of TGC in urologic scanning is to compensate for the hyperechogenicity of tissue distal to a fluid-filled structure such as the bladder or a large renal cyst. It is often necessary to decrease the TGC for that region of the image distal to the fluid-filled structure so that structures in that location can be accurately represented (Fig. 4.11).

Frequency adjustment allows a multifrequency probe to be switched between two or three main frequency ranges during scanning. For instance, a curved array probe for abdominal scanning will often have the ability to adjust from 2–4 to 3.5–5 to 4–6 mHz. These ranges are specifically designed to take advantage of greater axial resolution with the higher frequencies and greater depth of penetration with lower frequencies. It is useful during scanning to change between frequencies to determine which frequency range provides the best overall image quality (Fig. 4.12).

The frequency determines the axial resolution of the scan. Axial resolution is the ability to identify as separate, two objects in the direction of the

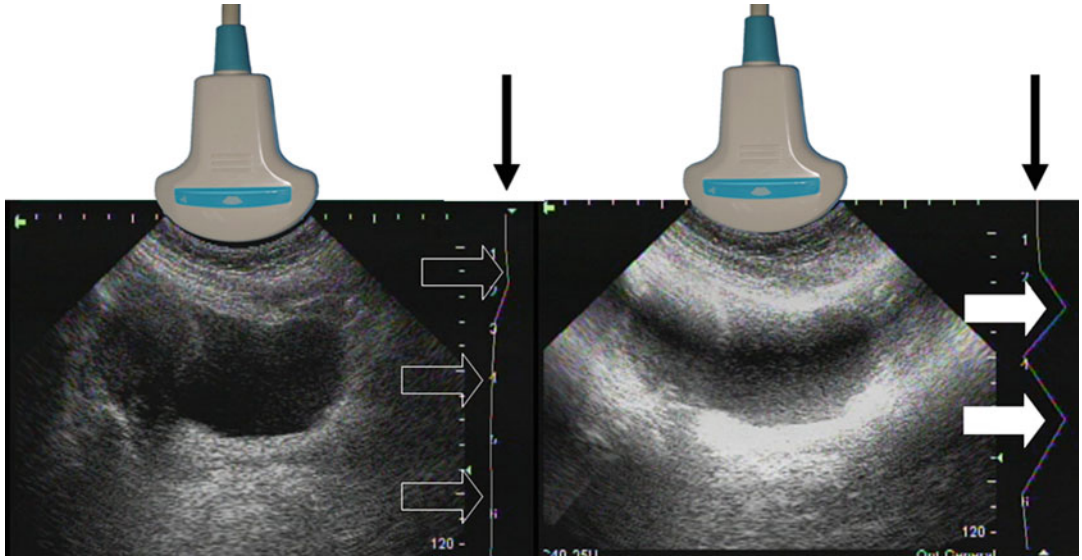

Fig. 4.10 Note how the shape of TGC curve (*black arrows* in the image on the left) corresponds to the pixel brightness at given regions of the scanned field. When the TGC curve is deviated to the right, (*large arrows* in the image on the right) the signals produced by sound waves returning from that corresponding region of the ultrasound field are amplified and displayed as "brighter" pixels. Acoustic output is unchanged by adjustments in time-gain compensation

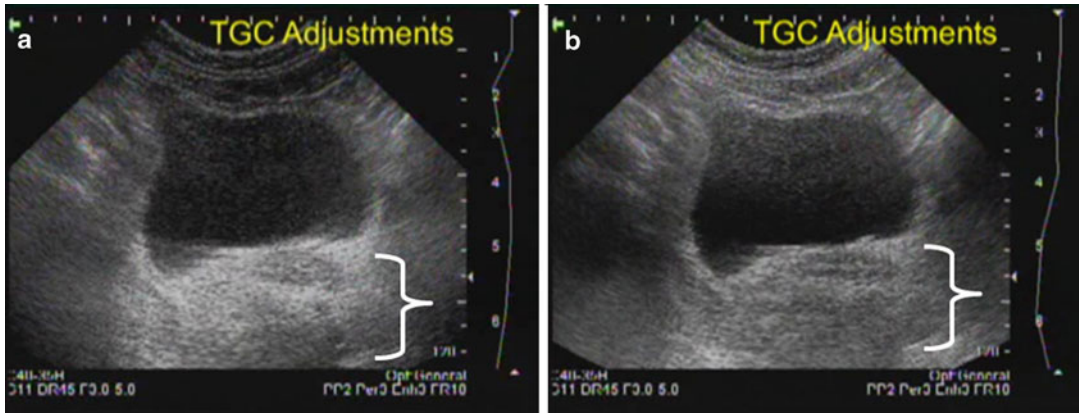

Fig. 4.11 (**a**) The fluid-filled bladder results in a region of decreased attenuation which produces a hyperechoic appearance of tissue posterior to the urinary bladder. (**b**) This artifact called "increased through transmission" can be corrected by decreasing the TGC curve in this region (*brackets*)

traveling sound wave. The higher the frequency, the better the axial resolution. The pulse that is sent from a transducer usually consists of two or three wavelengths and, as such, has a physical length. This pulse must fit completely between two objects in the axial plane in order to discriminate those objects as separate (Fig. 4.13).

Therefore, a pulse using a higher frequency wave has a shorter physical length than a pulse using a lower frequency wave. The shorter the pulse length, the better the axial resolution. A 5 mHz transducer produces a pulse length sufficient to produce an axial resolution of approximately approximately 1 mm (see insert Box).

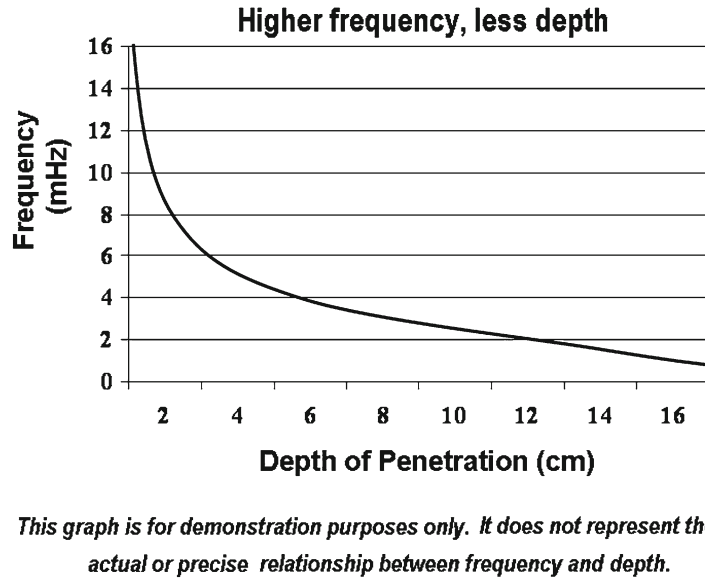

Fig. 4.12 The relative relationship between frequency and depth of penetration. Notice that to image a kidney 12 cm beneath the skin, a frequency of 2–4 mHz would be required to achieve an adequate depth of penetration

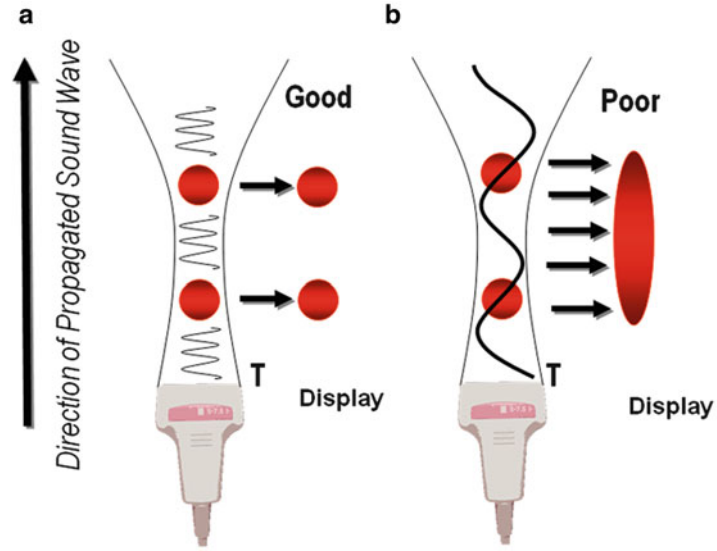

Fig. 4.13 (**a**) The shorter pulse length associated with this higher frequency wave is able to fit between the two objects in the axial plane providing good axial resolution. (**b**) The longer pulse length is unable to fit between the objects, thus depicting the two distinct objects as a single "blurred" echogenic focus

Axial Resolution

1 pulse = 3λ

$v = f\lambda$

For normal tissue velocity of 1,540 m/s and a frequency of 5 mHz,

$\lambda = v/f$

$\lambda = 1{,}540$ m/s/5 mHz

$\lambda = 0.34$ mm

$3\lambda = 1.02$ mm

$\therefore$ 1 pulse = 1.02 mm

Therefore, axial resolution at 5 mHz $\geq$ 1.02 mm.

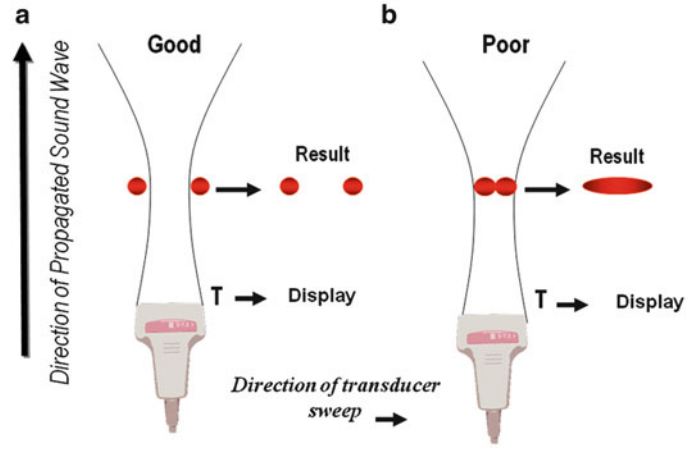

Fig. 4.14 Lateral resolution is optimized when beam width is narrow enough to fit between two objects equidistant from the transducer. In (**a**) the objects would be correctly displayed as separate objects. In (**b**) the beam width is too thick to fit between the objects, and they would be displayed as a single "blurred" focus

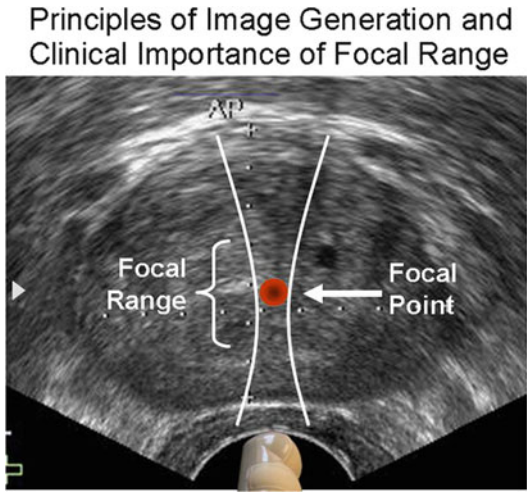

Fig. 4.15 The shape of the ultrasound beam determines its lateral resolution. The narrowest portion of the beam is its focal point or focal zone. The location of the narrowest point of the beam can be adjusted by manually setting foci

Focal zone adjustments are made in an attempt to bring the narrowest portion of the ultrasound beam into the location where maximal lateral resolution is desired. Lateral resolution is defined as the ability to discriminate as separate, two points which are equidistance from the transducer (Fig. 4.14).

Lateral resolution is a function of the width of the sound wave beam. The more focused the beam, the better the lateral resolution; that is, even closely spaced objects can be differentiated. Most transducers have a focal point producing the best lateral resolution and a focal range producing adequate lateral resolution (Fig. 4.15).

The width of the beam can be controlled by setting the location of focal zones. However, the thickness of the beam (known as the elevation or azimuth) is determined by the characteristics of the transducer crystals and design. In general, the focal zone should be placed at or just distal to the area that is of maximum clinical interest (Fig. 4.16).

It is possible to set multiple focal zones; however, this requires the software to sequentially interpret returning sound waves from specific locations of the scanning field (Fig. 4.17).

Multiple focal zones result in a slower frame refresh rate and may result in a display motion that is discontinuous. In most urologic scanning applications a slower refresh rate is not a significant liability. Multiple focal zones are most useful in urologic scanning when fine anatomic detail throughout a solid structure is desirable (notably, in testicular scanning). When it is desirable to produce and interpret a twinkle artifact during Doppler scanning, it is useful to place the focus just at or distal to the object producing the twinkle artifact (Chap. 5, page 57).

Depth/size function allows the user to select that portion of the scanned field which will be displayed on the monitor. By adjusting the depth of field, it is possible to allow the structure of interest to occupy the appropriate proportion of the visual field. By limiting the area of the scanned field from which returning echo signals will need to be

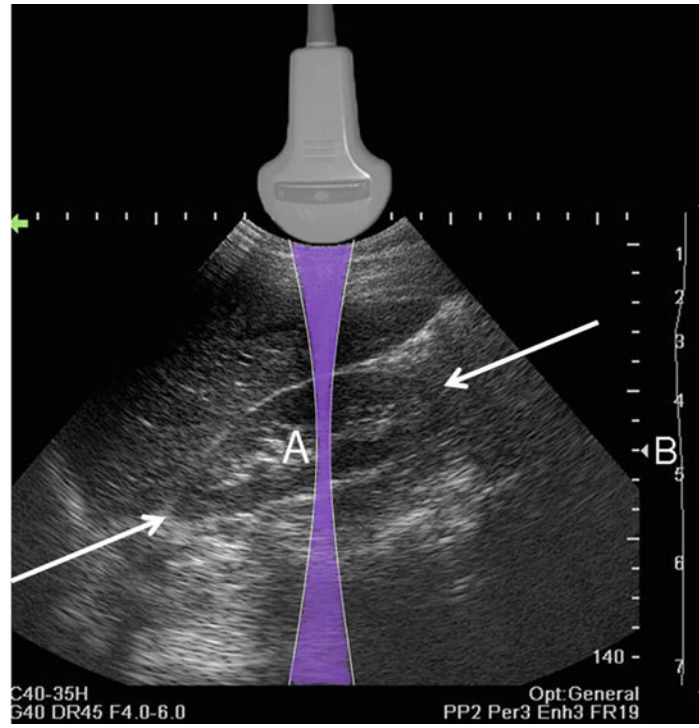

Fig. 4.16 The shape of the ultrasound beam is simulated in this drawing (*purple*). The focal zone (**A**) is located to produce the best lateral resolution of the medial renal cortex (*white arrows*). The location of the focal zone is designated by the *arrowhead* (**B**). The location of the focal zone can be adjusted by the operator

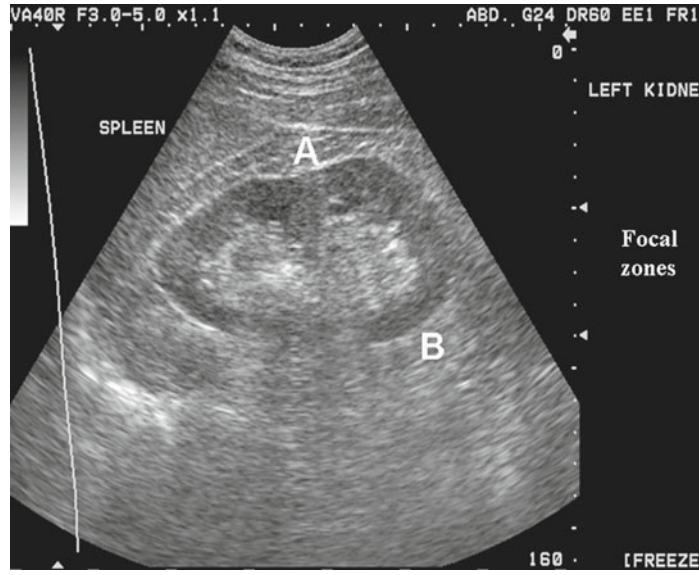

Fig. 4.17 In this sagittal renal ultrasound two focal zones (*arrowheads*) are set to correspond to the (**A**) lateral renal cortex and (**B**) the medial renal vortex

interpreted and displayed, the amount of work performed interpreting that returning information will be diminished and frame refresh rates will be improved. The depth/size function has no effect on the axial resolution of the image. Appropriate depth of field adjustments can improve the ability to visually discriminate certain structures during urologic scanning and improves the overall performance of the equipment (Fig. 4.18).

Field of view is an adjustment to limit the width of an image so that only a portion of the

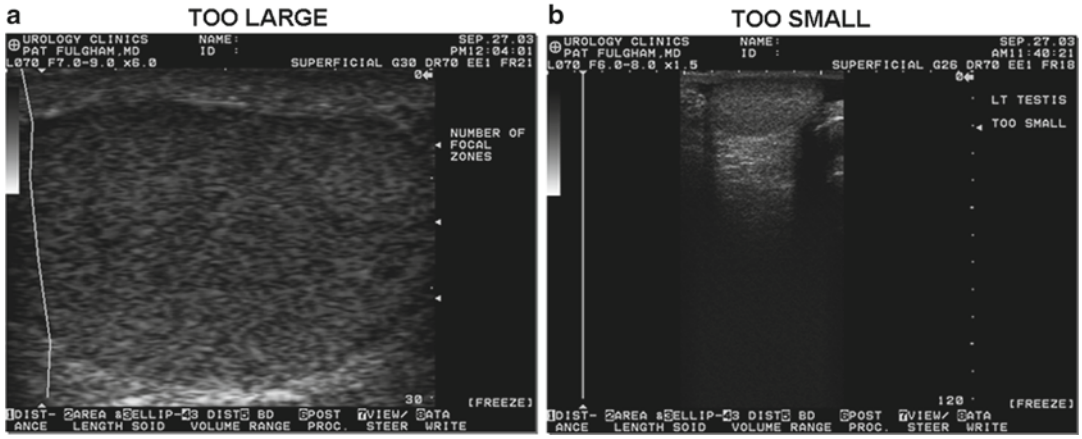

Fig. 4.18 (**a**) Depth of field has been set so that the testis fills the available display space but produces a grainy image. (**b**) Depth of field has been increased so that the testis occupies a very small portion of the available display. Tissue posterior to the testis which is not relevant occupies a large percentage of the display

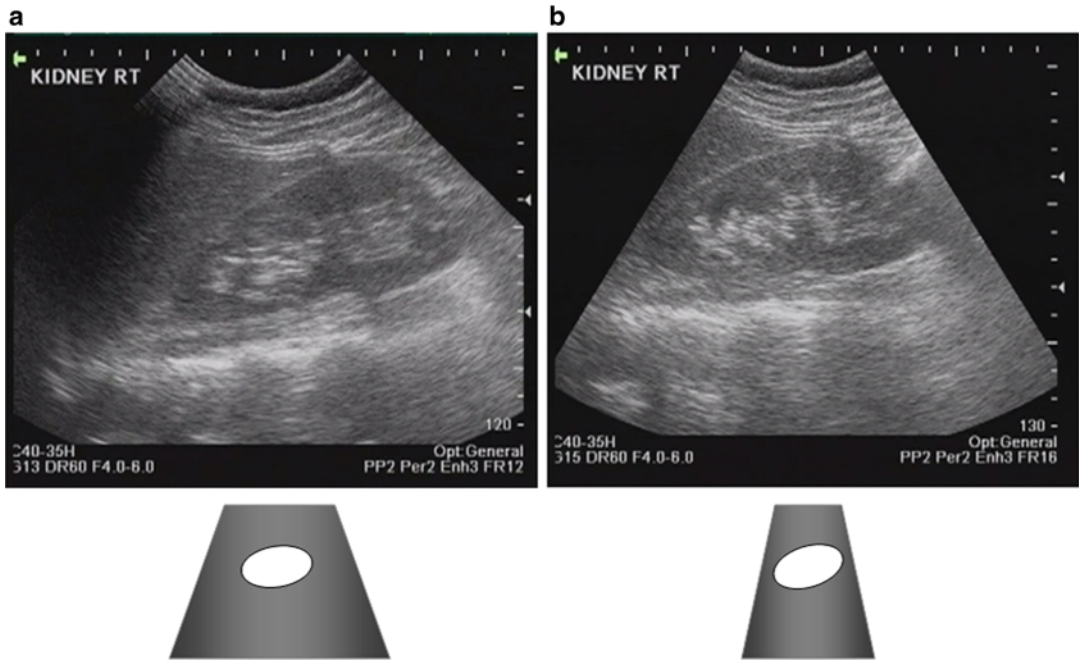

Fig. 4.19 The full ultrasound field is displayed in (**a**). Limiting the field of view to the kidney (**b**) decreases the time necessary to interpret returning echo information and improves the frame refresh rate

available ultrasound information is interpreted. As with changes in depth of field, narrowing the field of view will reduce the amount of work necessary to interpret the returning echo data and improve frame refresh rate. It also limits the visual distraction of tissues which are irrelevant to a specific exam (Fig. 4.19).

The **cine function** of most machines provides an opportunity to save a sequence of frames from the most recent scanning session and allows these frames to be played back one by one. This is a very useful feature when scanning organs such as the kidney which may be affected by respiratory motion. When a subtle

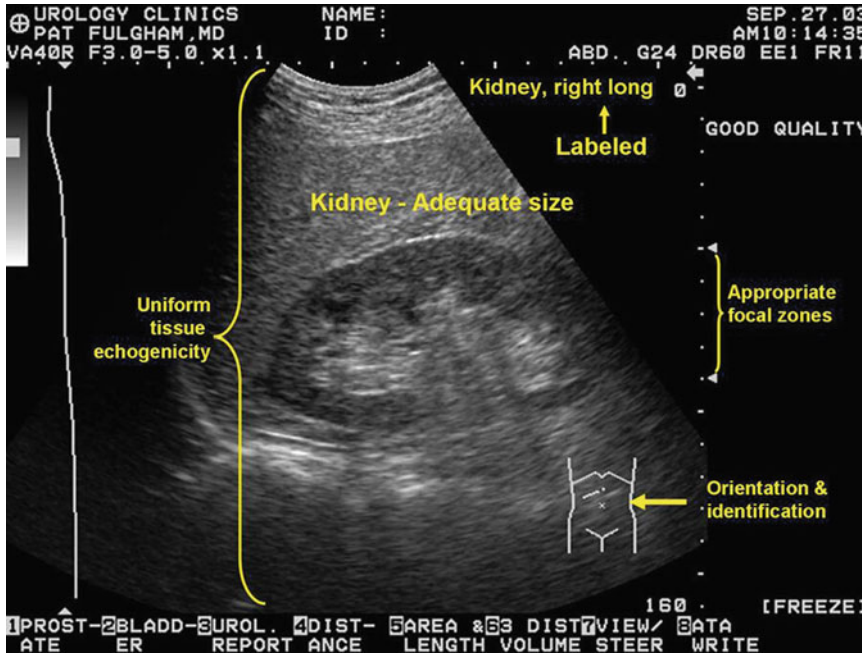

Fig. 4.20 This image displays the characteristics of a good-quality image by virtue of technical settings of user-controlled variables as well as proper labeling

finding is identified, the machine can be placed in the freeze mode and then the sequential images captured in the cine memory can be scanned backwards until the most appropriate image for measurement and documentation is identified. The cine function is invaluable in clinical office urology because it significantly decreases the time necessary to perform and document a complete examination.

Conclusion

Ultrasound equipment has preset applications for imaging of the prostate, kidneys, bladder, and testes. These presets allow scanning of most patients without the need to make individual adjustments. However, there are many clinical circumstances where the ability to make individual adjustments is invaluable to making a clinical diagnosis or clarifying an artifact. Most equipment allows users to store a large number of additional scanning protocols to account for commonly encountered challenges such as obese patients or pediatric patients.

Summary

A good-quality image is recognized by certain generally agreed upon characteristics (Fig. 4.20).

Ultrasound is ultimately an exercise in image recognition. Clinicians tend to see what they know and are familiar with. Great care must be taken to ensure optimal image quality so that the unexpected and unfamiliar may also be recognized and correctly diagnosed.

Reference

1. Guidance for Industry and FDA Staff Information for Manufacturers Seeking Marketing Clearance of Diagnostic Ultrasound Systems and Transducers. http://www.fda.gov/downloads/MedicalDevices/DeviceRegulationandGuidance/GuidanceDocuments/UCM070911.pdf (2008). Accessed 9 Sept 2008.

Renal Ultrasound

5

Jennifer Simmons and Pat F. Fulgham

Introduction

Technical innovations have resulted in the creation of lower-cost and portable ultrasound machines that have the potential to provide a valuable tool to assist in bedside evaluation. Point-of-service ultrasound is well suited for the expeditious diagnosis of renal disorders while facilitating subsequent therapeutic interventions such as percutaneous procedures and ablations. The combination of an accurate diagnostic tool with the clinical acumen of a well-trained urologist is likely to improve health-care delivery while reducing the cost of providing that care.

Renal ultrasound has been found to be a highly sensitive and specific test for hydronephrosis in both the adult and pediatric population, augmenting the clinical toolbox of the on-call urologist [1]. Additionally, renal ultrasound is valuable in the initial evaluation of hematuria and urolithiasis [2]. Asynchronous patient care (i.e., an initial history and physical examination separated in time and space from the ultrasound examination) requires that the physician have access to and remembers to review the imaging study at a second visit. Integration of ultrasound, performed by the urologist, into the initial clinical evaluation improves the efficiency of patient care while avoiding the pitfalls of segregating the diagnostic process into metachronous episodes.

This chapter details the applications and techniques of renal ultrasound necessary to integrate ultrasound into the daily practice of urology. The reader will be able to explore the technical process of generating an ultrasound image of the renal units in response to a specific clinical question.

Indications

The indications for renal ultrasound include [3]:

- Flank and/or back pain
- Hematuria
- Further evaluation of abnormal findings of the kidney on other imaging studies
- Planning and guidance for intraoperative procedures, i.e., transcutaneous renal biopsies, cyst aspiration, and ablation of renal masses
- Evaluation of postoperative renal transplant patients
- Intraoperative renal parenchymal and vascular imaging for ablation or resection of renal masses
- Abdominal trauma
- Follow-up of known or suspected abnormalities in the kidney
- Evaluation of asymptomatic microscopic hematuria in patients who are not candidates for IVP, CT, or MRI [4]
- Evaluation for and monitoring of urolithiasis [5]

J. Simmons, MD
Division of Urology, Geisinger Medical Center, Danville, PA, USA

P.F. Fulgham, MD, FACS (✉)
Department of Urology, Texas Health Presbyterian Dallas, 8210 Walnut Hill Lane Suite 014, Dallas, TX 75231, USA
e-mail: pfulgham@airmail.net; patfulgham@yahoo.com

P.F. Fulgham and B.R. Gilbert (eds.), *Practical Urological Ultrasound*, Current Clinical Urology,
DOI 10.1007/978-1-59745-351-6_5,

Equipment

Adequately performing and documenting a renal ultrasound requires familiarity with basic features of the ultrasound machine. For renal imaging in adults, a curved array transducer is used as seen in Fig. 5.1. A smaller-width transducer can offer superior contact with the body surface in very thin patients and may make it easier, than with a wide transducer, to scan between the ribs. Both types work well for most patients. Renal ultrasound scanning is performed at frequencies between 2.5 and 6 MHz. The kidney lies several centimeters below the skin surface so the lower frequencies will give superior penetration. For thin patients a higher frequency should be used. For patients with a large abdominal girth, a lower frequency should be used. With the lower frequencies penetration is improved but results in a decrease in the quality of linear (axial) resolution.

Most commonly, one or two focal zones are used for renal imaging. The focal zone should correspond to the area of interest in the field of view. The focal zone corresponds to the narrowest part of beam and gives the best lateral resolution at the region of interest. Adding focal zones slows down the refresh rate of the image. Other machine features commonly used during renal ultrasound exams are the measurement calipers, cine loop, and Doppler mode.

Patient Preparation

Patient preparation is helpful to facilitate an efficient exam. Fasting decreases intestinal contents and can allow for a more anterior approach to imaging the kidney, away from the thicker flank musculature. In the urology office, however, renal imaging is often used on short notice to investigate an acute problem during the appointment. Thus, it is usually impractical to have the patient fast several hours prior to the exam. For planned exams, such as upper tract imaging for hematuria workup or screening for postoperative hydronephrosis after impacted stone removal, one would ask the patient to fast for 6 h prior to the exam.

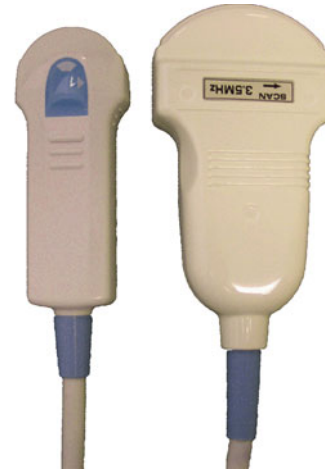

Fig. 5.1 Curved array transducers are used for the performance of renal ultrasound. Seen in this image are two different widths of curved array transducers, small footprint (*left*) and a large footprint (*right*)

The exam room should have the capability to dim the room lights and reduce the glare from natural light. The ultrasound image detail on the screen is dramatically improved by dim ambient light.

Patient positioning will depend on the indication for the exam to be performed. A focused unilateral follow-up exam such as for post-ESWL hematoma or for renal trauma can be done efficiently with the patient in the supine position. A bilateral exam will likely involve the patient's moving from supine to right lateral decubitus positions to allow access to the left kidney. Ultrasound for urolithiasis will involve imaging from the high posterior flank then moving anteriorly and inferiorly all the way to the ureterovesical junction (UVJ) looking for distal stones and ureteral jets.

The ultrasound machine should be positioned so the screen is easily seen by the operator and the keyboard and patient can be reached comfortably. Extreme care should be taken to avoid falls when rolling patients from side to side on standard exam tables. Typical exam tables are narrow and have no side rails. The examiner's attention will be focused on the ultrasound screen, so unsteady patients should be moved onto a stretcher with side rails or guarded on the opposite side by ancillary staff.

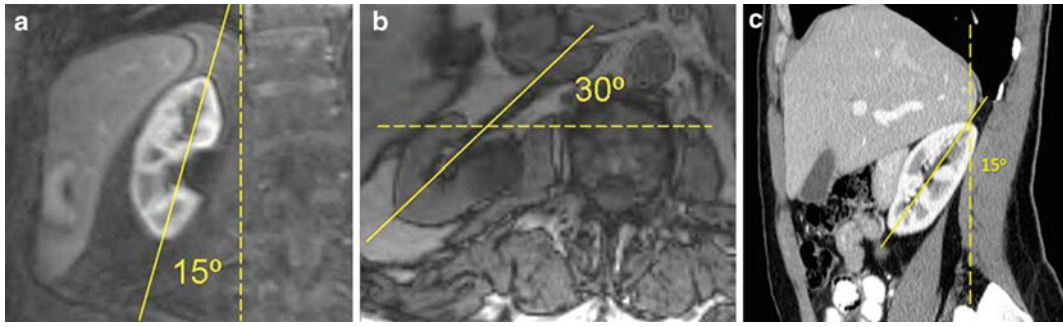

Fig. 5.2 (**a**) Coronal MRI showing that the lower pole is 15° lateral to the vertical plane. (**b**) Transverse MRI at the level of the renal hila showing that the axis of the kidney is 30° posterior to the true coronal plane. (**c**) MRI demonstrating that the lower pole of the kidney is anterior to the upper pole

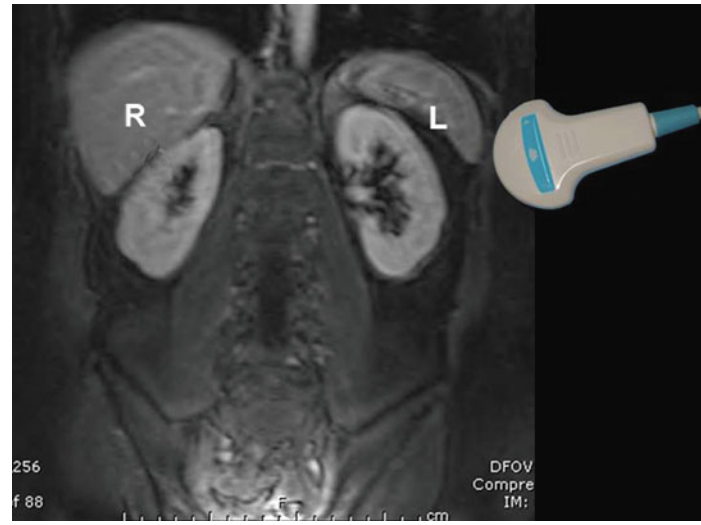

Fig. 5.3 Image of an MRI demonstrating the anatomical position of the kidney in the abdomen and proper position and angle of the ultrasound probe for imaging the left kidney. This probe position would generate a true midsagittal ultrasound image of the left kidney

Anatomic Considerations for Renal Imaging

Consider the orientation of the kidney in the retroperitoneum. The lower pole is 15° lateral to the upper pole in the coronal plane (Fig. 5.2a). In the transverse coronal plane, the hilum of the kidney is about 30° posteriorly rotated off the true coronal plane (Fig. 5.2b). Lifting of the kidney by the psoas muscle causes the lower pole to be more anterior than the upper pole (Fig. 5.2c). For longitudinal views of the kidney, the orientation of the ultrasound probe should match the long axis of the kidney (Fig. 5.3). This also allows for identification of the true midsagittal plane of the kidney.

Imaging the Right Kidney

Technique

Ultrasound of the right kidney is typically performed with the patient in the supine position. The transducer is placed in the mid-clavicular line at the level of the costal margin. Bowel gas in the transverse colon will often be encountered initially. The transducer is swept laterally using the liver as an acoustic window to image the upper pole of the right kidney. Figure 5.4 is an example of a right kidney viewed through a liver window. The homogenous composition of the liver offers excellent transmission of the sound waves with minimal distortion. As the transducer is moved

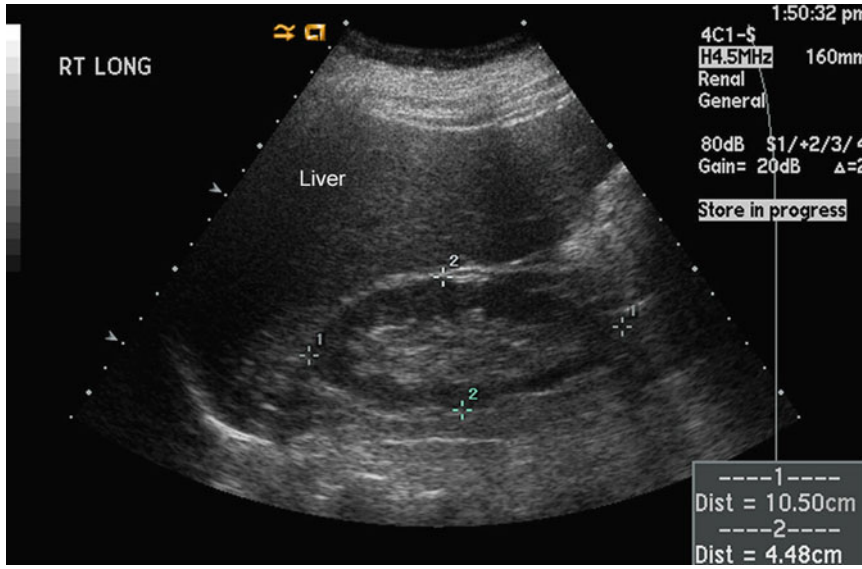

Fig. 5.4 Right kidney viewed using the liver as an acoustic window

more laterally the kidney can be more completely imaged without interference from bowel gas. An attempt should be made to find the true midsagittal plane of the right kidney. This serves as an anatomic landmark from which the remainder of the complete scan can be performed. The midsagittal plane of the kidney is characterized by the longest measureable sagittal axis of the kidney. The renal parenchyma is discontinuous medially at the level of the entry and exit of the renal vessels and the exit of the renal pelvis from the renal sinus.

Once the midsagittal plane is localized, the kidney should be scanned anteriorly and posteriorly until the entirety of the renal parenchyma has been evaluated. The upper pole and mid kidney can usually be viewed through the liver window. The lower pole frequently has to be viewed directly via a more lateral or posterior location. Figure 5.5 is an example of the lower pole of the left kidney viewed directly from the flank rather than through the spleen as an acoustic window. In the midsagittal plane the transducer should be rotated 90° counterclockwise to achieve the mid-transverse plane of the kidney. This is characterized by a horseshoe-shaped renal parenchyma discontinuous on the medial aspect at the level of the renal sinus. It is often possible to see the renal vein sonographically in this view. The renal artery is more difficult to visualize. Once the mid-transverse plane has been identified, the kidney is scanned through the upper pole and through the lower pole. This evaluation can be accomplished by moving the probe cephalad and caudad and by having the patient take a deep inspiration to bring the upper pole of the kidney into view.

Once the kidney has been completely evaluated in both planes, attention is turned to identifying and documenting normal and abnormal findings.

Imaging the Left Kidney

Technique

Ultrasound of the left kidney is typically performed with the patient in the right lateral decubitus position. Having the patient raise the left arm overhead will further open the intercostal spaces to allow for better imaging. The transducer is placed at the mid axillary or posterior axillary line. Bowel contents commonly prevent an anterior approach to viewing the left kidney. The left kidney image is often of less crisp detail due to attenuation and scattering by muscle in the flank and back. The spleen is frequently seen

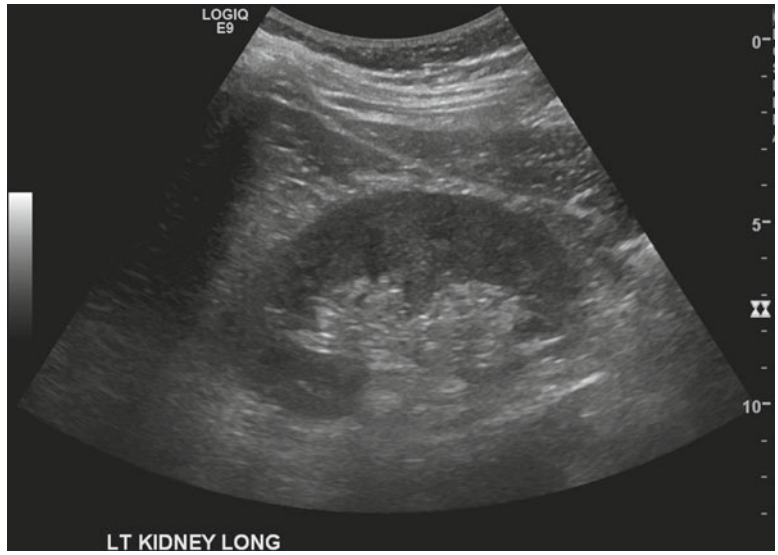

Fig. 5.5 Left kidney viewed directly via lateral flank approach (true midsagittal plane)

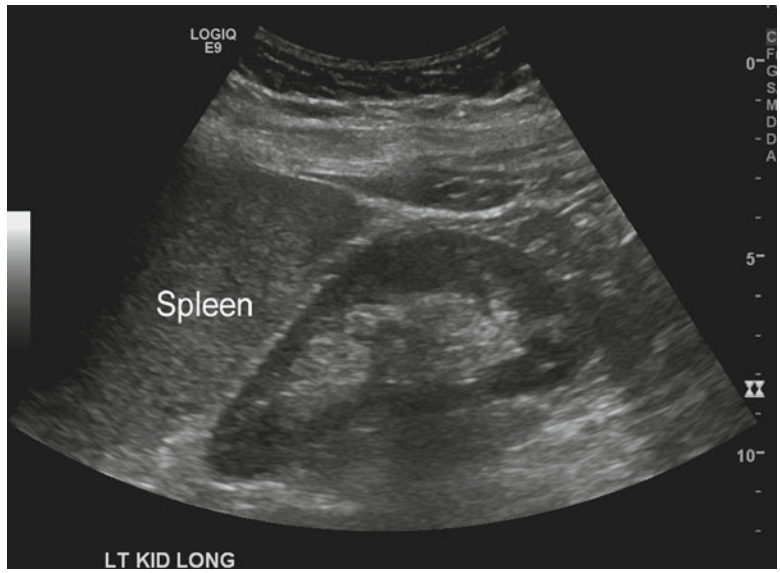

Fig. 5.6 The spleen is seen on this image cephalad to the left kidney

anterior and superior to the left kidney, but is not usually well positioned to use as an acoustic window (Fig. 5.6). The true midsagittal view of the left kidney is then located. This will be the plane of the longest sagittal length of the kidney (midsagittal). The renal capsule will appear discontinuous at the mid kidney medially at the site of the renal hilum. In the coronal view, cortical tissue is seen as a continuous ring around the hyperechoic pelvic sinus fat except at the renal hilum. Once the anterior and posterior surfaces have been fully imaged in the sagittal plane, one rotates the probe 90° counterclockwise to image in the axial plane. The left kidney assumes a horseshoe shape with the discontinuity of the parenchyma oriented medially at the location of the renal sinus. The upper and lower poles of the left kidney are imaged completely by moving the probe

cephalad and caudad and with targeted breathing by the patient as necessary. A deep inspiration and expiration will move the kidney several centimeters. Once the kidney has been completely evaluated in both planes, attention is turned to identifying and documenting normal and abnormal findings.

The goal of the ultrasound exam is to view the entirety of the kidney, including every capsular surface. When imaging in the transverse plane, the entire length of the kidney must be viewed. Through the use of directed patient breathing, scan from just above the superior pole of the kidney all the way inferior through the entire kidney to just below the lower pole. The cross-sectional diameter of the renal capsule becomes smaller as one reaches each pole, then disappears as the imaging beam goes beyond the edge of kidney. A good analogy is the way one would view the axial imaging of a CT scan. One would scroll through the kidney from just above the kidney to just below the kidney to avoid missing any exophytic lesions at the poles. When imaging in the longitudinal plane, one would fan the probe anteriorly and posteriorly to fully view the kidney from the anterior surface, through midline and on through the posterior surface. Seen in Fig. 5.7 is an example of the type of small exophytic peripheral lesion which could be missed with incomplete imaging of the full anterior and lateral surface of the left kidney.

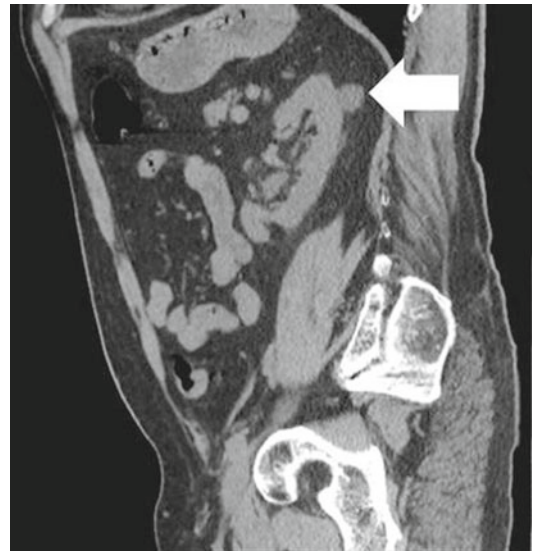

Fig. 5.7 This MRI demonstrates a small exophytic renal cyst (*arrow*) that could easily be missed on ultrasound if the full anterior and lateral surface of the left kidney is not evaluated

Normal Findings

Renal contours should be smooth and of an oval reniform shape. Any deviation from a smooth uniform contour should be noted and a representative image saved. All surfaces of the kidney should be scanned from top to bottom and from anterior to posterior.

The kidney measurements should be recorded. The transverse view of the mid kidney should be measured and the image saved. An image of the midline longitudinal length should be measured and the image saved. Care should be taken to ensure that the true midline longitudinal view of the kidney is obtained for accurate measurement of length. If the transducer is aligned in the true midsagittal plane, the longitudinal kidney image should be displayed in a horizontal plain on the screen. Thus positioned, there is less distortion related to the angle of insonation. Figure 5.8 demonstrates that there may be a substantial difference in the measurement of the long axis of the kidney if the kidney is imaged in a parasagittal plane vs. a true midsagittal plane. The true midsagittal plane is characterized by a medial discontinuity of the renal parenchyma representing the hiatus through which the renal vessels and collecting system enter and exit. Normal adult kidneys measure 10–12 cm longitudinally, 5–7 cm transversely, and 3 cm in the anteroposterior dimension [6, 7]. A table of normal pediatric age-adjusted renal sizes should be readily accessible for reference if one does pediatric imaging [8]. The right and left kidneys should be of similar size. Any size discrepancy should be noted in the report. A discrepancy in the long axis of over 1.5 cm is considered abnormal [9].

Renal cortical thickness should be relatively uniform throughout the kidney. Any bulges or indentations in the cortex should be noted on the report and captured as an image. Parenchymal

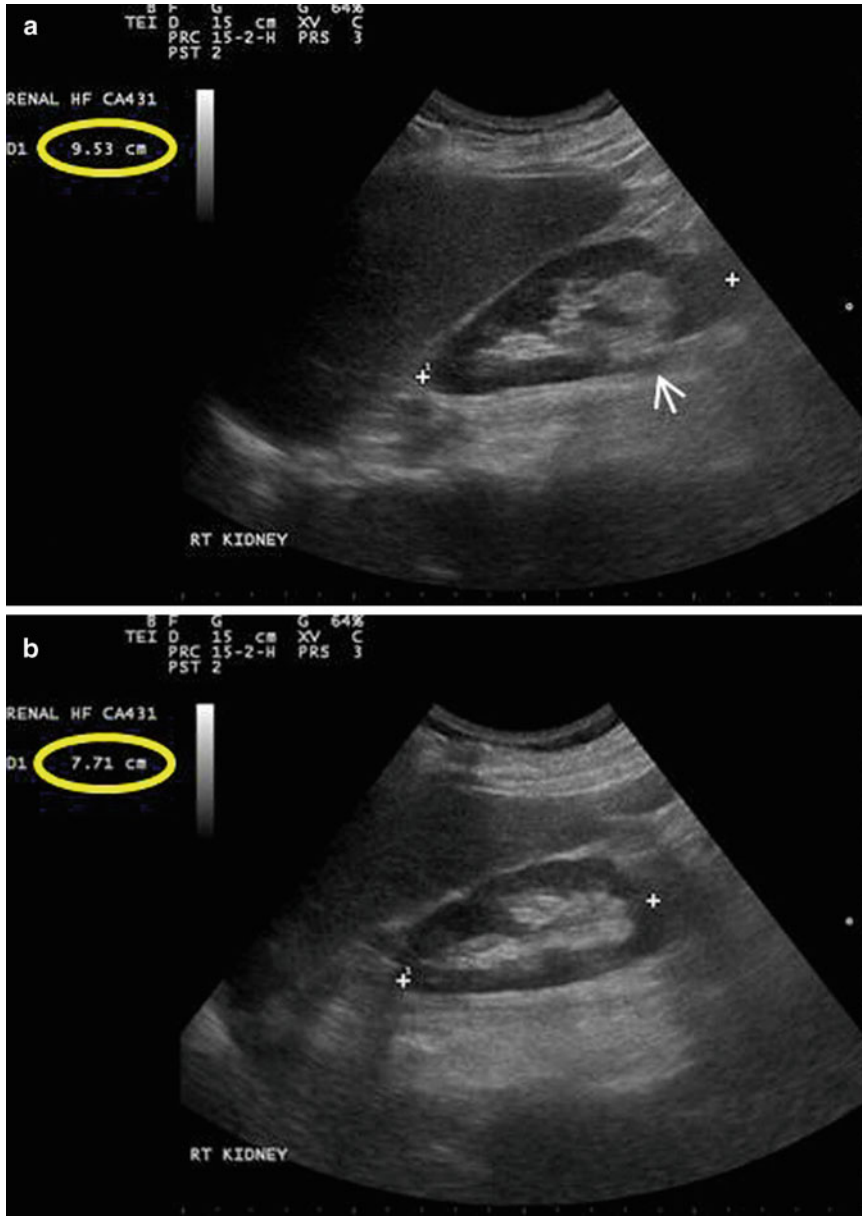

Fig. 5.8 An accurate measurement of renal length depends upon obtaining a truly midline renal image in the sagittal plane. In ultrasound image (**a**) the right kidney is in the true midline as noted by the medial discontinuity of the renal parenchyma. This represents the hiatus through which the renal vessels and collecting system enter and exit (*arrow*). The kidney on this view measures 9.53 cm. Ultrasound image (**b**) demonstrates the measurement of the same right kidney when it is not in the true midline. The kidney measures 7.71 cm

and cortical thickness should be noted. The cortical thickness is measured from the renal capsule to the base of the triangular medullary pyramids. The parenchymal thickness is measured from the renal capsule to the edge of the renal sinus. In adults, the medullary pyramids are often indistinct on ultrasound imaging, and thus measuring an accurate cortical thickness can be difficult [10]. Parenchymal thickness is often easier to measure in general. A renal parenchymal thickness under

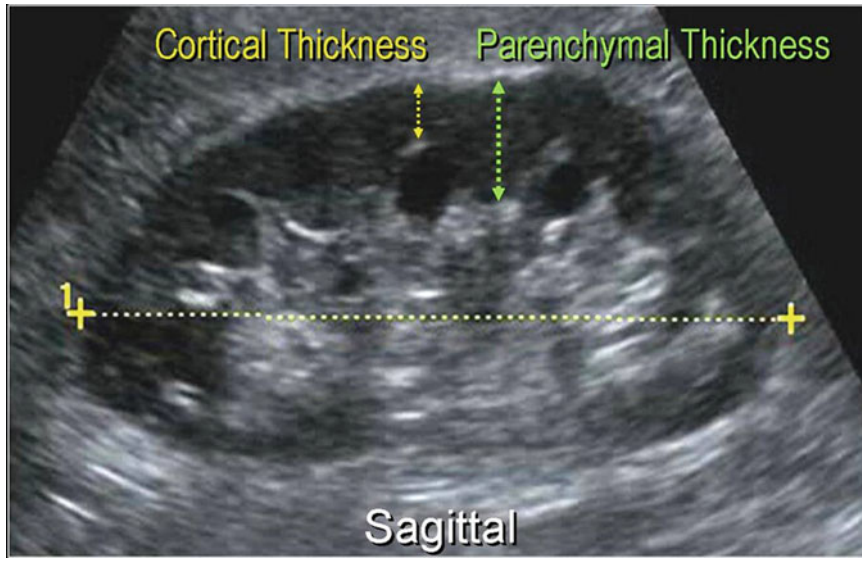

Fig. 5.9 Image demonstrating the difference between the measurement of the cortical thickness and parenchymal thickness

1 cm is considered to be abnormal [10]. Figure 5.9 demonstrates cortical vs. parenchymal thickness measurements.

The echotexture of the kidney should be noted. The normal adult renal cortex should appear hypoechoic or iso-echoic relative to the normal liver or normal spleen. The normal renal cortex should appear homogenous in echogenicity. The medullary pyramids should be hypoechoic compared to the renal cortex. This is much more pronounced in children than adults.

The renal sinus is hyperechoic compared to the renal cortex in normal kidneys. The renal sinus is highly echogenic due to its many different reflectors including blood vessels, sinus fat, and the collecting system.

Adjacent Structures

Renal ultrasound by urologists is usually performed for a specific clinical indication and is focused on the kidneys. Adjacent organs will be in the field of view and any remarkable findings of those organs should be noted.

The adrenal gland in adults is not normally visualized on ultrasound. A prominent adrenal gland seen on ultrasound should be considered potentially abnormal and further imaging with CT or MRI as appropriate should be considered.

It is not the intention of a focused urological examination to provide complete imaging of the liver, gallbladder, spleen, or aorta, but any abnormalities noted on these organs during the renal exam should be documented and pursued with further testing as appropriate. Often the urologist has an ongoing relationship with the patient. The urologist can both draw upon other relevant preexisting imaging and communicate the findings to the patient. As the clinical situation indicates, further follow-up imaging and/or referrals to appropriate specialists can be ordered.

Ultrasound Report

Report generation is a critical component of all renal ultrasound exams. The ultrasound report should be clearly identified as such in the medical record and should be signed by the interpreting physician. The report has four components: indications, equipment, findings, and impression.

Indications

The clinical history and reason for performing the study should be documented in the indication section.

Equipment

Each ultrasound report should identify the make and model of the machine and the probe used for the exam.

Findings

The *Findings* section should include a succinct description of the normal findings as well as any notable abnormalities. It should include measurements. Formal ultrasound terminology should be used. The ultrasound findings should be described in this section with diagnoses being reserved for the impression section of the report. For example, one should report "a 9 mm brightly hyperechoic focus in the lower pole of the right kidney with strong posterior acoustic shadowing" in the *Findings* and report "consistent with the appearance of a stone" in the *Impression*.

Impression

The *Impression* portion of the report should include an interpretation of the sonographic findings based on the clinical history and physical findings. When the urologist is the performing and interpreting physician, the impression may also include a *plan* for subsequent imaging or intervention.

Image Documentation

Representative images of the exam should be saved in the permanent patient record. These can be digital or hard copy images. Minimum image documentation will vary based on the clinical indication for the study but for a full evaluation of both kidneys it should include:

1. Right kidney:
   (a) Longitudinal view including length measurement.
   (b) Transverse view of the upper pole.
   (c) Transverse view of the renal pelvis.
   (d) Transverse view of the lower pole.
   (e) View showing the liver and right kidney on the same image, if possible.
2. Left kidney:
   (a) Longitudinal view including length measurement.
   (b) Transverse view of the upper pole.
   (c) Transverse view of the renal pelvis.
   (d) Transverse view of the lower pole.
   (e) View showing the spleen and left kidney on the same image, if possible.
3. Appropriate views of abnormalities, with measurements if indicated.

Doppler

Color and power Doppler are useful tools in renal imaging. The ability to confirm normal blood flow in the kidney can be useful in the follow-up of trauma, partial nephrectomy, and obstruction. The ability to characterize hypoechogenic structures in the kidney is useful. Renal hilar vessels can mimic the hypoechoic appearance of a distended renal pelvis. The use of the Doppler mode can quickly distinguish between vessels and hydronephrosis (Fig. 5.10). The use of Doppler to demonstrate renal artery stenosis is generally beyond the scope of office urologic practice.

Resistive Index

Resistive indices are calculated by quantifying the velocity of blood flow from the Doppler waveform of intrarenal arteries. The arcuate arteries running along the junction of the cortex and medulla or the interlobar arteries running between the medullary pyramids are targeted. Color or power Doppler can be used to identify a suitable vessel. The Doppler angle indicator is aligned with the long axis of the blood vessel being interrogated and the gate should be set at

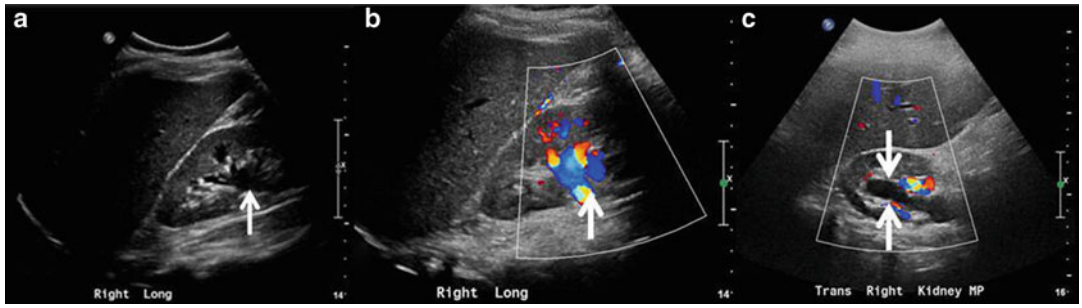

Fig. 5.10 The anechoic area (*arrow*) seen centrally in image (**a**) which has an appearance consistent with hydronephrosis is found to represent hilar vessels by color Doppler in image (**b**). In a different kidney, the central anechoic area (*arrows*) in the transverse image (**c**) remains anechoic (*arrow*) during application of Doppler indicating a dilated collecting system

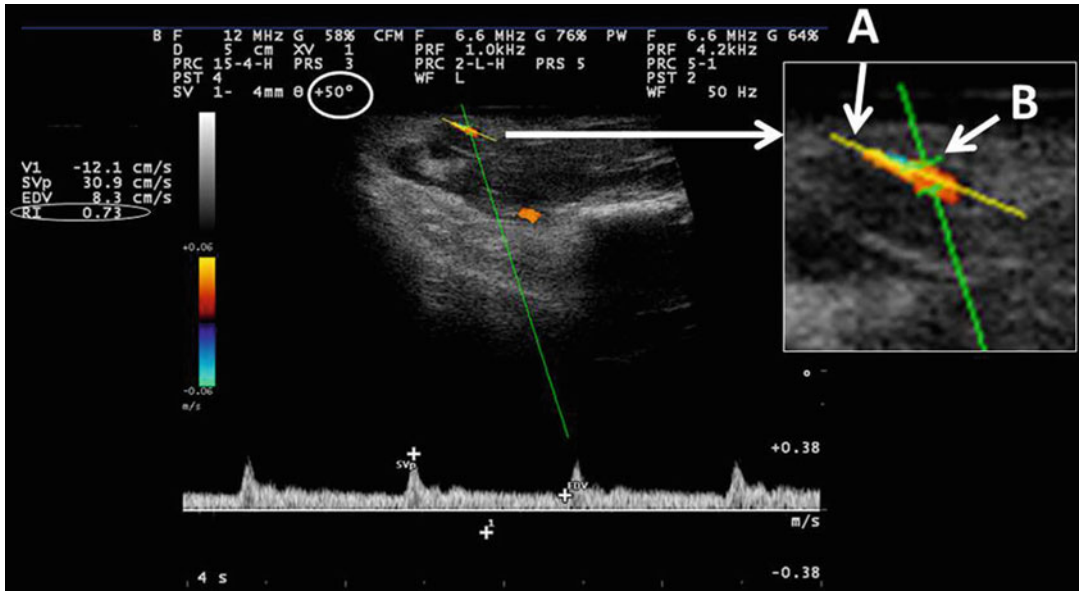

Fig. 5.11 The accurate calculation of the resistive index depends on (**a**) aligning the angle indicator (*yellow line*) with the long axis of the vessel being imaged and (**b**) ensuring that the gate (two parallel *green lines*) is set to about 3/4 of the vessel width. The goal is to achieve an angle of insonation (θ) of ≤60°. In this image the angle is 50° (*circle*). The resistive index is calculated as 0.73

no greater than 75% of the inner diameter of the vessel. The angle of insonation (θ) should always be ≤60°. The resultant waveform is analyzed (Fig. 5.11). The peak diastolic and end systolic velocities are marked. The formula to calculate RI is peak systolic velocity (PSV) minus the end-diastolic velocity (EDV) divided by the PSV [(PSV-EDV)/PSV]. A value of <0.7 is generally accepted as normal. Higher RIs can be seen in children and the elderly. Comparing side-to-side RIs, called resistive ratio, may be useful. A resistive ratio is the ratio between the RI of the affected kidney and the contralateral unaffected kidney. However, a difference in the RI of ≥0.1 on the symptomatic side compared to the asymptomatic side may be more important than a resistive ratio clinically [11–13]. Studies have shown acceptable sensitivity and specificity for RI in evaluating obstruction [14]. Ureteral obstruction causes elevated arterial resistance even preceding the development of significant hydronephrosis. Nonobstructive

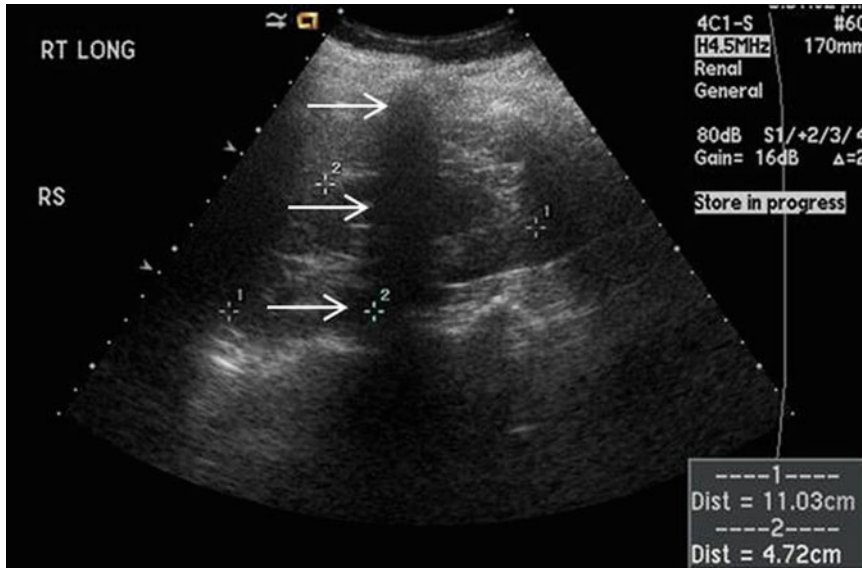

Fig. 5.12 Rib causing posterior acoustic shadowing (*arrows*) across this midsagittal image of the kidney

causes of renal pelvis dilation tend to demonstrate normal RIs. For example, pregnant women were shown to have normal RIs despite the development of hydronephrosis of pregnancy [15]. Studies show promise for evaluating renal colic in pregnancy when ionizing radiation is to be avoided [16, 17]. But the inability to distinguish acute vs. chronic obstruction limits the clinical utility of resistive indices in this setting.

The RI seems to rise reliably only in complete obstruction. Studies which included patients with partial obstruction showed much less ability to discriminate anatomic obstruction from functional ureteral dilation [18]. The resistive index is not reliable as an isolated finding to prove or disprove a clinically significant obstruction. Rather, it can be another useful finding to support or refute a working diagnosis during an ongoing clinical evaluation.

Artifacts

Imaging the retroperitoneum with ultrasound is a challenging task due to anatomic hurdles to sound wave transmission. It is necessary to recognize and account for several common ultrasound artifacts. Ribs may cause posterior acoustic shadowing. Positioning the transducer between the ribs may be necessary to obtain a complete view of the kidney. Probe manipulation techniques such as fanning (see Chap. 2) may be helpful for directing the beam between the ribs. A small-width curved array transducer is often helpful for imaging between the ribs. Positioning the patient in the lateral decubitus position with their ipsilateral arm extended above the head opens the intercostal spaces adequately in most patients. If additional extension is needed for particularly narrow intercostal spaces, a rolled towel or pillow under the contralateral side may facilitate further extension. Figure 5.12 demonstrates a persistent rib shadow. If a more favorable window cannot be found, then the examiner will have to move the kidney above and below the shadow with coached breathing to accomplish complete imaging of the kidney.

Stones 5 mm or larger will reliably be seen on ultrasound as a hyperechoic focus and will usually produce a posterior acoustic shadow. Small or narrow stones may fail to produce a strong acoustic shadow. Some calculi may display *twinkle artifact* during interrogation with color Doppler. Twinkle artifact is a mixed color flow signal around and behind a bright specular reflector. Twinkle artifact can be very useful when imaging a hyperechoic focus. Blood vessels near the collecting system such

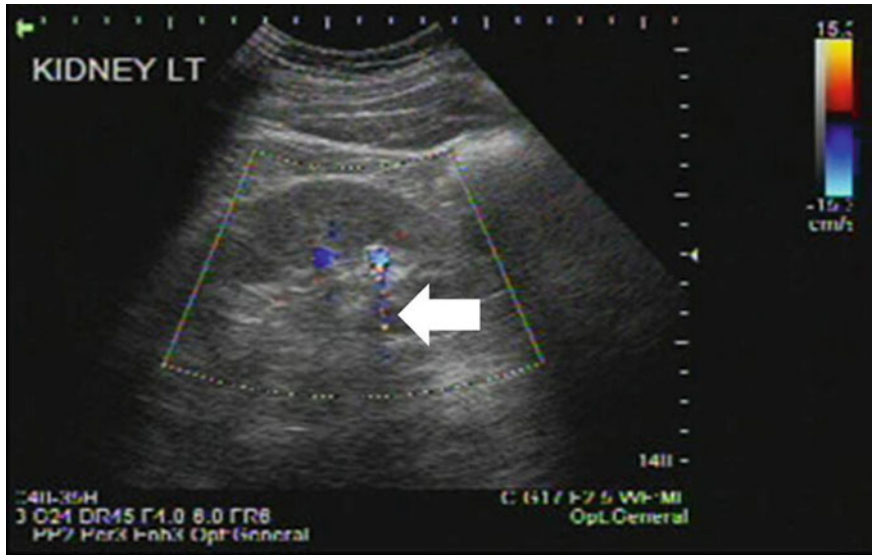

Fig. 5.13 Twinkle artifact (*arrow*) is the result of the interaction of sound waves with a highly echogenic object or an interface of significantly different impedance

as arcuate arteries often appear hyperechoic and can be very difficult to differentiate from small stones. Application of color Doppler will often produce a multicolored trail posterior to a stone (Fig. 5.13).

Stones appear differently on ultrasound compared to CT scan. Larger stones will appear as an intensely hyperechoic leading edge rim with complete shadowing posterior on ultrasound. Therefore, it can be difficult to accurately determine the three-dimensional shape and size of a stone (Fig. 5.14).

Reverberation artifact is the indistinct hazy shadow created by bowel gas. The colon lies anterior to each kidney and so this finding is often encountered anterior or medial to the kidney. Figure 5.15a, b demonstrate the reverberation artifacts typical of bowel gas. If shadowing from bowel gas is interfering with visualization of the kidney, the probe may be moved laterally and even posteriorly to image around it. Alternatively, the patient may be turned to the decubitus position.

Edging artifact is often strikingly demonstrated at the poles of the kidney. This artifact can also be seen off the edges of renal cysts (Fig. 5.16). Edging artifact occurs when sound waves strike a rounded surface at an angle which prevents reflection back to the probe.

Side lobe artifact, also called slice thickness artifact, can be seen as fine, hyperechoic echoes within a renal cyst. To differentiate this artifact from a complex cyst with tissue on the edge of the cyst, one can change the angle of insonation. If the finding is due to an anatomic structure, the finding on that surface of the cyst wall will persist regardless of the angle of insonation. The side lobe artifact may be minimized by adjusting the time gain compensation curve (Fig. 5.17).

Renal Findings

Renal scanning requires a good foundation of knowledge of both normal and abnormal findings. The kidney has a few normal variations which might be discovered on renal sonography. Some well-known normal variants are reviewed here. Pathologic findings in the kidney are quite familiar to urologists and may need to be further studied with additional imaging modalities.

Parapelvic Cysts

Parapelvic cysts are anechoic structures of varying size adjacent to or within the renal sinus. They are easily mistaken for hydronephrosis. The cysts sometimes penetrate deeply into the

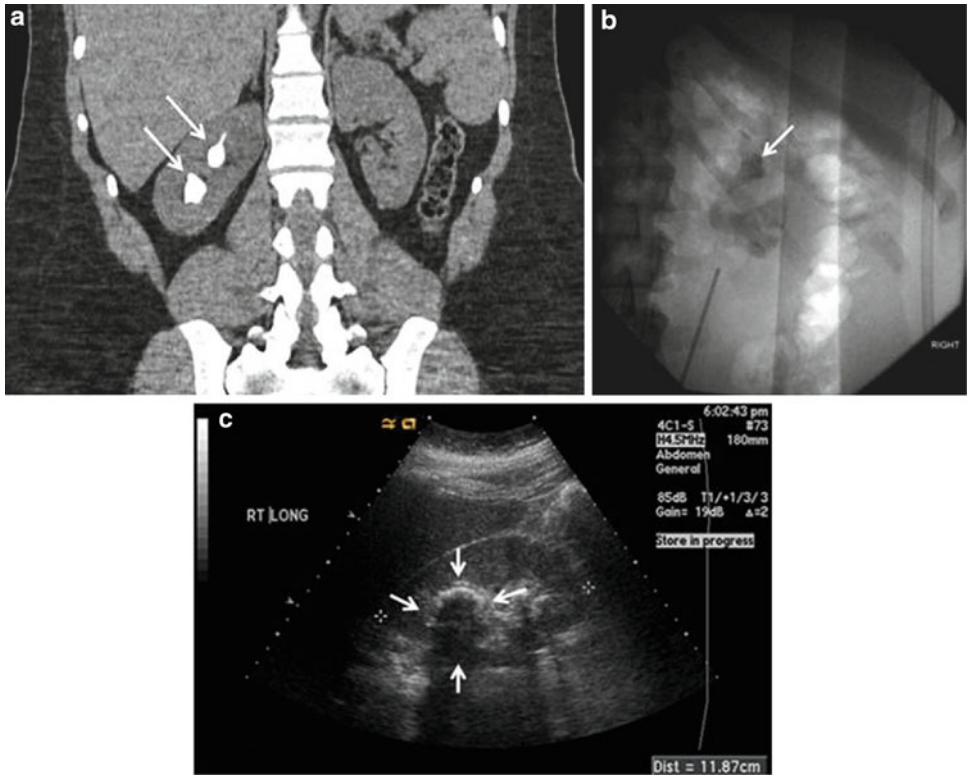

Fig. 5.14 (**a**) CT demonstrating two large caliceal stones in the right kidney (*arrows*). (**b**) Same stones on a plain radiograph. The stone is seen to be a partial staghorn calculus (*arrow*). (**c**) Ultrasound of the stone demonstrating bright leading edge (*top three arrows*) with posterior acoustic shadowing (*bottom arrow*) making it difficult to determine the three-dimensional structure of the stone

renal sinus mimicking dilated calyces (Fig. 5.18). One helpful difference is the location of the cyst in relation to the medullary pyramid. In hydronephrosis the long axis of the hypoechoic structure tends to line up pointing towards the renal papilla and pyramid (Fig. 5.19). Parapelvic cysts tend to have their long axis pointing in between pyramids. A CT scan or retrograde pyelogram may be necessary to differentiate parapelvic cysts from hydronephrosis.

An extrarenal pelvis can also be confused for hydronephrosis. Careful examination should demonstrate lack of dilation of the infundibuli and calyces. Ancillary imaging is often necessary to confirm the diagnosis.

A dromedary hump can be seen on the mid portion of the lateral surface of a small percent of left kidneys. This altered shape is believed to be the result of pressure from the spleen above this area molding the kidney during development, making the mid portion below the spleen bulge out. It is very rarely seen on the right mid kidney and in that case believed to be molding from the adjacent liver. This normal variant involves a bulging of the mid left lateral kidney contour; however, uniformity of the parenchymal thickness should be preserved (Fig. 5.20). The echotexture of the cortex of the bulge should also be unchanged from adjacent tissue. Any bulge in this location which distorts the parenchymal thickness or is varied in echogenicity compared to adjacent tissue should be considered pathologic.

Hypertrophied columns of Bertin are extensions of renal cortical tissue protruding deeply into the renal sinus. These columns are always located in between medullary pyramids and have the same echotexture as adjacent renal cortex (Fig. 5.21).

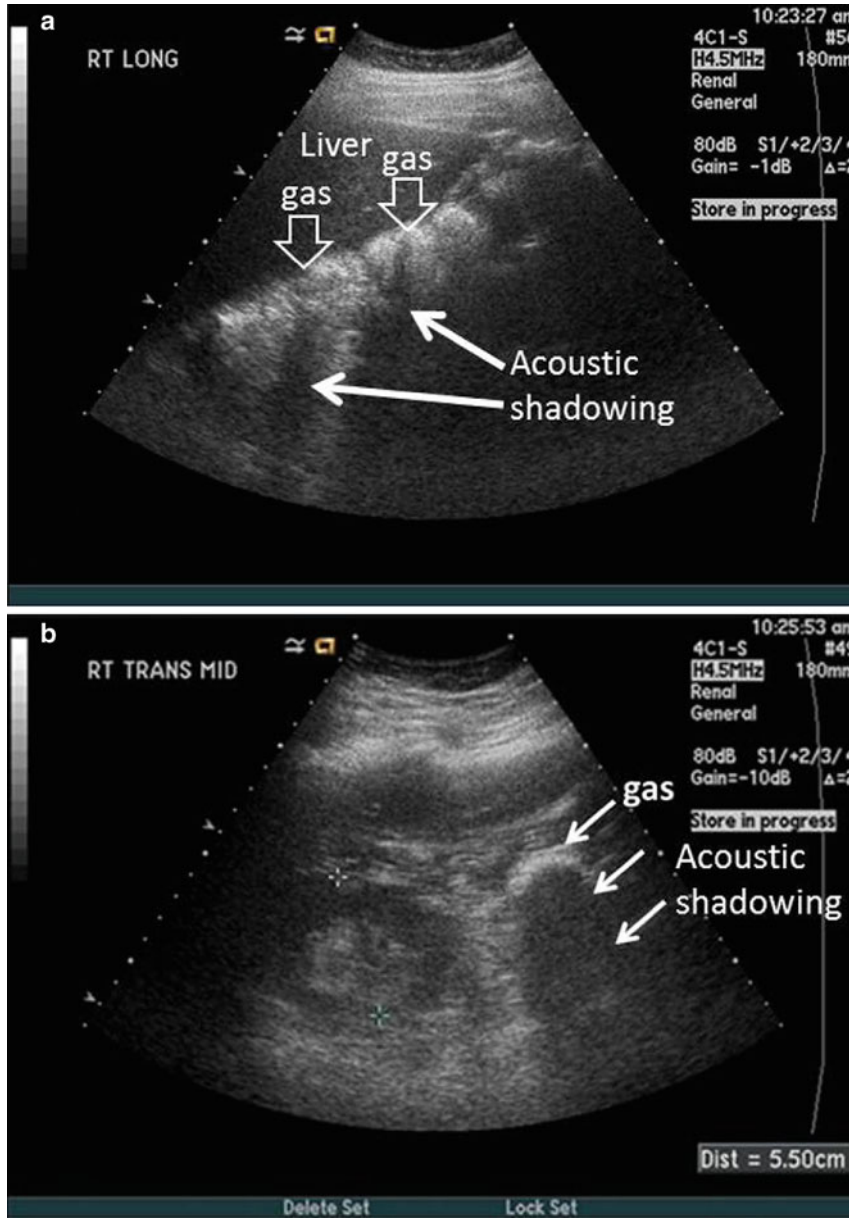

Fig. 5.15 (**a**) The characteristic shadow of bowel gas in the transverse colon shows a hyperechogenic focus corresponding to air bubbles in the bowel contents (*open arrows*) and a tracking black shadow of mixed echogenicity (*closed arrows*). (**b**) Bowel gas (*top arrow*) with dark posterior acoustic shadowing (*bottom two arrows*)

Junctional defects are areas of discontinuity in the parenchymal rim found most commonly in the anterior superior portion of the right kidney. They can rarely be seen on the posterior-inferior portion of the right kidney. The defect has a hyperechoic appearance, indents the renal surface slightly, and runs from edge of renal capsule to the renal sinus. It is often triangular in shape (Fig. 5.22). It is believed to be the result of an incomplete fusion of the upper and lower pole parenchymal masses during embryologic development.

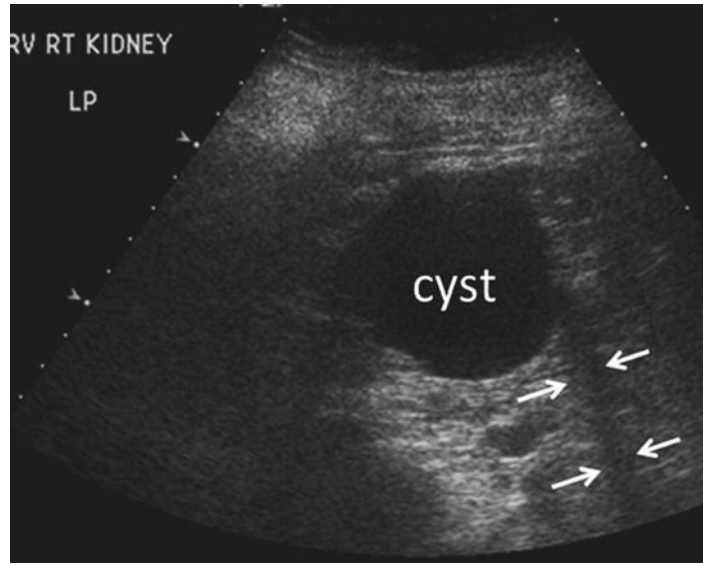

Fig. 5.16 Edging artifact (*arrows*) seen on the trailing edge of a renal cyst

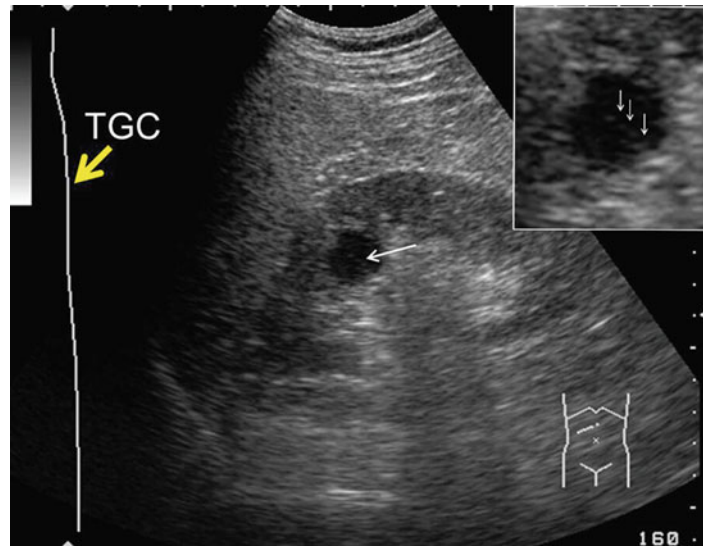

Fig. 5.17 Echoes within this renal cyst represent the side lobe artifact (*white arrows*). The time gain compensation curve (TGC) could be adjusted to minimize this artifact

It can be confused with a cortical scar. The hyperechoic junctional defect should communicate with the renal sinus, whereas cortical scars tend to occur over medullary pyramids and do not reach the sinus.

Persistent fetal lobulation (Fig. 5.23) appears as bulges in the capsular surface over the medullary pyramids and depressions of the surface in between the pyramids. The cortex is otherwise normal in thickness and uniform in echogenicity. This is a developmental variant of normal.

Renal Cysts

Renal cysts are extremely reliably imaged with ultrasound. A simple cyst is required to have three findings: (1) cyst contents are anechoic; (2) cyst walls are thin, smooth, and well defined; and (3) there is posterior acoustic enhancement beyond the cyst. The Bosniak classification was developed for describing renal cysts on CT scans but is often extended to describing cysts seen on ultrasound examinations [19, 20]. The Bosniak I renal cyst is a simple cyst as described above (Fig. 5.24).

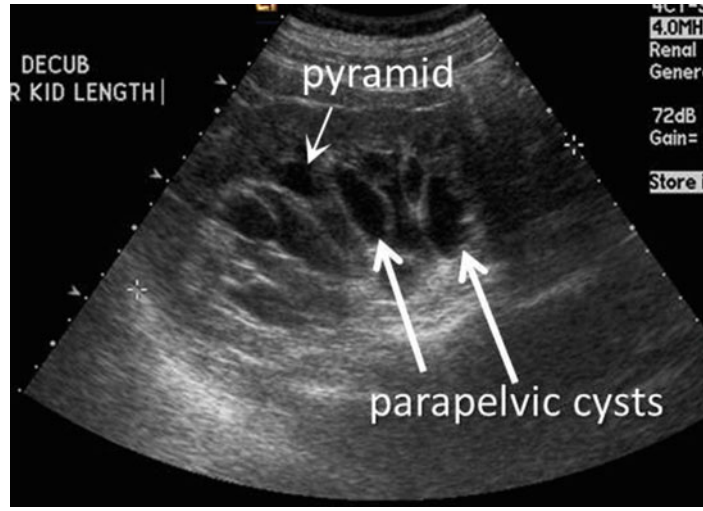

Fig. 5.18 Parapelvic cysts (*bottom two arrows*) with long axes which point between medullary pyramids (*top arrow*)

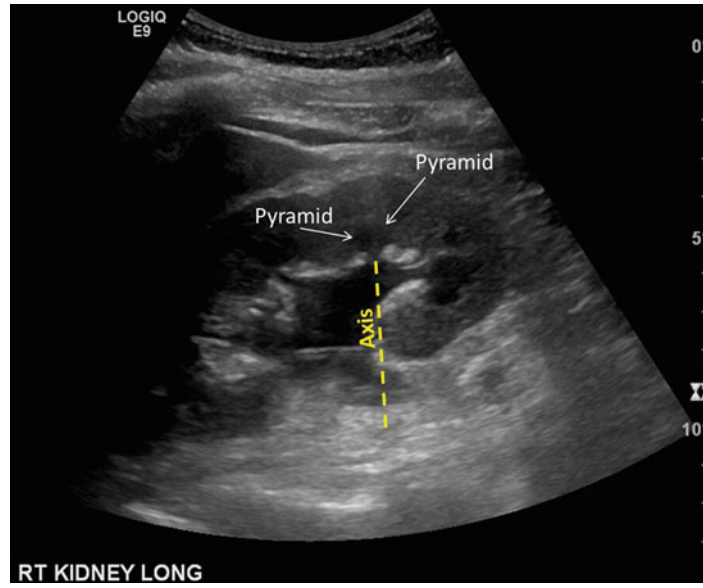

Fig. 5.19 The long axis (*yellow line*) of the hypoechoic pelvis and infundibulum points to a medullary pyramid (*white arrows*)

Bosniak II has small calcifications or thin septations or internal echoes (Fig. 5.25). Bosniak III contains thick calcifications, solid nodules, or thick septations (Fig. 5.26). Bosniak IV is a solid mass lesion with some cystic areas (Fig. 5.27). A renal ultrasound lacks the resolution to identify fine abnormal features which would upstage a cyst from Bosniak I to Bosniak II. Furthermore, ultrasound will not demonstrate enhancement which is a key element of the Bosniak classification system (Table 5.1 Bosniak cysts).

Renal Scars

Parenchymal scarring appears as a sharp depression in the outline of the kidney. Scars are always located over renal pyramids. The cortical thickness

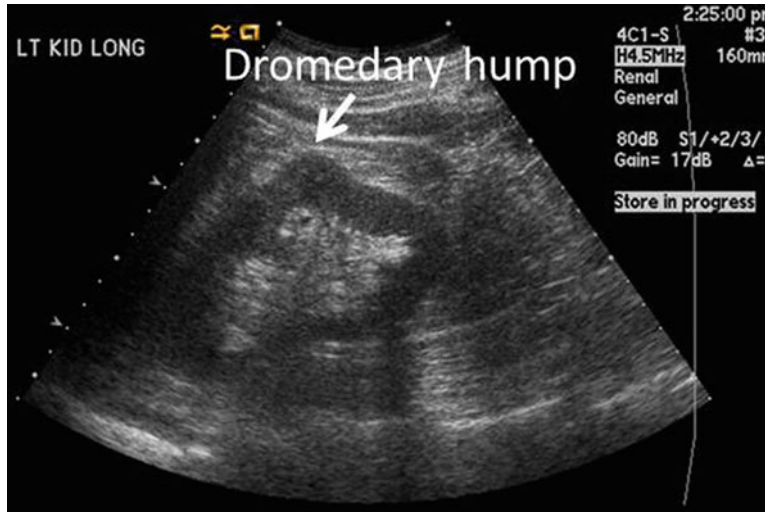

Fig. 5.20 Dromedary hump (*arrow*). The thickness of the renal parenchyma remains constant in dromedary hump

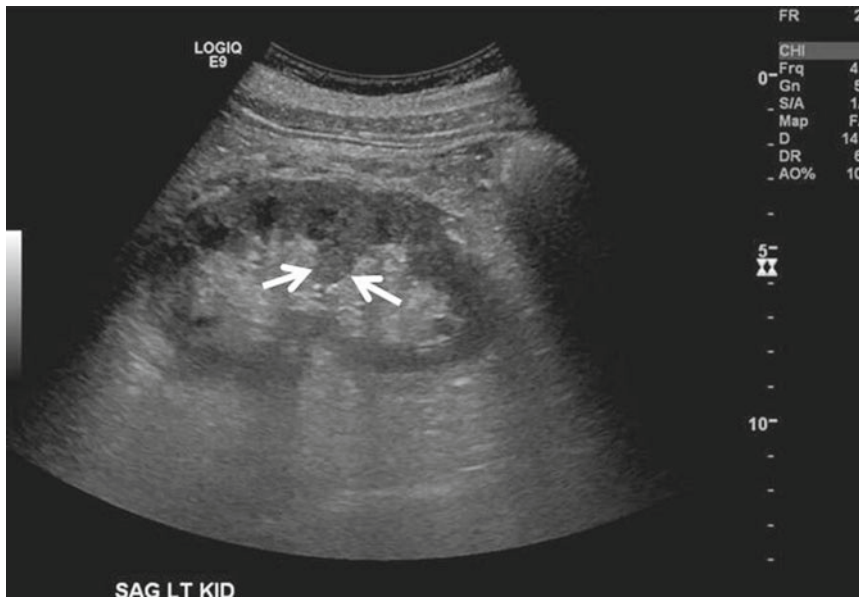

Fig. 5.21 Hypertrophied column of Bertin (*white arrows*). Note the tissue of normal renal parenchymal echogenicity extending into the renal sinus

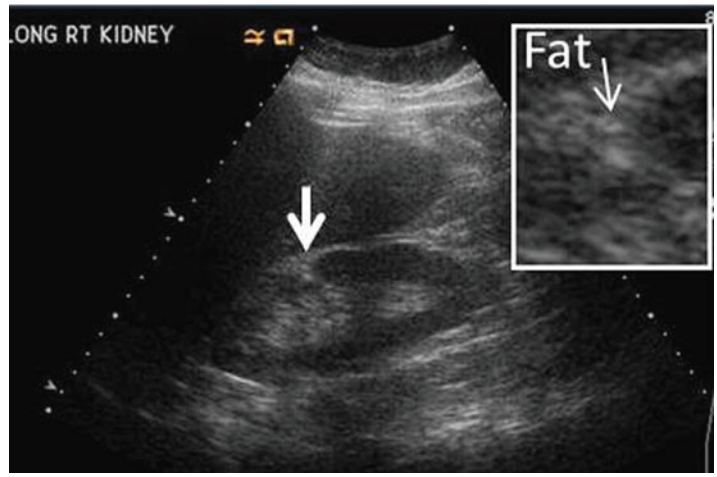

Fig. 5.22 Junctional defect with apparent invagination of perinephric fat (*arrow*)

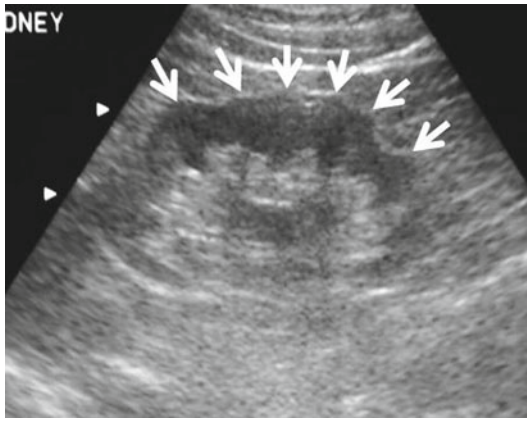

Fig. 5.23 The fetal kidney has 12–15 segments. The shape sometimes persists to adulthood as fetal lobulations (*arrows*)

is dramatically reduced or gone altogether at the scar. Figure 5.28 demonstrates a renal cortical scar.

Medical Renal Disease

Evidence of medical renal disease may be evident on renal ultrasound in several ways. Some medical renal disease causes the renal parenchyma to become hyperechoic. The normal cortex should be hypoechoic or iso-echoic to the liver. The increase in echogenicity is believed to be the result of increased collagen deposition common to most medical renal parenchymal diseases [10]. Some medical renal disease also causes loss of renal mass (Fig. 5.29) [21]. Parenchymal thickness and renal size decrease with age [10, 22, 23] (Table 5.2).

Renal Masses

Renal ultrasound has a role as an adjunct to cross-sectional imaging with CT and MRI for the management of renal masses. Ultrasound is not as sensitive as CT or MRI at initially detecting or characterizing renal masses. However, ultrasound can be very helpful in ongoing surveillance of known masses. The dangers of repeated ionizing radiation from CT scan is beginning to gain recognition [24–26]. When the size of a renal mass is the only variable being monitored, ultrasound is an attractive alternative to ionizing imaging studies for serial observation.

Intraoperative Ablation

Ultrasound is a standard intraoperative tool for guiding ablative renal therapies. Traditional extracorporeal or intracorporeal laparoscopic ultrasound imaging can be used in real time to guide accurate placement of probes for cryotherapy or radiofrequency ablation of renal masses. During partial nephrectomy ultrasound can be used to confirm the

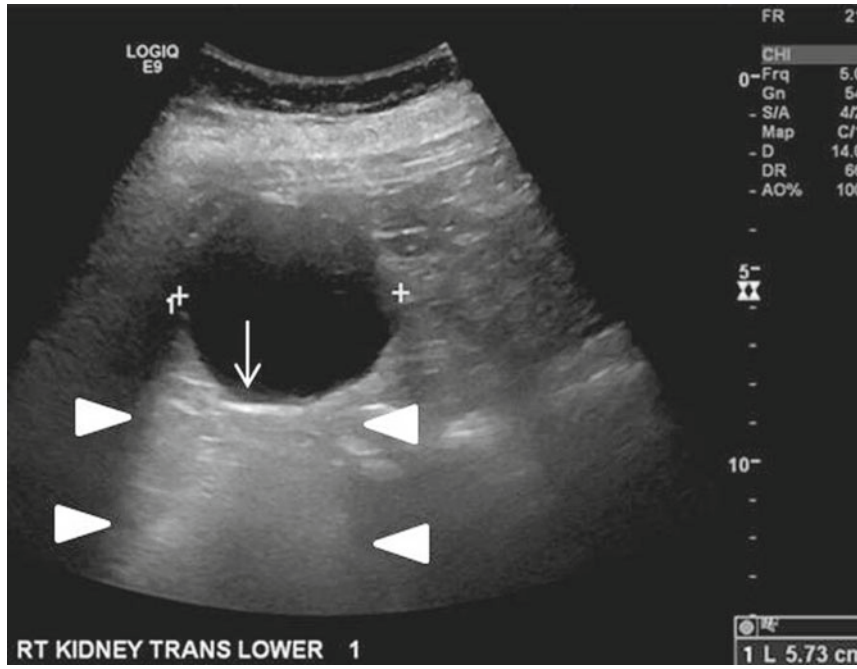

Fig. 5.24 Simple cyst (Bosniak I). Note the anechoic interior, bright back wall (*arrow*), and the increased posterior enhancement (*arrow heads*)

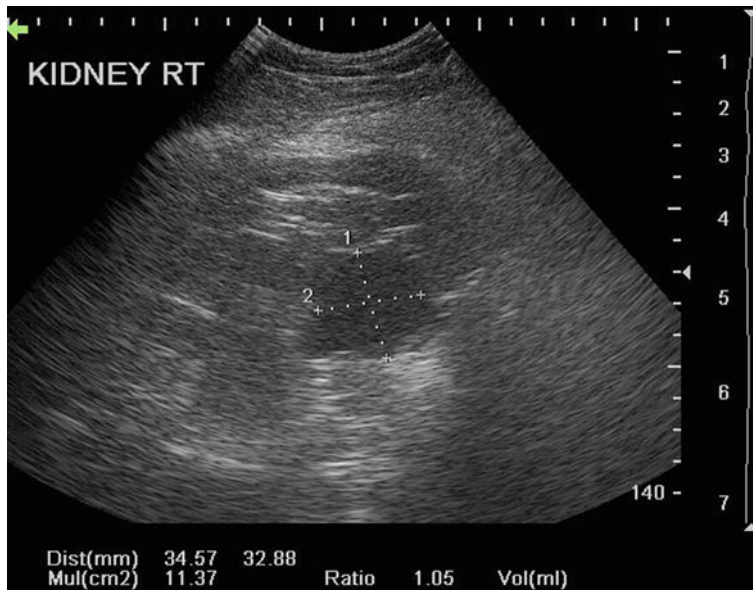

Fig. 5.25 Bosniak II cyst, in this case with irregular shape and thickened posterior wall

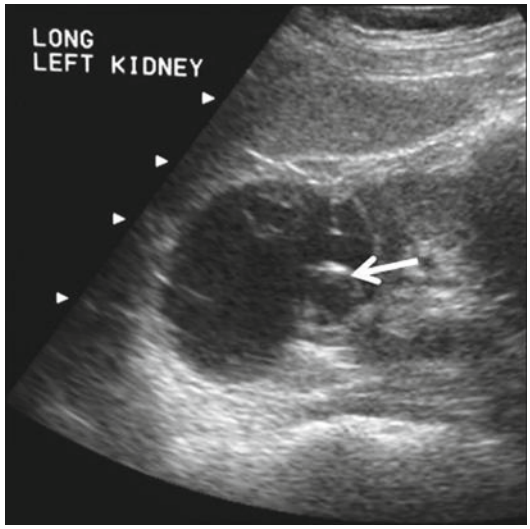

Fig. 5.26 Bosniak III cyst demonstrating a thick mural nodule (*arrow*) within the cyst

absence of blood flow following vascular occlusion and may be useful in selective vascular mapping.

Angiomyolipomas

Renal ultrasound is an excellent imaging study for confirming the diagnosis of fat-containing angiomyolipomas (AML) of the kidney. Figure 5.30 is an example of the typical hyperechoic appearance of a fat-rich AML. Size is the main criteria for surgical intervention. Ultrasound is an excellent imaging modality for following these lesions over time.

Stones

As mentioned previously, ultrasound does not give the complete two-dimensional visualization of stones in the way that plain films or CT scans do. For evaluation of acute renal colic, ultrasound compares well with stone-protocol CT scan in sensitivity and specificity when hydronephrosis is present, but less well without dilation [27–31].

Ultrasound is not as helpful as CT in diagnosing alternate causes of abdominal pain with the exception of gallstones. Furthermore, in most hospitals in the United States, CT is more readily available in the ER setting than is ultrasound. Ultrasound quality is also more variable depending on patient body habitus and sonographer skill level. Thus most cases of acute renal colic in the United States are initially imaged with spiral CT. Regardless of initial imaging study, ultrasound is an excellent clinical tool for subsequent follow-up. Stones are reliably seen in the kidney at sizes of 5 mm and up. Stones in the upper and mid ureter are usually difficult to visualize directly, but if causing hydronephrosis can be assumed to persist if the hydronephrosis remains.

Office ultrasound is quite useful for managing these patients with renal or ureteral calculi in the office setting [32].

Patients frequently do not recover small stones and renal colic can be episodic in nature. Thus it can be difficult to determine if a stone has passed. A targeted office ultrasound can quickly establish persistence or resolution of hydronephrosis and the presence or absence of an ipsilateral ureteral jet. It may require extended observation of the ureteral orifices before it can be concluded that a ureteral jet is absent. Distal stones can often be directly imaged posterior to the bladder or in the intramural portion of the distal ureter. Such information will aid in formulating the appropriate treatment plan. Patients with resolution of the hydronephrosis can be reassured their stone has likely passed. Those with persistent hydronephrosis can be scheduled for intervention or follow-up visits after further observation.

Hydronephrosis

Renal ultrasound has a sensitivity of 98% for the detection of hydronephrosis [33]. In the hands of the urologist, ultrasound is a useful tool for monitoring hydronephrotic disease processes. The surgeon who repaired the UPJ obstruction, performed the ureteral reimplant, or treated the ureteral stricture can use ultrasound with a high degree of confidence that hydronephrosis will be demonstrated if present. Ultrasound has been shown to be an effective tool for surveillance of ureteral strictures after endoscopic stone surgery [34]. The classification of hydronephrosis is summarized in Table 5.3 [35].

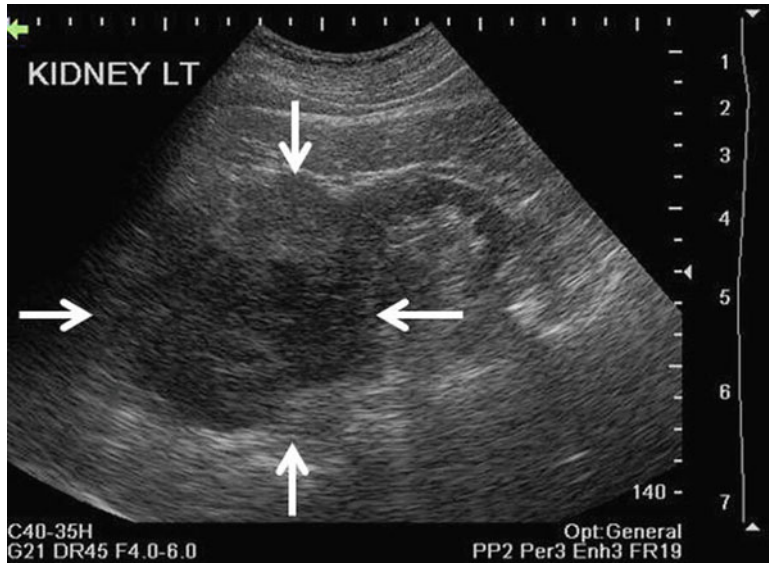

Fig. 5.27 Bosniak IV cyst demonstrating a solid mass (*arrows*) with hypoechogenic cystic components

Table 5.1 The Bosniak renal cyst classification system [20]

Category	Description
I	A benign simple cyst with a hairline thin wall that does not contain septa, calcifications, or solid components. It measures water density and does not enhance
II	A benign cyst that may contain a few hairline thin septa in which "perceived"[a] enhancement may be present. Fine calcification or a short segment of slightly thickened calcification may be present in the wall or septa. Uniformly high-attenuation lesions <3 cm (the so-called high-density cysts) that are well marginated and do not enhance are included in this group. Cysts in this category do not require further evaluation
IIF	(F for follow-up) Cysts that may contain multiple hairline thin septa or minimal smooth thickening of their wall or septa. Perceived enhancement of their septa or wall may be present. Their wall or septa may contain calcification that may be thick and nodular, but no measurable contrast enhancement is present. These lesions are generally well marginated. Totally intrarenal nonenhancing high-attenuation renal lesions >3 cm are also included in this category. These lesions require follow-up studies to prove benignity
III	"Indeterminate" cystic masses that have thickened irregular or smooth walls or septa in which measurable enhancement is present. These are surgical lesions; although some will prove to be benign (e.g., hemorrhagic cysts, chronic infected cysts, and multiloculated cystic nephroma), some will be malignant, such as cystic renal cell carcinoma and multiloculated cystic renal cell carcinoma
IV	These are clearly malignant cystic masses that can have all the criteria of category III but also contain enhancing soft-tissue components adjacent to, but independent of, the wall or septum. These lesions include cystic carcinomas and require surgical removal

[a]Not measurable enhancement—see text for details

Conclusion

Familiarity with the patient's history, symptoms, and prior imaging improves the urologist's ability to derive valid conclusions from ultrasound imaging. In-office ultrasound is a useful adjunct to more quickly move patients along their treatment path. Ultrasound for the evaluation of renal calculus will likely increase in use as the public becomes more cognizant of the long-term risks of imaging using ionizing radiation. Ultrasound offers significant cost savings compared to CT and MRI.

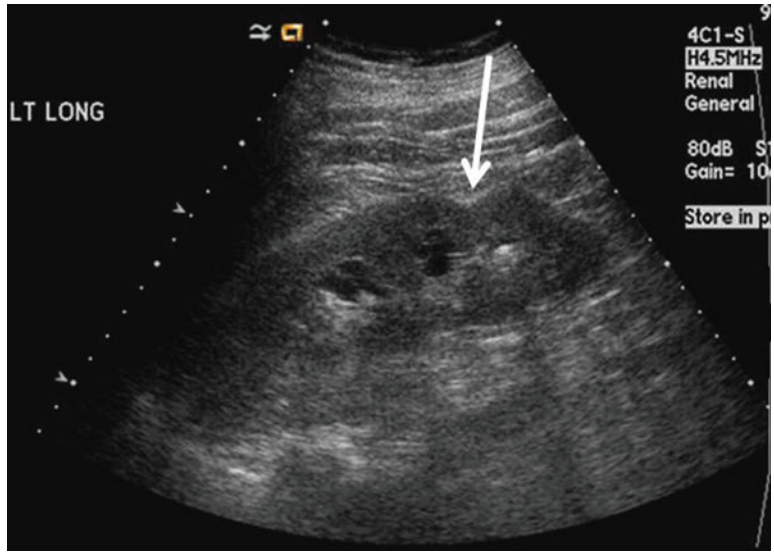

Fig. 5.28 Renal cortical scarring appears as a sharp depression (*arrow*) in the outline of the kidney usually overlying a calyx

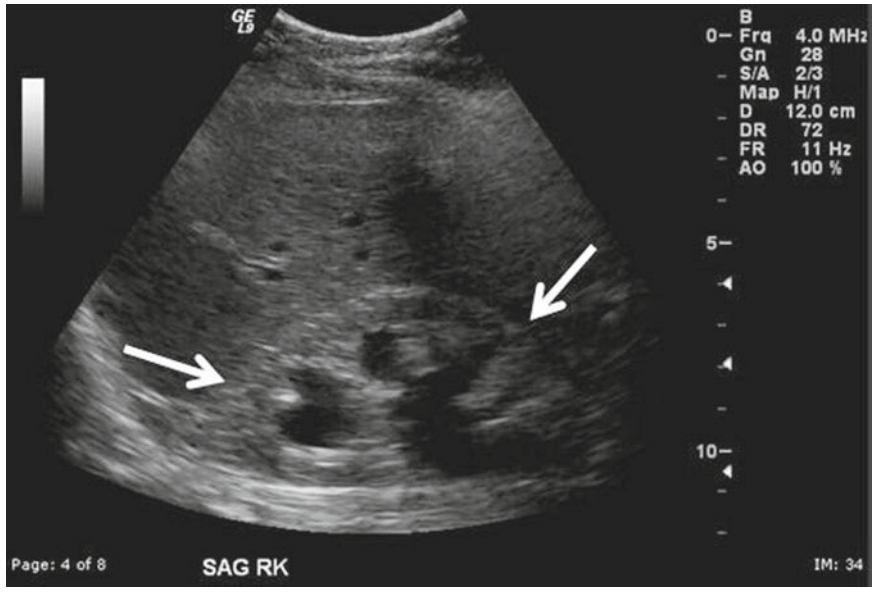

Fig. 5.29 Small hyperechogenic kidney (*arrows*) as a result of medical renal disease

Table 5.2 Effect of renal disease on sonographic appearance of the kidney [36]

Disease process	Echogenicity	Cortex	Renal size
Diabetic glomerulonephropathy	Normal/increased	Preserved	Enlarged
Renovascular disease	Increased	Thinned	Decreased
Obstructive uropathy	Increased	Thinned	Decreased

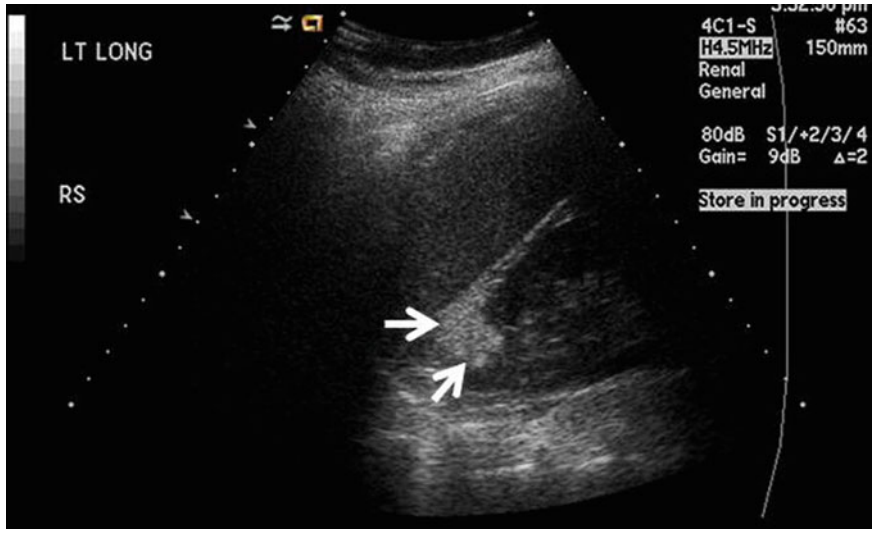

Fig. 5.30 An angiomyolipoma is typically a hyperechoic mass (*arrows*). The hyperechoicism is caused by the high fat content of the tumor

Table 5.3 Classification of hydronephrosis

Grade	Central renal complex	Renal parenchymal thickness
0	Intact	Normal
1	Slight splaying	Normal
2	Evident splaying confined within renal border	Normal
3	Wide splaying outside renal border; calices uniformly dilated	Normal
4	Further dilation of renal pelvis and calices	Thinned

Acknowledgments Dr Simmons wanted to acknowledge and thank Daniel Rukstalis, MD for his contributions to the chapter.

References

1. Surange RS, Jeygopal NS, Chowdhury SD, Sharma NK. Bedside ultrasound: a useful tool for the on-call urologist? Int Urol Nephrol. 2001;32(4):591–6.
2. Datta SN, Allen GM, Evans R, Vaughton KC, Lucas MG. Urinary tract ultrasonography in the evaluation of haematuria—a report of over 1000 cases. Ann R Coll Surg Engl. 2002;84(3):203–5.
3. AIUM Practice Guidelines, Ultrasound in the practice of urology. 2011. http://www.aium.org/resources/guidelines/urology.pdf. Accessed Mar 2013.
4. American Urological Association (AUA) Guideline: diagnosis, evaluation and follow-up of asymptomatic microhematuria (AMH) in adults: AUA Guideline. 2012. http://www.auanet.org/content/media/asymptomatic_microhematuria_guideline.pdf. Accessed May 2012.
5. American Urological Association (AUA) Guideline: clinical effectiveness protocols for imaging in the management of ureteral calculous disease: AUA technology assessment. 2012. http://www.auanet.org/content/media/imaging_assessment.pdf. Accessed Mar 2013.
6. Wein A. Campbell-Walsh urology, vol. 1. 9th ed. Philadelphia: Saunders; 2009.
7. Emamian SA, Nielsen MB, Pedersen JF, Ytte L. Kidney dimensions at sonography: correlation with age, sex, and habitus in 665 adult volunteers. Am J Roentgenol. 1993;160(1):83–6.
8. Han BK, Babcock DS. Sonographic measurements and appearance of normal kidneys in children. Am J Roentgenol. 1985;145(3):611–6.
9. Adam A, editor. Grainger and Allison's diagnostic radiology, No 1. 5th ed. Philadelphia: Elsevier; 2008.
10. Moghazi S, Jones E, Schroepple J, et al. Correlation of renal histopathology with sonographic findings. Kidney Int. 2005;67(4):1515–20.
11. Shokeir AA, Abdulmaaboud M. Resistive index in renal colic: a prospective study. BJU Int. 1999;83(4):378–82.
12. Rawashdeh YF, Djurhuus JC, Mortensen J, Horlyck A, Frokiaer J. The intrarenal resistive index as a

pathophysiological marker of obstructive uropathy. J Urol. 2001;165(5):1397–404.
13. Shokeir AA, Abdulmaaboud M. Prospective comparison of nonenhanced helical computerized tomography and Doppler ultrasonography for the diagnosis of renal colic. J Urol. 2001;165(4): 1082–4.
14. Horrigan TJ, Reese CS, Parres JA, Clarke HS, Desmond A, Kropp KA. A study of resistive indices in the arcuate arteries of the kidney over the course of gestation. J Perinatol. 1996;16(6):467–9.
15. Platt JF, Rubin JM, Ellis JH. Acute renal obstruction: evaluation with intrarenal duplex Doppler and conventional US. Radiology. 1993;186(3):685–8.
16. Andreoiu M, MacMahon R. Renal colic in pregnancy: lithiasis or physiological hydronephrosis? Urology. 2009;74(4):757–61.
17. Shokeir AA, Mahran MR, Abdulmaaboud M. Renal colic in pregnant women: role of renal resistive index. Urology. 2000;55(3):344–7.
18. Tublin ME, Bude RO, Platt JF. Review. The resistive index in renal Doppler sonography: where do we stand? Am J Roentgenol. 2003;180(4):885–92.
19. Bosniak MA. The current radiological approach to renal cysts. Radiology. 1986;158(1):1–10.
20. Israel GM, Bosniak MA. An update of the Bosniak renal cyst classification system. Urology. 2005;66: 484–8.
21. Shathabish S. A longitudinal study of kidney structure and function in adults. Nephrol Dial Transplant. 2010;25(4):1120–6.
22. Gourtsoyiannis N, Prassopoulos P, Cavouras D, Pantelidis N. The thickness of the renal parenchyma decreases with age: a CT study of 360 patients. Am J Roentgenol. 1990;155(3):541–4.
23. Akpinar IN, Altun E, Avcu S, Tuney D, Ekinci G, Biren T. Sonographic measurement of kidney size in geriatric patients. J Clin Ultrasound. 2003;31(6):315–8.
24. Berrington de Gonzalez A, Mahesh M, Kim KP, et al. Projected cancer risks from computed tomographic scans performed in the United States in 2007. Arch Intern Med. 2009;169(22):2071–7.
25. Smith-Bindman R, Lipson J, Marcus R, et al. Radiation dose associated with common computed tomography examinations and the associated lifetime attributable risk of cancer. Arch Intern Med. 2009;169(22):2078–86.
26. Smith-Bindman R. Is computed tomography safe? N Engl J Med. 2010;363(1):1–4.
27. Patlas M, Farkas A, Fisher D, Zaghal I, Hadas-Halpern I. Ultrasound vs CT for the detection of ureteric stones in patients with renal colic. Br J Radiol. 2001;74(886): 901–4.
28. Sheafor DH, Hertzberg BS, Freed KS, et al. Nonenhanced helical CT and US in the emergency evaluation of patients with renal colic: prospective comparison. Radiology. 2000;217(3):792–7.
29. Ripolles T, Agramunt M, Errando J, Martinez MJ, Coronel B, Morales M. Suspected ureteral colic: plain film and sonography vs unenhanced helical CT. A prospective study in 66 patients. Eur Radiol. 2004; 14(1):129–36.
30. de Souza LR, Goldman SM, Faintuch S, et al. Comparison between ultrasound and noncontrast helical computed tomography for identification of acute ureterolithiasis in a teaching hospital setting. Sao Paulo Med J Revista Paulista de Medicina. 2007; 125(2):102–7.
31. Katz SI, Saluja S, Brink JA, Forman HP. Radiation dose associated with unenhanced CT for suspected renal colic: impact of repetitive studies. Am J Roentgenol. 2006;186(4):1120–4.
32. AUA Guideline: clinical effectiveness protocols for imaging in the management of ureteral calculous disease: AUA technology assessment. http://www.auanet.org/content/media/imaging_assessment.pdf. Accessed Mar 2013
33. Ellenbogen PH, Scheible FW, Talner LB, Leopold GR. Sensitivity of gray scale ultrasound in detecting urinary tract obstruction. Am J Roentgenol. 1978; 130:731–3.
34. Manger JP, Mendoza PJ, Babayan RK, Wang DS. Use of renal ultrasound to detect hydronephrosis after ureteroscopy. J Endourol. 2009;23(9):1399–402.
35. Fernbach SK, Maizels M, Conway JJ. Ultrasound grading of hydronephrosis: introduction to the system used by the Society for Fetal Urology. Pediatr Radiol. 1993;23:478.
36. O'Neill Charles W. Atlas of renal ultrasonography. Philadelphia: W.B. Saunders Company; 2001. pp. 43, 47.

Scrotal Ultrasound

6

Rao S. Mandalapu, Peter N. Tiffany,
and Bruce R. Gilbert

Normal Ultrasound Anatomy of the Testis and Paratesticular Structures

The scrotum is separated into right and left hemiscrotal compartments by a septum called the median raphe. The normal scrotal wall thickness varies between 2 and 8 mm. The scrotal wall contains the following structures: rugated skin, superficial fascia, dartos muscle, external spermatic fascia, cremasteric fascia, and internal spermatic fascia. These layers are indistinguishable on a normal clinical exam. The tunica vaginalis consists of parietal and visceral layers normally separated by 2–3 mL of straw-colored fluid often referred to as a physiologic hydrocele. On ultrasound this fluid is often seen as a thin anechoic rim around the head of the epididymis [1]. The parietal and visceral layers join at the posterolateral aspect of the testis where the tunica attaches to the scrotal wall [2].

The testes descend into the scrotum at approximately the 28th week of gestational age through the inguinal canal along with the processus vaginalis. The processus vaginalis gradually closes through infancy and early childhood. The size and shape of the testis change with the age. Gonadal hormones influence testicular size in early life. Testicular volume gradually rises from birth to 5 months of age due to a peak in gonadotropic hormones [3, 4]. After the age of 5 months, the testicular volume steadily declines and reaches its minimum volume at approximately 9 months of age and remains approximately the same size until puberty [5]. The testis is rounded in newborns and gradually becomes ovoid with growth. The echogenicity of the testis increases in puberty due to the development of germ cell elements [6].

The adult testis is a smooth ovoid gland, approximately 4–5 cm long, 3 cm wide, 2–3 cm in the anterior–posterior (AP) dimension, and typically between 20 and 30 mL in volume. The testis exhibits medium homogenous echogenicity. A dense fibrous capsule, the tunica albuginea, envelops the testis, which is apparent as a thin echogenic line on ultrasound. The testis has approximately 250–400 conical lobules, which comprises seminiferous tubules and are separated by fibrous septa of tunica albuginea that extend from the mediastinum of the testis into the parenchyma of the testis [7]. Testicular lobules are occasionally identified on ultrasound as lines radiating from the mediastinum testis (Fig. 6.1). The seminiferous tubules contained within the lobules open into dilated spaces called rete testis within the mediastinum. The seminiferous tubules are long V-shaped tubules, both ends of which usually terminate in the rete testis (Fig. 6.2). The rete testis is

R.S. Mandalapu, MD
Department of Urology, Fox Chase Cancer Center, Temple University Hospital, Elkins Park, PA, USA

P.N. Tiffany, MD
Department of Urology, Winchester Hospital, Tufts University School of Medicine, Stoneham, MA, USA

B.R. Gilbert, MD, PhD (✉)
Hofstra North Shore LIJ School of Medicine, The Arthur Smith Institute for Urology, New Hyde Park, NY, USA
e-mail: bgilbert@gmail.com

P.F. Fulgham and B.R. Gilbert (eds.), *Practical Urological Ultrasound*, Current Clinical Urology,
DOI 10.1007/978-1-59745-351-6_6,

connected to the head (caput or globus major) of the epididymis with about 8–12 efferent ductules. The normal rete testis is sonographically evident in 18% of patients as a hypoechoic area with a striated configuration adjacent to the mediastinum testes [8]. The septa and mediastinum testes may appear as linear echogenic areas on ultrasonography [1] (Fig. 6.3).

The adult epididymis is 6–7 cm long and has three parts, the head (caput) measuring 10–12 mm in diameter, the body (corpus) measuring 2–4 mm in diameter, and the tail (cauda) about 2–5 mm in diameter. In the normal epididymis, the head is routinely identified located posterolateral to the upper pole of the testis. The caput epididymis is triangular in shape, often has the same echogenicity as the testis (Fig. 6.4). However, it can be heterogeneous with areas that are hyper or hypoechoic. The smaller corpus epididymis can be seen as a hypoechoic structure containing multiple echogenic linear structures representing the coiled epididymal tubule and lies posteriorly along the long axis of the testis.

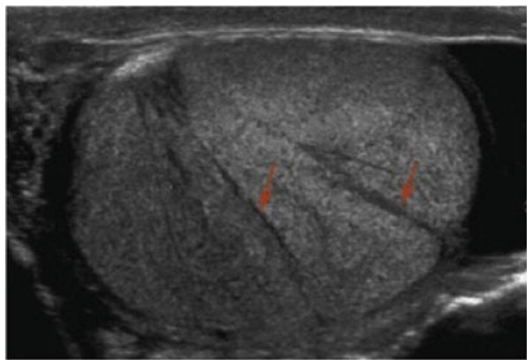

Fig. 6.1 Normal adolescent testis showing testicular lobules separated by fibrous septa (*arrows*)

The testicular appendages are the remnants of the mesonephric and paramesonephric ducts. There are four testicular appendages: the appendix testis, the appendix epididymis, the vas aberrans, and the paradidymis (Fig. 6.5). The appendix testis and the appendix epididymis are commonly seen on scrotal ultrasound [9].

The appendix testis (hydatid of Morgagni) is a small ovoid structure usually at the upper pole of the testis in the groove between the testis and the epididymis, better seen in the presence of fluid around the testis. The appendix testis is the vestigial remnant of the paramesonephric (Müllerian) duct (Fig. 6.6).

The appendix epididymis originates from the mesonephric (Wolffian) duct and is seen associated with the epididymal head on ultrasound images (Fig. 6.7).

The spermatic cord is normally seen superior to the posteromedial aspect of the testis and contains the vas deferens, the testicular and cremasteric

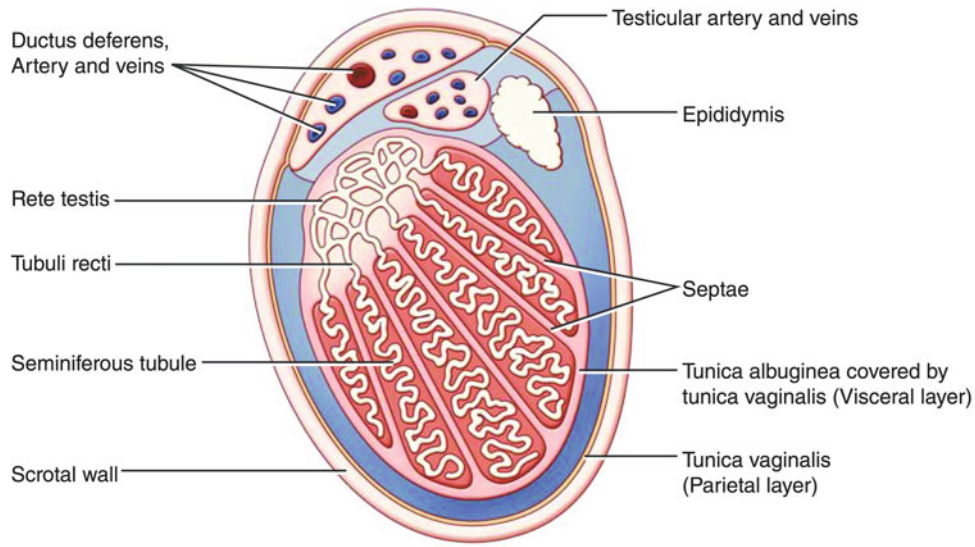

Fig. 6.2 Schematic cross section of the testis showing testicular lobules, seminiferous tubules, rete testis, and mediastinum testis

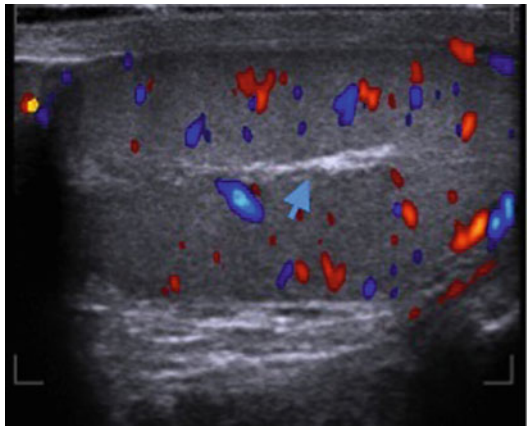

Fig. 6.3 The mediastinum testes appear as linear echogenic areas on ultrasonography (*arrow*)

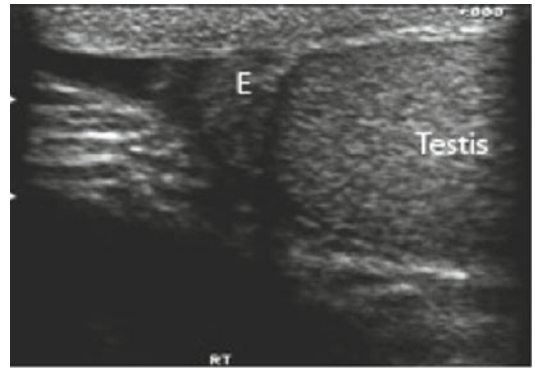

Fig. 6.4 The caput epididymis is *triangular* in shape (E) and is usually either isoechoic or slightly hypoechoic when compared to the testis

and deferential arteries, the pampiniform plexus of veins, genital branch of the genital femoral nerve, testicular plexus of the sympathetic trunk, and lymphatic vessels [7] (Fig. 6.8).

The blood supply to the scrotal structures is from the three primary arteries (Fig. 6.9). The testis is supplied by the gonadal artery or testicular artery, which arises from the aorta and courses through the scrotum with the spermatic cord. The deferential artery, which arises from the superior vesical artery, supplies the vas deferens and epididymis. The cremasteric artery, a branch of the inferior epigastric artery, supplies the scrotal sac and coverings of the spermatic cord. The veins draining the testis and epididymis converge to form the pampiniform plexus at the mediastinum on the superior pole of the testis. The pampiniform plexus is primarily drained by the testicular and external pudendal veins [10]. The testicular vein has no valves.

Color flow imaging can provide visual assessment of intratesticular and epididymal flow. Testicular vessels are noted to have a low impedance pattern on duplex Doppler with high levels of diastolic flow, reflective of the low vascular resistance of the testis. Power Doppler scanning is valuable because of its increased sensitivity to low flow and its independence from Doppler angle correction. Occasionally, it may be difficult to visualize intratesticular flow in the prepubertal testes, but capsular vessels are easy to identify. The resistive index of the intratesticular arteries decreases with age [1, 11]. Diastolic arterial flow may not be detectable in normal testes with volumes of 4 cm^3 or less. The RI of the testicular parenchymal arteries is typically equal to 1.0 due to undetectable diastolic arterial flow in smaller testes. Significant differences in mean RI between prepubertal and postpubertal testes has been reported [11].

Scanning Protocol and Technique

The patient is examined in the supine position. There are several different techniques to support the scrotum. The easiest is to use the patient's legs for support. Other approaches use towels placed across the patient's thighs or under the scrotum. The phallus is positioned up on the pubis held by the patient and/or covered by a towel (Figs. 6.10 and 6.11).

Transducer Selection

High-frequency (7.5–18 MHz) linear array transducers are most often used for scrotal scanning. Broad bandwidth transducers allow for multiple focal zones, eliminating the need for adjustment during the examination. Multiple frequency transducers allow the transducer to be set at one of several distinct frequencies. A linear array probe with a "footprint" able to measure the longitudinal length of testis is ideal. A curved array probe can

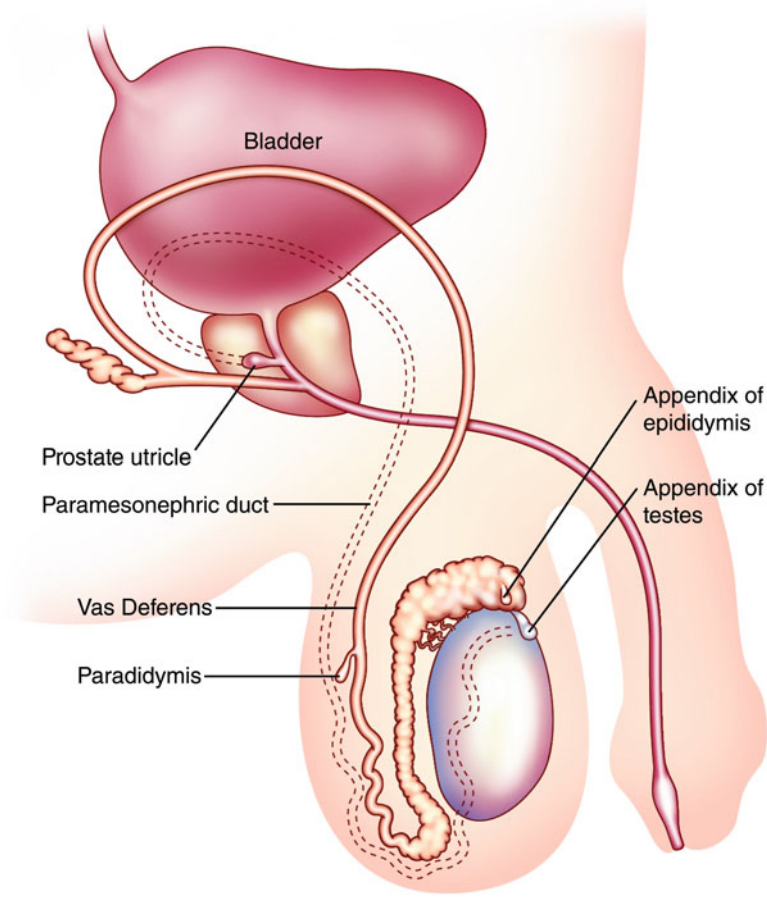

Fig. 6.5 Testicular appendages: appendix testis (Müllerian remnant) and the appendix epididymis and paradidymis (Wolffian remnant). There are also the cranial (originates from body of epididymis) and caudal (originates from tail of epididymis) vas aberrans not shown in this figure

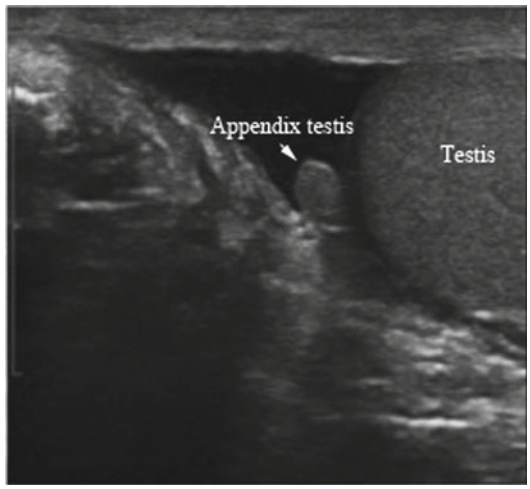

Fig. 6.6 Appendix testis is a small ovoid structure typically identified in a groove between the upper pole of the testis and the epididymis. It is better appreciated with hydrocele

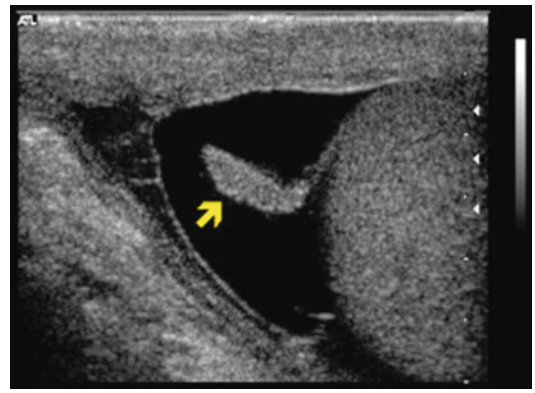

Fig. 6.7 Appendix epididymis (*arrow*) is nicely visualized when a small hydrocele is present. Differentiating an appendix epididymis from an appendix testis often requires the sonographer to visualize the origin of the structure in real time

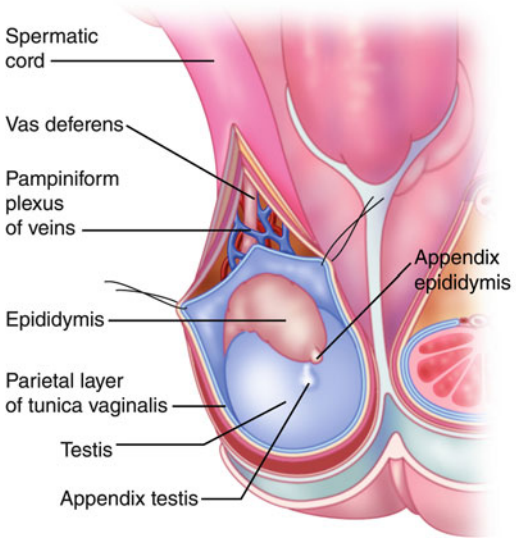

Fig. 6.8 Spermatic cord and paratesticular structures. The spermatic cord contains the vas deferens, the testicular and cremasteric and deferential arteries, the pampiniform plexus of veins, genital branch of the genital femoral nerve, testicular plexus of the sympathetic trunk, and lymphatic vessels

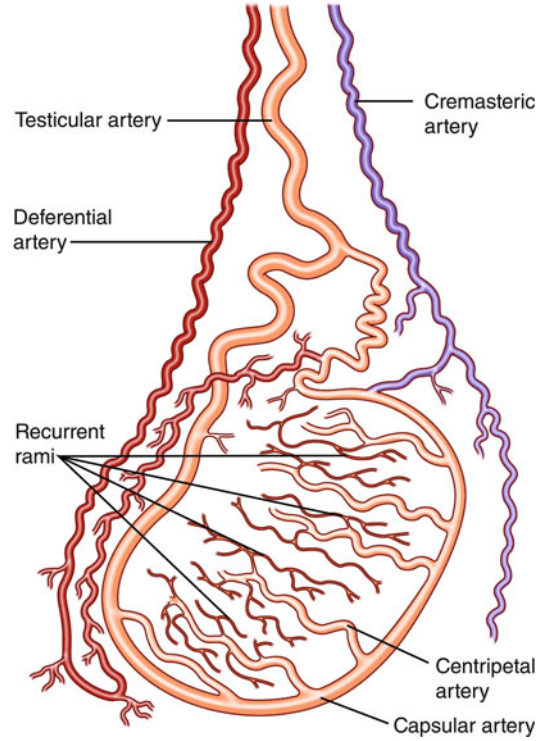

Fig. 6.9 Blood supply of testis. The testis is supplied by three sources of blood supply: *1*. the testicular artery, which arises from the aorta; *2*. the deferential artery, which arises from the superior vesical artery; and *3*. the cremasteric artery, a branch of the inferior epigastric artery

be used with a thickened scrotal wall or in the presence of scrotal edema or for large testis. The curved array transducer is also useful to compare echogenicity of the testes. However, the frequency is usually lower, resulting in a less detailed image. Color and spectral Doppler are essential elements of a complete scrotal ultrasound because they provide documentation of normal testicular blood flow and paratesticular findings.

Survey Scan

Evaluation of the scrotal contents is begun with a longitudinal survey scan, progressing medial to lateral to get an overall impression of the testis and paratesticular structures. The standard orientation of the image should be with the superior pole to the left and the inferior pole to the right on the monitor screen. If the testis is larger than the footprint of the transducer views of the superior and inferior portions of the testis including the epididymis in these regions, it should be documented. At least one image should visualize both testes to document the presence of two testes.

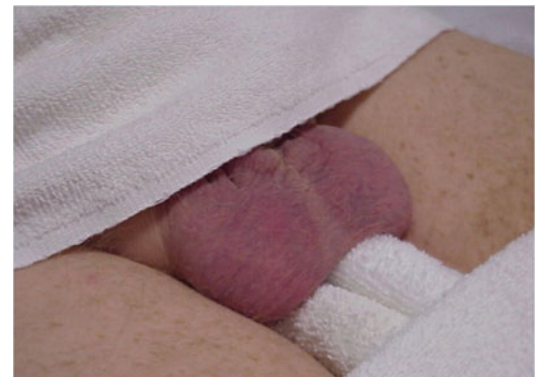

Fig. 6.10 Patient is placed in a supine position with towel placed under scrotum

The transverse view is obtained by rotating the transducer 90°. The standard orientation for the right testis is to have the lateral aspect to the left and the medial aspect to the right. Conversely, for the left testis, the lateral aspect should be to the

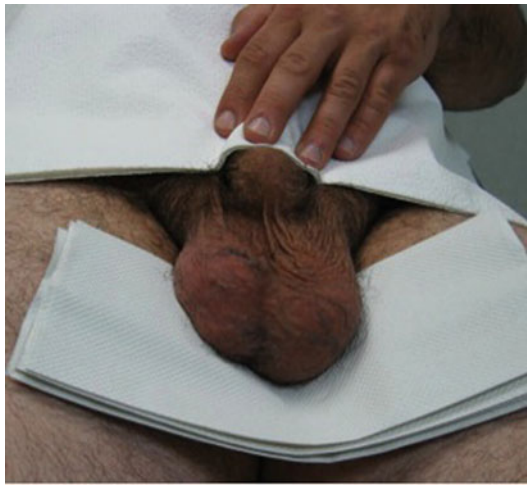

Fig. 6.11 Patient position with phallus support. The phallus is positioned up on the pubis held by the patient

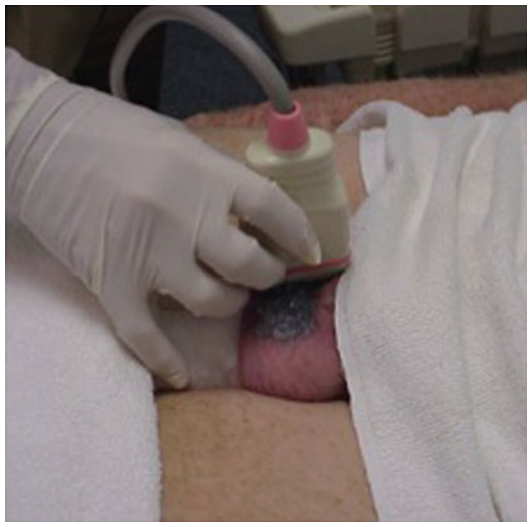

Fig. 6.12 Longitudinal view. Measurement should be made of the long axis at the mid-testis

right and the medial aspect to the left. Using the mid-testis as a starting point of the survey scan, one should proceed first toward the superior pole then back to the mid-testis before scanning to the inferior pole. Measurements of width and AP dimensions are taken and documented at the mid-testis. A measurement should also be made of the long axis at the mid-testis together with the mid-transverse AP measurement. If the equipment being used has split-screen capabilities, comparative views of echogenicity and blood flow can

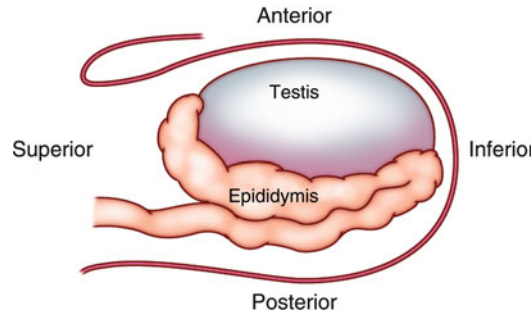

Fig. 6.13 Longitudinal schematic view

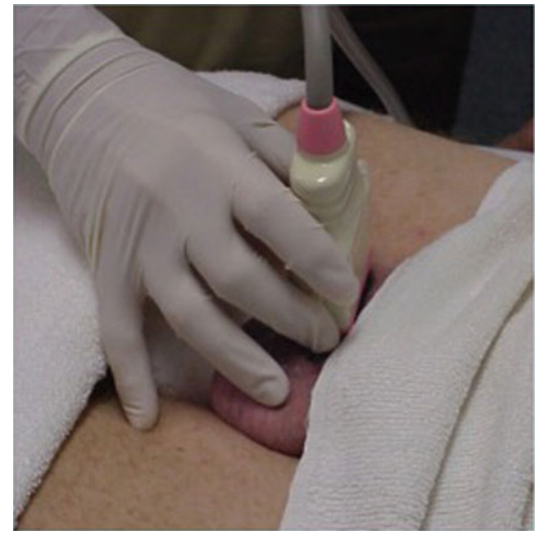

Fig. 6.14 Transverse view, mid-transverse anterior–posterior measurement should be documented

easily be made and documented (Figs. 6.12, 6.13, 6.14 and 6.15).

The use of color Doppler imaging should be considered an integral part of the scrotal ultrasound exam. Many inflammatory, neoplastic, and even benign conditions have characteristic flow patterns that can assist in diagnosis.

Color and Spectral Doppler

Color and spectral Doppler is an invaluable component of the scrotal US examination. There is an expanding literature suggesting that these modalities might be a noninvasive indicator of testicular function. Biagiotti et al. provided data suggesting

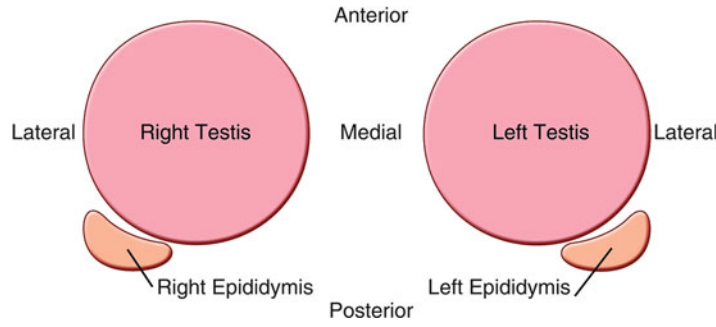

Fig. 6.15 Transverse schematic view

that RI and PSV were better predictors of dyspermia than FSH and testicular volume [12]. In a companion study they demonstrated that RI and PSV can differentiate obstructive azoospermia (OAS) from nonobstructive azoospermia (NOS) [12].

It is often difficult to interrogate intratesticular vessels when the intratesticular microcirculation is impaired. Unsal et al. [13] provided data supporting interrogation of the capsular vessel and capsular branches in lieu of the intratesticular vessels. They found that RI of both capsular vessel and capsular branches could serve as indicators of impaired testicular microcirculation. Pinggera et al. [14] examined semen quality and the RI of intratesticular arteries in 160 men. Of interest, their study indicated that 80 with a normal sperm count had an RI of 0.54 ± 0.05 while the 80 with impaired sperm counts had a statistically higher RI of 0.68 ± 0.06. In addition, Balci et al. [15] demonstrated that a decrease in RI, suggestive of an improved testicular microcirculation, was found after varicocele repair in patients with improvements in semen quality.

Documentation

The written report and archived images are a reflection of the quality of the examination. The old adage "If it's not documented, it wasn't done" should guide the sonographer in developing a quality report. The static images obtained during the evolving ultrasound exam should represent the sonographer's impression of the findings. If electronic storage space is available and the equipment allows, video clips, which demonstrate important findings, can and should be obtained. A quality report can aid in diagnosis and is therefore in the best interest of patients.

An earlier chapter on documentation provides examples of a template for documenting the scrotal ultrasound examination. In addition to the measurements and anatomical findings of the exam, it is essential to include patient identification information, the exam date, and the indications for performing the exam. The physician who performed the exam should sign the report.

Images should be attached to the report. Each image should include the date, the time, patient identification, and the transducer used and its frequency. The area of interest should be clearly identified. The orientation and measurements should be clearly labeled along with the pertinent anatomy and any abnormalities. There is no minimum number of images that are required for proper documentation. It is the best practice to provide images that depict the measurements being taken and the pathology being described. It is also essential, when two testes are present, to document this on a single image that shows both testes. This image also provides the best comparison of echogenicity between the two testes.

Indications

There are many specific indications for scrotal ultrasound (Tables 6.1 and 6.2). Scrotal ultrasound is also performed when the physical examination is inconclusive or difficult to complete (or both) because of patient discomfort or inability of the examiner to precisely identify the scrotal structures on palpation. In these instances the scrotal ultrasound examination is an integral part

Table 6.1 Indications for scrotal ultrasound

Assessment of scrotal mass
a. Scrotal wall lesions
1. Noninflammatory
a. Acute idiopathic scrotal wall edema (AISE)
b. Anasarca
c. Neoplastic
i Squamous cell carcinoma of the scrotum
2. Inflammatory
a. Cellulitis/scrotal wall abscess
b. Fournier's gangrene
c. Miscellaneous scrotal lesions
d. Epidermoid cysts of the scrotal wall
e. Pseudotumor of the scrotum
b. Extratesticular lesions
1. Varicocele
2. Hydrocele
3. Hematocele/pyocele
4. Inguinal hernia
5. Tumors of the spermatic cord
6. Epididymal lesions
a. Benign epididymal lesions
i. Epididymo-orchitis
ii. Sperm granuloma
iii. Epididymal cysts
iv. Spermatocele
v. Appendix epididymis
vi. Adenomatoid tumor
vii. Papillary cystadenoma
viii. Leiomyoma
b. Malignant epididymal lesions
i. Sarcoma of the epididymis
ii. Clear cell carcinoma of the epididymis
c. Testicular Lesions
i. Benign lesions of the testis
ii. Malignant lesions of the testis
2. Evaluation of male infertility
1. Varicocele
2. Impaired semen quality and azoospermia
3. Antisperm antibodies
4. Testicular atrophy
3. Testicular trauma
4. Torsion

of the physical examination of the male genitalia. In other situations, ultrasound evaluation is essential to diagnosis and treatment and well supported in the literature.

The indications listed are based primarily on clinical experience and/or evidence obtained from case series and rarely from comparative series with historical controls. In other words the decision on whether or not to obtain imaging is discretionary and not informed by a strong or clear body of evidence. "Appropriateness" criteria are desirable and high-level evidence-based studies are required in order to determine appropriateness. Part of the work of urologic imaging research in the future should look to assess the limitations of the current literature and then create an evidence base that will define the value of the imaging services critical to the practice of urology [16, 17]. Other specialty societies have begun the process of developing appropriateness criteria in a rigorous way in response to concerns about the use and misuse of imaging [18]. These efforts generate a more precise application of medical discoveries including advanced imaging technology.

Abnormal Ultrasound Findings

Scrotal Wall Lesions

Palpation of the scrotal contents can be difficult in patients with a thickened scrotal wall or scrotal wall edema or retracted scrotum. Scrotal ultrasound is particularly useful in the evaluation of the scrotal contents in these patients.

Noninflammatory

Acute idiopathic scrotal edema (AISE) is a self-limited disease of unknown origin. It presents with unilateral or bilateral scrotal swelling without pain and associated with unilateral or bilateral inguinal lymphadenopathy. It is thought to be a variant of angioneurotic edema, often associated with eosinophilia. Physical examination findings include scrotal skin swelling and erythema also extends to the inguinal and perianal area. AISE is a diagnosis of exclusion. The characteristic ultrasound findings for AISE, including edema of the scrotal wall with hypervascularity and compressibility, and enlargement of the inguinal lymph nodes with normal testis and epididymis [19, 20] (Fig. 6.16).

The other noninflammatory causes of scrotal wall edema include congestive heart failure, renal

Table 6.2 Ultrasound characteristics of nonneoplastic intratesticular masses

Intratesticular lesion	Ultrasound findings
Simple testicular cyst	Well-circumscribed, anechoic, increased through transmission
Epidermoid cyst	Classic appearance: an onion ring due to alternating layers of hypoechogenicity and hyperechogenicity
Tubular ectasia of the rete testis (TERT)	Avascular cystic dilations in the rete testis
Intratesticular varicocele	Anechoic, tortuous structure with a venous waveform on Doppler color flow study
Tunica albuginea cyst	Cyst at upper or lateral margin of testis, may be clinically palpable
Testicular hematoma	Avascular hyperechoic lesion within the testicular parenchyma
Congenital testicular adrenal rests	Bilateral hypoechoic or hyperechoic lesions with or without posterior acoustic shadowing

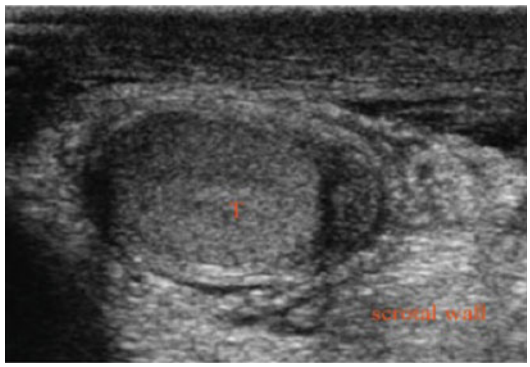

Fig. 6.16 Acute idiopathic scrotal wall edema: gray-scale ultrasound shows edema and diffusely thickened scrotal wall

failure, anasarca, hepatic failure, cirrhosis, nephrotic syndrome, and poor nutritional status.

The scrotal wall appears thickened in chronic venous or lymphatic obstruction secondary to filariasis, radiation, trauma, and surgery.

The scrotal ultrasound demonstrates scrotal wall thickness with layers of alternating hypo- and hyperechogenicity [21].

Inflammatory

Cellulitis/Scrotal Wall Abscess

Patients who are diabetic or immunocompromised are more susceptible to infection and scrotal wall cellulitis or abscess. The ultrasonography demonstrates thickening of the subcutaneous tissue and heterogeneity with increased blood flow on color Doppler study. The scrotal wall abscess appears on ultrasound as a well-defined mass with irregular hypoechoic lesion within the scrotal wall and no Doppler flow within the mass [1].

Fournier's Gangrene

Fournier's gangrene is a polymicrobial rapidly progressing necrotizing fasciitis which commonly involves perineum and genital regions. Fournier's gangrene is a urologic emergency with mortality up to 50% [22, 23]. Computer tomography remains the imaging modality of choice [24]. However, ultrasonography can provide valuable clues at the time of initial presentation. Ultrasonography shows marked thickening of the scrotal skin with multiple hyperechoic foci associated with shadowing, which are consistent with the presence of subcutaneous gas and is characteristic of Fournier's gangrene [25].

Miscellaneous Scrotal Skin Lesions

Henoch-Schonlein purpura (HSP) is a systemic vasculitis of unknown origin. It is characterized by a palpable skin rash, abdominal pain, and polyarthralgia. HSP has been reported to have scrotal wall swelling and ecchymosis in up to 38% of cases [26].

Epidermoid Cysts of the Scrotal Wall

Epidermoid cysts (also called follicular infundibular cysts, epidermal cysts, or epidermal inclusion cysts) are the most common cutaneous cysts of the scrotal wall. Epidermoid cysts result from the proliferation of epidermal cells within a circumscribed space of the dermis. The source of this epidermis is nearly always the infundibulum of the hair follicle [27]. These cysts may become infected and form scrotal wall abscesses.

Pseudotumor of the Scrotum

Scrotal fibrous pseudotumors are uncommon and are thought to be reactive, benign lesions. They are the second most common paratesticular mass, after adenomatoid tumor, and they may mimic a malignancy clinically. The sonographic appearance of the fibrous pseudotumor of the scrotum is variable depending on the contributing fibrous tissue components, the presence or absence of calcification, and the scrotal structure involved [28].

The pseudotumor of the scrotum is a benign condition; local excision of the mass is the treatment of choice [29]. However, preoperative diagnosis is seldom made in these patients due to the nonspecific clinical and sonographic findings.

Scrotal Wall Malignant Lesions

Squamous cell carcinoma (SCC) of the scrotum is an uncommon neoplasm. SCC is associated with occupational exposure in chimney sweepers and workers in the oil and chemical industries. It is also associated with exposure to radiation, HPV, and with immune-related conditions such as psoriasis [30].

The literature concerning scrotal SCC is limited. Ultrasound evaluation of these lesions is not well defined.

Extratesticular Lesions

Scrotal Hernia

Congenital inguinal hernia is due to failure of the processus vaginalis to obliterate which results in passage of intestinal loops or omentum or peritoneal fluid in the scrotal sac [7, 31, 32]. Right inguinal hernias are more common as the right processus vaginalis closes later. Scrotal ultrasound can be helpful in cases of inconclusive physical examination. Clinically occult contralateral hernia can be assessed with ultrasound [33]. Patients with a scrotal hernia usually present with mesenteric fat and/or bowel loops seen superior to the testis. Real-time imaging studies can demonstrate peristaltic activity or bowel motion or intestinal gas bubbles with their characteristic echogenic interfaces. Gray-scale ultrasound shows characteristic findings including highly echogenic fat suggestive of an omental hernia [33] (Figs. 6.17, 6.18 and 6.19).

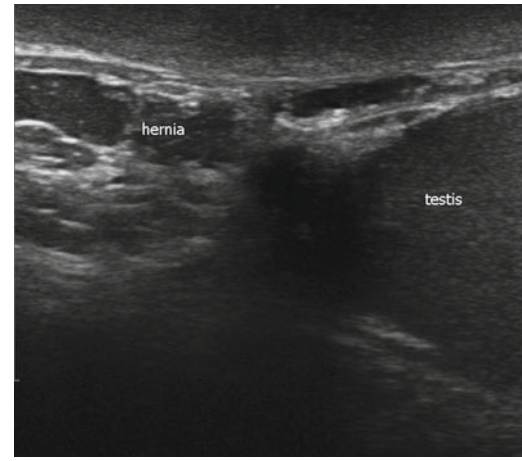

Fig. 6.17 Gray-scale ultrasound shows characteristic findings of highly echogenic omental fat suggestive of omental hernia

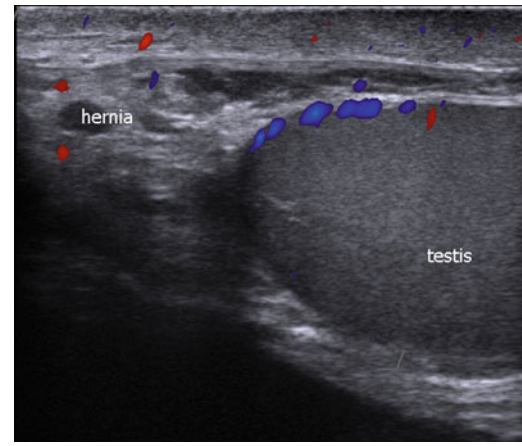

Fig. 6.18 Color Doppler study showing no increased blood flow to the inguinal hernia

Hydrocele

Hydrocele is the most common cause of painless scrotal swelling. A hydrocele is a serous fluid collection between the parietal and visceral layers of the tunica vaginalis. The tunica vaginalis is a mesothelium-lined sac that results from closure of the superior portion of the processus vaginalis. This fascial structure normally covers the entire testis except the posterior border. It has a visceral layer and an outer parietal layer that lines the internal spermatic fascia of the scrotal wall. Hydroceles can be congenital or acquired. The congenital

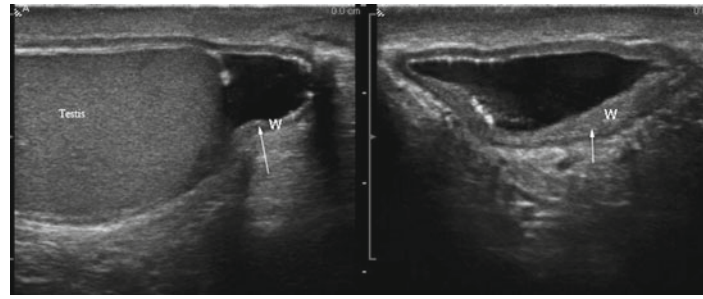

Fig. 6.19 Gray-scale ultrasound showing thickened hernia sac (W) in chronic inguinal hernia (*arrows*)

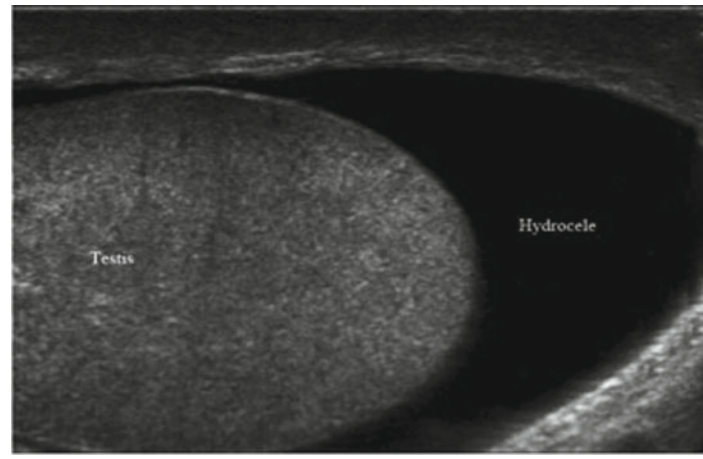

Fig. 6.20 Gray-scale ultrasound showing fluid collection in the hydrocele sac

hydrocele or communicating hydrocele occurs when a patent processus vaginalis allows fluid to pass from the peritoneal space into the scrotum [34]. The acquired hydrocele may be idiopathic with no identifiable cause. The incidence of hydroceles is about 1% of adult males. Hydroceles are usually anechoic on ultrasonography (Fig. 6.20). They may contain echogenic cholesterol crystals. The presence of septations is often associated with infection, trauma, or metastatic disease. Hydrocele may develop secondary to venous or lymphatic obstruction caused by infection, trauma, torsion, or tumor. About 10% of testicular tumors are accompanied by a hydrocele; clinical suspicion increases with new onset of hydrocele in men in their 30s or 40s [35]. Scrotal ultrasound is essential to rule out testicular pathology in these patients. The testis is often posteriorly displaced by the hydrocele. A massive hydrocele exerts a pressure effect that may compromise blood flow within the testis. Vascular resistance in intratesticular arteries is increased, and color Doppler ultrasound may demonstrate an increase in the caliber of capsular arteries. Fluid aspiration and surgical excision of hydrocele sac has been shown to restore normal blood flow to the testis [36].

Hematocele/Pyocele

A hematocele is an accumulation of blood within the tunica vaginalis. Hematoceles are usually secondary to trauma, torsion, tumor, and surgery. Hematoceles often present with scrotal discomfort and a hard scrotal mass and history of trauma. The ultrasonography shows a complex heterogeneous appearance and may demonstrate mass effect with distortion of the testis [37].

Pyocele is an accumulation of pus within the tunica vaginalis and is most often occurring because of untreated epididymo-orchitis. Pyoceles present with acute scrotal pain and symptoms of sepsis. A pyocele also appears heterogeneous on the ultrasonogram, and gas may be identified, causing hyperechoic reflections and shadowing [37] (Fig. 6.21).

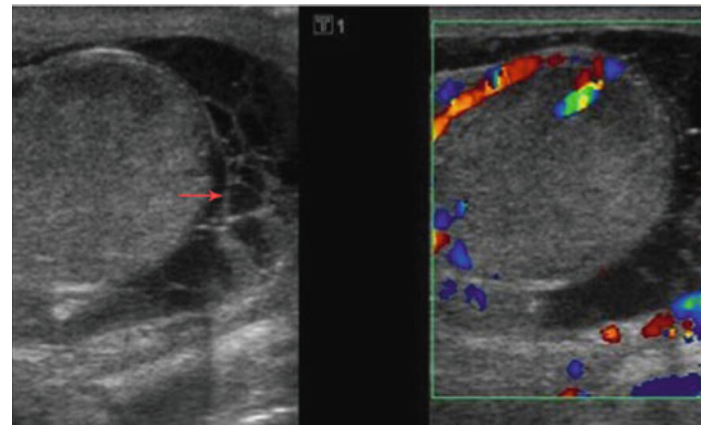

Fig. 6.21 A complex heterogeneous fluid collection with the tunica vaginalis on gray-scale ultrasound showing septations and no blood flow noted on Doppler study

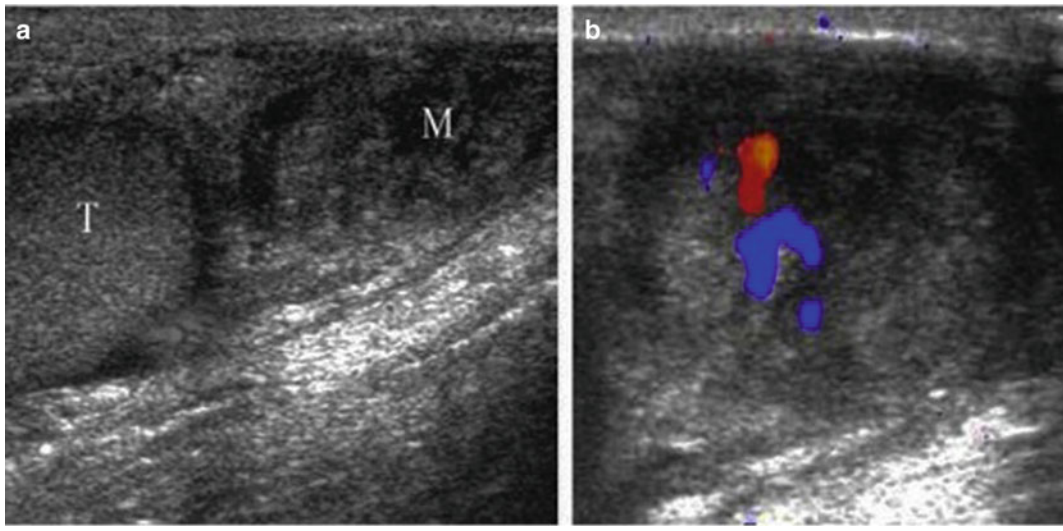

Fig. 6.22 (**a**) Leiomyosarcoma of the scrotum: gray-scale ultrasound appearance as an ill-defined solid mass with heterogeneous echotexture in the paratesticular space (*M* mass, *T* testis) (**b**) Doppler color flow shows increased vascularity within the mass

Tumors of the Spermatic Cord

Lipomas of the spermatic cord are very common benign tumors of the spermatic card. They can be unilateral or bilateral and often present an asymptomatic fullness of the spermatic cord. It is important to confirm that these masses do not represent inguinal hernias by noting the intact external inguinal ring on physical examination. If the physical examination is inconclusive, a scrotal ultrasound can be useful to rule out the presence of a hernia.

Rhabdomyosarcomas may occur in the spermatic cord in children, and liposarcoma is the most common malignant tumor arising in the spermatic cord in adults, although both are rare. Leiomyosarcomas in the paratesticular space also have been reported. The ultrasound appearance is an ill-defined solid mass with heterogeneous echotexture and increased vascular flow on Doppler color study (Fig. 6.22a, b).

Epididymal Lesions

Benign Epididymal Lesions

Epididymo-orchitis

Epididymitis is the most common cause of subacute unilateral scrotal pain in preadolescent and adolescent boys and adult men. On physical exam the epididymis can often be identified as

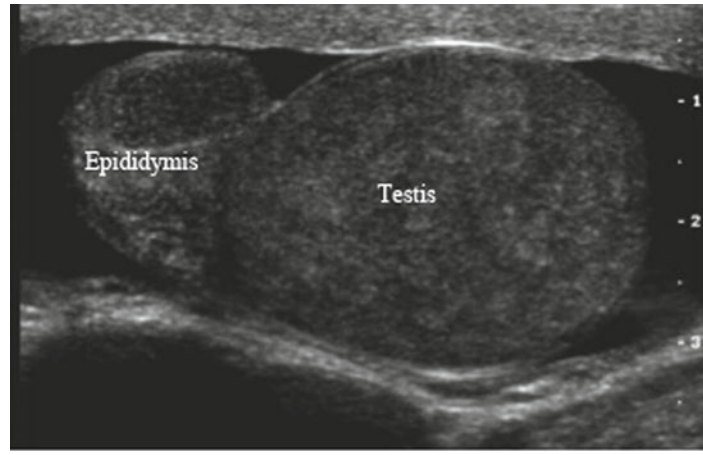

Fig. 6.23 Epididymo-orchitis: gray-scale image demonstrates enlarged and heterogeneous epididymis and testis

an enlarged and tender structure posterolateral to the testis. The pain is often relieved with elevation of the testis (Prehn's sign). Epididymitis in boys is not rare and is mostly an inflammatory phenomenon, presumably postinfectious, with a benign course. Serologic titers in boys diagnosed with acute epididymitis are commonly positive for enteroviruses and adenoviruses and *M. pneumonia*. Blunt trauma also is a potential cause of epididymal inflammation. Among sexually active males <35 years old, epididymitis often results from STDs especially *Chlamydia trachomatis* and *Neisseria gonorrhea*. In older men bacterial epididymitis can result from retrograde transit of bacteria down the vasa. Epididymitis can also be congestive in nature, e.g., postvasectomy. Rare infectious causes include brucellosis, TB, cryptococcus, syphilis, and mumps. Rare noninfectious causes include sarcoidosis and amiodarone [38, 39].

The body of the normal epididymis has slightly decreased echogenicity as compared to its head. In patients with acute epididymitis, the epididymis is enlarged with increased vascularity. Epididymitis may be focal or global, with enlargement and thickening of the epididymis. Gray-scale ultrasound demonstrates a hypoechoic or heterogeneous, enlarged epididymis (Fig. 6.23). The color flow Doppler shows increased vascularity with high-flow, low-resistance pattern. A reversal of flow during diastole occurs with venous infarction. A reactive hydrocele is often present. Complications include infectious spread

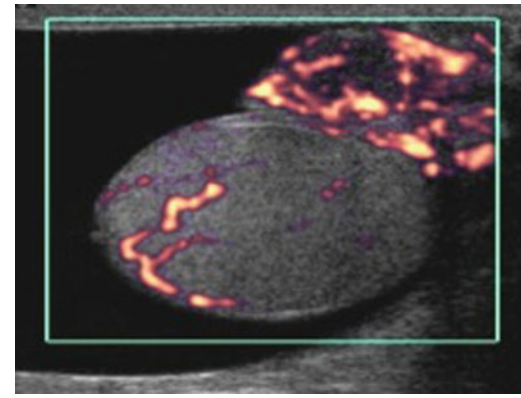

Fig. 6.24 Power Doppler ultrasound showing increased vascularity of the epididymis and the testis in epididymo-orchitis

to the testis resulting in epididymo-orchitis, abscess formation, testicular infarction (usually secondary to obstruction of venous flow followed by testicular atrophy), and chronic pain. Doppler ultrasound is often diagnostic (Fig. 6.24).

Patients with chronic epididymitis often present with persistent pain. In these men, ultrasound examination reveals an enlarged epididymis with increased echogenicity and possible areas of calcifications (Fig. 6.25).

Sperm Granuloma

Sperm are highly antigenic, and an intense inflammatory reaction occurs when they exit the vas deferens [40]. A sperm granuloma occur in at least 40% of postvasectomy patients [41]. Sperm granulomas are rarely symptomatic

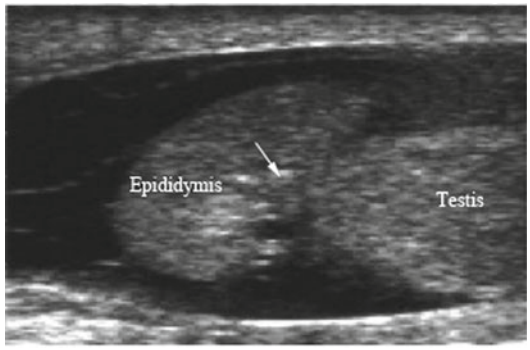

Fig. 6.25 Chronic epididymitis: gray-scale ultrasound showing increase of echogenicity and microcalcifications seen in the caput epididymis

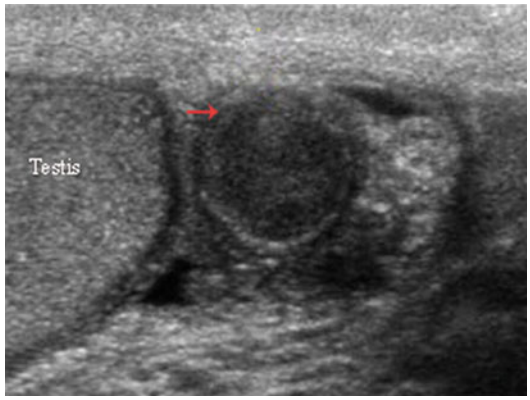

Fig. 6.26 Sperm granuloma: gray-scale ultrasound shows hypoechoic and nonvascular mass in the epididymis

(about 2–3% of vasectomy patients have pain that can be attributed to sperm granuloma) usually occurring 2–3 weeks postoperatively [42] (Fig. 6.26).

Epididymal Cyst

An epididymal cyst is a nonpainful cystic structure that, when large, displaces the testis inferiorly. Cysts of the epididymis occur in up to 40% of the men. True epididymal cysts account for 75% of these masses and contain lymphatic fluid. They are typically thin walled and well defined, usually with strong posterior acoustic enhancement and no internal echoes. These cysts are frequently multiple, occurring with similar frequency throughout the length of the epididymis (Fig. 6.27).

Spermatocele

The spermatoceles are benign cystic lesions, which contain spermatozoa, lymphocytes, and debris. Spermatoceles form as a result of efferent duct obstruction and usually located in the head of the epididymis. Ultrasonography cannot differentiate between epididymal cysts and spermatocele, but the spermatocele often has faint septations (Fig. 6.28).

Appendix Epididymis and Testis

The appendix epididymis originates from the mesonephric (Wolffian) duct and is seen associated with the epididymal head in 6% of ultrasound images. Sonography is important for distinguishing torsion of appendix epididymis which is self-limiting and does not threaten testicular viability. Clinically, the cremasteric reflex is preserved and a palpable nodule with bluish discoloration (blue dot) is often detected. Ultrasound shows a hyperechoic mass with central hypoechoic area adjacent to the testis or epididymis. Other associated findings include scrotal wall edema and epididymal enlargement. Blood flow in the peritesticular structures may be increased. The appendix testis is a Müllerian remnant. Doppler ultrasound is helpful to exclude torsion of the appendix testis since blood flow within the testis is normal in torsion of the appendix testis (Fig. 6.29).

Adenomatoid Tumor

Adenomatoid tumors are the most commontumors of the paratesticular tissues, Accounting for 30% of these lesions and up to 77% of the benign tumors arising from the epididymis. They are most commonly identified in men in their 20–40s. It has been suggested that they derive from vascular endothelium, the mesonephros, or Müllerian epithelium, although most recent reports consider them to be mesothelial in origin [43]. They are round, firm, smooth, discrete masses measuring 0.5–5 cm in diameter that are usually asymptomatic and slow growing. Ultrasonography can confirm the extratesticular nature of these masses. Adenomatoid tumors on ultrasound appears as an isoechoic mass with increased vascularity to the tumor (Fig. 6.30).

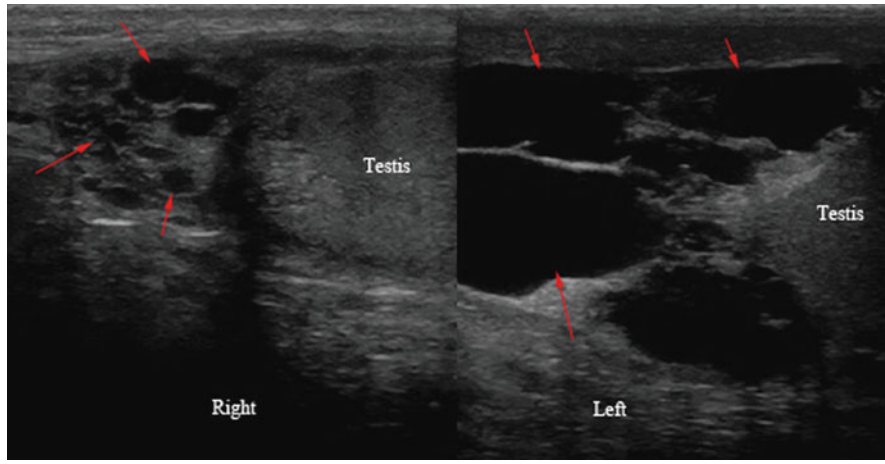

Fig. 6.27 Bilateral epididymal cysts: gray-scale ultrasound is showing hypoechoic cystic lesions (*arrows*) with no internal echoes in a patient with bilateral multiple epididymal cysts

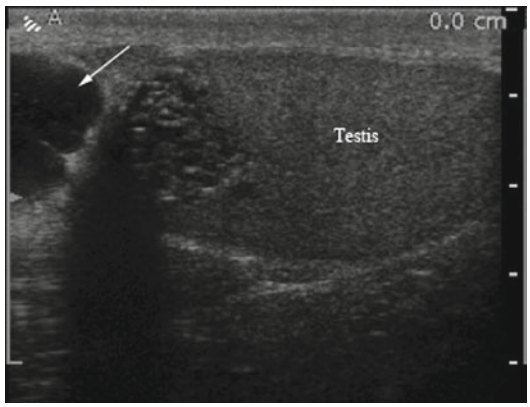

Fig. 6.28 Gray-scale ultrasound showing spermatocele with hypoechoic cystic lesion in the head of the epididymis (*arrow*)

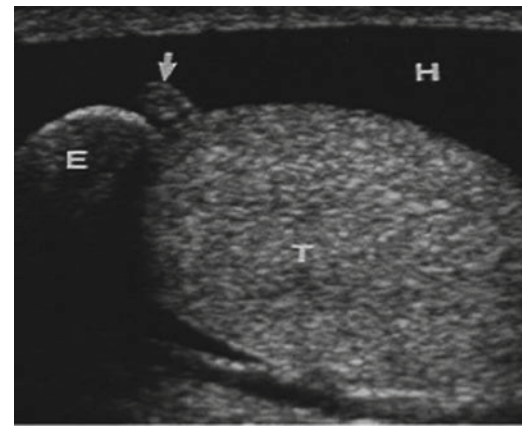

Fig. 6.29 Appendix of epididymis: ultrasound shows a hyperechoic mass with central hypoechoic area adjacent to the testis or epididymis. Inflammation of the appendix of epididymis is associated with hydrocele (H)

Papillary Cystadenoma

Papillary cystadenoma is a rare benign tumor of epithelial origin and is believed to arise from the efferent ductules of the head of the epididymis [44]. Papillary cystadenoma presents clinically as a firm, non-tender easily palpable mass in the epididymis. Two-thirds of papillary cystadenomas occur in patients with von Hippel-Lindau (VHL) syndrome and are frequently bilateral [45]. Unilateral presentation is seen very rarely in sporadic cases. These tumors are usually solid and echogenic on ultrasonography when they are small and hypoechoic and vascular, when large; however, a cystic appearance may also be seen occasionally [45].

Leiomyoma

Leiomyomas are benign epididymal solid tumors. Leiomyomas can also be bilateral and may accompany a hydrocele. These masses are smooth and firm and can grow to be large. The ultrasound appearance is a well-defined solid mass with heterogeneous echotexture located in paratesticular space.

Malignant Epididymal Lesions

Malignant tumors arising from the epididymis are very rare when compared to benign lesions with a proportion of 1:3 [46]. The exact incidence

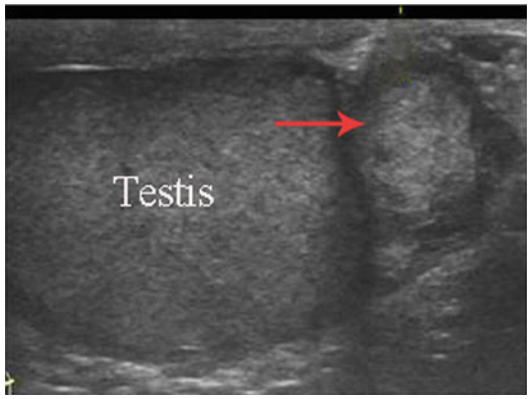

Fig. 6.30 Adenomatoid tumor of the testis shown as isoechoic mass in the lower pole of the testis

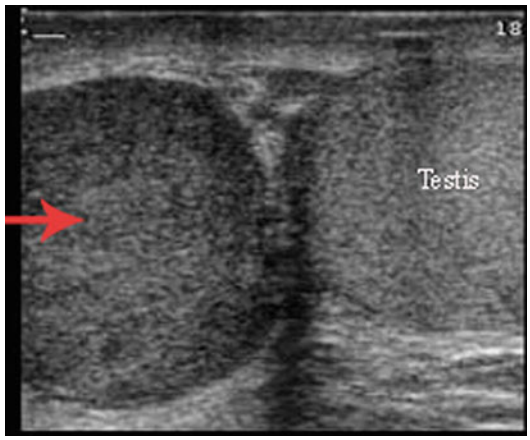

Fig. 6.31 Leiomyosarcoma of the epididymis: gray-scale ultrasound showing large hypoechoic mass in the epididymis with normal testis

of malignant tumors of the epididymis is uncertain because of the small number of reported cases.

Sarcoma of the Epididymis

More than half of the malignant neoplasms of the epididymis are sarcomas followed in frequency by carcinomas [46]. Fibrosarcoma of the epididymis has been reported in isolated case reports. Dowling et al. reported fibrosarcoma in a 60-year-old male confined to the epididymis on final pathology [47]. Leiomyosarcoma of the epididymis on ultrasound appears as a large hypoechoic mass (Fig. 6.31).

Clear Cell Carcinoma of the Epididymis

Primary clear cell carcinoma of the epididymis is very rare and has been reported in individual case reports. Kurihara et al. reported a unilateral scrotal mass histologically as a primary papillary adenocarcinoma of the epididymis with clear cell variant mimicking clear cell carcinoma of the kidney in an 82-year-old male. However, no evidence of renal cell carcinoma was found on repeated imaging studies [48]. Histologically these tumors are composed of complex tubulopapillary formations lined by cuboidal or columnar predominantly clear cells and may have large cysts with complex papillary glands lined by columnar cells with clear eosinophilic cytoplasm. Necrosis is common and the tumor may have invasive margins.

Testicular Lesions

Benign Lesions of the Testis

Testicular Torsion

Torsion occurs most frequently in adolescent boys, two-thirds of cases occur between 12 and 18 years of age. Acute scrotal symptoms in young boys are caused by epididymitis in 70% of cases. Ultrasound is helpful to differentiate testicular torsion from other causes of acute scrotal pain. The severity of torsion of the testis can range from 180 to 720°, but complete occlusion of blood flow is thought to occur after 450° of torsion [7]. Transient or intermittent torsion with spontaneous resolution sometimes occurs. Venous congestion or occlusion progresses to arterial occlusion, testicular ischemia, and infarction. The collateral blood flow is typically not adequate to provide viability to the testicle if the testicular artery is occluded.

Testicular torsion can be classified as extravaginal or intravaginal. The extravaginal form of torsion is found exclusively in newborn infants. Intravaginal torsion is more common and is due to a bell-and-clapper deformity in which the tunica vaginalis has an abnormally high insertion on the spermatic cord and completely encircles the testis, leaving the testis free to rotate within

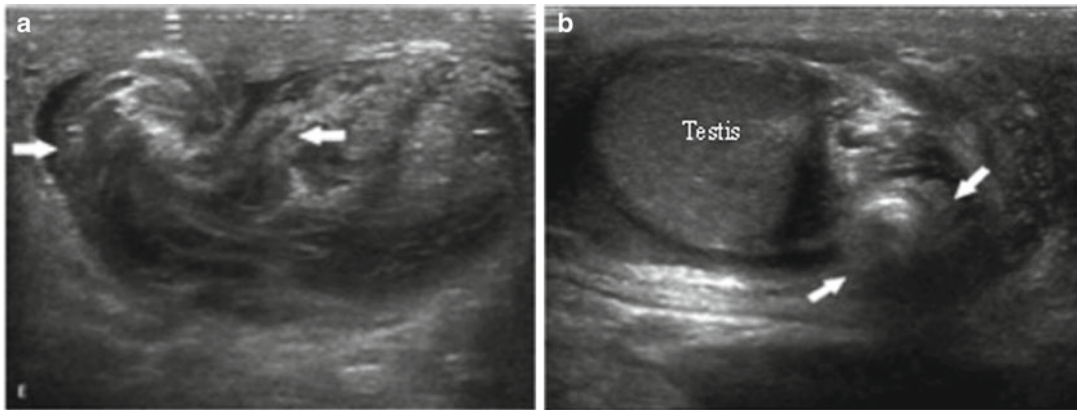

Fig. 6.32 (**a**, **b**) The spermatic cord immediately cranial to the testis and epididymis is twisted, which gives it a characteristic "torsion knot" or "whirlpool appearance" on gray-scale ultrasound

the tunica vaginalis. The deformity is bilateral in most cases. The spermatic cord immediately cranial to the testis and epididymis is twisted, which gives it a characteristic "torsion knot" or "whirlpool appearance" (Fig. 6.32a, b).

Intravaginal torsion may also occur in testes that are retractile or are not fully descended. Blunt trauma, sudden forceful rotation of the body, or sudden exertion also predispose to testicular torsion.

The torsion of a testicular or epididymal appendage is thought to be more common than torsion of the spermatic cord; the latter represents a true urologic emergency. There is a 90% chance of salvaging the testicle when ischemia has been present for less than 6 h, which decreases to 50% at 12 h and 10% at 24 h [49]. While irreversible testicular damage is presumed after 4 h of spermatic cord torsion, only 50% of men who were detorsed less than 4 h after their symptoms began were noted to have normal semen quality [50].

Torsion is a clinical diagnosis proven at surgery. Ultrasound does not diagnose torsion—only the urologist (or pathologist) can. Ultrasound should only be used to document findings. Many conditions (such as torsion–detorsion, intermittent torsion, persistent capsular flow, and color flow artifacts) can suggest apparent flow in the testicular parenchyma in cases where there is no viability sustaining.

Waldert et al. reported 298 boys presenting with an acute scrotum who underwent color flow study performed by urologists and then underwent exploratory surgery regardless of the sonographic findings. At surgery, 20% of boys were diagnosed with testicular torsion with 56% found with torsion of an appendage and 8% noted with epididymitis and 11% had no definite surgical diagnosis. Color Doppler sonography sensitivity, specificity, positive predictive value, and negative predictive value for testicular torsion were 96.8, 97.9, 92.1, and 99.1%, respectively. The two boys misdiagnosed as epididymo-orchitis were both noted with 90° torsion and no venous drainage but with residual arterial flow. Eighty-five percent of all testes were salvaged. Those with viable testes presented with a 4 h median duration of symptoms [51].

On gray-scale ultrasound, the affected testis usually appears hypoechoic (Fig. 6.33) and Doppler color flow study shows decreased or no flow in the affected testis (Fig. 6.34). Testicular size can vary from increased to decreased when compared to its counterpart depending upon the duration of the torsion. The sonographer should always compare the affected testis with the contralateral side using longitudinal, transverse, and coronal views. When the sonographer attempts to align the transducer parallel to flow, apical views can be particularly informative. Spectral waveform analysis with calculation of the RI is also helpful, but as stated previously, is not diagnostic. In patients with acute torsion, the epididymis may appear hypoechoic and enlarged, similar to epididymitis.

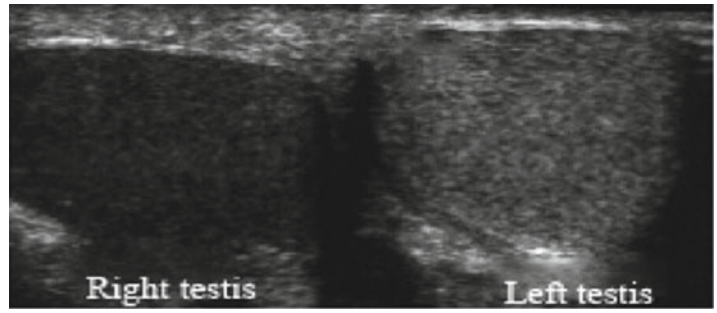

Fig. 6.33 Right testicular torsion with normal left testis for comparison of the echogenicity on gray-scale ultrasonogram

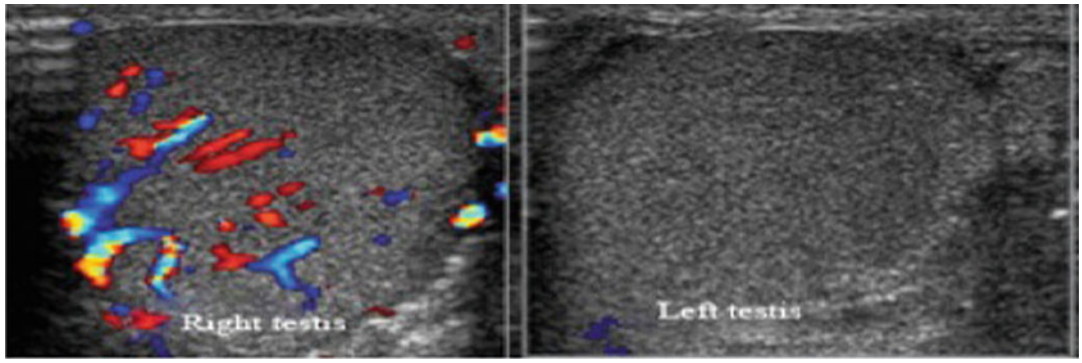

Fig. 6.34 Left testicular torsion: color Doppler ultrasound shows absent blood flow in the left testis

Primary Orchitis

The ultrasound findings in patients with orchitis include an enlarged testis with a homogenous appearance and a decreased resistive index (RI). The RI of the epididymal and testicular artery has been shown to be significantly lower in patients with epididymo-orchitis than in control subjects [52]. Orchitis may be diffuse or focal appearing as multiple hypoechoic lesions with increased testicular blood flow (Figs. 6.35 and 6.36). If inflammation progresses the pressure of intratesticular edema may compromise blood flow leading to infarction and ultrasound will demonstrate the absence of blood flow and surrounding reactive hyperemia [53].

Testicular Abscess

Persistent fever, scrotal pain, and swelling can be seen in approximately 5% of patients originally presenting with orchitis. These are the clinical hallmarks of a testicular abscess. The characteristic ultrasound appearance of a testicular abscess usually appears within 1–7 weeks after orchitis.

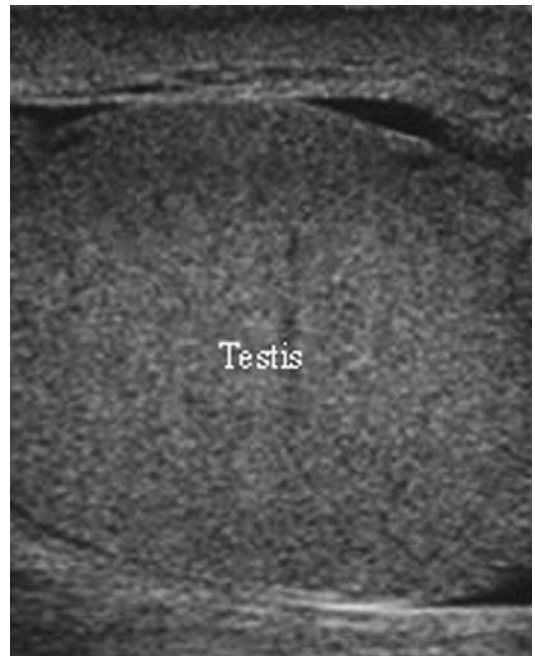

Fig. 6.35 Orchitis: gray-scale ultrasound showing homogenous enlargement of the testis with minimal hydrocele

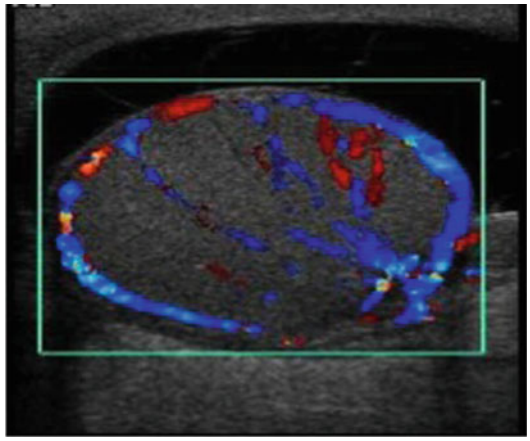

Fig. 6.36 Color Doppler study shows increased blood flow to the testicle with prominent capsular vessels

Ineffective treatment of epididymo-orchitis may result in a pyocele or a testicular or scrotal abscess, testicular infarction, and possibly fasciitis. A scrotal abscess may resemble a tumor; however, sonographic evidence of inflammation, as described above, and the absence of Doppler flow will often differentiate abscess from the tumor (Fig. 6.37).

Nonpalpable Testis

When the testis is nonpalpable in the scrotum, a search is initiated to confirm its presence or absence. Ultrasound is usually the initial diagnostic imaging modality because of its sensitivity in the inguinal canal where most undescended testes are found. If the absent testis is not identified within the inguinal canal, CT or MRI is often used in an attempt to locate an intra-abdominal testis. Surgical exploration, however, remains the "gold standard" for identifying an intra-abdominal testis.

A cryptorchid testis in the inguinal canal, identified by the presence of the mediastinum testis, is usually small in size (hypotrophic). It can be differentiated from an inguinal hernia by the absence of peristalsis, highly reflective omental fat, or both.

Testicular Microcalcification

The etiology of testicular microcalcification (TM) is unknown. It has been suggested that the calcified concretions within the lumen of seminiferous tubules originate from sloughing of degenerated intratubular cells and failure of the Sertoli cells to phagocytize the debris [54, 55].

Testicular microcalcification (TM) has been defined as five or more microcalcifications within the testicular parenchyma. TM appears on ultrasound as hyperechogenic lesions measuring between 1 and 3 mm-sized multiple foci within the testicular parenchyma. The prevalence of TM varies from 1.5 to 5.6% in asymptomatic healthy men, compared with 0.8–20% in infertile men [56]. Acoustic shadowing on ultrasound is often absent, likely due to the small size of the calcifications [57, 58] (Figs. 6.38 and 6.39). They are usually symmetrical but occur unilaterally in 20% of the cases. Goede et al. reported 2.4% prevalence of TM in young asymptomatic boys [59].

The risk of subsequent development of carcinoma in situ (CIS) and testicular germ cell tumor in patients presenting with TM is less clear [58, 60]. The association between TM and testicular germ cell tumors is well documented in several case studies. DeCastro et al. reported the prevalence of TM in healthy asymptomatic men aged between 18 and 35 years as 5.6% with an odds ratio of developing a testicular cancer of 317 compared with men with no TM on their 5 year follow-up study [61].

TM is also described in association with various benign conditions including varicocele, cryptorchidism, male pseudohermaphroditism, Klinefelter's syndrome, neurofibromatosis, and Down's syndrome [62].

Data from several investigators suggest that TM is a benign, nonprogressive condition, at least when followed for up to 45 months [61, 63]. However, several recent case reports have documented the development of testicular tumors in patients with TM when follow-up was extended for several years, suggesting the need for close follow-up in these patients [61, 64].

Bennett et al. demonstrated a direct relationship between the quantity of microliths and the incidence of testicular tumor at the initial presentation [65].

The risk of CIS of testis in men with history of undescended testis is approximately 2–4% [66]. If TM is present in these patients, the risk increases to 10% [67].

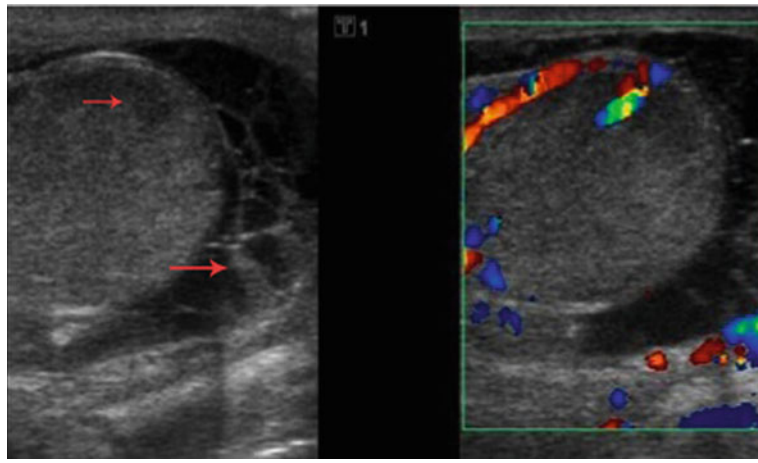

Fig. 6.37 Ultrasound findings show heterogeneous complex septate fluid collection. Color Doppler ultrasound shows no blood flow in the abscess and increased blood flow in the surrounding testicular parenchyma

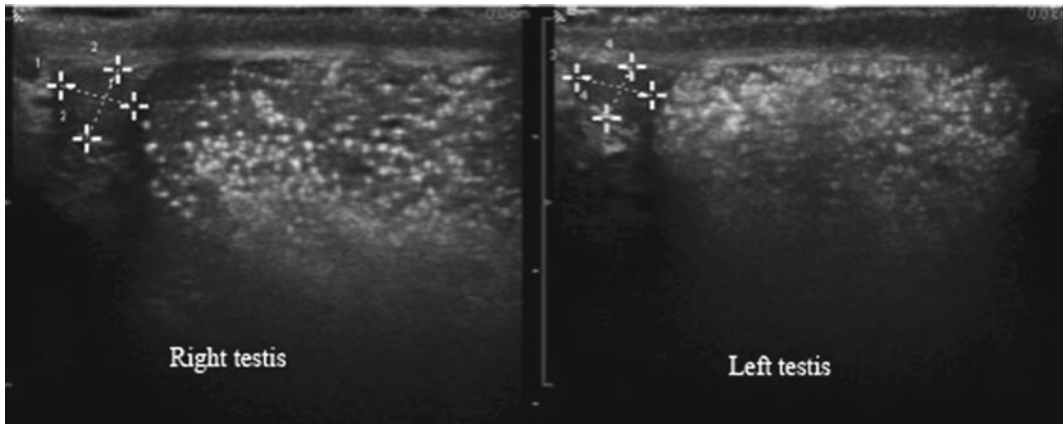

Fig. 6.38 Bilateral multiple microcalcifications of the testis with no acoustic shadowing

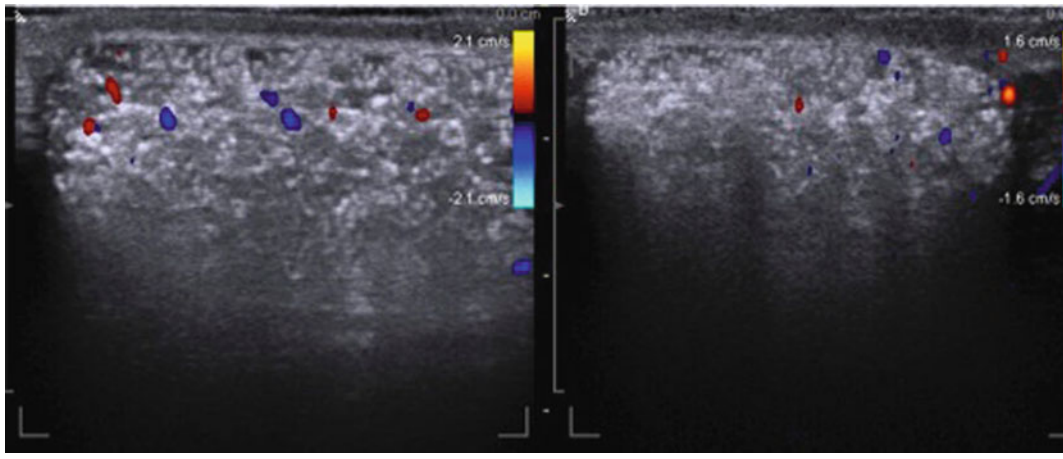

Fig. 6.39 Color Doppler study showing multiple microcalcifications

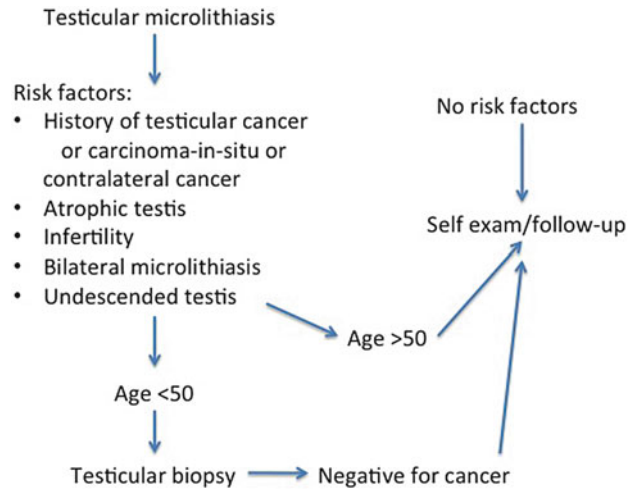

Fig. 6.40 Management of testicular microlithiasis

In men with infertility, atrophic testis, undescended testis, bilateral TM, and history of CIS or testicular cancer who have contralateral TM, there is an increased risk of developing a testicular cancer [56].

Men with TM and associated risk factors should be considered for long-term follow-up including testicular biopsy as indicated. Testicular microcalcification management and a follow-up algorithm have been shown in Fig. 6.40.

Testicular Macrocalcification

Intratesticular macrocalcifications can be secondary to the presence of a germ cell tumor, a "burnt-out" germ cell tumor, a Sertoli cell tumor, prior trauma, infection (TB), infarction, or inflammation (e.g., sarcoidosis) [68].

One theory to explain the genesis of the burned-out tumor suggests that the tumor outgrows its own blood supply and then subsequently involutes with fibrosis and dystrophic calcification [69] (Fig. 6.41).

Extratesticular calcifications can be found with the tunica vaginalis space and can result from inflammation of the tunica vaginalis or from a sloughed testicular appendage. These calcifications can be freely mobile and are known as scrotal pearls or scrotoliths.

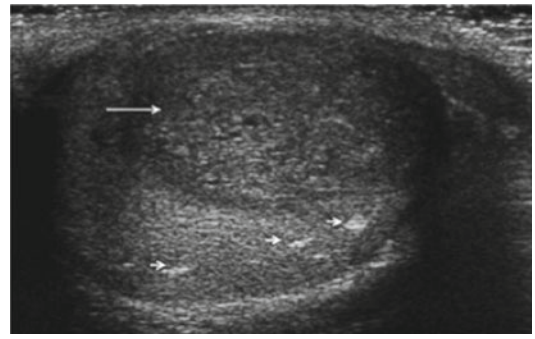

Fig. 6.41 Mixed germ cell tumor of the testis with areas of burnt-out tumor (*small arrows*)

Cystic Lesions

Testicular Cysts

Testicular cysts occur in approximately 8–10% of patients [70]. They are mostly benign cysts associated with extratesticular spermatoceles often incidentally found on ultrasound [71]. The common causes for the testicular cysts include trauma, surgery, and inflammation. They usually occur at the mediastinum testis and are simple cysts on ultrasound; testicular cysts have an imperceptible wall, and display an anechoic through transmission, with sizes ranging from 2 mm to 2 cm in diameter [72] (Fig. 6.42).

Cystic teratoma may resemble testicular cysts but appear on ultrasound as a cystic mass with solid

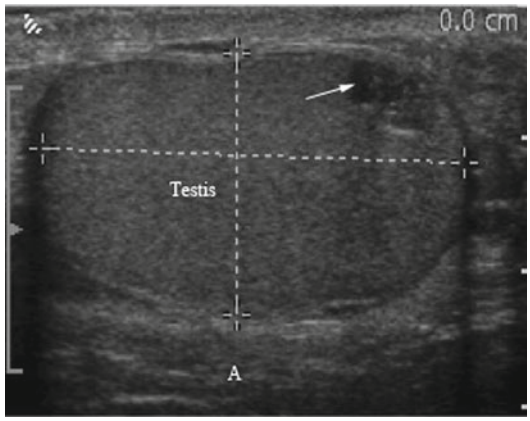

Fig. 6.42 Testicular cysts are benign simple cysts often secondary to trauma, surgery, or inflammation

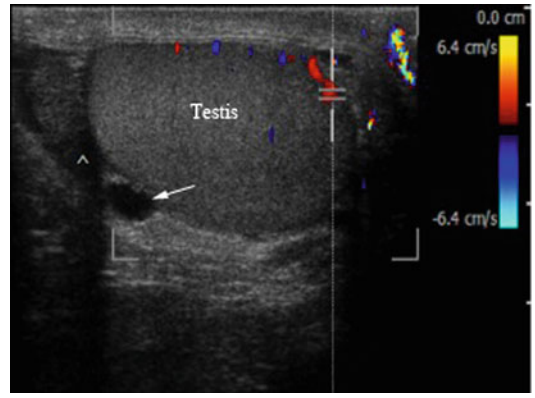

Fig. 6.44 Tunica albuginea cyst is within the layers of the tunica. They appear as simple cysts on ultrasound (*arrow*)

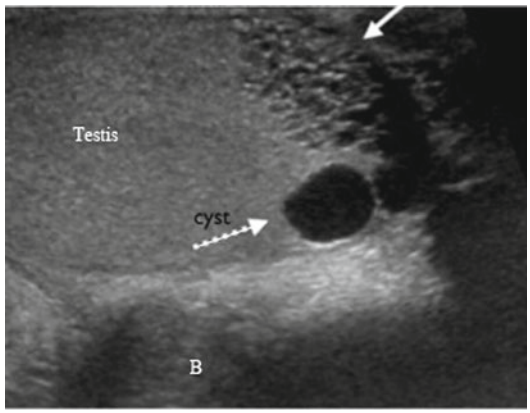

Fig. 6.43 Cystic teratoma on ultrasound appears as a cystic mass with solid components and the mass localized within the testicular parenchyma

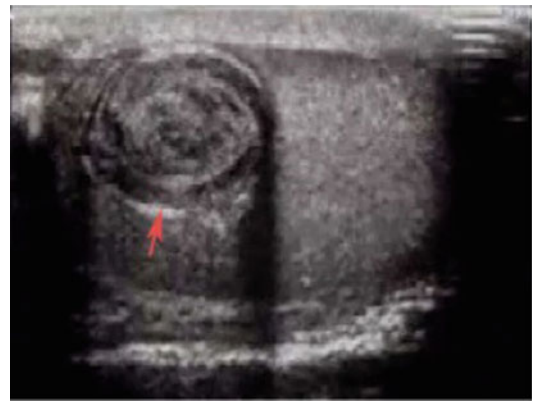

Fig. 6.45 The characteristic sonographic appearance of the epidermoid cyst—an onion ring configuration due to alternating layers of hypo- and hyperechogenicity

components. Cystic teratoma occurs in children and adults. In children, cystic teratoma behaves as a benign tumor, whereas in adults and adolescents it has been known to metastasize [73] (Fig. 6.43).

Cysts of the Tunica Albuginea

Tunica albuginea cysts arise from within the layers of the tunica albuginea. They are benign cysts and are clinically palpable by virtue of their location. These cysts meet the criteria for a simple cyst by ultrasound [74, 75] (Fig. 6.44).

Epidermoid Cysts

Epidermoid cysts of the testis are rare benign germ cell tumors, accounting for 1–2% of resected benign tumors of the testis. Epidermoid cysts usually present between 20 and 40 years of age. They are often unilateral; bilateral occurrences are very rare [76].

Epidermoid cysts are variable on sonographic appearance attributable to variations in maturation and keratin content. The characteristic sonographic appearance of the epidermoid cyst is an onion ring configuration due to alternating layers of hypo- and hyperechogenicity without internal flow [9, 77, 78] (Figs. 6.45 and 6.46). An epidermoid cyst of less than 3 cm in size with negative tumor markers can be managed conservatively by enucleation provided that frozen sections are obtained to confirm the diagnosis [79].

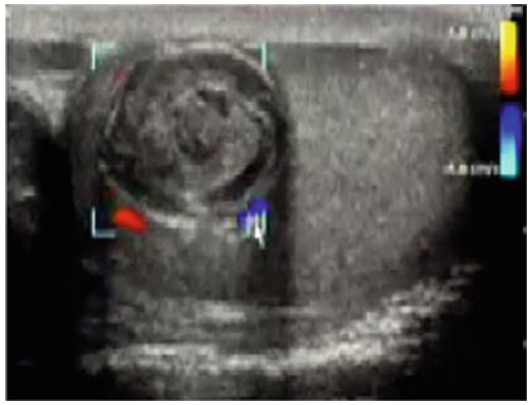

Fig. 6.46 Doppler flow study shows no blood flow in the mass

Tubular Ectasia of Rete Testis

Tubular ectasia of the rete testis (TERT) is a benign clinical entity in which cystic dilation of rete testis results from partial or complete obliteration of the efferent ducts. The pathogenesis is thought to be due to obstruction at the level of, or distal to, the efferent ductules at the epididymal head. This subsequently leads to dilation in the proximal ductal system manifesting as tubular ectasia [80, 81].

TERT often present an asymptomatic finding in men older than 50 years with unremarkable physical examination of the testes. It is often bilateral and asymmetric, and it is identified by its typical location in or around the mediastinum testis. On ultrasound, it is seen as multiple anechoic, avascular structures within the mediastinum and is often associated with ipsilateral spermatoceles [77] (Figs. 6.47 and 6.48). It is important to differentiate this benign cystic tumor from malignant cystic tumors of the testis and thus avoid unnecessary orchidectomy. Cystic malignant tumors, most commonly the cystic teratomas, can be distinguished sonographically by the presence of multiple cystic areas, often surrounded by a soft tissue mass. They are almost always unilateral and are anywhere in testicular parenchyma, not limited to the mediastinum [82]. They can be further confirmed by measuring serum tumor markers.

Intratesticular Varicocele

Intratesticular varicocele has been defined as dilated veins radiating from the mediastinum testis into the testicular parenchyma [83, 84]. It is often a clinically occult condition that may occur in association with extratesticular varicocele. The sonographic features of intratesticular varicoceles are similar to those of extratesticular varicoceles. Color flow Doppler sonography demonstrates tubular or serpentine vascular structures more than 2 mm in diameter with a positive Valsalva maneuver (Figs. 6.49 and 6.50). Kessler et al. reported that the Valsalva maneuver plays an important role in the diagnosis of intratesticular varicocele because in most cases the retrograde flow will not show up spontaneously on color flow Doppler sonography [85]. Patients with intratesticular varicocele may have testicular pain in up to 50% of cases secondary to venous congestion, resulting in stretching of the tunica albuginea. Bucci et al. reported a 2% incidence of intratesticular varicocele in their series of 342 patients who were evaluated with color Doppler ultrasound as part of a fertility evaluation [84].

Das et al. found 39% bilateral intratesticular varicoceles in a large cohort of 1,040 men who underwent scrotal ultrasound [86]. Color flow Doppler sonography helps to differentiate intratesticular varicocele from the tubular ectasia of rete testis adjacent to the mediastinum.

Intratesticular Abscess

Patients with an intratesticular abscess present with an acutely painful scrotum and associated fever. An intratesticular abscess most frequently results from epididymo-orchitis [87]. Ultrasonography is the imaging modality of choice and demonstrates a hypoechoic lesion within the testis marked by low-level echoes and shaggy margins. Color flow Doppler demonstrates absent vascularity in the abscess with increased peripheral hyperemia [72].

Intratesticular Hematoma

Blunt trauma of the scrotum is a common injury among younger men. Physical examination may be difficult in these patients with scrotal trauma due to tenderness and swelling of the scrotum. Scrotal ultrasound is the standard imaging modality to evaluate testicular integrity. The sensitivity and specificity of ultrasonography for testicular

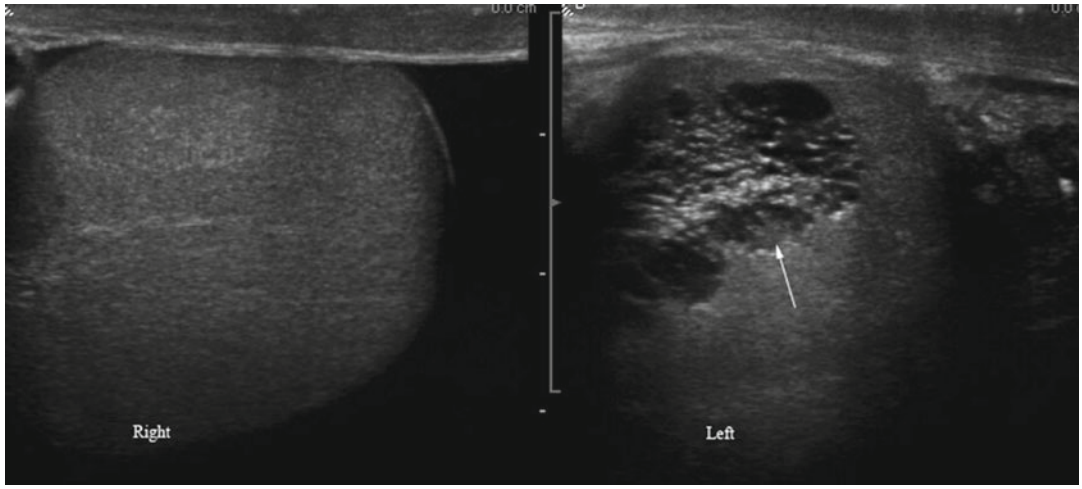

Fig. 6.47 Left-sided tubular ectasia of the rete testis on gray-scale ultrasound (*arrow*)

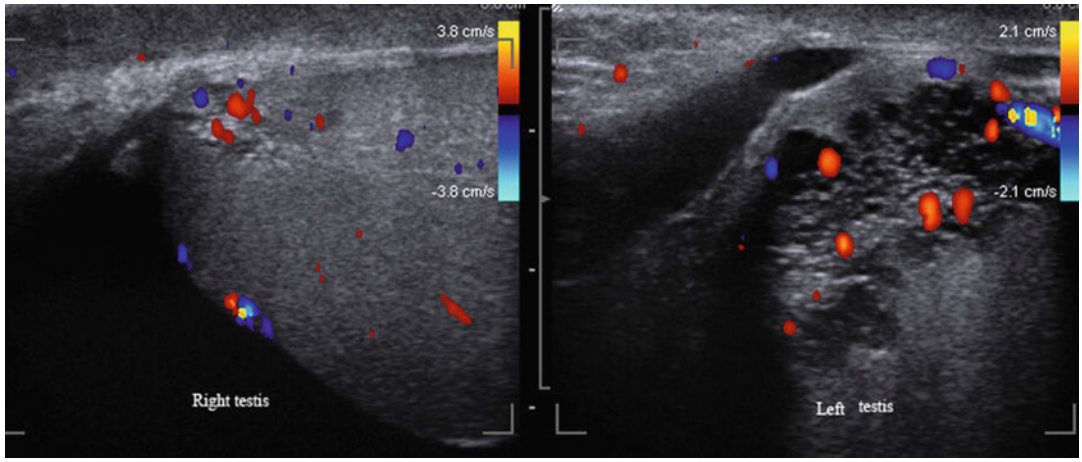

Fig. 6.48 Doppler color flow study shows normal blood flow to the tubular ectasia of the rete testis

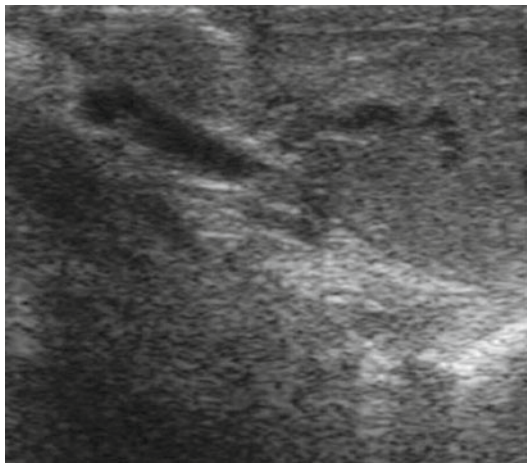

Fig. 6.49 Intratesticular varicoceles are dilated veins within the testicular parenchyma. Gray-scale ultrasound shows dilated veins

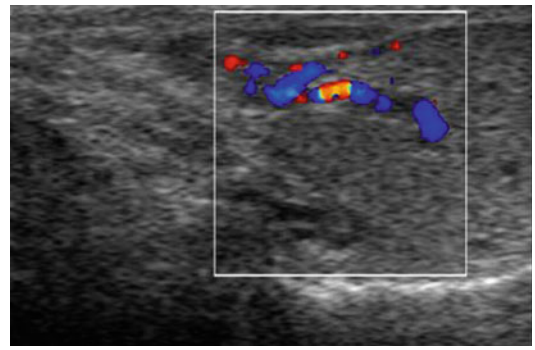

Fig. 6.50 Color Doppler flow study showing dilated intratesticular veins

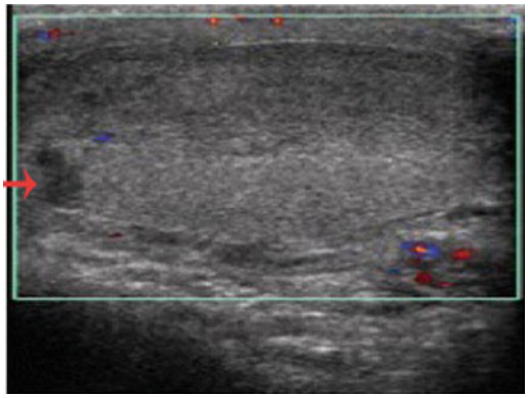

Fig. 6.51 Intratesticular hematoma: gray-scale ultrasound showing hypoechoic area on longitudinal and mid-transverse views with no blood flow on Doppler color flow study

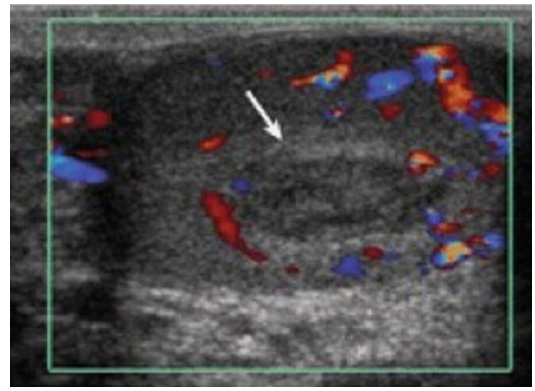

Fig. 6.52 Intratesticular hematoma: gray-scale ultrasound showing hypoechoic area on longitudinal and mid-transverse views with no blood flow on Doppler color flow study

hematoma has been reported to be 93.5 and 100%, respectively.

Intratesticular hematoma can be diagnosed with gray-scale ultrasound, which demonstrates an intact tunica albuginea with intratesticular hypoechoic areas showing no blood flow on Doppler color flow study (Figs. 6.51 and 6.52).

Congenital Testicular Adrenal Rests

Congenital adrenal hyperplasia (CAH) is an autosomal recessive disease characterized by deficiency of adrenocortical enzymes. More than 90% of cases of CAH are caused by 21-hydroxylase deficiency [88, 89]. Congenital testicular adrenal rests are seen in about 29% of patients with CAH [90]. An increase in adrenocorticotropic hormone (ACTH) levels causes hyperplasia of adrenal remnants in the testes in patients with CAH and results in the development of intratesticular masses. Sonographically, these masses appear as hypoechoic intratesticular masses in both testes and Doppler color flow shows increased vascularity [90, 91] (Figs. 6.53 and 6.54). Intratesticular masses are typically located in the region of the mediastinum testis [91]. Scrotal ultrasound is the diagnostic modality of choice for their diagnosis. Congenital testicular adrenal rests most commonly present as bilateral intratesticular masses. The differential diagnosis for these masses includes testicular tumors, which are extremely rare on both testes [59]. Therefore, congenital adrenal rests must be considered in patients with CAH and clinically followed by ultrasound to demonstrate stable masses [92]. These masses typically regress with treatment.

Sarcoidosis

Involvement of the testis and epididymis with sarcoid is rare. Clinically it presents as a painless epididymal or testicular mass or as epididymitis. Sonographically the lesion is an irregular hypoechoic mass that may be calcified, multifocal, and bilateral [93].

Malignant Lesions of the Testis

Testicular malignancies are accounts for approximately 1% of all the malignancies in men. The predicted 5-year survival rate is currently at 95.3%, due to early patient self-detection and testicular tumor sensitivity to chemotherapy and radiotherapy. The most common presentation is of a painless scrotal mass, with pain being reported in only 10% of cases [94]. Ultrasonography is the gold standard imaging modality. Early diagnosis is crucial to a favorable outcome.

Germ Cell Tumors

Germ cell tumors account for 95% of testicular malignancies and can be divided into seminomatous and nonseminomatous groups; the remainder is made up of sex cord-stromal tumors, lymphoma, and metastases.

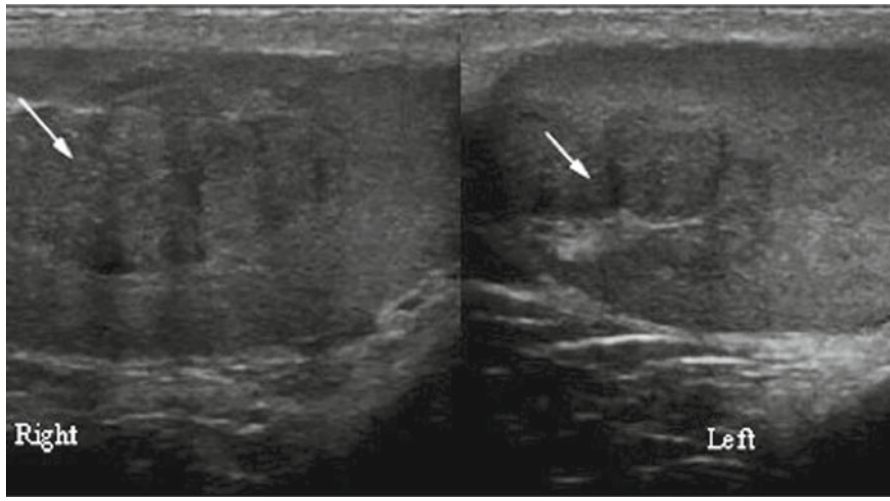

Fig. 6.53 Testicular adrenal rests are typically bilateral. Ultrasound features are hypoechoic lesions located in the region of the mediastinum testis (*arrow*)

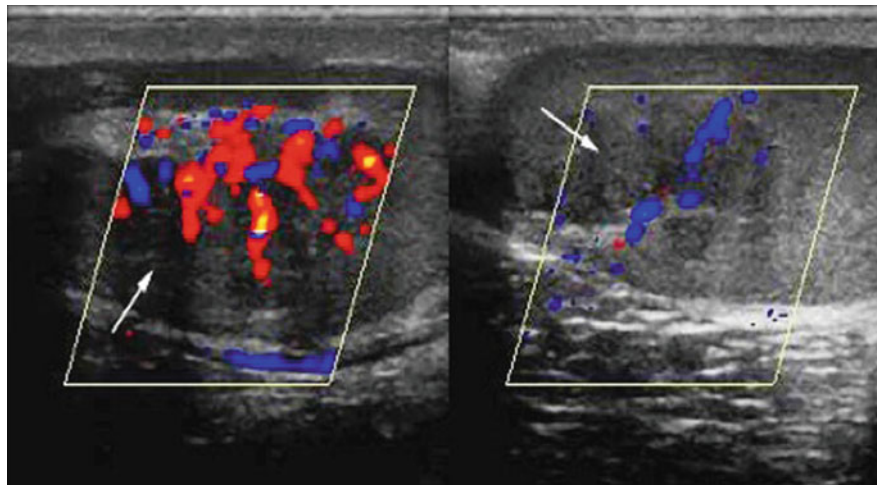

Fig. 6.54 Testicular adrenal rests: Doppler color flow study shows increased vascularity

Seminoma

Seminoma is the most common germ cell tumor, accounting for up to 50% of all germ cell tumors, and occurs in men predominantly between the ages of 35 and 45. Bilateral seminomatous germ cell tumors are rare and are reported only in 2% of the cases [95]. They commonly present as a painless scrotal mass. On gross pathology, they are lobulated and pale in color and may vary in size from small well-defined lesions to masses that completely replace normal testicular parenchyma. Microscopically, the cells are comparatively uniform with clear cytoplasm and a characteristic lymphocyte infiltration [95].

The sonographic appearance typically is a homogenous, well-defined hypoechoic lesion. Cystic areas are found only in 10% of cases [96]. Larger tumors tend to be more heterogeneous and may be poorly marginated and diffusely infiltrative and multifocal (Figs. 6.55 and 6.56).

Nonseminomatous Germ Cell Tumors

Nonseminomatous germ cell tumors (NSGCT) generally occur in younger men between ages 25

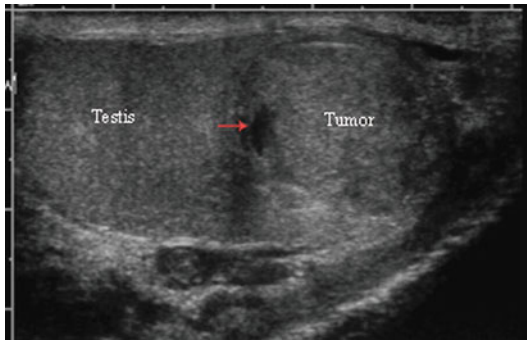

Fig. 6.55 Testicular germ cell tumor showing heterogeneous appearance on gray-scale ultrasound

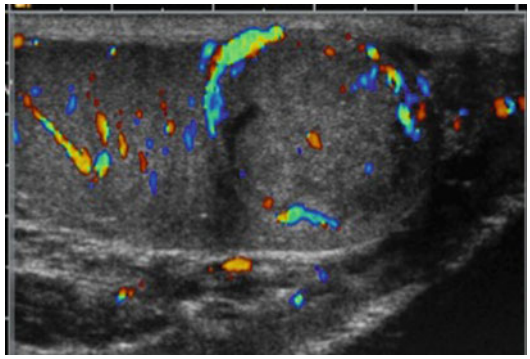

Fig. 6.56 Doppler flow study shows increased blood flow within the tumor

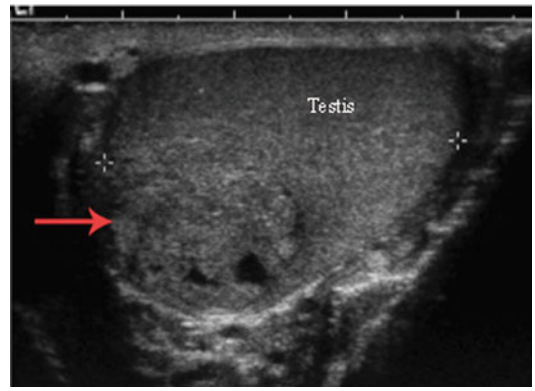

Fig. 6.57 Non-seminomatous germ cell tumor showing heterogeneous appearance on gray-scale ultrasound

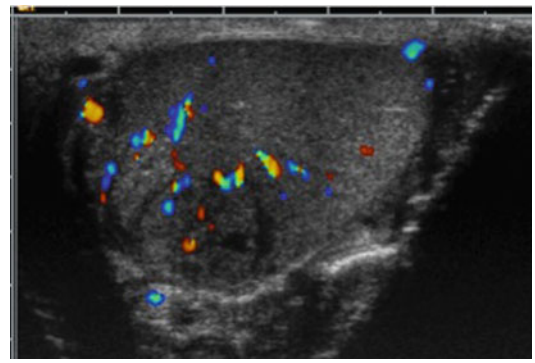

Fig. 6.58 Color Doppler flow study shows increased blood flow within the tumor

and 35. NSGCT are often mixed germ cell tumors comprised of embryonal carcinoma, yolk sac tumor, choriocarcinoma, and teratoma. They can be locally aggressive with invasion of the tunica albuginea, epididymis, or the spermatic cord.

The ultrasonographic findings reflect the diversity of the components and the tumors characteristically appear irregular with a heterogeneous parenchyma pattern, representing calcification, hemorrhage, fibrosis, and cystic lesions [97, 98] (Figs. 6.57 and 6.58).

Pure embryonal cell carcinoma makes up 2–3% of all germ cell tumors. An embryonal cell carcinoma is an aggressive tumor with ultrasonographic findings often demonstrating heterogeneous echo texture. These tumors are characteristically smaller in size than a seminoma usually without enlargement of the testis [99].

Yolk sac tumors also known as endodermal sinus tumors, usually occur in children younger than 2 years [99]. Histologically, yolk sac tumors are predominantly solid, yellow-gray friable tumors with a characteristic but highly variable range of histological patterns [100].

Yolk sac tumor shows periodic acid-Schiff (PAS) positive globules, focal areas of positive alpha-fetoprotein immunostaining, prominent intracellular and extracellular hyaline globules, and Schiller-Duval bodies (SD bodies), characterized by a small central blood vessel surrounded by two layers of tumor cells [100, 101]. The sonographic appearance of yolk sac tumors of the testis is nonspecific; thus it is difficult to differentiate from other solid tumors of the testes based solely on sonography.

Choriocarcinoma is associated with an elevated human chorionic gonadotropin level and carries the worst prognosis of all germ cell

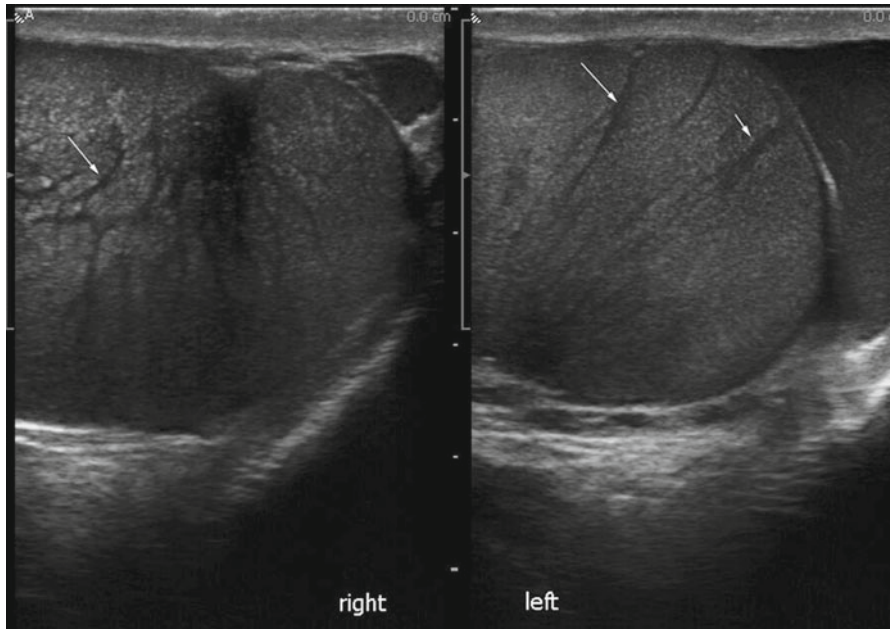

Fig. 6.59 Gray-scale ultrasound showing bilateral testicular lymphoma. Right testis was measuring 64.5 cm^3 and the left testis was measuring 69.0 cm^3. *Arrows* showing dilated vascular markings

tumors, with early metastatic spread to the lung, liver, gastrointestinal tract, and brain.

Teratoma is the second most common pediatric testicular tumor. Mature teratoma is often benign in children. Teratoma will demonstrate endodermal, mesodermal, and ectodermal components in a disorganized arrangement [97]. Echogenic foci in these tumors represent elements of its embryologic composition—immature bone, fat, and fibrosis.

Non-germ cell tumors are rare, but most commonly arise from Leydig or Sertoli cells. Leydig cells are the principle source of male testosterone. Leydig cell tumors represent fewer than 3% of all testis tumors.

Sertoli cell tumors represent approximately 1% of testicular tumors and can occur in children and adults. In addition to a testicular mass, gynecomastia frequently develops. Leydig or Sertoli cell tumors are rarely malignant.

Testis-sparing resection can be considered in these patients. Intraoperative ultrasonography is an essential component of organ-preserving surgery for nonmalignant testicular tumors.

Testicular Lymphoma

Primary testicular lymphoma is the most common testicular malignancy in men aged >60 [102–104].

The most common histological type is large B-cell non-Hodgkin's lymphoma. Scrotal ultrasound demonstrates diffuse enlargement of the testis and the Doppler color flow study shows increased vascularity (Figs. 6.59 and 6.60a).

Orchiectomy has historically been advocated as the diagnostic and therapeutic procedure of choice. This treatment recommendation was recently changed to a combined modality of systemic doxorubicin-based chemotherapy, prophylactic intrathecal chemotherapy, and orchidectomy or scrotal radiotherapy [103].

Incidentally Discovered Nonpalpable Testicular Lesions

Incidentally noted solid testicular masses that are not palpable are usually benign (Table 6.2). Significant risk factors for the presence of malignancy include size >1 cm, ipsilateral atrophy, history of cryptorchidism, history of contralateral

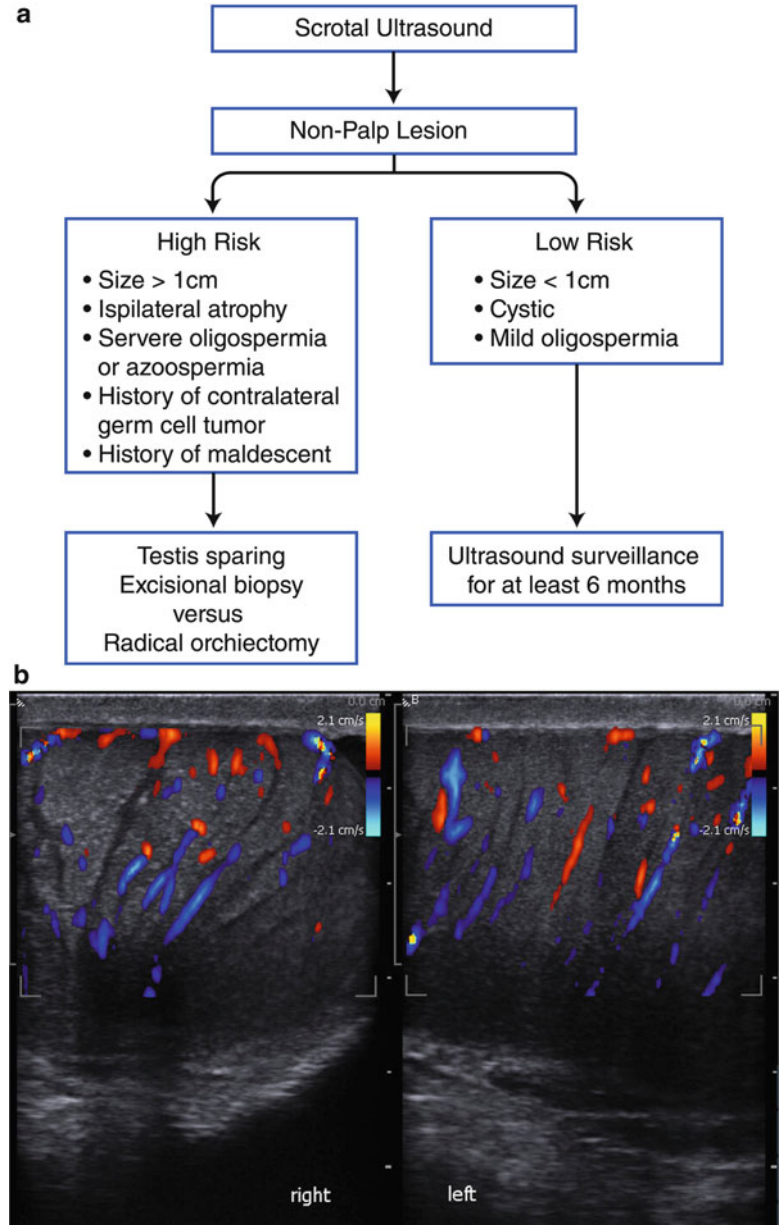

Fig. 6.60 (**a**) Management of incidental finding of nonpalpable testicular mass. (**b**) Doppler color flow study showing increased vascularity in both the testes

germ cell tumor, and severe oligospermia or azoospermia [105]. Patients at low risk for malignancy can be managed with active ultrasound surveillance for at least 6 months. If during the active surveillance period, the lesion size should increase significantly, then testis-sparing excisional biopsy or radical orchiectomy must be considered [106, 107]. Figure 6.60b depicts a rational approach to the evaluation of the nonpalpable testicular lesion. Patients at high risk can be managed with ultrasound-guided testis-sparing excisional biopsy or radical orchiectomy (Mammen et al. AUA Update Series, pages 14–19, 2009) [108] (Fig. 6.61).

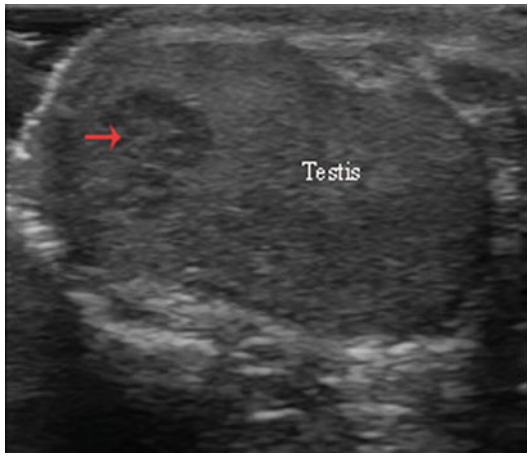

Fig. 6.61 Non-palpable intratesticular tumor shown as a hypoechoic lesion on gray-scale ultrasound

Special Indications

Male Infertility

In men with impaired fertility, ultrasound can provide diagnostic information and provide documentation prior to and after intervention. Additionally, recent literature supports the use of spectral Doppler ultrasound in providing information about intratesticular blood flow and function [14, 52, 109, 110].

Varicocele

A varicocele is a dilatation of the testicular vein and the pampiniform venous plexus within the spermatic cord. With bilateral varicoceles, the larger varicocele is often on the left side, most likely related to the angle of insertion in to the left renal vein and the length of the left testicular vein [111, 112]. The left testicular vein is 8–10 cm longer than the right, with a proportional increase in pressure head. Varicoceles have been found to be a bilateral condition in more than 80% of cases in some series [112, 113].

Congenitally absent or incompetent venous valves have been thought to be the primary cause of varicocele. Subsequent studies have shown that there are men who have incompetent or absent testicular vein valves without varicocele and men with varicocele who have competent valves [114, 115]. Dilation of the testicular vein can cause functional incompetence as a result of loss of coaptation, even with the normal venous valves [116]. However, it remains difficult to differentiate between cause and effect in anatomic analysis, as evidenced by recent studies, which documented significant histologic changes in the vein wall of the pampiniform plexus that appeared to have a linear correlation with the varicocele grade [117] (Fig. 6.62).

The most common presentation of a varicocele is due to an investigation of male subfertility and less frequently due to scrotal pain. A varicocele is present in about 15% of normally fertile men, in 30–40% of men with primary subfertility, and in as many as 80% of men with secondary subfertility [118, 119]. Clinically significant varicoceles are associated with impairments in semen quality that can include a decrease in sperm count, sperm motility, and the number of morphologically normal sperm. In particular, an increased number of tapered (elongated) heads with an increase in the number of immature (round) germinal forms appearing in the ejaculate are usually present [118].

Clinically detectable varicocele has been associated with testicular hypotrophy or atrophy, an abnormal gonadotropin axis, histologic changes in the testis, abnormal spermatogenesis, and infertility. The exact mechanism whereby a varicocele induces pathologic change has yet to be elucidated [120]. However, increased testicular temperature, hypoxia, reflux of adrenal and renal metabolites, and the generation of reactive oxygen species (ROS) have been postulated as possible effects of a varicocele on spermatogenesis [120].

Ultrasound characteristics include the findings of multiple, hypoechoic serpiginous tubular structures of varying diameters best visualized superior and posterolateral to the testis [121]. Color flow Doppler is important in documenting the presence and size of a varicocele as well as differentiating an intratesticular varicocele from a dilated rete testis [86, 122]. The presence of bilateral varicoceles is often best identified by scrotal ultrasound [123, 124] (Figs. 6.63 and 6.64a). Tarhan et al. reported an increase in blood flow velocity in the testicular artery and decrease in resistive indices in the

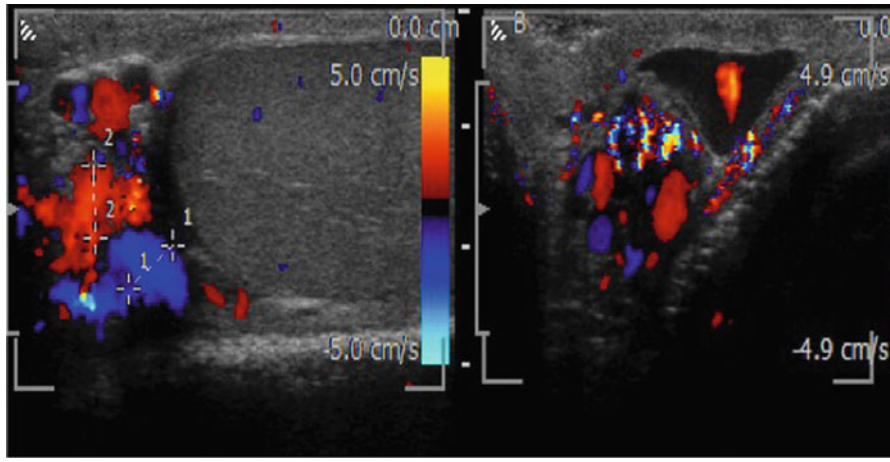

Fig. 6.62 Varicocele: Doppler color flow study showing low-reflective dilated veins on the superior and posterolateral aspect of the testis

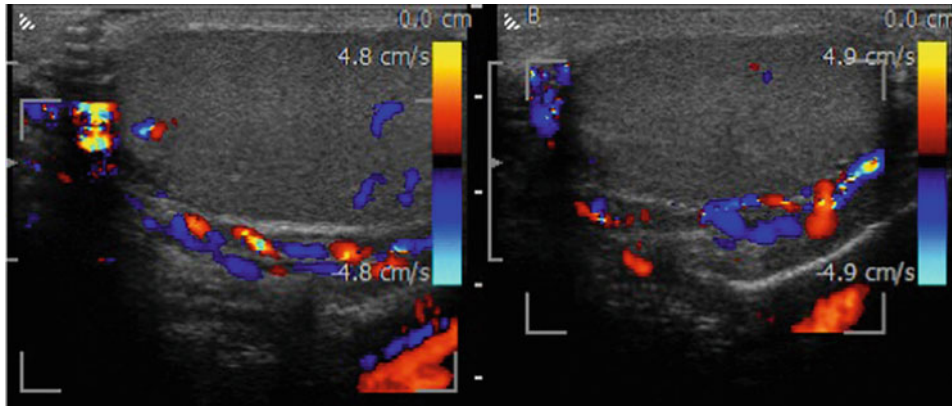

Fig. 6.63 Bilateral varicoceles: color Doppler ultrasound characteristics are the findings of multiple, low-reflective serpiginous tubular structures of varying diameters visualized posterolateral to the testis

intratesticular branches in patients with clinically significant varicoceles after microscopic ligation [110]. However, no statistically significant difference was noted in blood flow velocity and resistive indices in subclinical varicoceles after surgery when compared to control group [13, 110, 125]. Intratesticular arterial resistance is decreased by varicocele ligation suggesting an increased blood flow into the testicular tissue. Interrogation with Doppler color flow study in men with varicoceles before surgery can provide important diagnostic information about the varicocele's effect on testicular function and the potential therapeutic efficacy of surgical intervention.

Tarhan et al. reported the effect of varicocelectomy on testicular blood flow and sperm quality in patients who underwent left varicocelectomy. The mean values of blood flow velocities in the left testicular artery (peak systolic and end diastolic) increased and resistance indices in the left intratesticular arteries decreased significantly after surgery [15, 110]. No significant difference was detected between the preoperative and postoperative blood flow parameters in the right intratesticular arteries. In the semen analysis, statistically significant increases were found in sperm concentration, normal morphology percentage, and total motile sperm concentration 3 months after varicocelectomy [110]. Pinggera

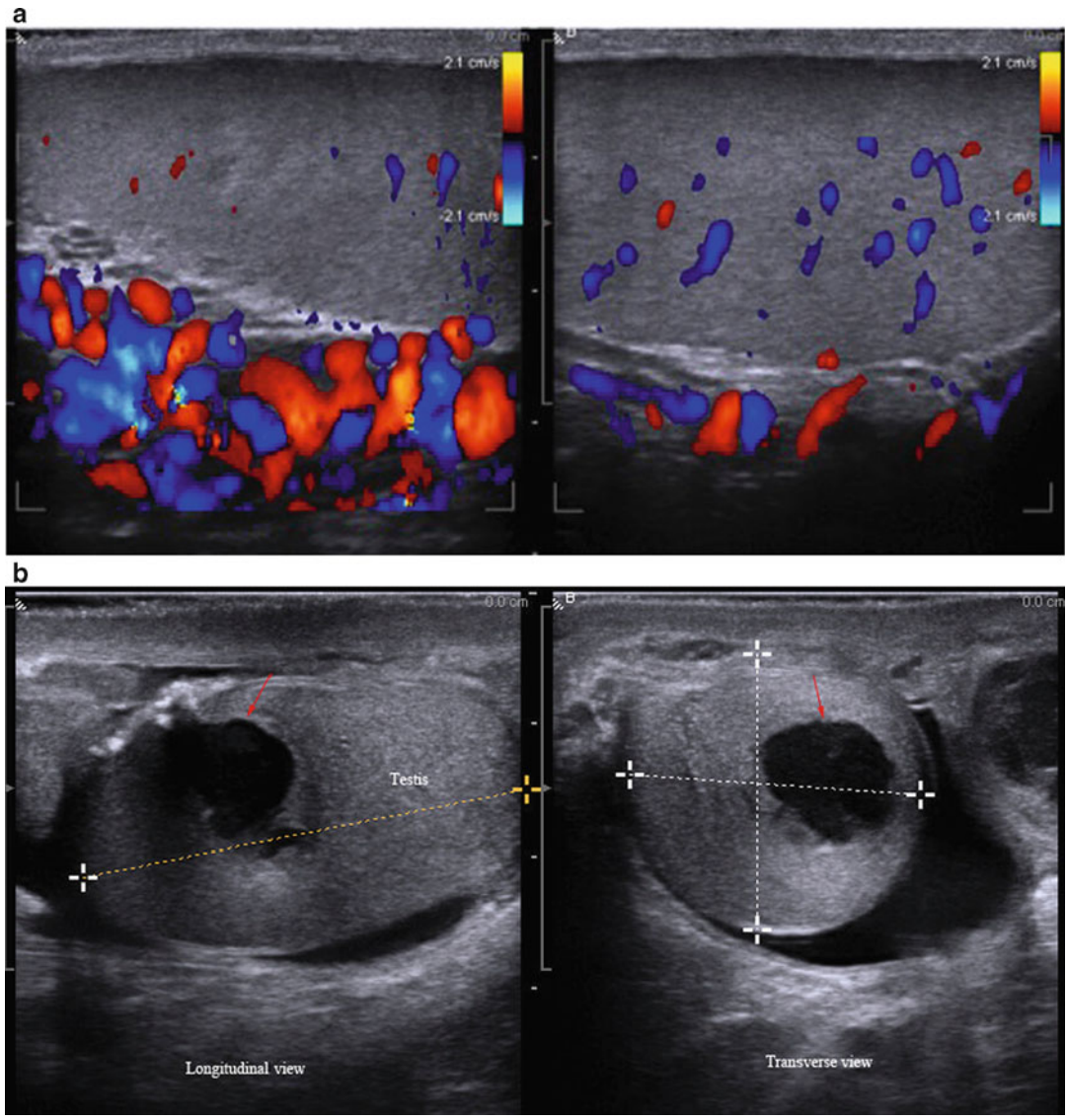

Fig. 6.64 (**a**) Doppler color flow study showing bilateral varicoceles. This is a large right varicocele in a 34-year-old male (**b**) Gray-scale ultrasound showing large hypoechoic area (*arrows*) within the testicular parenchyma on follow-up ultrasound in a patient who underwent testicular biopsy. These findings were consistent with intratesticular hematoma, which needs serial sonographic follow-up until the hematoma is resolved

et al. reported that the mean resistive index (RI) of intratesticular arteries is 0.54 in men with normal sperm counts and the mean RI of 0.68 in men with abnormal sperm counts. The data suggest that an RI of >0.6 is associated with pathological sperm counts [14].

In patients who experience the sudden onset of a varicocele or whose varicocele persists in the supine position, further imaging of the retroperitoneum is warranted to identify etiologic factors.

Impaired Semen Quality and Azoospermia

Poor semen quality can be a sign of underlying disease. Varicocele, ductal obstruction, and testicular tumors are examples of associated pathology easily demonstrated by ultrasound that may or may not be

identified by physical examination. Ultrasound, being a noninvasive, real-time imaging modality, is often used in the comprehensive evaluation of men with impaired semen quality to document the presence or absence of pathology, especially when the physical exam is inconclusive or suggestive of intrascrotal pathology. In men with azoospermia, ultrasound as an initial imaging modality can often define the underlying etiology as obstructive or NOS [126]. Ultrasound is useful in patients with congenital bilateral absence of the vas deferens (CBAVD) to assess other mesonephric developmental defects and associated conditions such as congenital renal agenesis [127, 128].

Romeo et al. reported elevated inhibin-B levels in patients with untreated varicocele. The inhibin-B levels directly correlate to testicular volume. Inhibin levels directly reflect the function of the Sertoli cells and integrity of seminiferous tubules [129]. Inhibin levels have been shown to improve after varicocelectomy corresponding to improved semen parameters also noted in men after varicocelectomy [130].

Varicocele repair improves the seminal parameters in approximately 70% of the patients, with the improvement in motility being the most common [110, 131, 132].

Evers et al. evaluated the effect of varicoceles treatment on pregnancy rate in subfertile couples in a Cochrane review. This study suggested that there is no evidence that treatment of varicoceles in men with otherwise unexplained subfertility improves the couple's chance of conception [133].

Testicular Biopsy

Testicular biopsy is a diagnostic surgical procedure used to distinguish between OAS and NOS. Testicular biopsy is also performed for sperm retrival for in vitro fertilization and cryopreservation. The most common complication associated with the testicular biopsy or testicular sperm extraction is intratesticular hematoma [134] (Fig. 6.64b).

Antisperm Antibodies

About 10% of men presenting with subfertility are found to have antisperm antibodies, compared with 2% or fewer of fertile men [135, 136]. Several common causes of antisperm antibodies, including OAS, congenital bilateral absence of the vas deferens, epididymitis, genital trauma, and cryptorchidism can be evaluated with scrotal ultrasound [137–139].

Testicular Atrophy

This condition may be related to age, trauma, torsion, infection, inflammation, hypothyroidism, drug therapy, or chronic disease. While the appearance of the testis on ultrasound is variable and related to the underlying cause, it is usually characterized by decreased echogenicity with a normal appearing epididymis (Figs. 6.65 and 6.66).

Testicular Trauma

Testicular trauma accounts for less than 1% of all trauma-related injuries. Physical examination may be difficult in patients with scrotal trauma due to tenderness and swelling of the scrotal contents. Scrotal ultrasound remains the standard imaging study to evaluate testicular and epididymal integrity and assess the vascular status of the testis [140, 141]. The characteristic ultrasound findings of scrotal trauma are thickening of the scrotal wall, asymmetry, irregularity, poorly defined testicular borders (contour abnormality), interruption of the tunica albuginea, heterogeneous testicular echogenicity, and intra- or extratesticular hematoma with variable echogenicity (Figs. 6.67 and 6.68). A discrete line or hypoechoic stripe in the testicular parenchyma is a direct evidence of testicular rupture with disruption of the tunica albuginea [142].

Buckley and McAninch reported 100% sensitivity and 93.5% specificity for testicular rupture related to blunt trauma when comparing ultrasound results to the findings at surgical exploration [143] (Figs. 6.69 and 6.70). Guichard et al. reported the sensitivity and specificity of ultrasound for testis rupture as 100 and 65%, respectively, when compared to surgical findings [144]. They further noted that ultrasonography allowed the diagnosis of a hematocele with a sensitivity of 87% and a specificity of 89%, testicular hematoma with a sensitivity of 71% and specificity of 77%, and testis avulsion with a sensitivity of 100% and a specificity of 97%. Ultrasonography results for epididymis injuries were poor [144].

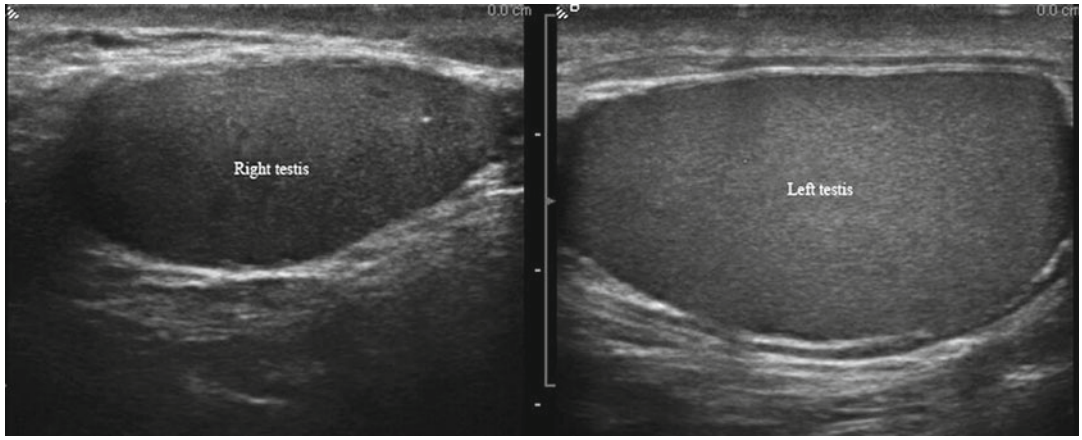

Fig. 6.65 Atrophic right testis: gray-scale ultrasound shows decreased echogenicity when compared to the left testis

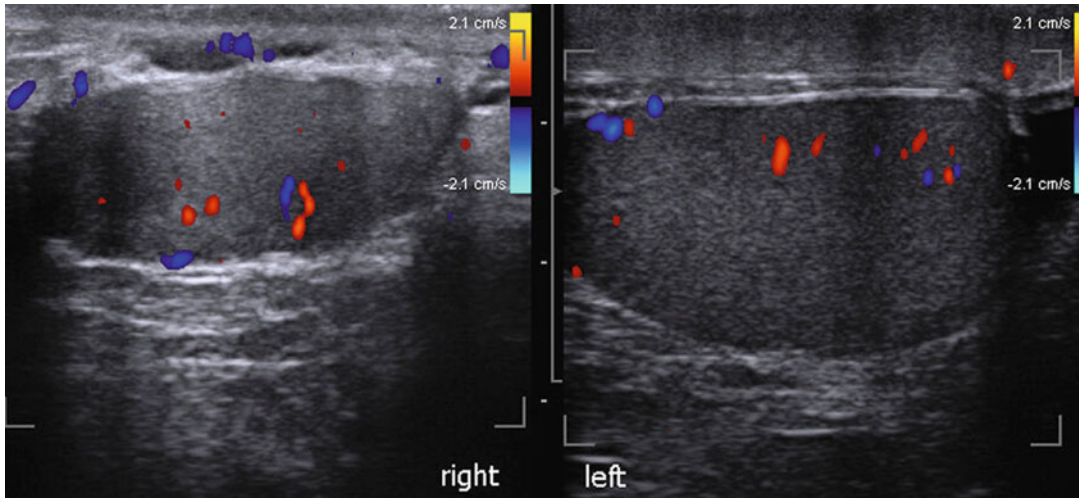

Fig. 6.66 Doppler color flow study shows right-sided atrophic testis in a 31-year-old male with history of cryptorchidism with normal blood flow to the testicular parenchyma

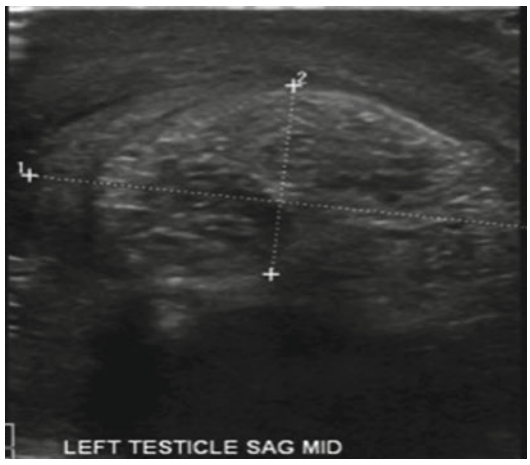

Fig. 6.67 Gray-scale ultrasound showing hypoechoic areas suggesting intratesticular hematoma following blunt trauma of the scrotum

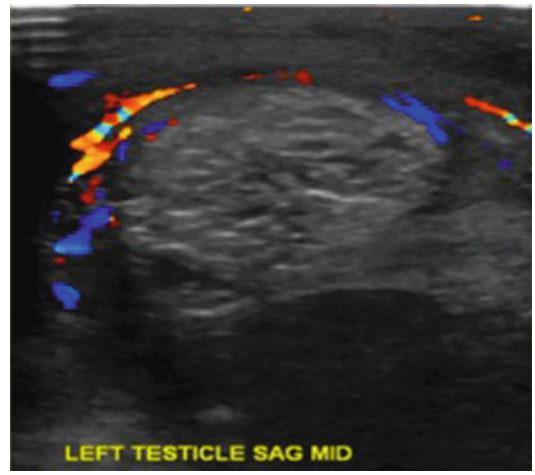

Fig. 6.68 Doppler flow study showing no blood flow within the intratesticular hematoma

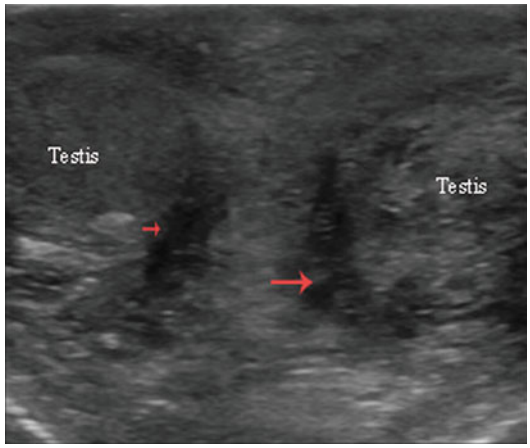

Fig. 6.69 Gray-scale ultrasound shows disruption of the left tunica vaginalis (*arrow*)

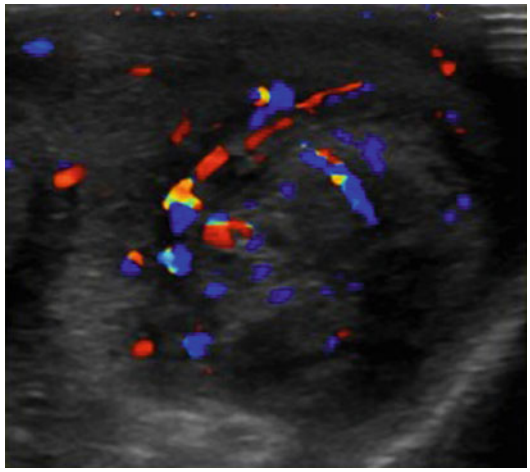

Fig. 6.70 Doppler color flow study showing testicular rupture following a blunt trauma scrotum. There is no increased blood flow noted in the testicular rupture

Ultrasound has several shortcomings including the fact that it is operator-dependent. Alternatively, magnetic resonance imaging (MRI) had 100% diagnostic accuracy for the diagnosis of testicular rupture [145].

The current management strategy for testicular rupture advocates early surgical intervention with the goal of preventing testicular loss. These recommendations are also applied in boys with a hematocele since up to 80% of significant hematoceles are due to testicular rupture [146]. The goal is to avert infection, necrosis, atrophy, and impaired fertility if managed conservatively [141].

References

1. Dogra V, Bhatt S. Acute painful scrotum. Radiol Clin North Am. 2004;42(2):349–63.
2. Smart JM, et al. Ultrasound findings of masses of the paratesticular space. Clin Radiol. 2008;63(8):929–38.
3. Hadziselimovic F, et al. The importance of mini-puberty for fertility in cryptorchidism. J Urol. 2005;174(4 Pt 2):1536–9; discussion 1538–9.
4. Raivio T, et al. Serum androgen bioactivity in cryptorchid and noncryptorchid boys during the postnatal reproductive hormone surge. J Clin Endocrinol Metab. 2003;88(6):2597–9.
5. Kuijper EA, et al. Ultrasonographically measured testicular volumes in 0- to 6-year-old boys. Hum Reprod. 2008;23(4):792–6.
6. Aso C, et al. Gray-scale and color Doppler sonography of scrotal disorders in children: an update. Radiographics. 2005;25(5):1197–214.
7. Dogra VS, et al. Sonography of the scrotum. Radiology. 2003;227(1):18–36.
8. Thomas RD, Dewbury KC. Ultrasound appearances of the rete testis. Clin Radiol. 1993;47(2):121–4.
9. Bhatt S, et al. Imaging of non-neoplastic intratesticular masses. Diagn Interv Radiol. 2011;17:52–63.
10. Wishahi MM. Anatomy of the venous drainage of the human testis: testicular vein cast, microdissection and radiographic demonstration. A new anatomical concept. Eur Urol. 1991;20(2):154–60.
11. Paltiel HJ, Rupich RC, Babcock DS. Maturational changes in arterial impedance of the normal testis in boys: Doppler sonographic study. AJR Am J Roentgenol. 1994;163(5):1189–93.
12. Biagiotti G, et al. Spermatogenesis and spectral echo-colour Doppler traces from the main testicular artery. BJU Int. 2002;90(9):903–8.
13. Unsal A, et al. Resistance and pulsatility index increase in capsular branches of testicular artery: indicator of impaired testicular microcirculation in varicocele? J Clin Ultrasound. 2007;35(4):191–5.
14. Pinggera GM, et al. Assessment of the intratesticular resistive index by colour Doppler ultrasonography measurements as a predictor of spermatogenesis. BJU Int. 2008;101(6):722–6.
15. Balci A, et al. Long-term effect of varicocele repair on intratesticular arterial resistance index. J Clin Ultrasound. 2008;36(3):148–52.
16. Nielsen ME. Use and misuse of imaging by urologists. J Urol. 2010;184(1):12–4.
17. Douglas PS. Improving imaging: our professional imperative. J Am Coll Cardiol. 2006;48(10):2152–5.
18. Hendel RC, et al. ACCF/ACR/SCCT/SCMR/ASNC/NASCI/SCAI/SIR 2006 appropriateness criteria for cardiac computed tomography and cardiac magnetic resonance imaging: a report of the American College of Cardiology Foundation Quality Strategic Directions Committee Appropriateness Criteria Working Group, American College of Radiology, Society of Cardiovascular Computed Tomography,

Society for Cardiovascular Magnetic Resonance, American Society of Nuclear Cardiology, North American Society for Cardiac Imaging, Society for Cardiovascular Angiography and Interventions, and Society of Interventional Radiology. J Am Coll Cardiol. 2006;48(7):1475–97.
19. Lee A, et al. Acute idiopathic scrotal edema: ultrasonographic findings at an emergency unit. Eur Radiol. 2009;19(8):2075–80.
20. Thomas AC, et al. Ultrasound findings of acute idiopathic scrotal edema. Scientific World Journal. 2004;4 Suppl 1:9–10.
21. Grainger AJ, Hide IG, Elliott ST. The ultrasound appearances of scrotal oedema. Eur J Ultrasound. 1998;8(1):33–7.
22. Malik AM, et al. The spectrum of presentation and management of Fournier's gangrene–an experience of 73 cases. J Pak Med Assoc. 2010;60(8):617–9.
23. Sorensen MD, et al. Fournier's gangrene: management and mortality predictors in a population based study. J Urol. 2009;182(6):2742–7.
24. Levenson RB, Singh AK, Novelline RA. Fournier gangrene: role of imaging. Radiographics. 2008;28(2):519–28.
25. Rajan DK, Scharer KA. Radiology of Fournier's gangrene. AJR Am J Roentgenol. 1998;170(1):163–8.
26. Hara Y, et al. Acute scrotum caused by Henoch-Schonlein purpura. Int J Urol. 2004;11(7):578–80.
27. Swygert KE, et al. Melanoma in situ involving an epidermal inclusion (infundibular) cyst. Am J Dermatopathol. 2007;29(6):564–5.
28. Germaine P, Simerman LP. Fibrous pseudotumor of the scrotum. J Ultrasound Med. 2007;26(1):133–8.
29. Seethala RR, et al. Diffuse fibrous pseudotumor of the testicular tunics associated with an inflamed hydrocele. Arch Pathol Lab Med. 2003;127(6):742–4.
30. Lowe FC. Squamous-cell carcinoma of the scrotum. Urol Clin North Am. 1992;19(2):397–405.
31. Jones ME, et al. Risk of congenital inguinal hernia in siblings: a record linkage study. Paediatr Perinat Epidemiol. 1998;12(3):288–96.
32. Rescorla FJ, et al. The "other side" of pediatric hernias: the role of laparoscopy. Am Surg. 1997;63(8):690–3.
33. Erez I, et al. Preoperative ultrasound and intraoperative findings of inguinal hernias in children: a prospective study of 642 children. J Pediatr Surg. 2002;37(6):865–8.
34. Osifo OD, Osaigbovo EO. Congenital hydrocele: prevalence and outcome among male children who underwent neonatal circumcision in Benin City, Nigeria. J Pediatr Urol. 2008;4(3):178–82.
35. Wampler SM, Llanes M. Common scrotal and testicular problems. Prim Care. 2010;37(3):613–26, x.
36. Mihmanli I, et al. Testicular size and vascular resistance before and after hydrocelectomy. AJR Am J Roentgenol. 2004;183(5):1379–85.
37. Garriga V, et al. US of the tunica vaginalis testis: anatomic relationships and pathologic conditions. Radiographics. 2009;29(7):2017–32.
38. Somekh E, Gorenstein A, Serour F. Acute epididymitis in boys: evidence of a post-infectious etiology. J Urol. 2004;171(1):391–4; discussion 394.
39. Bohm MK, Gift TL, Tao G. Patterns of single and multiple claims of epididymitis among young privately-insured males in the United States, 2001 to 2004. Sex Transm Dis. 2009;36(8):490–2.
40. Adams CE, Wald M. Risks and complications of vasectomy. Urol Clin North Am. 2009;36(3):331–6.
41. Greek G. Vasectomy. A safe, effective, economical means of sterilization. Postgrad Med. 2000;108(2):173–6, 179.
42. Schwingl PJ, Guess HA. Safety and effectiveness of vasectomy. Fertil Steril. 2000;73(5):923–36.
43. Akbar SA, et al. Multimodality imaging of paratesticular neoplasms and their rare mimics. Radiographics. 2003;23(6):1461–76.
44. Aydin H, et al. Clear cell papillary cystadenoma of the epididymis and mesosalpinx: immunohistochemical differentiation from metastatic clear cell renal cell carcinoma. Am J Surg Pathol. 2005;29(4):520–3.
45. Alexander JA, Lichtman JB, Varma VA. Ultrasound demonstration of a papillary cystadenoma of the epididymis. J Clin Ultrasound. 1991;19(7):442–5.
46. Salm R. Papillary sarcinoma of the epididymis. J Pathol. 1969;97(2):253–9.
47. Dowling KJ, Lieb HE. Fibrosarcoma of epididymis. Urology. 1985;26(3):307–8.
48. Kurihara K, et al. Papillary adenocarcinoma of the epididymis. Acta Pathol Jpn. 1993;43(7–8):440–3.
49. Ringdahl E, Teague L. Testicular torsion. Am Fam Physician. 2006;74(10):1739–43.
50. Bartsch G, et al. Testicular torsion: late results with special regard to fertility and endocrine function. J Urol. 1980;124(3):375–8.
51. Waldert M, et al. Color Doppler sonography reliably identifies testicular torsion in boys. Urology. 2010;75(5):1170–4.
52. Jee WH, et al. Resistive index of the intrascrotal artery in scrotal inflammatory disease. Acta Radiol. 1997;38(6):1026–30.
53. Yagil Y, et al. Role of Doppler ultrasonography in the triage of acute scrotum in the emergency department. J Ultrasound Med. 2010;29(1):11–21.
54. Nakagawa A, et al. In vivo analysis of phagocytosis of apoptotic cells by testicular Sertoli cells. Mol Reprod Dev. 2005;71(2):166–77.
55. Drut R, Drut RM. Testicular microlithiasis: histologic and immunohistochemical findings in 11 pediatric cases. Pediatr Dev Pathol. 2002;5(6):544–50.
56. van Casteren NJ, Looijenga LH. Dohle GR Testicular microlithiasis and carcinoma in situ overview and proposed clinical guideline. Int J Androl. 2009;32(4):279–87.
57. Dagash H, Mackinnon EA. Testicular microlithiasis: what does it mean clinically? BJU Int. 2007;99(1):157–60.
58. Middleton WD, Teefey SA, Santillan CS. Testicular microlithiasis: prospective analysis of prevalence and associated tumor. Radiology. 2002;224(2):425–8.

59. Goede J, et al. Prevalence of testicular microlithiasis in asymptomatic males 0 to 19 years old. J Urol. 2009;182(4):1516–20.
60. von Eckardstein S, et al. Sonographic testicular microlithiasis as an indicator of premalignant conditions in normal and infertile men. J Androl. 2001;22(5):818–24.
61. DeCastro BJ, Peterson AC, Costabile RA. A 5-year followup study of asymptomatic men with testicular microlithiasis. J Urol. 2008;179(4):1420–3; discussion 1423.
62. Kocaoglu M, et al. Testicular microlithiasis in pediatric age group: ultrasonography findings and literature review. Diagn Interv Radiol. 2005;11(1):60–5.
63. Furness PD, 3rd, et al. Multi-institutional study of testicular microlithiasis in childhood: a benign or premalignant condition? J Urol. 1998;160(3 Pt 2):1151–4; discussion 1178.
64. Frush DP, Kliewer MA, Madden JF. Testicular microlithiasis and subsequent development of metastatic germ cell tumor. AJR Am J Roentgenol. 1996;167(4):889–90.
65. Bennett HF, et al. Testicular microlithiasis: US follow-up. Radiology. 2001;218(2):359–63.
66. Dieckmann KP, Skakkebaek NE. Carcinoma in situ of the testis: review of biological and clinical features. Int J Cancer. 1999;83(6):815–22.
67. Husmann DA. Cryptorchidism and its relationship to testicular neoplasia and microlithiasis. Urology. 2005;66(2):424–6.
68. Comiter CV, et al. Burned-out primary testicular cancer: sonographic and pathological characteristics. J Urol. 1996;156(1):85–8.
69. Angulo JC, et al. Clinicopathological study of regressed testicular tumors (apparent extragonadal germ cell neoplasms). J Urol. 2009;182(5):2303–10.
70. Gooding GA, Leonhardt W, Stein R. Testicular cysts: US findings. Radiology. 1987;163(2):537–8.
71. Hamm B, Fobbe F, Loy V. Testicular cysts: differentiation with US and clinical findings. Radiology. 1988;168(1):19–23.
72. Dogra VS, et al. Benign intratesticular cystic lesions: US features. Radiographics. 2001;21 Spec No: S273–81.
73. Carver BS, Al-Ahmadie H, Sheinfeld J. Adult and pediatric testicular teratoma. Urol Clin North Am. 2007;34(2):245–51; abstract x.
74. Chou SJ, et al. Cysts of the tunica albuginea. Arch Androl. 2004;50(2):89–92.
75. Tammela TL, et al. Cysts of the tunica albuginea–more common testicular masses than previously thought? Br J Urol. 1991;68(3):280–4.
76. Khalid M, et al. Concomitant bilateral testicular epidermoid cysts. Saudi Med J. 2008;29(6):907–9.
77. Dogra VS, et al. Testicular epidermoid cysts: sonographic features with histopathologic correlation. J Clin Ultrasound. 2001;29(3):192–6.
78. Malvica RP. Epidermoid cyst of the testicle: an unusual sonographic finding. AJR Am J Roentgenol. 1993;160(5):1047–8.
79. Loya AG, Said JW, Grant EG. Epidermoid cyst of the testis: radiologic-pathologic correlation. Radiographics. 2004;24 Suppl 1:S243–6.
80. Nistal M, Mate A, Paniagua R. Cystic transformation of the rete testis. Am J Surg Pathol. 1996;20(10):1231–9.
81. Nair R, et al. Tubular ectasia of the rete testis: a diagnostic dilemma. Ann R Coll Surg Engl. 2008;90(7):W1–3.
82. Bree RL, Hoang DT. Scrotal ultrasound. Radiol Clin North Am. 1996;34(6):1183–205.
83. Atasoy C, Fitoz S. Gray-scale and color Doppler sonographic findings in intratesticular varicocele. J Clin Ultrasound. 2001;29(7):369–73.
84. Bucci S, et al. Intratesticular varicocele: evaluation using gray scale and color Doppler ultrasound. World J Urol. 2008;26(1):87–9.
85. Kessler A, et al. Intratesticular varicocele: gray scale and color Doppler sonographic appearance. J Ultrasound Med. 2005;24(12):1711–6.
86. Das KM, et al. Intratesticular varicocele: evaluation using conventional and Doppler sonography. AJR Am J Roentgenol. 1999;173(4):1079–83.
87. Desai KM, Gingell JC, Haworth JM. Localised intratesticular abscess complicating epididymo-orchitis: the use of scrotal ultrasonography in diagnosis and management. Br Med J (Clin Res Ed). 1986;292(6532):1361–2.
88. Mouritsen A, et al. Testicular adrenal rest tumours in boys, adolescents and adult men with congenital adrenal hyperplasia may be associated with the CYP21A2 mutation. Int J Androl. 2010;33(3):521–7.
89. Claahsen-van der Grinten HL, et al. Prevalence of testicular adrenal rest tumours in male children with congenital adrenal hyperplasia due to 21-hydroxylase deficiency. Eur J Endocrinol. 2007;157(3):339–44.
90. Dogra V, Nathan J, Bhatt S. Sonographic appearance of testicular adrenal rest tissue in congenital adrenal hyperplasia. J Ultrasound Med. 2004;23(7):979–81.
91. Proto G, et al. Bilateral testicular adrenal rest tissue in congenital adrenal hyperplasia: US and MR features. J Endocrinol Invest. 2001;24(7):529–31.
92. Dieckmann KP, et al. Bilateral testicular germ cell tumors. Report of nine cases and review of the literature. Cancer. 1986;57(6):1254–8.
93. Datta SN, et al. A case of scrotal sarcoidosis that mimicked tuberculosis. Nat Clin Pract Urol. 2007;4(4):227–30.
94. Metcalfe PD, et al. Pediatric testicular tumors: contemporary incidence and efficacy of testicular preserving surgery. J Urol. 2003;170(6 Pt 1):2412–5; discussion 2415–6.
95. Horwich A, Shipley J, Huddart R. Testicular germ-cell cancer. Lancet. 2006;367(9512):754–65.
96. Schwerk WB, Schwerk WN, Rodeck G. Testicular tumors: prospective analysis of real-time US patterns and abdominal staging. Radiology. 1987;164(2):369–74.
97. Woodward PJ, et al. From the archives of the AFIP: tumors and tumorlike lesions of the testis: radiologic-pathologic correlation. Radiographics. 2002;22(1):189–216.

98. Shah A, et al. Re: new ultrasound techniques for imaging of the indeterminate testicular lesion may avoid surgery completely. Clin Radiol. 2010;65(6):496–7.
99. Frush DP, Sheldon CA. Diagnostic imaging for pediatric scrotal disorders. Radiographics. 1998;18(4):969–85.
100. Ulbright TM, Roth LM. Recent developments in the pathology of germ cell tumors. Semin Diagn Pathol. 1987;4(4):304–19.
101. Thava V, Cooper N, Egginton JA. Yolk sac tumour of the testis in childhood. Br J Radiol. 1992;65(780):1142–4.
102. Hasselblom S, et al. Testicular lymphoma–a retrospective, population-based, clinical and immunohistochemical study. Acta Oncol. 2004;43(8):758–65.
103. Vural F, et al. Primary testicular lymphoma. J Natl Med Assoc. 2007;99(11):1277–82.
104. Zucca E, et al. Patterns of outcome and prognostic factors in primary large-cell lymphoma of the testis in a survey by the International Extranodal Lymphoma Study Group. J Clin Oncol. 2003;21(1):20–7.
105. Carmignani L, et al. High incidence of benign testicular neoplasms diagnosed by ultrasound. J Urol. 2003;170(5):1783–6.
106. Muller T, et al. Management of incidental impalpable intratesticular masses of <or = 5 mm in diameter. BJU Int. 2006;98(5):1001–4.
107. Hallak J, et al. Organ-sparing microsurgical resection of incidental testicular tumors plus microdissection for sperm extraction and cryopreservation in azoospermic patients: surgical aspects and technical refinements. Urology. 2009;73(4):887–91; discussion 891–2.
108. Toren PJ, et al. Small incidentally discovered testicular masses in infertile men–is active surveillance the new standard of care? J Urol. 2010;183(4):1373–7.
109. Lefort C, et al. [Ischemic orchiditis: review of 5 cases diagnosed by color Doppler ultrasonography]. J Radiol. 2001;82(7):839–42.
110. Tarhan S, et al. Long-term effect of microsurgical inguinal varicocelectomy on testicular blood flow. J Androl. 2011;32(1):33–9.
111. Shafik A, et al. Testicular veins: anatomy and role in varicocelogenesis and other pathologic conditions. Urology. 1990;35(2):175–82.
112. Gat Y, et al. Induction of spermatogenesis in azoospermic men after internal spermatic vein embolization for the treatment of varicocele. Hum Reprod. 2005;20(4):1013–7.
113. Gat Y, et al. Varicocele, hypoxia and male infertility. Fluid Mechanics analysis of the impaired testicular venous drainage system. Hum Reprod. 2005;20(9):2614–9.
114. Wishahi MM. Anatomy of the spermatic venous plexus (pampiniform plexus) in men with and without varicocele: intraoperative venographic study. J Urol. 1992;147(5):1285–9.
115. Braedel HU, et al. A possible ontogenic etiology for idiopathic left varicocele. J Urol. 1994;151(1):62–6.
116. Gorenstein A, Katz S, Schiller M. Varicocele in children: "to treat or not to treat"–venographic and manometric studies. J Pediatr Surg. 1986;21(12):1046–50.
117. Iafrate M, et al. Varicocele is associated with an increase of connective tissue of the pampiniform plexus vein wall. World J Urol. 2009;27(3):363–9.
118. The influence of varicocele on parameters of fertility in a large group of men presenting to infertility clinics. World Health Organization. Fertil Steril. 1992;57(6):1289–93.
119. Benoff S, Gilbert BR. Varicocele and male infertility: part I. Preface. Hum Reprod Update. 2001;7(1):47–54.
120. Robinson SP, Hampton LJ, Koo HP. Treatment strategy for the adolescent varicocele. Urol Clin North Am. 2010;37(2):269–78.
121. Cornud F, et al. Varicocele: strategies in diagnosis and treatment. Eur Radiol. 1999;9(3):536–45.
122. Tasci AI, et al. Color doppler ultrasonography and spectral analysis of venous flow in diagnosis of varicocele. Eur Urol. 2001;39(3):316–21.
123. Kadyrov ZA, et al. [Bilateral varicocele: epidemiology, clinical presentation and diagnosis]. Urologiia. 2007;3:64–8.
124. Gat Y, et al. Physical examination may miss the diagnosis of bilateral varicocele: a comparative study of 4 diagnostic modalities. J Urol. 2004;172(4 Pt 1):1414–7.
125. Akcar N, et al. Intratesticular arterial resistance and testicular volume in infertile men with subclinical varicocele. J Clin Ultrasound. 2004;32(8):389–93.
126. Donkol RH. Imaging in male-factor obstructive infertility. World J Radiol. 2010;2(5):172–9.
127. Honig SC, Lipshultz LI, Jarow J. Significant medical pathology uncovered by a comprehensive male infertility evaluation. Fertil Steril. 1994;62(5):1028–34.
128. McCallum T, et al. Unilateral renal agenesis associated with congenital bilateral absence of the vas deferens: phenotypic findings and genetic considerations. Hum Reprod. 2001;16(2):282–8.
129. Romeo C, et al. Altered serum inhibin b levels in adolescents with varicocele. J Pediatr Surg. 2007;42(2):390–4.
130. Ozden C, et al. Effect of varicocelectomy on serum inhibin B levels in infertile patients with varicocele. Scand J Urol Nephrol. 2008;42(5):441–3.
131. Sakamoto H, et al. Effects of varicocele repair in adults on ultrasonographically determined testicular volume and on semen profile. Urology. 2008;71(3):485–9.
132. Zucchi A, et al. Varicocele and fertility: relationship between testicular volume and seminal parameters before and after treatment. J Androl. 2006;27(4):548–51.
133. Evers JH, Collins J, Clarke J. Surgery or embolisation for varicoceles in subfertile men. Cochrane Database Syst Rev. 2009(1):CD000479.
134. Schlegel PN, Su LM. Physiological consequences of testicular sperm extraction. Hum Reprod. 1997;12(8):1688–92.

135. Gilbert BR, Witkin SS, Goldstein M. Correlation of sperm-bound immunoglobulins with impaired semen analysis in infertile men with varicoceles. Fertil Steril. 1989;52(3):469–73.
136. Sinisi AA, et al. Prevalence of antisperm antibodies by SpermMARtest in subjects undergoing a routine sperm analysis for infertility. Int J Androl. 1993;16(5):311–4.
137. Urry RL, et al. The incidence of antisperm antibodies in infertility patients with a history of cryptorchidism. J Urol. 1994;151(2):381–3.
138. Heidenreich A, et al. Risk factors for antisperm antibodies in infertile men. Am J Reprod Immunol. 1994;31(2–3):69–76.
139. Zini A, et al. Anti-sperm antibody levels are not related to fertilization or pregnancy rates after IVF or IVF/ICSI. J Reprod Immunol. 2011;88(1):80–4.
140. Deurdulian C, et al. US of acute scrotal trauma: optimal technique, imaging findings, and management. Radiographics. 2007;27(2):357–69.
141. Cubillos J, et al. A conservative approach to testicular rupture in adolescent boys. J Urol. 2010;184(4 Suppl):1733–8.
142. Bhatt S, Dogra VS. Role of US in testicular and scrotal trauma. Radiographics. 2008;28(6):1617–29.
143. Buckley JC, McAninch JW. Use of ultrasonography for the diagnosis of testicular injuries in blunt scrotal trauma. J Urol. 2006;175(1):175–8.
144. Guichard G, et al. Accuracy of ultrasonography in diagnosis of testicular rupture after blunt scrotal trauma. Urology. 2008;71(1):52–6.
145. Kim SH, et al. The efficacy of magnetic resonance imaging for the diagnosis of testicular rupture: a prospective preliminary study. J Trauma. 2009;66(1):239–42.
146. Chandra RV, et al. Rational approach to diagnosis and management of blunt scrotal trauma. Urology. 2007;70(2):230–4.

Penile Ultrasound

7

Soroush Rais-Bahrami and Bruce R. Gilbert

Introduction

Penile ultrasound is commonly used in the diagnostic workup of a patient with erectile dysfunction (ED) but also plays an important role by providing an anatomic and functional vascular assessment in a multitude of other conditions including Peyronie's disease, high-flow priapism, penile fracture, penile urethral strictures, urethral stones, or diverticula, or masses involving deep tissues of the penis. As a component of the evaluation for ED, penile Doppler ultrasound (PDU) is performed to assess the quality of arterial blood flow and sufficiency of veno-occlusive mechanisms, both necessary for an adequate erection. More recently, this imaging modality is playing a central role in the early detection and diagnosis of otherwise silent coronary artery disease (CAD) in men who present with ED as their initial symptom. PDU is also an essential component of the assessment of external genitalia in trauma situations where high-flow priapism or penile fracture is suspected. Penile ultrasound provides a readily available, minimally invasive diagnostic modality that evaluates both the structural anatomy and functional hemodynamics at a reasonable cost.

S. Rais-Bahrami, MD
Hofstra North Shore LIJ School of Medicine, The Arthur Smith Institute for Urology, New Hyde Park, NY, USA

B.R. Gilbert, MD, PhD (✉)
Hofstra North Shore LIJ School of Medicine, The Arthur Smith Institute for Urology, 450 Lakeville Road, Suite M41, New Hyde Park, NY 11042, USA
e-mail: bgilbert@gmail.com

Ultrasound Settings

Penile ultrasound is best performed with a high-frequency linear array transducer with an ultrasound frequency of 7.5–18 MHz which allows for high resolution images of the penis and internal vascular structures. Color and spectral Doppler are essential elements of penile ultrasonography in addition to B-mode ultrasound. 3D ultrasound is a developing technique that has the potential for better defining anatomic and vascular changes occurring with disease processes of the penis.

When available, split screen visualization allows for comparison of laterality very similar to scrotal ultrasound discussed earlier. This is very important in penile ultrasound, but more specifically in PDU whereby the differences between vascular diameter, velocity of blood flow, and measurement of resistive index can be elegantly displayed in a single view for comparison of the right and left sides.

Scanning Technique

Scanning technique, as with any ultrasound examination, is operator-dependent and hence may vary greatly. Nevertheless, it is essential for

P.F. Fulgham and B.R. Gilbert (eds.), *Practical Urological Ultrasound*, Current Clinical Urology,
DOI 10.1007/978-1-59745-351-6_7, © Springer Science+Business Media New York 2013

each practitioner to establish a routine protocol to which they fastidiously adhere. This allows for data to be comparable across serial examinations of the same patient and between studies performed on different patients with similar pathologies. Also, a routine protocol allows practitioners to provide anticipatory guidance to patients prior to beginning the study. A technique for patient preparation, routine survey scanning, and indication-specific scanning protocols for penile ultrasound is presented.

Patient Preparation

The patient should lie comfortably on the examination table in a supine position with legs together providing support for the external genitalia. An alternative position is dorsal lithotomy with the penis lying on the anterior abdominal wall. Regardless of the patient position preferred, the area of interest should remain undraped for the duration of the examination. Care should be taken to cover the remainder of the patient as completely as possible including the abdomen, torso, and lower extremities. Ample amounts of ultrasonographic acoustic gel should be used between the transducer probe and the surface of the penis to allow uninterrupted transmission of sound waves, thus producing a high-quality image.

Penile Ultrasound Protocol

As with other ultrasound exams, penile ultrasound uses specific scanning techniques and images targeting the clinical indication prompting the study. Irrespective of the indication for penile ultrasound, routine scanning during penile ultrasound should include both transverse and longitudinal views of the penis by placing the transducer probe on the dorsal or ventral aspect of the penis. The technique presented here uses a dorsal approach, which is easier for the flaccid phallus. However, the ventral approach is often better with a fully erect phallus. The goal is to visualize the cross-sectional view of the two corpora cavernosa dorsally and the corpus spongiosum ventrally along the length of the penis from the base of the penile shaft to the glans penis.

The corpora cavernosa appear dorsally, as two homogeneously hypoechoic circular structures, each surrounded by a thin (usually less than 2 mm) hyperechoic layer representing the tunica albuginea that envelops the corpora. The corpus spongiosum is a ventrally located circular structure with homogeneous echotexture, usually more echogenic than the corpora cavernosa [1]. It is best visualized by placing the ultrasound transducer probe on the ventral aspect of the penis; however, it is easily compressible so minimal pressure should be maintained while scanning. For routine anatomic scanning of the penis with ultrasound, all three corpora can be sufficiently viewed from a single dorsal approach to the penile shaft. A survey scan is first performed prior to obtaining static images at the proximal (base), midportion, and distal (tip) of the corpora cavernosal bodies for documentation (Figs. 7.1, 7.2 and 7.3). The value of the survey scan cannot be over stated. It often provides the perspective that is necessary to assure absence of coexisting pathology. A careful survey scan of the phallus will identify abnormalities of the cavernosal vessels, calcified plaques, and abnormalities of the spongiosa tissue.

Still images recommended as representative views of this initial surveying scan include one transverse view at the base of the penile shaft, one at the mid-shaft, and a third at the distal shaft just proximal to the corona of the glans penis (Fig. 7.1a, b). Each image should show transverse sections of all three corporal bodies. As noted in the labeled images, orientation by convention is for the right corporal body to be on the left side of the display (as viewed by the sonographer) while the left corporal body is located on the right side of the display. Figure 7.2 demonstrates two mid-shaft views: one with the transducer on the dorsal phallus and the other with the transducer on the ventral phallus. A longitudinal projection splitting the

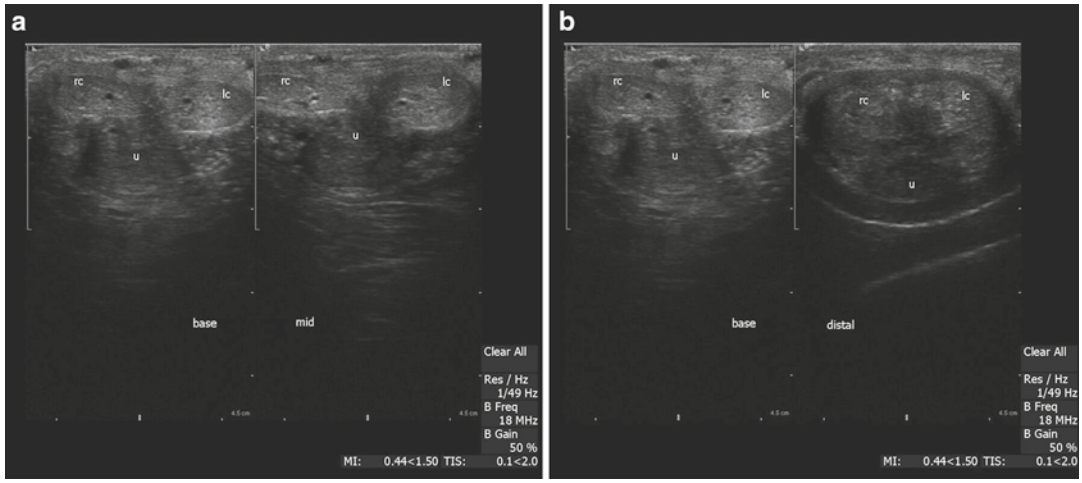

Fig. 7.1 (**a**) Survey scan with transverse views through the base and mid-shaft of the penis. In this image, the transducer is on the dorsal penile surface and demonstrates the right and left corpora cavernosa (rc and lc) and urethra (u). (**b**) Survey scan with transverse views through the base and distal shaft regions of the penis. In this image the transducer is on the dorsal penile surface and demonstrates the right and left corpora cavernosa (rc and lc) and urethra (u)

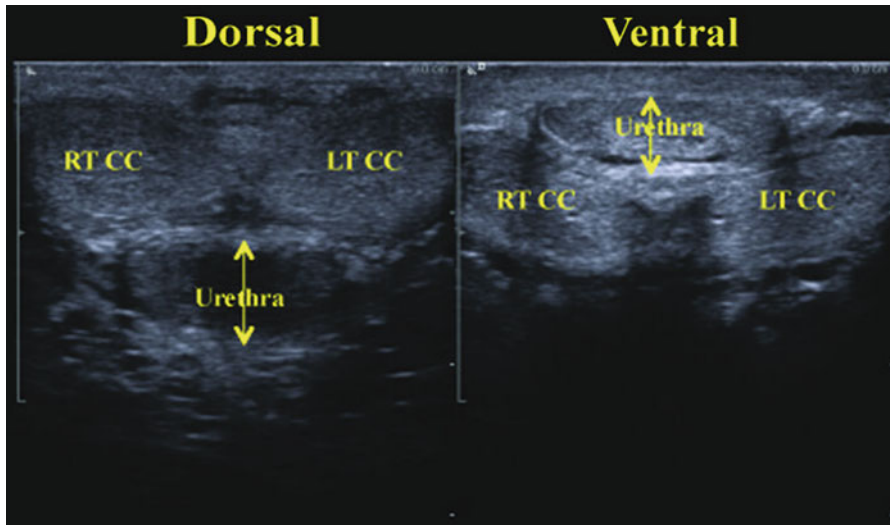

Fig. 7.2 Demonstrates two mid-shaft views. The *left*-side image demonstrates the view with the transducer on the dorsal phallus and the *right*-side image with the transducer on the ventral surface of the phallus depicting the right corpus cavernosa (RT CC), left corpus cavernosa (LT CC), and urethra

screen view helps to compare the right and left corporal bodies. Figure 7.3 demonstrates a dorsal approach with measurements of the cavernosal artery diameter. By convention, the orientation is constant, with the projection of the right corporal body on the left side of the display while the left corporal body is located on the right side of the display.

Protocol box: suggested baseline penile Doppler images

- Survey scan (with cine loops if possible):
  - Transverse: proximal to distal.
  - Longitudinal: left lateral to right lateral.
- Baseline images in both transverse and longitudinal views with cavernosal

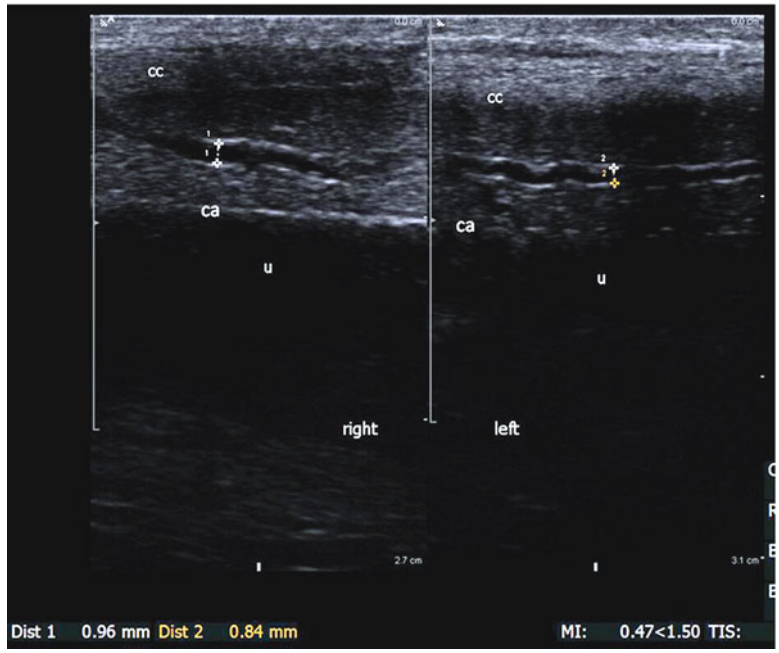

Fig. 7.3 Longitudinal view of corpora cavernosa (cc) in split screen view, displaying right corpus cavernosum on *left* and left corpus cavernosum on *right* of screen. Cavernosal artery (ca) diameter at baseline is measured bilaterally with calipers

artery internal diameter and spectral flow parameters: peak systolic velocity (PSV), end-diastolic velocity (EDV), and resistive index (RI). Video clips (cine) are valuable for independent review.
- Longitudinal and transverse survey scan of the phallus with video clips.
- Split screen base (proximal), mid, and distal view of phallus in transverse plane.
- Split screen longitudinal view of left and right corpora cavernosa.
- Flaccid phallus.
- Inner diameter measurements of left and right cavernosal artery and mid phallus.
- Spectral Doppler waveform with PSV, EDV, and Ri.
- Optional: acceleration time.

Focused Penile Ultrasound by Indication

There are several accepted indications for penile ultrasound, each with specialized focus beyond the routine survey scan as previously described. General guidelines for the use of penile ultrasound are delineated by the "Consensus Statement of Urologic Ultrasound Utilization" put forth by the American Urologic Association [2]. These indications can be further classified as either vascular, structural, or urethral pathology in nature (Table 7.1).

Erectile Dysfunction

PDU has been a vital part of the assessment of patients with ED. Some practitioners immediately turn to intracavernosal injection therapy with vasoactive agents in patients who have failed a course of oral phosphodiesterase-5 inhibitors. However, PDU may be used as a diagnostic tool in conjunction with commencement of injection therapy. PDU allows for a baseline evaluation of the functional anatomy as well as providing a real-time assessment of the dynamic changes experienced in response to the dosing of vasoactive medications. In cases where intracavernosal injection of vasoactive substances does not

Table 7.1 Indications for penile and urethral ultrasound

Vascular pathology
Erectile dysfunction (ED)
Cavernosal artery diameter
Flow velocity
Peak systolic velocity (PSV)
End-diastolic velocity (EDV)
Resistive index (Ri)
Priapism
High flow (arterial)
Low flow (ischemic)
Penile trauma/fracture
Dorsal vein thrombosis
Structural pathology
Penile fibrosis/Peyronie's disease
Plaque assessment (number, location, echogenicity, and size)
Perfusion abnormalities
Perfusion surrounding plaques
Penile mass
Primary penile tumors
Metastatic lesions to the penis
Penile foreign body (size, location, echogenicity)
Penile urethral disease
Urethral stricture (location, size)
Perfusion surrounding plaques
Calculus/foreign body
Urethral diverticulum/cyst/abscess

prompt a penile erection, documentation provided by PDU will be a foundation for other management options including use of vacuum constriction devices or insertion of a penile prosthesis.

Possibly one of the most compelling reasons for the performance of PDU in men presenting with ED is the finding that impaired penile vascular dynamics, as documented on PDU, may be associated with a generalized vessel disease that often predates cardiovascular disease by 5–10 years [3–5]. Significantly, early treatment of metabolic factors (e.g., hypertension, dyslipidemia, hyperglycemia) can delay and possibly prevent the development of cardiovascular disease [6, 7]. Therefore, the physician evaluating ED has a unique opportunity to diagnose vascular impairment at a time when lifestyle changes and possible medical intervention have the potential to change morbidity and mortality of cardiovascular disease. As suggested by Miner, there might be a "window of curability" in which the significant risk of future cardiovascular events might be averted through early diagnosis and treatment [8–10].

In cases of diagnostic study for ED, emphasis is directed toward the cavernosal arteries. However, the initial survey scan is essential to evaluate for plaques, intracavernosal lesions, and urethral pathology as well as evaluation of the dorsal penile vessels. The cavernosal arteries are visualized within the corpora cavernosa, and the depth of these arteries can be easily defined within the corpora during transverse scanning to ensure a comprehensively represented assessment of diameter at different points along its course. Color Doppler examination of the penis should be performed in both transverse and longitudinal planes of view. Using the transverse views as a guide to cavernosal artery depth, turning the transducer probe 90° then provides longitudinal views of each corpus cavernosum separately, allowing for identification of the cavernosal arteries in longitudinal section (Fig. 7.3). The diameter of the cavernosal artery should be measured on each side. Color flow Doppler makes recognition of the location and direction of blood flow easy. Measurements of vessel diameter to assess the peak systolic flow velocity (PSV) as well as end-diastolic flow velocity (EDV) allow for the assessment of a vascular resistive index (RI) (Fig. 7.4). The diameter of the cavernosal artery ranges from 0.2 to 1.0 mm in a flaccid penis [11, 12]. PSV varies at different points along the length of the cavernosal artery, typically with higher velocities occur more proximally [13]. Hence, assessment of the PSV and EDV should be recorded at the junction of the proximal one-third and the distal two-thirds of the penile shaft. In the flaccid state, cavernosal artery PSV normally measures 5–15 cm/s, at baseline. This should be assessed and compared to the pharmacostimulated state [14, 15].

Intracavernosal injection therapy should then be given. At regimented serial time points following the injection of vasoactive medication, cavernosal artery dimensions, and flow velocities should be recorded to assess the response to pharmacologic stimulation. After prepping the lateral aspect of the penile shaft

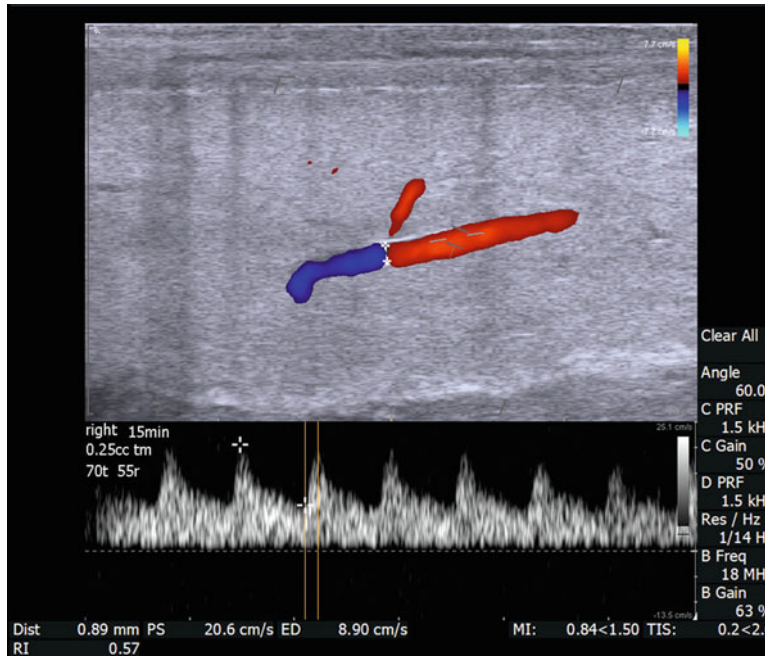

Fig. 7.4 The right cavernosal artery is imaged 15 min after intracavernosal injection of 0.25 mL of the trimix. The measured vessel diameter is 0.89 mm. The direction of flow and a dorsal branch of the cavernosal artery is easily appreciated with color Doppler. Also documented on this image is measurement of arterial diameter (0.89 mm), PSV (20.6 cm/s), EDV (8.9 cm/s), and calculated RI (0.57) are shown. Please note that the angle of incidence is electronically made to be 60° by both electronic steering of the transducer and aligning the cursor to be parallel to the flow of blood through the artery. In addition the width of the caliper is adjusted to be approximately ¾ the width of the artery for best sampling

with an alcohol or povidone-iodine prep pad, a finely measured volume of a vasoactive agent should be injected into one corpus cavernosum (in the distal two-thirds of the penile shaft) using a 29 or 30 gauge ½″ needle. Pressure should be held on the injection site for at least 2 min to prevent hematoma formation.

Vasoactive agents used for pharmacologic stimulation of erection include prostaglandin E1, papaverine, or trimix (combination of prostaglandin E1, papaverine, and phentolamine) [16]. As with every medication administration, the expiration date of the medication should be reviewed, patient allergies should be evaluated, and the dosage administered should be documented. We obtain an informed consent after the patient is counseled about the known risk for developing a low-flow priapism and appropriate follow-up if this were to arise [17]. This protocol requires the patient to stay in the office until penile detumescence occurs. A treatment protocol for low-flow priapism is given in Table 7.2. Of note, for patients in which we have given a vasoactive agent and have had to treat for low-flow priapism, aspiration, irrigation, and injection of intracorporal phenylephrine are usually successful to reverse

Table 7.2 Treatment protocol for low-flow priapism caused by pharmacologic induction by vasoactive agents

Observation: If no detumescence in 1 h, then
• Aspiration: With a 19 or 21 gauge butterfly needle aspirate 30–60 cc corporal blood. A sample should be sent for diagnostic cavernosal blood gas to confirm low-flow, ischemic state. Repeat in ½h if 100% rigidity returns
• Pharmacologic detumescence:
Phenylephrine 100–500 μg injected in a volume of 0.3–1 cc every 3–5 min for a maximum of 1 h
Monitor for acute hypertension, headache, reflex bradycardia, tachycardia, palpitations, and cardiac arrhythmia
Serial noninvasive blood pressure and continuous electrocardiogram monitoring are recommended

the priapism state. In our experience, when required, corporal aspiration alone has been uniformly successful in the setting of pharmacologically induced priapism following diagnostic duplex penile ultrasonography.

Arteriogenic ED is a form of peripheral vascular disease, commonly associated with diabetes mellitus and/or coronary artery disease. PSV is the most accurate measure of arterial disease as the cause of ED. The average PSV after intracavernosal injection of vasoactive agents in healthy volunteers without ED ranges from 35 to 47 cm/s, with a PSV of 35 cm/s or greater signifying arterial sufficiency following pharmacostimulation [18–23]. Primary criteria for arteriogenic ED include a PSV less than 25 cm/s, cavernosal artery dilation less than 75%, and acceleration time >110 ms. In cases of equivocal PSV measurements, particularly when PSV is between 25 and 35 cm/s included, asymmetry of greater than 10cm/s in PSV comparing the two cavernosal arteries, focal stenosis of the cavernosal artery, cavernosal artery, and cavernosal-spongiosal flow reversal [24].

Veno-occlusive insufficiency, also referred to as venous leak, can only be diagnosed in cases of ED where the patient was confirmed to have appropriate arterial function as measured by PSV. PDU parameters to assess the presence of veno-occlusive insufficiency as the cause of ED are EDV and RI. Antegrade EDV greater than 5 cm/s in the cavernosal artery demonstrated throughout the study, especially at the most turgid level of erection achieved, is suggestive of a venous leak [25, 26]. This is only true if PSV is normal. Arteriogenic dysfunction by definition fails to produce a fully tumescent and rigid phallus. In the setting of venous leak, EDV is always greater than 0. The definitive test for venous leak is the DICC (dynamic infusion cavernosography and cavernosometry). However, when both arteriogenic and venogenic dysfunction exists, interpretation of DICC is difficult. On PDU an RI of less than 0.75, measured 20 min following maximal pharmacostimulation, has been found to be associated with a venous leak in 95% of patients [27]. In the absence of a venous leak, a fully erect penis should have an EDV nearing zero, and hence the RI should approach or exceed (when reverse flow occurs) 1.0 (Fig. 7.5). In cases of diagnostic PDU with intracavernosal pharmacostimulation where an RI of 1.0 or greater is achieved, we recommend immediate treatment or prolonged observation to achieve detumescence because of the high specificity of absent diastolic flow for priapism [28].

In cases where arterial function and venous leak may be coexistent processes, indeterminate results may be yielded on PDU, and a mixed vascular cause of ED may be assumed. However, venous competence cannot be accurately assessed in a patient with arterial insufficiency (Fig. 7.6).

As previously discussed, arteriogenic ED has been found to correlate directly with other systemic cardiovascular diseases, both coronary artery disease (CAD) and peripheral vascular disease (PVD), in a number of population studies [29, 30]. Researchers have postulated the common risk factor of atherosclerotic vascular disease and impaired endothelium-dependent vasodilation by way of the nitric oxide pathway as the underlying pathophysiologic explanation for the remarkable overlap between these disease processes [31–33]. Also, hypogonadism has been noted as a common etiology for organic erectile dysfunction and disorders leading to metabolic syndrome [34, 35]. Vessel compliance is compromised in arteriogenic ED as it is in CAD. Patients with severe vascular etiology ED have an increased cavernosal artery diameter of less than 75% (with overall luminal diameter rarely above 0.7 mm) following injection of vasoactive agents into the corpora cavernosa [22, 36].

Studies have demonstrated that vasculogenic ED may actually provide a lead time on otherwise silent and undiagnosed cardiovascular disease [29, 37, 38]. ED has also been found to predict metabolic syndrome in men with normal body weight, as defined by body mass index (BMI) less than 25 kg/m [2], suggesting that the early diagnosis and intervention of vasculogenic ED might avert significant morbidity and provide a public health benefit by reducing the significant risk of cardiovascular and metabolic syndrome risk in men with ED [3, 5, 10, 39–42].

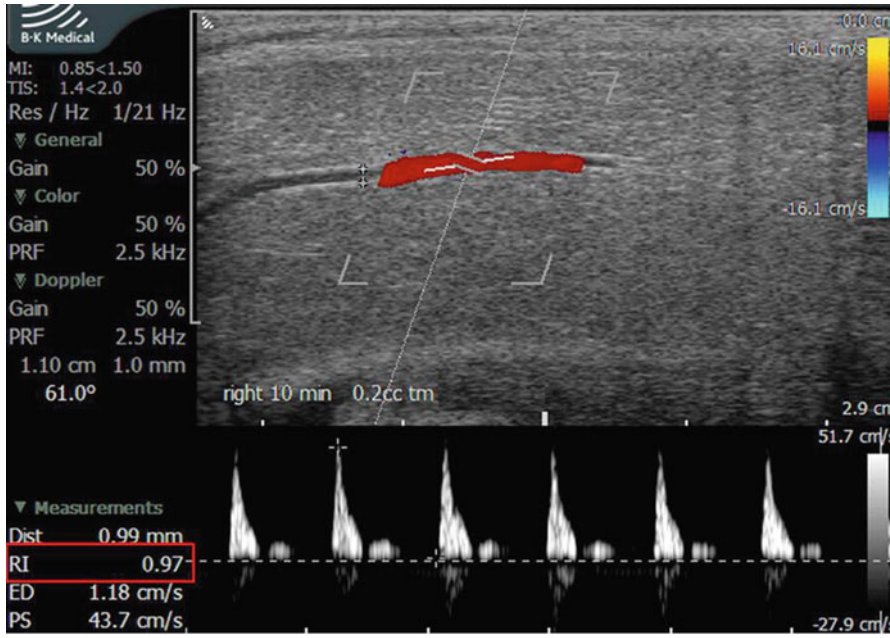

Fig. 7.5 In a fully erect phallus the RI should approach or exceed 1.0. If this condition persists, it is termed low-flow priapism. Color Doppler ultrasound findings in low-flow priapism demonstrate poor flow or absent flow in the cavernosal artery of the penis with moderate flow in the dorsal artery and vein. Also, there is no flow within the corpora cavernosa

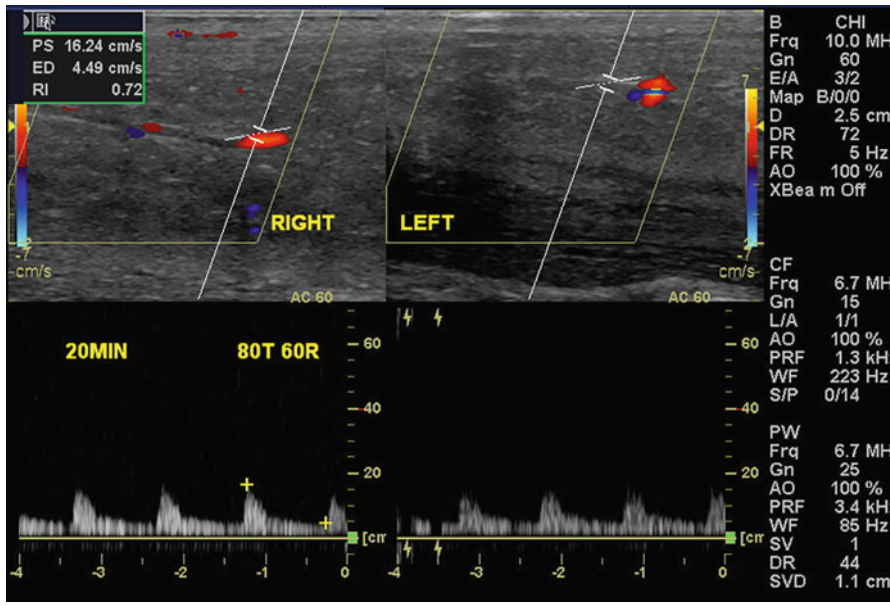

Fig. 7.6 With maximal stimulation, a PSV less than 25 cm/s suggests significant arteriogenic dysfunction. Referral for evaluation of cardiovascular disease is recommended

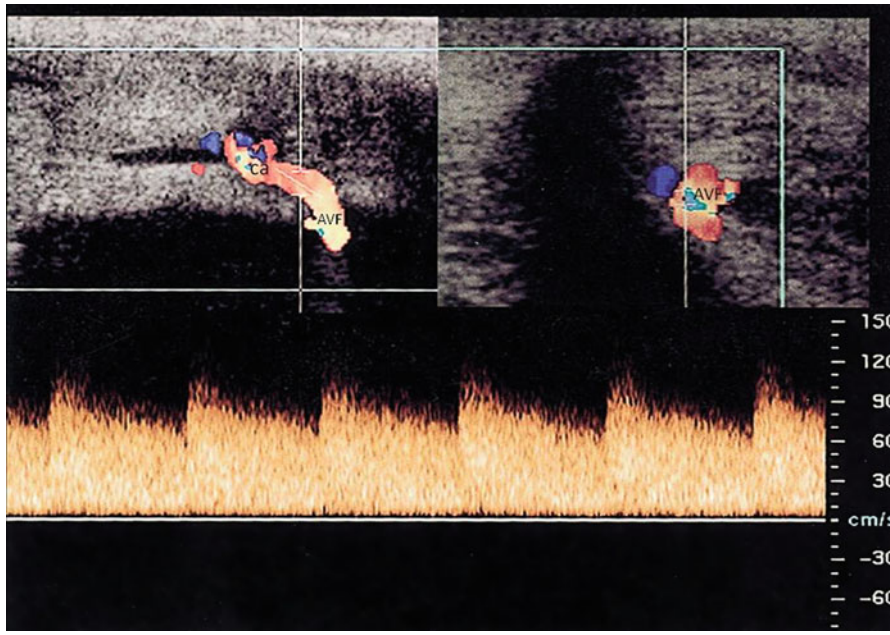

Fig. 7.7 Color Doppler ultrasound findings in a high-flow priapism demonstrating high-flow velocity in the cavernosal artery (ca) feeding the arteriovenous fistula (AVF)

Protocol box: suggested postinjection images when evaluating erectile dysfunction

- 5 and 10 min
  - Inner diameter measurements of left and right cavernosal artery and mid phallus.
  - Spectral Doppler waveform with PSV, EDV, and RI.
  - Optional: acceleration time.
- 15 and 20 min (second injection if indicated)
  - Inner diameter measurements of left and right cavernosal artery and mid phallus.
  - Spectral Doppler waveform with PSV, EDV, and Ri.
  - Optional: acceleration time.
- 25 and 30 min (third injection if indicated)
  - Inner diameter measurements of left and right cavernosal artery and mid phallus.
  - Spectral Doppler waveform with PSV, EDV, and Ri.
- Optional: acceleration time.

Priapism

Priapism can be differentiated as low-flow (ischemic) or high-flow (arterial) using PDU. Ultrasound plays an adjunct role to an illustrative history which may commonly indicate the likely underlying mechanism of priapism. Like laboratory tests including a cavernosal blood gas, PDU provides documentable findings that may guide further treatment. High-flow priapism is commonly a result of pelvic or perineal trauma which results in arterial fistulization between the cavernosal artery and the lacunae of the corpus cavernosum. Unlike low-flow priapism, which is a medical emergency associated with severely compromised venous drainage from the corpora cavernosa, high-flow priapism does not result in venous stasis and rapid risk of tissue necrosis. Ultrasound used to aide in the definitive diagnosis and localization of the cause of high-flow priapism can expedite treatment with selective angioembolization [43]. In cases of high-flow priapism PDU reveals normal or increased blood flow within the cavernosal arteries and irregular, turbulent flow pattern between the arteries into the cavernosal body at the site of an arterial-

lacunar fistula (Fig. 7.4). In contrast, a low-flow priapism on PDU would present with absent or very high-resistance flow within the cavernosal artery (Fig. 7.7).

A transperineal approach should also be used in cases of suspected high-flow priapism to fully evaluate the proximal aspects of the corpora cavernosa. Ultrasonography of these deep structures may reveal ateriocavernosal fistula following perineal trauma, not evident by routine scanning of the penile shaft.

Penile Fracture

Similar to priapism, the diagnosis of penile fracture is largely clinical, based upon the history gathered combined with the physical examination findings. However, PDU may play an important diagnostic role in more elusive cases, expediting a definitive diagnosis and early surgical management [44, 45]. Penile fracture can be seen on ultrasonography as a break point in the normally thin, hyperechoic tunica albuginea with altered echotexture in the adjacent area in the corpus cavernosum (Fig. 7.8a, b). This area of injury is also void of blood flow on color flow Doppler. Penile ultrasound can be used to measure the resultant hematoma that extrudes from the break point in the tunica albuginea (Fig. 7.8c).

In cases of both conservative management and postsurgical exploration and repair, PDU can be used as a minimally invasive follow-up study to ensure progressive healing, resorption of the hematoma, and intact blood flow on serial evaluations. Also, PDU allows for a dynamic anatomic assessment of erectile function following penile fracture in patients who have ED.

Dorsal Vein Thrombosis

Occasionally, dorsal vein thrombosis, often called Mondor's phlebitis, occurs with the triad of clinical symptoms of inflammation, pain, and fever resulting in patient consultation. There is often some induration and tenderness over the involved vein. The etiology has been variously ascribed to neoplasm, mechanical injury during intercourse,

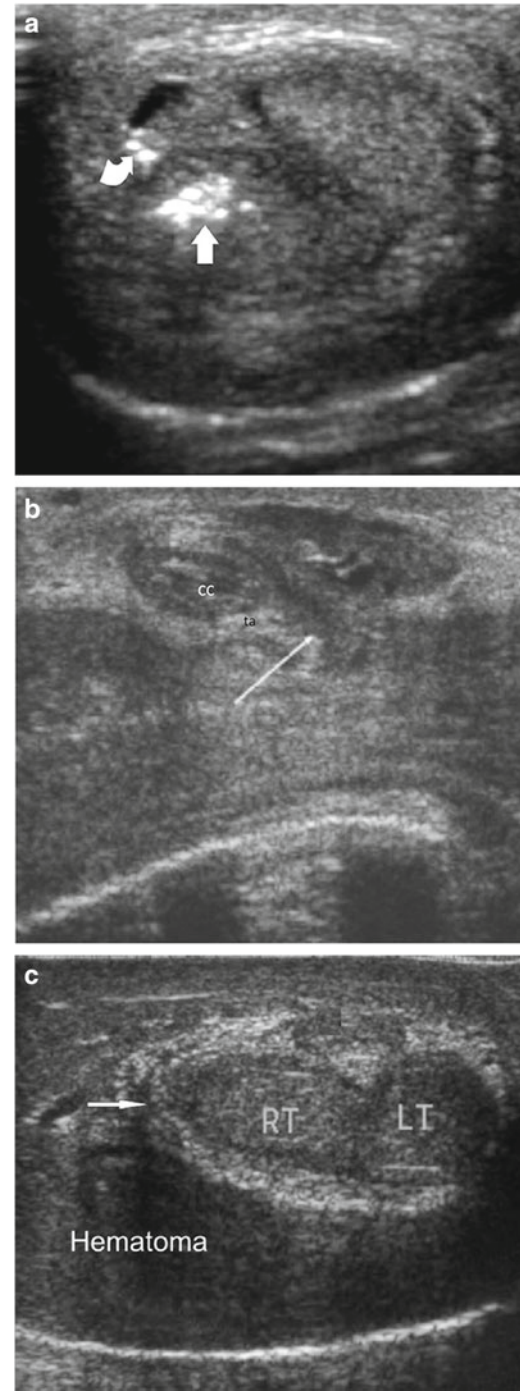

Fig. 7.8 Penile fracture depicted at the level of a tunica albugineal tear and presence of air spreading from urethral lumen through the corpus spongiosum (**a**, *curved arrow*) and right corpus cavernosum (**a**, *straight arrow*). In (**b**) the fracture is shown (*long arrow*) with tissue bulging above the tunica albuginea. The hematoma in (**c**) is seen outside of the right (RT) and left (LT) corporal bodies. The *arrow* indicates the tunical disruption

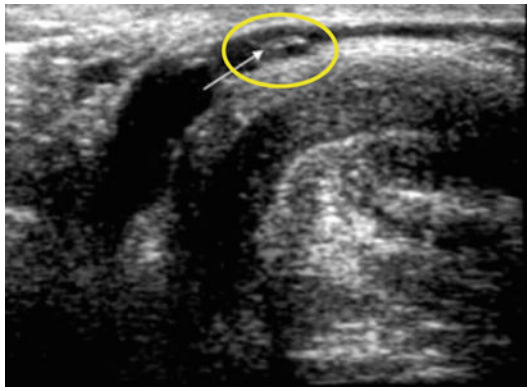

Fig. 7.9 Thrombosis of the dorsal penile vein (Mondors' phlebitis) is shown by the *arrow*

sickle cell disease, varicocele surgery, and herpes simplex infection. Occlusion of the vein can be visualized on ultrasound (Fig. 7.9) and followed with serial imaging as required to document resolution which usually occurs spontaneously as patency is reacquired in 6–8 weeks [46–50].

Peyronie's Disease

Penile ultrasonography can be used as an adjunct to a complete history and physical examination in the assessment of a patient with Peyronie's disease. Fibrotic plaques can be visualized as hyperechoic or hypoechoic areas of thickening of the tunica albuginea (Fig. 7.10a) [51, 52]. At times these plaques have elements of calcification, which cause a distinct hyperechoic focus with posterior shadowing on ultrasound (Fig. 7.10b). Ultrasonography can aid to confirm the presence of plaques palpated on physical examination and allows for accurate measurement of these lesions. Whenever possible, measurement of the plaque length, width, and depth should be obtained and documented. PDU can be used to assess perfusion around the area of plaques. Hyperperfusion is suggestive of active inflammation.

Many men with Peyronie's disease have coexistent ED. Men with Peyronie's disease and ED most commonly have veno-occlusive insufficiency secondary to the fibrotic plaques present, but arterial insufficiency or mixed vascular abnormalities can also be implicated as the cause of ED [53]. Comprehensive assessment of the underlying cause of ED using PDU provides guidance for the most appropriate patient-specific treatment course. In men with normal erectile function, plication or grafting procedures may be preferred. In men with concomitant Peyronie's disease and ED, reconstructive procedures may be undertaken with added care to define perforating collateral vasculature from the dorsal artery system. In more severe cases penile implant may be indicated.

Penile Masses

Most commonly masses discovered on physical examination are benign entities such as Peyronie's plaques, subcutaneous hematomas, or cavernosal herniation through tunica albuginea defects.

Cancerous lesions of the penis are rare. Nevertheless, primary penile carcinomas with deep invasion and more rarely metastatic lesions may present as masses within the penile deep tissues. Penile carcinoma is usually identified by inspection as most arise as a superficial skin lesion. Ultrasound usually identifies these lesions as hypoechoic ill-defined lesions with increased blood flow relative to surrounding tissues. Although not indicated for staging purposes, ultrasound can aid in assessment of anatomic relationships of the mass to deep structures, at times identifying depth of penetration in cases where the tumor clearly invades the tunica albuginea and corporal bodies [54, 55].

Metastatic deposits within the penis are exceedingly rare, but appear on ultrasound similar to primary penile carcinomas as hypoechoic lesions with hyperperfusion (Fig. 7.11a). However, metastatic lesions in the penis are rarely contiguous with the skin surface and are more commonly well circumscribed compared to primary penile cancers (Fig. 7.11b) [56].

Penile Urethral Pathologies

Penile ultrasound has been used as an adjunct to the physical examination to better diagnose and define specific urethral pathologies. Direct

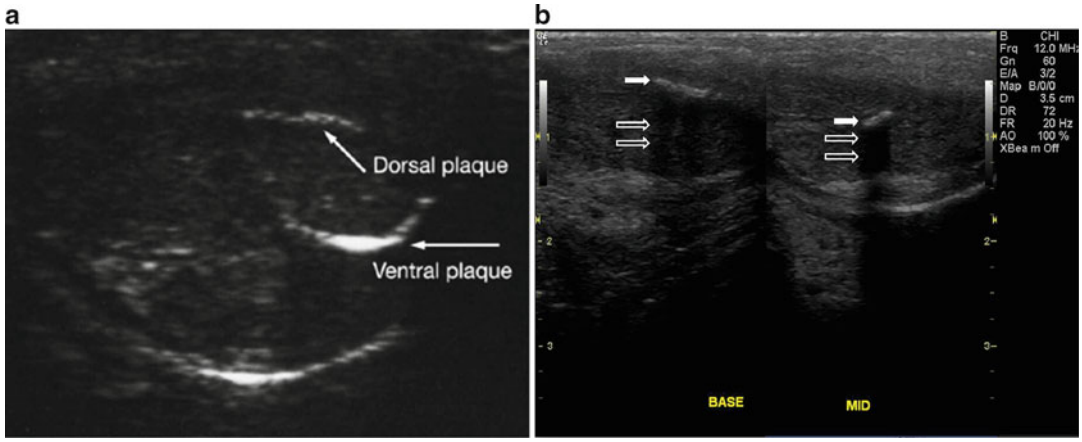

Fig. 7.10 (**a**) Hyperechoic areas on the dorsal and ventral surface of the left corpora cavernosa consistent without posterior shadowing consistent with non-calcified plaques. (**b**) A calcified plaque (*arrows*) at the base and midportion of the phallus with posterior shadowing (*open arrows*)

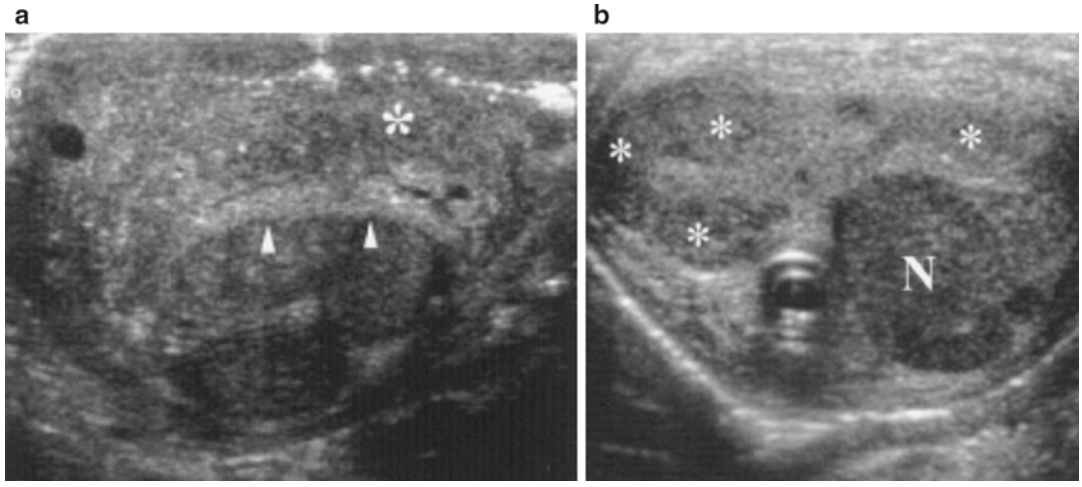

Fig. 7.11 (**a**) Squamous cell carcinoma of the penis (*asterisk*) confined to subepithelial tissue. The tunica albuginea of the corpora cavernosa (*arrowheads*) is intact. (**b**) Bladder cancer metastatic to penis with diffuse (*asterisk*) and nodular (N) involvement of the corpora cavernosa

urethral visualization using a cystoscope is the preferred diagnostic test for many urologists. However, ultrasound can provide an economically sound and noninvasive alternative for the assessment of urethral stricture, foreign bodies including urethral calculi, and urethral and periurethral diverticula, cysts, and abscesses.

Urethral strictures are the result of fibrous scarring of the urethral mucosa and surrounding spongiosal tissues which contract and narrow the luminal diameter of the urethral channel. Common causes of penile urethral strictures are infections, trauma, and congenital narrowing. Urethral trauma resulting in stricture disease includes, but is not limited to, straddle injury, passage of stones or foreign bodies, and iatrogenic instrumentation including catheterization and cystoscopy. Although retrograde urethrography is the standard imaging modality for urethral stricture disease (both anterior and posterior segments), penile ultrasound provides a more accurate assessment of stricture length and diameter in the anterior segment [57–59]. Furthermore, penile ultrasound allows for assessment of stricture involvement within the

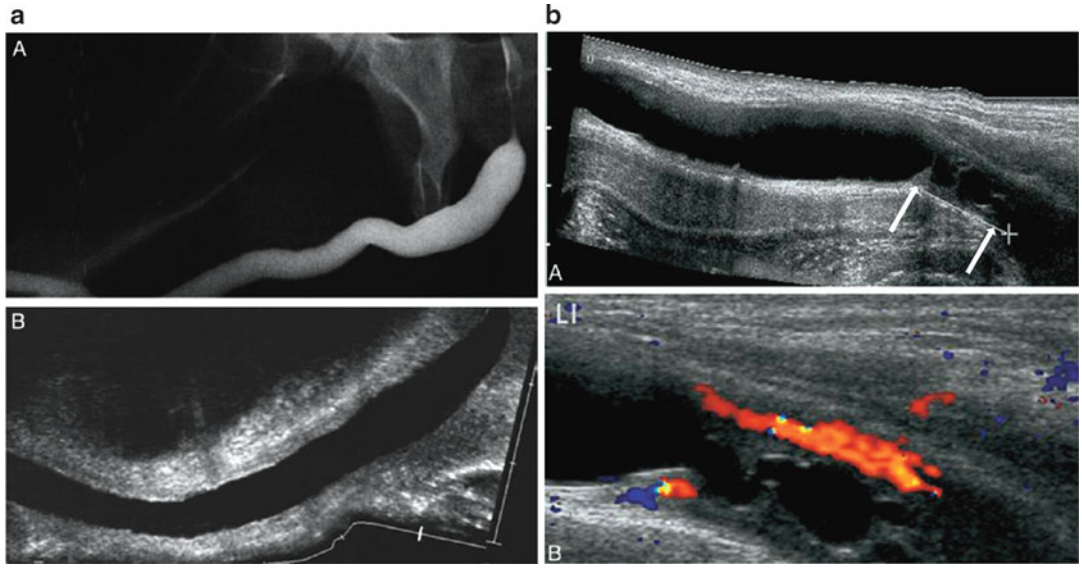

Fig. 7.12 (**a**) Normal Radio-urethrography (*top*) and sonourethrography (*bottom*). (**b**) Urethral stricture (*arrow*) with sonourethrography (*top*) and sonourethrography with color Doppler (*bottom*). Note the lumenal perfusion detail given by sonourethrography

periurethral spongy tissue whereas a classic urethrogram only assesses the luminal component of the pathology (Fig. 7.12a, b) [60]. On B-mode ultrasonography, strictures appear as hyperechoic areas surrounding the urethra without evidence of Doppler flow, consistent with findings of fibrosis. However, the fibrotic stricture segment may have surrounding Doppler flow demonstrating hyperemia from inflammation. With distension of the urethra with saline or lubricating jelly, areas of narrowing can be appreciated, corresponding to the location of a stricture (Fig. 7.12b top).

Urethral foreign bodies or calculi suspected based upon patient history and physical examination can be easily confirmed with penile ultrasound. Shape, size, and location of these obstructing bodies can be assessed, and a therapeutic plan can be made based upon the data obtained [61].

Urethral and periurethral diverticuli, cysts, and abscesses can be delineated with penile ultrasound with ease. A contrast medium such as normal saline or lubricating jelly is needed to provide a differential in ultrasound impedance to identify urethral or periurethral diverticula with the best sensitivity [62]. Cysts and abscesses around the urethra can be visualized using penile ultrasound without the insertion of contrast material. However, at times contrast material can be useful in identifying whether the structures noted are separate from the urethra once distended.

Importance of the Angle of Insonation

The Doppler shift (FD) is a change in frequency between the transmitted sound wave F_T and received sound wave F_R resulting from the interaction between the frequency of the sound waves transmitted by the transducer (F_T), the velocity of blood (V_{BF}), the cosine of the angle of incidence (θ) between the vector of the transmitted sound wave from the transducer and the vector of blood flow, as well as the speed of sound in tissue (c) as given by the equation

$$\mathrm{FD} = F_R - F_T = \frac{(2 * F_T * V_{BF} * \cos\theta)}{c}.$$

This concept of a Doppler shift is used to measure blood flow velocity whereby the shift in sound-wave frequency is detected by the ultrasound transducer after encountering active blood flow.

However, several factors influence the resultant frequency shift and hence the measured velocity. These include the incident frequency of the ultrasound beam used, speed of sound in soft

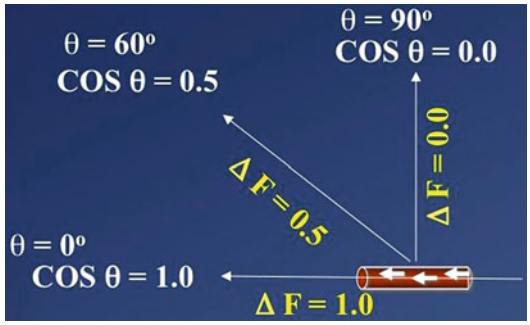

Fig. 7.13 Doppler angle: The change in Doppler frequency (ΔF) is directly related to the cosine of the angle of insonance (θ). The angle of insonance (the angle between the incident beam and the vector of blood flow) must be less than 60° for accurate measurements of blood flow velocity

tissues, the velocity of the moving reflectors (i.e., blood in a vessel), and the angle between the incident beam and vector of blood flow (θ) called the angle of insonation.

The angle of insonation is inversely related to Doppler shift. Hence, as the angle of insonation increases, approaching 90°, the Doppler shift decreases; and therefore the calculated blood flow velocity decreases to 0. The Doppler angle is therefore a significant technical consideration in performing duplex Doppler examinations, and an ideal angle of insonance between 0 and 60° is required (Fig. 7.13).

Clinical pearl: even if the angle of insonance is not corrected, the RI will be accurate. However, PSV and EDV will be inaccurate.

Proper Documentation

Complete and meticulous documentation of every ultrasound examination is an element of a comprehensive study. Documentation often entails a series of representative static images or cine series (when electronic storage space and technology allows) that are archived with an associated report documenting pertinent findings and indicated measurements and calculations. The combination of images and a written document of findings allows for optimal diagnosis aiding in patient care, archival reference in the patient medical record, and appropriate billing of services provided. Table 7.3 represents some diagnoses and associated ICD-9 codes for these diagnoses prompting or resulting from penile ultrasound evaluations.

Table 7.3 ICD-9 diagnosis codes for cases prompting penile ultrasound examination

594.2	Urethral stone
597.0	Urethral abscess
598.9	Urethral stricture
599.2	Urethral diverticulum
607.3	Priapism
607.84	Erectile dysfunction
607.85	Peyronie's disease
939.0	Foreign body in urethra
959.13	Penile fracture

An example report of a PDU performed as an element of an ED workup is shown in the Appendix. Each report must include patient identification (i.e., name, medical record number, date of birth, etc.), date of the examination, type of examination performed, indications for the examination, and pertinent findings and diagnoses. It is mandatory to include complete identification of the patient and study. Each report should also be undersigned by the ultrasonographer and physician interpreter of the study to document who performed the study and who read the results in cases where a technician performs the study saving images for a physician's interpretation. Copies of the printed images should be attached to the report or electronically stored images and/or videos should be referenced in the written report. The ultrasound images should be labeled with the date and time of the study, patient identification, and applicable anatomic labeling.

Conclusion

With a proper understanding of penile anatomy and functional physiology, penile ultrasound provides a real-time imaging modality assessing the static anatomic features and vascular dynamics. As a diagnostic modality, ultrasound provides urologists a vital tool in the office assessment of ED, Peyronie's disease, penile urethral strictures, and masses of the penis as well as an acute care setting evaluation of a penile trauma patient. It is essential that urologists maintain proficient PDU skills in their diagnostic armamentarium.

Appendix

A sample report template for a penile Doppler ultrasound performed as a diagnostic element in a case of erectile dysfunction.

				PATIENT LABEL					
PENILE ULTRASOUND									
DATE OF SERVICE:					BP:				
PROCEDURE:					Pulse:				
INDICATION:									
US MACHINE:				TRANSDUCER:					
B-MODE FINDINGS (ATTACH IMAGES)									
RIGHT CORPORA CAVERNOSUM				LEFT CORPORA CAVERNOSUM					
AP LONGITUDINALH (cm)				AP LONGITUDINAL (cm)					
PLAQUE_MASS (size,location):				PLAQUE_MASS (size,location):					
SIZE:	LOCATION:			SIZE:	LOCATION:				
ECHOGENICITY:				ECHOGENICITY:					
CALCIFICATIONS (quantity)				CALCIFICATIONS (quantity)					
INTRACORPORA COMMENTS:									
TRANSVERSE	AP	Width		TRANSVERSE	AP	Width			
PROXIMAL (cm)				PROXIMAL (cm)					
MID (cm)				MID (cm)					
DISTAL (cm)				DISTAL (cm)					
LESION (Y/N):	TYPE:			LESION (Y/N):	TYPE:				
SIZE:	LOCATION:			SIZE:	LOCATION:				
ECHOGENICITY:				ECHOGENICITY:					
COMPARATIVE ECHOGENICITY									
CORPORACAVERNOSUS COMMENTS									
BULBOCAVERNOSUS COMMENTS									
COLOR DOPPLER/DUPLEX FINDINGS (ATTACH IMAGES)									
INDICATION FOR COLOR/DUPLEX STUDY:									
COMMENTS:									
PSV	EDV	RI	Dia (mm)	Time	PSV	EDV	RI	DIA (mm)	Tum/Rig
				Baseline					
				5 MIN					
				10 MIN					
				15 MIN					
				20 MIN					
				30 MIN					
				40 MIN					
PHYSICIAN INTERPRETATION									
DATE/TIME									
			PHYSICIAN SIGNATURE						
					Bruce R. Gilbert, MD, PhD.				

References

1. Doubilet PM, Benson CB, Silverman SG, et al. The penis. Semin Ultrasound CT MR. 1991;12:157.
2. http://www.auanet.org/content/guidelines-and-quality-care/policy-statements.cfm
3. Shin D, Pregenzer Jr G, Gardin JM. Erectile dysfunction: a disease marker for cardiovascular disease. Cardiol Rev. 2011;19:5.
4. Tomada N, Tomada I, Botelho F, et al. Are all metabolic syndrome components responsible for penile hemodynamics impairment in patients with erectile dysfunction? The role of body fat mass assessment. J Sex Med. 2011;8(3):831–9.
5. Corona G, Monami M, Boddi V, et al. Male sexuality and cardiovascular risk. A cohort study in patients with erectile dysfunction. J Sex Med. 2010; 7:1918.
6. Wing RR. Long-term effects of a lifestyle intervention on weight and cardiovascular risk factors in individuals with type 2 diabetes mellitus: four-year results of the Look AHEAD trial. Arch Intern Med. 2010;170: 1566.
7. Hayashi T, Farrell MA, Chaput LA, et al. Lifestyle intervention, behavioral changes, and improvement in cardiovascular risk profiles in the California WISEWOMAN project. J Womens Health (Larchmt). 2010;19:1129.
8. Miner MM. Erectile dysfunction: a harbinger or consequence: does its detection lead to a window of curability? J Androl. 2011;32:125.
9. Inman BA, Sauver JL, Jacobson DJ, et al. A population-based, longitudinal study of erectile dysfunction and future coronary artery disease. Mayo Clin Proc. 2009;84:108.
10. Billups KL, Bank AJ, Padma-Nathan H, et al. Erectile dysfunction as a harbinger for increased cardiometabolic risk. Int J Impot Res. 2008;20:236.
11. Patel U, Lees WR. Penile sonography. In: Solibiati L, Rizzatto G, editors. Ultrasound of superficial structures. London: Churchill Livingstone; 1995. p. 229–42.
12. Wilkins CJ, Sriprasad S, Sidhu PS. Colour Doppler ultrasound of the penis. Clin Radiol. 2003;58:514.
13. Kim SH, Paick JS, Lee SE, et al. Doppler sonography of deep cavernosal artery of the penis: variation of peak systolic velocity according to sampling location. J Ultrasound Med. 1994;13:591.
14. Roy C, Saussine C, Tuchmann C, et al. Duplex Doppler sonography of the flaccid penis: potential role in the evaluation of impotence. J Clin Ultrasound. 2000;28:290.
15. Mancini M, Bartolini M, Maggi M, et al. Duplex ultrasound evaluation of cavernosal peak systolic velocity and waveform acceleration in the penile flaccid state: clinical significance in the assessment of the arterial supply in patients with erectile dysfunction. Int J Androl. 2000;23:199.
16. van Ahlen H, Peskar BA, Sticht G, et al. Pharmacokinetics of vasoactive substances administered into the human corpus cavernosum. J Urol. 1994;151:1227.
17. Patel U, Amin Z, Friedman E, et al. Colour flow and spectral Doppler imaging after papaverine-induced penile erection in 220 impotent men: study of temporal patterns and the importance of repeated sampling, velocity asymmetry and vascular anomalies. Clin Radiol. 1993;48:18.
18. Broderick GA, Lue TF. The penile blood flow study: evaluation of vasculogenic impotence. In: Jonas U, Thon WF, Stief CG, editors. Erectile dysfunction. Berlin: Springer; 1991.
19. Shabsigh R, Fishman IJ, Shotland Y, et al. Comparison of penile duplex ultrasonography with nocturnal penile tumescence monitoring for the evaluation of erectile impotence. J Urol. 1990;143:924.
20. Benson CB, Vickers MA. Sexual impotence caused by vascular disease: diagnosis with duplex sonography. AJR Am J Roentgenol. 1989;153:1149.
21. Lue TF, Hricak H, Marich KW, et al. Vasculogenic impotence evaluated by high-resolution ultrasonography and pulsed Doppler spectrum analysis. Radiology. 1985;155:777.
22. Mueller SC, Lue TF. Evaluation of vasculogenic impotence. Urol Clin North Am. 1988;15:65.
23. Pescatori ES, Hatzichristou DG, Namburi S, et al. A positive intracavernous injection test implies normal veno-occlusive but not necessarily normal arterial function: a hemodynamic study. J Urol. 1994;151:1209.
24. Benson CB, Aruny JE, Vickers Jr MA. Correlation of duplex sonography with arteriography in patients with erectile dysfunction. AJR Am J Roentgenol. 1993; 160:71.
25. Bassiouny HS, Levine LA. Penile duplex sonography in the diagnosis of venogenic impotence. J Vasc Surg. 1991;13:75.
26. Quam JP, King BF, James EM, et al. Duplex and color Doppler sonographic evaluation of vasculogenic impotence. AJR Am J Roentgenol. 1989;153:1141.
27. Naroda T, Yamanaka M, Matsushita K, et al. [Clinical studies for venogenic impotence with color Doppler ultrasonography–evaluation of resistance index of the cavernous artery]. Nippon Hinyokika Gakkai Zasshi. 1996;87:1231.
28. Cormio L, Bettocchi C, Ricapito V, et al. Resistance index as a prognostic factor for prolonged erection after penile dynamic colour Doppler ultrasonography. Eur Urol. 1998;33:94.
29. Feldman HA, Johannes CB, Derby CA, et al. Erectile dysfunction and coronary risk factors: prospective results from the Massachusetts male aging study. Prev Med. 2000;30:328.
30. Blumentals WA, Gomez-Caminero A, Joo S, et al. Should erectile dysfunction be considered as a marker for acute myocardial infarction? Results from a retrospective cohort study. Int J Impot Res. 2004;16:350.

31. Sullivan ME, Thompson CS, Dashwood MR, et al. Nitric oxide and penile erection: is erectile dysfunction another manifestation of vascular disease? Cardiovasc Res. 1999;43:658.
32. Solomon H, Man JW, Jackson G. Erectile dysfunction and the cardiovascular patient: endothelial dysfunction is the common denominator. Heart. 2003;89:251.
33. Montorsi P, Montorsi F, Schulman CC. Is erectile dysfunction the "tip of the iceberg" of a systemic vascular disorder? Eur Urol. 2003;44:352.
34. Guay AT. The emerging link between hypogonadism and metabolic syndrome. J Androl. 2009;30:370.
35. Traish AM, Guay AT. Are androgens critical for penile erections in humans? Examining the clinical and preclinical evidence. J Sex Med. 2006;3:382.
36. Lue TF, Tanagho EA. Physiology of erection and pharmacological management of impotence. J Urol. 1987;137:829.
37. O'Kane PD, Jackson G. Erectile dysfunction: is there silent obstructive coronary artery disease? Int J Clin Pract. 2001;55:219.
38. Mulhall J, Teloken P, Barnas J. Vasculogenic erectile dysfunction is a predictor of abnormal stress echocardiography. J Sex Med. 2009;6:820.
39. Zambon JP, Mendonca RR, Wroclawski ML, et al. Cardiovascular and metabolic syndrome risk among men with and without erectile dysfunction: case–control study. Sao Paulo Med J. 2010;128:137.
40. Mottillo S, Filion KB, Genest J, et al. The metabolic syndrome and cardiovascular risk a systematic review and meta-analysis. J Am Coll Cardiol. 2010;56:1113.
41. Bohm M, Baumhakel M, Teo K, et al. Erectile dysfunction predicts cardiovascular events in high-risk patients receiving telmisartan, ramipril, or both: The ONgoing Telmisartan Alone and in combination with Ramipril Global Endpoint Trial/Telmisartan Randomized AssessmeNt Study in ACE iNtolerant subjects with cardiovascular Disease (ONTARGET/TRANSCEND) Trials. Circulation. 2010;121:1439.
42. Batty GD, Li Q, Czernichow S, et al. Erectile dysfunction and later cardiovascular disease in men with type 2 diabetes: prospective cohort study based on the ADVANCE (Action in Diabetes and Vascular Disease: Preterax and Diamicron Modified-Release Controlled Evaluation) trial. J Am Coll Cardiol. 2010;56:1908.
43. Kang BC, Lee DY, Byun JY, et al. Post-traumatic arterial priapism: colour Doppler examination and superselective arterial embolization. Clin Radiol. 1998; 53:830.
44. Asgari MA, Hosseini SY, Safarinejad MR, et al. Penile fractures: evaluation, therapeutic approaches and long-term results. J Urol. 1996;155:148.
45. El-Bahnasawy MS, Gomha MA. Penile fractures: the successful outcome of immediate surgical intervention. Int J Impot Res. 2000;12:273.
46. Atan A, Gungor S, Ozergin O, et al. Idiopathic penile mondors' disease: a case report. Int Urol Nephrol. 2002;34:97.
47. Dicuio M, Pomara G, Ales V, et al. Doppler ultrasonography in a young patient with penile Mondor's disease. Arch Ital Urol Androl. 2005;77:58.
48. Sasso F, Gulino G, Basar M, et al. Penile Mondors' disease: an underestimated pathology. Br J Urol. 1996;77:729.
49. Nachmann MM, Jaffe JS, Ginsberg PC, et al. Sickle cell episode manifesting as superficial thrombophlebitis of the penis. J Am Osteopath Assoc. 2003; 103:102.
50. Luzzi GA, Pattinson J, Wathen CG. Penile Mondor's disease and inherited thrombophilia. Int J STD AIDS. 2006;17:70.
51. Brock G, Hsu GL, Nunes L, et al. The anatomy of the tunica albuginea in the normal penis and Peyronie's disease. J Urol. 1997;157:276.
52. Chou YH, Tiu CM, Pan HB, et al. High-resolution real-time ultrasound in Peyronie's disease. J Ultrasound Med. 1987;6:67.
53. Kadioglu A, Tefekli A, Erol H, et al. Color Doppler ultrasound assessment of penile vascular system in men with Peyronie's disease. Int J Impot Res. 2000;12:263.
54. Horenblas S, Kroger R, Gallee MP, et al. Ultrasound in squamous cell carcinoma of the penis; a useful addition to clinical staging? A comparison of ultrasound with histopathology. Urology. 1994;43:702.
55. Lont AP, Besnard AP, Gallee MP, et al. A comparison of physical examination and imaging in determining the extent of primary penile carcinoma. BJU Int. 2003;91:493.
56. Lan SK, Lin CW, Ho HC, et al. Penile metastasis secondary to nasal NK/T-cell lymphoma. Urology. 2008;72:1014.
57. Gallentine ML, Morey AF. Imaging of the male urethra for stricture disease. Urol Clin North Am. 2002;29:361.
58. Morey AF, McAninch JW. Role of preoperative sonourethrography in bulbar urethral reconstruction. J Urol. 1997;158:1376.
59. Choudhary S, Singh P, Sundar E, et al. A comparison of sonourethrography and retrograde urethrography in evaluation of anterior urethral strictures. Clin Radiol. 2004;59:736.
60. Morey AF, McAninch JW. Sonographic staging of anterior urethral strictures. J Urol. 2000;163:1070.
61. Kim B, Kawashima A, LeRoy AJ. Imaging of the male urethra. Semin Ultrasound CT MR. 2007; 28:258.
62. Bearcroft PW, Berman LH. Sonography in the evaluation of the male anterior urethra. Clin Radiol. 1994; 49:621.

Transabdominal Pelvic Ultrasound

8

R. Ernest Sosa and Pat F. Fulgham

Introduction

Transabdominal pelvic ultrasound provides instant noninvasive imagery of the lower urinary tract for the assessment of urologic conditions. It is useful in evaluating patients with lower urinary tract symptoms. The examining physician gains valuable information about the anatomy and function of a patient's bladder and prostate. In the female patient, bladder hypermobility can be assessed. Urologists performing and interpreting bladder ultrasound will have a specific clinical question in mind as a reason for performing the scan. In order to obtain a good-quality diagnostic image and render an interpretation of the ultrasound findings, it is important to have an understanding of ultrasound machine settings, patient positioning, probe manipulation, normal ultrasound anatomy, and common artifacts.

R. Ernest Sosa, MD
Chief, Division of Urology, Veterans Administration Healthcare System, New York Harbor, Manhattan, NY, USA

P.F. Fulgham, MD, FACS (✉)
Department of Urology, Texas Health Presbyterian Dallas, 8210 Walnut Hill Lane Suite 014, Dallas, TX 75231, USA
e-mail: pfulgham@airmail.net; patfulgham@yahoo.com

Indications

Ultrasound of the bladder is performed for a variety of clinical indications (Table 8.1). When the bladder is full, it provides information about bladder capacity as well as bladder wall thickness. The presence of bladder wall pathology such as tumors, trabeculations, and diverticula and the presence of bladder stones or of a foreign body can also be ascertained. Imaging of the ureteral orifices using Doppler can confirm the presence of ureteral efflux of urine. The presence of a ureterocele or a stone in the distal ureter or the presence of distal ureteral dilation may also be appreciated. In the male patient, prostate size and morphology may be evaluated. In the female patient, bladder hypermobility can be assessed. In male and female patients, the proper position of a urethral catheter in the bladder can be confirmed (Fig. 8.1). The presence of blood clot and tumor in the bladder can also be determined (Fig. 8.2).

Pelvic ultrasound may also be useful to guide procedures such as deflation of a retained catheter balloon or for guiding the placement of a suprapubic catheter [1].

Patient Preparation and Positioning

The patient should have a full bladder but should not be uncomfortably distended. A bladder volume of approximately 150 cc is optimal. The patient is placed in the supine position on the

P.F. Fulgham and B.R. Gilbert (eds.), *Practical Urological Ultrasound*, Current Clinical Urology,
DOI 10.1007/978-1-59745-351-6_8,

Table 8.1 Indications for bladder ultrasound

1. Measurement of bladder volume
2. Measurement of post-void residual
3. Measurement of prostate size and morphology
4. Assessment of anatomic changes associated with bladder outlet obstruction a. Bladder wall thickness b. Bladder wall trabeculation c. Bladder wall diverticula d. Bladder stones
5. Documentation of efflux of urine from the ureteral orifices
6. Evaluation of pediatric posterior urethral valves
7. Assessment of correct position of a urethral catheter
8. Guidance for placement of a suprapubic tube
9. Assessment for completeness of the evacuation of bladder clots
10. Evaluation of hematuria
11. Evaluation for bladder tumors
12. Evaluation for distal ureteral dilation
13. Evaluation for foreign body in bladder
14. Evaluation for distal ureteral stone
15. Evaluation for ureterocele
16. Evaluation for complete bladder emptying
17. Assessment for bladder neck hypermobility in women
18. Evaluation of pelvic fluid collections
19. Guidance for transperineal prostate biopsy
20. Imaging of prostate when the rectum is absent or obstructed

examining table. The abdomen is exposed from the xiphoid process to just below the pubic bone. The patient may place their arms up above their head or by their side on the table. The room should be at a comfortable temperature. The lights are dimmed. A paper drape placed over the pelvic area and tucked into the patient's clothing will protect the clothing and allow for easy cleanup after the procedure. The examiner assumes a comfortable position to the patient's right.

Equipment and Techniques

The appropriate mode for performing pelvic ultrasound is selected on the ultrasound equipment, and the patient's demographics are entered into demographic fields. A curved-array transducer is utilized for the pelvic ultrasound study (Fig. 8.3). The advantage of the curved-array transducer is that it requires a small skin surface for contact and produces a wider field of view. In the adult patient, a 3.5–5.0 MHz transducer is utilized to examine the bladder. For the pediatric patient, particularly for a small, young child, a higher frequency transducer is desirable, particularly for a small, young child.

An even coating of warm conducting gel is placed on the skin of the lower abdominal wall or on the probe face. Prior to beginning the ultrasound examination the transducer is most often held in the examiner's right hand. The orienting notch on the transducer is identified (Fig. 8.3). The orientation of the transducer may be confirmed by placing a finger on the contact surface near the notch. The image produced by contact with the finger should appear on the left side of the screen indicating the patient's right side in the transverse plane and the cephalad direction in the sagittal plane.

Various techniques for probe manipulation are useful in ultrasound (Fig. 8.4). The techniques of rocking and fanning are non-translational, meaning the probe face stays in place while the probe body is rocked or fanned to evaluate the area of interest. The techniques of painting and skiing are translational, meaning the probe face is moved along the surface of the skin to evaluate the area of interest. All four techniques are useful for avoiding obstacles like the pubic bone or bowel gas and for performing a survey scan.

Ultrasound of the bladder may be started in the transverse view with the notch on the transducer to the patient's right (Fig. 8.5). The transducer is placed on the lower abdominal wall with secure but gentle pressure. If the pubic bone is in the field of view, the bladder may not be fully visualized. The pubic bone will reflect the sound waves resulting in acoustic shadowing which obscures the bladder. The pubic bone may be avoided by varying the angle of insonation using the fanning technique until a full transverse image is obtained. In the transverse view of the bladder, the right side of the bladder should appear on the left side of the screen. The machine settings may be adjusted until the best-quality image is obtained.

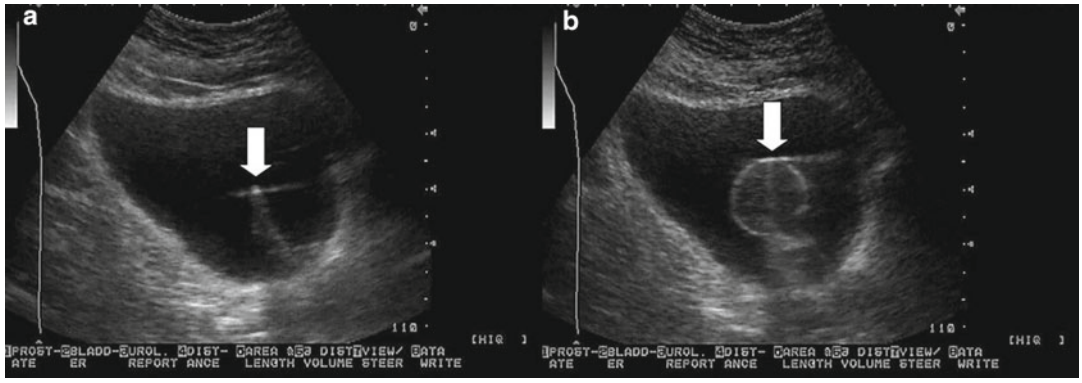

Fig. 8.1 (**a**) The tip of the balloon catheter is seen in the bladder (*arrow*). (**b**) Image of the inflated balloon in the bladder (*arrow*)

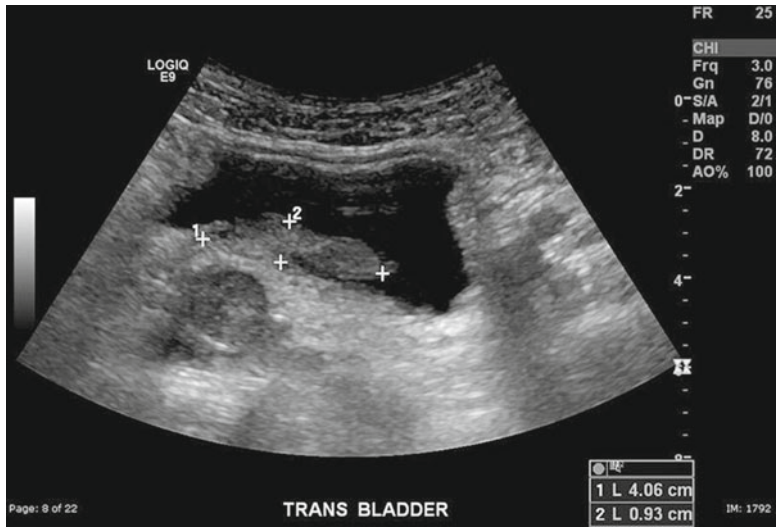

Fig. 8.2 Residual blood clot in the bladder after irrigation for clot retention

Fig. 8.3 Curved-array transducer with orienting notch (*arrow*)

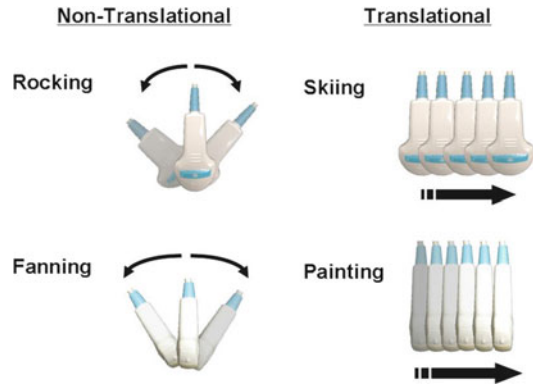

Fig. 8.4 Various techniques for probe manipulation

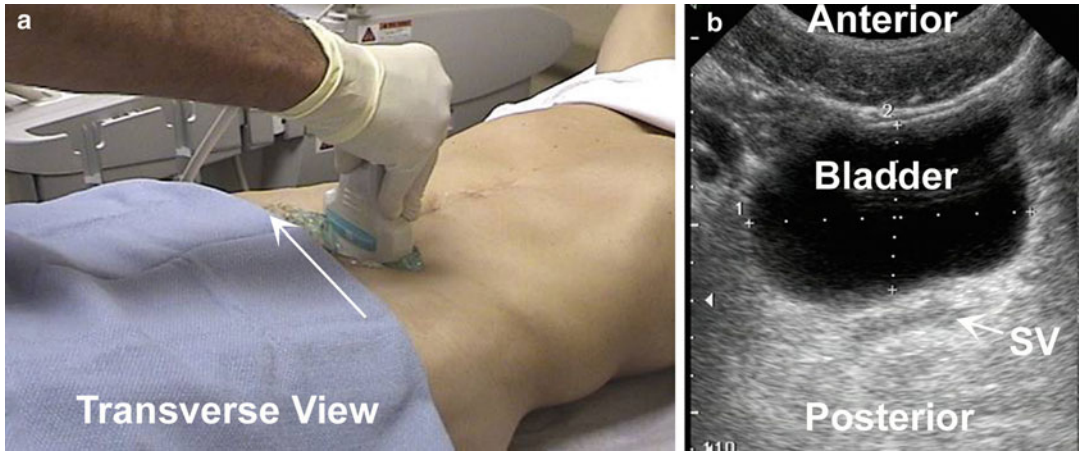

Fig. 8.5 (**a**) Position of transducer for obtaining a transverse image. Notch (*arrow*) is directed toward patient's right. (**b**) Transverse image of the bladder with measurements of the width (*1*) and height (*2*) of the bladder. *SV* seminal vesicles

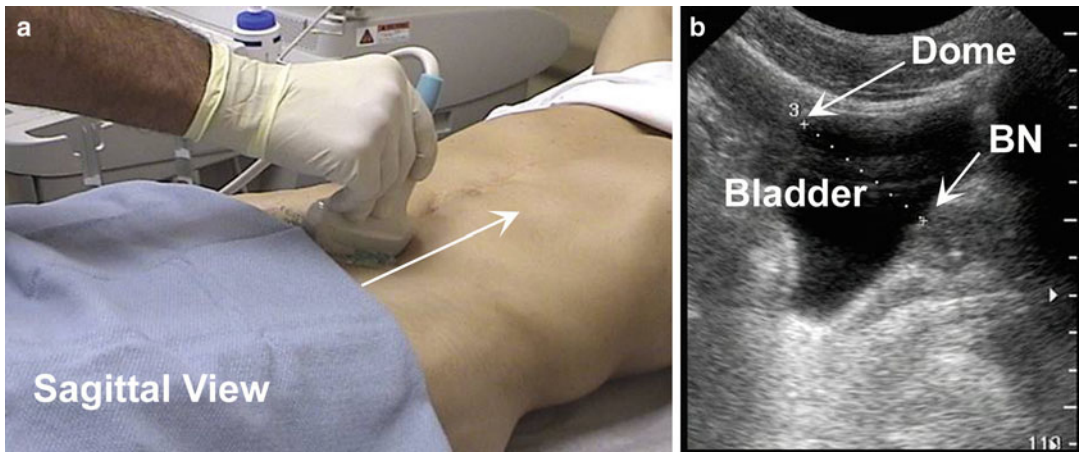

Fig. 8.6 (**a**) Position of the transducer with the notch to the patient's head. (**b**) Sagittal image of the bladder with length of the bladder (*3*) from the dome on the *left* to the bladder neck (BN) at the *right*

Survey Scan of the Bladder

A survey scan should be conducted prior to addressing specific clinical conditions to determine if any additional or incidental pathology is present. The survey scan is performed in the transverse view then the sagittal view, the length. When starting with a transverse view, the sagittal view is obtained by rotating the transducer 90° clockwise with the probe notch pointing toward the patient's head (Fig. 8.6). The rocking technique may be used to facilitate viewing the bladder in the sagittal view.

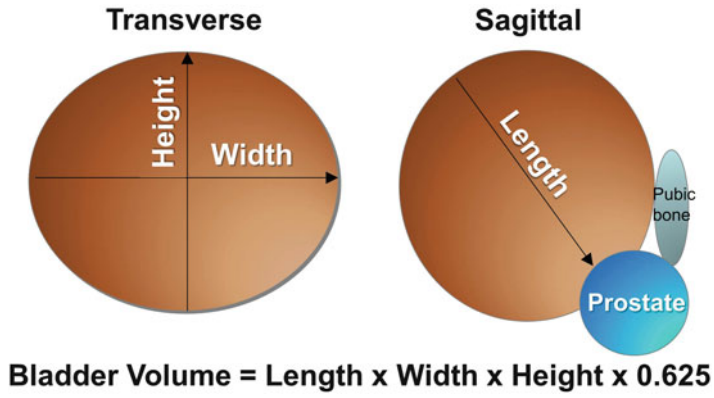

Fig. 8.7 The formula for calculating bladder volume = width (*1*) × height (*2*) × length (*3*) × 0.625

Measurement of Bladder Volume

The bladder volume is obtained by first locating the largest transverse diameter in the mid-transverse view (Fig. 8.7). The width and the height are measured. The transducer is then rotated 90° clockwise to obtain the sagittal view. In the mid-sagittal view the length of the bladder is measured using the dome and the bladder neck as the landmarks. These measurements may be made using a split screen so that both measurements are on the same screen. These images are printed or saved electronically. The bladder volume is calculated by multiplying the width, height, and length measurements by 0.625. When the specified measurements are obtained, the calculated bladder volume will usually be automatically displayed. When measuring urine volume in the bladder, the report should indicate whether the volume is a bladder volume measurement or a post-void residual urine volume measurement.

Measurement of Bladder Wall Thickness

Measurement of bladder wall thickness is taken, by convention, when the bladder is filled to at least 150 cc. Bladder wall thickness may be measured at a number of different locations. In this case the bladder wall thickness is measured along the posterior wall on the sagittal view (Fig. 8.8). If the bladder wall thickness is less than 5 mm when the bladder is filled to 150 cc, there is a 63% probability that the bladder is not obstructed. However, if the bladder wall thickness is over 5 mm at this volume, there is an 87% probability that there is bladder outlet obstruction. Nomograms are available to calculate the likelihood of urodynamically demonstrated bladder outlet for bladder wall thickness at various bladder volumes [2].

Evaluation of Ureteral Efflux

The efflux of urine from the distal ureters can be appreciated using power or color Doppler. By positioning the probe in the sagittal view (orienting notch toward the patient's head) and then twisting the probe approximately 15° to one side or the other, the probe is aligned with the direction of urine efflux from the ureteral orifice. This will often demonstrate efflux. Ureteral "jets" of urine can be seen on gray scale but are more easily seen using Doppler. These jets are seen as a yellow/orange streak when power Doppler is used (Fig. 8.9). These jets would appear red on color Doppler.

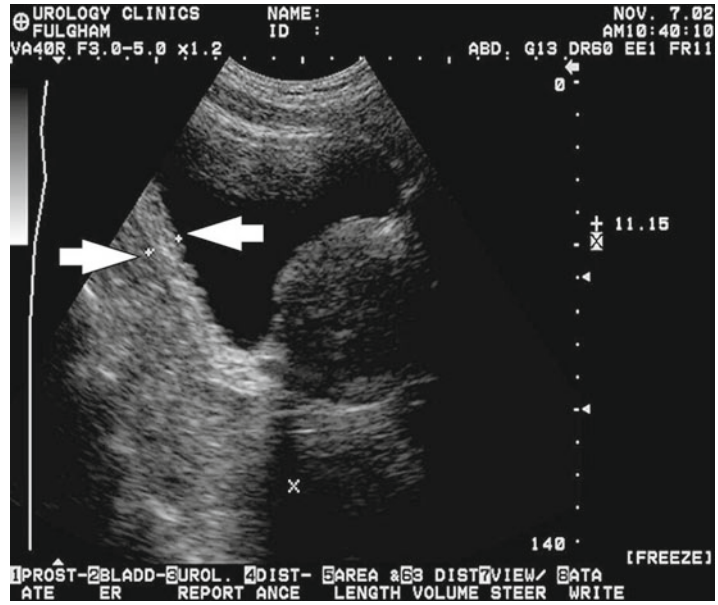

Fig. 8.8 Bladder wall thickness, in this case, is measured (*arrows*) along the posterior wall. In this image the wall measures 11.15 mm in thickness

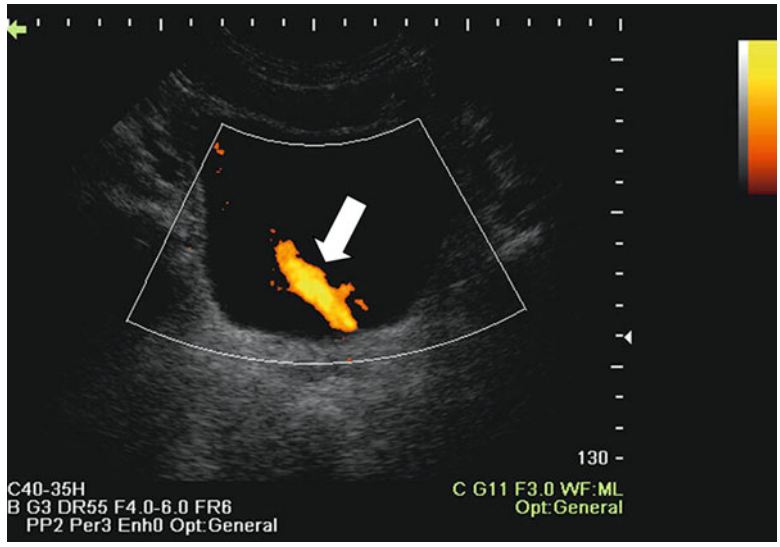

Fig. 8.9 Ureteral jet (*arrow*) demonstrated using power Doppler

Common Abnormalities

Bladder Stones

Many of the abnormalities appreciated on bladder ultrasound are the result of bladder outlet obstruction or urethral obstruction. Bladder stones may be easily visualized on ultrasound (Fig. 8.10). A stone will reflect sound waves resulting in a shadow posterior to the stone. A technique of having the patient turn on their side will cause the stone to move thus proving it to be a stone and not a fixed bladder wall lesion such as a bladder tumor with dystrophic calcification.

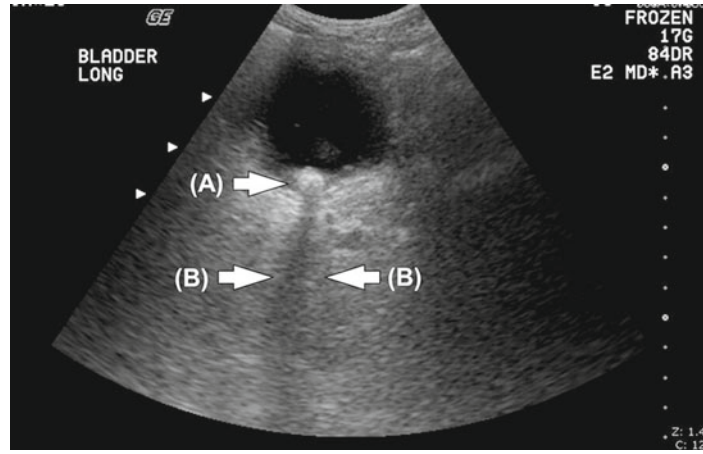

Fig. 8.10 A hyperechoic bladder calculus (**A**) is seen in this image along with the posterior acoustic shadowing from the calculus (**B**)

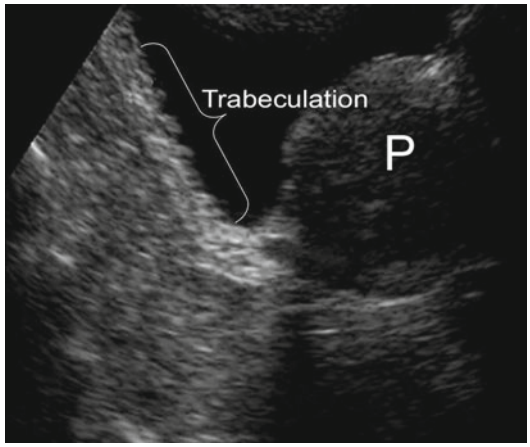

Fig. 8.11 Trabeculation of the bladder is demonstrated in this sagittal image

Trabeculation and Diverticula

Trabeculation of the bladder wall may be seen in response to distal obstruction. This finding is often best observed on the sagittal view (Fig. 8.11). **Bladder diverticula** may be demonstrated on ultrasound (Fig. 8.12). Using the Doppler mode, the flow of urine in and out of the diverticulum may be seen (Fig. 8.12b).

Ureteral Dilation

The distal ureters may be examined sonographically for the presence of distal ureteral dilation (Fig. 8.13). Ureteral dilation is a nonspecific finding with multiple possible causes including primary congenital dilation, reflux, obstruction at the bladder neck from prostatic enlargement or at the urethra from posterior urethral valves, or urethral stricture disease. In some cases the obstruction may be caused by distal ureteral scar tissue, a tumor, or a distal ureteral stone (Fig. 8.14). The ureters are also evaluated in the sagittal view and are located in the bladder base. **Ureteroceles** may be well seen as rounded fluid-filled membranes (Fig. 8.15). Associated congenital abnormalities, such as duplication or ectopy may also be detected.

Neoplasms

Ultrasound of the bladder can determine the presence of focal lesions, such as bladder tumors (Fig. 8.16). The sensitivity of ultrasound for bladder tumor detection is dependent on the location and size of the tumor. Tumors located in the anterior

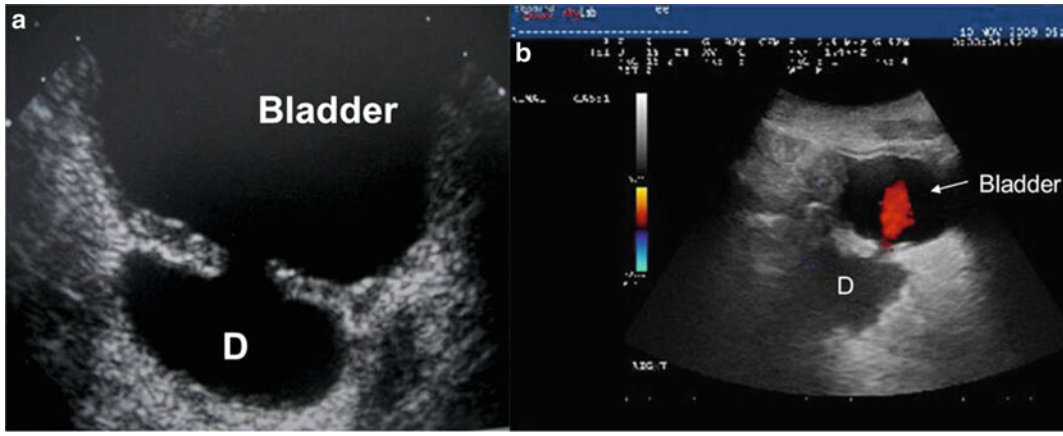

Fig. 8.12 (**a**, **b**) Bladder diverticula (D) are seen. (**b**) The Doppler mode is used to demonstrate the flow of urine out of the diverticula (D). The flow of urine is from the diverticula into the bladder as indicated by the *red* color. Flow toward the transducer is assigned the color *red* in this case

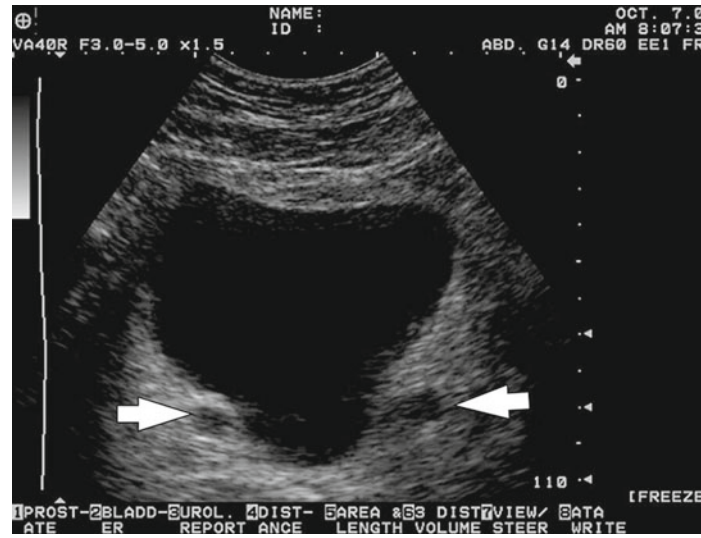

Fig. 8.13 Dilated distal ureters (*arrows*) on this transverse view of the bladder. The cause of the dilation in this case was bladder outlet obstruction

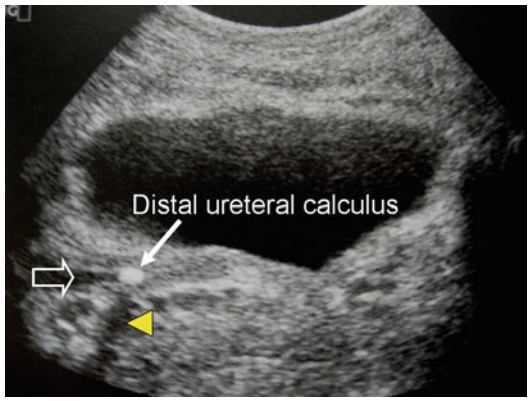

Fig. 8.14 Dilated distal ureter seen on this transverse view of the bladder is a hypoechoic structure (*open arrow*) parallel to the floor of the bladder. Shadowing (*yellow arrowhead*) is seen posterior to a distal ureteral calculus (*white arrow*)

region of the bladder will have the lowest detection rate on ultrasound (47%) whereas tumors located in the lateral side walls of the bladder have the highest detection rates [3]. The diameter of the bladder tumor also affects detection rate. Detection is most reliable for tumors >5 mm in diameter. In one study, the detection rate for tumors >5 mm was the highest for tumors located in the right lateral wall (100%) and lowest in the anterior wall (61%) [4].

Ultrasound may be helpful in the **staging of bladder carcinoma**. Although direct observation of the depth of bladder wall invasion is difficult, some predictions of invasiveness may be obtained by measuring ***contact length*** (length of the base of the tumor that is in contact with the distended

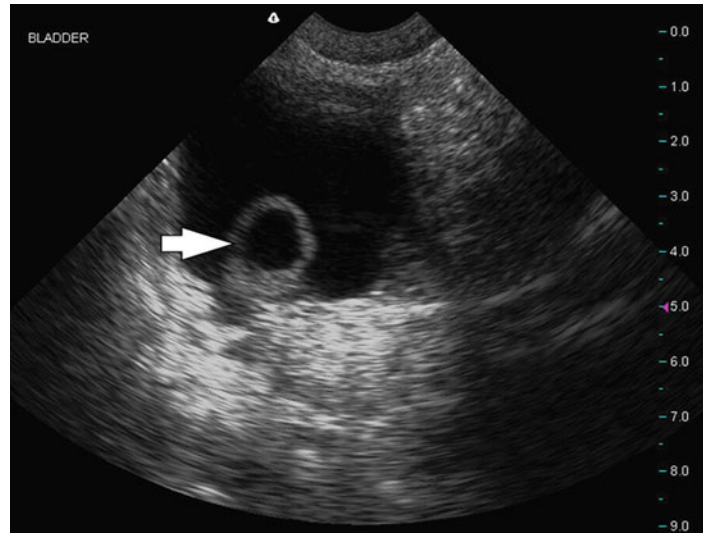

Fig. 8.15 Ureterocele (*arrow*) is seen as a hyperechoic structure surrounding fluid. This ureterocele is thickened. Many ureteroceles appear as a thin hyperechoic membrane on ultrasound

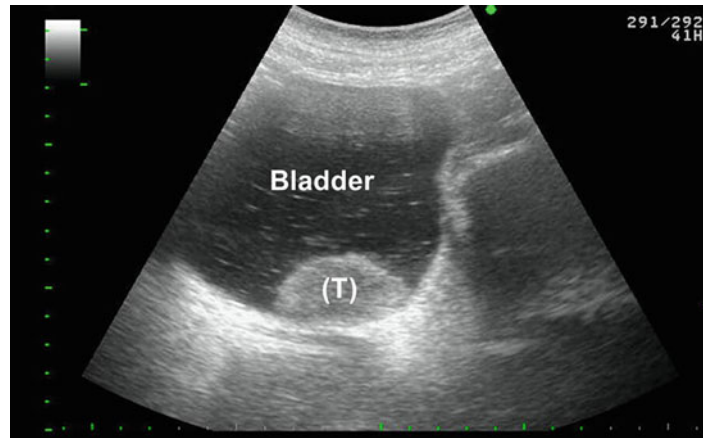

Fig. 8.16 A bladder wall lesion (T) consistent with transitional cell carcinoma. The lack of shadowing suggests a soft tissue abnormality

bladder wall) and ***height*** (distance from the base of the tumor to the luminal margin of the tumor). A ***height-to-contact-length ratio*** may be calculated. This ratio is correlated with the likelihood of muscle invasion (Fig. 8.17). In a study by Ozden et al., it was determined that a contact length of greater than 41.5 mm and a height-to-contact-length ratio of less than 0.605 were the cutoff values for differentiating superficial from invasive tumors with a sensitivity rate of 81% [5]. Tumors smaller than 0.5 cm that are flat and/or near the bladder neck may be missed [4].

Foreign Bodies and Perivesical Processes

Transabdominal ultrasound of the pelvis may be very useful in identifying foreign bodies in the bladder or in assessing perivesical pathology.

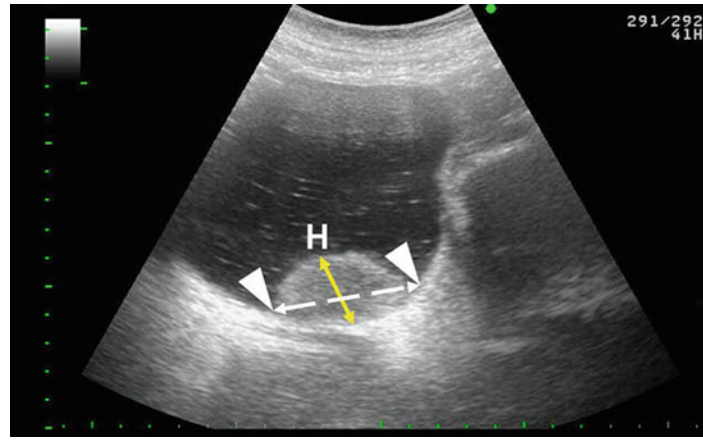

Fig. 8.17 Contact length (*arrow* heads) is the width of a tumor that is in contact with the bladder wall. The tumor height (H) is obtained by measuring the distance from the base to the luminal margin of the tumor (*yellow arrow*)

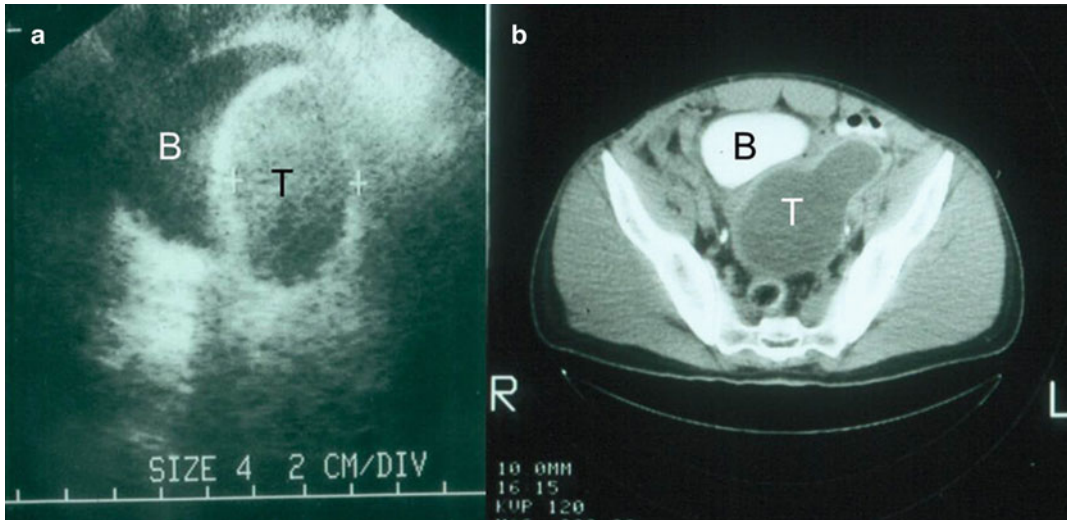

Fig. 8.18 Metastatic lesion from testicular tumor (T) adjacent to the bladder (B) shown on ultrasound in image (**a**) and on CT scan in image (**b**)

Perivesical neoplasms and fluid collections are best appreciated when the bladder is full (Fig. 8.18).

Evaluation of the Prostate Gland

Once examination of the bladder has been concluded attention is given to the prostate gland. The prostate is evaluated in both the transverse and sagittal views. To view the prostate, however, the ultrasound probe may need to be angled more steeply behind the pubic bone. It may be necessary to apply more pressure to the probe in cases where the abdomen is protuberant. The height and width of the prostate are measured in the transverse view (Fig. 8.19). The length of the prostate is measured by rotating the transducer 90° clockwise into the sagittal position, making sure to maintain the indicator on the probe toward the patient's head (Fig. 8.20). The volume of the prostate is automatically determined by most ultrasound equipment but may also be calculated using the formula: length × width × height × 0.523.

Intravesical prostatic protrusion (IPP) is measured on the sagittal view. IPP is present when the middle lobe extends into the bladder lumen (Fig. 8.21). IPP has been shown to correlate with

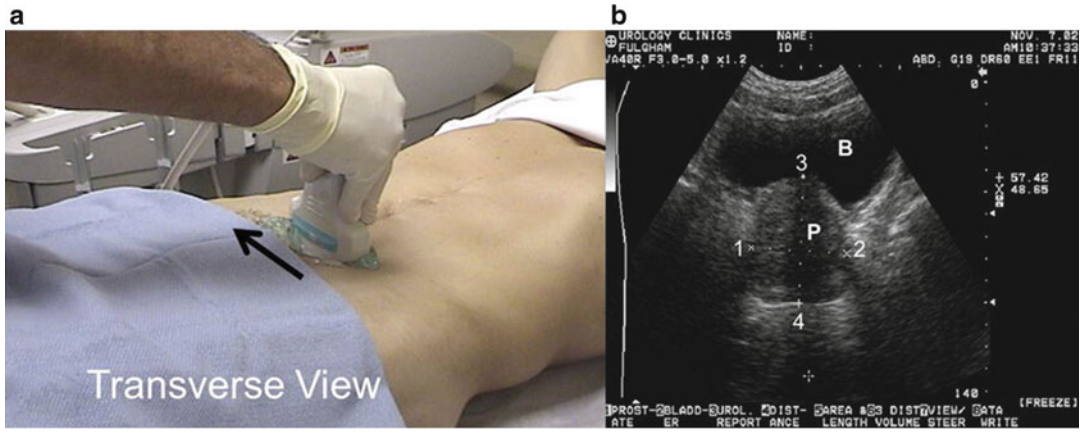

Fig. 8.19 (**a**) The probe is positioned for evaluating the prostate in the transverse view. The orienting notch on the transducer is to the patient's right side (*black arrow*). In image (**b**) a full bladder (B) is helpful for visualizing the prostate (P). The width (*1–2*) and the height (*3–4*) are obtained

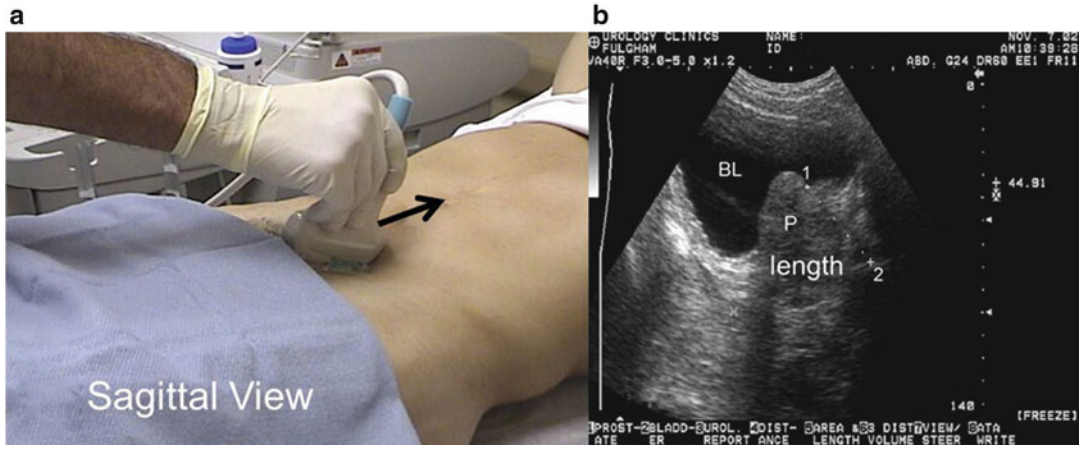

Fig. 8.20 (**a**) The probe is positioned for measuring prostate length. The notch is directed toward the patient's head (*black arrow*). (**b**) The length of the prostate (P) is measured as indicated by calipers *1–2* in this sagittal view

bladder outlet obstruction as demonstrated by urodynamic evaluation [6–8]. The prostate should be carefully evaluated for calcifications in the parenchyma, lucent lesions, cysts, and solid mass effects. Further characterization of prostatic abnormalities can be made with digital rectal examination, transrectal ultrasound, and computerized tomography if necessary. Other structures which may be evaluated include the seminal vesicles and ejaculatory ducts, though they are typically better seen on transrectal ultrasound of the prostate.

Documentation

Proper documentation is imperative to creating a permanent record of the study. The images obtained should be of sufficient and uniform quality with appropriate labeling of structures. It is important that the report of the study state the indications for the study, description of findings, measurements, impression/assessment, and the signature and name of the interpreting physician.

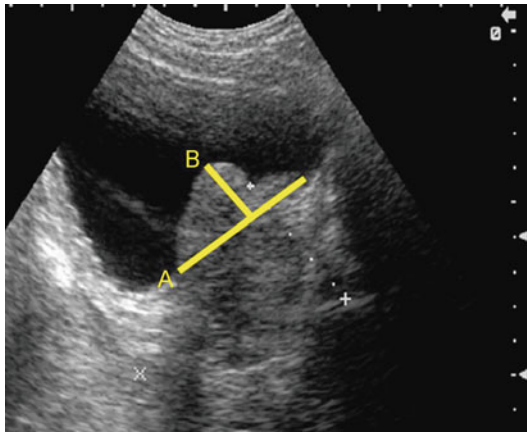

Fig. 8.21 The IPP is measured by first drawing a line (*A*) across the bladder neck. The protrusion of the prostate is determined by measuring the perpendicular length from line *A* to the luminal tip of the prostate, line (*B*)

Image Documentation

- Measurement of bladder volume, if indicated (this may be performed using a split screen)
  - Midsagittal view length measurement from dome of the bladder to the bladder neck
  - Mid-transverse view with height and width measurements
- Measurement of bladder wall thickness, if indicated
- Documentation of the presence of ureteral jets, if indicated
- Documentation of any abnormalities
- Calculated bladder volume or post-void residual, if indicated
- Measurement of prostate volume (this may be performed using a split screen)
  - Midsagittal view with height measurement
  - Mid-transverse view with measurement of width and length
- Seminal vesicles: transverse and longitudinal views for length and width measurements, if indicated
- Measurement of IPP, if appropriate

Ultrasound Report

- Patient identification (name, date of birth, other facility identifiers)
- Date of study

Fig. 8.22 An example of an automated bladder scanner. The automated bladder scan is useful for obtaining a post-void residual but is not considered a diagnostic ultrasound study

- Facility name, location
- Ordering physician
- Indication
- Findings: bladder measurements, prostate measurements, bladder wall thickness, and abnormalities
- Impression/assessment
- Name of interpreting physician and signature

Automated Bladder Scanning

A handheld device to obtain a bladder volume or a post-void residual is an important piece of equipment for the urologist's office. It allows for a quick measurement of post-void residual and can be performed by office staff. However, this is not a diagnostic ultrasound study and is only performed if the intent of the study is to determine the bladder volume or post-void residual (Fig. 8.22). A diagnostic ultrasound machine may also be used to determine post-void residual. Automated bladder ultrasound may be useful for determining if a patient has an adequate pre-void bladder volume (>150 mL) prior to executing a urinary flow rate determination.

Automated bladder scanners may be inaccurate in a number of clinical circumstances

Table 8.2 Potential causes of inaccuracy by automated scanning devices

1. Obesity
2. Ascites
3. Clot retention
4. Bladder diverticulum
5. Perivesical fluid collection a. Urinoma b. Hematoma c. Lymphocele d. Ovarian cyst
6. Distortion or compression of bladder by perivesical mass

(Table 8.2). The presence of ascites, urinomas, or bladder diverticula may result in inaccurate determinations of residual urine. Tumor, blood clots, or distortion of the bladder by extrinsic mass may also produce inaccurate results. Findings on automated scans which seem inappropriate to the clinical findings should be verified by manually performed transabdominal pelvic ultrasound.

Conclusion

Transabdominal pelvic ultrasound is a valuable tool in the practice of urology. It allows for the immediate assessment of many urologic conditions and assists the urologist in immediate diagnosis and treatment.

References

1. Jacob P, Rai BP, Todd AW. Suprapubic catheter insertion using an ultrasound-guided technique and literature review. BJU Int. 2012;110(6):779–84.
2. Manieri C, Carter S, Romano G, Trucchi A, Valenti M, Tubaro A. The diagnosis of bladder outlet obstruction in men by ultrasound measurement of bladder wall thickness. J Urol. 1998;159:761–5.
3. Ozden E, Turgut AT, Turkolmez K, Resorlu B, Safak M. Effect of bladder carcinoma location on detection rates by ultrasonography and computed tomography. Urology. 2007;69(5):889–92.
4. Itzchak Y, Singer D, Fischelovitch Y. Ultrasonographic assessment of bladder tumors. I. Tumor detection. J Urol. 1981;126(1):31–3.
5. Ozden E, Turgut AT, Yesil M, Gogus C, Gogus O. A new parameter for staging bladder carcinoma: ultrasonographic contact length and height-to-length ratio. J Ultrasound Med. 2007;26:1137–42.
6. Franco G, De Nunzio C, Costantino L, Tubaro A, Ciccariello M, et al. Ultrasound assessment of intravesical prostatic protrusion and detrusor wall thickness—new standards for noninvasive bladder outlet obstruction diagnosis? J Urol. 2010;183:2270–4.
7. Chia SJ, Heng CT, Chan SP, Foo KT. Correlation of intravesical prostatic protrusion with bladder outlet obstruction. BJU Int. 2003;914(4):371–4.
8. Lieber MM, Jacobson DJ, McGree ME, et al. Intravesical prostatic protrusion in men in Olmsted County, Minnesota. J Urol. 2004;182(6):2819–24.

Suggested Reading

Hoffer M, editor. Ultrasound teaching manual: the basics of performing and interpreting ultrasound scans. Stutgart, NY: Georg Thieme; 2005.
Middleton W. General and vascular ultrasound. 2nd ed. Philadelphia: Mosby; 2007.
Block B. The practice of ultrasound: a step by step guide to abdominal scanning. Stutgart, NY: Georg Thieme; 2004.

Pelvic Floor Ultrasound

9

Chad Baxter and Farzeen Firoozi

Introduction

Pelvic ultrasound is increasingly used to evaluate pelvic floor disorders and has several advantages in contrast to other imaging modalities such as magnetic resonance imaging (MRI) and cystourethrography. Ultrasound is relatively inexpensive, widely available, and offers real-time, dynamic imaging of pelvic anatomy without radiation. Most urologists are trained in transrectal ultrasonography. However, those skills are easily translated to translabial pelvic ultrasonography. This chapter focuses on 2D ultrasound imaging and technique as it is the most widely available and familiar to urologists. However, the expanding prevalence of 3D and 4D ultrasound reconstructions of pelvic anatomy will likely advance the understanding of pelvic floor pathology and our appreciation and use of pelvic ultrasound.

This chapter describes the translabial pelvic ultrasound examination by anatomic compartments. Normal and commonly encountered aberrant findings of the anterior, central, and posterior compartments are described. Imaging of surgically placed materials including transvaginal mesh and urethral bulking agents concludes the chapter.

Anterior Compartment

The anterior compartment includes the urethra, bladder neck, bladder, and retropubic space of Retzius, as well as the surrounding supportive muscular and connective tissue.

Indications for Anterior Compartment Ultrasound

The indications for anterior compartment ultrasound are urinary incontinence, urinary retention, urethral diverticulum, urethral stricture, urethral hypermobility, vaginal cyst, cystocele, mesh extrusion, mesh erosion, and pelvic pain.

Technique

Ultrasonographic examination of the anterior compartment is most commonly performed translabially with a 5–8 cm, 3.5–5 MHz, curved array transducer. Alternatively, the ultrasonographer may select a 7.5 MHz linear array transducer. In contrast to a transvaginal technique, translabial ultrasound examination is noninvasive and does not distort the pelvic anatomy. We typically perform the exam with the patient in the dorsal lithotomy position.

C. Baxter, MD
Department of Urology, David Geffen School of Medicine at UCLA, Santa Monica, CA, USA

F. Firoozi, MD (✉)
Department of Urology, Hofstra Northshore–LIJ School of Medicine, The Arthur Smith Institute for Urology, Center of Pelvic Health and Reconstructive Surgery, 450 Lakeville Road, Lake Success, NY 11042, USA
e-mail: Ffiroozi@nshs.edu

P.F. Fulgham and B.R. Gilbert (eds.), *Practical Urological Ultrasound*, Current Clinical Urology,
DOI 10.1007/978-1-59745-351-6_9, © Springer Science+Business Media New York 2013

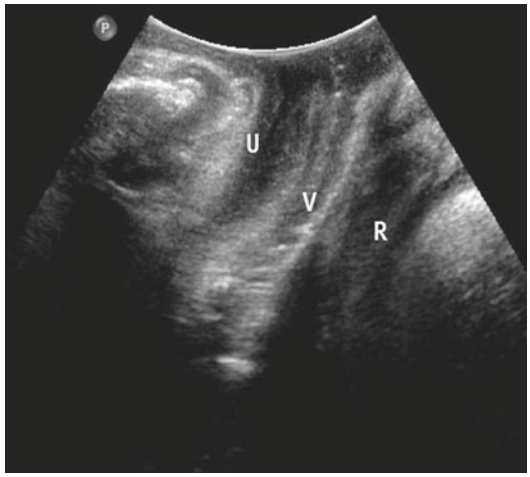

Fig. 9.1 Two-dimensional orientation of translabial ultrasound image in midsagittal line. *U* urethra; *V* vagina; *R* rectum

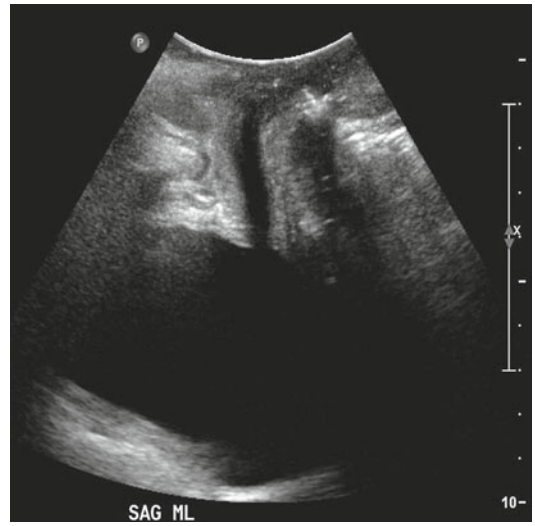

Fig. 9.2 Hypoechoic urethra

Conventional ultrasonography orients the 2D image in the midsagittal line with the pubic symphysis in the upper-left portion of the image (Fig. 9.1).

Normal Ultrasound Anatomy

Urethra

The urethral complex appears immediately caudal to the symphysis and includes the urethral mucosa, smooth muscle, and surrounding vasculature (Fig. 9.2). The normally oriented urethra is parallel to the incident ultrasound beam and appears hypoechoic. With increasing degrees of urethral hypermobility, the urethra moves more perpendicular to the ultrasound beam, and the urethral complex progressively appears less hypoechoic.

The fibers of the rhabdosphincter are oriented transversely to the incident beam in the normally oriented urethra, and the rhabdosphincter thus appears hyperechoic. With progressive urethral hypermobility, rhabdosphincter orientation shifts in relation to the ultrasound energy and may become less hyperechoic [1]. Periurethral connective tissue appears hyperechoic relative to the urethral complex, though clearly less echogenic than the adjacent inferoposterior margin of the pubis. Frequently observed punctate echogenicities within the urethra that are likely calcified periurethral glands appear to be of no clinical significance [2].

Bladder Neck

Multiple techniques are described, but the position of the bladder neck may be most reliably described relative to the inferoposterior margin of the symphysis pubis [3]. Though bladder fullness influences examination findings, volumes have not been standardized. A full bladder may reduce sensitivity in demonstrating the degree of bladder neck mobility, and an empty bladder makes it more difficult to identify the location of the bladder neck [4].

Bladder neck descent (BND) is conventionally determined by measuring the displacement of the bladder neck from rest to maximum Valsalva relative to the inferoposterior symphysis pubis margin (Fig. 9.3). The normal amount of BND has yet to be defined with numerous proposed cutoffs ranging between 15 and 30 mm. It does appear that the greater the BND, the more likely the patient is to have stress urinary incontinence. Many variables confound the measurement of BND, including Valsalva maneuver effort, bladder fullness, parity, and recruitment of levator ani contraction at time of Valsalva [5]. Alternatively, bladder neck mobility may be

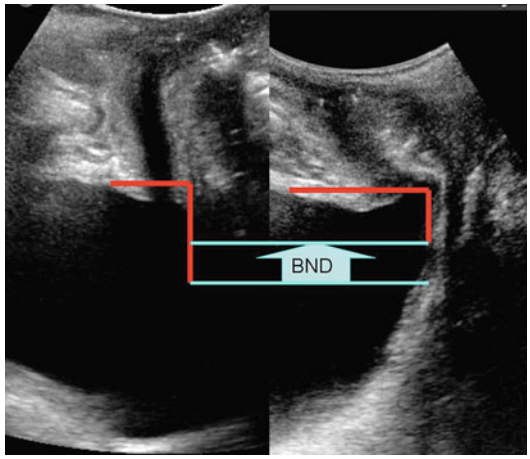

Fig. 9.3 Bladder neck descent. *Left side* image without Valsalva maneuver, *right side* image with Valsalva

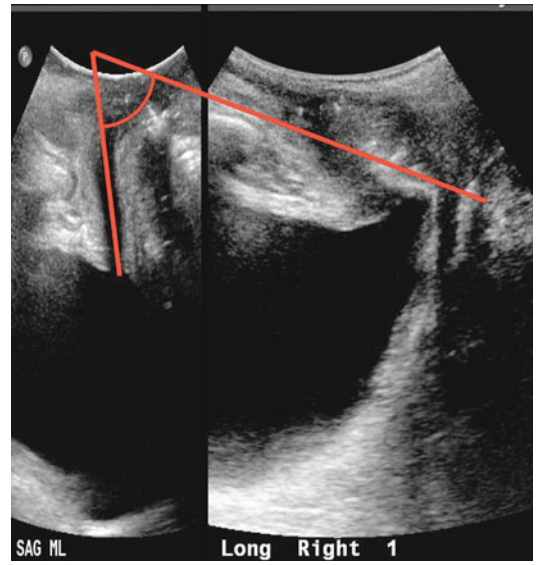

Fig. 9.4 Retrovesical angle measurement describing urethral rotation

measured by retrovesical angle (RVA). This angle measures urethral rotation around the urethral axis as demonstrated (Fig. 9.4). Normal RVA values, as commonly observed in continent patients, range from 90° to 120° [6].

Abnormal funneling of the bladder neck and proximal urethra may also be observed both at rest and with Valsalva maneuver and with or without significant BND or enlarged RVA.

Bladder

The bladder is examined for position, wall thickness, intravesical volume, intravesical lesions, and adjacent ureterectasis of the distal ureters. In patients without prolapse, the bladder is positioned above the inferior margin of the symphysis pubis. Cystocele may be understaged if the bladder is examined only when fully distended, particularly in patients with stenosis of the vaginal introitus, as this will prevent the bladder from descending during Valsalva maneuvers. If the bladder is examined while partially or completely distended, the luminal surface of the posterior wall in a partially filled bladder appears hyperechoic due to through-transmission of the incident beam. The bladder lumen should be examined for echogenic material such as debris secondary to infection, or urolithiasis. While bladder ultrasound is inadequate for complete oncologic screening, the urothelial surface should be examined for neoplasm. The inter-ureteric ridge is also commonly apparent. The distal ureter may be visualized posterior to the ridge with lateral movement of the transducer. Inspection of the ureter at this level may reveal ureterectasis, possibly indicative of vesicoureteral reflux, ureteric obstruction, or normal physiology. Doppler flow ultrasonography may reveal the presence of a ureteral urine jet. The absence of a ureteral jet does not establish ureteral obstruction; thus the clinical utility of a ureteral jet is debated [7].

Much has been made of detrusor wall thickness (DWT). Association between DWT and the presence of urodynamically proven detrusor overactivity, obstruction, stress incontinence, and p_{det}/Q_{max} has been described [8]. In a compliant bladder, DWT lessens with increased bladder filling. No consensus exists regarding bladder volume at which DWT is calculated. DWT is calculated most commonly by measuring the wall thickness at three discreet locations: posterior wall, dome, and anterior wall (Fig. 9.5). Some authors consider normal DWT to be 5 mm or less [9], but this is controversial [10].

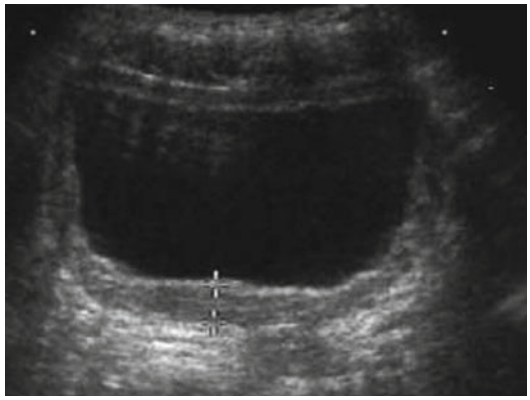

Fig. 9.5 Bladder wall thickness

Common Abnormal Findings

Urethra

As mentioned above, urethral hypermobility may be suspected by static ultrasound imaging and confirmed with dynamic ultrasonography with Valsalva maneuvering. Periurethral tissues should be homogeneous and without hypoechoic, cystic-appearing lesions. Periurethral lesions may include urethral diverticulum as well as nearby Gartner's duct cysts. Large urethral diverticula are readily imaged with ultrasound. (Typically, diverticula arise from the dorsal aspect of the urethra.) Less frequently, they arise ventrally from the urethra. Ultrasound is not as sensitive as MRI for small diverticula, but ultrasound can confirm an otherwise palpable suburethral fluctuance suggestive of diverticulum [11, 12].

Gartner's duct cysts and Bartholin's gland lesions may be readily distinguished from urethral diverticula. The former lesions are stationary on Valsalva maneuver while the diverticula are affixed to the urethra and thus commonly mobile on Valsalva. Diverticula of the urethra are commonly septated and contain heterogeneously echogenic material. Bartholin's and Gartner's cysts are typically homogeneous in appearance [13]. Urethral ultrasonography may also reveal the presence and extent of periurethral fibrosis. This may be important in patients with urethral stricture desiring reconstruction, or in planning extent of urethrolysis, or anti-incontinence surgery (Fig. 9.6).

Bladder

Bladder ultrasonography may reveal bladder diverticula as well. These may appear as periureteral cystic lesions near the trigone and interureteric ridge or along the posterolateral walls and dome. Ureteroceles may also be visualized, particularly with ureterectasis. Bladder calculi may also be identified as hyperechoic intravesical filling defects with posterior shadowing.

Papillary bladder lesions may be identified as intravesical echogenic foci attached to the bladder wall (Fig. 9.7). These lesions are best imaged with a full bladder and may easily be missed without bladder distension.

Bladder ultrasound may reveal significant detrusor fibrosis and thinning of the wall, perhaps suggestive of patients at risk for bladder rupture during planned hydrodistension.

Ultrasonography may also be valuable in office-based imaging of vesicovaginal fistulae. Particularly in radiation-induced fistula where physical exam is often precluded by patient discomfort and distal vaginal stenosis, office-based ultrasound may prove useful in identifying extent of fibrosis and ischemia.

With increasing use of mesh in vaginal reconstruction, hyperechoic mesh is increasingly encountered. With 3D reconstruction, the lattice-structure of the mesh is visible. This is more thoroughly explored later in the chapter.

Apical and Posterior Compartments

Basics of Apical and Posterior Prolapse Assessment

Translabial ultrasound can be used for the assessment of apical and posterior vaginal wall prolapse [14, 15]. A full sonographic assessment of the apical portion of the vagina includes the uterus.

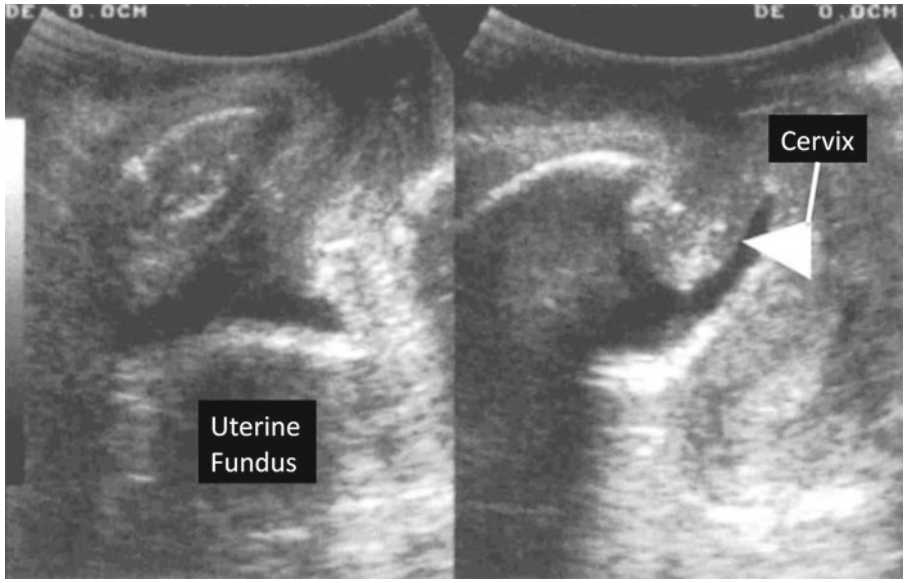

Fig. 9.6 Uterine fundus is easily visualized in image to the *left*. Prolapse of the cervix and uterus is noted with Valsalva maneuver

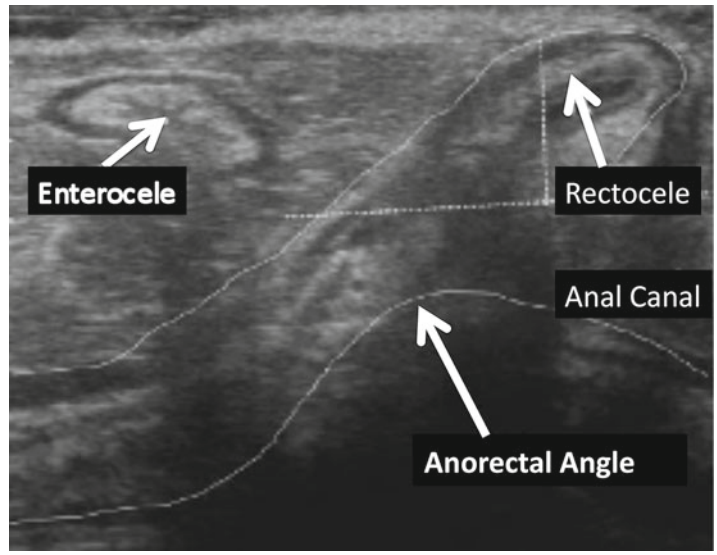

Fig. 9.7 An enterocele is noted in the *left upper* portion of the ultrasound image. In addition, a rectocele is also noted in the *upper-right* portion of the image

The uterus can be difficult to visualize due to a few factors: it is iso- to hypoechoic making it similar and difficult to discern from vaginal tissues, a retroverted position can be obscured by a rectocele or hidden by rectal contents, and overall it is small in size in postmenopausal women. There are some clues that can be used to localize the uterus. The cervix is typically seen as a specular echo which represents its leading edge. A specular reflector reflects sound waves with minimal scatter usually producing a bright linear echo. The uterus can also be identified by

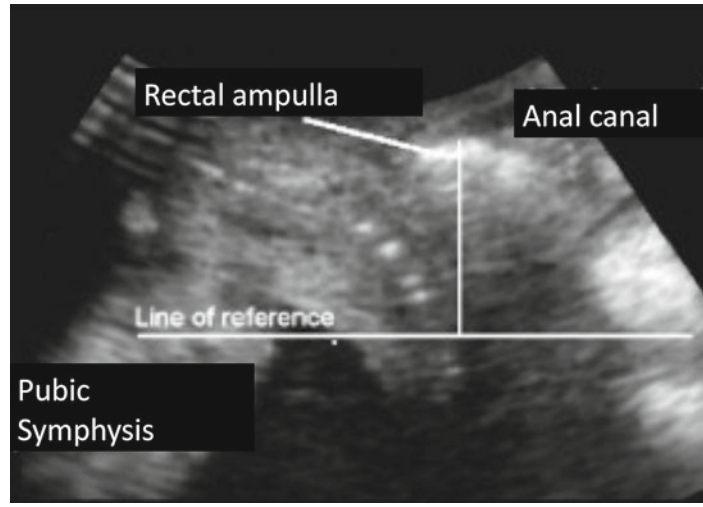

Fig. 9.8 The inferior margin of the pubic symphysis is used as a line of reference. Perineal hypermobility is noted with descent of the rectal ampulla

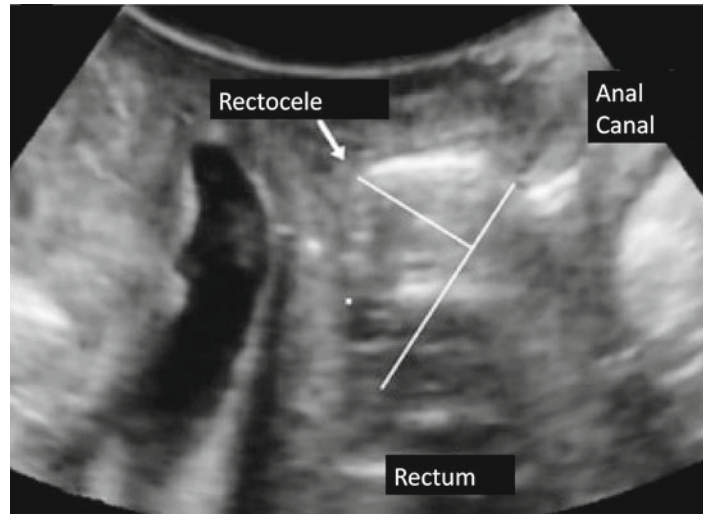

Fig. 9.9 Normal position of the posterior vaginal wall is delineated with the *oblique white line*. A rectocele is noted with prolapse of the true posterior vaginal wall into the vagina

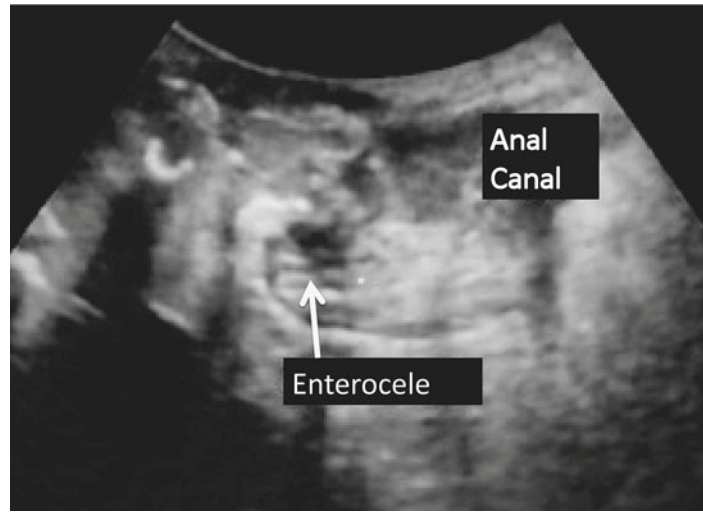

Fig. 9.10 The *white arrow* points to the vault prolapse which contains small bowel (enterocele)

locating nabothian follicles which are oftentimes seen within the cervix. Translabial ultrasound can be readily used to locate the cervix, especially in patients with prolapse (Fig. 9.8). The same can be said for identifying a prolapsed vault posthysterectomy.

Quantification of apical prolapse is performed using the cervix or pouch of Douglas and the posterior wall using the leading edge of rectocele. We use the inferior margin of the pubic symphysis as a line of reference for measuring the degree of descent. Translabial ultrasound measurement of apical and posterior compartment prolapse has been shown to correlate well with validated prolapse quantification systems, with correlations of $r = 0.77$ for uterine prolapse and $r = 0.53$ for posterior prolapse [16]. Some have shown that posterior compartment descent to 15 mm or more below the pubic symphysis has been a radiographic cutoff for significant descent as it relates to symptomatic prolapse [17].

Although correlations between clinical prolapse staging and translabial ultrasound for posterior compartment prolapse are not as strong when compared to anterior or apical compartment prolapse, we are able to use this form of imaging to separate a true or false rectocele. That is to say we can distinguish a rectocele sonographically from other findings such as a rectovaginal septum defect or perineal hypermobility without any actual fascial defects (Fig. 9.8). True rectoceles, which occur as a result of fascial defects, are located consistently very close to the anorectal junction, typically transversely oriented (Fig. 9.9).

Enterocele

A major strength of translabial ultrasound for apical and posterior compartment assessment of prolapse is the ability to distinguish rectocele from enterocele [18]. An enterocele is readily diagnosed sonographically by visualizing within the herniated small bowel, fluid-containing peritoneum, omentum, or sigmoid anterior to the anorectal junction (Fig. 9.10). While MRI is very sensitive for radiographically mapping all vaginal compartment prolapse, it can be cost-prohibitive. Although not expensive, a defecogram can show an enterocele easily, but not before exposing the patient to a significant amount of radiation. Translabial ultrasound can be used easily and inexpensively to diagnose an enterocele with no radiation exposure. From a surgical planning standpoint, ultrasound identification of herniated contents can apprise the surgeon of what to expect during repair of the prolapse.

Imaging Implant Materials

Midurethral Slings

One of the unique aspects of sonography of the pelvic floor is the ability to detect synthetic materials, namely mesh, that can be difficult if not impossible to localize with computed tomography, MRI, or X-ray imaging [19]. This has proven very useful in the last decade, as the popularity of midurethral synthetic slings have risen exponentially due to the relative ease of the procedure and overall high success rates [20]. Sonographic imaging adds to the overall information on postoperative assessment of outcome, specifically by elucidating in vivo biomechanical characteristics. From a clinical standpoint, ultrasonography can shed light on assessment of complications after sling placement, which may include erosion, voiding dysfunction, and recurrence of stress incontinence. In addition, ultrasound can confirm the presence of a sling in patients unsure of previous anti-incontinence procedures performed in the past.

Both xenografts and allografts are difficult to visualize due to the iso-echoic nature of these implants. Synthetic slings, on the other hand, are hyperechoic and much more visible on ultrasound (Fig. 9.11). Using translabial ultrasound the entire intrapelvic contents can be visualized, from the pubic rami to anterior to the urethra and back through the contralateral side [21]. Another advantage of translabial ultrasound for synthetic slings is the ability to

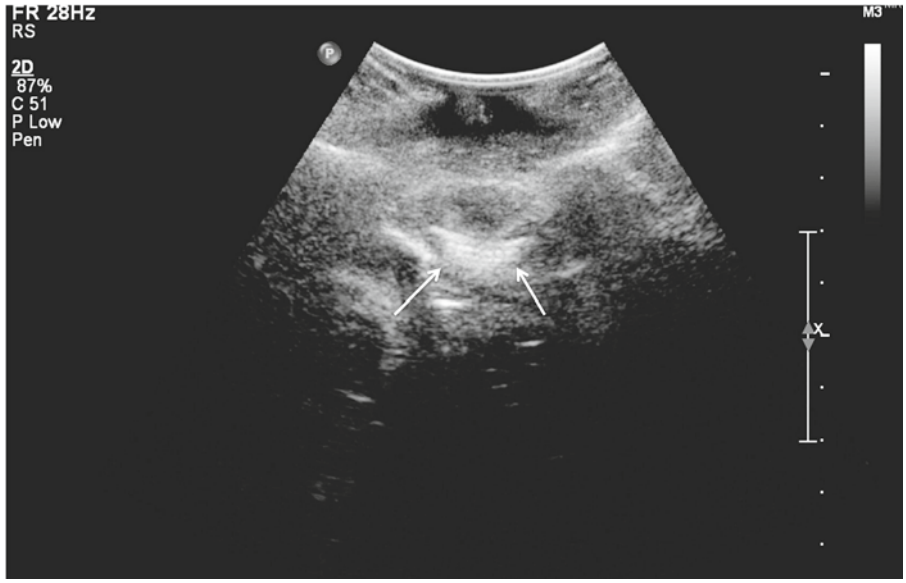

Fig. 9.11 Mesh is delineated by the two white arrows. The orientation can be seen hugging the urethra in a hammock fashion

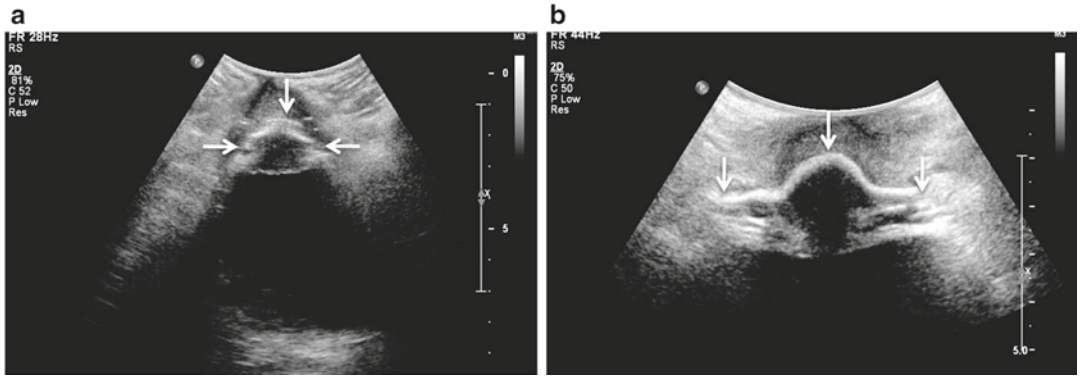

Fig. 9.12 (**a**) This image demonstrates the mesh sling pointed to by three *white arrows*, with a retropubic course which a TVT sling. (**b**) This image reveals the three *white arrows* pointing to the mesh sling in a horizontal orientation denoting a TOT sling

characterize orientation of the sling, which includes asymmetry, varying width, tape twisting, and effect of tape division. With the use of rendered volumes of 2D imaging, TVT (transvaginal taping) and TOT (transobturator taping) slings can be easily distinguished from one another. One of the techniques utilized to discern a TVT from TOT is to follow the tape with oblique parasagittal views until the levator ani insertion is reached—TOT slings typically traverse the muscle (Fig. 9.12). Varying echogenicity can be characteristic of some types of slings (e.g., relatively less echogenic IVS when compared to a TVT™ or Sparc™, when trying to determine sling type when imaging patients). The typical c-shape of all retropubic slings is pretty consistent, seen most clearly during a Valsalva maneuver. The tighter the c-shape, the

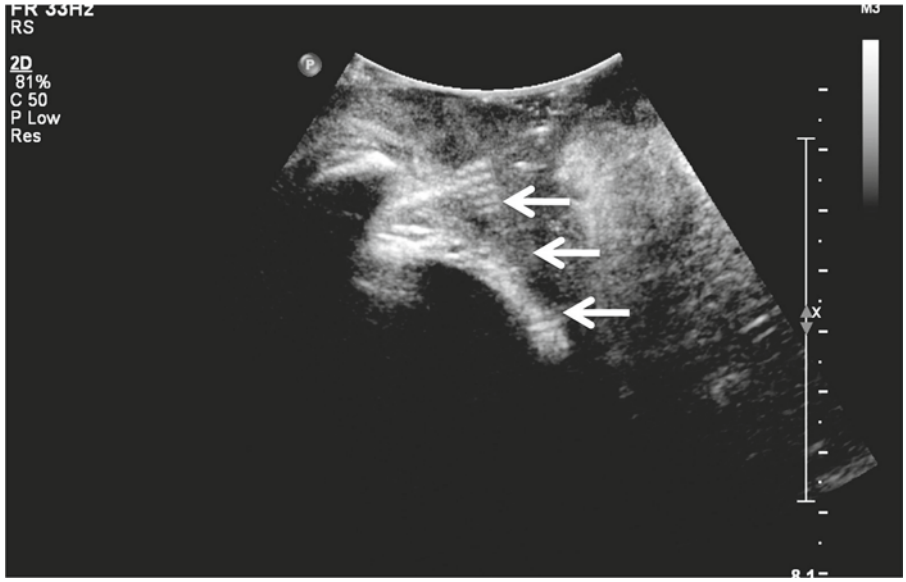

Fig. 9.13 The three *white arrows* map the anterior position of this anterior Prolift™ mesh

more tensioned the tape tends to be in patients. With regard to positioning, even though a midurethral location for a sling is thought by most to be the ideal position, some studies have shown that this is not necessarily the case [22].

Prolapse Mesh Kits

The use of mesh for augmentation of prolapse surgery has become commonplace. A majority of the commercial mesh kits currently available are polypropylene, which is highly echogenic and easily seen on ultrasound. Commercial mesh kits utilize mesh arms that traverse the obturator foramen, levator sidewall, and pararectal space by the use of external trocars. A recent trend has been the development of trocarless systems, which have mesh arms that anchor internally to the same fixed structures.

One of the uses of ultrasound in this new era of mesh augmented prolapse repairs is the evaluation of their success anatomically. A study done by Shek et al. used ultrasound to assess the outcomes of using mesh for repair of large and/or recurrent cystoceles [23]. The implant material was able to be imaged in all patients. In 10% of the patients, the authors were able to note cystocele recurrence dorsal to the mesh, with 8% of the patients demonstrating significant descent ventral to the mesh. Interestingly, they were also able to demonstrate dislodgement of the superior anterior arms by showing mesh axis alteration of more than 90° of rotation of the cranial margin in the ventrocaudal direction; this occurred in 10% of their patients. This study is an example of the potential future role of ultrasound in assessing outcomes of prolapse surgery. In the future, it may also serve as a tool in optimizing surgical techniques for the use of mesh to augment prolapse surgery.

Along with the increase in use of mesh, there has been a surge in complications related to the use of mesh in prolapse surgery [24]. Mesh erosion involving the vaginal wall and other pelvic structures such as the bladder and bowel have been reported [25]. Involvement of pelvic structures such as the bladder and bowel can be easily delineated with the use of ultrasound (Fig. 9.13). Ultrasound certainly plays a role in mapping the location of mesh in order to plan surgical removal of the mesh (Fig. 9.13). Other

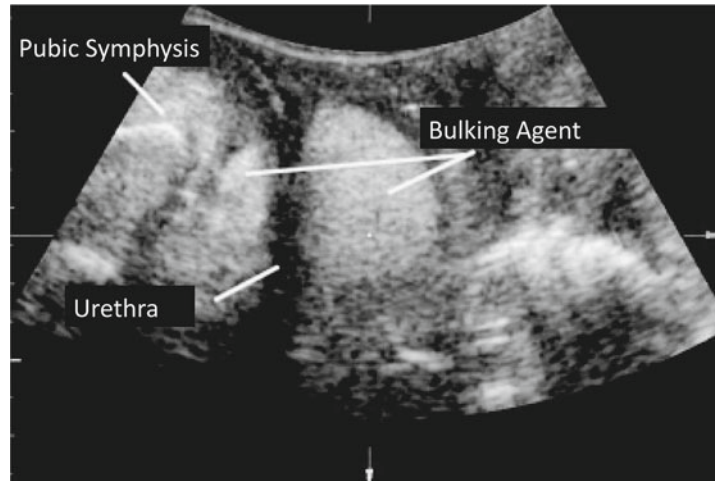

Fig. 9.14 This view reveals a periurethral bulking agent (Macroplastique™), which is echogenic and seen circumferentially around the urethra

mesh complications such as dyspareunia and vaginal/pelvic pain have been described [26]. Ultrasound can be used to assess the need for any further resection of mesh if the patient remains symptomatic. As the role of mesh in prolapse surgery becomes better defined, ultrasonography will become increasingly important in assessing outcomes, improving surgical technique, and aiding in the management of complications.

Periurethral Bulking Agents

Most injectables used as periurethral bulking agents for the management of stress incontinence are highly echogenic (Fig. 9.14). A popular injectable, Microplastique™, can be easily seen as a hyperechoic donut shape encircling the urethra. Even though useful in locating injectables, translabial ultrasound has not been shown in any studies to correlate well with treatment success.

Acknowledgement The authors wish to thank Dr. Shlomo Raz, MD who has provided many of the images from his personal collection.

References

1. Mitterberger M, Pinggera GM, Mueller T, et al. Dynamic transurethral sonography and 3D reconstruction of the rhabdosphincter and urethra. J Ultrasound Med. 2006;25:315–20.
2. Yang JM, Huang WC. The significance of urethral hyperechogenicity in female lower urinary tract symptoms. Ultrasound Obstet Gynecol. 2004;24(1):67–71.
3. Dietz HP, Eldridge A, Grace M, Clarke B. Test-retest reliability of the ultrasound assessment of bladder neck mobility. Int Urogynecol J. 2003;14 Suppl 1:S57–8.
4. Dietz HP, Wilson PD. The influence of bladder volume on the position and mobility of the urethrovesical junction. Int Urogynecol J. 1999;10(1):3–6.
5. Oerno A, Dietz HP. Levator co-activation is an important confounder of pelvic organ descent on Valsalva. In: ICS annual scientific meeting (abstract), Christchurch; 2006.
6. Alper T, Cetinkaya M, Okutgen S, Kokcu A, Lu E. Evaluation of urethrovesical angle by ultrasound in women with and without urinary stress incontinence. Int Urogynecol J. 2001;12(5):308–11.
7. Delair SM, Kurzrock EA. Clinical utility of ureteral jets: disparate opinions. J Endourol. 2006;20(2):111–4.
8. Kuhn A, Genoud S, Robinson D, et al. Sonographic transvaginal bladder wall thickness: does the measurement discriminate between urodynamic diagnoses? Neurourol Urodyn. 2011;30(3):325–8.
9. Lekskulchai O, Dietz HP. Normal values for detrusor wall thickness in young Caucasian women. In: International continence society annual scientific meeting (abstract), Montreal; 2005.
10. Blatt AH, Titus J, Chan L. Ultrasound measurement of bladder wall thickness in the assessment of voiding dysfunction. J Urol. 2008;179(6):2275–8.
11. Gerrard ER, Lloyd LK, Kubricht WS, et al. Transvaginal ultrasound for the diagnosis of urethral diverticulum. J Urol. 2003;169(4):1395–7.
12. Ockrim JL, Allen DJ, Shah PJ, et al. A tertiary experience of urethral diverticulectomy: diagnosis, imaging, and surgical outcomes. BJU Int. 2009;103(11):1550–4.

13. Tunn R, Petri E. Introital and transvaginal ultrasound as the main tool in the assessment of urogenital and pelvic floor dysfunction: an imaging panel and practical approach. Ultrasound Obstet Gynecol. 2003;22(2):205–13.
14. Creigton SM, Pearce JM, Stanton SL. Perineal video-ultrasonography in the assessment of vaginal prolapse: early observations. Br J Obstet Gynaecol. 1992;99(4):310–3.
15. Dietz HP, Haylen BT, Broome J. Ultrasound in the quantification of female pelvic organ prolapse. Ultrasound Obstet Gynecol. 2001;18(5):511–4.
16. Bump RC, Mattiason A, Bo K, et al. The standardization of terminology of female pelvic organ prolapse and pelvic floor dysfunction. Am J Obstet Gynecol. 1996;175(1):10–7.
17. Dietz HP. What's "normal" pelvic organ descent, and what's prolapse? In: ICS annual scientific meeting, Christchurch; 2006.
18. Dietz HP, Steensma AB. Posterior compartment prolapse on two-dimensional and three-dimensional pelvic floor ultrasound: the distinction between true rectocele, perineal hypermobility and enterocele. Ultrasound Obstet Gynecol. 2005;26:73–7.
19. Halsaka M, Otcenasek M, Martam A, et al. Pelvic anatomy changes after TVT procedure assessed by MRI. Int Urogynecol J. 1999;10 Suppl 1:S87–8.
20. Kaum HJ, Wolff F. TVT: on midurethral tape positioning and its influence on continence. Int Urogynecol J. 2002;13(2):110–5.
21. Dietz HP, Wilson PD. The "iris effect"; how two-dimensional and three-dimensional ultrasound can help us understand anti-incontinence procedures. Ultrasound Obstet Gynecol. 2004;23(3):267–71.
22. Ng CC, Lee LC, Han WH. Use of three-dimensional ultrasound to assess the clinical importance of midurethral placement of the tension-free vaginal tape (TVT) for the treatment of incontinence. Int Urogynecol J. 2005;16(3):220–5.
23. Shek K, Dietz HP, Rane A. Transobturator mesh anchoring for the repair of large or recurrent cystocele. In: ICS annual scientific meeting, Christchurch; 2006.
24. Achtari OA, O'Reilly B, Schierlitz L, et al. Mesh erosion following vaginal repair: is I avoidable? Int Urogynecol J. 2003;14 Suppl 1:S65.
25. Firoozi F, Goldman HB. Transvaginal excision of mesh erosion involving the bladder after mesh placement using a prolapse kit: a novel technique. Urology. 2010;75(1):203–6.
26. Ridgeway B, Walters M, Paraisa MF, et al. Early experience with mesh excision for adverse outcomes after transvaginal mesh placement using prolapse kits. Am J Obstet Gynecol. 2008;199:703–7.

Transrectal Ultrasound of the Prostate

10

Edouard J. Trabulsi, Xiaolong S. Liu, and Akhil K. Das

Definition and Scope

Transrectal ultrasound (TRUS), first described by Watanabe and colleagues in the 1960s, is an essential tool for the diagnosis of prostate cancer, as well as for image-guided prostate interventions [1]. By the 1970s TRUS imaging had achieved wide use in clinical practice. Most commonly, TRUS is used to guide core needle biopsy for prostate cancer diagnosis. This was first described by Hodge in 1989 when he advocated the systematic biopsy of the prostate gland [2]. Treatment modalities including brachytherapy, cryotherapy, and high-intensity focused ultrasound (HIFU) also rely on TRUS to appropriately treat prostate cancer patients [3]. In addition, TRUS provides valuable information for follow-up and treatment of benign prostatic hyperplasia (BPH) and can be helpful in the evaluation of patients with idiopathic infertility [4–8]. This chapter will discuss the indications and techniques for TRUS, proper documentation, anatomy of the prostate, and new ultrasonographic technologies. The topic of TRUS with prostate biopsy is covered in a separate chapter.

E.J. Trabulsi, MD, FACS (✉) • X.S. Liu • A.K. Das
Department of Urology, Thomas Jefferson University, Kimmel Cancer Center, 1025 Walnut Street, Suite 1102, Philadelphia, PA 19107, USA
e-mail: edouard.trabulsi@jefferson.edu

Indications

The list of potential indications for TRUS evaluation is lengthy but falls into the following general categories: prostate cancer diagnosis and treatment, BPH management and workup, infertility evaluation, and non-oncologic interventions such as prostatic abscess drainage or aspiration of prostatic or ejaculatory duct cysts.

The evaluation of a patient with an elevated serum prostate-specific antigen (PSA) commonly includes a TRUS evaluation with ultrasound-guided prostate biopsy. To be effective with TRUS evaluation of the prostate, the urologist must have expertise in recognizing normal and abnormal anatomy. Hypoechoic areas of the prostate should be recognized and specifically targeted for biopsy, as the likelihood that these areas harbor cancer is higher [9]. Absence of hypoechoic lesions does not preclude biopsy, and the clinical significance of hypoechoic areas of the prostate has been questioned in the modern era. In particular, a large study of nearly 4,000 patients from Wayne State University demonstrated that the prostate cancer detection rate of targeted biopsies of hypoechoic lesions was the same as biopsies from isoechoic regions [10]. Other TRUS findings suggestive of prostate cancer include lobar asymmetry, capsular bulging, deflection of the junction between the transition zone (TZ) and peripheral zone (PZ), and any area of increased vascularity (Fig. 10.1). A systematic evaluation of the entire prostate gland with volume measure-

P.F. Fulgham and B.R. Gilbert (eds.), *Practical Urological Ultrasound*, Current Clinical Urology,
DOI 10.1007/978-1-59745-351-6_10,

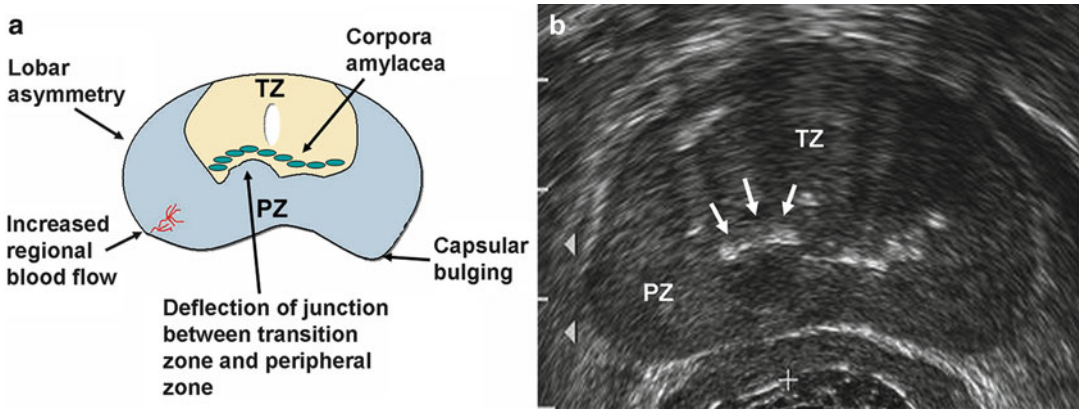

Fig. 10.1 TRUS findings suspicious for prostate cancer. (**a**) Lobar asymmetry, capsular bulging, increased blood flow, and deflection of the junction between the TZ and PZ can all be indicators of prostate cancer on TRUS. (**b**) Transverse image of the prostate demonstrating upward deflection of the junction between the TZ and PZ. The corpora amylacea (*arrows*) indicate this junction and also demarcate the border between the inner and outer gland

ment and evaluation of the seminal vesicles (SV) and surrounding structures should be performed prior to performing any prostate biopsy.

TRUS is used to evaluate the anatomy and calculate the volume of the prostate in symptomatic BPH prior to surgical therapy or minimally invasive therapy (MIT) for BPH [11, 12]. The size and anatomy of the prostate can recommend or exclude certain MIT procedures for patients. Specific volume limits are used to stratify patients for transurethral resection of the prostate (TURP), MITs such as transurethral microwave therapy (TUMT) and transurethral radiofrequency needle ablation (TUNA), or open simple prostatectomy. In addition to prostate volume measurements, the presence or absence of a large intravesical median lobe of the prostate, visualized on TRUS, may influence the choice of technique for surgical treatment of BPH.

Additionally, minimally invasive prostate cancer treatment options are dependent on TRUS technology to accurately monitor and guide treatment planning and delivery [13]. TRUS clarifies the anatomy for the clinician; specifically, it provides an accurate volume assessment of the prostate gland prior to any procedure. Certain patients may be excluded from some treatment options for prostate cancer or may require hormonal downsizing prior to treatment based on TRUS findings. For cryotherapy, real-time TRUS is vital to accurately place probes and monitor the freezing area during the procedure [14]. Similarly, in brachytherapy, real-time TRUS is used to calculate the prostate volume and construct the plan for seed implantation. Continuous real-time TRUS is also used during high-intensity focused ultrasound (HIFU) treatment for prostate cancer, a popular minimally invasive prostate cancer treatment in Europe that is currently in clinical trials in the USA [15, 16]. As part of image-guided radiotherapy for prostate cancer, TRUS is used to accurately place prostate markers, such as fiducial markers, within the prostate for daily monitoring of prostate position and accurate image-guided treatment planning, as shown in Fig. 10.2 [17, 18].

In patients with azoospermia or ejaculatory dysfunction, TRUS may help diagnose cysts of the SV or ejaculatory ducts as well as obstruction of the vasa deferentia. Accurate diagnosis of these rare conditions can change the management strategy for infertility patients [6–8]. Another uncommon but useful application of TRUS is the diagnosis of prostatic abscesses which can be associated with prostatitis or epididymitis [19, 20]. These abscesses can then be aspirated or surgically unroofed during transurethral or transrectal procedures (see Fig. 10.10).

Recently, measurement of the Resistive Index (RI) of prostatic vessels using TRUS was shown to be correlated with the outlet obstruction seen

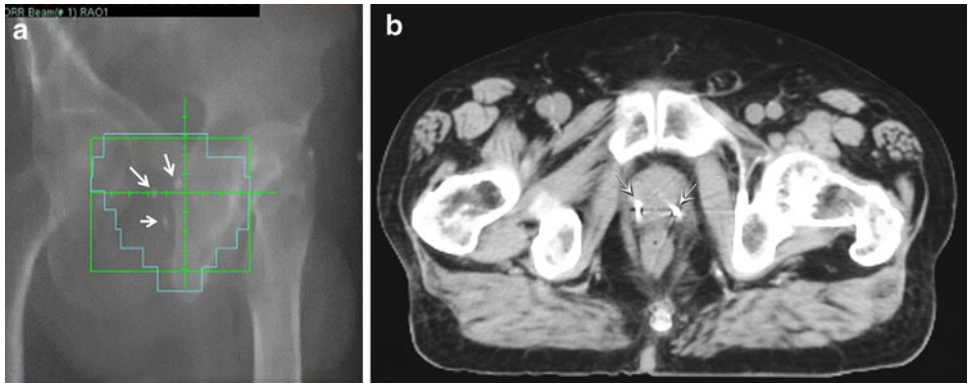

Fig. 10.2 (**a**) Port film after fiducial marker placement in the prostate. Three markers (*arrows*) are visible on plain film within the prostate and are used for daily position adjustments during radiotherapy treatment. (**b**) Axial CT image shows 2 of 3 markers (*arrows*) in the base of the prostate

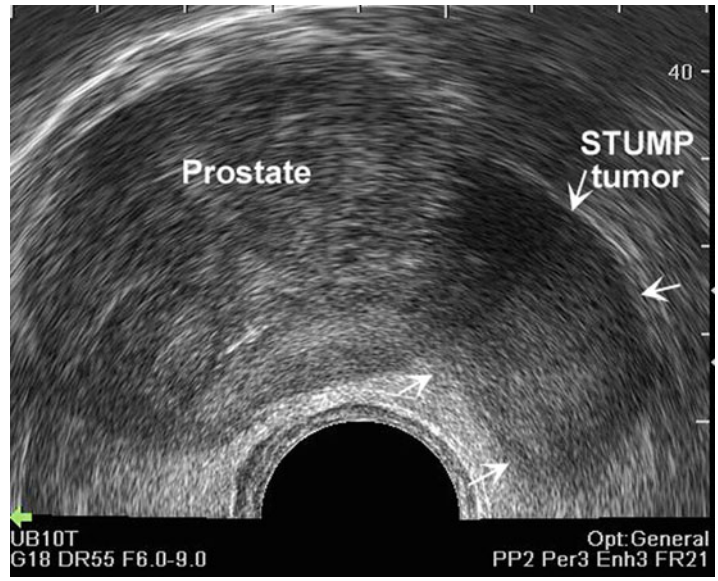

Fig. 10.3 Axial view at the base of the prostate demonstrates a slightly hypoechoic solid mass adjacent to the left lateral margin of the gland. This was subsequently shown by biopsy to be a stromal tumor of uncertain malignant potential (STUMP)

in men with BPH [21]. In men with lower urinary tract symptoms, the RI was significantly higher in those with BPH and infravesical obstruction than in those with a normal prostate.

Techniques

A complete TRUS evaluation of the prostate includes scanning in both the sagittal and transverse planes to obtain a volume calculation. The central zone and the PZ are evaluated for hypoechoic lesions and contour abnormalities. The SVs and the vasa deferentia are also visualized during the ultrasound procedure. Any abnormalities are measured, and ectasia, if present, is documented. Additionally, the rectal wall is examined for abnormal thickening or focal lesions, as occasional rectal tumors and periprostatic tumors can be encountered on TRUS of the prostate (Fig. 10.3).

Prior to the transrectal ultrasound procedure, patients are typically asked to do a cleansing enema at home before the procedure. The enema helps decrease the amount of stool in the rectum, thereby producing a superior acoustic environment

for prostate imaging. Although an enema is not absolutely mandatory, it is helpful in obtaining optimal images during TRUS. In patients undergoing real-time imaging for cryotherapy, brachytherapy, or HIFU, preoperative or intraoperative enema is important for *adequate* real-time imaging and image guidance during the procedure. If any invasive procedure is planned, antiplatelet and anticoagulation medications such as ASA, NSAIDs, clopidogrel, warfarin, vitamin E, and fish oil should be stopped at least 1 week prior to the procedure, thereby reducing the risk of bleeding with the procedure. Antibiotics given prior to the procedure may reduce the risk of bacteremia and sepsis.

Patients are positioned either in the left lateral decubitus or the lithotomy position. Most clinicians would prefer the left lateral decubitus position, especially for a straightforward TRUS. In this position, an arm board is usually placed parallel to the table and a pillow is placed between the knees to help maintain the position. The buttocks should be flush with the end of the table to allow manipulation of the probe. Next, a digital rectal exam should be performed prior to insertion of the TRUS probe. Finding a rectal stricture or rectal bleeding might delay the performance of the TRUS until the etiology is known and evaluated by the urologist. In addition, any palpable contour abnormalities of the prostate should be documented, including descriptive identifiers and their location on the gland.

The lithotomy position is used with patients who are undergoing brachytherapy or cryotherapy. Although TRUS is often performed in the lateral decubitus position, the lithotomy position is preferred for patients in whom color flow and power Doppler imaging of the prostate is planned [22]. Because the vascularity pattern of the prostate is influenced by patient positioning and gravity, the lithotomy position can help more accurately identify areas of neovascularity and increased blood flow for targeted biopsies of the prostate.

Gray-scale TRUS has been the most common modality used for imaging of the prostate. Although Doppler imaging with color flow, power Doppler and harmonic imaging have been advocated in the diagnosis of prostate cancer, their exact role for other treatment modalities such as cryotherapy or brachytherapy is still under investigation. These techniques will be further discussed in a separate section of this chapter.

There are two different types of probes available for TRUS: a side-fire probe and an end-fire probe. Either type of probe transmits mid-level frequencies between 6 and 10 MHz. Models with new biplane probe technology provide a simultaneous image of both sagittal and transverse images during the transmission period. By increasing the frequency, the axial resolution is improved. As the frequency of the probe is increased, however, the depth of tissue penetration declines, and the portion of the image that has adequate returning echo amplitude is closer to the transducer [23]. Increased resolution may be helpful in patients who have peripheral zone cancers which may be identified as a hypoechoic nodule with TRUS. However, the anterior portions of the prostate furthest from the probe may be less well seen secondary to attenuation. Lower frequency transducers, such as 4 MHz transducers, have a greater depth of penetration (between 2 and 8 cm) but with lower resolution. Lower frequency transducers improve the anterior delineation of larger glands with deeper tissue penetration, thus increasing the accuracy of volume measurements but provide poorer resolution.

A coupling medium, which is usually ultrasound gel or a lubricant, is placed between the probe and the rectal surface. This is essential since ultrasound waves propagate inefficiently through air and are completely reflected when they strike an interface between tissues or materials of a significantly different impedance. Most probes are also covered with a protective condom. A coupling medium is placed between the probe and the condom, as well as the condom and rectal mucosa.

Any TRUS scanning protocol must involve the prostate and should be performed in both the transverse and the sagittal planes. By advancing the probe in a cephalad direction in the rectum, images of the prostate base, the seminal vesicles, and the bladder neck are obtained. By pulling the probe caudally toward the anal sphincter, the

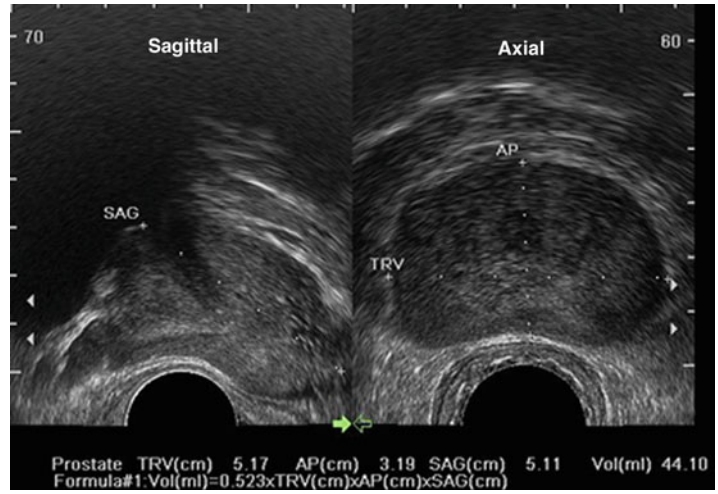

Fig. 10.4 Prostate volume measurements require the measurement of the prostate in three dimensions. In axial view the width (TRV) and height (AP) of the prostate are measured. In sagittal view the length (SAG) is measured

prostatic apex and proximal urethra are visualized. Transverse imaging with end-fire, side-fire, and some biplane probes is accomplished by angling the handle of the probe, right or left, using the anal sphincter as a fulcrum. Angling the probe toward the scrotum produces more cephalad images while angling the probe toward the sacrum produces more caudal images.

There are also two approaches to probe manipulation for sagittal imaging. One method is rotation of the probe either clockwise or counterclockwise. Clockwise rotation visualizes the left side of the prostate, and counterclockwise rotation yields images of the right side. Sagittal images can also be viewed by angling the probe up or down the anal sphincter which functions as a fulcrum. If the patient is placed in the left lateral decubitus position, angling the butt of the probe up or toward the ceiling images the left side of the prostate while angling the butt of the probe down or toward the floor images the right side. In either case, a survey scan of the prostate from base to apex, as well as the lateral aspects of the prostate, is performed first. This would include survey views of the seminal vesicles and bladder. The cine loop obtained while performing the survey scan can be easily saved along with the digital images obtained during the rest of the study. Storing the video of the survey scan provides the urologist with an overview of the entire prostate prior to biopsy or treatment, when subsequently reviewing the study.

Prostate volume is often calculated after the survey scan of the prostate is completed. Volume calculation requires measurement in three dimensions (Fig. 10.4).

The transverse and anterior posterior (A–P) dimensions are measured at the point of the widest diameter in the axial plane. The longitudinal dimension is measured in the sagittal plane just off the midline as sometimes the bladder neck may obscure the cephalad extent of the gland. Most formulas to assess prostate volumes assume an ideal geometric shape of the gland. These shapes can include an ellipse ($\pi/6 \times$ transverse diameter $\times$ A–P diameter $\times$ longitudinal diameter), a sphere ($\pi/6 \times$ the transverse diameter^3), or an egg-shaped spheroid ($\pi/6 \times$ transverse diameter$^2 \times$ the A–P diameter). Despite the inherent inaccuracies that arise from these geometric hypotheses, these formulas reliably estimate the gland volume and weight with correlation coefficients greater than 0.90 when compared to prostatectomy specimen weights (based on the assumption that 1 cm^3 equals 1 g of prostate tissue) [24]. By calculating the prostate volume, one can then derive the PSA density (PSAD) which is the ratio of serum PSA to prostate volume. The PSAD can help improve prostate cancer detection specificity and has been shown to be higher in patients diagnosed with cancer on initial and repeat prostate biopsies [25].

In patients undergoing brachytherapy, more accurate gland volume may be required.

This is accomplished by a technique called planimetry. With the patient in the lithotomy position, the probe is mounted to a stepping device and transverse images are obtained at set intervals. This is done throughout the length of the gland. The cross-sectional volume of each step is determined by measuring the circumference of the 5 mm slice and calculating its volume. The sum of the slice volumes is the volume of the entire gland.

TRUS imaging of the prostate alone is a relatively benign procedure. Other than patient discomfort due to the physical presence of an ultrasound probe in the rectum, there is little patient risk in receiving a stand-alone TRUS. However, complications can result after TRUS coupled with penetration of the rectal wall (e.g., fiducial marker placement). These include hematuria, hematospermia, rectal bleeding, and urinary retention. Hematuria after needle biopsy occurs in roughly 47% of patients and typically resolves after 5–7 days [26]. Hematospermia can be observed in up to 36% of biopsies and small traces of blood may even persist up to several months [26]. Rectal bleeding is usually mild and controllable with digital or TRUS probe pressure. Recent studies put the incidence of bleeding at 1–5%. Bleeding requiring transfusion, bacteremia requiring IV antibiotics, and other more major complications are uncommon, but antibiotic-resistant organisms are becoming more common and troublesome, raising questions about the appropriate antibiotic prophylactic coverage for these procedures [27]. Fortunately, most complications are generally minor and usually self-limited.

Documentation

A standard protocol should be used when documenting a transrectal ultrasound procedure. The report of the procedure should include the indication for the procedure. The technique should be described and the position of the patient should be documented. The machine and the probes used in the procedure should be described. The anatomy of surrounding structures including seminal vesicles, vasa deferentia, and the perirectal space should be evaluated and the findings documented. The measurements of the prostate gland including height, width, and length along with the calculated volume should be documented. Any abnormal findings should be noted. If color or power Doppler is performed, those findings should be documented. The report should be signed by the urologist. A sample TRUS documentation sheet is shown in Fig. 10.5.

Images of the prostate should be captured and stored electronically or printed and maintained with the report. Images of the prostate in the axial and sagittal views should be documented at the apex, mid, and base. Images depicting the measurement of prostatic volume should be documented. The prostatic urethra and periprostatic tissues should be demonstrated and, when indicated, the vasa deferentia. Images demonstrating any abnormalities such as hypoechoicism, hyperechoicism, or increased regional blood flow on Doppler should be documented. Measurements of abnormalities should be taken and documented.

Normal Anatomy

The prostate gland lies beneath the pubis between the bladder neck and the urogenital diaphragm just anterior to the rectum in an ideal position to be imaged via TRUS. Traditionally, the prostate gland is described using histological/anatomical zonal architecture [28] (Fig. 10.6).

These divisions consist of the anterior fibromuscular stroma (AFS), which is devoid of glandular tissue, transition zone (TZ), central zone (CZ), and peripheral zone (PZ). Typically the prostate on TRUS is divided into the inner gland, consisting of the AFS, TZ, periurethral tissue, and CZ, and the outer gland which is the PZ. In the young male, the TZ comprises 5–10% of normal prostate volume. The TZ increases with age and often accounts for the obstructive symptomatology associated with benign prostatic hypertrophy (BPH). Approximately 20% of prostate cancers originate in the TZ (Fig. 10.4). The CZ surrounds the ejaculatory ducts and accounts for a minority of cancers. Finally, the PZ makes up 75% of the prostate volume and is the source of the great

a

PATIENT LABEL

PROSTATE ULTRASOUND

DATE OF SERVICE: | PSA:

INDICATION:

US MACHINE: | TRANSDUCER:

B-MODE

DRE

	LEFT	RIGHT
SIZE		
LEFT		
RIGHT		

SEMINAL VESICLE

LENGTH (cm)	
WIDTH (cm)	
DESCRIPTION	

TRANSVERSE PROSTATE

BASE:

MID-GLAND:

APEX:

SAGITTAL PROSTATE

ANTERIOR

MID-GLAND

POSTERIOR

MID-SAGITTAL PROSTATE MEASUREMENTS

HEIGHT (cm)

WIDTH (cm)

LENGTH (cm)

VOLUME (cm^3)

COLOR DOPPLER/DUPLEX FINDINGS (ATTACH IMAGES)

INDICATION FOR COLOR/DUPLEX STUDY: | URETERAL JETS (R/L):

	LEFT	RIGHT	COMMENTS:
SV:			
BASE:			
APEX:			
MASS:			

PSV	EDV	RI	LOCATION	PSV	EDV	RI
			BASE			
			MIDDLE			
			APEX			
			AVERAGE			

PHYSICIAN INTERPRETATION

DATE/TIME

PHYSICIAN SIGNATURE

b

PATIENT LABEL

TRUS PROCEDURE RECORD

DATE OF SERVICE:		RM IN:	
PROCEDURE:	PROSTATE U/S; U/S GUIDANCE/TRUS NEEDLE BX	TIME OUT:	
DIAGNOSIS:	ELEVATED PSA / ABNORMAL DRE / FOLLOW UP	START:	
PHYSICIAN:		FINISHED	
ASSISTANT:		RM OUT:	
LAST ASPIRIN USE		LAST PSA:	
ALLERGIES:		BP:	
VALVES/PROSTHETICS:		PULSE:	

PATEINT TOOK NECESSARY PREPARATIONS AND ANTIBIOTICS FOR PROCEDURE — PARENT SIGNATURE

DATE/TIME	Temp	HR	BP	RR	COMMENTS

POST PROCEDURE INSTRUCTIONS & INFORMATION GIVEN — PARENT SIGNATURE — WITNESS SIGNATURE

PATIENT POST PROCEDURE PAIN SCORE: / 10

PHYSICIAN ORDERS

DATE/TIME	ORDER	SIGNATURE	GIVEN BY

PROCEDURE NOTE

PSA | DRE

SEE DICTATED NOTE

TRANSRECTAL U/S GUIDED NEEDLE BX OF PROSTATE

1% LIDOCAINE (cc)____ | 2% LIDOCAINE(cc)____

LEFT (#cores)	RIGHT (#cores)
_____BASE	_____BASE
_____MID	_____MID
_____APEX	_____APEX
_____TRANSITION ZONE	_____TRANSITION ZONE
_____TOTAL LEFT	_____TOTAL LEFT
	_____TOTAL CORES

PATIENT FOLLOW-UP:

PHYSICIAN INTERPRETATION

DATE/TIME

PHYSICIAN SIGNATURE

Fig. 10.5 Sample TRUS documentation sheets

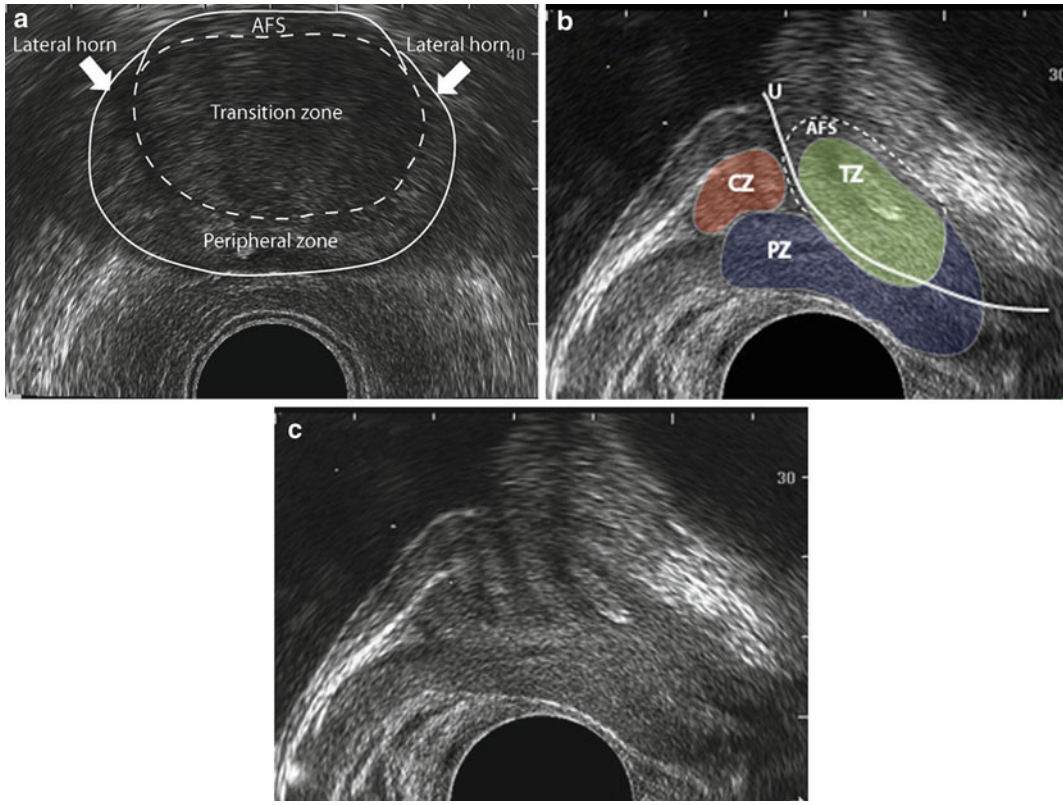

Fig. 10.6 Image (**a**) demonstrates the zonal anatomy of the prostate in axial view. The anterior fibromuscular stroma (AFS) is just between the capsules anteriorly. Image (**b**) demonstrates the zonal anatomy of the prostate in the midsagittal plane. *U* urethra; *CZ* central zone; *TZ* transition zone; *PZ* peripheral zone; *AFS* anterior fibromuscular stroma. Image (**c**) is the same as image (**b**) without the drawing overlay

majority of prostate carcinoma. Unfortunately, these zonal regions can sometimes be difficult to distinguish using ultrasound imaging.

The prostatic inner gland has a more heterogeneous appearance on ultrasound whereas the outer gland has a more homogenous appearance. Frequently, hyaline concretions known as *corpora amylacea* [29] (Fig. 10.7) highlight the plane between the outer gland and the inner gland [11]. These small, multiple, diffuse hyaline concretions are normal and often an incidental ultrasonographic finding of the prostate. Generally, they represent a common, normal ultrasound finding rather than a pathological entity [30]. Larger prostatic calculi may be associated with symptoms and can be related to underlying inflammation. These larger calculi may require further evaluation and treatment.

The prostatic urethra traverses the length of the gland in the midline and thus must be imaged in the sagittal plane to be viewed in its entirety along its course. Generally, the distended urethral lumen is hypoechoic in appearance. Periurethral calcifications may produce a thin echogenic outline. Smooth muscle of the internal sphincter extends from the bladder neck encircling the urethra to the level of the verumontanum. These muscle fibers may be visualized sonographically as a hypoechoic ring around the upper prostatic urethra producing a funnel-like appearance proximally. The urethra angles anteriorly and runs the remainder of the gland to the exit at the apex of the prostate. This angle gives the prostatic urethra an anterior concave appearance when viewed along the entire course of the sagittal plane.

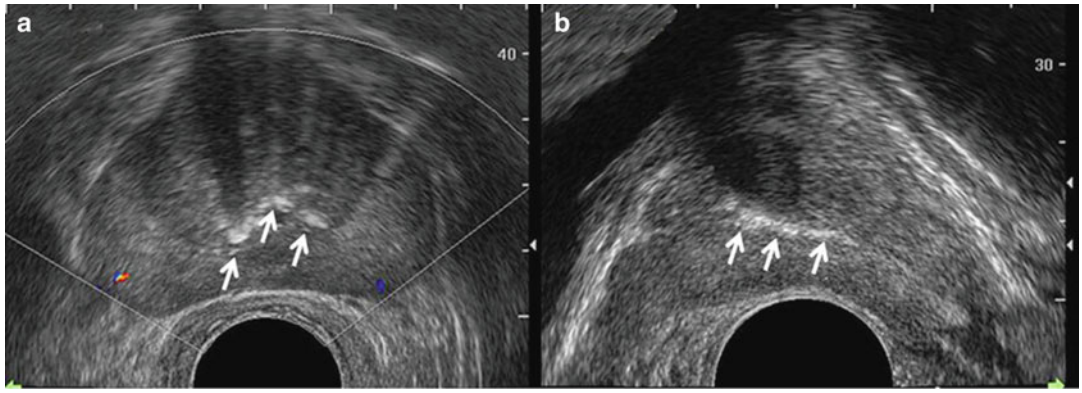

Fig. 10.7 Corpora amylacea (*arrows*) within the prostate. In the axial view (**a**) of the prostate the corpora amylacea are seen surrounding the urethra and there is acoustic shadowing. On sagittal view (**b**) the corpora amylacea can be seen to track along the urethra

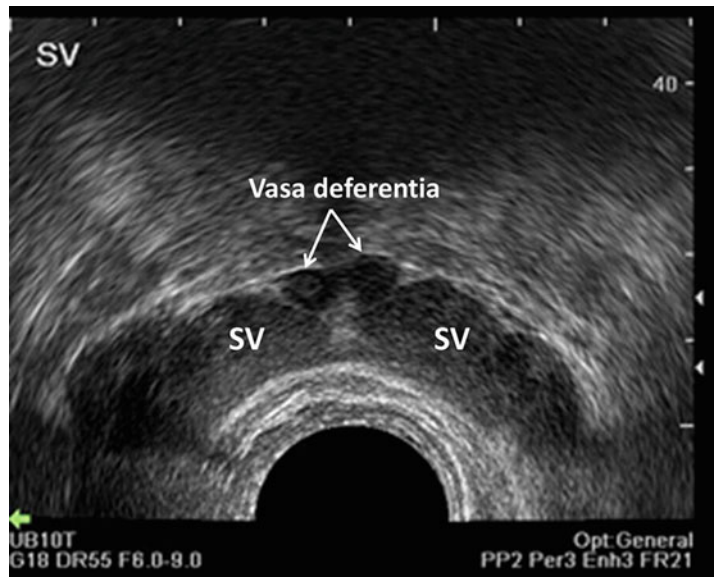

Fig. 10.8 Axial view of the prostate showing the seminal vesicle (SV) and vasa deferentia

The seminal vesicles (SV) are positioned posteriorly to the base of the prostate (Fig. 10.8). They have a smooth saccular appearance that should be symmetrical. The normal SV measures approximately 4.5–5.5 cm in length and 2.2 cm in width. Solid lesions in the SV can be concerning for malignancy, while cystic masses of the SV are generally benign [31–33]. Solid lesions are even more worrisome if there is a history of primary neoplasm elsewhere. Infectious etiologies such as schistosomiasis should be considered in patients with solid SV masses who have lived in areas of endemic infestation [34]. The vasa deferentia can be visualized in a transverse plane just above the ipsilateral SV before diving caudally toward the prostate near the midline. Each vas lies just medial to the tapering ipsilateral SV before the two structures fuse to form the ejaculatory duct. The ejaculatory ducts enter the gland posteriorly and empty into the urethra at the level of verumontanum. These ducts are occasionally seen as hypoechoic structures on TRUS. Their course parallels the prostatic urethra proximal to the verumontanum.

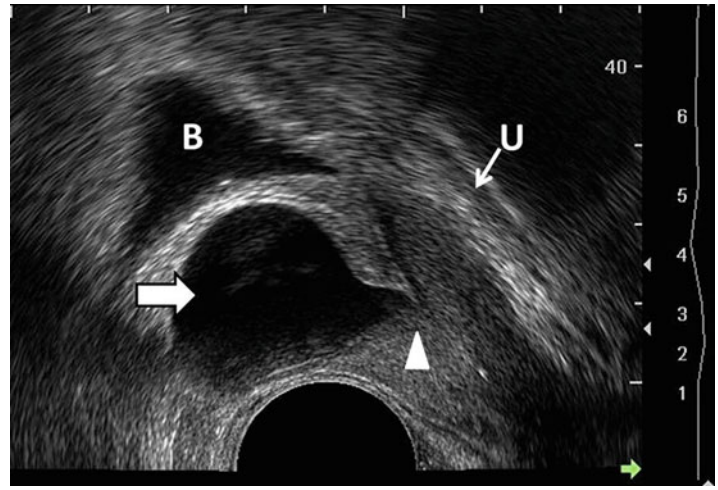

Fig. 10.9 Utricular cyst. A sagittal view of the prostate demonstrates a utricular cyst (*arrow*) in the midline arising from the vicinity of the verumontanum (*caret*). *B* bladder, the hyperechoic structure to the right is the ureter (U)

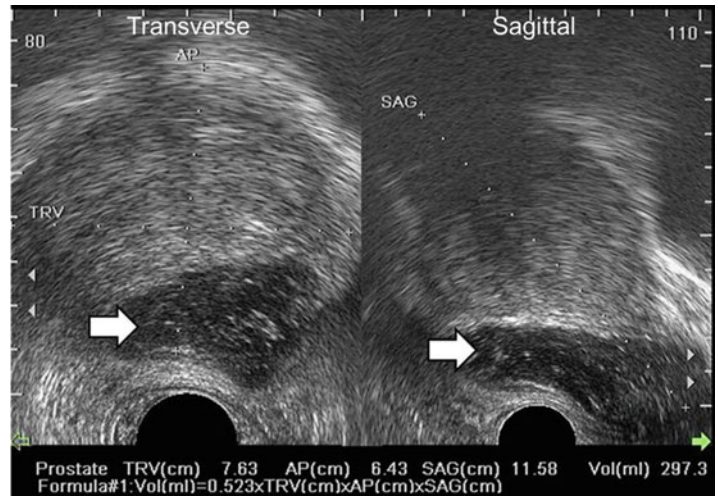

Fig. 10.10 Prostate abscesses (*arrows*) are seen as hypoechoic areas on axial and sagittal views

Abnormal Anatomy

The most common finding on TRUS is a variety of cystic lesions of the prostate. Prostatic cysts may be acquired or congenital in nature and are rarely clinically significant. Congenital prostatic cystic lesions can originate from either Mullerian or Wolffian structures. Those that arise from Mullerian structures include enlarged prostatic utricles (appear as a midline anechoic structure projection from the posterior urethra at the level of the verumontanum) (Fig. 10.9) and Mullerian duct cysts (also appear as a midline anechoic structure) which result from failure of the Mullerian ducts to properly fuse with the urethra [35, 36]. Lesions that originate from Wolffian structures include seminal vesicle cysts and vas deferens cysts. Seminal vesicle cysts may be associated with renal agenesis in up to two thirds of men [37].

Prostatic abscesses typically appear hypoechoic on TRUS. These collections can contain inhomogeneous material with internal septations [20]. This appearance with the constellation of signs and symptoms, including fever, pain, and persistent infection, is consistent with prostatic abscess. These abscesses are routinely amenable to TRUS-guided transrectal drainage as a treatment modality (Fig. 10.10).

The appearance of the prostate after external-beam radiation, brachytherapy, and androgen ablation varies compared to normal prostate anatomy. The radiated prostate can be diffusely hypoechoic, and typical zonal anatomy is difficult to identify [38]. After brachytherapy, seeds should be evenly distributed throughout the gland and appear hyperechoic on TRUS with posterior shadowing [39]. Overall prostate volume can decline up to 50% with brachytherapy. Androgen ablation can result in an average 30% volume loss in patients with prostate cancer [40].

Enhanced Imaging Techniques

Despite the most meticulous and systematic approach to TRUS, the sensitivity of prostate biopsy remains disappointingly low, with false negative rates of 25% or higher in multiple studies [41, 42]. In an attempt to improve the sensitivity of ultrasound-guided prostate biopsy, enhanced ultrasonographic techniques have been utilized to better identify areas of the prostate containing cancer.

Neoplastic prostate tissue is histologically distinct from normal prostate tissue, differentiated by a loss of glandular architecture, increased cellular density, and increased microvascularity [43]. The loss of glandular architecture reduces the content of reflective interfaces, causing a hypoechoic appearance on TRUS [43]. Increased cellular density may change the normal elasticity of prostate tissue which may be measurable by real-time elastography [44]. Hypervascularity and tumor-associated angiogenesis may be appreciated on Doppler and/or contrast-enhanced Doppler examination or other advanced techniques.

Doppler Ultrasound

Color and power Doppler have both been used to enhance TRUS biopsy detection of prostate cancer [45, 46]. Color Doppler measures the frequency shift in ultrasound waves as a function of the velocity and direction of vascular flow. Increased blood flow as a result of increased microvascularity to cancerous tissue is the theoretical justification for the use of color and power Doppler sonography [43]. Amplified flow patterns to areas of tumor, which harbor an increased number and size of blood vessels, is the hallmark of prostate cancer detection using Doppler imaging (Fig. 10.11).

Targeted biopsies of the prostate can then be performed where there is enhanced flow. Power Doppler reflects the integrated amplitude or power of the Doppler signal. Power Doppler is more sensitive to low-velocity flow than color Doppler because it displays information about the amount of blood forming at a given velocity rather than the relative frequency shift caused by that velocity. Several studies have shown an increased sensitivity of power Doppler to detect cancer [47, 48]. Unfortunately, when looking at the overall picture, the use of color and power Doppler has yielded mixed results. Sensitivity for tumor detection lies anywhere from 13 to 49% in recent studies, and ultrasound abnormalities have been shown in many patients with subsequently demonstrated benign pathology [45, 46, 49, 50]. These findings may be due to patient position and the presence of benign conditions, such as prostatitis, that result in increased blood flow to the prostate thereby clouding the picture for targeted cancer biopsies using this technique.

Contrast-Enhanced Ultrasound

Microbubble contrast agents for use in contrast-enhanced TRUS were first developed in the 1980s [50]. They are composed of tiny bubbles of injectable gas contained within a supporting shell such as a lipid or a surfactant microsphere. Contrast microbubbles are on the order of 1–10 μm in size and thus able to penetrate even the smallest microvessels. These contrast agents consist of microbubbles of gas which irregularly reflect the ultrasound signal and are thereby able to show the increased microvascularity and vascular density correlated to prostate cancer (Fig. 10.12) [51].

Studies comparing systematic biopsy versus contrast-enhanced color flow Doppler sonography using microspheres to target areas of

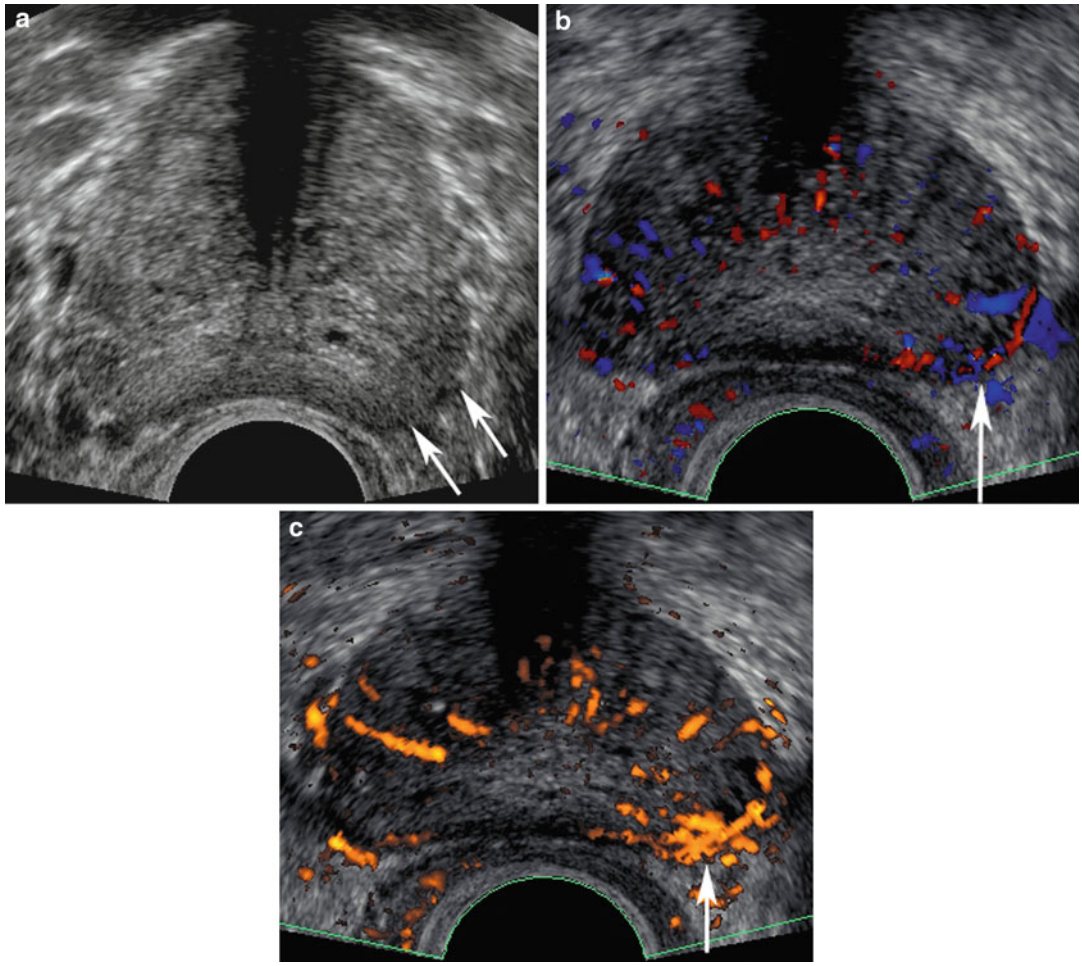

Fig. 10.11 Gleason 3+3 prostate adenocarcinoma. Several transverse images through the midgland of the prostate. (**a**) Conventional gray-scale imaging demonstrates a slightly hypoechoic lesion along the left midgland (*arrows*). (**b**) Color Doppler demonstrates increased vascular flow to this area, corresponding to area of probable cancer. (**c**) Power Doppler shows increased flow to the same left midgland area, confirming hypervascularity

increased neovascularity for directed biopsies were twice as likely to yield positive results and higher Gleason grades [52–54] when compared to systematic biopsies. Flash replenishment technology takes advantage of the ability of ultrasound waves to periodically "destroy" the microbubbles and provide a clean viewing field on the monitor. Low energy pulses show blood vessels refilling with contrast, permitting optimal visualization of vascular flow to cancerous cells. Increased positive core rates for targeted biopsies over systematic biopsy have been reported in the literature utilizing this flash replenishment technique [55].

3D Ultrasound

Experience with three-dimensional (3D) ultrasound of the prostate has been limited. Currently the use of specialized ultrasound probes is required for 3D visualization of the prostate. In addition to the standard axial and sagittal planes, 3D ultrasound provides an additional coronal plane. The use of 3D ultrasound for prostate biopsy has demonstrated mixed results. In a study by Hamper et al., 16 patients underwent both 2D and 3D TRUS-guided biopsy of the prostate [56]. The authors noted only a subjective improvement

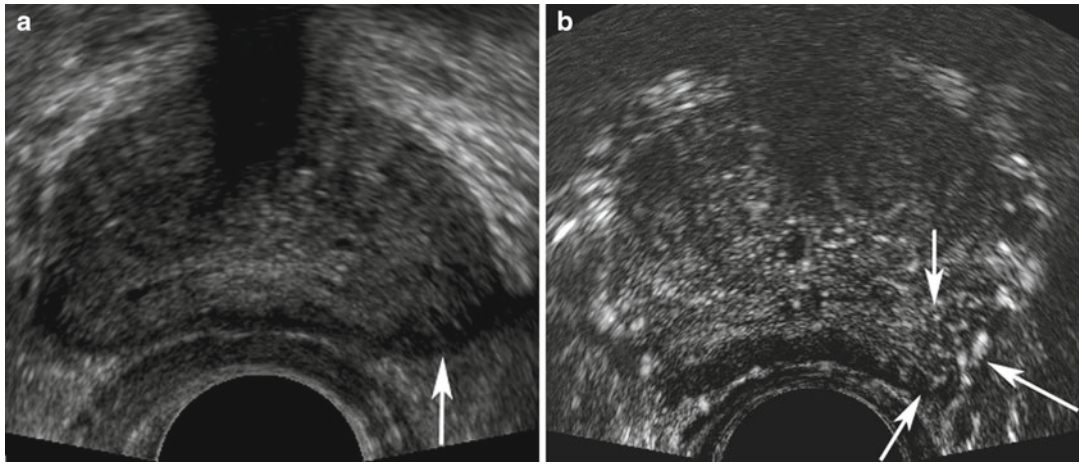

Fig. 10.12 Transverse image through the midgland of the prostate. (**a**) Gray-scale imaging demonstrates a hypoechoic contour bulge of the left midgland suspicious for prostate cancer (*arrow*). (**b**) After microbubble contrast injection, gray-scale imaging reveals a slightly larger area of parenchymal enhancement with visualization of hypervascularity (*arrows*). On biopsy, this area revealed (Gleason 4 + 4 = 8) prostate adenocarcinoma

in the ability to identify hypoechoic areas of the prostate while using 3D. Further studies utilizing 3D need to be performed to better elucidate its role in TRUS of the prostate.

Elastogram

Prostate cancer typically results in both glandular architecture loss and increased cellular density. Decreased tissue elasticity is a product of these changes. Decreased tissue elasticity may be measurable using ultrasound elastography. Ultrasound elastography, also called strain imaging, is a method of signal processing using a special ultrasound probe that generates an elastogram. Lower-density tissues allow greater displacement when compressed with the ultrasound probe while higher-density tissues allow for less displacement (Fig. 10.13).

The elastogram is created by compression and decompression of the prostate by the TRUS operator using the probe. This difference in compressibility allows for the use of elastography in targeted prostate biopsy [57]. A study published in 2008 reported a sensitivity of 86% and specificity of 72% in detecting prostate cancer, with a negative predictive value of 91.4% using ultrasound elastography [58]. Compared to microbubble enhancement or flow-based imaging techniques (e.g., Doppler), elastograms provide a less subjective target and thus show promise in the future of TRUS-guided prostate biopsy.

Although gray-scale TRUS imaging is the current gold standard for prostate imaging, new technologies have emerged in the field of ultrasonography to better guide the urologist in prostate cancer imaging and detection. With more patients undergoing evaluation for elevated PSA each year and thus likely receiving a TRUS with needle biopsy of the prostate, it is crucial that new technologies be developed to more accurately and efficiently identify suspicious areas concerning for malignancy. Reliable techniques showing no suspicious areas might obviate a biopsy. No current advanced ultrasound technique has been shown to be capable of replacing standard systematic biopsy. Fusion technologies combining ultrasound images with other modalities such as MRI or CT show promise for combining the advantage of real-time ultrasound-directed biopsy with the greater resolution of the other modalities. However, with continued research and improvement we may be able to one day reduce the number of specimens needed for prostate cancer detection or altogether eliminate the need for biopsy in those patients without cancer.

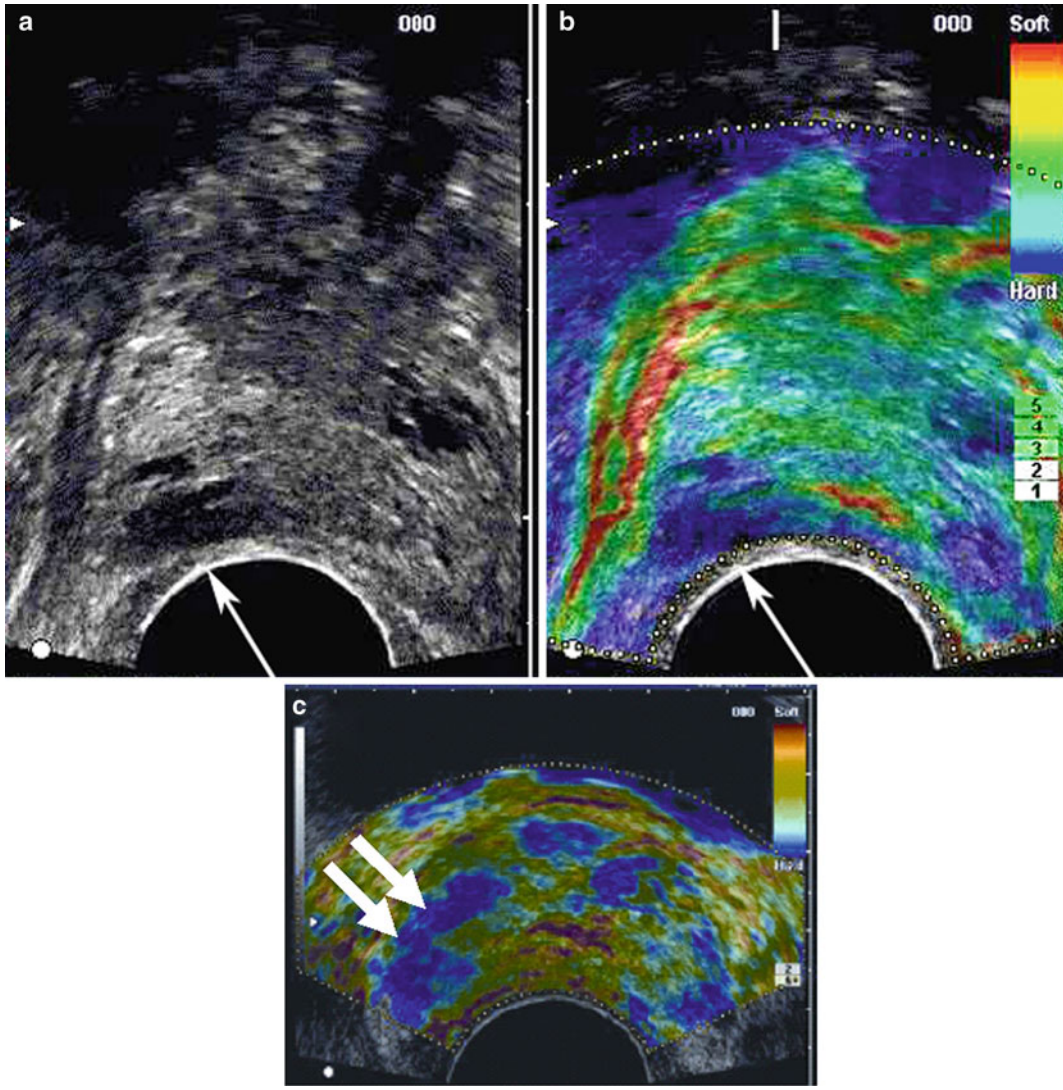

Fig. 10.13 (**a**) Gray-scale image reveals a hypoechoic lesion in right midgland (*arrow*). This lesion corresponds to an area of increased tissue stiffness (*dark blue*) on the corresponding elastogram (**b**). A targeted biopsy of this region revealed prostate adenocarcinoma. Note the color scale in the upper right corner of (**b**) and (**c**) indicating relative tissue "firmness." (**c**) In a different prostate an elastogram depicts an area of increased firmness (*arrows*) concerning for neoplasm

Conclusion

Transrectal ultrasound imaging plays a crucial role in the evaluation and management of both benign and malignant pathologies of the prostate. The development and use of TRUS has greatly enhanced the armamentarium of the urologist. With future research, newer technologies can hopefully further refine the use of TRUS in the diagnosis and treatment of prostatic conditions.

References

1. Watanabe H, et al. [Diagnostic application of ultrasonotomography to the prostate]. Nihon Hinyokika Gakkai Zasshi. 1968;59(4):273–9.

2. Hodge KK, et al. Random systematic versus directed ultrasound guided transrectal core biopsies of the prostate. J Urol. 1989;142(1):71–4. discussion 74–5.
3. Beerlage HP. Alternative therapies for localized prostate cancer. Curr Urol Rep. 2003;4(3):216–20.
4. Wasserman NF. Benign prostatic hyperplasia: a review and ultrasound classification. Radiol Clin North Am. 2006;44(5):689–710. viii.
5. Stravodimos KG, et al. TRUS versus transabdominal ultrasound as a predictor of enucleated adenoma weight in patients with BPH: a tool for standard preoperative work-up? Int Urol Nephrol. 2009;41(4): 767–71.
6. Smith JF, Walsh TJ, Turek PJ. Ejaculatory duct obstruction. Urol Clin North Am. 2008;35(2):221–7. viii.
7. Raviv G, et al. Role of transrectal ultrasonography in the evaluation of azoospermic men with low-volume ejaculate. J Ultrasound Med. 2006;25(7):825–9.
8. Zahalsky M, Nagler HM. Ultrasound and infertility: diagnostic and therapeutic uses. Curr Urol Rep. 2001; 2(6):437–42.
9. Frauscher F, Klauser A, Halpern EJ. Advances in ultrasound for the detection of prostate cancer. Ultrasound Q. 2002;18(2):135–42.
10. Onur R, et al. Contemporary impact of transrectal ultrasound lesions for prostate cancer detection. J Urol. 2004;172(2):512–4.
11. Issa M, Oesterling J. Radiofrequency thermal therapy for benign prostatic hyperplasia by transurethral needle ablation of the prostate. In: Narayan P, editor. Benign prostatic hyperplasia. London: Churchill Livingstone; 2000. p. 269–80.
12. Wheelahan J, et al. Minimally invasive non-laser thermal techniques for prostatectomy: a systematic review. The ASERNIP-S review group. BJU Int. 2000;86(9):977–88.
13. Eggener SE, et al. Focal therapy for localized prostate cancer: a critical appraisal of rationale and modalities. J Urol. 2007;178(6):2260–7.
14. Aus G. Current status of HIFU and cryotherapy in prostate cancer—a review. Eur Urol. 2006;50(5): 927–34. discussion 934.
15. Marberger M, et al. New treatments for localized prostate cancer. Urology. 2008;72(6 Suppl):S36–43.
16. Polascik TJ, Mouraviev V. Focal therapy for prostate cancer. Curr Opin Urol. 2008;18(3):269–74.
17. Dehnad H, et al. Clinical feasibility study for the use of implanted gold seeds in the prostate as reliable positioning markers during megavoltage irradiation. Radiother Oncol. 2003;67(3):295–302.
18. Linden RA, et al. Technique of outpatient placement of intraprostatic fiducial markers before external beam radiotherapy. Urology. 2009;73(4):881–6.
19. Oliveira P, et al. Diagnosis and treatment of prostatic abscess. Int Braz J Urol. 2003;29(1):30–4.
20. Lim JW, et al. Treatment of prostatic abscess: value of transrectal ultrasonographically guided needle aspiration. J Ultrasound Med. 2000;19(9):609–17.
21. Kojima M, et al. Doppler resistive index in benign prostatic hyperplasia: correlation with ultrasonic appearance of the prostate and infravesical obstruction. Eur Urol. 2000;37(4):436–42.
22. Halpern EJ, et al. High-frequency Doppler US of the prostate: effect of patient position. Radiology. 2002;222(3):634–9.
23. Kossoff G. Basic physics and imaging characteristics of ultrasound. World J Surg. 2000;24(2):134–42.
24. Terris MK, Stamey TA. Determination of prostate volume by transrectal ultrasound. J Urol. 1991;145(5): 984–7.
25. Djavan B, et al. Optimal predictors of prostate cancer on repeat prostate biopsy: a prospective study of 1,051 men. J Urol. 2000;163(4):1144–8. discussion 1148–9.
26. Rodriguez LV, Terris MK. Risks and complications of transrectal ultrasound guided prostate needle biopsy: a prospective study and review of the literature. J Urol. 1998;160(6 Pt 1):2115–20.
27. Batura D, et al. Adding amikacin to fluoroquinolone-based antimicrobial prophylaxis reduces prostate biopsy infection rates. BJU Int. 2011;107(5):760–4.
28. McNeal JE. The zonal anatomy of the prostate. Prostate. 1981;2(1):35–49.
29. Christian JD, et al. Corpora amylacea in adenocarcinoma of the prostate: incidence and histology within needle core biopsies. Mod Pathol. 2005;18(1):36–9.
30. Halpern E. Anatomy of the prostate gland. In: Halpern E, Cochlin D, Goldberg B, editors. Imaging of the prostate. London: Martin Dunitz; 2002. p. 3–15.
31. Geramoutsos I, et al. Clinical correlation of prostatic lithiasis with chronic pelvic pain syndromes in young adults. Eur Urol. 2004;45(3):333–7. discussion 337–8.
32. Sheih CP, et al. Seminal vesicle cyst associated with ipsilateral renal malformation and hemivertebra: report of 2 cases. J Urol. 1993;150(4):1214–5.
33. Narayana A. Tumors of the epididymis, seminal vesicles, and vas deferens (spermatic cord). In: Culp D, Loening S, editors. Genitourinary oncology. Philadelphia, PA: Lea & Febiger; 1985. p. 385–98.
34. Al-Saeed O, et al. Seminal vesicle masses detected incidentally during transrectal sonographic examination of the prostate. J Clin Ultrasound. 2003;31(4): 201–6.
35. Cochlin DL. Cysts and congenital anomalies of the prostate and ejaculatory ducts. In: Halpern EJ, Cochlin DL, Golberg BB, editors. Imaging of the prostate. London: Martin Dunitz; 2002. p. 115–28.
36. McDermott V, Orr JD, et al. Duplicated Mullerian duct remnants associated with unilateral renal agenesis. Abdom Imaging. 1993;18(2):193–5.
37. King BF, Hattery RR, et al. Congenital cystic disease of the seminal vesicle. Radiology. 1991;178(1): 207–11.
38. Egawa S, Wheeler TM, et al. The sonographic appearance of irradiated prostate cancer. Br J Urol. 1991; 68(2):172–7.
39. Stone NN, Stock RG. The effect of brachytherapy, external beam irradiation and hormonal therapy on prostate volume. J Urol. 2007;177(3):925–8.

40. Whittington R, Broderick GA, et al. The effect of androgen deprivation on the early changes in prostate volume following transperineal ultrasound guided interstitial therapy for localized carcinoma of the prostate. Int J Radiat Oncol Biol Phys. 1999; 44(5):1107–10.
41. Chen ME, et al. Optimization of prostate biopsy strategy using computer based analysis. J Urol. 1997; 158(6):2168–75.
42. Daneshgari F, et al. Computer simulation of the probability of detecting low volume carcinoma of the prostate with six random systematic core biopsies. Urology. 1995;45(4):604–9.
43. Bigler SA, Deering RE, Brawer MK. Comparison of microscopic vascularity in benign and malignant prostate tissue. Hum Pathol. 1993;24(2):220–6.
44. Taylor LS, et al. Three-dimensional sonoelastography: principles and practices. Phys Med Biol. 2000; 45(6):1477–94.
45. Newman JS, Bree RL, Rubin JM. Prostate cancer: diagnosis with color Doppler sonography with histologic correlation of each biopsy site. Radiology. 1995; 195(1):86–90.
46. Halpern EJ, Strup SE. Using gray-scale and color and power Doppler sonography to detect prostatic cancer. AJR Am J Roentgenol. 2000;174(3):623–7.
47. Cho JY, Kim SH, Lee SE. Diffuse prostatic lesions: role of color Doppler and power Doppler ultrasonography. J Ultrasound Med. 1998;17(5):283–7.
48. Okihara K, et al. Ultrasonic power Doppler imaging for prostatic cancer: a preliminary report. Tohoku J Exp Med. 1997;182(4):277–81.
49. Nelson ED, et al. Targeted biopsy of the prostate: the impact of color Doppler imaging and elastography on prostate cancer detection and Gleason score. Urology. 2007;70(6):1136–40.
50. Furlow B. Contrast-enhanced ultrasound. Radiol Technol. 2009;80(6):547S–61.
51. Brawer MK, et al. Predictors of pathologic stage in prostatic carcinoma. The role of neovascularity. Cancer. 1994;73(3):678–87.
52. Frauscher F, et al. Detection of prostate cancer with a microbubble ultrasound contrast agent. Lancet. 2001;357(9271):1849–50.
53. Frauscher F, et al. Comparison of contrast enhanced color Doppler targeted biopsy with conventional systematic biopsy: impact on prostate cancer detection. J Urol. 2002;167(4):1648–52.
54. Mitterberger M, et al. Comparison of contrast enhanced color Doppler targeted biopsy to conventional systematic biopsy: impact on Gleason score. J Urol. 2007;178(2):464–8. discussion 468.
55. Linden RA, et al. Contrast enhanced ultrasound flash replenishment method for directed prostate biopsies. J Urol. 2007;178(6):2354–8.
56. Hamper UM, et al. Three-dimensional US of the prostate: early experience. Radiology. 1999;212(3): 719–23.
57. Krouskop TA, et al. Elastic moduli of breast and prostate tissues under compression. Ultrason Imaging. 1998;20(4):260–74.
58. Pallwein L, et al. Sonoelastography of the prostate: comparison with systematic biopsy findings in 492 patients. Eur J Radiol. 2008;65(2):304–10.

Ultrasound for Prostate Biopsy

11

Christopher R. Porter

Introduction

The evaluation of prostatic conditions prior to the advent of sonographic techniques relied on palpation of the gland and "blind" sampling techniques via needle aspiration and biopsy. With the development of B-mode ultrasound in the 1950s, and probes capable of providing images to the clinician in real-time, gray-scale ultrasound became the standard method of prostate imaging for most prostate conditions. The position of the prostate in the pelvis, tucked as it were beneath the pubis and anterior to the rectum, lends itself to the application of a transrectal approach. The transrectal approach to imaging the gland has become the standard of care for diagnostic evaluation of prostatic conditions, prostate biopsy, and therapeutic approaches to prostate cancer.

The urologists' application of transrectal ultrasound (TRUS) is ubiquitous: virtually all urologists' offices, whether they are in a private small group setting or in the academic setting, have one or more ultrasound units with probes appropriate for transrectal imaging.

This chapter will focus on TRUS-guided prostate biopsy. The chapter will encompass the initial evaluation of the gland, the techniques used to perform prostate biopsy, and the references for documenting the exam and patient safety.

C.R. Porter, MD, FACS (✉)
Department of Surgery, Virginia Mason Medical Center, 1100 9th Ave, C7 URO, Seattle, WA 98111, USA
e-mail: Christopher.Porter@vmmc.org

History

TRUS-guided prostatic biopsy is the standard method for early detection of adenocarcinoma of the prostate. Prostate biopsy was first described in 1930 using a transperineal approach [1]. Seven years later the first transrectal biopsy was performed by Astraldi [2]. TRUS was first described in 1955 [3] and was widely used in practice by the 1970s [4]. Hodge described the first systematic biopsy template (sextant) in 1989 [5]. Further refinements have included an extended-core biopsy scheme as well as refinements to pain control strategies.

Anatomy

Grossly the prostate is situated anterior to the rectum and beneath the pubic arch. Laterally the prostate is bordered by the levator ani and inferiorly by the bladder neck. Prostatic glandular anatomy is typically described in terms of zonal architecture. The anterior fibromuscular stroma (AFS) is devoid of glandular tissue. The transition zone (TZ), which makes up 5–10% of normal prostate volume, gives rise to benign prostatic hyperplasia (BPH) and is the zone or origin for 20% of prostate cancers. The central zone (CZ) surrounds the ejaculatory ducts, makes up 20%

P.F. Fulgham and B.R. Gilbert (eds.), *Practical Urological Ultrasound*, Current Clinical Urology,
DOI 10.1007/978-1-59745-351-6_11,

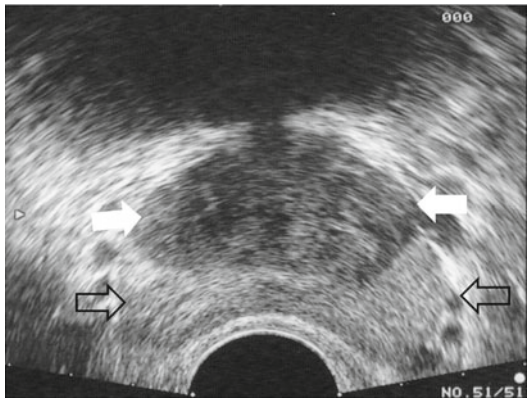

Fig. 11.1 Transrectal ultrasound image (7.5 MHz) of the prostate. Hypoechoic region anteriorly corresponds to transition zone (*white arrows*). Peripheral zone (relatively more hyperechoic) lies posteriorly (*open arrows*)

of the prostate volume, and gives rise to a minority of prostate cancers (5%). The peripheral zone (PZ) makes up to 75% of the normal prostate volume and is the source of the majority of prostate cancers. These zonal distinctions are not always evident on ultrasound examination; however, in the presence of BPH, the PZ may be differentiated from the CZ. The paired seminal vesicles (SV), which are generally symmetrical in appearance, are located posteriorly (Fig. 11.1).

Technique Preparation

Patients undergoing a prostate needle biopsy should refrain from taking antiplatelet/anticoagulation medications (i.e., ASA/NSAIDs/clopidogrel/warfarin) 7 days prior to the procedure. Other medications including over-the-counter medications and herbal products which may affect clotting time should also be avoided. A list of medications which should be avoided prior to biopsy is included in Appendix.

Crawford et al. [6] have demonstrated that antibiotics 24 h prior to and continuing 24–48 h post-procedure reduce bacterial septicemia. Recently, there has been a rise in septicemia rates from the modern-day prophylaxis rate of less than 1% [7]. This has been due in part to an increased incidence of extended-spectrum beta-lactamase-producing (ESBL) *Escherichia coli* that tend to be resistant to ciprofloxacin, ceftriaxone, sulbactam/ampicillin, and cefazolin. Generally imipenem and piperacillin–tazobactam are the effective agents against ESBL-producing *E. coli* [8, 9]. Prophylaxis against infective endocarditis, with appropriate antibiotics—usually gentamicin and ampicillin [10]—is recommended by the American Heart Association for patients at high risk for infective endocarditis. This includes patients (1) with prosthetic cardiac valves or prosthetic material used for cardiac valve repair, (2) those with previous infective endocarditis, (3) patients with congenital heart defects, and (4) cardiac transplant recipients with valve regurgitation [11]. The American Academy of Orthopedic Surgeons (AAOS) guidelines [12] state that clinicians should consider antibiotic prophylaxis for all total joint replacement patients prior to any invasive procedure that may cause bacteremia. For genitourinary procedures, the AAOS recommends ciprofloxacin 60 min prior to the biopsy. Prophylactic antibiotic use may need to be modified based on local patterns of bacterial resistance.

An enema may be given the night prior to and the morning of the procedure. Reduced rectal contents will increase visibility by reducing interference and have been demonstrated to reduce the rate of bactermia [13].

Anesthesia

It is accepted that transrectal ultrasound prostate biopsy can be painful [14, 15]. Patient perception of this procedure is a major source of anxiety and a deterrent for undergoing biopsy. Nijs demonstrated 18% of patients in a population-based screening program refused biopsy due to anticipated pain [16]. Nash first conducted randomized, double-blind studies evaluating the effect of infiltration of 1% lidocaine in the vascular pedicles of 64 patients undergoing PNB [17]. The mean pain scores on the side injected with drug were significantly lower than the control side. Numerous investigators have demonstrated decreased pain with various pre-procedural periprostatic local anesthetic strategies (including a meta-analysis of 14 studies examining 994 procedures) [17–20]. Conversely, a small number of studies have shown no benefit [21–23]. There have been several different periprostatic

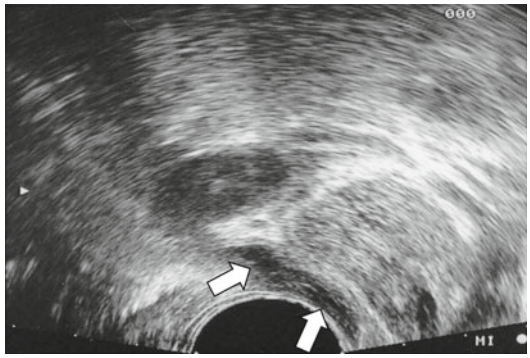

Fig. 11.2 Transrectal ultrasound image (7.5 MHz) of the prostate—sagittal view. Hypoechoic region posterior to the gland represents local anesthetic injection site (*arrows*)

injection techniques described. The most common strategy involves injection of local anesthetic between the base of the prostate and the seminal vesicles, causing a wheal between the corresponding seminal vesicle and the prostate gland from the rectal wall [24–26]. Other authors have described injecting the prostatic plexus in the area of the apex of the prostate, [18, 27] A majority of studies advocate bilateral injections [19, 24–26]. The administered anesthetic described varies from 1 to 2% lidocaine [17, 18, 22, 25] with a meta-analysis showing cumulative anesthetic dose varying from 2.5 to 20 mL [20] (Fig. 11.2).

Transrectal Biopsy Technique

Patients are typically placed in the left lateral decubitus position. Digital rectal exam is performed, and any palpable lesions are noted with respect to their location on the gland. Usually a 7.5 MHz probe is used. The probe is activated and placed using the ultrasound image to guide the probe gently beyond the anal sphincter and adjacent to the prostate. It is recommended to perform this slowly and carefully to minimize patient discomfort. TRUS should be performed in the sagittal and the transverse planes using gray-scale ultrasound. The gland is then inspected using color and power Doppler in both planes for the presence of lesions demonstrating increased flow with respect to other PZ areas of the gland. Abnormalities are recorded by image-saving mechanisms (either paper hard copy or electronic). Localization of all lesions is performed in real time with image documentation. Following instillation of local anesthesia, prostate volume calculations should be carried out. These volumes can be calculated through a variety of formulas that assume the prostate to be that of a geometric shape. These formulas estimate weight as well as volume, as 1 cm^3 equals 1 g of prostatic tissue [28]. The specific gravity of prostate tissue is approximately 1.02 g/cm^3.

Formulas for estimated weight and volume of the prostate gland:

a. Ellipse: ($\pi/6 \times$ transverse diameter $\times$ AP diameter $\times$ longitudinal diameter)
b. Sphere: ($\pi/6 \times$ transverse diameter^3)
c. Prolate (egg shaped): ($\pi/6 \times$ transverse diameter2 $\times$ AP diameter)

Volume measurements of the TZ and bladder volume may be carried out and recorded depending on the preference of the physician. The integrity of the surrounding structures should be evaluated which include examination of the bladder wall, seminal vesicles, and anal canal up to the level of the prostate.

PSA Density

Calculating prostate volume allows the use of PSA density (PSAD) defined as the ratio of serum PSA-to-prostate volume. PSAD is thought to improve cancer detection (sensitivity) and reduce the number of unnecessary prostate needle biopsies (PNB) (specificity). Djavan and colleagues demonstrated that PSAD and TZ PSAD were significantly higher in subjects diagnosed with prostate cancer on initial and repeat biopsies [29]. The authors routinely calculate PSAD and record it in real time; however, their data do not support basing the decision to perform prostate biopsy solely on this parameter.

Prostatic and Paraprostatic Cysts

As the prostate is examined focal cystic areas can often be noted. These cysts can vary in size and, when associated with BPH, are due to cystic dilatation of TZ glands. Other common cysts include acquired prostatic retention cysts which represent

dilatation of glandular acini. Acquired prostatic retention cysts may occur in any zone and are not associated with BPH. Other cysts are less common but have important associations or implications. Utricular and Mullerian duct cysts are congenital midline or paramedian cysts. Utricular cysts are intraprostatic in nature. Arising from a dilated utricle originating at the verumontanum, these communicate with the urethra and can be associated with cryptorchidism and hypospadias [30]. Mullerian duct cysts are located retrovesically and originate from Mullerian remnants. They have no communication with the urethra and can be associated with calculi and renal agenesis [31]. Ejaculatory cysts, arising from an obstructed ejaculatory duct, can be located in a midline or paramedian position. These can be associated with seminal vesicle obstruction and may contain calculi. Seminal vesicle cysts are found lateral to the prostate and are secondary to congenital hypoplasia of the ejaculatory duct [32]. Unilateral in nature, they may contain calculi and are associated with renal agenesis and epididymitis. Prostatic abscesses can be associated with surgery, prostatitis, or epididymitis [33].

Hypoechoic Lesions

The gland should be examined for hypoechoic lesions. The classic appearance of prostate cancer is a round/oval hypoechoic lesion located in the PZ. Contemporary series have noted that the presence of these lesions is a less sensitive sign for prostate cancer than once thought, with hypoechoic lesions being malignant at a rate of 17–57% [34]. However, a continued valuable asset of TRUS is directed biopsy of these lesions. Absence of hypoechoic lesions is not a contraindication to biopsy as 39% and 1% of prostate cancer are isoechoic and hyperechoic, respectively [35]. TRUS has a known poor specificity in regard to the presence of a hypoechoic lesion. Entities which also have a hypoechoic appearance on TRUS include granulomatous prostatitis [36], prostatic infarction, [37] lymphoma, [38] and TZ BPH [39] (Fig. 11.3).

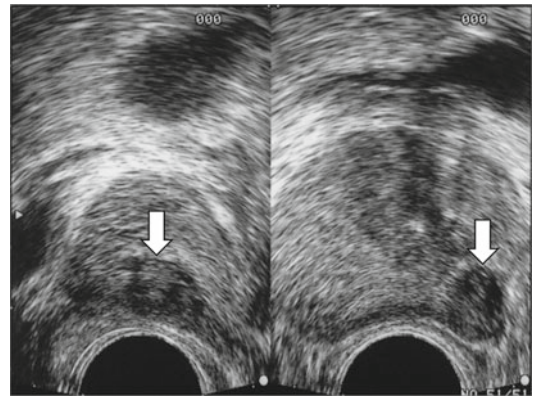

Fig. 11.3 Transrectal ultrasound image (7.5 MHz) of the prostate—transverse view (*left*) and sagittal view (*right*). Hypoechoic lesion in the peripheral zone posterolaterally represents an area of increased suspicion for malignancy (*arrows*)

Color Doppler

Color Doppler (CD) is a tool that attempts to allow TRUS to differentiate benign from malignant tissue. CD measures the frequency shift in sound waves as a measurement of the velocity of blood flow. This capitalizes on the hypervascular appearance of prostate cancer due to increased microvessel density secondary to increased angiogenesis versus benign tissue [40]. Cornud et al. [41] noted that in patients with clinical T1c disease, high-risk pathologic features (ECE, pT3b) were present more often in tumors visualized with CD versus those with the absence of a positive CD signal. Another study demonstrated a 2.6 times increased detection of prostate cancer versus conventional gray-scale ultrasound. [34] Halpern and Strup [42] demonstrated CD sensitivity and specificity to diagnose prostate cancer at 27.3 and 83.9%, respectively. This is an improvement in specificity with respect to gray-scale imaging (sensitivity 44.4%, specificity 70.5%). However, 45% of cancers still went undetected by any ultrasound modality. Arger [43] has suggested that pathologic groups based on Gleason scores, high (8–10), intermediate (5–7), and low (2–4), were not separable by vascular measurement. While several studies [41]

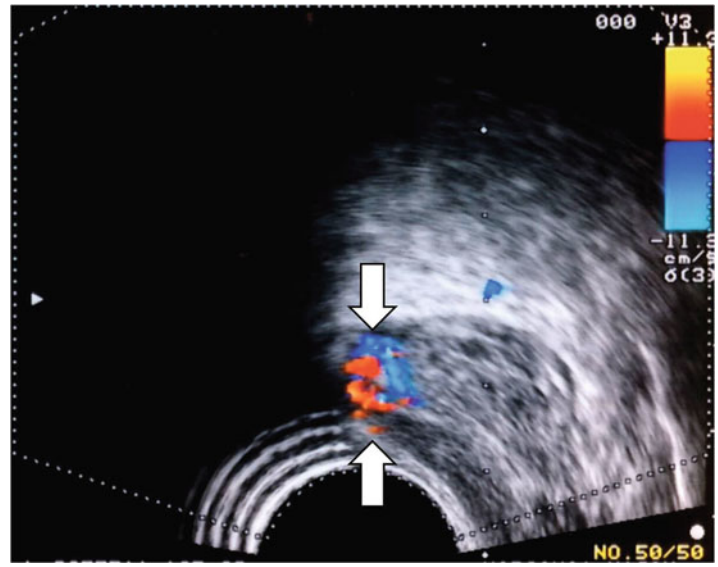

Fig. 11.4 Transrectal ultrasound image, color Doppler, of the prostate—sagittal view. Colored area (*arrows*) in the posterior lateral aspect of the gland represents an area of increased vascular flow relative to the surrounding parenchyma

[44] [45] have demonstrated increased cancer detection using CD-targeted focal biopsy strategies, there remain enough questions to preclude replacement of a systemic biopsy approach [46] (Fig. 11.4).

Biopsy Strategies

The advent of the sextant biopsy technique, that is, systematic biopsy of the apex, mid, and base of the prostate on each side of the gland, represented an improvement in prostate cancer detection over site-specific biopsies of hypoechoic lesions or palpable abnormalities [5]. With this limited template, there is still concern for a high false-negative rate, with Levine et al. [47] demonstrating in a repeat biopsy series a false-negative rate of 30% of men with an abnormal digital rectal examination (DRE) and/or elevated serum PSA. Refinements have focused on the importance of increased number of cores, as well as including laterally directed biopsies. Many groups have reported series (Table 11.1) in which improved cancer detection rates are achieved by including additional laterally directed cores and/or increasing the cores taken from 6 to as many as 13. [47–51]

Investigators [52, 53] have demonstrated a lack of usefulness for TZ and SV sampling on initial biopsy with only 2.1 and 3.7%, respectively, of biopsies being positive. The spatial distribution of cancer foci of prostate cancers with negative initial biopsies or with a gland volume larger than 50 cc may vary compared to that of prostate carcinomas diagnosed on initial biopsy. In these cases special emphasis on the apico-dorsal peripheral and transitional zones should be considered [54, 55]. Biopsy of the SV is not recommended unless a palpable abnormality is appreciated.

It is generally recommended that 10–12 biopsies of the gland be obtained with attention to the anterior horns. Technique is important in obtaining laterally directed biopsies. It should be recalled that the tru-cut needle travels between 17 mm and 24 mm depending on the manufacturer's standard. The user must appropriately guide the angle of the biopsy to maximize its position laterally on the gland, particularly when the anterior horns are approached (Fig. 11.5).

Repeat Biopsy

For the patient who has had a previous negative biopsy but has a persistent PSA elevation or abnormal DRE, an additional biopsy may be considered. During repeat biopsy the standard extended-core biopsy protocol should be carried out. Additionally any sites of ultrasound abnormality and any sites of high-grade prostatic

Table 11.1 Prostate cancer detection rates with extended-core biopsy

Study	Number of cores/biopsy	Prostate cancer detection %
Eskew [48]	6	26.1
	13	40.3
Babian [49]	6	20
	11	30
Presti [51]	6	33.5
	8	39.7
	10	40.2
Naughton [50]	6	26
	12	27

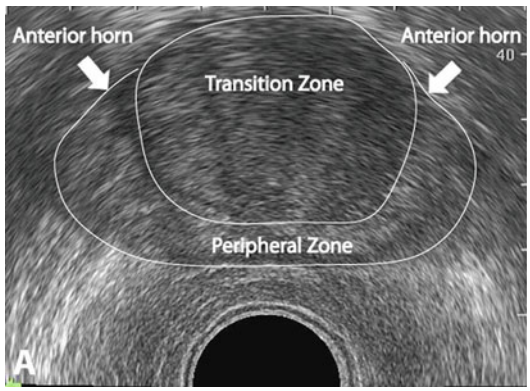

Fig. 11.5 Transrectal ultrasound image (7.5 MHz) of the prostate—transverse view. White arrow depicts the anterior horns of the prostate

intraepithelial neoplasia (HGPIN) or ASAP should be sampled [56]. The aforementioned strategy of apico-dorsal peripheral and TZ biopsies should be included. It is well established that as successive biopsies are obtained, a decreased rate of prostate cancer detection will be observed with each additional biopsy [57]. A large series of over 1,100 men undergoing biopsy as directed by PSA screening found an initial prostate cancer detection rate of 34% [58]. This declined to 19, 8, and 7% on biopsies 2–4, respectively. This was echoed by Djavan in the European Prostate Cancer Detection Study [59]. 1,051 men with a PSA value of 4–10 ng/mL had a detection rate of 22% on primary biopsy. This declined to 10, 5, and 4% on subsequent biopsies 2, 3, and 4. The use of free and total PSA, along with prostate cancer antigen-3 (PCA3), may allow risk stratification of patients for additional prostate biopsy. Catalona et al. [60] proposed the use of the percentage of free PSA to reduce unnecessary biopsies in patients with PSA values between 4.0 and 10.0 ng/mL and a palpably benign gland. In this study Catalona suggested that patients with a free PSA of less than 25% were significantly more likely to have a positive biopsy. PCA3 encodes a prostate-specific messenger ribonucleic acid (mRNA) that serves as the target for a novel urinary molecular assay for prostate cancer detection [61]. It has also shown promise as an aid in prostate cancer diagnosis in identifying men with a high probability of a positive (repeat) biopsy. Urine is collected after DRE, and PCA3 mRNA concentration is measured. Haese et al. [62] compared PCA3 to percent-free PSA and biopsy results in 463 men undergoing repeat biopsy. The overall positive repeat biopsy was 28%. The probability of a positive repeat biopsy increased with rising PCA3 scores. The PCA3 score (cut point of 35) was superior to percent-free PSA (cut point of 25%) for predicting repeat prostate biopsy outcomes.

Saturation Biopsy

Saturation biopsy has a role in maximizing prostate cancer detection rates in select patients at high risk for prostate cancer in the setting of a negative biopsy. Protocols have been described using both transrectal and transperineal approaches [63]. Various series have shown detection rates of 30–34% [64–67]. A drawback to this procedure is the need for the biopsies to be performed under sedation in a hospital setting. However, there are

circumstances that warrant more extensive gland sampling. These include (1) a persistent rise in serum PSA and (2) new DRE abnormalities and low volume cancers for which a surveillance approach is being considered. The standard transrectal approach has a theoretical limitation due to its limited ability to obtain anterior prostatic tissue particularly at the apex. The technique described below focuses on the transperineal approach with glandular mapping.

Transrectal Ultrasound-Guided Transperineal Prostate Biopsy Using the Brachytherapy Template

Indications for transrectal ultrasound-guided/transperineal prostate biopsy (TRUS/TPB) include men with further worrisome serum PSA changes or DRE abnormalities after one or more negative standard biopsies or those considering active surveillance for prostate cancer. The TRUS/TPB includes stereotactic TPB using a standard brachytherapy template and the ultrasound device together with a brachytherapy stepper device [68].

Patients are appropriately counseled on the risks and benefits of the procedure, and surgical consent is obtained. Similar pre-biopsy precautions are taken as per those outlined for the transrectal technique.

Under general anesthesia, patients are placed in the lithotomy position. Intravenous antibiotics are administered. A DRE is again performed and any lesions noted. As in the case of transrectal biopsies the prostate is scanned in gray scale and color Doppler, and any abnormalities are recorded. The transrectal probe is placed in a brachytherapy stepper device and synchronized with the ultrasound device. Prostate volumes are again obtained and recorded. The prostate is divided into 12 sections: 4 quadrants at the base, mid-gland and apex, respectively. Tissue cores are harvested using a biopsy gun beginning at the apical quadrants. Twenty-four core samples are targeted in both the sagittal and axial views. Specimens are placed in individual jars and reported accordingly. Patients are discharged with oral antibiotics and analgesics.

TRUS Biopsy After Definitive Treatment and Hormonal Ablative Therapy

External beam radiotherapy (EBRT) decreases the size of the prostate gland. Small areas of cancer which have moderate or severe radiation effects tend to appear isoechoic while large (greater than 4 mm) foci of cancer usually show little radiation effect, and these foci typically appear hypoechoic [69]. In situations that are worrisome for biochemical relapse and where the urologist and patient are seeking proof of local relapse, prostate needle biopsy is usually performed as described in the transrectal ultrasound-guided manner.

With the exception of the presence of well-distributed foreign bodies, long-term changes after brachytherapy resemble EBRT [70]. Biopsies of the gland are obtained in the same fashion as described above.

Whittington [70] described the effect of LHRH analogs on prostate tissue. The median decrease in prostate volume as a result of androgen deprivation was 33%. The reduction in volume was greatest in men with the largest initial gland volume (59%) and least in men with the smallest glands (10%). It is rare that further biopsies will be required after hormonal ablation; however, if biopsies are required, it is very important to notify the pathologist as to the presence of hormonal ablation given the histologic changes that usually occur in these situations.

After radical prostatectomy, the presence of lesions (hyper or hypoechoic) interrupting the tapering of the bladder to the urethra, representing the anastomotic plane, is considered worrisome for recurrence [71]. One notable exception is nodules anterior to the anastomosis which may be the ligated dorsal venous complex [72]. Biopsies of the bladder neck—urethral anastomosis are possible. The target for biopsy is usually small, and care is required to accurately map the anatomy prior to biopsy. The typical area of concern is between the bladder neck and the external sphincter. The urologist is reminded to exhibit extreme caution around the sphincter.

Complications

Transrectal ultrasound-guided needle biopsy is safe for diagnosing prostate cancer. Complications do arise after a prostate needle biopsy with few major but frequent minor self-limiting complications (Table 11.2).

Vagal response, secondary to pain/anxiety, occurs in 1.4–5.3% of patients. [67] Vagal response is generally responsive to hydration and placing the patient in the Trendelenburg position. Hematuria is quite common immediately following biopsy (71%), with 47% of patients having limited hematuria resolving over 3–7 days [73]. Hematospermia is observed in 9–36% of biopsies and may persist for several months [7, 72]. Rectal bleeding is observed in 2–8% of biopsies [7, 73]. Frequently, the bleeding is mild and can be controlled with digital pressure. In severe cases where bleeding is not controlled with conservative approaches, bleeding may be managed with rectal packing [74], using a tampon or gauze, or can be addressed with endoscopic injection of vasoconstrictive agents or ligation of bleeding vessels during colonoscopy [75]. Acute urinary retention requiring catheter drainage occurs up to 0.4% of the time [75]. Men with enlarged prostates or with severe baseline lower urinary tract symptoms are at an increased risk [73, 76]. In the pre-prophylaxis era, Thompson [76] demonstrated a bacteremia rate of 100% with a bacteriuria rate of 87%. This decreased to 44% and 16%, respectively, with enema alone [77]. Crawford et al. [6] administered 48 h of carbenicillin and noted bacteriuria to decrease from 36 to 9% versus the control group. The treatment group's incidence of fever was 17% compared to a rate of 48% in the control group. Antibiotic prophylaxis is now standard of care. Berger demonstrated fever (>38.5 °C) in 0.8% of 4,303 patients receiving a 5-day course of ciprofloxacin [7]. Similarly, a study administering 1–3 days of ciprofloxacin noted a fever incidence of 0.6% [78]. Seeding of prostate cancer in the needle tract is rare but is reported in the literature. It is seen more commonly in the form of perineal recurrences after transperineal biopsy [79, 80] but has been reported after TRUS biopsy [81]. Perineal recurrence has a poor prognosis [80], while rectal seeding has been shown to be responsive to hormonal therapy as well as EBRT [82]. Hara demonstrated increased circulating PSA mRNA in men following positive biopsy; [83] however, the risk of developing metastatic disease is thought to be low [56].

Table 11.2 Complication Rates in TRUS biopsies.

Complication	Incidence
Vagal response secondary to pain/anxiety	1.4–5.3% [67]
Hematuria	71%
	47% resolved over 3–7 days [73]
Hematospermia	9–36% [7, 72]
Rectal bleeding	2–8% [7, 73]
Acute urinary retention	0.4% [75]
Bacteremia (with enema)	44% [77]
Bacteriuria (with enema)	16% [77]

Pathologic Findings

HGPIN and ASAP

High-grade intraepithelial neoplasia (HGPIN) is detected on needle biopsy in 1–25% of patients [84]. HGPIN was thought to be a precursor lesion for adenocarcinoma, and historically, its presence prompted rebiopsy at 3–6 months in the absence of prostate cancer in the biopsy specimen [85–87]. Lefkowitz et al. noted that with extended 12-core biopsy technique, the repeat biopsy cancer detection rate was 2.3% and recommended repeat biopsy was not indicated for HGPIN in the absence of any other findings [88]. Atypical small acinar proliferation (ASAP) demonstrates proliferation of gland without atypia [89, 90] and has an incidence of 5% of men undergoing biopsy. The association of ASAP with prostate cancer is stronger than with HGPIN, [91, 92] with the cancer detection rates on subsequent biopsies ranging from 51 to 75%. [93, 94]

Predicting Outcomes Following Local Treatment

The pathologic elements obtained during needle biopsy including the number of cores positive, the percent involvement of each core, and the location of positive cores may contribute important prognostic information. Clinical understaging by TRUS needle biopsy occurs [95] but is reduced in the era of extended-core strategies [96]. Studies have demonstrated the number of cores positive and/or the percent of cores positive, to have a correlation to prostate cancer extracapsular extension (ECE), surgical margin status, tumor volume and stage, seminal vesicle involvement, and the presence of lymph node metastasis [97–100]. Length of tumor tissue involved in each core can be measured. Longer tumor lengths, or higher percentage of core positivity, have been strongly associated with the presence of ECE, SV involvement, and biochemical recurrence following treatment [101–104]. Biopsy site-specific percent cores positivity is predictive of sextant site of extension [105], which can aid in identification of appropriate candidates for nerve-sparing surgery.

Summary

Transrectal biopsy technique using prophylactic antibiotics, local analgesia, and an extended-core technique is safe and allows detection of prostate cancer while providing important prognostic information.

Appendix: List of Medications to be Avoided Prior to Biopsy

Aminosalicylic acid (*Paser*)	*Topical medication (cream, gel, ointment, etc.)*
Aspirin (***numerous***, *e.g.*, *Bayer*, *Bufferin*, *Ecotrin*, *Fiorinal*, *Aspergum*, *Alka-Seltzer*, *Percodan*, *Anacin*, *Goody's*, *Zorprin*)	**Diclofenac** (*Flector*, *Solaraze*, *Voltaren*)
Celecoxib (*Celebrex*)	**Trolamine** (*e.g.*, *Aspercreme*, *Mobisyl*, *Myoflex*)
Choline magnesium trisalicylate	**Methyl salicylate** (*e.g.*, *Salonpas*, *Icy Hot*)
Clopidogrel (*Plavix*)	*Ophthalmic medication*
Cilostazol (*Pletal*)	**Bromfenac** (*Xibrom*)
Diclofenac (*Cataflam*, *Voltaren*, *Arthrotec*)	**Diclofenac** (*Voltaren*)
Diflunisal	**Flurbiprofen** (*Ocufen*)
Dipyridamole (*Aggrenox*, *Persantine*)	**Ketorolac** (*Acular*)
Etodolac (*Lodine*)	**Nepafenac** (*Nevanac*)
Fenoprofen	*Injectable medication*
Flurbiprofen	**Enoxaparin** (*Lovenox*)
Ibuprofen (*e.g.*, *Advil*, *Midol*, *Motrin*)	**Dalteparin** (*Fragmin*)
Indomethacin (*Indocin*)	**Fondaparinux** (*Arixtra*)
Ketoprofen (*Orudis*)	**Heparin** (*HepFlush*, *Hep-Lock*)
Ketorolac (*Toradol*)	**Tinzaparin** (*Innohep*)
Magnesium salicylate (*e.g.*, *Doan's*, *Momentum*)	**Ketorolac** (*Toradol*)
Meclofenamate	*Herbals/natural products***
Mefenamic acid (*Ponstel*)	**Aloe**
Meloxicam (*Mobic*)	**Bilberry**
Nabumetone (*Relafen*)	**Cayenne**
Naproxen (*e.g.*, *Aleve*, *Naprosyn*, *Pamprin*, *Treximet*)	**Dong quai**
Oxaprozin (*Daypro*)	**Feverfew**
Piroxicam (*Feldene*)	**Fish oil**
Salicylamide (*e.g.*, *BC Fast Pain Relief*, *Lobac*)	**Flaxseed oil**

(continued)

(continued)

Salsalate	**Garlic**
Sulindac (*Clinoril*)	**Ginger**
Ticlopidine (*Ticlid*)	**Ginkgo biloba**
Tolmetin	**Ginseng**
Warfarin (*Coumadin*, *Jantoven*)	**Glucosamine**, **chondroitin**
-Many OTC headache, allergy, and cough and cold products also contain aspirin, ibuprofen, or naproxen	**Golden seal**
-Tylenol is okay. Take as instructed	**Supplement oils**
	Vitamin E
	**Includes pills, liquids, teas, etc.

Prior to surgery it is important to review *all medications* you are taking with your physician as some products may increase your risk of bleeding. These include prescription, over-the-counter (OTC), and herbal products. Please notify your physician if you are taking any of the following medications. *Medications are listed by their generic name, with some common brand names in parenthesis.
Always consult your healthcare provider if you are unsure if you are taking a medication that may increase your bleeding risk.

References

1. Ferguson R. Prostatic neoplasms; their diagnosis by needle puncture and aspiration. Am J Surg. 1930;9:507.
2. Astraldi A. Diagnosis of cancer of the prostate; biopsy by rectal route. Urol Cutaneous Rev. 1937;41:421.
3. Wild J, Reid J. Fourth annual conference in ultrasound therapy. Philadelphia, 1955.
4. Wantanabe H, Kato H, Kato T. Diagnostic application of ultrasonotomography to the prostate. Nippon Hinyokika Gakkai Zasshi. 1968;59:273.
5. Hodge KK, McNeal JE, Terris MK, et al. Random systematic versus directed ultrasound guided transrectal core biopsies of the prostate. J Urol. 1989;142:71.
6. Crawford ED, Haynes Jr AL, Story MW, et al. Prevention of urinary tract infection and sepsis following transrectal prostatic biopsy. J Urol. 1982;127:449.
7. Berger AP, Gozzi C, Steiner H, et al. Complication rate of transrectal ultrasound guided prostate biopsy: a comparison among 3 protocols with 6, 10 and 15 cores. J Urol. 2004;171:1478.
8. Cannon Jr GM, Smaldone MC, Paterson DL. Extended-spectrum beta-lactamase gram-negative sepsis following prostate biopsy: implications for use of fluoroquinolone prophylaxis. Can J Urol. 2007;14:3653.
9. Ozden E, Bostanci Y, Yakupoglu KY, et al. Incidence of acute prostatitis caused by extended-spectrum beta-lactamase-producing Escherichia coli after transrectal prostate biopsy. Urology. 2009;74(1):119–23.
10. Dajani AS, Taubert KA, Wilson W, et al. Prevention of bacterial endocarditis: recommendations by the American Heart Association. Clin Infect Dis. 1997;25:1448.
11. Nishimura RA, Carabello BA, Faxon DP, et al. ACC/AHA 2008 guideline update on valvular heart disease: focused update on infective endocarditis: a report of the American College of Cardiology/American Heart Association Task Force on Practice Guidelines: endorsed by the Society of Cardiovascular Anesthesiologists, Society for Cardiovascular Angiography and Interventions, and Society of Thoracic Surgeons. Circulation. 2008;118:887.
12. Bratzler DW, Houck PM. Antimicrobial prophylaxis for surgery: an advisory statement from the National Surgical Infection Prevention Project. Clin Infect Dis. 2004;38:1706.
13. Lindert KA, Kabalin JN, Terris MK. Bacteremia and bacteriuria after transrectal ultrasound guided prostate biopsy. J Urol. 2000;164:76.
14. De Sio M, D'Armiento M, Di Lorenzo G, et al. The need to reduce patient discomfort during transrectal ultrasonography-guided prostate biopsy: what do we know? BJU Int. 2005;96:977.
15. Soloway MS. Do unto others–why I would want anesthesia for my prostate biopsy. Urology. 2003;62:973.
16. Nijs HG, Essink-Bot ML, DeKoning HJ, et al. Why do men refuse or attend population-based screening for prostate cancer? J Public Health Med. 2000;22:312.
17. Nash PA, Bruce JE, Indudhara R, et al. Transrectal ultrasound guided prostatic nerve blockade eases systematic needle biopsy of the prostate. J Urol. 1996;155:607.
18. Schostak M, Christoph F, Muller M, et al. Optimizing local anesthesia during 10-core biopsy of the prostate. Urology. 2002;60:253.
19. Trucchi A, De Nunzio C, Mariani S, et al. Local anesthesia reduces pain associated with transrectal

prostatic biopsy. A prospective randomized study. Urol Int. 2005;74:209.
20. Hergan L, Kashefi C, Parsons JK. Local anesthetic reduces pain associated with transrectal ultrasound-guided prostate biopsy: a meta-analysis. Urology. 2007;69:520.
21. Bozlu M, Atici S, Ulusoy E, et al. Periprostatic lidocaine infiltration and/or synthetic opioid (meperidine or tramadol) administration have no analgesic benefit during prostate biopsy. A prospective randomized double-blind placebo-controlled study comparing different methods. Urol Int. 2004;72:308.
22. Vanni AP, Schaal CH, Costa RP, et al. Is the periprostatic anesthetic blockade advantageous in ultrasound-guided prostate biopsy? Int Braz J Urol. 2004;30:114.
23. Walsh K, O'Brien T, Salemmi A, et al. A randomised trial of periprostatic local anaesthetic for transrectal biopsy. Prostate Cancer Prostatic Dis. 2003;6:242.
24. Adamakis I, Mitropoulos D, Haritopoulos K, et al. Pain during transrectal ultrasonography guided prostate biopsy: a randomized prospective trial comparing periprostatic infiltration with lidocaine with the intrarectal instillation of lidocaine-prilocaine cream. World J Urol. 2004;22:281.
25. Obek C, Ozkan B, Tunc B, et al. Comparison of 3 different methods of anesthesia before transrectal prostate biopsy: a prospective randomized trial. J Urol. 2004;172:502.
26. Rabets JC, Jones JS, Patel AR, et al. Bupivacaine provides rapid, effective periprostatic anesthesia for transrectal prostate biopsy. BJU Int. 2004;93:1216.
27. Nambirajan T, Woolsey S, Mahendra V, et al. Efficacy and safety peri-prostatic local anesthetic injection in trans-rectal biopsy of the prostrate: a prospective randomized study. Surgeon. 2004;2:221.
28. Terris MK, Stamey TA. Determination of prostate volume by transrectal ultrasound. J Urol. 1991;145:984.
29. Djavan B, Zlotta A, Remzi M, et al. Optimal predictors of prostate cancer on repeat prostate biopsy: a prospective study of 1,051 men. J Urol. 2000;163:1144.
30. Zagoria RJ. Genitourinary Radiology. In: Thrall JH, editor. The Requisites. 2nd ed. Philadelphia, PA: Mosby; 2004. p. 335–8.
31. Gregg DC, Sty JR. Sonographic diagnosis of enlarged prostatic utricle. J Ultrasound Med. 1989;8:51.
32. McDermott V, Orr JD, Wild SR. Duplicated Mullerian duct remnants associated with unilateral renal agenesis. Abdom Imaging. 1993;18:193.
33. King BF, Hattery RR, Lieber MM, et al. Congenital cystic disease of the seminal vesicle. Radiology. 1991;178:207.
34. Frauscher F, Klauser A, Volgger H, et al. Comparison of contrast enhanced color Doppler targeted biopsy with conventional systematic biopsy: impact on prostate cancer detection. J Urol. 2002;167:1648.
35. Shinohara K, Scardino PT, Carter SS, et al. Pathologic basis of the sonographic appearance of the normal and malignant prostate. Urol Clin North Am. 1989;16:675.
36. Terris MK, Macy M, Freiha FS. Transrectal ultrasound appearance of prostatic granulomas secondary to bacillus Calmette-Guerin instillation. J Urol. 1997;158:126.
37. Purohit RS, Shinohara K, Meng MV, et al. Imaging clinically localized prostate cancer. Urol Clin North Am. 2003;30:279.
38. Varghese SL, Grossfeld GD. The prostatic gland: malignancies other than adenocarcinomas. Radiol Clin North Am. 2000;38:179.
39. Ramey JR, Halpern EJ, Gomella LG. Ultrasonography and biopsy of the prostate. In: Wein AJ, editor. Campbell-Walsh urology, vol. 3. 9th ed. Philadelphia, PA: Saunders; 2007. p. 2883–95.
40. Bigler SA, Deering RE, Brawer MK. Comparison of microscopic vascularity in benign and malignant prostate tissue. Hum Pathol. 1993;24:220.
41. Cornud F, Hamida K, Flam T, et al. Endorectal color Doppler sonography and endorectal MR imaging features of nonpalpable prostate cancer: correlation with radical prostatectomy findings. AJR Am J Roentgenol. 2000;175:1161.
42. Halpern EJ, Strup SE. Using gray-scale and color and power Doppler sonography to detect prostatic cancer. AJR Am J Roentgenol. 2000;174:623.
43. Arger PH, Malkowicz SB, VanArsdalen KN, et al. Color and power Doppler sonography in the diagnosis of prostate cancer: comparison between vascular density and total vascularity. J Ultrasound Med. 2004;23:623.
44. Okihara K, Kojima M, Nakanouchi T, et al. Transrectal power Doppler imaging in the detection of prostate cancer. BJU Int. 2000;85:1053.
45. Kelly IM, Lees WR, Rickards D. Prostate cancer and the role of color Doppler US. Radiology. 1993;189:153.
46. Halpern EJ, Frauscher F, Strup SE, et al. Prostate: high-frequency Doppler US imaging for cancer detection. Radiology. 2002;225:71.
47. Levine MA, Ittman M, Melamed J, et al. Two consecutive sets of transrectal ultrasound guided sextant biopsies of the prostate for the detection of prostate cancer. J Urol. 1998;159:471.
48. Eskew LA, Bare RL, McCullough DL. Systematic 5 region prostate biopsy is superior to sextant method for diagnosing carcinoma of the prostate. J Urol. 1997;157:199.
49. Babaian RJ, Toi A, Kamoi K, et al. A comparative analysis of sextant and an extended 11-core multisite directed biopsy strategy. J Urol. 2000;163:152.
50. Naughton CK, Miller DC, Mager DE, et al. A prospective randomized trial comparing 6 versus 12 prostate biopsy cores: impact on cancer detection. J Urol. 2000;164:388.
51. Presti Jr JC, Chang JJ, Bhargava V, et al. The optimal systematic prostate biopsy scheme should include 8

rather than 6 biopsies: results of a prospective clinical trial. J Urol. 2000;163:163.
52. Terris MK, Pham TQ, Issa MM, et al. Routine transition zone and seminal vesicle biopsies in all patients undergoing transrectal ultrasound guided prostate biopsies are not indicated. J Urol. 1997;157:204.
53. Epstein JI, Walsh PC, Sauvageot J, et al. Use of repeat sextant and transition zone biopsies for assessing extent of prostate cancer. J Urol. 1997;158:1886.
54. Mazal PR, Haitel A, Windischberger C, et al. Spatial distribution of prostate cancers undetected on initial needle biopsies. Eur Urol. 2001;39:662.
55. Chang JJ, Shinohara K, Hovey RM, et al. Prospective evaluation of systematic sextant transition zone biopsies in large prostates for cancer detection. Urology. 1998;52:89.
56. Katsuto Shinohara VM, Chi T, Carroll P. Prostate Needle Biopsy Techniques and Interpretation. In: Voegelzang S, Shipley D, Linehan, editors. Genitourinary Oncology. 3rd ed. Philadelphia, PA: Lippincott; 2006. p. 111–9.
57. Djavan B, Remzi M, Marberger M. When to biopsy and when to stop biopsying. Urol Clin North Am. 2003;30:253.
58. Keetch DW, Catalona WJ, Smith DS. Serial prostatic biopsies in men with persistently elevated serum prostate specific antigen values. J Urol. 1994;151:1571.
59. Djavan B, Ravery V, Zlotta A, et al. Prospective evaluation of prostate cancer detected on biopsies 1, 2, 3 and 4: when should we stop? J Urol. 2001;166:1679.
60. Catalona WJ, Partin AW, Slawin KM, et al. Use of the percentage of free prostate-specific antigen to enhance differentiation of prostate cancer from benign prostatic disease: a prospective multicenter clinical trial. JAMA. 1998;279:1542.
61. Wang R, Chinnaiyan AM, Dunn RL, et al. Rational approach to implementation of prostate cancer antigen 3 into clinical care. Cancer. 2009;115(17):3879–86.
62. Haese A, de la Taille A, van Poppel H, et al. Clinical utility of the PCA3 urine assay in European men scheduled for repeat biopsy. Eur Urol. 2008;54:1081.
63. Bott SR, Henderson A, McLarty E, et al. A brachytherapy template approach to standardize saturation prostatic biopsy. BJU Int. 2004;93:629.
64. Lane BR, Zippe CD, Abouassaly R, et al. Saturation technique does not decrease cancer detection during follow up after initial prostate biopsy. J Urol. 2008;179:1746.
65. Borboroglu PG, Comer SW, Riffenburgh RH, et al. Extensive repeat transrectal ultrasound guided prostate biopsy in patients with previous benign sextant biopsies. J Urol. 2000;163:158.
66. Stewart CS, Leibovich BC, Weaver AL, et al. Prostate cancer diagnosis using a saturation needle biopsy technique after previous negative sextant biopsies. J Urol. 2001;166:86.
67. Fleshner N, Klotz L. Role of "saturation biopsy" in the detection of prostate cancer among difficult diagnostic cases. Urology. 2002;60:93.
68. Moran, et al. Re-biopsy of the Prostate With Stereotactic Transperineal Technique. J Urol. 2006;176:1376–81.
69. Egawa S, Wheeler TM, Scardino PT. The sonographic appearance of irradiated prostate cancer. Br J Urol. 1991;68:172.
70. Whittington R, Broderick GA, Arger P, et al. The effect of androgen deprivation on the early changes in prostate volume following transperineal ultrasound guided interstitial therapy for localized carcinoma of the prostate. Int J Radiat Oncol Biol Phys. 1999;44:1107.
71. Kapoor DA, Wasserman NF, Zhang G, et al. Value of transrectal ultrasound in identifying local disease after radical prostatectomy. Urology. 1993;41:594.
72. Goldenberg SL, Carter M, Dashefsky S, et al. Sonographic characteristics of the urethrovesical anastomosis in the early post-radical prostatectomy patient. J Urol. 1992;147:1307.
73. Rodriguez LV, Terris MK. Risks and complications of transrectal ultrasound guided prostate needle biopsy: a prospective study and review of the literature. J Urol. 1998;160:2115.
74. Maatman TJ, Bigham D, Stirling B. Simplified management of post-prostate biopsy rectal bleeding. Urology. 2002;60:508.
75. Brullet E, Guevara MC, Campo R, et al. Massive rectal bleeding following transrectal ultrasound-guided prostate biopsy. Endoscopy. 2000;32:792.
76. Raaijmakers R, Kirkels WJ, Roobol MJ, et al. Complication rates and risk factors of 5802 transrectal ultrasound-guided sextant biopsies of the prostate within a population-based screening program. Urology. 2002;60:826.
77. Thompson PM, Pryor JP, Williams JP, et al. The problem of infection after prostatic biopsy: the case for the transperineal approach. Br J Urol. 1982;54:736.
78. Desmond PM, Clark J, Thompson IM, et al. Morbidity with contemporary prostate biopsy. J Urol. 1993;150:1425.
79. Moul JW, Bauer JJ, Srivastava S, et al. Perineal seeding of prostate cancer as the only evidence of clinical recurrence 14 years after needle biopsy and radical prostatectomy: molecular correlation. Urology. 1998;51:158.
80. Moul JW, Miles BJ, Skoog SJ, et al. Risk factors for perineal seeding of prostate cancer after needle biopsy. J Urol. 1989;142:86.
81. Bastacky SS, Walsh PC, Epstein JI. Needle biopsy associated tumor tracking of adenocarcinoma of the prostate. J Urol. 1991;145:1003.
82. Koppie TM, Grady BP, Shinohara K. Rectal wall recurrence of prostatic adenocarcinoma. J Urol. 2002;168:2120.
83. Hara N, Kasahara T, Kawasaki T, et al. Frequency of PSA-mRNA-bearing cells in the peripheral blood of patients after prostate biopsy. Br J Cancer. 2001;85:557.
84. Meng MV, Shinohara K, Grossfeld GD. Significance of high-grade prostatic intraepithelial neoplasia on prostate biopsy. Urol Oncol. 2003;21:145.

85. Oyasu R, Bahnson RR, Nowels K, et al. Cytological atypia in the prostate gland: frequency, distribution and possible relevance to carcinoma. J Urol. 1986;135:959.
86. Prange W, Erbersdobler A, Hammerer P, et al. Significance of high-grade prostatic intraepithelial neoplasia in needle biopsy specimens. Urology. 2001;57:486.
87. Davidson D, Bostwick DG, Qian J, et al. Prostatic intraepithelial neoplasia is a risk factor for adenocarcinoma: predictive accuracy in needle biopsies. J Urol. 1995;154:1295.
88. Lefkowitz GK, Sidhu GS, Torre P, et al. Is repeat prostate biopsy for high-grade prostatic intraepithelial neoplasia necessary after routine 12-core sampling? Urology. 2001;58:999.
89. Helpap BG, Bostwick DG, Montironi R. The significance of atypical adenomatous hyperplasia and prostatic intraepithelial neoplasia for the development of prostate carcinoma. An update. Virchows Arch. 1995;426:425.
90. Helpap B, Bonkhoff H, Cockett A, et al. Relationship between atypical adenomatous hyperplasia (AAH), prostatic intraepithelial neoplasia (PIN) and prostatic adenocarcinoma. Pathologica. 1997;89:288.
91. Iczkowski KA, Chen HM, Yang XJ, et al. Prostate cancer diagnosed after initial biopsy with atypical small acinar proliferation suspicious for malignancy is similar to cancer found on initial biopsy. Urology. 2002;60:851.
92. Iczkowski KA, MacLennan GT, Bostwick DG. Atypical small acinar proliferation suspicious for malignancy in prostate needle biopsies: clinical significance in 33 cases. Am J Surg Pathol. 1997; 21:1489.
93. Alsikafi NF, Brendler CB, Gerber GS, et al. High-grade prostatic intraepithelial neoplasia with adjacent atypia is associated with a higher incidence of cancer on subsequent needle biopsy than high-grade prostatic intraepithelial neoplasia alone. Urology. 2001;57:296.
94. Park S, Shinohara K, Grossfeld GD, et al. Prostate cancer detection in men with prior high grade prostatic intraepithelial neoplasia or atypical prostate biopsy. J Urol. 2001;165:1409.
95. Javidan J, Wood DP. Clinical interpretation of the prostate biopsy. Urol Oncol. 2003;21:141.
96. Makhlouf AA, Krupski TL, Kunkle D, et al. The effect of sampling more cores on the predictive accuracy of pathological grade and tumour distribution in the prostate biopsy. BJU Int. 2004;93:271.
97. Wills ML, Sauvageot J, Partin AW, et al. Ability of sextant biopsies to predict radical prostatectomy stage. Urology. 1998;51:759.
98. Ravery V, Boccon-Gibod LA, Dauge-Geffroy MC, et al. Systematic biopsies accurately predict extracapsular extension of prostate cancer and persistent/recurrent detectable PSA after radical prostatectomy. Urology. 1994;44:371.
99. Badalament RA, Miller MC, Peller PA, et al. An algorithm for predicting nonorgan confined prostate cancer using the results obtained from sextant core biopsies with prostate specific antigen level. J Urol. 1996;156:1375.
100. D'Amico AV, Whittington R, Malkowicz SB, et al. Clinical utility of percent-positive prostate biopsies in predicting biochemical outcome after radical prostatectomy or external-beam radiation therapy for patients with clinically localized prostate cancer. Mol Urol. 2000;4:171.
101. Naya Y, Slaton JW, Troncoso P, et al. Tumor length and location of cancer on biopsy predict for side specific extraprostatic cancer extension. J Urol. 2004;171:1093.
102. Freedland SJ, Aronson WJ, Terris MK, et al. Percent of prostate needle biopsy cores with cancer is significant independent predictor of prostate specific antigen recurrence following radical prostatectomy: results from SEARCH database. J Urol. 2003; 169:2136.
103. Freedland SJ, Csathy GS, Dorey F, et al. Percent prostate needle biopsy tissue with cancer is more predictive of biochemical failure or adverse pathology after radical prostatectomy than prostate specific antigen or Gleason score. J Urol. 2002;167:516.
104. Freedland SJ, Csathy GS, Dorey F, et al. Clinical utility of percent prostate needle biopsy tissue with cancer cutpoints to risk stratify patients before radical prostatectomy. Urology. 2002;60:84.
105. Elliott SP, Shinohara K, Logan SL, et al. Sextant prostate biopsies predict side and sextant site of extracapsular extension of prostate cancer. J Urol. 2002;168:105.

Pediatric Urologic Ultrasound

12

Lane S. Palmer

Introduction

Ultrasound maintains its position as the primary imaging study of the genitourinary tract in children despite technological advances in computerized tomography (CT) and magnetic resonance imaging (MR). Some of the attributes of ultrasound that help to maintain this position include its ease and rapidity to perform, noninvasive nature, reproducibility, and its avoidance of ionizing radiation. These are all important, particularly in the small child whose behavior may preclude a second chance to properly image the abnormality. The commonplace performance of prenatal ultrasound leads to the need for postnatal sonographic confirmation of possible urologic pathology. The other commonly ordered studies, voiding cystourethrography (VCUG), diuretic renography, CT, and MR are ordered mainly based upon the results of the ultrasound.

Ultrasound Performance in Children

Definitions and scope: The kidney is just one component to be evaluated in sonogram of the retroperitoneum in children or in adults; the other components include adrenals, ureters (when visible), and any masses. Similarly, the bladder is one component of a pelvic ultrasound which also includes the surrounding organs such as the rectum, ovaries, and uterus. The scrotal ultrasound examination includes images of the testis, the epididymis, and the spermatic cord.

The definitions of the complete and limited examinations are the same regardless of the age of the patient. The complete ultrasound of the retroperitoneum consists of a B-mode scan of the kidneys, abdominal aorta, common iliac artery origins, and inferior vena cava, including any abnormalities. The components of the complete ultrasound examination of the pelvis are gender-specific and include uterus and adnexal structures, endometrium in girls, prostate and seminal in boys, and the bladder and any pelvic pathology in both sexes. In contrast, the limited examination assesses one or more elements but not all of the components of the complete examination or the reevaluation of one or more previously demonstrated abnormalities. An examination performed simply to determine a post-void volume is not considered an imaging study and is often performed with automated equipment for that specific purpose.

Indications: **Ultrasound is the most common imaging study performed of the pediatric urinary tract**. There are several indications for performing renal and bladder sonograms in children that can be further divided into investigative, screening, and surveillance indications

L.S. Palmer, MD (✉)
Hofstra North Shore-LIJ School of Medicine,
Cohen Children's Medical Center of New York,
1999 Marcus Avenue, M18, Lake Success, NY 11050, USA
e-mail: lpalmermd@gmail.com

P.F. Fulgham and B.R. Gilbert (eds.), *Practical Urological Ultrasound*, Current Clinical Urology,
DOI 10.1007/978-1-59745-351-6_12,

Table 12.1 Indications for ultrasound in children

Renal and bladder
• Urinary tract infection—febrile or recurrent nonfebrile
• Prenatal GU abnormality
• Voiding dysfunction
• Renal colic
• Palpable abdominal mass
• Single umbilical artery
• Hypertension
• Hematuria
• Proteinuria
• Azotemia
• Family history polycystic kidney disease
• Hemihypertrophy
• Urinary retention
• Syndrome associated with renal involvement (e.g., tuberous sclerosis, CHARGE, VACTERL, WAGR, etc.)
• Surveillance of
– Vesicoureteral reflux
– Nephrolithiasis
– Hydronephrosis
– Cystic renal disease
– Neurogenic bladder dysfunction (e.g., myelodysplasia)
– Obstructive uropathy (e.g., posterior urethral valves)
Scrotal
• Palpable intrascrotal mass
• Scrotal pain
• Scrotal swelling
• Varicocele
• Testicular asymmetry

(Table 12.1). Most commonly, ultrasound is the first imaging study of the child with a febrile UTI [1] or one with an abnormality noted on prenatal sonogram or in the boy with scrotal pain.

Technique

Kidneys: The kidneys are imaged in both longitudinal and transverse planes with the child primarily in the supine position. If the child is able to follow commands, **the kidneys are best imaged with the child making a deep inspiration pushing the kidney caudally below the ribs**. If the child cannot follow commands, the images might be better obtained with a bolster placed under the flank or with the child turned on the side and the arm raised above the head to open up the space between the ribs and the iliac crest allowing better access to the kidney. Images must be taken with the child in the prone position for better visualization of the kidney between the ribs. The right kidney is imaged along the anterior axillary line using the liver as an acoustic window while the left kidney is imaged along the posterior axillary line using the spleen as an acoustic window. Imaging is done with a curved linear-array robe. In children under age 18 months or so, a 6–12 MHz probe is used, while older children are better imaged using a 3.5–5 MHz probe.

Bladder: The bladder is imaged with the child in the supine position using a curved array probe (7.7–11 MHz for children under 18 months or 3.5–5 mHz for older children) which makes small skin contact and is easy to angle to gather the most information. The sonographer performs the study in both the transverse and longitudinal directions with the bladder at least partially filled looking for a normal bladder and surrounding organs and documenting any luminal, intraluminal, or extraluminal abnormalities. The transverse images are taken moving from the pubis to the umbilicus in 1–2 cm intervals, while the longitudinal images are taken moving from the midline in either direction in 1–2 cm intervals. Measurements are made in the transverse plane measuring the height and width of the urine within the bladder and then the length in the sagittal plane. These three measurements are multiplied together and then multiplied by 0.65 [2] to calculate the bladder volume. Efflux of urine from the ureteral orifices can be demonstrated by applying the Doppler mode over the appropriate location on the bladder floor.

Scrotum: Ultrasound imaging of the scrotum is performed with the child supine and the scrotum supported by a folded towel placed between the thighs. In older children and adolescents, the penis position is maintained suprapubically with a second towel or held in position by the patient. Scanning should be performed with 7–18 MHz high-frequency linear-array transducer. **Both testes and epididymides should be compared for size, echogenicity, masses, and vascularity and imaged in both the transverse and longitudinal axes**.

Table 12.2 Documentation of ultrasound examination

Kidneys						
Size	_____×_____		_____×_____			
Abnormal location	No	Pelvic		Horseshoe		
Hydronephrosis	No	Grade	1	2	3	4
Malrotated	No	Yes				
Duplication	No	Yes				
Proximal ureteral dilation	No	Yes				
Cortical thinning	No	Yes				
Abnormal cortical echotexture		No	Yes			
Cortical cyst	No	Size_____mm		UP_____	MP____	LP___
Stones	No	Size_____mm		UP_____	MP____	LP___
Mass	No	Yes				
Bladder						
Pre-void volume_____cc	Post-void volume			_____cc		
Thickened bladder	No	Yes				
Distal ureteral dilation		No	Yes			
Bladder mass	No	Yes				
Pelvic mass	No	Yes				
Bladder stones	No	Yes				
Scrotal						
Right	Left					
Testis size:_____x_____x_____						
Testis mass	No	Yes	_____mm	Location_____		
Microcalcifications	No	Yes				
Varicocele	No	Yes	_____mm			
Epididymal cyst	No	Yes	_____mm			
Hernia	No	Yes				
Hydrocele	No	Yes				

Spectral Doppler analysis of the intratesticular vasculature of both testes is performed when indicated. In patients presenting with acute scrotum, the asymptomatic side should be scanned first so that gray scale and color Doppler gain settings are set optimally and to obtain a baseline for comparison with the affected side. In the presence of a suspected varicocele, having the child perform the Valsalva maneuver or placing the child in the upright position can improve the evaluation of venous distention.

Documentation: The documentation of the ultrasound examination should be as complete and systematic as the examination itself. Mention should be made of normal and abnormal findings. All measurements that were taken should be documented. An example of some components of documentation of the kidneys, bladder, and scrotum is shown in Table 12.2.

Kidney

Normal Anatomy

The proper evaluation of kidney assesses the location, orientation, axis, size, echogenicity of the parenchyma and the integrity of its contour, the nature of the central echogenic focus, and the absence of a visible proximal ureter (Fig. 12.1).

Normal kidneys lie in the retroperitoneum along the psoas, orientated parallel to it; both are oblique such that the upper pole of the kidney is posterior to the lower pole. The size of the kidney is age-dependent and is determined by measuring the distance between the two poles and compared to published nomograms [3]. From a sonographic perspective, the most important neighbor is the anterior relationship to the liver on the right side

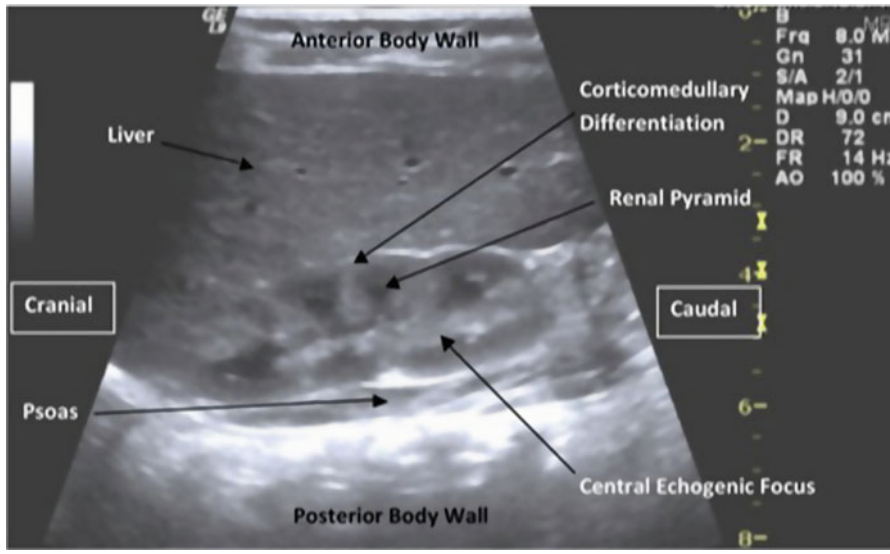

Fig. 12.1 Sagittal view of a normal kidney demonstrating a normal position in the flank and a normal axis, with good corticomedullary differentiation, a collapsed central echogenic focus, and hypoechoic pyramids oriented radially about the perimeter

and the spleen on the left side. During the first several months of life, the echogenicity of the renal parenchyma may be isoechoic or hyperechoic in comparison to the adjacent liver or spleen and then becomes hypoechoic in comparison.

The renal cortex can be distinguished from the medulla by the presence of a line, reflecting the subtle differences in echogenicity. The presence of this corticomedullary differentiation is an indicator of normal architecture and a marker of parenchymal integrity.

The contour of the pediatric kidney can be smooth but is often lobulated. The lobes of parenchyma consist of a central pyramid covered by cortical parenchyma and the columns of Bertin are located between these pyramids. The lobulated appearance regresses with time and the contour becomes smooth.

The renal pyramids are seen as hypoechoic areas radially distributed surrounding the central echogenic focus (CEF) that are most commonly seen in infants and also regress with time. The CEF consists of the renal pelvis, hilar vasculature and lymphatics, and sinus fat (accounting for its hyperechoic appearance). In the sagittal plane, there is ordinarily a single CEF surrounded by a symmetric thickness of parenchyma. The CEF should be collapsed upon itself unless it is distended with urine and the walls of the renal pelvis separate. The proximal ureter should ***not*** normally be visible on sonogram.

Renal Anomalies

Anomalies or abnormalities of the kidneys in children can be described developmentally as either congenital or acquired and then again anatomically by number, location, vascular, parenchymal, and collecting system.

Unilateral Renal Agenesis

Unilateral renal agenesis is most commonly detected in children during imaging performed (1) prenatally, (2) for a urinary complaint, (3) during screening for associated anomalies, or (4) incidentally during evaluation of unrelated conditions. On ultrasound, the renal fossa is empty of a reniform structure and may instead be occupied by bowel. Otherwise the surrounding organs are normal in appearance. It is important that the person performing the study then scans the pelvis to determine if the kidney is ectopic in position. In infants, **the adrenal will be prominent and in the normal**

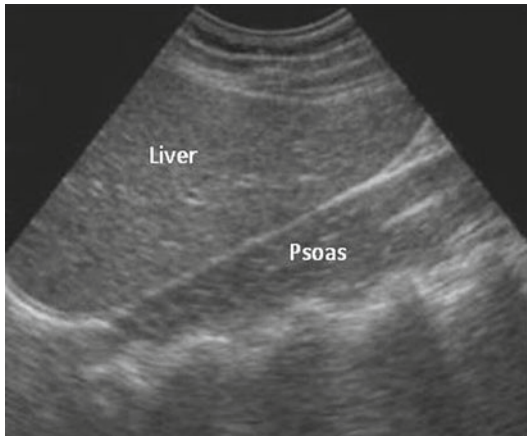

Fig. 12.2 An empty renal fossa demonstrating the psoas muscle posterior and the normal liver anterior and superior

anatomical position. The remaining kidney will be large reflecting compensatory hypertrophy. The diagnosis can be confined by nuclear scintigraphy (DMSA), MR, or CT, although Krill et al. found that measuring the polar size of the kidney on ultrasound offers sufficient accuracy in predicting a solitary kidney [4]. VCUG is indicated because of the significant incidence of vesicoureteral reflux in the remaining renal unit [5] (Fig. 12.2).

Renal Ectopia

Kidneys begin their embryologic journey in the bony pelvis with the renal pelvis oriented anteriorly and then reach the renal fossa and finish their medial rotation by the ninth week of gestation. However, this process may abort anywhere along the course of ascent. Similarly, the metanephric blastema may cross over to the contralateral side and may attach to the other metanephric blastema (crossed-fused ectopia).

A normal-appearing reniform kidney may be seen in the pelvis behind the bladder (Fig. 12.3). However, because of the associated malrotation of a pelvic or crossed (fused, non-fused) kidney, the cortex may appear variable in echogenicity and in corticomedullary differentiation. Also, or for the same reason, measurement of polar length may be artificially small.

The horseshoe kidney is the most common fusion anomaly in children (Fig. 12.4). This may be suspected when both malrotated kidneys are positioned caudal to their usual position. Horseshoe kidneys are at risk for UPJ obstruction and Wilms' tumor and these may be detected easily by ultrasound. The isthmus between the two kidneys may be thick on ultrasound; function of the isthmus can be evaluated by nuclear scintigraphy.

Renal Vein Thrombosis

Ultrasound is well-suited for evaluating the kidney with suspected renal vein thrombosis. Risk factors for renal vein thrombosis include dehydration, traumatic delivery, and sepsis. During the acute phase, during which there is considerable edema, ultrasound will demonstrate an enlarged kidney with loss of corticomedullary differentiation (Fig. 12.5). The parenchyma is hypoechoic early in the process due to edema but becomes hyperechoic as fibrosis sets in. Thrombi in smaller vessels are seen as radiating linear echogenic bands in the parenchyma. At later phases, atrophy will be seen as well as calcifications in the area of the thrombi. Venous flow is absent when Doppler is applied.

Infection and Scarring

Urinary tract infections are a leading indication for ordering renal ultrasound in children. The spectrum of the clinical presentation of UTIs is variable and often matches the ultrasound findings. In many cases, the sonogram of the kidneys and bladder is completely normal. In some cases, all is normal except for some self-limited mild hydronephrosis or hydroureter as a result of the dilating effect of bacteria-released endotoxins. When there is diffuse pyelonephritis, the kidney will be enlarged and hypoechoic (either diffusely or multifocal) with loss of corticomedullary differentiation will be seen (Fig. 12.6).

Following a pyelonephritic episode, particularly when associated with vesicoureteral reflux, the healing parenchyma may leave a scar. **The scar needs to be large to be detected on ultrasound**: **the indented contour in the area(s) of scar reflecting cortical loss**. This contraction of parenchyma may be focal or in severe cases involves the

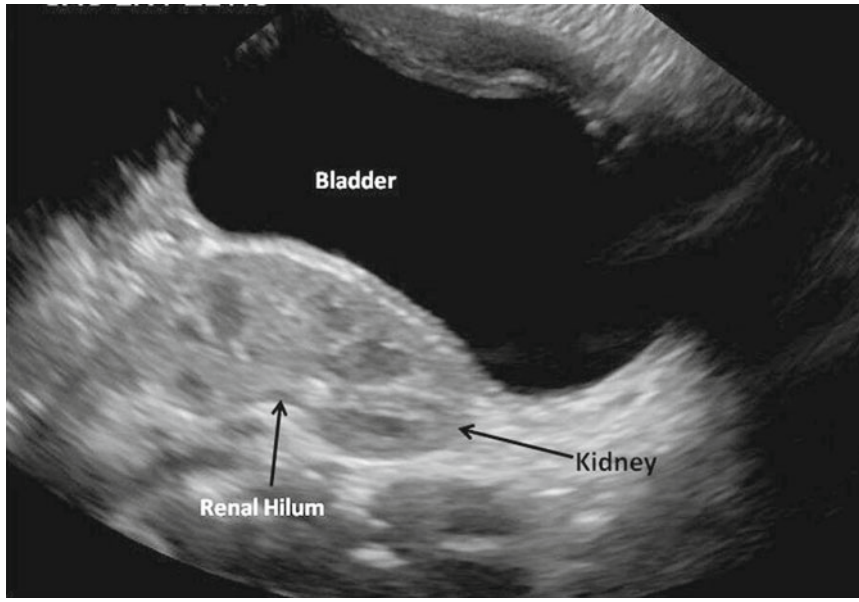

Fig. 12.3 The presence of an ectopic kidney in the pelvis situated posterior to the urinary bladder. The kidney has normal contour and echogenicity but is malrotated due to incomplete medial rotation during ascent

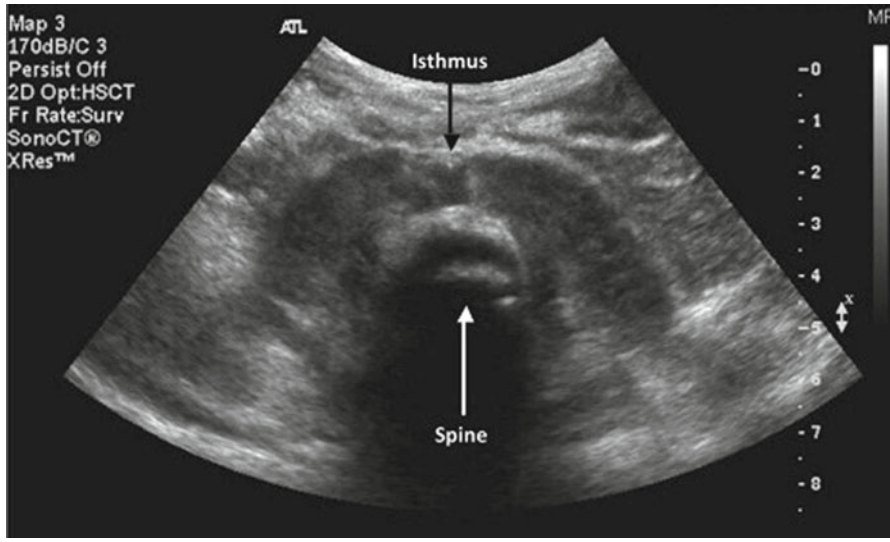

Fig. 12.4 Transverse view demonstrating the caudal location of malrotated and fused kidneys, i.e., a horseshoe kidney. The isthmus is identified in the midportion of the kidney and the spine located posteriorly

entire kidney. In such cases the size of the kidney will also contract. One needs to avoid confusing these scars with persistent fetal lobulations. Scarring typically occurs *over* calyces (the point of retrograde entry of bacteria to the parenchyma) while the contour indentations associated with fetal lobulations are *between* the calyces (reflecting the adjacent lobes of renal development) (Fig. 12.7).

Renal Cystic Diseases

There are several conditions in which renal cysts are prominent. The more important ones in children are multicystic dysplastic kidney (MCDK) and polycystic kidney disease (both autosomal recessive and autosomal dominant).

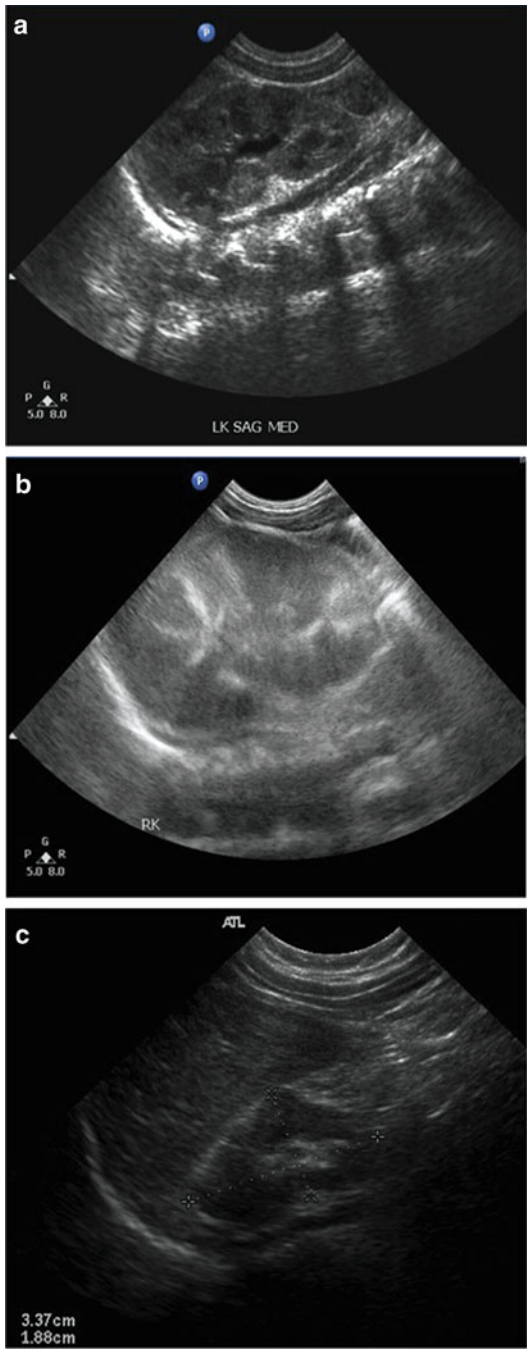

Fig. 12.5 Sequence of renal sonograms from a neonate with renal vein thrombosis. (**a**) Sagittal view of the left kidney demonstrating normal echogenicity and pyramids with grade 1 hydronephrosis. (**b**) Sagittal view of the right kidney taken at the same time as (**a**) demonstrates a larger kidney with poor corticomedullary differentiation. (**c**) 6 months later, the left kidney has become atrophic and continues to have poor corticomedullary differentiation

Multicystic dysplastic kidney: The classic ultrasound findings are those of multiple noncommunicating cysts of variable size (Fig. 12.8). The largest cysts are located in the periphery of the kidney thus helping to distinguish this from severe hydronephrosis where the larger hypoechoic areas are located centrally. However, despite this difference, it may be very difficult to distinguish between the two entities. There is a paucity of renal parenchyma in the MCDK which has minimal to no function as documented by nuclear scintigraphy. The natural history of an MCDK is involution with subsequent contraction or even disappearance of the kidney as followed by ultrasound. Associated contralateral renal abnormalities may be seen in about 40 % of the cases, and vesicoureteral reflux may be present in the stump of the MCDK or in the contralateral kidney; therefore, VCUG is indicated [6].

Polycystic Kidney Disease

The genetics of the two diseases are self-evident in their names and their clinical courses are different. The ultrasound features of autosomal recessive polycystic kidney disease (ARPCKD) type include extremely large, reniform kidneys that are homogeneous and hyperechoic. The multiple reflective interfaces of the ectatic dilated renal tubules cause the characteristic hyperechoic appearance. Autosomal-dominant polycystic kidney disease (ADPCKD) demonstrates bilateral multiple renal cysts of variable size. At the youngest ages, the cysts are fewer in number and the renal parenchyma relatively normal with respect to corticomedullary differentiation and echogenicity. However, with time, the cysts grow in size and number leading to compression of the renal parenchyma and possible distortion of the renal pelvis (Fig. 12.9).

Renal Tumors

Mesoblastic nephroma and Wilms' tumor (Fig. 12.10) are the more important solid renal masses in children. The benign mesoblastic

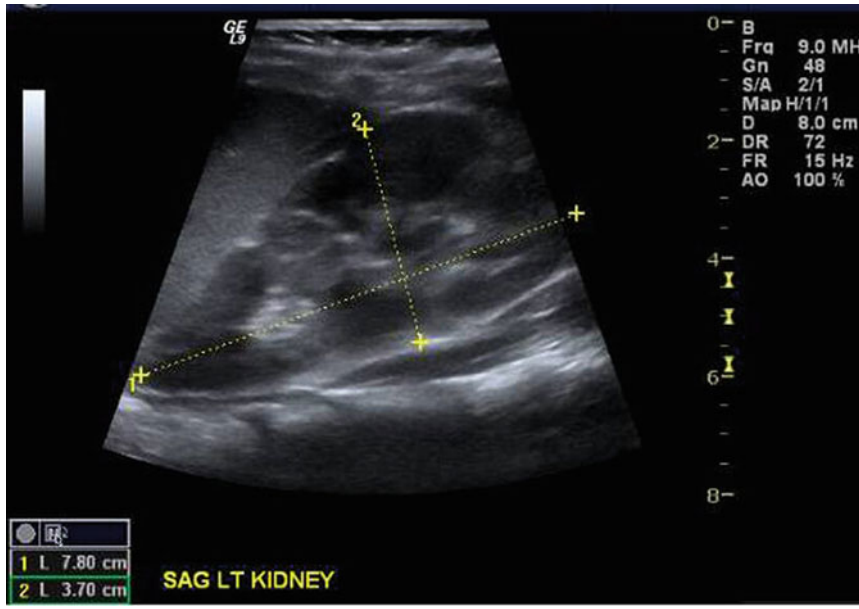

Fig. 12.6 Sagittal view of the kidney of a hospitalized, febrile (103.4°F), 3-year-old girl whose catheterized urine culture grew 100,000 *E. coli*. The kidney is enlarged (7.8 cm) and has disturbed echogenicity due to edema and inflammation

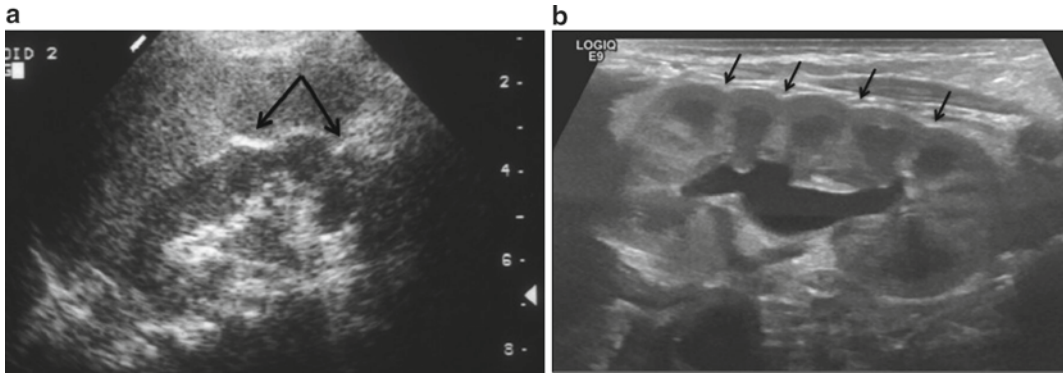

Fig. 12.7 (**a**) Sagittal view of the right kidney of a child with a history of febrile urinary tract infections. Scarring is identified in the upper pole of the kidney (*black arrows*). (**b**) Comparison sonogram demonstrating indentations of the renal contour (*black arrows*) that represent fetal lobulations positioned between the pyramids and not over the calyces

nephroma is the most common solid renal mass in children under 3 months while the malignant Wilms' tumor is the most common solid renal mass in childhood. They commonly present as abdominal or flank masses and their ultrasound features are similar. These are heterogeneous intrarenal masses of variable size that are mainly solid and hyperechoic, but areas of necrosis and hemorrhage lead to areas that are hypoechoic. Cystic variants of Wilms' tumor will demonstrate anechoic areas. Hydronephrosis may be present with either mass. The contralateral kidney may demonstrate involvement in Wilms tumor. Tumor thrombus may be present in the renal vein.

Stones

Urolithiasis is not unique to children and has the same features as in adults. Stones are detected as hyperechoic foci with posterior shadowing; the

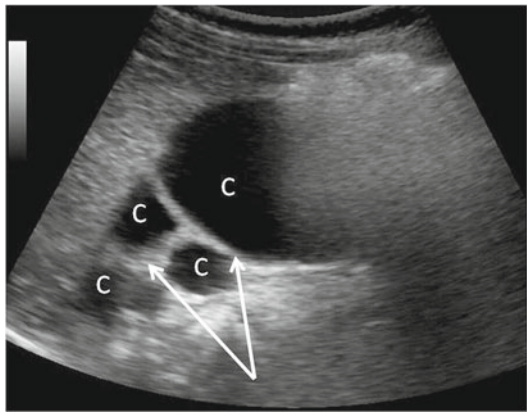

Fig. 12.8 Multicystic dysplastic kidney with multiple-sized anechoic areas of variable sizes without identifiable parenchyma in the periphery and hyperechoic parenchyma (*arrows*) between the cysts (C)

shadowing distinguishes the stone from fat or blood vessels. The axial resolution of ultrasound allows for its detection of medium-sized or large stones; sometimes an apparently single stone is actually 2 or more smaller stones in close proximity. Hydronephrosis proximal to the stone can be seen.

Hydronephrosis

Dilation of the renal pelvis goes by a variety of monikers: pyelectasis, pelviectasis, pelvis dilation, and hydronephrosis. Regardless of the name, **renal pelvic dilation is the most common ultrasound abnormality of the kidney seen prenatally or postnatally** [7]. Prenatally dilation of the renal pelvis is measured in millimeters in the anteroposterior dimension; the risk of a significant uropathy increases with the age of gestation [8] or size of the pelvis [9]. Postnatally, hydronephrosis is divided into grades using systems such as that outlined by the Society for Fetal Urology (Fig. 12.11). By the SFU system, the lowest grade of hydronephrosis refers to slight pelvic dilation and the highest grade refers to extension of the dilatation into the calyces and the presence of renal parenchymal thinning [10].

Hydronephrosis may be primary or secondary and either obstructive or nonobstructive. VCUG and/or diuretic renography helps to define the nature of the hydronephrosis. In contrast to higher grades of hydronephrosis, milder grades (1, 2) are unlikely to be obstructive. The most common cause of obstruction is at the ureteropelvic junction either due to a congenital intrinsic narrowing or from a lower pole vessel crossing anterior to the ureter. When UPJ obstruction is suspected, the ultrasound will demonstrate a large centrally located hypoechoic area (renal pelvis) extending into and blunting the calyces (grade III). As mentioned above, if the renal parenchyma is compressed and thinned compared with the contralateral kidney, this constitutes grade IV hydronephrosis and is likely due to obstruction. In cases of intermittent obstruction, the SFU grade of hydronephrosis may be lower than expected [11]. The diagnosis of obstruction is only suspected by ultrasound but not made without the adjuvant use of other provocative studies such as furosemide nuclear scintigraphy, magnetic urography, or even retrograde pyelogram or excretory urography (Case Study 1).

Case Study 1

Child with ureteropelvic junction obstruction. (a) Preoperative sagittal view of a left renal ultrasound demonstrates SFU grade 4 hydronephrosis—extension into the calyces with parenchymal thinning (arrow). (b) The diuretic MAG 3 renogram demonstrates a right kidney with rapid uptake and drainage while the left one (*) shows persistent tracer. The drainage curve of the left kidney remains flat, even after furosemide injection while the right kidney drained before injection. (c) Intraoperative retrograde pyelogram demonstrates a dilated renal pelvis and narrowing at the ureteropelvic junction (arrow). (d) Postoperative ultrasound image of the left kidney showing resolution of the hydronephrosis and minimal residual calyceal dilation (*).

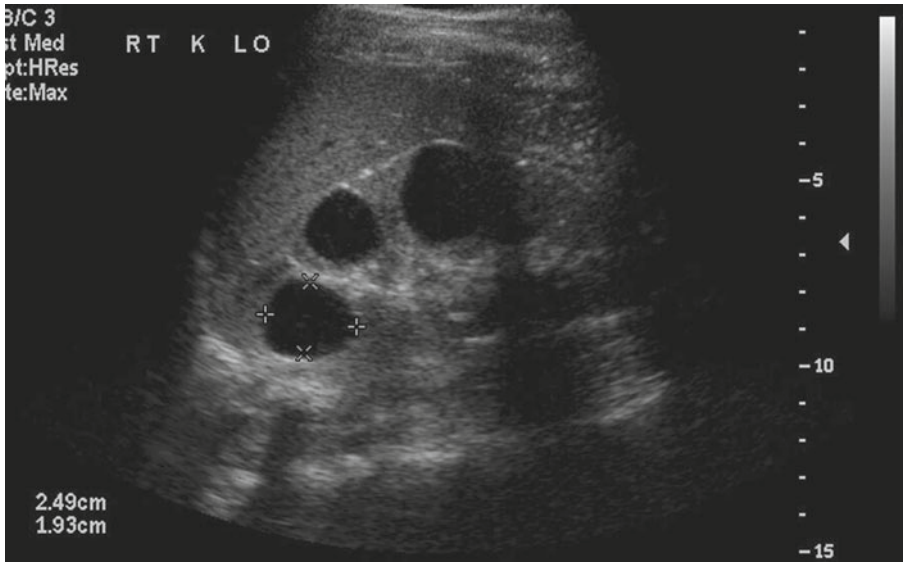

Fig. 12.9 Sagittal view of a renal ultrasound of a teenager with ADPCK demonstrating replacement of the renal parenchyma with several cysts of variable size

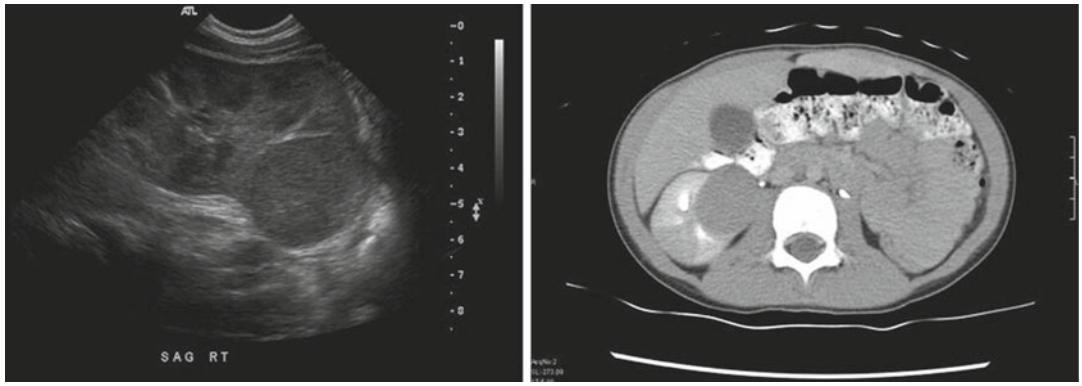

Fig. 12.10 Sonogram and corresponding CT of a 2-year-old child with a right-sided Wilms' tumor. The lower pole exophytic mass is seen as a homogeneous mass in this case. However, other cases may demonstrate a heterogeneous mass reflecting bleeding and necrosis replacing the majority of the renal parenchyma

Collecting System Duplication

The presence of a duplicated collecting system is very common [12]. Most duplication anomalies are inconsequential and are discovered incidentally on prenatal ultrasound or later when ultrasound is performed for urologic or non-urologic reasons. However, some duplication anomalies can be clinically significant such as in cases of ureterocele and ectopic ureters that are associated with the upper pole moiety and ureteropelvic junction obstruction and reflux that are associated with the lower pole moiety. These significant duplications may be detected prenatally or after their clinical presentation leads to the performance of an ultrasound.

The ultrasound must include the kidney and the bladder to best document the nature of the duplication. In the simplest case, there are two central echogenic foci separated by a bar of renal parenchyma isoechoic to the rest of the normal parenchyma, no hydronephrosis, and the proximal ureters are not identifiable (Fig. 12.12).

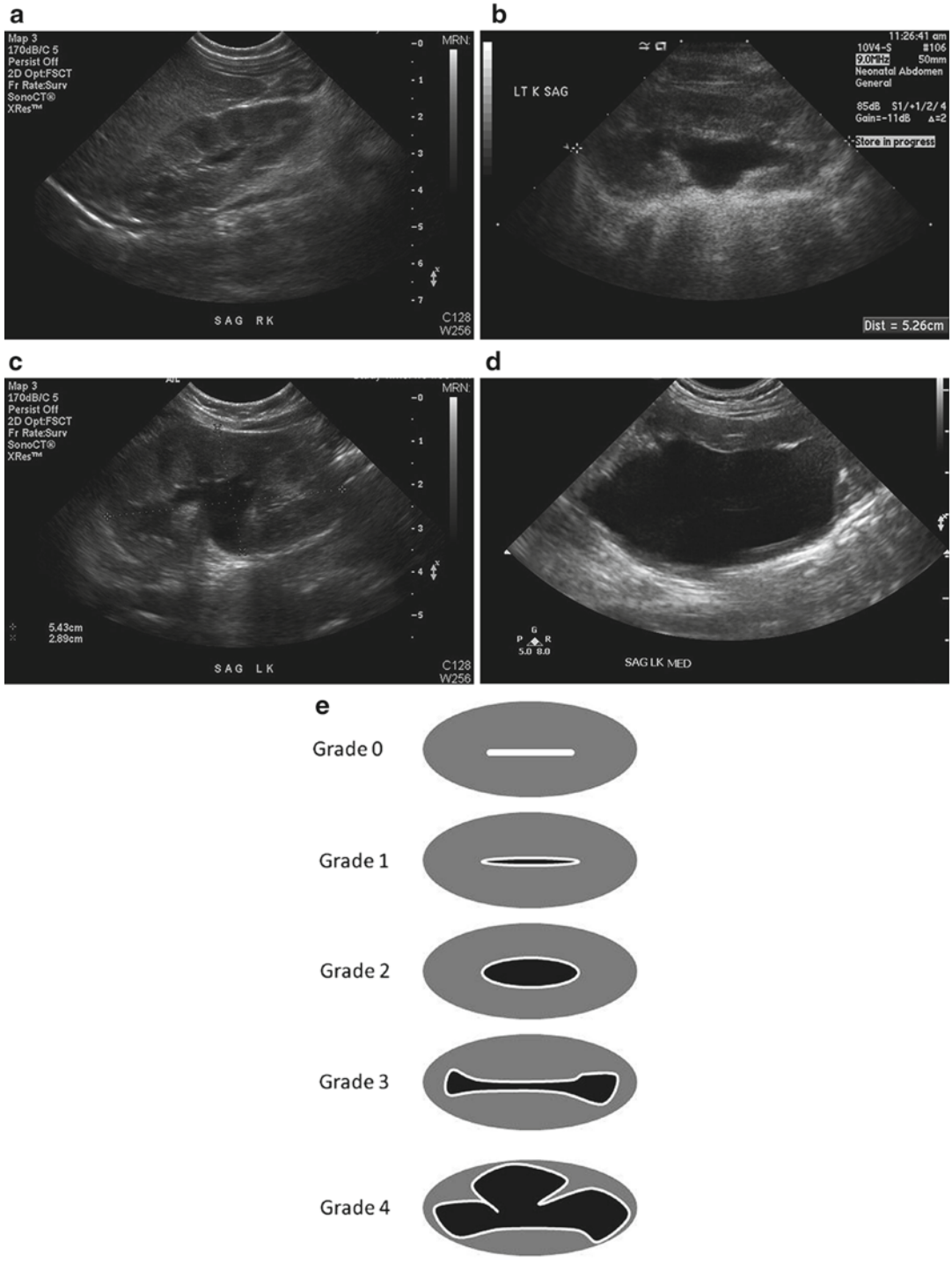

Fig. 12.11 Society for Fetal Urology grading system: (**a**) 1-mild pelvic dilation; (**b**) 2-moderate pelvic dilation; (**c**) 3-dilation extending into the calyces and normal parenchyma; (**d**) 4-calyceal dilation and thinning of the parenchyma compared to the contralateral kidney; and (**e**) a schematic representation of these grades is depicted for comparison with the images above

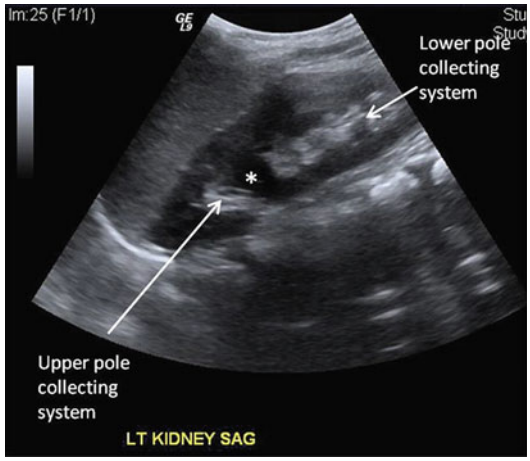

Fig. 12.12 Renal duplication. Sagittal ultrasound demonstrating two central echogenic foci separated by a bar of normal renal parenchyma (*asterisk*)

The bladder is normal in thickness and contour without any defects within it and the distal ureters are not visible. In the more complex cases, ultrasound identifies hydronephrosis in either upper or lower pole moieties, dilation and possible tortuosity of the proximal and/or distal ureters, upper pole scarring or dysplasia (shrunken hyperechoic region), or ureterocele. VCUG and diuretic renogram supplement the ultrasound in better defining the complete anomaly.

Bladder

Normal Bladder

The bladder should be smooth in contour and thin walled. In general, thickened bladders reflect bladder outlet obstruction as seen in neurogenic states or posterior urethral valves; however, bladder wall thickness is of arguable clinical value. The urine will be hypoechoic and there should be an absence of debris, masses, or significant post-void residual urine. The area inferior to the bladder contains the rectum and the presence of stool should be noted (Fig. 12.13a–c).

Ureterocele

Ureteroceles have a variable effect on the urinary tract and thus on the findings at ultrasound. **Bladder ultrasound is most effective in making the radiographic diagnosis of ureterocele** [13]: **a round thin-walled cystic structure at the bladder base perhaps with the dilated ureter leading into it**. An everting ureteroceles may be confused for bladder diverticulum [14]. Hydroureter is present when the ureterocele delays the passage of urine or is associated with reflux. The contralateral ureter may also be dilated when the ureterocele encroaches upon the contralateral orifice retarding the passage of urine, or undermines the antireflux mechanism, or causes obstruction of the bladder neck. The renal ultrasound may demonstrate a single system (males more likely) or a duplicated system (females more likely). Hydronephrosis of variable grade may be seen ipsilateral and/or contralateral to the kidney with the ureterocele (Case Study 2).

Case Study 2
This 3-month-old female was born with prenatally detected left hydronephrosis. The postnatal imaging included (a) sagittal image of the kidney that reveals a duplicated left collecting system with hydronephrosis isolated to the upper pole. (b) The bladder sonogram demonstrates a very large ureterocele (*) presumed to be from the left side (this was confirmed cystoscopically). (c) The VCUG demonstrates vesicoureteral reflux into the lower pole moiety only with displacement of the lower pole by the dilated upper pole segment. The area of the upper pole system is marked as *

Vesicoureteral Reflux

Vesicoureteral reflux is the most common anomaly detected following abnormal prenatal renal ultrasound or after a urinary tract infection. Ultrasound may demonstrate variable degree of

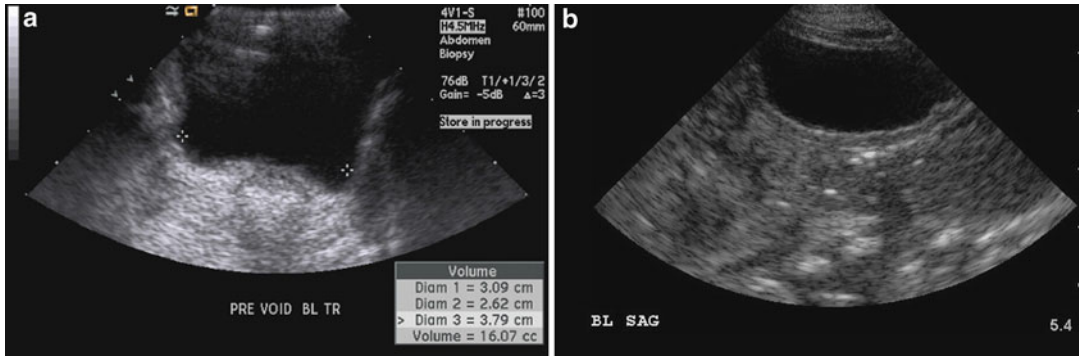

Fig. 12.13 Pre- and post-void images of a normal bladder. (**a**) demonstrates transverse and sagittal images of a thin-walled bladder without debris and intraluminal or extraluminal abnormalities. (**b**) The bladder empties its volume to completion and stool is seen in the rectal vault

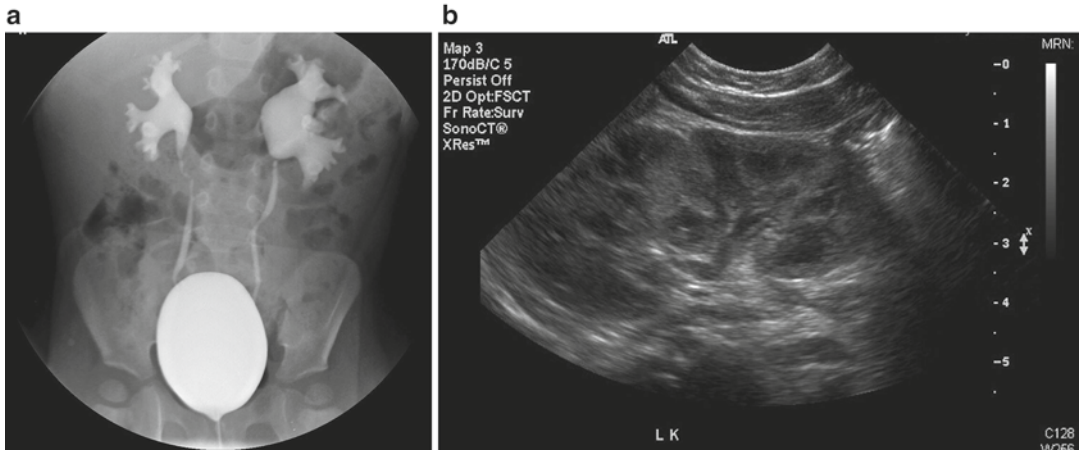

Fig. 12.14 VCUG from a young child with bilateral vesicoureteral reflux, grade 3 on the *right* and grade 4 on the *left* (**a**). The sonogram of the kidneys was completely normal as seen here of the *left side*, the side with the higher grade of reflux (**b**)

hydronephrosis or hydroureteronephrosis. However, the grade of hydronephrosis does not necessarily correlate with the grade of vesicoureteral reflux (Fig. 12.14) [15]. Notwithstanding this fact, renal ultrasound is often used to screen older siblings of probands with reflux. When reflux is associated with renal scarring, ultrasound can document advanced scarring where irregular renal contour, loss of corticomedullary differentiation, or a shrunken kidney may be seen. Scarring is best documented by areas of decreased uptake during nuclear scintigraphy (DMSA). Ultrasound may be useful as a postoperative study to document that the kidneys appear the same as the preoperative images [16].

Posterior Urethral Valves

Posterior urethral valves are not diagnosed by ultrasound, but the effect of the valves on the bladder, ureters, and kidneys can be detected and can be profound. Bladder wall thickening may be seen reflecting detrusor hypertrophy. Dilation of the ureters is variable and may be present due to the obstructive phenomena

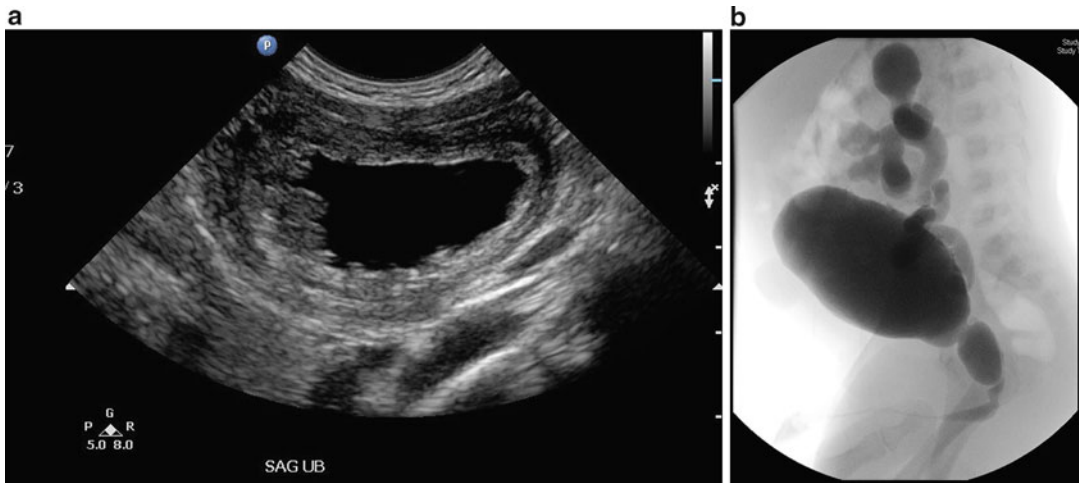

Fig. 12.15 Neonate with posterior urethral valves confirmed and treated cystoscopically. This transverse sonographic image of the bladder highlights the much thickened muscular wall (**a**). Other features included a dilated posterior urethra and bilateral hydroureteronephrosis. The VCUG shown demonstrates irregular-shaped bladder with dilated posterior urethra and sudden change in caliber at the location of the valve and high-grade vesicoureteral reflux (**b**)

and/or vesicoureteral reflux. When present, hydroureters may be seen distally as hypoechoic areas posterior to the bladder and may be traced proximally, in severe cases, to the ureteropelvic junction. At the level of the kidney, hydronephrosis of all grades may be seen. In the presence of renal damage, the parenchyma may be hyperechoic and thinned with the loss of corticomedullary differentiation, or cystic changes. When suspected on prenatal ultrasound, oligohydramnios and a dilated prostatic urethra may be present in addition to the above findings [17] (Fig. 12.15a, b).

Neurogenic Bladder

The sonographic images of urinary tract of children with neurogenic bladders are similar to those seen in posterior urethral valves. Ultrasound will often demonstrate bladder wall thickening, associated hydronephrosis, or hydroureteronephrosis due to reflux or high bladder pressures. Ultrasound studies in both conditions will provide information regarding the post-void residual and thus the bladder's ability to empty. As in posterior urethral valves, there is spectrum of effect on the urinary tract and the findings outlined above may be seen to varying degrees.

Scrotum

The details of scrotal ultrasound and varicoceles will be discussed in greater detail in Chap. 8. However, it is important to outline the findings associated with the more common scrotal pathologies in children.

Undescended Testis

Ultrasound is of limited utility for the evaluation of cryptorchidism. Since a majority of undescended testes are located in the inguinal canal, high-frequency (18 mHz) linear-array transducers are often able to identify gonads in this location. The presence or absence of a testis on sonogram should only confirm the findings at physical examination. The features of the testis would be similar to that of the normally descended testis unless

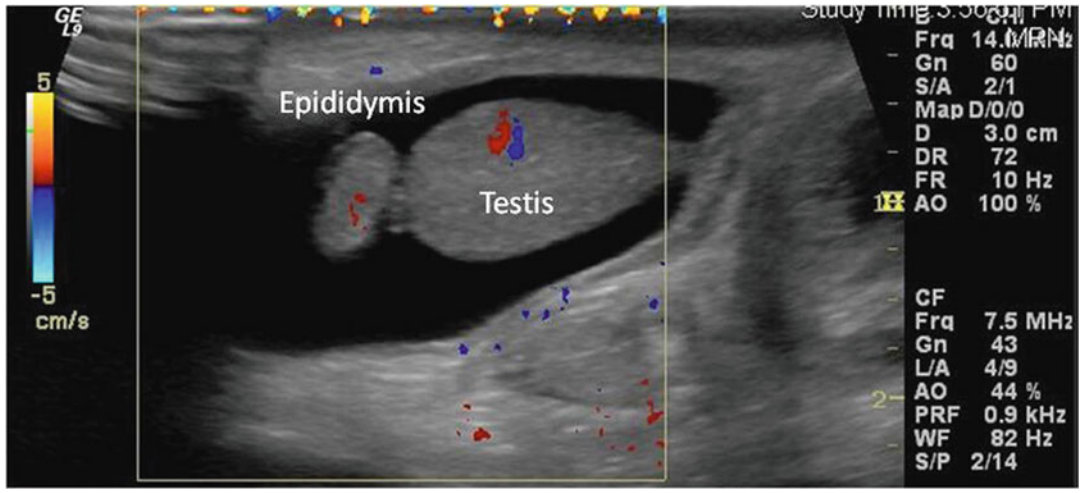

Fig. 12.16 Sagittal view of a scrotal ultrasound from a neonate with a nonpalpable right testis. The testis was identified in the scrotum with adequate blood flow documented by Doppler. The difficulty in palpating the testis stemmed from the large surrounding hydrocele (anechoic area surrounding the testis)

atrophy has occurred. In these cases, the testis size is smaller and the parenchyma is hyperechoic.

Hydrocele

Hydroceles in children are commonly communicating with the abdomen via a patent processus vaginalis; otherwise they are isolated from the abdomen and surround the testes. The diagnosis is typically one based on history and physical examination. However, ultrasound can be a useful adjunct in which there is an anechoic fluid collection located in the anterolateral position of the affected hemiscrotum (Fig. 12.16). Longstanding hydroceles may become septated and proteinaceous debris found in the hydrocele fluid. Septations appear on sonogram as hyperechoic linear or curvilinear areas separating the hypoechoic or anechoic fluid while the debris appears as scattered punctuate hyperechoic structures within the fluid. Large communications with the abdomen may be seen as the probe is moved proximally within the inguinal canal as a fluid-filled anechoic tubular structure.

Intersex

In the child with ambiguous genitalia, the goal of imaging is to identify gonads and Müllerian structures. Ultrasound may distinguish testicle from ovary in the case of a palpable gonad by its oval shape, larger size, and the presence of an epididymis. Ovaries are more echogenic and follicular cysts may be identified (Fig. 12.17). Ultrasound is less reliable than MR to assess an intra-abdominal gonad. Pelvic ultrasound may be useful in identifying a well-developed uterus; otherwise it is a difficult structure to properly identify when it is rudimentary.

Acute Testicular Pain

Ultrasound is an excellent modality to help define the nature of acute scrotal pain and swelling, i.e., distinguish between torsion of the spermatic cord or an inflammatory process (epididymo-orchitis or torsion of the appendix testis). Its rapidity and excellent sensitivity and specificity make it the

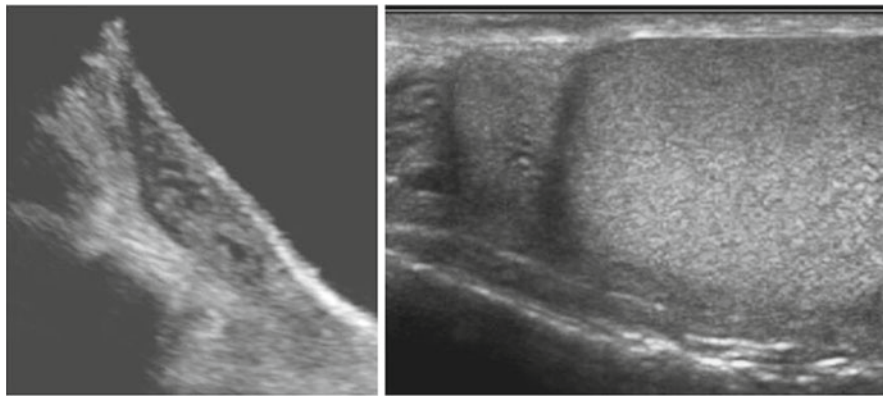

Fig. 12.17 Comparative images of an ovary (*left*) and testis (*right*). Ovaries tend to be oblong and follicles are sometimes present. The testis is oval and the presence of the epididymis helps to make the distinction

first line of imaging in many institutions [18]. The unaffected testis/epididymis should be imaged first and compared to the affected side with respect to symmetry, architecture, and perfusion.

Case Study 3

Sonographic images from two adolescent boys presenting to the Emergency Department with acute scrotal pain and swelling. (a) Longitudinal views of the testes of a 13-year-old male presenting with 4 h of acute scrotal pain and swelling of the right side. The ultrasound demonstrates similar echogenicity of the two sides. However, Doppler signal is present within the left testis while there is no signal identified within the right testis, only in the surrounding tissue; this is consistent with torsion. (b) Color flow study of the spermatic cord demonstrates point at which flow is no longer detected. (c) Longitudinal view of the testis of a 16-year-old male with 1 day of acute right-sided scrotal pain. There is significant increased Doppler signal in the testis and in the epididymis which is consistent with an inflammatory process such as epididymo-orchitis.

The sonographic findings of testicular torsion evolve with time. The study should start with the evaluation of the unaffected side. Early in the time course, the affected testis will have normal size and echogenicity. Sometimes, the point of torsion on the cord can be identified [19]. This is followed by an increase in testis and epididymal size and a decrease in echogenicity. The extent of hypoechogenicity increases with time. Reactive hydroceles and thickening of the overlying scrotal skin may be present. **The nonsalvageable testis appears heterogeneous as infarction and necrosis ensues** [20] and Doppler flow may be detected due to hyperemia of the skin and surrounding soft tissue. Ultimately, the testis will contract. While the sine qua non of testicular torsion is the unilateral absence of Doppler flow on the affected side, decreased flow may be seen in cases of partial torsion or may reflect technical limitations of documenting flow in the normal testes.

Inflammation of the epididymis and/or testis in children may be infectious in nature or secondary to trauma or torsion of an appendage. Sonographically, the epididymis (more commonly at the caput) and/or testis may be enlarged and hypoechoic. Color Doppler will demonstrate increased flow to these structures or only to the epididymis. As in cases of spermatic cord torsion, comparison to the unaffected contralateral hemiscrotum is imperative. The actual torsed appendage (Fig. 12.18) may be seen as a hypoechoic structure at the junction of the epididymis and testis [21]. Reactive hydroceles and scrotal skin thickening may be present on the sonogram.

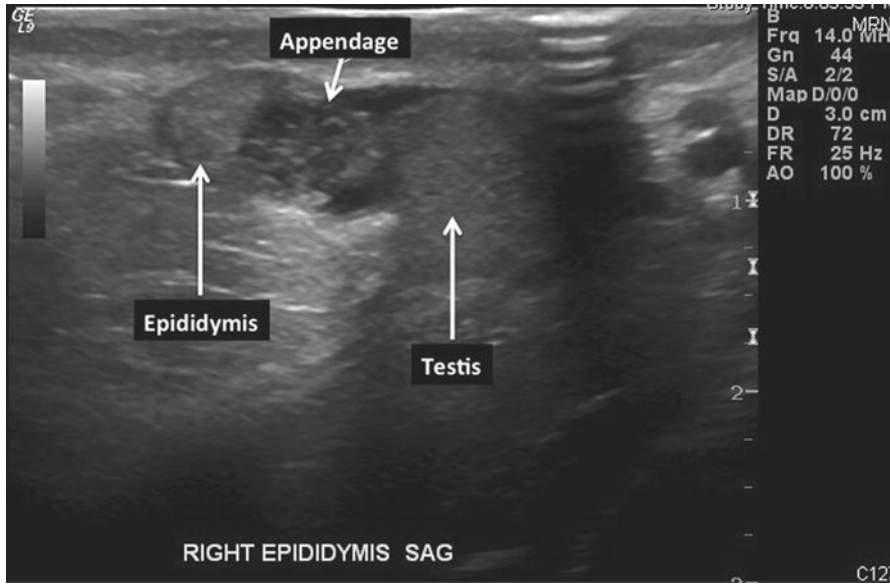

Fig. 12.18 Sagittal view of the testis in an adolescent male with acute onset of scrotal pain. A hypoechoic lesion is found superior to the testis and inferior or overlying the epididymis consistent with an appendage. Blood flow was present to tall structures except to the torsed appendage

Conclusion

Ultrasound continues to have a pivotal role in managing children with urologic conditions. The practicing urologist needs to understand the nuances in performing and interpreting these studies in children. It is imperative for urologists to know the ultrasound findings associated with the more common urologic conditions in childhood of the kidney, bladder, and scrotum.

References

1. Giorgi Jr LJ, Bratslavsky G, Kogan BA. Febrile urinary tract infections in infants: renal ultrasound remains necessary. J Urol. 2005;173(2):568–70.
2. Li-Ing B, et al. Bladder shape impact on the accuracy of ultrasonic estimation of bladder volume. Arch Phys Med Rehabil. 1998;79:1553–6.
3. Rosenbaum DM, Korngold E, Teele RL. Sonographic assessment of renal length in normal children. AJR Am J Roentgenol. 1984;142(3):467–9.
4. Krill A, Salami S, Rosen L, Friedman SC, Gitlin J, Palmer LS. Evaluating compensatory hypertrophy: a growth curve specific for solitary functioning kidneys. J Urol. 2012;188(4 Suppl):1613–7.
5. Cascio S, Paran S, Puri P. Associated urological anomalies in children with unilateral renal agenesis. J Urol. 1999;162(3 Pt 2):1081–3.
6. Damen-Elias HA, Stoutenbeek PH, Visser GH, Nikkels PG, de Jong TP. Concomitant anomalies in 100 children with unilateral multicystic kidney. Ultrasound Obstet Gynecol. 2005;25(4):384–8.
7. Mandell J, Blyth BR, Peters CA, Retik AB, Estroff JA, Benacerraf BR. Structural genitourinary defects detected in utero. Radiology. 1991;178(1):193–6.
8. Ismaili K, Hall M, Donner C, Thomas D, Vermeylen D, Avni FE. Brussels Free University Perinatal Nephrology study group. Results of systematic screening for minor degrees of fetal renal pelvis dilatation in an unselected population. Am J Obstet Gynecol. 2003;188(1):242–6.
9. Odibo AO, Raab E, Elovitz M, Merrill JD, Macones GA. Prenatal mild pyelectasis: evaluating the thresholds of renal pelvic diameter associated with normal postnatal renal function. J Ultrasound Med. 2004;23(4):513–7.
10. Fernbach SK, Maizels M, Conway JJ. Ultrasound grading of hydronephrosis: introduction to the system used by the Society for Fetal Urology. Pediatr Radiol. 1993;23(6):478–80.
11. Rooks VJ, Lebowitz RL. Extrinsic ureteropelvic junction obstruction from a crossing renal vessel: demography and imaging. Pediatr Radiol. 2001;31(2):120–4.
12. Campbell MF. Anomalies of the ureter. In: Campbell MF, Harrison JH, editors. Urology. 3rd ed. Philadelphia: WB Saunders; 1970. p. 1512.
13. Cremin BJ. A review of the ultrasonic appearances of posterior urethral valve and ureteroceles. Pediatr Radiol. 1986;16:357.

14. Zerin JM, Baker DR, Casale JA. Single-system ureteroceles in infants and children: imaging features. Pediatr Radiol. 2000;30:139–46.
15. Blane CE, DiPietro MA, Zeim JM, et al. Renal sonography is not a reliable screening examination for vesicoureteral reflux. J Urol. 1993;150:752–5.
16. Grossklaus DJ, Pope JC, Adams MC, Brock JW. Is postoperative cystography necessary after ureteral reimplantation? Urology. 2001;58(6):1041–5.
17. Dinneen MD, Dhillon HK, Ward HC, Duffy PG, Ransley PG. Antenatal diagnosis of posterior urethral valves. Br J Urol. 1993;72(3):364–9.
18. Siegel MJ. The acute scrotum. Radiol Clin North Am. 1997;35(4):959–76.
19. Baud C, Veyrac C, Couture A, et al. Spiral twist of the spermatic cord: a reliable sign of testicular torsion. Pediatr Radiol. 1998;28:950–4.
20. Kaye JD, Levitt SB, Gitlin JS, Friedman SC, Freyle J, Palmer LS. Parenchymal echotexture predicts testicular salvage after torsion - a new paradigm to determine the need for emergent exploration. J Urol. 2008;180 (4, 2 of 2):1733–1736.
21. Strauss S, Faingold R, Manor H. Torsion of the testicular appendages: sonographic appearance. J Ultrasound Med. 1997;16:189–92.

Ultrasound of the Gravid and Pelvic Kidney

13

Majid Eshghi

This chapter addresses the assessment of hydronephrosis and renal colic during pregnancy, as well as the assessment of conditions associated with congenital pelvic and transplant kidneys utilizing ultrasound imaging.

Ultrasound Evaluation During Pregnancy

The hormonal changes during pregnancy caused by estrogen, progestational, and prostaglandin-like agents are considered to be a contributing factor towards hydronephrosis and ureterectasis. Additionally, the anatomic location of the sigmoid colon on the left side provides a buffering effect on the left ureter and typically leads to less hydronephrosis. The growing size of the uterus in a limited pelvic space is considered to be the primary reason for dilation of the ureters and hydronephrosis. It is also thought that increasing gestational age and the growth of the uterus out of the pelvis contribute to a decrease in the pressure exerted on the ureters. This stabilization of the hydronephrosis results in a decrease in flank pain experienced during the late stage of pregnancy.

The pregnancy-induced hormonal and associated physiological changes result in a **decrease in renal vascular resistance**, **and an increase in cardiac output which in turn leads to increased renal plasma flow**. Along with these changes, there is also a **130 % increase in the size of the kidneys** and glomerular surface area under the influence of prolactin and its growth hormone-type effect. Another physiologic outcome is hypercalciuria, secondary to **approximately 30–50 % increased GFR**. The calcium filtration and intestinal calcium absorption are related to the high levels of placenta calcitriol. During the pregnancy, there is also an increase in inhibitors of stone formation, such as citrate, magnesium, and glycosaminoglycans. In spite of hypercalciuria and dilation of the upper tract, **gravid and nongravid patients are at equal risk for development of urolithiasis** with similar stone composition [1–5].

The hydronephrosis of pregnancy usually begins in the **second trimester and affects 90 % of pregnancies by the 26–28th weeks**. Dilatation increases up to the 30th week of gestation and remains stable for the remaining 8–10 weeks. The incidence of dilation is greatest in nulliparous patients [6, 7]. The hydronephrosis subsides within the 6 weeks after parturition, but sometimes it may persist longer. **As a rule**, **there is more dilation on the right** (**85 %**) **than the left** (**15 %**). **The ureteral dilation does not occur below the pelvic brim** [8]. It is also believed that the gravid uterus compresses the ureters at the pelvic brim. Other factors that can be contributory are dextrorotation of the uterus and ureteral **compression by the uterine and gonadal**

M. Eshghi, MD, FACS, MBA (✉)
Department of Urology, New York Medical College, Westchester Medical Center, 100 Woods Road, Munger Pavillion, Room 456, Valhalla, New York, NY 10595, USA
e-mail: Majid_Eshghi@nymc.edu

P.F. Fulgham and B.R. Gilbert (eds.), *Practical Urological Ultrasound*, Current Clinical Urology,
DOI 10.1007/978-1-59745-351-6_13,

vessels, which become quite engorged during pregnancy (ovarian vein syndrome). The elevated baseline or resting ureteral pressures recorded above the pelvic brim decrease in prone position—and ureteral contractile pressures recorded during pregnancies argue against ureteral atony caused by progesterone. It has been observed that **ureters that do not cross the pelvic brim such as those connected to pelvic kidneys or in an ileal conduit urinary diversion do not develop hydronephrosis**, nor does it occur in quadrupeds [9]. These findings also argue against the role that hormones play during the early stages of gestation. Finally, the hydronephrosis can be considered to be the result of a combination of the above factors. Increased hydration has been shown to increase the degree of hydronephrosis. There are other conditions that can simulate urolithiasis symptoms during pregnancy, namely, acute pyelonephritis, renal vein thrombosis (RVT), and renal rupture [10–13].

The indications for ultrasonography of the kidney will include bilateral or unilateral flank pain, unilateral colicky pain, and less frequently, hematuria. **Ultrasound evaluation helps in differentiating physiologic hydronephrosis from obstruction secondary to calculus disease**. There are occasional situations where the colicky pain may be caused by papillary necrosis and in rare cases of HELLP syndrome (Hemolysis, Elevated Liver Enzymes, and Low Platelets). The one condition of the placenta that can be responsible for hematuria is placenta percreta that involves the bladder or ureter. Placenta accreta and increta do not extend beyond the uterus. Other general indications for ultrasonography during pregnancy include oliguria, anuria, urinary tract infection, pyelonephritis, and urinary retention (which is more commonly seen postpartum) [5, 14–21].

Resistive index (**RI**) is a useful tool for the assessment of obstruction either in gravid or nongravid kidneys. RI measures intrarenal impedance and it is calculated from the following formula:

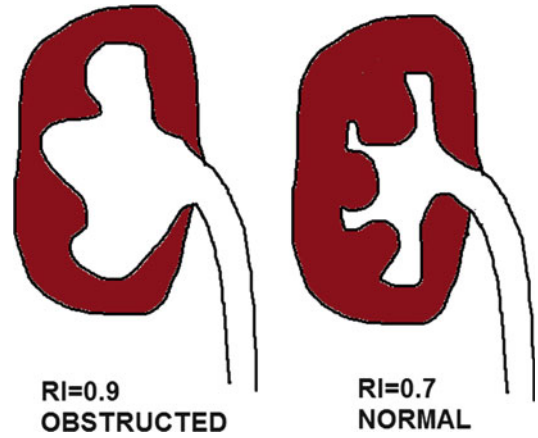

Fig. 13.1 Schematic diagram indicating an obstructed right kidney with associated elevated resistive index

$$\mathrm{RI} = \frac{\mathrm{PSV} - \mathrm{EDV}}{\mathrm{PSV}}$$

The resistive index (RI) is the peak systolic velocity (PSV) minus the end-diastolic velocity (EDV) divided by the PSV. The proper **location of measuring RI is at the corticomedullary junction where renal arcuate arteries and/or interlobar arteries along the medullary pyramids** are assessed usually at an angle of 50–60° [22]. **The normal RI is equal to or more than 0.7, and typically, an RI of more than 0.9 indicates renal dysfunction**. **RI increases with decreasing diastolic flow**. In normal pregnancy there is no appreciable change in RI. Therefore in a hypothetical situation of absence of flow in diastole, the resistive index equals 1.0. **In the early stages of obstruction, RI is often elevated and usually occurs within 6 h** after clinical acute obstruction [8]. From a technical point of view, compression of the kidney can cause elevation of RI, and this is typically noted in transplanted pelvic kidneys that are superficially located (Fig. 13.1) [23–26].

Diuretic Doppler ultrasound is a modification of conventional Doppler sonography to assess physiological responses of obstructed and nonob-

$$\text{Resistive index (RI)} = \frac{\text{Peak systolic velocity (PSV)} - \text{End diastolic velocity (EDV)}}{\text{Peak systolic velocity (PSV)}}$$

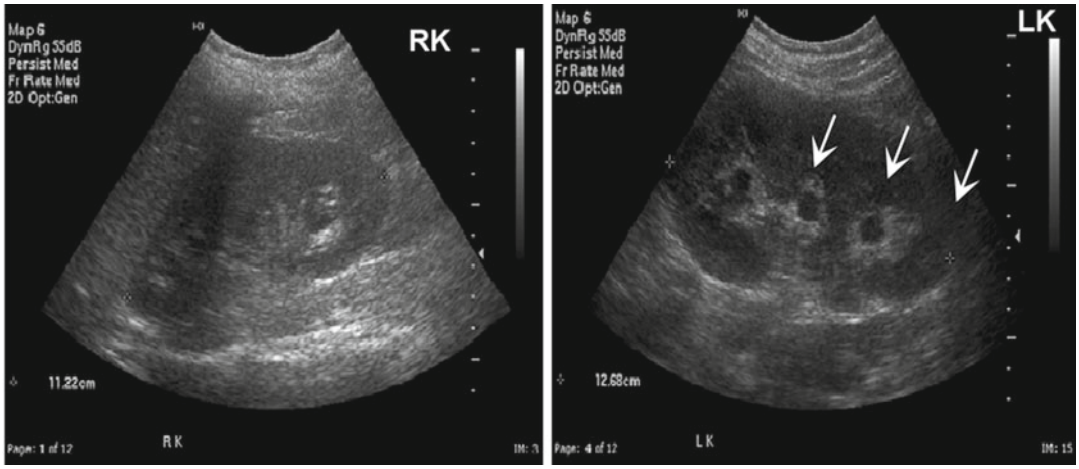

Fig. 13.2 30-year-old female, G2P1, at 28 weeks of gestation, presenting with left flank pain. The right kidney (RK) shows no hydronephrosis, whereas the left kidney (LK) demonstrates calyceal dilation (*arrows*)

structed kidneys to diuretic stimulation. Furosemide-enhanced diuresis leads to significant increases in the RI of obstructed kidneys, while having no effect on that of nonobstructed kidneys in adults or children. Saline loading followed by furosemide results in a divergent response with an increased RI in obstructed and a decreased RI in nonobstructed kidneys. Other factors causing elevated RI are renal medical disease, diabetic nephropathy, and external factors such as fasting and exsanguination. Recent studies documented decrease in RI with increasing heart rate and stable blood pressure and increasing RI with pulse pressure widening [27–30].

Resistive index is usually normal in a pregnant patient. The elevation of obstruction-related RI is thought to be due to increased renal vascular resistance secondary to elevated prostaglandins. It is recommended that, for the assessment of RI, patients **should avoid the use of NSAIDs prior to ultrasound imaging**. NSAIDs may interfere with interpretation which may be due to blocking prostacyclin synthesis resulting in decreased renal blood flow and mask the expected changes in RI [31]. Several NSAIDs (e.g., ketorolac, indomethacin) have been shown, in animal models, to reverse both the early vasodilation and subsequent vasoconstriction of acute ureteric obstruction [32, 33]. Measurement of RI is usually most evident during the first 6–48 h of obstruction. **A difference of more than 0.1 from side to side is suggestive of obstruction**. The overall sensitivity of RI for the assessment of obstruction is 42–100%, and it is less sensitive for partial versus complete obstruction.

Another method for assessing the obstruction in a gravid kidney is the measurement of the renal pelvic dilation. Pathological obstruction is suspected if **the cross-sectional (AP) measurement of the renal pelvis exceeds 27 mm on the right or 18 mm on the left during the second and third trimester**. It is therefore **imperative to obtain images of the gravid kidney from both sagittal and cross-sectional views**. Pathological obstruction is suspected if the AP measurement exceeds 18 mm on the right and 15 mm on the left side during the first trimester. The cross-section measurement of the renal pelvis should be in the midpole where the maximum dilation can best be assessed [34] (Figs. 13.4 and 13.5). The frequency of developing hydronephrosis is not related to the number of pregnancies [12, 35]. These changes should be interpreted in correlation with qualitative and objective clinical manifestations. Predominately left renal pelvic dilation with left flank pain suggests obstruction. Right flank pain with minimal to no pelvic dilation suggests no pathological obstruction (Figs. 13.2).

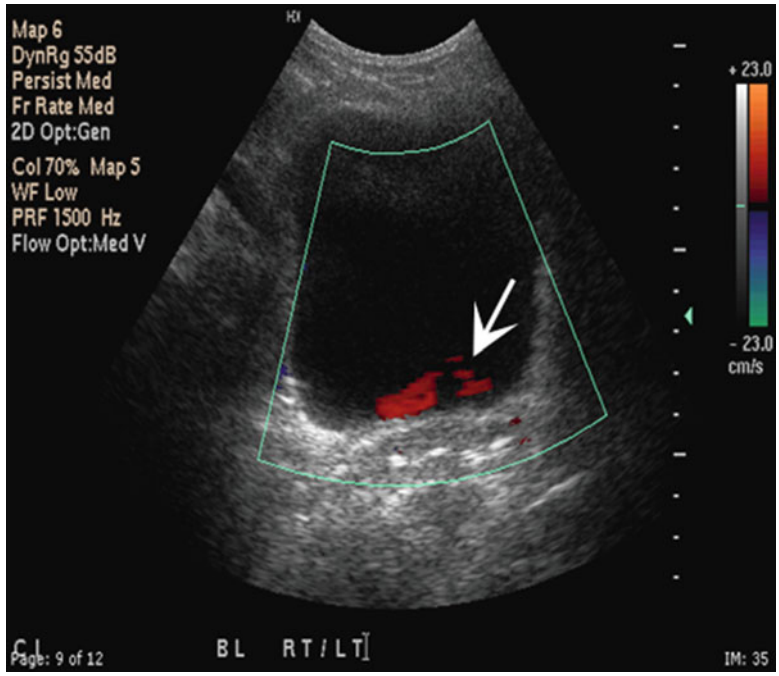

Fig. 13.3 Ureteral jets in the previous patient, note sluggish jet from the *left* side (*arrow*)

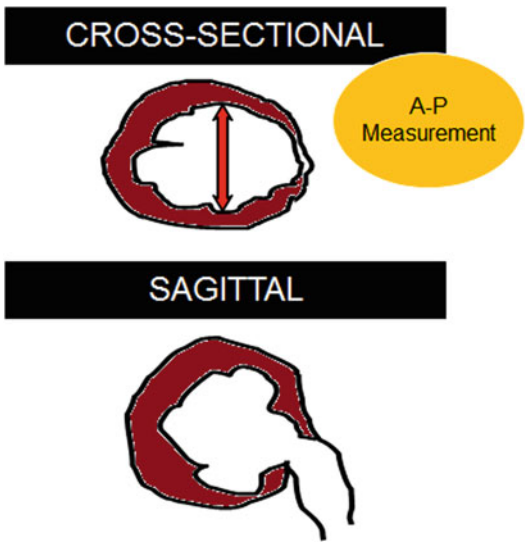

Fig. 13.4 Diagram depicting renal pelvic measurements

Table 13.1 The grading of hydronephrosis during pregnancy

Grading	
Grade 0	hydronephrosis 0–5 mm, minimal separation of central echo complex
Grade 1	hydronephrosis 6–10 mm
Grade 2	hydronephrosis 11–15 mm
Grade 3	hydronephrosis equal or more than 16 mm. A large sonolucent sac occupies a major portion of the kidney.

Table 13.2 AP Renal Pelvic and Calyceal Measurements suggesting obstruction

	Right Kidney	Left Kidney	Calyceal diameter
First Trimester	>18 mm	>15 mm	>10 mm
Second and Third Trimester	>27 mm	>18 mm	>10 mm

AP renal pelvic and calyceal measurements suggesting obstruction

In early pregnancy, there is no significant difference in calyceal dilation. With the increase of gestational age, the degree of hydronephrosis increases on the right side and decreases on the left [36] (Table 13.2).

Example: Grade 1 hydronephrosis is detected bilaterally in 53% of patients. For grade 2, the ratio changes to 35% on the right and 14% on the

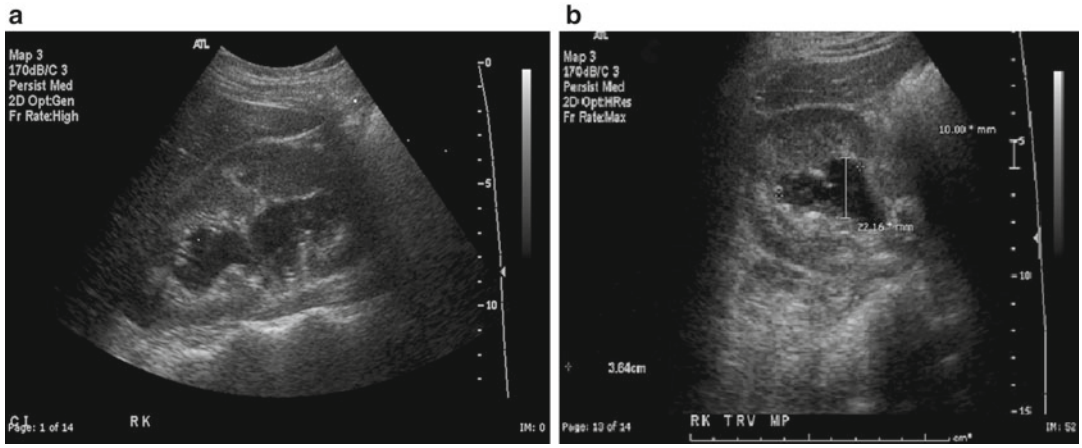

Fig. 13.5 Sagittal (**a**) and transverse (**b**) midpole ultrasound images of a pregnant patient with right flank pain, AP measurement of 27.16 indication obstruction

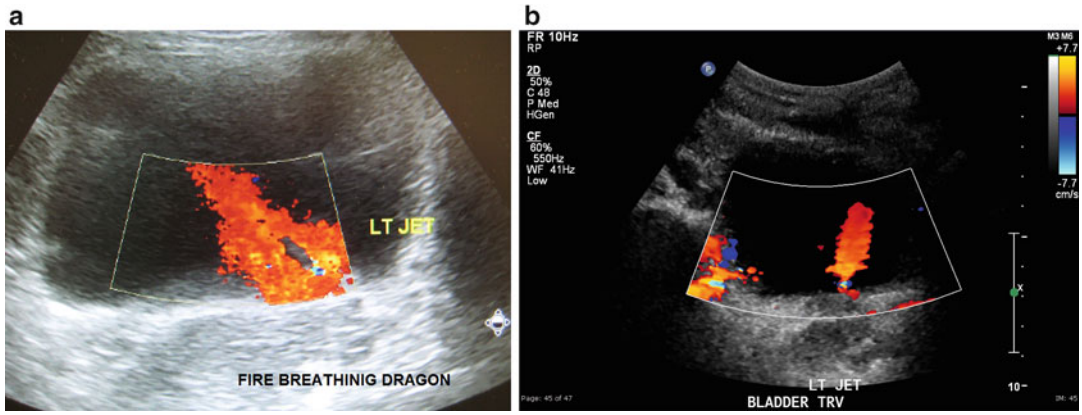

Fig. 13.6 (**a**) A strong left ureteral jet: pulsatile egress of urine into bladder gives the appearance of a dragon-breathing fire. (**b**) A strong left ureteral jet (*arrows*) in a patient with a left double pigtail ureteral stent. Note that the direction of the jet is slightly towards left of bladder and vertical secondary to changes in the orientation of the orifice with the stent in place

left. The following graph shows the mean calyceal diameter of the right and the left kidneys as plotted against gestational age (Table 13.3).

Ureteral Jets: One of the more recent applications of Doppler is imaging of the base of the bladder and trigone for detection of pulsatile (peristaltic) egress of urine from the ureteral orifices (Figure 13.3). Ureteral jets can be well documented even after placement of double pigtail ureteral stent (Fig. 13.6a, b). This application is quite useful in assessing the patency of the ureter. Ureteral jets can be assessed during the follow-up and observation period of medical expulsive therapy, in anticipation of spontaneous stone passage. This application is very valuable in management of pregnant patients with renal colic as it eliminates radiation exposure. Presence, clinical utility, value, and accuracy of ureteral jets, at times, remain controversial. This is due to the significant variability of ureteral jets frequency in normal volunteers [37–41].

The drawback to assessment with ureteral jets is that it may add significant scanning time to a standard renal bladder study, but in

Table 13.3 This table describes renal calyceal dilation as it relates to gestational age

Gestational age (week)	Observed percentiles				Adjusted percentiles			
	Right		Left		Right		Left	
	50th	70th	90th	90th	50th	75th	90th	90th
4–6	0.0	3.0	5.0	2.1	1.4	2.4	3.4	0.1
7–8	0.0	0.0	5.0	0.0	0.3	3.2	4.5	2.2
9–10	0.0	0.0	4.0	0.0	1.2	4.0	5.7	3.5
11–12	0.0	5.0	7.0	6.0	2.0	4.9	7.0	4.5
13–14	0.0	5.8	8.0	6.9	2.7	5.7	8.4	5.3
15–16	0.0	1.0	8.9	4.9	3.0	6.7	9.8	6.0
17–18	5.0	9.5	12.0	8.8	3.7	7.6	11.2	6.6
19–20	0.0	8.0	11.0	7.7	4.2	8.6	2.6	7.1
21–22	5.0	9.0	13.8	6.8	4.6	9.6	13.9	7.1
23–24	8.0	12.0	15.0	8.2	4.9	10.5	15.1	7.9
25–26	7.0	13.0	16.7	8.0	5.3	11.4	16.2	8.2
27–28	7.0	13.0	21.0	9.0	5.6	12.2	17.2	8.4
29–30	7.0	11.0	16.0	9.0	5.9	13.0	18.0	8.6
31–32	8.0	15.5	19.4	8.2	6.1	13.7	18.7	8.7
33–34	4.5	13.0	20.5	8.5	6.4	14.3	19.3	8.8
35–36	6.0	15.0	19.0	8.0	6.6	14.8	19.7	8.9
37–38	5.0	14.0	20.4	8.0	6.8	15.2	19.8	8.9
39–42	7.0	14.0	17.0	9.2	7.1	15.5	19.8	8.7

the case of a pregnant patient this is the most viable option. Unlike other scanning to obtain accurate results protocols, there is no defined, standard adequate scanning time. In well-hydrated patients' ureteral jets can often be documented within a few minutes of scanning the bladder. To indicate that there is an absence of ureteral jets adequate scanning time needs to be allowed. **Usually a minimum of 10 min is recommended to adequately document absence of ureteral jets** [41]. Thirty minutes may be required to document asymmetry of jet frequency in order for it to be a true finding. The patients must be adequately hydrated. The urine density differences contributes to visualization of ureteral jet [39]. Some of the other theories discussed in relation to ureteral jets include that **frequency decreases during normal pregnancy**. **Findings suggestive of ureteral obstructions are asymmetry of ureteral jets and absence or sluggish continuous flow from the affected side**. Lack of ureteral jets suggesting obstruction is after 10 min of observation with no obvious flow in a well-hydrated patient whereas in partial obstruction, there is sluggish trickling along the trigone versus strong upward jet towards opposite bladder wall.

Some of the above-mentioned signs that are indicative of obstruction can be seen in asymptomatic pregnant women. They may be attributed to diminished ureteral smooth muscle tone and extrinsic ureteral compression by the gravid uterus. **There is no correlation between the degree of hydronephrosis and mean jet frequency** [41] (Fig. 13.7). Transvaginal sonography demonstrating dilated distal ureter or presence of stone can further document obstruction specifically if combined with Doppler showing twinkling artifact [42–44] (Fig. 13.7).

Absence of ureteral jets is reported in 33.2–50% of asymptomatic pregnant women.

The absence of ureteral jets may be attributed to the patient's **supine position** and ureteral compression, which can be alleviated by placing the patient in the **contralateral decubitus position** [45]. True obstruction of the ureter would not respond to a change in patient position (Figs. 13.8a, b).

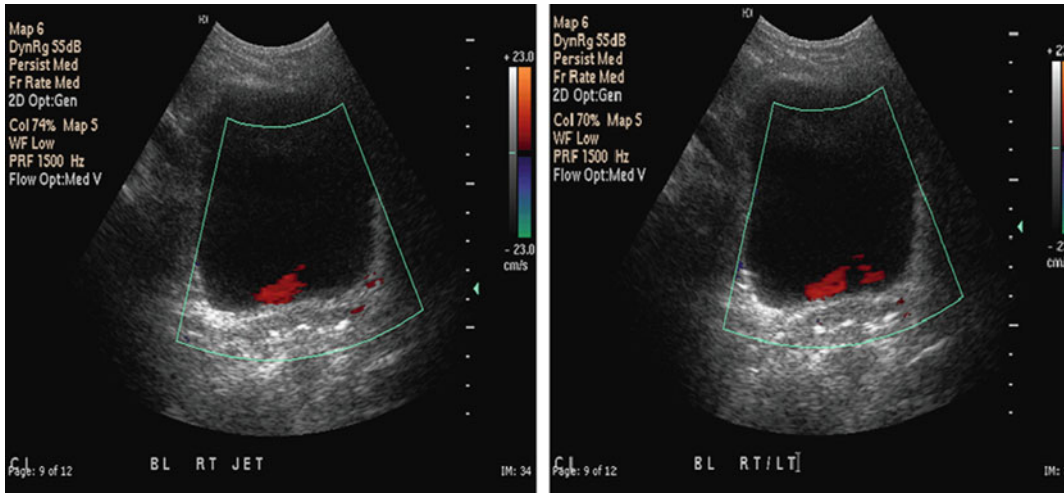

Fig. 13.7 *LT*: Presence of right ureteral jet from an unobstructed right gravid kidney. *RT*: Very sluggish left ureteral jet in an unobstructed left gravid kidney

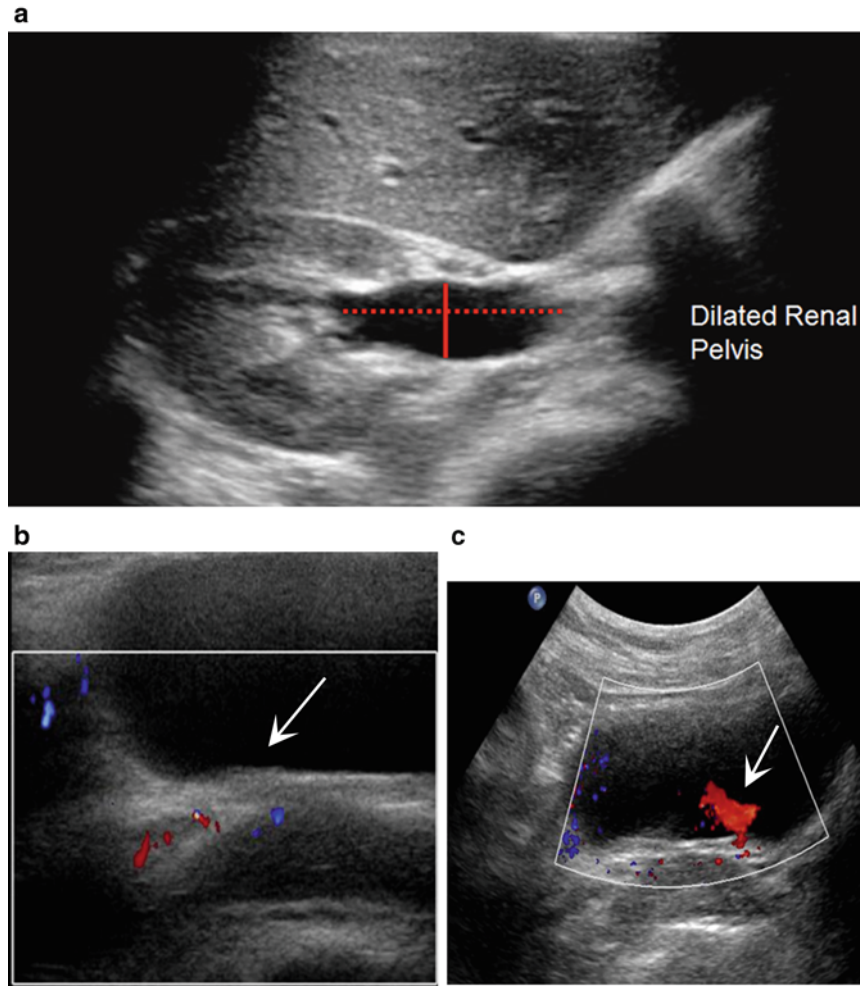

Fig. 13.8 (**a**) Hydronephrosis on the right side with dilation of the renal pelvis due to acute ureteral obstruction. (**b**) Absence of Rt. ureteral jet (*arrow*). (c) Presence of a strong Lt ureteral jet (*arrow*)

Ultrasound-Guided Ureteroscopy During Pregnancy

Symptomatic pregnant patients may require ureteroscopy or stenting for relief of obstruction. It is best to avoid radiation during ureteroscopy [46]. The following steps are recommended to help the physician achieve this goal:

- The patient is placed on the operating table in a dorsolithotomy position on a dedicated cystoscopy table with a lead apron under the patient and wrapped around the abdomen only exposing the upper portion of the affected kidney. This is for possible emergency use of C-arm fluoroscopy to assess the renal area while protecting the fetus. A 3.5/5 MgH transducer is used scanning the flank area as well as the right or left lower quadrant.
- After the placement of the guidewire, the ultrasound imaging of the kidney can show motion of the wire, indicating the proper location of the guidewire.
- If a ureteral catheter is advanced to the renal pelvis, injection of a few milliliters of air will create a bubbling effect, thus confirming the proper location of the catheter.
- Distal ureteral stones can be monitored with lower quadrant ultrasound imaging at the time of ureteroscopy.
- Transvaginal sonography can be helpful in assessing the distal ureter if transabdominal ultrasound is inadequate.
- Proper location of the stent may also be confirmed using sonography.

Case Study: Sonography of the lower pelvis on the right side in a pregnant patient with right flank pain shows echo and shadowing, which is suggestive of the presence of ureteral stone (9c). This patient had undiagnosed, complete duplication of the right collecting system, with two stones obstructing both ureters. After ureteroscopy and stone removal of one stone, intraoperative ultrasound continued to show persistence of an echogenic area. Further evaluation of the trigone revealed a second orifice and ureter with an obstructing stone (Fig. 13.9 a–f).

At the completion of the procedure, a stent can be placed and the proximal location of the stent can be confirmed with ultrasound (Fig. 13.9g).

Ultrasound Evaluation of Pelvic Kidneys

Pelvic kidneys are either congenital or transplanted. The transplant kidney can be either autotransplant, deceased donor, living-related, or living unrelated in patients with end-stage renal disease requiring dialysis.

The anatomy of the congenital pelvic kidneys is different from the surgically implanted pelvic kidneys. **Congenital kidneys** are **located centrally** and like cross fused ectopia have **normal ureteral orifices**. Renal ultrasound can reveal common problems with pelvic kidneys, such as stone formation and hydronephrosis due to malrotation and poor drainage. Sonography of the congenital pelvic kidneys can be difficult or impossible because it is superimposed by the bowel, but the assessment of ureteral jets is simple due to the normal location of orifices.

On the other hand, transplant kidneys are commonly placed extraperitoneally in the right or left lower quadrants. This anatomic arrangement provides for an easy imaging target since the distance between the skin and the kidney is short, without bowel interposition. The transplant kidney ureters are implanted into the bladder, commonly in the anterior lateral location using a modified Lich-Gregoir technique. Depending on the technique of anastomosis, there may be a **nipple artifact** in the bladder, which can be detected via ultrasound. Stones can be formed at this site which produces an echo during imaging. Doppler application reveals significant **twinkle artifact** [44] (Figs. 13.10 and 13.11).

Post surgery, the hilar anatomy of a transplant kidney differs from the native kidney. In these kidneys, the **pelvis is more anterior**, **whereas the artery and vein are situated more posteriorly**. Ultrasound imaging of the transplant kidneys is performed from the anterior abdominal wall with the patient in the supine position. In the posttransplant kidney, the renal artery and vein have a different orientation. The renal artery is anastomosed to either the internal iliac end to end or external iliac artery end to side. The renal vein is anastomosed to the external iliac vein end to side.

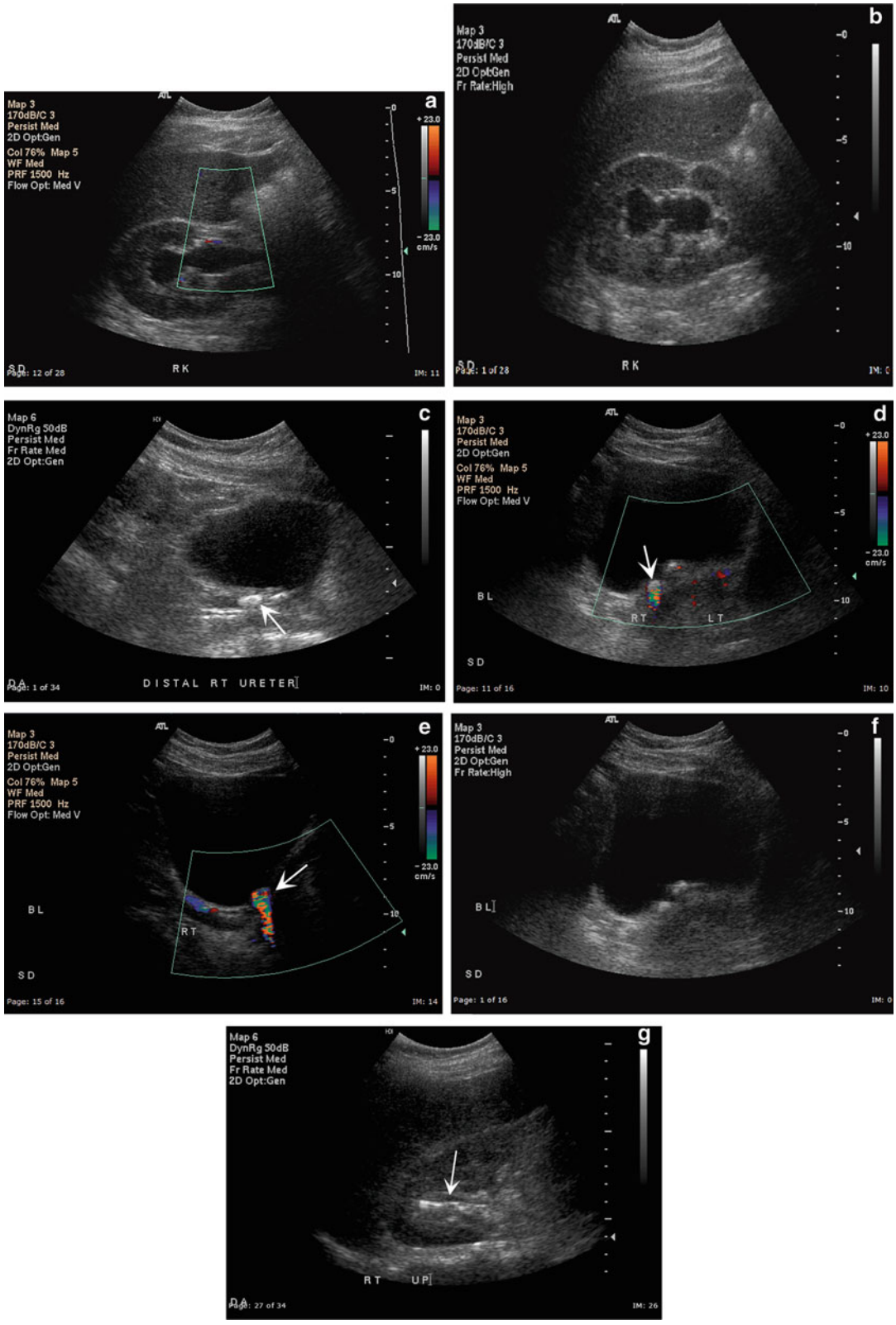

Fig. 13.9 (**a**) Ultrasound reveals dilated upper pole. (**b**) Hydronephrotic mid- and lower pole. (**c**) Pelvic ultrasound detecting two stones in the vicinity of the distal ureter(s). (**d**) Twinkle artifact confirming the first stone (*arrow*). (**e**) Twinkle artifact confirming the second stone (*arrow*). (**f**) AP view of bladder showing separation of two orifices with stone in each. (**g**) Stent in upper pole (*arrow*)

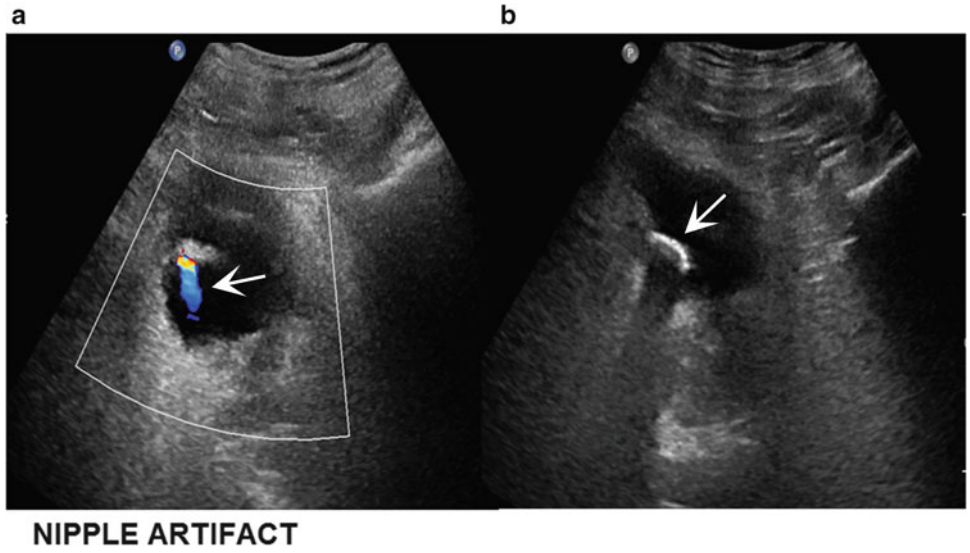

Fig. 13.10 Stone at the stump of a ureteral implant (**b**) with echo and posterior shadowing (*arrow*). Note the "twinkling" artifact with the Doppler wave (**a**)

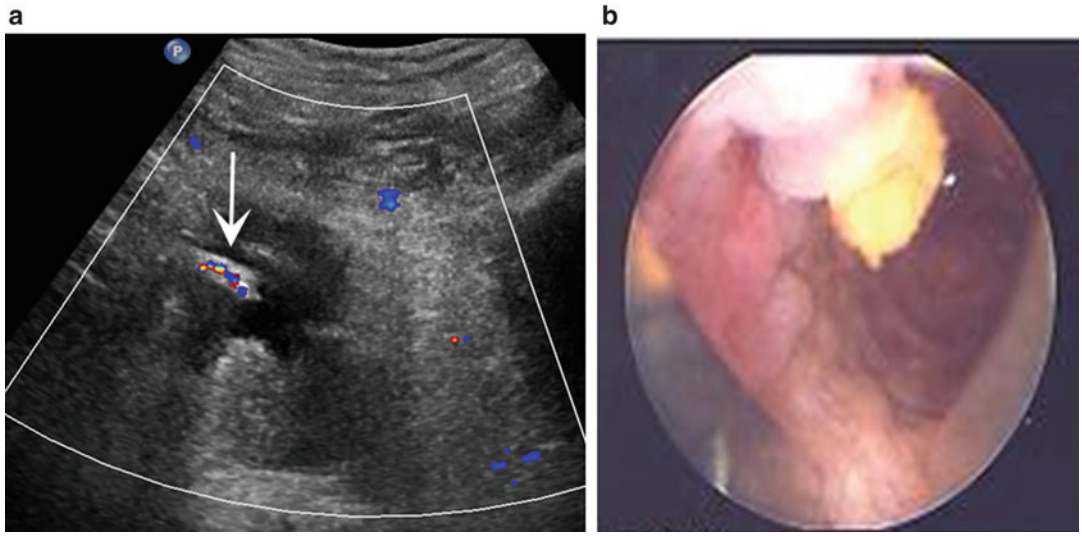

Fig. 13.11 A nipple artifact (**a**) at the anterolateral aspect of the bladder on sonography (*arrow*) represents the location of an implanted ureter. Endoscopic view of stone (*arrow*) formation at implant (**b**) site

Doppler evaluation of the transplant kidney and renal vasculature is usually the first method for studying the kidney during the postoperative period for routine follow-up or when there is dysfunction in the transplant kidney. These applications include the assessment for rejection, renal artery stenosis, and thrombosis of the renal artery or vein. Obviously some of the drainage complications in a transplant kidney such as ureteral obstruction, leakage, urinoma, and lymphocele can also be identified with ultrasound imaging [47].

Peak systolic velocity (**PSV**) in transplant kidneys is usually 100 ± 25 cm/s. In cases of renal artery stenosis (RAS), the PSV is between 180 and 200 cm/s.

Causes of elevated RI	
Parenchymal	Acute rejection Acute tubular necrosis pyelonephritis
Vascular	Renal vein thrombosis Hypotension
Urological	Ureteral obstruction
Technical	Graft compression

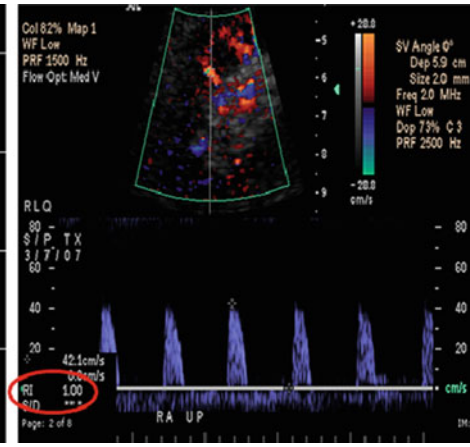

Fig. 13.12 Table showing causes of elevated RI. Doppler evaluation showing RI of 1.00 indicated a lack of diastolic blood flow (right image)

Renal aortic ratio (**RAR**) is another tool to assess the degree of renal artery stenosis, and it is calculated from the following equation:

$$\frac{\text{Renal peak systolic velocity (RPSV)}}{\text{Aortic peak systolic velocity (APSV)}}$$

RAR is considered normal up to 3.0, but a **ratio of more than 3.5 generally indicates renal artery stenosis** [7].

RI: A resistive index of more than 0.9 usually indicates renal transplant dysfunction. **Causes of elevated RI** in renal transplants can be seen in the accompanying table (Fig. 13.12).

Power Doppler (**PD**), also known as nondirectional Doppler, is useful for assessing **low flow states**, or when optimal Doppler angles cannot be obtained. **PD is 3–5 times more sensitive** in depicting flow in all arteries than the color Doppler imaging (CDI) [5, 48]. Unlike CDI, **PD does not provide information relative to velocity or direction** of the blood flow. In transplant kidneys, PD is an invaluable tool for the evaluation of **vascular thrombosis**, **occlusion of vessels**, and evaluation of the parenchymal flow. Unlike the CDI red and blue color scheme, **PD** typically has a single **salmon color** appearance (Fig. 13.16). The color schema can be changed by the sonographer. Color red is customarily assigned to arterial and color blue to venous flow.

Ultrasonic Findings in Transplant Complications

- **Acute tubular necrosis** (**ATN**): In this condition, the kidney is grossly edematous, echo poor, with a lack of corticomedullary differentiation. **RI is elevated to over 0.8** (Fig. 13.13). Nuclear scan is the primary imaging modality for ATN assessment.
- **Acute rejection**: Grayscale and spectral ultrasound imaging typically reveals **graft enlargement** due to edema, decreased cortical echogenicity, and swelling of the medullary pyramids resulting in **loss of corticomedullary differentiation**. The renal sinus fat may show edema as well on spectral Doppler imaging.
- **Chronic rejection**: Imaging of a chronically rejected kidney shows a small graft, **thin**, **echogenic renal cortex**, and relative sparing of medullary pyramids. **In chronic rejection RI is typically normal or slightly elevated** [47].
- **Foreign body**: Chronically infected and obstructed kidneys can develop organized amorphous intrarenal debris or fungus balls. This can be a rapid process due to the patient's immunocompromised state. Sonography can detect these foreign bodies readily (Fig. 13.14).
- **Renal vein thrombosis**: This is a surgical emergency and occurs in less than 1–2% of cases. Early detection of RVT is critical because it

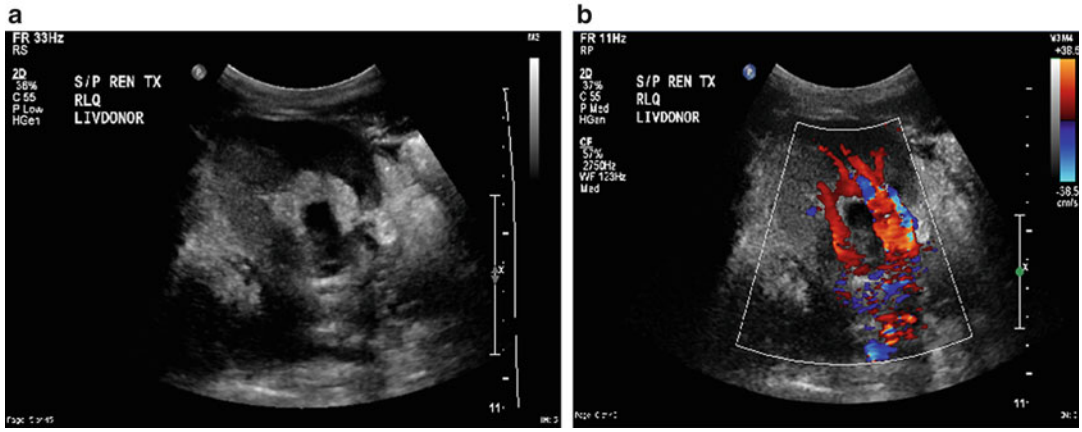

Fig. 13.13 Transverse gray-scale image of a kidney two days posttransplant with decreased urine output secondary to acute tubular necrosis (**a**). Note that the renal vascular supply is intact (**b**)

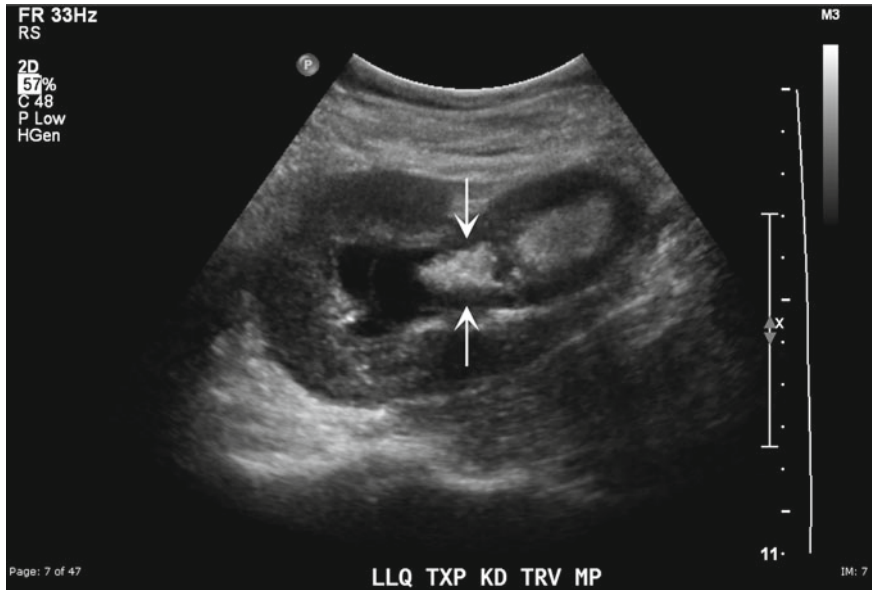

Fig. 13.14 A left lower quadrant transplant kidney obstructed with infectious amorphous debris. Filling defects in the center and the pelvic portion of the collection system are readily visible (*arrows*)

requires immediate surgical exploration. **Doppler evaluation is diagnostic** in these cases, since there are no collateral pathways in transplanted kidneys. The findings include **enlarged kidney with absent venous flow on color Doppler or power Doppler** and distended and thrombus-filled main renal vein. On arterial Doppler, wave will be prolonged, and in a U-shape or plateau-like pattern, due to a **diagnostic reversal of arterial flow in diastole** (Figs. 13.15a, b) [49–51].

- **Renal artery thrombosis** (**RAT**): A rare condition occurring in less than 1%, usually due to technical reasons. The patients are **anuric and hypertensive** and Doppler ultrasound imaging reveals the **absence of arterial flow** (Fig. 13.16) [47].
- **Renal artery stenosis**: This condition is usually accompanied by a rise in serum creatinine,

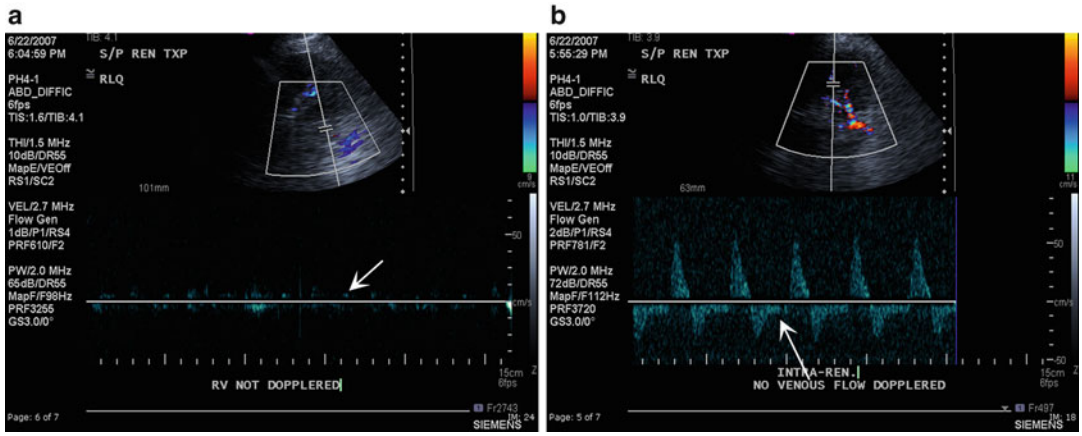

Fig. 13.15 (**a**, **b**) Renal vein thrombosis. Doppler imaging of the renal hilum in a patient with renal vein thrombosis showing the absence of venous flow (*arrow*) (**a**) and spectral Doppler shows reversal of arterial flow (below the line) in diastole (*arrow*) (**b**)

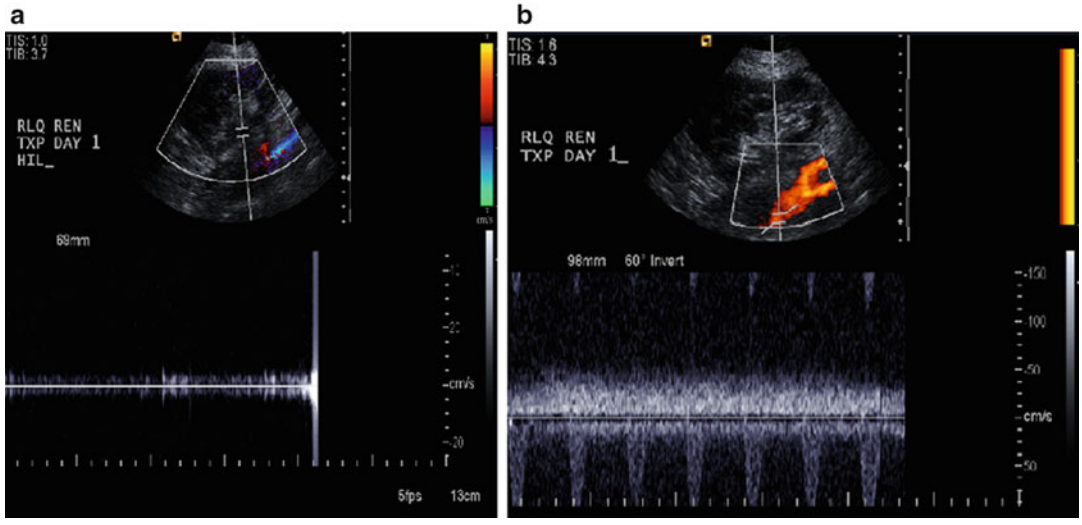

Fig. 13.16 (**a**, **b**) Patient with sudden drop of urine output on the first day post renal transplantation (**a**). Doppler imaging of the renal hilum reveals the absence of flow in the transplanted renal artery (**b**). Power Doppler (*salmon color*) shows good flow in the iliac vessels. Renal artery thrombosis was confirmed at the time of surgical exploration

hypertension, and a bruit over the graft can be auscultated. Grayscale ultrasound findings suggest the appearance of a **structurally normal kidney**, whereas the **CDI of renal artery displays a high-velocity jet exceeding peak flow in the iliac artery** (post stenotic jet effect). A pathologically low RI within the graft equal to or less than 0.6 may be highly specific for stenosis of over 50% since the actual flow is low within the kidney. **Parvus Tardus**, which is a small amplitude wave form with a prolonged systolic rise (slow upstroke), is indicative of proximal renal artery stenosis. **Parvus Tardus is usually identified within the renal parenchyma downstream from significant stenosis** [52–54] (Fig. 13.17).

- **Ureteral obstruction**: Ureterovesical anastomotic stricture is the most common type

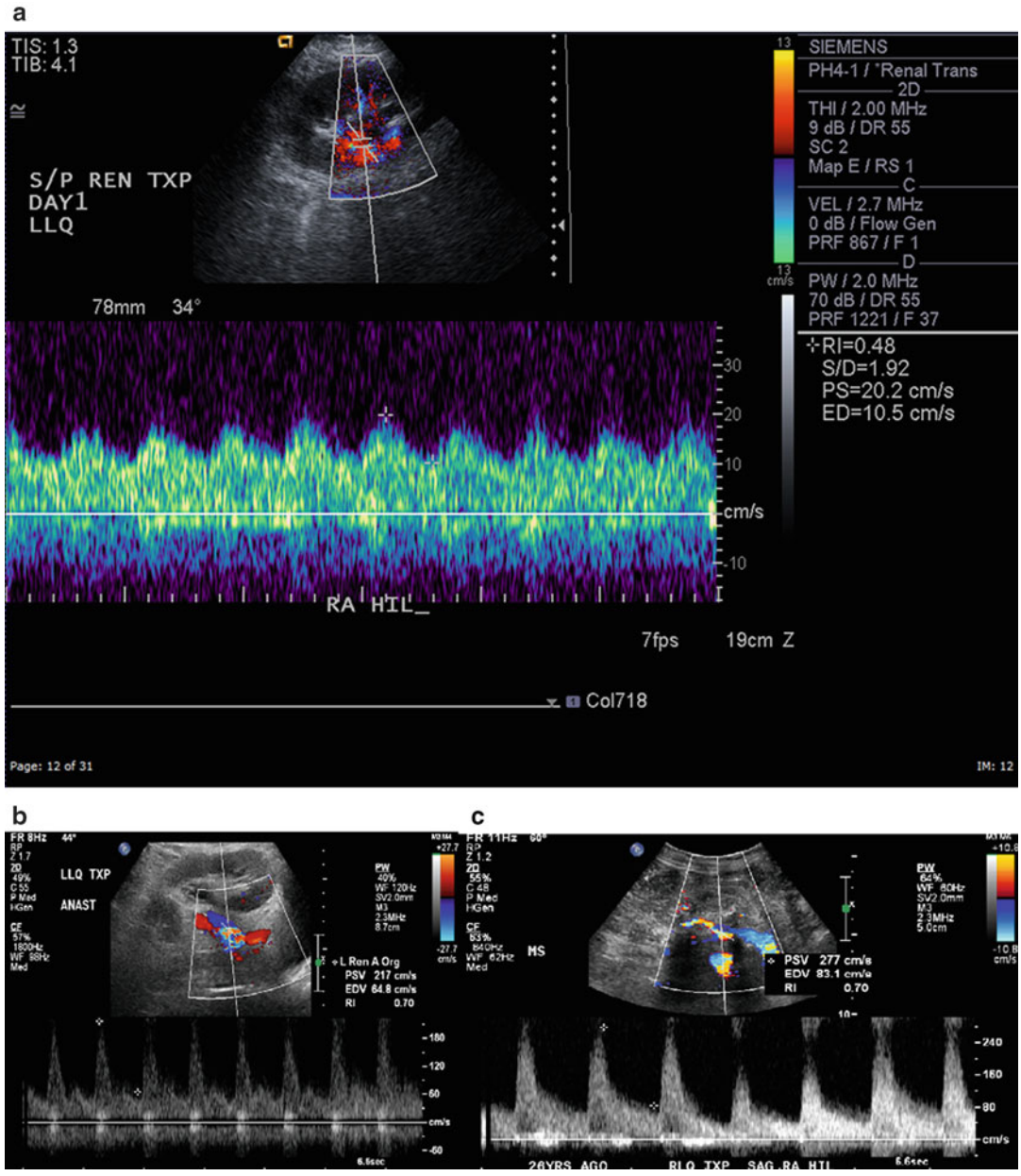

Fig. 13.17 (**a**) Spectral Doppler in a transplant patient with RAS showing a prolonged systolic rise or Parvus Tardus (slow upstroke). (**b**) Arterial anastomotic stenosis PSV=217 cm/s past anastomosis. (**c**) Main renal arterial stenosis PSV=277 cm/s measurement distal to stenosis

usually secondary to a tight anastomosis (early) or ischemia (late) (Fig. 13.18). In the acute phase of obstruction, RI is elevated whereas in the late phase it is usually normal. Stone disease, upper ureteral ischemic stricture, and lymphocele causing extraluminal compression occur less commonly. With malrotation of the transplant kidney, some patients develop ureteral obstruction at the level of the ureteropelvic junction. Even in

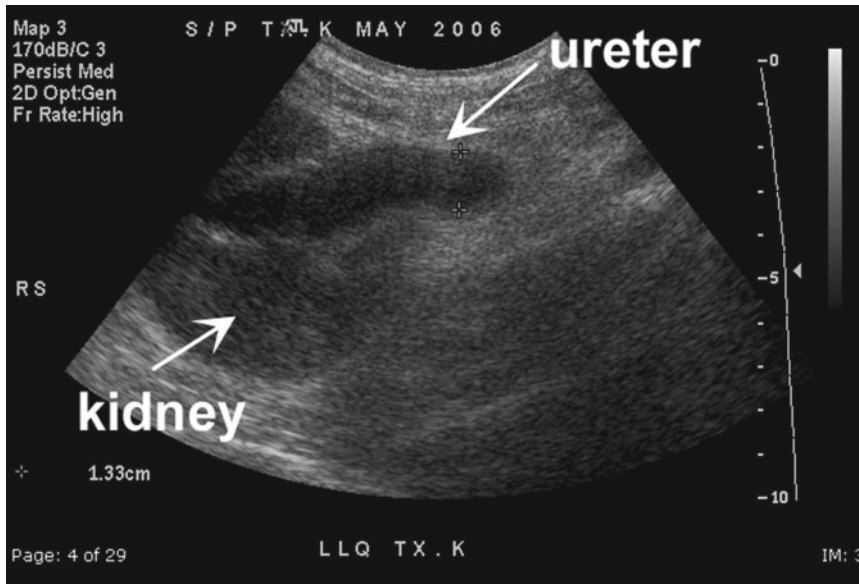

Fig. 13.18 Ultrasound image of a left lower quadrant kidney showing hydronephrosis and dilation (1.33 cm diameter) of the ureter due to ureterovesical anastomotic stricture

normal circumstances, due to tilted retroperitoneal lie of the graft, it is not unusual to find a mild degree of hydronephrosis or calyceal dilation in either pole of a transplanted kidney without clinical evidence of obstruction or changes in serum creatinine (Fig. 13.19).

- **UPJ obstruction**: Hydronephrosis due to UPJ obstruction has been diagnosed in patients after transplant, even in the absence of preoperative obstruction in donor. The clinical and ultrasound findings are similar to congenital UPJ obstruction in native kidneys (Fig. 13.20).
- **Lymphocele**: The most common fluid collection in transplant patients (5–15%), which can cause hydronephrosis or a pelvic collection. Lymphocele can cause graft dysfunction, **extraluminal ureteral obstruction**, lower extremity edema, pelvic discomfort, and **bladder displacement**—mimicking symptoms suggestive of LUTS or prostatic outlet obstruction. Pelvic ultrasound shows a collection, usually **between the transplant kidney and a displaced bladder**. It may also cause hydronephrosis (Fig. 13.21). Lymphocele in other locations may not cause similar findings.
- **Renal transplant stones**: The localization of the stone in the transplant kidney is similar to congenital kidneys, which shows an echogenic area with posterior shadowing and twinkle artifact. A Ureteral jet can be documented by aiming the Doppler at lateral and anterior aspect of the bladder at the site of ureteroneocystostomy (Fig. 13.22).
- **AV fistula**: Percutaneous renal biopsy of the transplant kidneys is commonly preformed to rule out possible rejection versus nephrotoxicity. The most significant complications of percutaneous needle biopsy are acute bleeding and AV fistula formation. Doppler ultrasound findings of AV fistula include **high-velocity**, **whirling flow pattern**, **mosaic color pattern** due to AV shunting, spectral broadening, and **turbulent flow with mirror-imaging**. The shunting will result in increased diastolic flow velocities (80 cm/s)

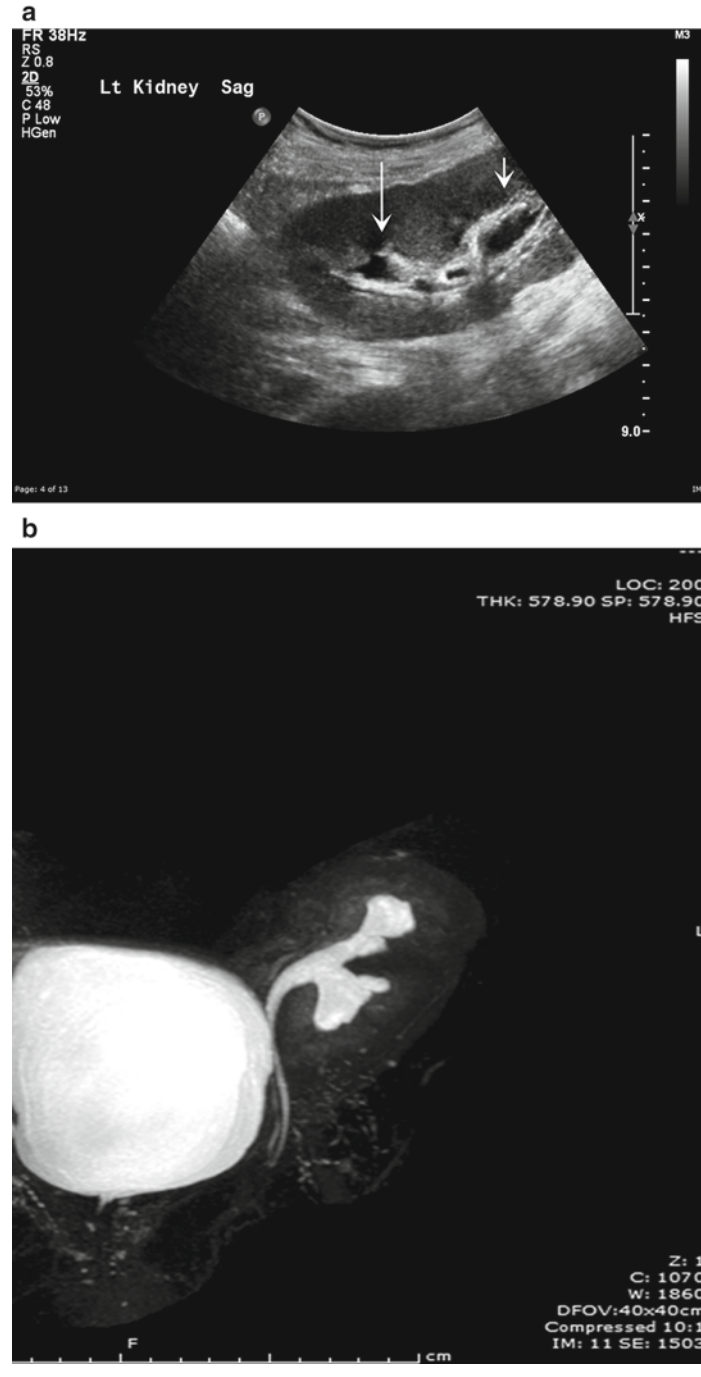

Fig. 13.19 Nonobstructed left lower quadrant renal transplant with mild hydronephrosis. (**a**) Grayscale sonogram showing calyceal dilation (*arrows*). (**b**) Non-contrast MR urogram with hydration rules out obstruction

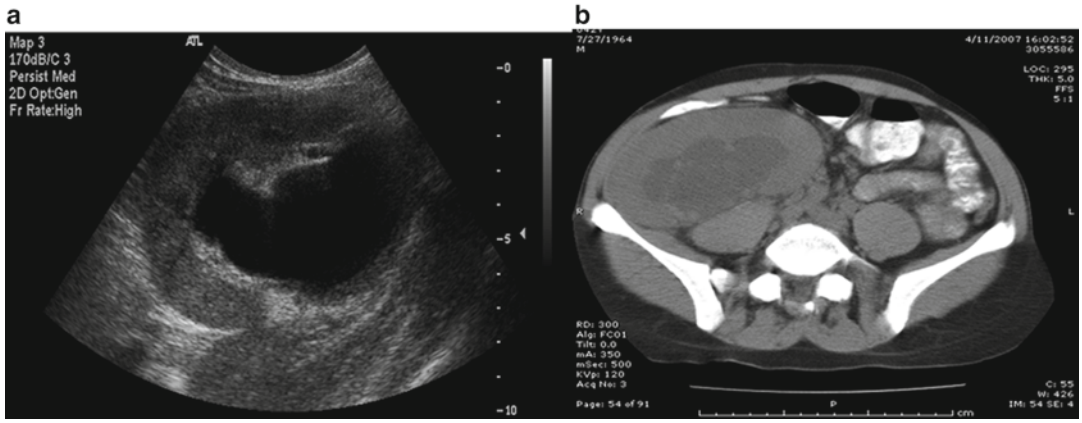

Fig. 13.20 Renal ultrasound and CT scan of a right lower quadrant transplant kidney (**a**) with UPJ obstruction. Corresponding CT scan of the same kidney (**b**)

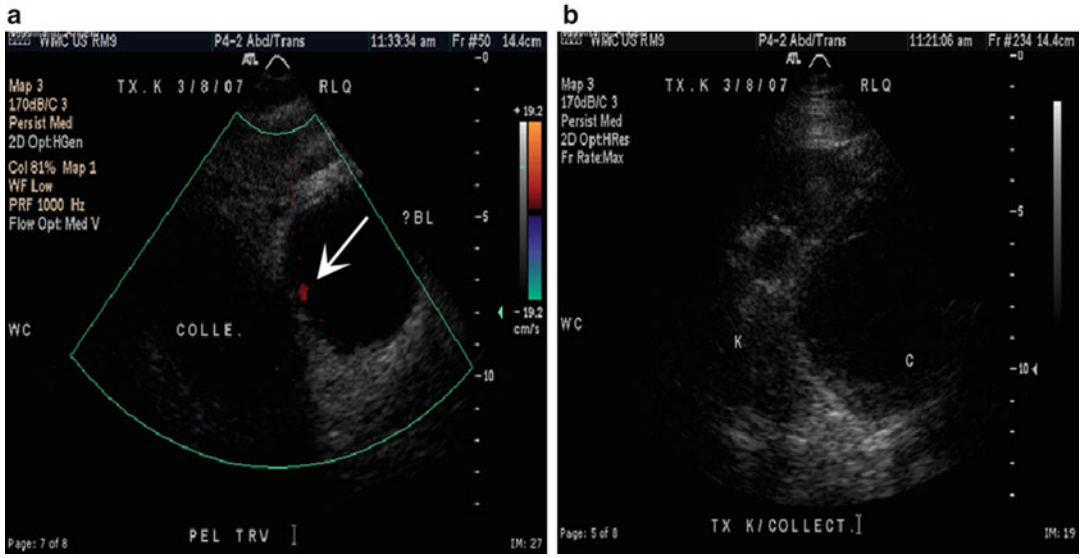

Fig. 13.21 (**b**) Right lymphocele (C) collection next to the RLQ transplant kidney. (K) and the bladder (**a**). Note a sluggish ureteral jet from the transplant ureter (*arrow*)

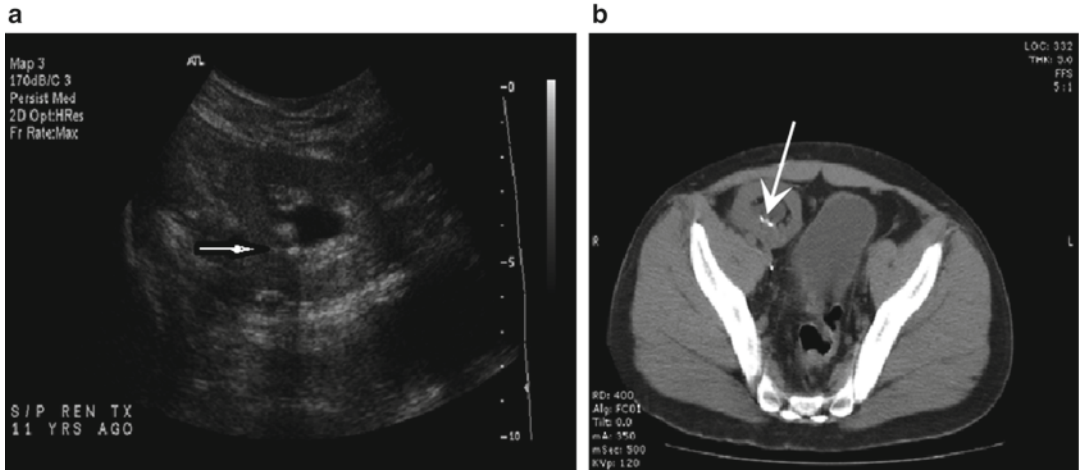

Fig. 13.22 Ultrasound (**a**) and (**b**) CT image comparison of transplant renal stone (*arrows*)

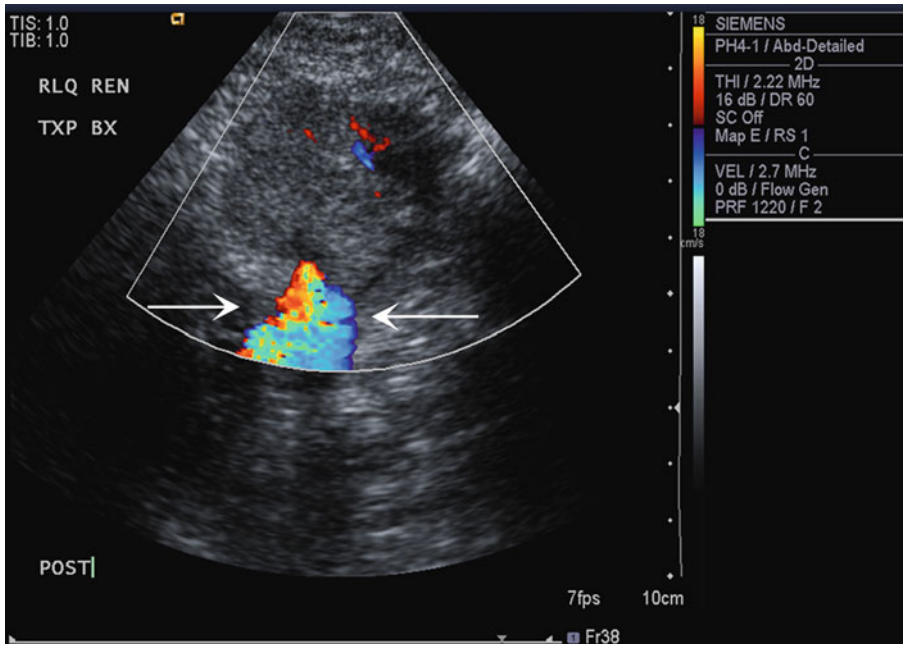

Fig. 13.23 Doppler imaging of a right lower quadrant renal transplant kidney demonstrating arteriovenous fistula, secondary to percutaneous renal needle biopsy. Note the mosaic pattern due to AV shunting and high-velocity whirling flow pattern (*arrows*)

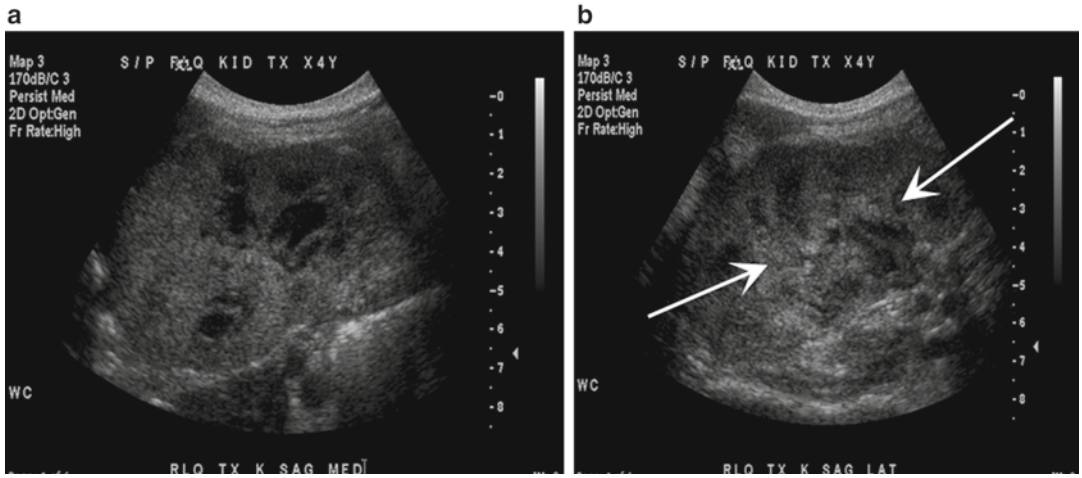

Fig. 13.24 Classic findings of chronic pyelonephritis (**a**). Note the loss of corticomedullary junction which should normally be seen at location arrows (**b**)

due to abnormal arteriovenous communications (Fig. 13.23) [47].

- **Acute pyelonephritis**: Acute and chronic infections can occur in transplant kidneys with similar image findings as native kidneys, which include graft enlargement, changes in echogenicity, and loss of corticomedullary junction (Fig. 13.24).

Acknowledgement The author would like to thank A. Arsanjani, MD, D. Lankford, MD and M. Degen, MD for assistance in preparing these manuscripts.

References

1. Schaeffer AJ, Schaeffer EM. Infections of the urinary tract. In: Kavoussi L, Novick A, Partin A, Peters C, editors. Campbell-Walsh Urology, vol. 1. 10th ed. Philadelphia, PA: Elsevier Saunders; 2011. p. 257–326.
2. Coe FL, Parks JH, Lindhemer MD. Nephrolithiasis during pregnancy. N Engl J Med. 1978;298:324–6.
3. Pearle M, Lotan Y. Urinary lithiasis: etiology, epidemiology, and pathogenesis. In: Kavoussi L, Novick A, Partin A, Peters C, editors. Campbell-Walsh urology, vol. 2. 10th ed. Philadelphia, PA: Elsevier Saunders; 2011. p. 1257–86.
4. Ferrandino M, Pietrow P, Preminger G. Evaluation and medical management of urinary lithiasis. In: Kavoussi L, Novick A, Partin A, Peters C, editors. Campbell-Walsh urology, vol. 2. 10th ed. Philadelphia, PA: Elsevier Saunders; 2011. p. 1287–323.
5. Fulgham P, Bishoff J. Urinary tract imaging: basic principles. In: Kavoussi L, Novick A, Partin A, Peters C, editors. Campbell-Walsh urology, vol. 1. 10th ed. Philadelphia, PA: Elsevier Saunders; 2011. p. 99–139.
6. Fried AM, Woodring JH, Thompson DJ. Hydronephrosis of pregnancy: a prospective sequential study of the course of dilation. J Ultrasound Med. 1983;2(6):255–9.
7. Rasmussen PE, Nielsen FR. Hydronephrosis during pregnancy: a literature survey. Eur J Obstet Gynecol Reprod Biol. 1988;27(3):249.
8. Schulman A, Herlinger H. Urinary tract dilation in pregnancy. Br J Radiol. 1975;48:638–45.
9. MacNeily AE, Goldenberg SL, Allen GJ, et al. Sonographic visualization of the ureter in pregnancy. J Urol. 1991;146:298–301.
10. Park SJ, Yi BH, Lee HK, et al. Evaluation of patients with suspected ureteral calculi using sonography as an initial diagnostic tool. J Ultrasound Med. 2008;27:1441–50.
11. Singh I, Strandhoy JW, Assimos DG. Pathophysiology of urinary tract obstruction. In: Wein AJ, editor. Campbell-Walsh urology. 10th ed. Philadelphia, PA: Elsevier Saunders; 2011. p. 1087–121.
12. Peake SL, Roxburgh HB, Langlois SL. Ultrasonic assessment of hydronephrosis of pregnancy. Radiology. 1983;146:167–70.
13. Nyholm JL, Brost BC, Watson WJ. Maternal hydration status affects pelvic calyceal diameter in pregnancy. Am J Perinatol. 2008;25(3):157–9.
14. Ellenbogen PH, Scheible FW, Tainer LB, et al. Sensitivity of gray scale ultrasound in detecting urinary tract obstruction. AJR Am J Radiol. 1978;130:731–3.
15. Boridy I, Maklad N, Sandler C. Suspected urolithiasis in pregnant women: Imaging algorithm and literature review. AJR Am J Radiol. 1996;167:869–75.
16. Deyoe LA, Cronan JJ, Breslaw BH, et al. New techniques of ultrasound and color Doppler in the prospective evaluation of acute renal obstruction: Do they replace the intravenous urogram? Abdom Imaging. 1995;20:58–63.
17. Tublin ME, Dodd GE, Verdile VP. Acute renal colic: diagnosis with duplex Doppler ultrasound. Radiology. 1994;193:697–701.
18. Platt JF, Rubin JM, Ellis JH, et al. Distinction between obstructive and non obstructive pyelocaliectasis with duplex Doppler sonography. AJR Am J Roentgenol. 1989;153:997–1000.
19. Calenoff L, Lin PJ, Ward WF. Radiology in obstetrical practice. In: Silvio A, editor. Obstetric practice. CV Mosby: St. Louis; 1980. p. 242.
20. Hill MC, Rich JI, Mardiat JG, Finder CA. Sonography vs. excretory urography in acute flank pain. AJR Am J Radiol. 1985;144:1235–8.
21. Shokeir AA, Abdulmaaboud M. Prospective comparison of nonenhanced helical computerized tomography and Doppler ultrasonography for the diagnosis of renal colic. J Urol. 2001;165:1082–4.
22. Olin JW, Piedmonte MR, Young JR, et al. The utility of duplex ultrasound scanning of the renal arteries for diagnosing significant renal artery stenosis. Ann Intern Med. 1995;122:833–8.
23. Tublin ME, Buda RO, Platt JI. The resistive index in renal Doppler sonography: where do we stand? AJR Am J Radiol. 2003;180:885–92.
24. Hertzberg BS, Carroll BA, Bowie JP, et al. Doppler US assessment of maternal kidneys: analysis of intrarena1 resistivity indexes in normal pregnancy and physiologic pelvicaliectasis. AJR Am J Radiol. 1993;186:689–92.
25. Soria Gálvez F. Usefulness of renal resistive index in the diagnosis and evolution of the obstructive uropathy Experimental study. Actas Urol Esp. 2007;31(1):38–42.
26. Shokeir AA. Renal colic in pregnant women: role of renal resistive index. J Urol. 2000;55(3):344–7.
27. Renowden SA, Cochlin DC. The effect of intravenous furosemide on Doppler wave form in normal kidneys. J Ultrasound Med. 1992;11:65.
28. Shokeir AA, Provost AP, El Azab M, et al. Renal Doppler ultrasound in children with obstructive uropathy: effect of intravenous normal saline fluid load and furosemide. J Urol. 1996;156:1455.
29. Farmakides G, Schulmand H, Schneider E. Surveillance of pregnant hypertensive patient with Doppler flow velocimetry. Clin Obstet Gynecol. 1992;35:387–94.
30. Mallek R, Bankier AA, Etele-Hainz A, et al. Distinction between obstructive and non obstructive hydronephrosis: value of diuresis duplex Doppler sonography. AJR Am J Radiol. 1996;166:113–7.
31. Jerde TJ, Calamon-Dixon JL, Bjorling DE, et al. Celecoxib inhibits ureteral contractility and prostanoid release. Urology. 2005;65:185.
32. Pozniak MA, Kelcz F, Stratta RJ, Oberley TD. Extraneous factors affecting resistive index. Invest Radiol. 1988;23:899–904.

33. Sjodin JG. Clinical experience of indomethacin in pain from ureteral stone. Scan J Urol Nephrol. 1983;75:35–6.
34. N'Guyen Tand Lung R, Cirarci-Vigneron N, Rabbe A, et al. Interet de l'echographie du rein maternel pendant la grassesse. Annual Radiology (Paris). 1986;20:381–3.
35. Grenier NL, Parient JL, Trillaud H, et al. Dilatation of the collecting system during pregnancy: physiologic vs obstructive dilatation. Eur Radiol. 2000;10(2): 271–9.
36. Faudes A, Bricola-Rilho M, Pinto E, et al. Dilatation of urinary tract during pregnancy: proposal of a curve of maximal caliceal diameter by gestational age. Am J Obstet Gynecol. 1998;178:1082–8.
37. Burge HL, Middleton WB, McClennan BL, et al. Ureteral jets in healthy patients and in patients with unilateral ureteral calculi: comparison with color Doppler ultrasound. AJR Am J Radiol. 1991;180: 437–42.
38. Cox IH, Erickson SJ, Foley WD, et al. Ureteral jets: evaluation of normal flow dynamics with color Doppler sonography. AJR Am J Roentgenol. 1992;158:1051–5.
39. Baker SM, Middleton WD. Color Doppler sonography of ureteral jets in normal volunteers: Importance of the relative specific gravity of urine in the ureter and bladder. AJR Am J Roentgenol. 1992;159:773–5.
40. Dubbins PA, Kurtz AB, Darby J, Goldberg B. Ureteric jet effect: the echographic appearance of urine entering the bladder. AJR Am J Radiol. 1981;140:513–5.
41. Delair SM, Kurzrock EA. Clinical utility of ureteral jets: disparate opinions. J Endourol. 2006;20(2):111–4.
42. Laing FC, Benson CB, DiSalvo DN, et al. Distal ureteral calculi: detection with vaginal ultrasound. AJR Am J Radiol. 1994;192:545–8.
43. Damani N, Wilson SR. Non gynecologic application of transvaginal US. Radiographics. 1999;19: S179–200.
44. Lee JY, Kim SH, Cho JY, et al. Color and power Doppler twinkling artifacts from urinary stones: clinical observation and phantom studies. AJR Am J Radiol. 1992;159:773–5.
45. Karabulut N, Karabulut A. Color Doppler evaluation of ureteral jets in normal second and third trimester pregnancy: Effect of patient position. Br J Radiol. 2002;75(892):351–5.
46. Swartz HM, Reichling BA. Hazards of radiation exposure for pregnant women. JAMA. 1978;239: 1907–8.
47. Dudd III GD, Tublin ME, Shah A, et al. Imaging vascular complications associated with renal transplants. AJR Am J Radiol. 1991;157:449–59.
48. Schwaighafer B, Kainberger F, Fruehwald F, et al. Duplex sonography of normal renal allografts. Acta Radiol. 1989;30:53.
49. Braun B, Weilemann LS, Weigand W. Ultrasonographic demonstration of renal vein thrombosis. AJR Am J Radiol. 1989;138:157–8.
50. Kaveggia LP, Parrella RR, Grant EG, et al. Duplex Doppler sonography in renal allograph: the significance of reversed flow in diastole. AJR Am J Radiol. 1990;155:295–8.
51. Reuther G, Wanjura D, Bauer H. Acute renal vein thrombosis in renal allografts: detection with duplex Doppler ultrasound. AJR Am J Radiol. 1989;170: 557–8.
52. Kohler TR, Zierler RE, Martin RL, et al. Non invasive diagnosis of renal artery stenosis by ultrasonic duplex scanning. Vasc Surg. 1986;4:450–6.
53. Gottlieb RH, Lieberman JL, Paico RC, et al. Diagnosis of renal artery stenosis in transplanted kidneys: value of Doppler waveform analysis of the intrarenal arteries. AJR Am J Radiol. 1995;165:1441–6.
54. Nazzal MM, Hoballah JJ, Miller EV, et al. Renal hilar Doppler analysis is of value in the management of patients with renovascular disease. Am J Surg. 1997;174:164–8.
55. House MK, Dowling RJ, King P. Using Doppler sonography to reveal renal artery stenosis. An evaluation of optimal imaging parameters. AJR Am J Radiol. 1999;173:761–5.

Intraoperative Urologic Ultrasound

14

Fernando J. Kim, Kyle Rove, and David E. Sehrt

Types of Transducers (Fig. 14.1)

Linear: The linear array scanners produce sound waves parallel to each other which generate a rectangular image. The width of the image and number of scan lines are the same at all tissue levels. Thus coupled with high-frequency settings, this probe has great near-field resolution. The linear transducer can be used for viewing surface texture of the liver. The disadvantage of this probe is the tendency for artifacts when applied to a curved part of the body which generate air gaps between skin and transducer.

Sector/vector: It produces a fanlike image that is narrow near the transducer and increases in width with deeper penetration. It is useful when scanning between the ribs as it fits in the intercostal space. The disadvantage is poor near-field resolution.

Curved: The curved probe is a compromise of the linear and sector scanners. The density of the scan lines decreases with greater distance from the transducer, but not to the level as sector scanners. Often imaging requires greater depth of the acoustic waves, so lower frequencies (3–5 MHz) are used. This lower frequency also allows scanning for patients with various body habitus. The curved probe may be difficult to use in curved regions of the body, e.g., the spleen behind the left costal margin.

Laparoscopic ultrasound (*LUS*): Laparoscopy with the assistance of ultrasound avoids unnecessary open surgery and improves selection of patients for renal and adrenal tumor resection. The diameter is less than 10 mm to allow introduction through a 10–11-mm laparoscopic port. The length is typically 35–50 cm and with articulating tips to allow imaging to any location in the abdominal cavity. LUS enables direct contact of the probe with the target tissue thus enabling the use of high-frequency (6–10 MHz) waves to improve resolution with a depth of 4–10 cm. LUS may be used to identify and characterize tumors, guide biopsy needles, probes, and monitor the freezing zone during cryoablation. Challenges of LUS include limitations of the small working space resulting in images from oblique planes.

Transrectal ultrasound: (a) *End fire* is a linear array whose direction of maximum radiation is along the axis of the array; it may be either unidirectional or bidirectional; the elements of the array are parallel and in the same plane, as in a fishbone antenna. (b) *Biplane is* composed of two arrays: one linear for imaging of the longitudinal plane and a highly curved one to image the

F.J. Kim, MD, FACS (✉) • D.E. Sehrt, BS
Department of Surgery/Urology, University of Colorado Health Science Center, Denver Health Medical Center, Tony Grampsas Cancer Center, 777 Bannock Street MC 0206, Denver, CO 80204, USA
e-mail: fernando.kim@dhha.org

K. Rove, MD
Department of Urology, University of Colorado Health Science Center, Aurora, CO, USA

P.F. Fulgham and B.R. Gilbert (eds.), *Practical Urological Ultrasound*, Current Clinical Urology,
DOI 10.1007/978-1-59745-351-6_14, © Springer Science+Business Media New York 2013

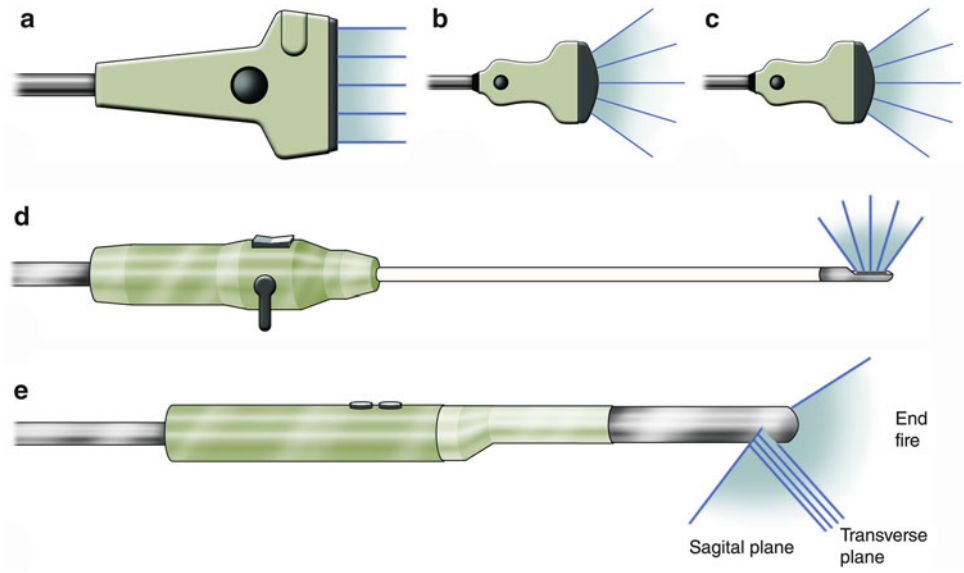

Fig. 14.1 Ultrasound probes used in urology. (**a**) Linear array (**b**) section/vector (**c**) curved array (**d**) laparoscopic (**e**) transrectal biplane

transverse plane. These two planes allow simultaneous visualization of perpendicular planes in real time.

The Kidneys

The same principles and techniques to perform renal procedures guided by ultrasonography apply to interventional techniques.

Percutaneous Nephrostomy and Percutaneous Nephrolithotomy

Percutaneous access to the renal collecting system was first described in 1955 by Goodwin et al. as a means to either drain or stent an obstructed urinary system [2]. Beyond the usual indications for an obstructed urinary system, percutaneous nephrostomy (PCN) can be used to access the collecting system in an antegrade manner for definitive treatment of nephrolithiasis, commonly performed by laser lithotripsy [3]. Generally, for percutaneous approach the left kidney is more challenging than the right due to the rib cage as described previously during the Kidney US chapter. Reports show that only 11% of urologists perform their own PCN access and majority uses fluoroscopic guidance, but given appropriate training and use of ultrasound guidance, this technique still remains well within the realm of the urologist as seen in some European and Asian countries [4–6].

Ultrasound probe: For adult abdominal scanning, a curved-array transducer 3–5 MHz is used. For pediatric patients, a higher-frequency transducer may be utilized. The use of color Doppler provides good visualization of vascular structures within the kidney, and the probes usually allow attachments that can display the path of the needle towards the target (calyx or stone).

Technique: Hydronephrosis on ultrasound will demonstrate enlarged renal calyces and pelvis that appear black (hypoechoic), indicating the presence of fluid. While acute hydronephrosis generally does not affect renal parenchyma, chronic obstruction of the urinary tract can result in thinning of the renal cortex (atrophy) and blunting of the renal papillae. Renal stones are identified as hyperechoic structure on US with shadowing, and color Doppler can identify vascular structures (Fig. 14.2). Presence of these

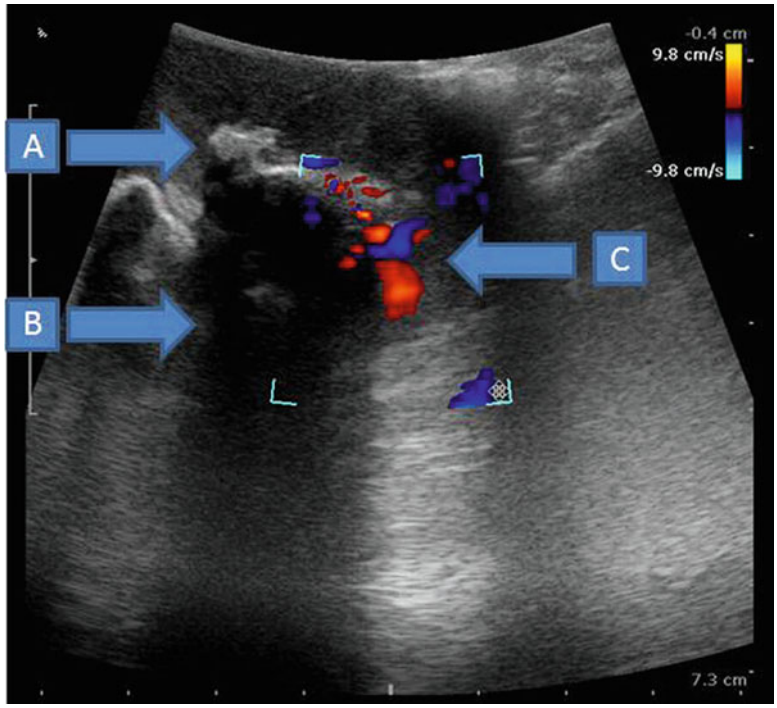

Fig. 14.2 Large hyperechoic renal stone with acoustic shadowing and color Doppler of vessels. (**a**) Large renal stone (**b**) acoustic shadowing (**c**) vessels on color Doppler

findings on ultrasound examination should be noted. Additionally, the operator should attempt to visualize the ureter, which may be dilated depending on etiology.

There are several described techniques, but the two most common are a one-stab technique and the Seldinger technique for placement of a PCN tube. The one-stab technique is usually reserved for moderately to severely dilated collecting systems. Meanwhile the Seldinger technique can be applied with or without dilation of the tract [7]. Both techniques are performed with the patient in a prone, prone-oblique position (Fig. 14.3). Recently, the supine position has been popularized for percutaneous nephrolithotomy (PCNL) [8]. The one-punch technique involves the use of ultrasound imaging to guide placement of a hollow 18-gauge needle with a sharp, beveled edge mounted to a pigtail catheter. Once inserted into the hydronephrotic collecting system and a flash of urine is obtained, the catheter can be slid over the needle and the needle subsequently removed [9]. Real-time ultrasound is used at all times to monitor the target and

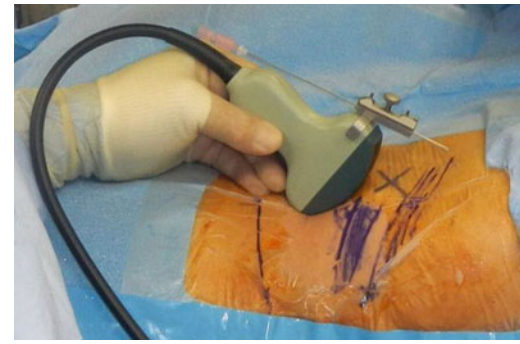

Fig. 14.3 Percutaneous nephrolithotomy with needle-probe attachment. *Blue* marking of ribs

ensure that the needle, wire, and dilators enter the calyx and do not violate other structures (Fig. 14.4). If only drainage is needed, a 12-French PCN tube can then be inserted over the wire with curl confirmation on ultrasound imaging. Imaging can be enhanced by injecting sterile saline to identify the collecting system under US guidance. Further serial dilation or inflating balloon dilators can be performed with dilators up to the size of the instrument sheath (24 °F), ensuring

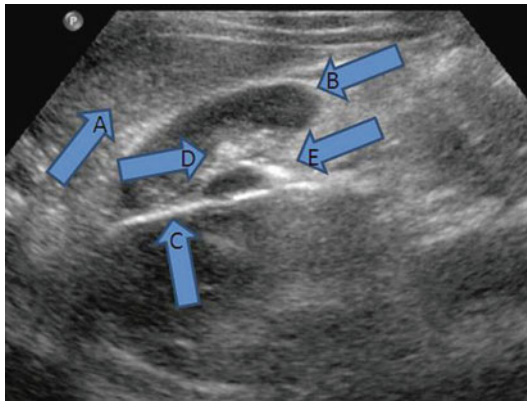

Fig. 14.4 Transverse view of the right kidney. (**a**) Liver (**b**) right kidney (**c**) percutaneous needle (**d**) collecting system (**e**) stone

that the wire remains in place for access purposes throughout the operation. In case of staghorn calculi, ultrasound guidance towards the stone or puncture of an alternate calyx may be required. The patient in a prone position allows the US probe to examine from the most lateral side of the abdomen under the rib cage and scan medially to enable a global view of the anatomy. The serious limitation of the ultrasound probe is the two-dimensional view of the kidney, calices, and the path which the needle may traverse injuring a viscera. The risk factors for colonic perforation are the following: the presence of colonic distension due to previous intestinal bypass surgery, female sex, elderly, thin patients, the presence of a horseshoe kidney, and previous renal surgery placing the colon in a more retroperitoneal position. The incidence of colonic injury is also greater on the left side, with a lower caliceal puncture, and with an extreme lateral origin of the percutaneous puncture [10]. Nevertheless, no statistically significant evidence has shown the implication of these factors in the development of colonic injury. Moreover, injuries to the spleen may occur on the left and liver on the right PCNL or PCN.

Clinical data: There has been one randomized trial that compared ultrasound-guided PCNL access to traditional fluoroscopic access and found comparable results with less exposure to ionizing radiation but longer access time (11.0 min vs. 5.5 min) [11]. In a large series of ultrasound-guided PCN by urologists, complications included urinary tract infection (1.1%), hemorrhage (1.9%), sepsis (0.76%), inferior vena cava injury (0.15%), gall bladder injury (0.15%), and death (0.3%). Overall, major complications occurred in 3.3% of patients (3–6.7% in various series) and minor complications in 5% (5–38% in various series) [12–14]. Successful PCN has been reported in these series as 90–95%. PCN and PCNL under ultrasound guidance are safe and highly successful techniques in the hands of a trained urologist.

Percutaneous Renal Biopsy

Renal biopsy can be divided in two groups of patients: (1) patients with an abnormal mass to rule out malignancy or (2) patients with medical renal disease that requires histologic diagnosis. In both groups of patients ultrasound imaging aids significantly to identify the suspected area. As discussed in other chapters of this book, the left renal US is often more challenging than the contralateral side due to the anatomic position.

Ultrasound probe: The use of curved-array 3.5–5-MHz probes with or without color Doppler provides good visualization and allows attachments that can display the path of the needle placement towards the target.

Technique: The technique is similar to PCNL. The target is different: (a) solid mass to rule out malignancy or (b) renal cortex to evaluate medical renal disease. As a general rule, percutaneous renal biopsy can be easily performed in nonobese patients and also transplanted kidneys since they are placed in the iliac fossa. The technique is similar to percutaneous renal procedures. If the colon is causing visual obstruction, rotate the patient and scan the kidney from posterior to anterior until the target is visualized. Preparation of the patient by fasting the night prior to the procedure may further improve visualization.

Clinical data: In the analysis of 623 renal biopsies guided by real-time ultrasound, the effectiveness

was 97.6% with 110 complications. Fourteen (2.24%) were major complications (Clavien ≥3): 9 cases of renal hematoma, 2 cases with macroscopic hematuria (which required blood transfusion), 1 case of intestinal perforation (which required exploratory laparotomy), 1 nephrectomy, and 1 case of a dissecting hematoma. The author concluded that the risk factors for developing major complications were the following: diastolic blood pressure ≥90 mmHg, RR 7.6 (95% CI 1.35–43); platelet count ≤120 × 103/μL; RR 7.0 (95% CI 1.9–26.2); and blood urea nitrogen (BUN) ≥60 mg/dL, RR 9.27 (95% CI 2.8–30.7) [15].

Laparoscopic Ablative and Partial Nephrectomy

Historically, radical nephrectomy has been the treatment of choice for patients with renal masses, but our understanding and appreciation of nephron-sparing surgery for small renal masses ≤4 cm (and more recently, ≤7 cm in select patients) with regard to cancer control and preservation of renal function has increased dramatically in recent years [16–18]. There has been a recent migration towards nephron-sparing approaches as innovations with minimally invasive techniques continue [19]. The application of probe ablation therapies such as cryoablation and radio-frequency ablation, although promising, is currently not the treatment option of choice when compared to partial nephrectomy due the lack of long-term outcome data. Although percutaneous approach of the kidney for ablative procedures is feasible, the preferred imaging modality used to treat the renal masses by interventional radiologists has been CT scan. However amongst urologists, a laparoscopic approach using ultrasonography is more commonly implemented. Therefore, we will describe the use of laparoscopic ultrasonography for these procedures.

In the early 1990s, cryotherapy was reintroduced for the treatment of prostate cancer after study in animals and human trials in the 1970s and 1980s. On the basis of these experimental and clinical studies, an optimal drop in temperature of −40 °C is required to achieve total cell death [20]. Although many theories were suggested for the underlying mechanism of the cryoablative tissue effect, the vascular component of initial vasoconstriction followed by reperfusion injury (increased capillary permeability) triggered by the thawing phase is considered to be the primary mechanism of tissue damage. However, intracellular crystallization and subsequent water shifting during the thawing phase also contribute significantly to the rupture of the cell membrane and irreversible cellular death [21].

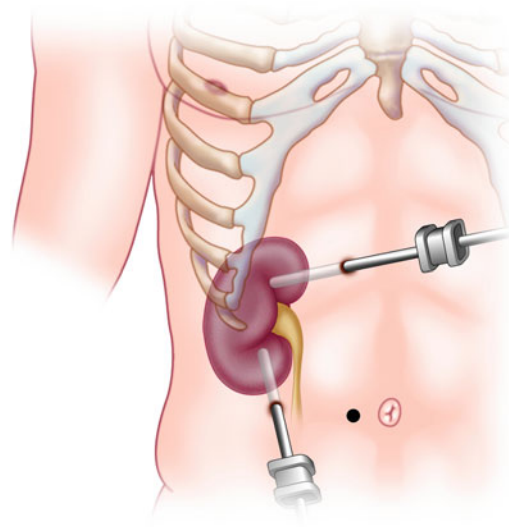

Fig. 14.5 Laparoscopic ultrasonic probe placement through a 10-mm trocar

Ultrasound probe: Laparoscopic renal ultrasound will often be performed with a 6–10-MHz linear array transducer. Endoluminal probes of 10–12 MHz may be used for transureteral evaluations. The 7.5-MHz flexible side-viewing laparoscopic transducer offers distinct capability to contour the organ. The rigid 7.5-MHz linear side-viewing laparoscopic transducer is easier to operate and is preferred by surgeons. Both types of transducers use a 10-mm laparoscopic port for introduction to the abdominal cavity (Fig. 14.5).

Technique: LUS imaging and orientation may not be intuitive and easy to understand the exact position of the lesion or particular regions of the target. The universal orientation left/cephalad also applies to LUS, but prior to the scan one should

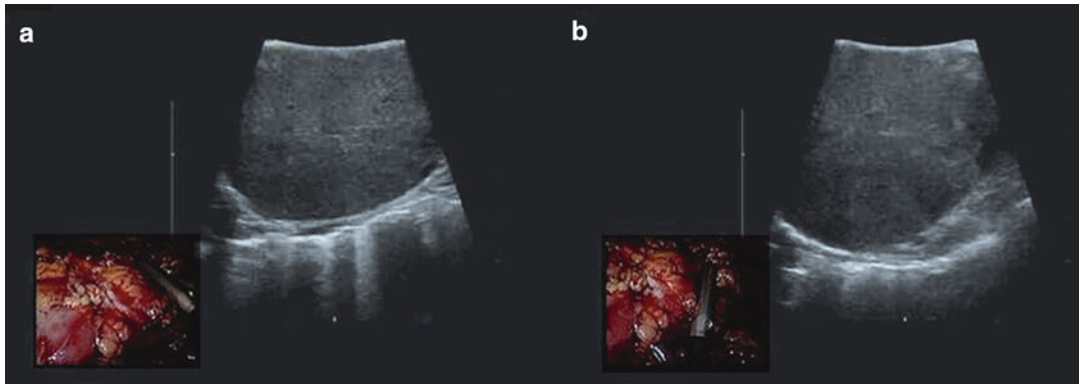

Fig. 14.6 Picture-in-picture of laparoscopic US during partial nephrectomy evaluates tumor size and depth to ascertain safe surgical margins. (**a**) lateral aspect of the renal tumor (**b**) medial aspect of the renal tumor

tip the end of the LUS to visualize the left side of the monitor and run along the crystals of the probe to translate the images of the US with the location in the monitor. For example, if only the tip of the LUS probe is touching the lesion, the image will be displayed only on the right side of the monitor. As the probe travels from the tip to the base of the probe, the image will be displayed in the entirety of the monitor (Fig. 14.6).

Indications for ultrasound-guided ablative therapy include small tumors (≤4 cm in diameter), older age, higher-risk patient, solitary kidney, and surgically scarred abdomen. Larger tumors and proximity to hilar vessels may be relative contraindications to ablative kidney surgery.

The size and optimal port placement are pivotal for LUS evaluation of renal lesions. The port size must be at least 10 mm. Generally, the posterior lesions are more challenging to be scanned. Either right or left side upper pole posterior lesions are best evaluated through an ipsilateral midclavicular or subxiphoid port. Anterior lesions can be evaluated almost through any port position. For a renal lesion biopsy and ablation, the needle or ablation probes are passed percutaneously through the abdominal wall. In general, multiple core biopsies (between 3 and 5) are taken with a 14- or 18-gauge needle under visual and ultrasonic guidance. Equally, the "rocking" maneuver allows the identification of the hyperechoic needle/probes and visualization of ablated tissue (Fig. 14.7).

Clinical data: A cryosystem consisting of argon (freezing phase) and helium (thawing phase) gases (Joule-Thomson effect) was used. Ultrasonic evaluation of the kidney should reveal suspect lesions. Simple cysts are generally spherical or ovoid, lack internal echoes, have a smooth, thin wall, and should show enhancement of the posterior wall indicating the presence of water. Lesions of suspect nature can include those with multiple septae, calcifications, or heterogeneous appearance that differentiates the lesion from healthy renal parenchyma [22]. The cryoneedles are introduced under real-time ultrasound guidance and will appear as hyperechoic structures with resultant shadowing. The borders of the ice ball can be readily identified on ultrasound as a hyperechoic rim (Fig. 14.8) which is generated by the interface between frozen and unfrozen tissues. The ice ball should be extended 1 cm beyond the visible border of treated lesions circumferentially to ensure negative margins. When thawed, the lesion will continue to remain hyperechoic compared with the surrounding kidney parenchyma [23]. All lesions should undergo two cycles of freezing and thawing.

The Adrenal Gland

Ultrasonography of the adrenal gland is technically difficult and is better evaluated by other imaging studies, i.e., CT scan and MRI [24]. LUS is a valuable adjunct to laparoscopic

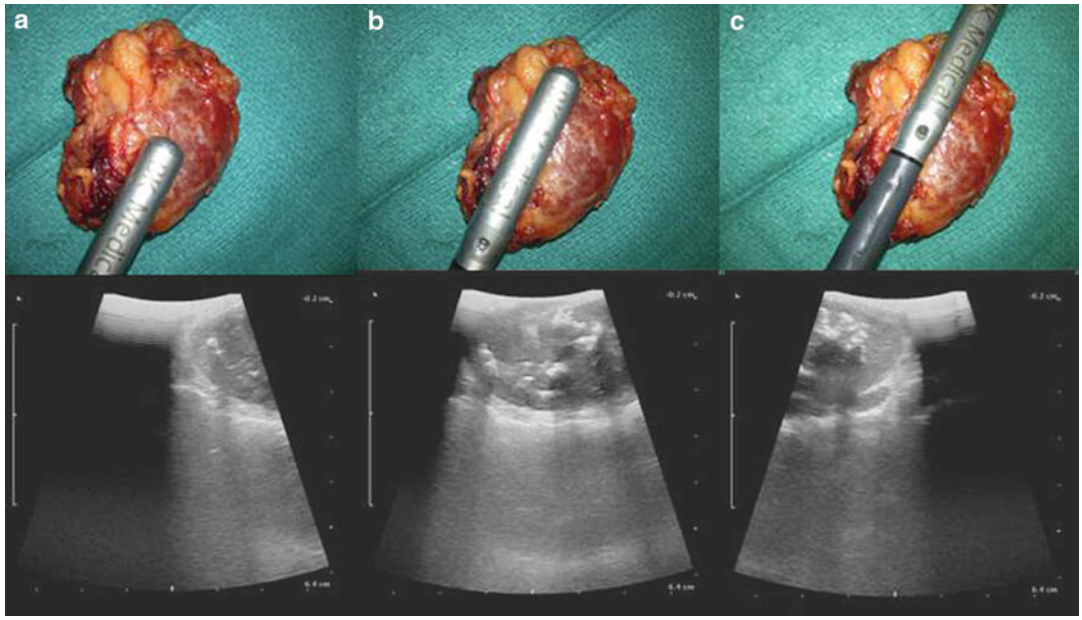

Fig. 14.7 Using the skiing technique across renal mass. The universal orientation of the laparoscopic probe is as follows: tip of the transducer is left and cephalad; therefore in (**a**) the distal end of the probe will demonstrate the adrenal mass on the right side of the monitor. When the transducer allows larger surface area contact, the image will show in the monitor (**b**) until only the base of the transducer is touching the adrenal mass and displaying the image on the left corner of the monitor (**c**) proximal end will demonstrate the adrenal mass on the left side of the monitor

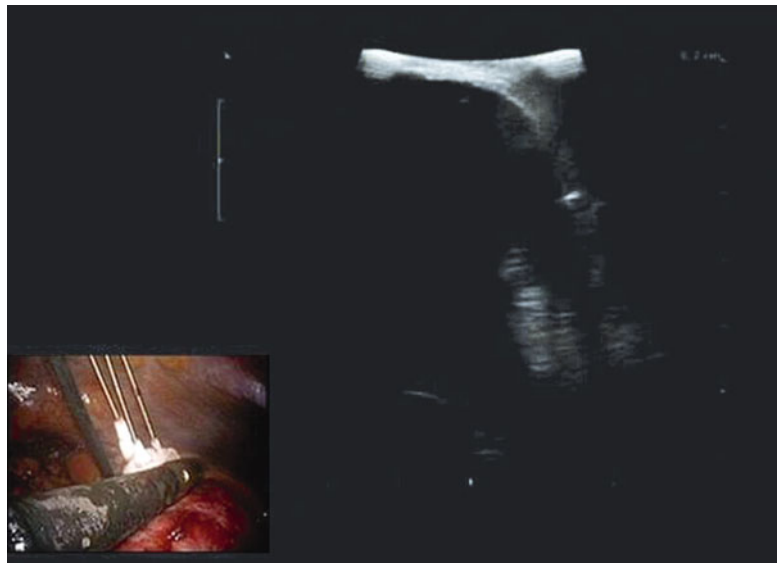

Fig. 14.8 Hyperechoic rim represents the outer layer of the ice ball. The homogeneous hypoechoic image is the ice ball that can be appreciated as the probes move towards the normal renal parenchyma

adrenalectomy facilitating tumor localization and identification of adjacent structures to direct the dissection particularly for partial adrenalectomies. Although large lesions on either side are easily identified, laparoscopic US may facilitate identification of small tumors in obese patients and right-sided lesions that are usually partially retrocaval.

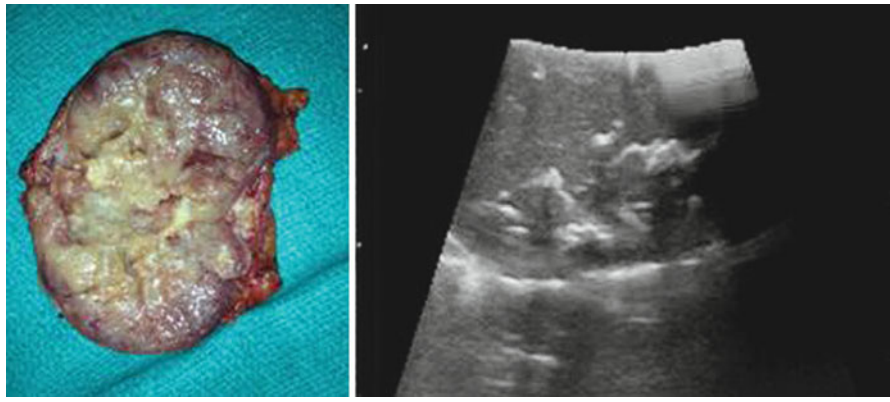

Fig. 14.9 An adrenal gland with ovarian metastasis. Gross anatomy with internal calcifications identified during laparoscopic adrenalectomy and use of LUS

Ultrasound probe: Although the flexible side-viewing 7.5-MHz rigid laparoscopic transducer offers distinct capability to contour the organ, often surgeons find the rigid, linear side-viewing transducer the simplest and most convenient to use in adrenal surgery.

Technique: In the transabdominal technique, the patient is placed in the modified flank position with 3–4 trocars inserted subcostally on the right and three trocars on the left, on an axis between the midclavicular and the midaxillary lines. After the dissection along the gutter to deviate the liver or the spleen medially to expose the suprarenal retroperitoneum, the laparoscopic transducer is inserted through the 10- or 12-mm port on the anterior axillary line or subxiphoid port. If the adrenal gland has not been identified, the upper pole of the kidney should be scanned demonstrating characteristic appearance of its parenchyma with the cortex and the collecting system. Then the transducer is advanced cephalad in the longitudinal plane until the adrenal gland is identified. Large tumors are easily identified and the value of intraoperative sonography in these cases is in elucidating their relationship with the kidney, aorta, spleen, and the tail of the pancreas on the left and the kidney, inferior vena cava, and the liver on the right side, respectively. The use of flow color Doppler also helps to identify the aorta and the inferior vena cava. Nonsecreting and secreting adenomas have a similar ultrasonographic appearance. They are usually less than 3 cm and have a very low echodensity. They sometimes contain cystic and calcified areas. Pheochromocytomas may appear as solid or cystic or may have both solid and cystic components. Hypoechoic areas represent necrosis and hyperechoic areas indicate hemorrhage. The ultrasound appearance of adrenal hyperplasia is of smooth enlargement with a normal echo pattern. Adrenal cortical carcinoma of 3–6 cm shows a homogeneous echo pattern similar to renal cortical tissue. Larger lesions vary in ultrasonographic appearance, having a heterogeneous appearance with focal or scattered hypoechoic or hyperechoic zones representing areas of tumor necrosis, hemorrhage, or, rarely, calcification. Metastatic adrenal tumors usually have an ovoid shape and variable echogenicity (Fig. 14.9). Adrenal cysts appear as anechoic masses with enhanced posterior sound transmission, whereas myelolipomas are highly echogenic because of their fat content. Although the use of LUS facilitates tumor evaluation and identification of adjacent structures, especially large vessels, in cases or pheochromocytoma and adrenal cortical carcinomas, compression of the adrenal gland may have very harmful effects either triggering catecholamine release or rupture of the malignant tumor causing spread of cancer.

Clinical experience: Contrast-enhanced ultrasonography has been employed in Europe and

other countries to evaluate hypervascularity and correlate with malignancy. Hijioka et al. reported their experience on contrast-enhanced endoscopic ultrasonography (CE-EUS) to identify adrenal mass hypervascular lesions and perform EUS-guided fine needle aspiration (EUS-FNA). They concluded that this imaging modality can assist in the diagnosis of metastatic lesions, i.e., clear cell carcinoma leading to adrenalectomy and confirmation of metastatic clear cell carcinoma of the kidney [25]. Additional reports of ultrasound and/or CT scan-guided percutaneous cryoablation of adrenal masses have shown encouraging cost-effective outcomes. This procedure was associated with very low morbidity and local tumor recurrence rates and increased overall survival. Even as an adjunct to systemic therapies, it seems that percutaneous cryoablation of adrenal masses appeared cost-effective for palliation [26].

The Bladder

Suprapubic Tube Placement or Suprapubic Aspiration

Aspiration or trocar suprapubic tube placement (SPT) or "punch" suprapubic tube, as they are commonly referred, can offer quick drainage of the urinary bladder. The clinical scenario that necessitate SPT placement is the inability of the patient to void (posterior urethral disruption, urethral stricture) or when invasive urethral procedure may trigger sepsis (acute prostatitis) or autonomic dysreflexia (spinal cord injury patients) [27, 28]. The primary risk associated with this technique is perforation of bowel overlying the urinary bladder and open SPT approach must be applied in these patients.

Ultrasound probe: The use of curved-array 3.5–5-MHz probes with or without color Doppler provides good visualization and allows attachments that can display the path of the introducing needle towards the bladder. In the absence of this type of probe a linear array can be used to rule out bowel interposition between the skin and the bladder.

Technique: For ultrasound-guided trocar (SPT) placement or aspiration, the urologist should inquire the past surgical history of the patient, as prior abdominal operations could signify increased risk for bowel overlying the urinary bladder. On exam, the patient should have a distended bladder prior to the procedure and no scars that include the lower abdomen. Typical ultrasonography findings should include a variable-thickness bladder wall and dark homogeneous fluid content representing urine. One may survey the infraumbilical area and detect bowel contents represented by dark dynamic shadowing images representing peristalsis with gas content or any intervening tissue planes or heterogeneous echogenicity between the abdominal wall and urinary bladder. Presence of large blood clots also interferes with the hypoechoic characteristic of a full bladder. Further ruptured bladders will be difficult visualizing since the bladder may be empty. "Rocking" of the US probe will verify needle and catheter placement in a full bladder, and immediate urine drainage should be observed after initial puncture. The US probe follows the universal left/cephalad position and it should be positioned approximately three fingerbreadths above the pubic bone allowing the SPT needle to be placed between the US probe and the pubic bone (Fig. 14.10).

However some cases may require exploratory laparotomy, thus allowing for direct visual placement of suprapubic cystotomy tube. In instances where surgery is not needed, however, percutaneous SPT may be desirable. Trocar SPT or "punch" suprapubic tube, as they are commonly referred, can offer quick drainage of the urinary bladder. The primary risk associated with placement is perforation of bowel overlying the urinary bladder. While blind techniques have certainly been described in the past, modern access to ultrasonography can assist the urologist in an outpatient, operative, or emergency room setting in mitigating risk. Alternatives to straight ultrasound-guided placement include optional cystoscopic visualization and the previously mentioned open cystotomy and SPT.

For ultrasound-guided trocar SPT, the urologist or proceduralist should inquire as to the

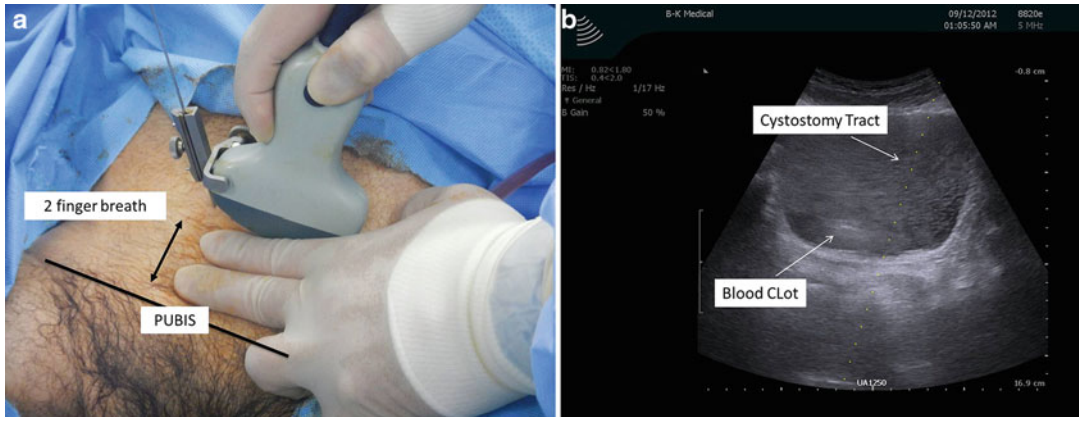

Fig. 14.10 (**a**) Placement of a suprapubic catheter. (**b**) The clear visualization of the full bladder demonstrates no interposing bowel

patient's past surgical history, as prior abdominal operations could signify increased risk for adhesions, particularly with respect to bowel overlying the urinary bladder. On exam, the patient should have a distended bladder prior to beginning the procedure. Typical ultrasonography findings should include a variable-thickness abdominal wall and dark, fluid-filled urinary bladder.

Clinical data: A total of 140 pediatric patients less than 2 years old that required suprapubic aspiration (SPA) were randomized to either an ultrasound-guided or ultrasound-unguided (control) protocol. The aspirations under ultrasound guidance were performed under ultrasound examination during insertion of the needle. SPA had an overall success rate in 90% of attempts (63/70) in the ultrasound-guidance group compared with 64% (45/70) in the no-ultrasound group ($p < 0.05$). There were fewer passes made in those patients who had the procedure done under ultrasound guidance ($p < 0.05$). Ozkan et al. demonstrated the use of ultrasonography as an assistant tool for SPA in centers where portable ultrasound guidance is available, in particular, for infants more than 1 month old [29]. There are several clinical scenarios for SPT including traumatic injury (posterior urethral disruption, intraperitoneal bladder perforation), short-term use for neurogenic bladder, and urinary retention (as in setting of stricture or other bladder outlet obstruction) [27, 28].

The Prostate

Transrectal Ultrasound

The advent of US technology has improved visualization, and 3D reconstruction of the prostate via transrectal US is under development. The transrectal probes are slimmer and offer a real-time simultaneous sagittal and transverse view of the prostate. Moreover, the prostate can be visualized by either a suprapubic or transrectal approach. The former does not offer complete evaluation of the prostate but may assist to define the presence of an intravesical prostate. We have recently demonstrated the correlation of US anatomical findings and comparative cadaveric anatomy of the external urethral sphincter. The rhabdosphincter can be appreciated in the US images as a hyperechoic triangle at the apex of the prostate (Fig. 14.11), and the cadaveric models demonstrated a significant amount of muscle fibers overlapping the prostatic apex [30].

Ultrasound probe: A biplane or end-fire transrectal ultrasound probe with frequency range of 6.0–9.0 MHz should be used to evaluate the prostate and surrounding structures. Prostate size and morphology may also be evaluated using a transabdominal approach with a curved linear array probe. The transrectal probe should be able to accommodate a needle guide for transrectal ultrasound-guided biopsy. The needle guide may be a single-use or a reusable device.

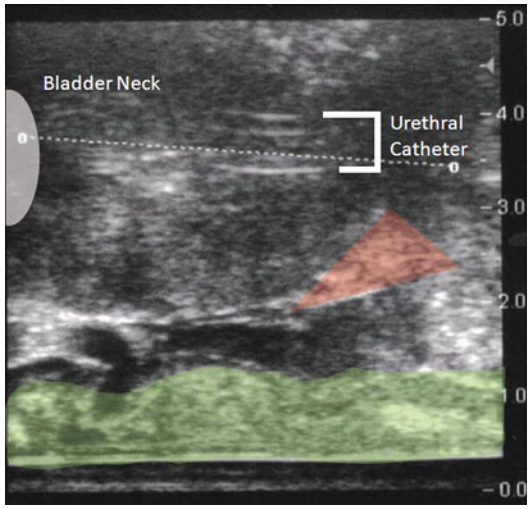

Fig. 14.11 Measurement of prostatic urethral length from the bladder neck to the prostate apex. The external sphincter is highlighted in *red*, the bladder neck in *white*, and the rectal wall in *green*

Technique: For optimal evaluation during transrectal ultrasound imaging, one must prepare the patient, giving instructions to clean the rectal vault. Presence of stool and gas compromises visualization. Fleet enema is recommended the night prior and the morning of the study. Slow introduction of the transrectal probe with lubrication in the rectum should be performed by gentle rotation and forward movement until the prostate is visualized. When a stepper is used, one may verify the correct model to use with different probes. Different techniques will be dependent on patient's position from lateral decubitus to lithotomy. The surgeon has to adjust and standardize images to transverse and sagittal views.

Transperineal Prostate Biopsies

The transperineal needle biopsy of the prostate is popular in Europe more than in the United States. While transperineal needle biopsy of the prostate was described as early as 1963, a grid-based, systematic, ultrasound-guided approach was not described until 2001 by Igal et al. Present biopsies involve the simultaneous use of image guidance via transrectal ultrasound with systematic sampling by either the standard sextant or whole gland mapping biopsies [31, 32]. Moreover, Barzell et al. describe extended biopsy technique with transrectal ultrasonography as an option for men with low-volume, low-grade, histologically proven prostate cancer who may be considering experimental targeted focal therapy. Prior to biopsy, the patient should undergo TRUS measurements of the prostate to ensure that the gland is not too large (<65 cm^3) and is not obstructed by the pubic arch. If the gland is too large or perineal access is partially obstructed, the patient can be started on 5α-reductase inhibitors and reevaluated every 3 months until the prostate is fully accessible. The procedure is generally performed in the clinic under local anesthesia with the patient in high lithotomy and use of a standard 5-mm interval brachytherapy perineal grid and a standard 18-gauge prostate needle biopsy gun. Five mm was determined to be the optimal grid size to ensure very few lesions are missed [33]. Cross-sectional ultrasound images are captured using a standard transrectal ultrasound probe, and these images are used to reconstruct the prostate in three dimensions by denoting borders of the gland. During the procedure, the urologist should note position of the urethra to avoid perforation with the biopsy gun. Care must be taken to ensure complete gland coverage by taking deeper (base) and shallow (apex) passes at the same grid position, as the length of the gland may be longer than a single pass of a standard 18-gauge biopsy needle. Each biopsy is labeled with *x*–*y*–*z* coordinates and placed in separate jars for histological analysis. Specialized software can then be used to combine pathology results (i.e., cancerous foci) with 3D model of the prostate generated from transrectal ultrasound images.

Cryotherapy

Cryotherapy was first proposed and used as a treatment for cancer in the nineteenth century. Using a combination of salt and ice applied to cervical and breast tumors, patients experienced less pain and decreased tumor size. Ultimately, conversion of air (oxygen and nitrogen) to their liquid forms and the ability to store them in adequate

quantities for regular use brought about a resurgence in use in the early twentieth century. The first cryoprobe was built by Cooper and Lee in 1961 and circulated liquid nitrogen, allowing them to freeze tissues that were in contact with the probe, and the first use in the prostate was in 1964 [34]. The advent of ultrasound as a monitoring tool made cryotherapy as an ablative tool more attractive for the treatment of prostate cancer. The AUA recognized cryotherapy for localized prostate cancer as a standard treatment option in 1996. Current devices are labeled third generation and use urethral warmers, a combination of argon (cooling) and helium (warming) gases taking advantage of the Joule-Thomson effect, and TRUS guidance.

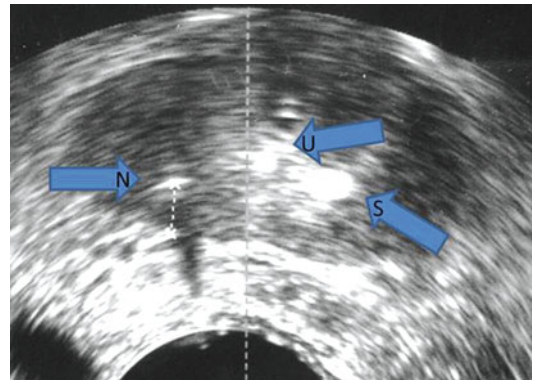

Fig. 14.12 Hyperechoic cryoablation needle (*N*) is observed and the distance to the prostate capsule may be measured. Additional left prostate stone (*S*) is visualized as well as the Foley catheter in the urethra (*U*)

Technique: With the patient in exaggerated lithotomy position, a brachytherapy template guide is placed on the perineum. A multifrequency biplanar transrectal ultrasound probe on a stepper is used for visualization of the prostate, urethra, bladder neck, and rectum. Temperature monitors are placed near Denonvilliers' fascia, external urinary sphincter, and neurovascular bundles, to monitor for appropriate level of freezing and avoid of thermal damage to these sensitive structures. Current recommendations state that temperature of these structures should remain above 15 °C. Cryoneedles are inserted under TRUS visualization into the grid to encompass either the entire gland or, in cases where focal therapy is desired, in the area of concern, identified by prior transperineal mapping biopsies (Fig. 14.12). Lastly, the urethral warmer is placed under cystoscopic guidance. For full-gland treatment, 2–4 mm of periprostatic tissues should be included in the treatment zone to ensure adequate cancer control. At the time of cystoscopy, the urethra is inspected for possible perforation of the needles or thermocouples, so that they can be moved prior to starting the freezing cycles. Freezing is carried out in an anterior-to-posterior direction to maintain TRUS visibility down to −40 °C for two freeze–thaw cycles. Visual guidance with ultrasound, though, has limitations that should be acknowledged prior to use [35, 36]. Ultrasound imaging cannot capture tissue temperature information during the procedure and changes visible in these images do not reliably correspond to specific temperature regions. Therefore, the temperature probes are placed before the cryoprobes. The identification of the external urinary sphincter must be well recognized by the surgeon to ensure proper probe placement to prevent urinary incontinence due to sphincter damage. We described the US findings and correlated with the studies in human cadaveric external urethral sphincter. The hyperechoic triangle distal to the apex of the prostate is the rhabdosphincter that has an important segment in the prostatic apex. The sphincter can be well demonstrated by pressing with the thumb over the base of the scrotum under the pubic arch [30]. Constant changes of views from sagittal to transverse and vice versa are required to evaluate the real-time progression of the ice ball to prevent rectal and urinary sphincter injury. The typical cryolesion is described as a well-marginated, hyperechoic rim with acoustic shadowing in the middle (Fig. 14.13). This hyperechoic rim obstructs the leading edge of frozen tissue, obscuring the true extent of affected area. Color Doppler may be useful to monitor blood flow around the rectum; however, this is not thought to be an objective monitoring tool. Complete thaw of the ice ball allows the visualization of the prostate as the beginning of the procedure.

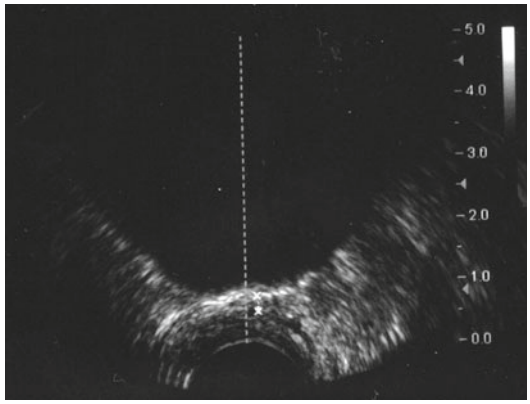

Fig. 14.13 Hyperechoic rim features of the external aspect of the ice ball during cryoablation of the prostate and the hypoechoic lesion representing the ice ball

Brachytherapy

Brachytherapy, or the placement of radioactive materials or seeds within the prostate, was first suggested by Alexander Graham Bell in 1908 [37–40]. Introduction of transrectal ultrasound-guided imaging offered the possibility of uniform distribution of the radioactive seeds for either permanent low-dose therapy (iodine-125, palladium-103) or temporary high-dose therapy (iridium-192) deposited into the prostate gland through a perineal template grid [41–43]. The introduction of image guidance also ensures seeds are not placed in close proximity to the urethra, nerves, or rectum, limiting side effects like lower urinary tract symptoms, erectile dysfunction, and fecal urgency. Ultrasound imaging during or at time of seed placement will generally reveal the hyperechoic needle and resultant shadowing. Similarly, seeds appear as small hyperechoic points. Assuring adequate dosimetry through appropriate placement of seeds remains paramount and has been shown to highly operator-dependent. However, computer-based planning systems coupled with TRUS imaging has allowed for precise and predictable seed placement that is reproducible (Fig. 14.14) [44]. Intraoperative preplanning replaces the need for an office visit with a planning session just prior to implantation in the operating room [45]. Because the exact number

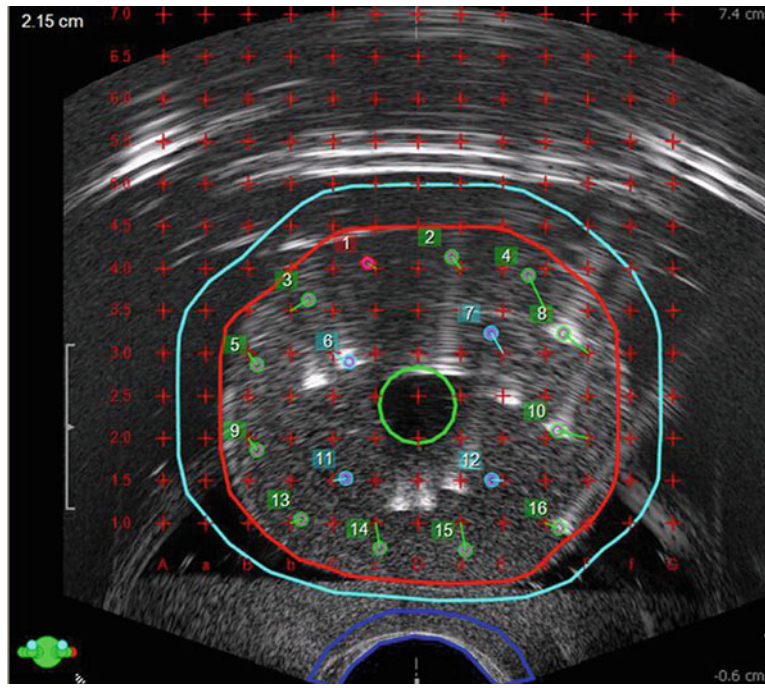

Fig. 14.14 Brachytherapy planning grid with positions of the brachy seeds. Seeds are visualized as hyperechoic objects

of required seeds is unknown prior to entering the OR, an approximate number are ordered according to a nomogram of gland volume derived from prior TRUS (at time of prostate biopsy) or CT. Biplanar TRUS imaging is performed in the exaggerated lithotomy position in the operating room and is fed to the treatment planning system. Transperineal implantation is then performed according to this plan. Biplanar TRUS imaging via US probe on a stepper is used to guide the needles throughout the procedure with confirmation of placement via fluoroscopy, since TRUS routinely cannot visualize anywhere from 2 to 45% of seeds during or after placement [46]. There are newer technologies that are under investigation looking at TRUS-fluoroscopy fusion imaging to verify seed placement and accurately verify dosimetry results during brachytherapy.

High-Intensity Focused Ultrasound

High-intensity focused ultrasound (HIFU) was first used over 15 years ago for the treatment of benign prostatic hypertrophy, and subsequently in 1996, Gelet et al. used this new technology for the treatment of patients with localized, low-grade adenocarcinoma of the prostate [47, 48]. HIFU is one such technique that can be used to focally ablate cancerous lesions using ultrasound energy to cause mechanical and thermal injury to the targeted tissue. HIFU, when used for the treatment of localized prostate cancer, uses a multifrequency ultrasound transducer placed in the rectum to generate acoustical energy that is focused on the tissue target, creating high temperatures and irreversible coagulative necrosis. HIFU utilizes a "trackless" principle, whereby tissue outside the focal plane is not damaged; the transrectal probe sits on the rectal mucosa and sends acoustical energy through the intervening tissues, only heating the tissue volume targeted by the probe [49]. The probe is repositioned mechanically as needed to target the prostate in its entirety. HIFU is performed with the patient placed under spinal or general anesthesia with prostate volumes greater than 40 cm^3 [50]. (Notably, study protocols of US trials do not permit the use of TURP prior to HIFU.) The prostate is visualized using real-time diagnostic images generated by the probe using lower, nondestructive acoustical energies (0.1–100 mW/cm^2). Once the target areas are identified, the prostate tissue is ablated with high energies (1,300–2,200 W/cm^2) focused in a small 1–3-mm-wide by 5–26-mm-long focal plane. Each pulse heats the tissue to 80–98 °C over a 3-s period. The gland is revisualized with lower ultrasound energies between ablative pulses. The probe is then moved and rotated in a semi-automated manner (device-dependent) using lower-energy diagnostic images to target adjacent prostate tissue. The end goal is to create overlapping lesions until the whole gland is treated. HIFU destroys target tissue through the thermal and mechanical effects of nonionizing, acoustical radiation (i.e., sound waves) delivered to target tissues after focusing by an acoustic lens, bowl-shaped transducer, or electronic phased array. Although not shown, the ablated area will become hyperechoic on lower-energy imaging. Because HIFU utilizes nonionizing radiation, it can be repeated one or more times during multiple sessions. The thermal effects are achieved by heating tissues to 60°C or higher, resulting in near-instantaneous coagulative necrosis and cell death [51]. By focusing the energy, more destruction occurs within the focal plane, but tissues outside the target area are spared of damage as energy intensities are far lower.

Laparoscopic Radical Prostatectomy

Ukimura, Gill, and colleagues recently described the use of real-time TRUS imaging of the prostate during laparoscopic prostatectomy, allowing for visualization of key structures such as the neurovascular bundles, bladder neck, and apex of the prostate, thus aiding in dissection [52].

Their report on intraoperative use of TRUS imaging for 25 consecutive patients notes the use of high-frequency 2D ultrasound imaging, power Doppler imaging, and 3D ultrasound imaging to aid in the identification of these key structures. In particular, the authors note that intraoperative use

of ultrasound aided in three primary aspects of the laparoscopic prostatectomy. Ultrasound aided in identification of the correct plane between the posterior bladder neck and base of the prostate, thus allowing for laparoscopic visualization of seminal vesicles and vasa deferentia. Secondly, the authors described the ability to identify the distal protrusion of the prostate apex posterior to the membranous urethra in difficult cases, thus enhancing apical dissection to ensure negative margins. Finally, the authors note that intraoperative ultrasound offered the ability to identify hypoechoic nodules abutting the prostate capsule, allowing the surgeon to perform a wide dissection around these locations.

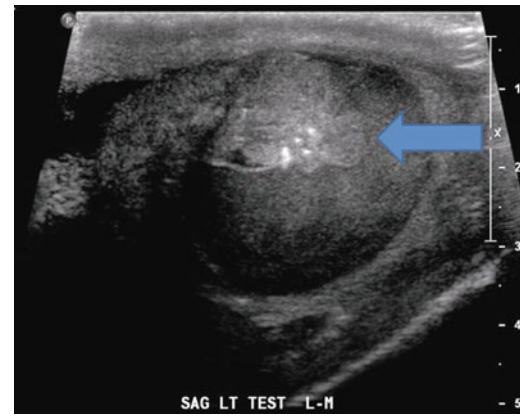

Fig. 14.15 *Blue arrow* depicts heterogeneous hyperechoic lesion of intratesticular mass (non-seminomatous germ cell tumor) with calcification

The Testis

Traditionally, patients with palpable or suspicious testicular masses would undergo radical orchiectomy, but investigators began to explore partial orchiectomy after intraoperative biopsy to confirm a lesion as benign or malignant, thus preserving testicular function in those where radical surgery is deemed unnecessary. Two recently published series show that the most common type of testicular tumor in prepubertal children is teratoma, a benign germ cell tumor (GCT).

Ultrasound probe: A high-frequency broadband linear transducer (4–12 MHz) can perform both power and spectral Doppler ultrasonography. Imaging of the scrotum, penis, and urethra is performed with a 7–12-MHz linear array transducer. The length of the transducer may vary from 4 to 8 cm. Equipment with Doppler capabilities is required for demonstrating blood flow in the evaluation of testicular torsion.

Technique: Technique and ultrasound probe for testis evaluation is described in detail in an earlier chapter. The linear array US is used intraoperatively after the testis is delivered via inguinal approach if malignancy is suspected. The cord is temporarily clamped and the testicle may be placed on ice (to minimize ischemia reperfusion injury) while the evaluation of the lesion is done. The goal is to delineate and determine respectability of the abnormal mass (hypoechoic/hyperechoic lesion compared to healthy parenchyma) (Fig. 14.15) that can be round or irregular and intratesticular. Dissection through the tunica albuginea and enucleation of the lesion with 2–5-mm margins should be carried out. The lesion should be sent for frozen section analysis by surgical pathology, and a determination of whether radical or partial orchiectomy is appropriately made. In the case of benign pathology, the tunica should be inspected for hemostasis and the incision closed. Finally, ultrasound may be used to inspect the affected area to ensure adequate resection of the lesion.

Clinical data: Organ-sparing approaches generally remain an option for a highly selected group of patients with testicular GCT only—men with bilateral testicular cancer or GCT in a solitary testis. Partial orchiectomy should be performed in such patients if the size and location of the mass are amenable to surgery. Partial orchiectomy of GCT provides a number of potential benefits over radical surgery: reduced need for androgen substitution, less psychological stress, preservation of fertility, and a durable cure rate. Partial orchiectomy of benign testicular lesions reduces the proportion of patients who are overtreated with radical orchiectomy. CIS detected in the testes remaining after partial orchiectomy can be treated with radiation therapy. Up to 40%

of patients will need hormonal replacement after this treatment. It should be emphasized that bilateral orchiectomy remains the best chance of cure in men with a solitary testis but comes at the cost of morbidity. Men should only undergo partial orchiectomy if one is certain that the lesion is benign. In this regard, size is important as masses larger than 2 cm in diameter are extremely suspicious for malignancy. Also, the lack of blood flow, serial growth, risk factors for GCT, and being impalpable all favor this approach [53].

The Renal Pelvis and Ureters

Stent Placement During Pregnancy and Patients in the ICU

Urolithiasis during pregnancy remains relatively common, affecting about 1 in 200 pregnancies [54]. While a majority of stones can be successfully managed conservatively with hydration, pain control, and antibiotics if necessary (70–80% will pass spontaneously owing mostly to physiologic dilatation of the ureters during pregnancy), the rest may require urologic intervention. Intravenous hydration may be necessary in cases of prolonged nausea and vomiting, and pain control should consist of acetaminophen with narcotic. Nonsteroidal anti-inflammatory medications should be avoided as they interfere with prostaglandin synthesis, which is required to maintain a patent ductus arteriosus until birth. In a portion of cases, renal colic and not urolithiasis may be the underlying cause of pain and necessitate urologic intervention [55]. Stent placement remains the most common of modern urologic interventions with various types of lithotripsy or PCN comprising the remainder. The urologist should note that stones and intervention may each increase the risk of preterm premature rupture of membranes and preterm labor. Minimally invasive techniques for managing patients who fail conservative treatment fall into two categories: temporary urinary drainage for obstructed urinary systems and procedures that facilitate stone removal. Stent placement has been performed using ultrasound guidance negating the need for ionizing radiation from intraoperative fluoroscopy and the concomitant risk to a fetus, particularly during the first trimester. When deciding on appropriate intervention for stones, diversion is usually recommended for stones that reside proximally in the collecting system [56]. Additionally, in cases of infected hydronephrosis or urosepsis, diversion is the mainstay of treatment. Cystoscopy for retrograde placement or PCN for antegrade placement of stents can be performed under local or regional anesthesia, thus minimizing the risk to the mother and fetus. Ureteral stents are placed at the time of cystoscopy, and ultrasound has been described as a valid tool for image guidance and confirmation of final stent position within the renal pelvis and bladder. Stent placement has been performed using ultrasound guidance negating the need for ionizing radiation from intraoperative fluoroscopy and the concomitant risk to a fetus, particularly during the first trimester.

Ultrasound probe: The use of a curved-array 3.5–5-MHz probe with or without color Doppler provides good visualization of the hydronephrosis calyx and or stone.

Technique: The technique, ultrasound probe, and limitations are similar to any renal ultrasound evaluation, with the special attention to the well-being of two instead of one patient. Fetal monitoring must be performed during the procedure with the assistance of the obstetric team. On renal ultrasound, stents appear as hyperechoic structures, and final placement with curls in the renal pelvis and bladder can be easily visualized as the cystoscope operator introduces and advances the ureteral stent up to the kidney. Additionally, one can evaluate the ureteral orifices with Doppler ultrasound of the bladder to confirm the presence of ureteral jets. Visualization of ureteral jets is an acceptable method of confirming the patency of the urinary tract. Patient can be awake or lightly sedated for the procedure with the assistance of the anesthesiologist and obstetric team to monitor the fetus. While one operator performs the cystoscopy, the radiologist or a second surgeon should perform the renal ultrasonography. The sonographer will

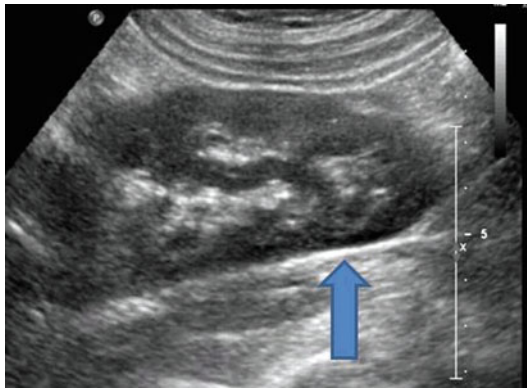

Fig. 14.16 Right ureteral stent placement under ultrasound guidance (*blue arrow*)

detect the hydronephrotic kidney and visualize the guide wire and stent placement real time (Fig. 14.16). Patients that are extremely unstable with septic shock due to impacted stone may have a stent placement using flexible cystoscopy and US guidance. In this case a single-J ureteral stent is preferable due to the stiffness and easier manipulation. Notably, stents should be changed every 4–6 weeks during pregnancy, as there is an increased propensity during pregnancy for stents to encrust.

Clinical data: One series of 300 pregnant women with renal colic, of whom 44 ultimately underwent ureteral stenting for symptomatic control or urinary obstruction, showed that stents placed during the second trimester were tolerated more (13/15 or 86.7%) as compared to those placed during the third trimester (14/26 or 53.8%) [55]. Our unpublished series includes five patients requiring ureteral stent placement in the intensive care unit. Three patients had a right-sided upper tract impacted stones, and two were left-sided (distal and mid ureter) stones. All patients were intubated and unstable. The use to flexible cystoscopy and single-J ureteral stents allowed prompt drainage of purulent urine and resolution of the septic shock. Placement of the left stents was more challenging due to the inability to move the patient to different positions and due to their high body mass index, but visualization of stent and flow during collection of intrarenal urine for culture was identified by color Doppler US. Moreover, the single-J stent allows repositioning that can be verified with simple abdominal X-ray (KUB).

Conclusion

Intraoperative use of ultrasound imaging has become standard in many different urologic interventions. Understanding its role in urologic surgery and interpreting key findings on ultrasound are essential to the successful use of this adjunct imaging technology. As newer devices, probes, and software are developed, we feel that use of ultrasound in the operating room will continue to expand into new areas.

References

1. http://www.auanet.org/content/guidelines-and-quality-care/policy-statements/c/consensus-statement-on-urologic-ultrasound-utilization.cfm.
2. Goodwin WE, Casey WC, Woolf W. Trocar (needle) nephrostomy in hydronephrosis. JAMA. 1955;157:891–4.
3. Gu Z, Qi J, Shen H, Liu J, Chen J. Percutaneous nephroscopic with holmium laser and ultrasound lithotripsy for complicated renal calculi. Lasers Med Sci. 2010;25:577–80.
4. Gupta S, Gulati M, Uday Shankar K, et al. Percutaneous nephrostomy with real-time sonographic guidance. Acta Radiol. 1997;38:454–7.
5. Bird VG, Fallon B, Winfield HN. Practice patterns in the treatment of large renal stones. J Endourol. 2003;17:355–61.
6. Skolarikos A, Alivizatos G, Papatsoris A, et al. Ultrasound-guided percutaneous nephrostomy performed by urologists: 10-year experience. Urology. 2006;68:495–9.
7. Alken P, Hutschenreiter G, Günther R. Percutaneous kidney stone removal. Eur Urol. 1982;8:304–11.
8. Miano R, Scoffone C, De Nunzio C, Germani S, Cracco C, Usai P, et al. Position: prone or supine is the issue of percutaneous nephrolithotomy. J Endourol. 2010;24:931–8.
9. Wah T. Percutaneous nephrostomy and antegrade ureteric stenting. Controversies and Consensus in Imaging and Intervention. 2005;3:20–2. Retrieved from www.c2i2.digithalamus.com (Feb 2012)
10. El-Nahas AR, Shokeir AA, El-Assmy AM, Shoma AM, Eraky I, El-Kenawy MR, et al. Colonic perfora-

tion during percutaneous nephrolithotomy: study of risk factors. Urology. 2006;67(5):937–41.
11. Basiri A, Ziaee A, Kianian H, et al. Ultrasonographic versus fluoroscopic access for percutaneous nephrolithotomy: a randomized clinical trial. J Endourol. 2008;22:281–4.
12. Radecka E, Magnusson A. Complications associated with percutaneous nephrostomies: a retrospective study. Acta Radiol. 2004;45:184–8.
13. von der Recke P, Nielsen MB, Pedersen JF. Complications of ultrasound guided nephrostomy: a 5-year experience. Acta Radiol. 1994;35:452–4.
14. Lewis S, Patel U. Major complications after percutaneous nephrostomy—lessons from a departmental audit. Clin Radiol. 2004;59:171–9.
15. Torres Muñoz A, Valdez-Ortiz R, González-Parra C, Espinoza-Dávila E, Morales-Buenrostro LE, Correa-Rotter R. Percutaneous renal biopsy of native kidneys: efficiency, safety and risk factors associated with major complications. Arch Med Sci. 2011;7:823–31.
16. Fergany AF, Hafez KS, Novick AC. Long-term results of nephron sparing surgery for localized renal cell carcinoma: 10-year followup. J Urol. 2000;163:442–5.
17. Lau WK, Blute ML, Weaver AL, Torres VE, Zincke H. Matched comparison of radical nephrectomy vs nephron-sparing surgery in patients with unilateral renal cell carcinoma and a normal contralateral kidney. Mayo Clin Proc. 2000;75:1236–42.
18. Huang WC, Levey AS, Serio AM, Snyder M, Vickers AJ, Raj GV, et al. Chronic kidney disease after nephrectomy in patients with renal cortical tumours: a retrospective cohort study. Lancet Oncol. 2006; 7:735–40.
19. Lee CT, Katz J, Shi W, Thaler HT, Reuter VE, Russo P. Surgical management of renal tumors 4cm or less in a contemporary cohort. J Urol. 2000;163:730–6.
20. Baust JG, Gage AA, Clarke D, et al. Cryosurgery—a putative approach to molecular-based optimization. Cryobiology. 2004;48:190–204.
21. Baust JG, Gage AA. The molecular basis of cryosurgery. BJU Int. 2005;95:1187–91.
22. Curry NS, Bissada NK. Radiologic evaluation of small and indeterminant renal masses. Urol Clin North Am. 1997;24:493–505.
23. Onik G, Reyes G, Cohen J, Porterfield B. Ultrasound characteristics of renal cryosurgery. Urology. 1993; 42:212–5.
24. Lockhart ME, Smith JK, Kenney PJ. Imaging of adrenal masses. Eur J Radiol. 2002;41(2):95–112.
25. Hijioka S, Sawaki A, Mizuno N, Hara K, Mekky MA, El-Amin H, et al. Contrast-enhanced endoscopic ultrasonography (CE-EUS) findings in adrenal metastasis from renal cell carcinoma. J Med Ultrason. 2011;38:89–92.
26. Bang HJ, Littrup PJ, Goodrich DJ, Currier BP, Aoun HD, Heilbrun LK, et al. Percutaneous cryoablation of metastatic renal cell carcinoma for local tumor control: feasibility, outcomes, and estimated cost-effectiveness for palliation. J Vasc Interv Radiol. 2012; 23:770–7.
27. Rosenstein D, McAninch JW. Urologic emergencies. Med Clin North Am. 2004;88:495–518.
28. Borrelli J, Brandes SB. Pelvic fractures: assessment and management for the urologist. AUA Update Series. 2004;23:82–6.
29. Ozkan B, Kaya O, Akda R, Unal O, Kaya D. Suprapubic bladder aspiration with or without ultrasound guidance. Clin Pediatr (Phila). 2000;39(10): 625–6.
30. Miano R, Kim FJ, De Nunzio C, Mauriello A, Sansalone S, Vespasiani G, et al. Morphological evaluation of the male external urethral sphincter complex by transrectal ultrasound: feasibility study and potential clinical applications. Urol Int. 2012; 89(3): 275–82.
31. Coppola R. Diagnosis of prostatic carcinoma by means of transperineal needle biopsy. Riforma Med. 1963;77:1282–4.
32. Igel TC, Knight MK, Young PR, et al. Systematic transperineal ultrasound guided template biopsy of the prostate in patients at high risk. J Urol. 2001; 165:1575–9.
33. Crawford ED, Wilson SS, Torkko KC, et al. Clinical staging of prostate cancer: a computer-simulated study of transperineal prostate biopsy. BJU Int. 2005; 96:999–1004.
34. Gonder MJ, Soanes WA, Smith V. Experimental prostate cryosurgery. Invest Urol. 1964;14:610–9.
35. Onik G, Cobb C, Cohen J, et al. US characteristics of frozen prostate. Radiology. 1988;168:629–31.
36. Littrup P, Monti J, Mody A, et al. Prostatic cryotherapy: ultrasonic and pathologic correlation in the canine model. Urology. 1994;44:175–84.
37. Scardino P, Carlton C. Combined interstitial and external irradiation for prostatic cancer. In: Javadpour N, editor. Principles and management of urologic cancer. Baltimore: Williams & Wilkins; 1983. p. 392–408.
38. Whitmore Jr WF, Hilaris B, Grabstald H. Retropubic implantation to iodine 125 in the treatment of prostatic cancer. J Urol. 1972;108:918–20.
39. DeLaney TF, Shipley WU, O'Leary MP, Biggs PJ, Prout Jr GR. Preoperative irradiation, lymphadenectomy, and 125iodine implantation for patients with localized carcinoma of the prostate. Int J Radiat Oncol Biol Phys. 1986;12:1779–85.
40. Aronowitz JN. Dawn of prostate brachytherapy: 1915–1930. Int J Radiat Oncol Biol Phys. 2002;54: 712–8.
41. Holm HH, Juul N, Pedersen JF, Hansen H, Stroyer I. Transperineal Iodine-125 seed implantation in prostatic cancer guided by transrectal ultrasonography. J Urol. 1983;130:283–6.
42. Ho A, Burri R, Cesaretti J, et al. Radiation dose predicts for biochemical control in intermediate-risk prostate cancer patients treated with low-dose-rate brachytherapy. Int J Radiat Oncol Biol Phys. 2009; 75:16–22.
43. Potters L, Roach III M, Davis B, et al. Postoperative nomogram predicting the 9-year probability of prostate cancer recurrence after permanent prostate brachyther-

apy using radiation dose as a prognostic variable. Int J Radiat Oncol Biol Phys. 2010; 76:1061–5.
44. Hinnen KA, Jan JB, van Roermund JG, et al. Long-term biochemical and survival outcome of 921 patients treated with I-125 permanent prostate brachytherapy. Int J Radiat Oncol Biol Phys. 2009;76:1433–8.
45. Nag S, Ciezki JP, Cormack R, et al. Intraoperative planning and evaluation of permanent prostate brachytherapy: report of the American Brachytherapy Society. Int J Radiat Oncol Biol Phys. 2001;51: 1422–30.
46. Han BH, Wallner K, Merrick G, Butler W, Sutlief S, Sylvester J. Prostate brachytherapy seed identification on post-implant TRUS images. Med Phys. 2003;30: 898–900.
47. Rove KO, Sullivan K, Crawford ED. High-intensity focused ultrasound: ready for primetime. Urol Clin North Am. 2010;37:27–35.
48. Gelet A, Chapelon JY, Bouvier R, et al. Local control of prostate cancer by transrectal HIFU therapy: preliminary results. J Urol. 1999;161:156–62.
49. Warwick R, Pond J. Trackless lesions in nervous tissues produced by high intensity focused ultrasound (high-frequency mechanical waves). J Anat. 1968; 102:387–405.
50. Chaussy C, Thuroff S. The status of high-intensity focused ultrasound in the treatment of localized prostate cancer and the impact of a combined resection. Curr Urol Rep. 2003;4:248–52.
51. Dewhirst MW, Viglianti BL, Lora-Michiels M, et al. Basic principles of thermal dosimetry and thermal thresholds for tissue damage from hyperthermia. Int J Hyperthermia. 2003;19:267–94.
52. Ukimura O, Gill IS, Desai MM, et al. Real-time transrectal ultrasonography during laparoscopic radical prostatectomy. J Urol. 2004;172:112–8.
53. Zuniga A, Lawrentschuk N, Jewett MA. Organ-sparing approaches for testicular masses. Nat Rev Urol. 2010;7:454–64.
54. Cormier CM, Canzoneri BJ, Lewis DF, et al. Urolithiasis in pregnancy: current diagnosis, treatment, and pregnancy complications. Obstet Gynecol Surv. 2006;61:733–41.
55. Andreoiu M, Macmahon R. Renal colic in pregnancy: lithiasis or physiological hydronephrosis? Urology. 2009;74:757–61.
56. Loughlin KR, Kerr LA. The current management of urolithiasis during pregnancy. Urol Clin North Am. 2002;29:701–4.

Index

P.F. Fulgham and B.R. Gilbert (eds.), *Practical Urological Ultrasound*, Current Clinical Urology,
DOI 10.1007/978-1-59745-351-6, © Springer Science+Business Media New York 2013